Phytochemical and biological activity studies on Salvia viridis L

Rungsimakan, Supattra

Award date:
2011

Awarding institution:
University of Bath

Phytochemical and biological activity studies on *Salvia viridis* L.

Supattra Rungsimakan

A thesis submitted for the degree of Doctor of Philosophy

University of Bath

Department of Pharmacy and Pharmacology

November 2011

Table of contents

Abstract

Six new compounds were isolated from the aerial and root parts of *S. viridis* L. cv. Blue Jeans. Two new triterpenoids, lup-20(29)-ene-2α-acetate-3β-ol, and lup-20(29)-ene-2α-ol-3β-acetate were found in the aerial part together with lup-20(29)-ene-2α-3β-diol, ursolic acid, oleanolic acid, β-sitosterol and β-sitosterol glucoside. Three new diterpenoids, 1-oxomicrostegiol, viroxocane, viridoquinone, together with five known diterpenoids, ferruginol, salvinolonyl 12-methyl ether, microstegiol, 7α-acetoxy-14-hydroxy-8,13-abietadiene-11,12-dione and 7α,14-dihydroxy-8,13-abietadiene-11,12-dione were found in roots. 1-Docosyl ferulate, 2",3"-di-*O*-acetyl-martynoside and a mixture of 2-(4'-alkoxy-phenyl) ethyl alkanoates were also isolated from roots. Seven caffeic acid derivatives, five flavonoid glycosides, and salidroside were found in the crude aerial fraction. Four caffeic acid derivatives were known phenylpropanoids, i.e. trans-, cis-verbascoside, leucosceptoside A and martynoside, which are now reported in the genus *Salvia* for the first time. The others were caffeic acid, rosmarinic acid and 6-*O*-caffeoyl-glucose. A new flavonoid glycoside, luteolin-7-*O*-α-rhamnopyranosyl-(1→6)-β-galactopyranoside was also identified in the aerial part with four known flavone glycosides: luteolin-7-*O*-β-glucopyranoside, luteolin-7-*O*-β-galactopyranoside, luteolin-7-*O*-rutinoside and apigenin-7-*O*-β-glucopyranoside.

Verbascoside (acteoside), which is a major component in this plant, showed a significant protective effect against UVA induced damage in a human skin fibroblast model in vitro. It exhibited 1.4 fold protective effect against UVA induced necrosis with 1.4 fold higher in cell survival. 50 μM Verbascoside showed the same protective effect as 100 μM DFO at a high intensity UVA dose (500 kJ/m^2). Further determination of organelle specific protection suggested a mechanism of action in mitochondria.

Two terpenoids, lup-20(29)-ene-2α-acetate-3β-ol and 7α,14-dihydroxy-8,13-abieta-diene-11,12-dione, exhibited antibacterial activity against *Enterococcus faecalis* with MIC 50 μM. Microstegiol was also active against *Staphylococcus aureus* with MIC 50 μM. Ursolic acid, oleanolic acid and ferruginol showed appreciable antibacterial activity against three Gram-positive bacteria, *Staphylococcus aureus*, *Enterococcus faecalis*, and *Bacillus cereus* with MIC 12.5-50 μM. The other diterpenoids were active against all three Gram-positive bacteria with MIC 100-200 μM. None of crude fractions was active against three Gram-negative bacteria, *Klebsiella pneumoniae*, *Proteus vulgaris*, and *Escherichia coli*.

Acknowledgements

I would like to express my gratitude to Dr Michael G Rowan for his great supervision. He is an excellent exemplar of a hard-working and optimistic scientist as well as a dedicated teacher. His kind and understanding personality has encouraged me to continually carry on laboratory work, and gain many essential skills. I am truly impressed by his keenness towards scientific knowledge, and I have also been inspired by his brilliant out of the box ideas.

I am also grateful to Dr Charareh Pourzand for being so great to me. She gave valuable suggestions for the in vitro cell culture experiment and has kindly devoted herself to help me develop many crucial skills. I also thank Dr Asma Aroun for cell culture experiments; Jo Carter for microbiology lab work; Dr Adrian Rogers for flow cytometric analysis. Working with them had become a good experience for me and I have learned many practical techniques.

I would like to express my thanks to Dr Tim Woodman for NMR experiments; Chris Rehbein for Mass Spectrometry, and also the technical staffs: Don Perry, Kevin Smith, Barry Crowley, Patricia Higgins, Susan Alston and the others in the Department of Pharmacy and Pharmacology, University of Bath for their help, and hospitality. I also thank Bridget Stein, EPSRC National Mass Spectrometry Service Centre, School of Medicine, University of Swansea for GC-CI-MS analysis.

I greatly appreciate the friendliness of colleagues: Dr Emma Casey, Dr Vinod Kumar, Dr Gerta Cami-Kobeci, Dr Quan Yang, Dr Manda Tsang, Chris Roche, Marco Mottinelli, Katerina Kumpan, Flora Bunga, Elina Ridzwan, Nour Alhusein, Tina Radka, Jin Zhang and Chieu Ming Long. I thank Abdelkader Metwally, Dr Sawanya Buranaphalin, and Dr Noppadon Adjimatera for their advice and friendship.

I gratefully thank the Thai Government for granting a PhD studentship.

Finally, my greatest gratitude goes to my family for their loving care, support, and encouragement.

List of abbreviations

°C	Degree Celsius
ACh	Acetylcholine
ATCC	American Type Culture Collection
br	Broad
$CDCl_3$	Chloroform-deuterated
CD_3OD	Methanol-deuterated
CECT	Spanish Type Culture Collection
CH_3OH	Methanol
cm	Centimetre
COSY	Correlated Spectroscopy
d	Doublet
dd	Doublets of doublet
ddd	Doublets of doublet of doublet
dt	Doublets of triplet
DEPT	Distortionless Enhancement by Polarization Transfer
DFO	Desferrioxamine
DMAPP	Dimethylallyl diphosphate
DMSO	Dimethylsulfoxide
DMSO-d6	Dimethylsulfoxide-deuterated
D_2O	Deuterated-water
DPPH	2,2-Diphenyl-1-picrylhydrazyl
EC_{50}	50% Effective Concentration
EMEM	Earle's modified Minimal Essential Medium
FPP	Farnesyl diphosphate
g	gram
GC-CI-MS	Gas Chromatography Chemical Ionisation Mass Spectrometry
GGPP	Geranylgeranyl diphosphate
GPP	Geranyl diphosphate
h	Hour
HMBC	Heteronuclear Multiple Bond Correlation
HMQC	Heteronuclear Multiple Quantum Correlation
HPLC	High Performance Liquid Chromatography

HR-ESI-MS	High Resolution Electrospray Mass Spectrometry
H2BC	Heteronuclear two Bond Correlation
Hz	Hertz
IC_{50}	50% Inhibitory Concentration
INT	*p*-Iodonitrotetrazolium chloride
IPP	Isopentenyl diphosphate
J	Coupling constant
kJ/m^2	KiloJoule per metre square
m	Multiplet
MEP	Methylerythritol phosphate
mg	Milligram
MHz	MegaHertz
MIC	Minimum Inhibition Concentration
min	Minute
ml	Millilitre
mM	Millimolar
mm	Millimetre
MS	Mass Spectrometry
MTT	3-(4,5-Dimethylthiazol-2-yl)-2,5-diphenyl tetrazolium bromide
MVA	Mevalonic acid
MW	Molecular weight
m/*z*	Mass by charge
NMR	Nuclear Magnetic Resonance
nm	Nanometre
NOESY	Nuclear Overhauser Effect Spectroscopy
NR	Neutral red
PBS	Phosphate Buffered Saline
PFP	Pentafluorophenyl
ppm	Part per million
q	Quartet
Rf	Retention factor
ROS	Reactive Oxygen Species
S.	*Salvia*
t	Triplet

TLC	Thin Layer Chromatography
Tris	Tris (hydroxymethyl) methylamine
µm	Micron
µl	Microlitre
µM	Micromolar
UV	Ultraviolet
UVA	Ultraviolet A
UVB	Ultraviolet B
UVC	Ultraviolet C
1D	One dimensional
2D	Two dimensional

Chapter 1
Introduction

Salvia, or Sage, has been used as traditional medicine and in culinary purposes for a long time. This plant belongs to family Lamiaceae (or Labiatae), subfamily Nepetoideae, and tribe Mentheae. They are perennial, annual, or biennial shrubs, or herbs with erect stems up to 170 cm, lobed or pinnate or simple leaves, 2-8 flowers in axillary verticillasters with various coloured bracts (Hedge, 1972). There are over 900 species of *Salvia* around the world, half of them are widely distributed in Central and South America (500 species) while the others are in Central Asia and Mediterranean (250 species), Eastern Asia (90 species), and South Africa region (30 species) (Walker et al., 2004).

The name *Salvia* is derived from the Latin word "*salvere*" meaning "to save" because of its medicinal properties (Dweck, 2000). Sage is traditionally used to treat common ailments, for instance, flatulence, stomach ache, mouth and throat infection, and also for culinary purposes (Barnes et al., 2007).

Figure 1.1 *Salvia viridis* L. cv. Blue Jeans (Synonym *S. horminum* L.)

The root of *S. miltiorrhiza* Bunge (Danshen) has been used in traditional Chinese medicine to treat coronary heart disease, cerebrovascular disease, various types of hepatitis, chronic renal failure, dysmenorrheal, and to stimulate blood circulation (Jiang et al., 2005; Li et al., 2008). Turkish *Salvia* species have been used as stomachic, diuretic, hemostatic, spasmolytic, carminative, mouth and throat infections including colds (Topcu et al., 2008). The Greek sage (*S. fruticosa* Miller) has been known as a spice or ingredient of folk remedies for toothache and intestinal complaints (Karousou et al., 2000). Infusions of certain *Salvia* species in South Africa have been used to treat colds, cough, flu, colic, diarrhoea, indigestion, abdominal complaints, and bacterial infections (Kamatou et al., 2008).

Many species have been investigated for their biologically active chemical constituents. Phytochemical studies on *Salvia* species have been extensively carried out, and their main chemical constituents can be classified as polyphenols, and terpenoids. The major compounds of aerial parts are flavonoids, triterpenoids and volatile substances, mainly monoterpenes whereas diterpenoids are commonly found in roots (Topcu, 2006). Certain types of phenolic acid, i.e. caffeic acid derivatives, have predominantly been found in this genus (Lu and Foo, 2002).

1.1. Terpenoids in the genus *Salvia*

Terpenoids are ubiquitous secondary metabolites in the plant kingdom. Many of them possess biological activities. A terpene containing oxygen atom is defined as a terpenoid, but the terms of terpenoid, and terpene can be interchangeable. Terpenoids can be classified into groups according to the number of carbon atoms in their skeleton, i.e. hemiterpenes (C_5), monoterpene (C_{10}), sesquiterpenes (C_{15}), diterpenes (C_{20}), sesterterpenes (C_{25}), triterpenes (C_{30}), and tetraterpenes (C_{40}). These are derived from isoprene (C_5) unit which are attached to another one by head to tail, or tail to tail linkages. Terpenoids are biosynthesised from dimethylallyl diphosphate (DMAPP), and isopentenyl diphosphate (IPP), and then rearrangement by cyclization reaction of the units (Dewick, 2009). Biosynthesis pathways of terpenoids are shown in Figures 1.3-1.6.

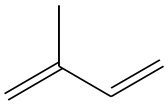

Figure 1.2 Isoprene

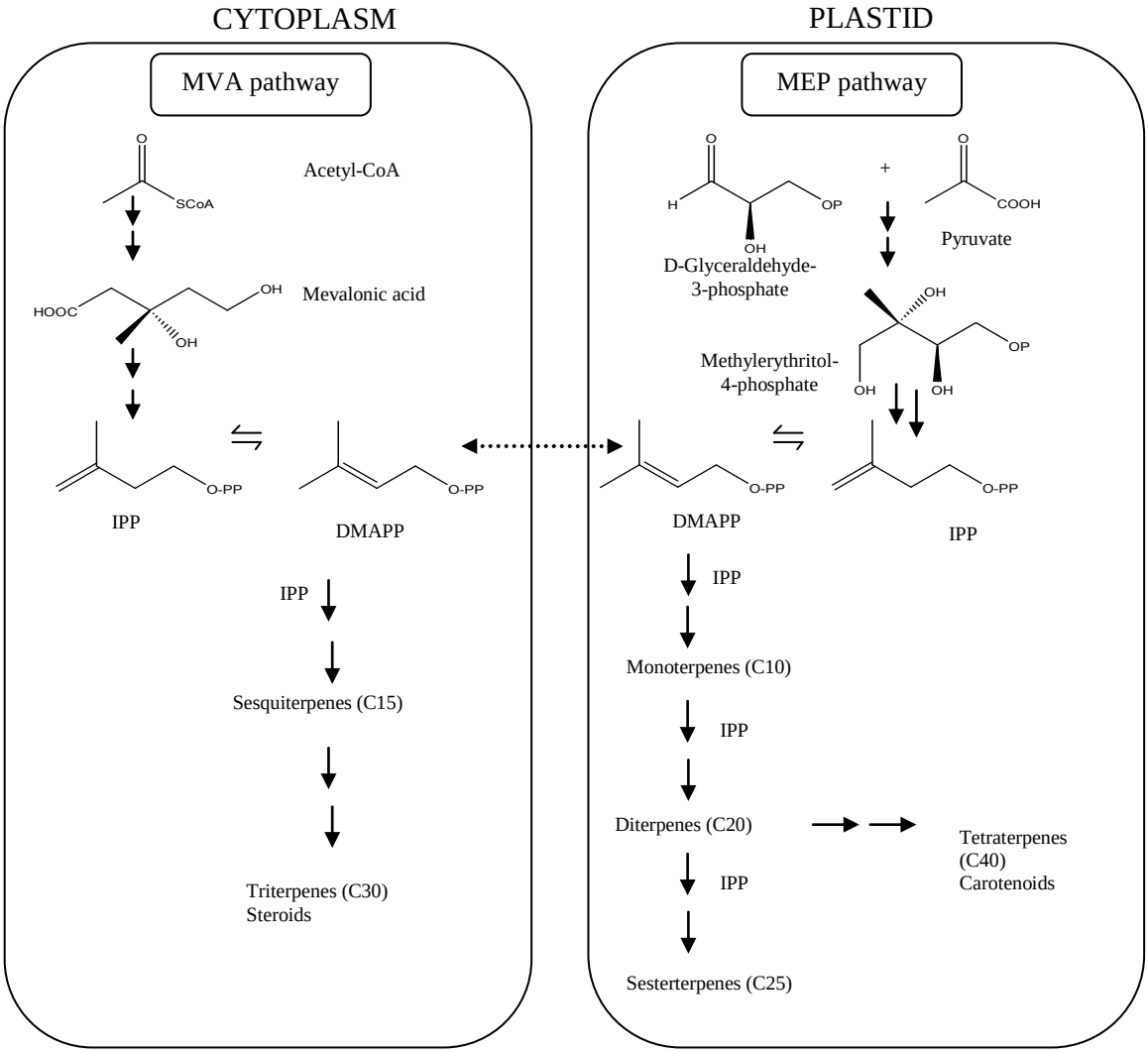

Figure 1.3 Biosynthesis pathways of terpenoids

Within plant cells, these two precursors, IPP and DMAPP, may be derived via the mevalonic acid (MVA) pathway in the cytoplasm, and via the methylerythritol phosphate (MEP) pathway in plastids (Bartram et al., 2006; Ikeda et al., 2008) as shown in Figure 1.3. The terpene synthases that are responsible for monoterpenes and diterpene biosynthesis are predominantly located in plastid whereas sesquiterpene synthases are mostly in the cytosol (Tholl, 2006). All terpenes are originally derived from DMAPP with further incorporation of IPP to yield geranyl diphosphate (GPP; C10), and farnesyl diphosphate (FPP; C15). The rearrangement of GPP with carbocation reactions catalyzed by the monoterpene synthase

enzymes results in a variety of monoterpenoids as shown in Figure 1.4. The cyclization of GPP into the menthyl/α-terpinyl cation is the key step in the formation of various derived monoterpenoids (Dewick, 2009).

GGPP (geranylgeranyl diphosphate; C20) is biosynthesized from FPP by further incorporation of IPP and is the essential precursor to generate diterpenes as shown in Figure 1.5. The cyclization reactions of GPP mediated by carbocation formation include the diterpene synthase enzymes and rearrangement of products derive distinctive diterpene skeletons (Dewick, 2009). Figure 1.5 shows two different chair conformation arrangements of GGPP. One is catalyzed by the enzyme (-)-copalyl diphosphate synthase (ene-kaurene synthase A), and the other is by (+)-copalyl diphosphate synthase (abietadiene synthase). Consequently, the two products that arise, i.e. (-)-copalyl PP, and (+)-copalyl PP (labdadienyl PP) respectively, are the main starting compounds for various types of diterpenoids. The (+)-copalyl PP is the substrate for reactions catalyzed by the enzyme KSL (kaurene synthase-like diterpene synthases) to yield abietane type ditepenoids such as ferruginol, and further modified to tanshinone derivatives (Wang and Wu, 2010).

FPP is the crucial precursor for sesquiterpene (C15), and triterpenes (C30) as shown in Figure 1.6. Sesquiterpene essential oils are biosynthesized by sesquiterpene cyclase enzymes to yield β-caryophyllene, α-humulene, and germacrenes (Dewick, 2009). The dimerization of FPP by tail to tail attachment yields squalene, the key intermediate in triterpenoid biosynthesis. The cyclization of intermediate, 2,3-oxidosqualene, results in various polycyclic triterpenes, and sterols (Volkman, 2005; Dewick, 2009). Figure 1.6 shows the pathway of pentacyclic tripenoid biosynthesis. The dammarenyl cation is generated from 2,3-oxidosqualene, and further rearranged and cyclized by the aid of the enzyme lupeol synthase, and β-amyrin synthase to yield the final products of lupeol, β-amyrin, and α-amyrin. These products are further oxidized to triterpenic acids, betulinic acid, oleanolic acid, and ursolic acid respectively.

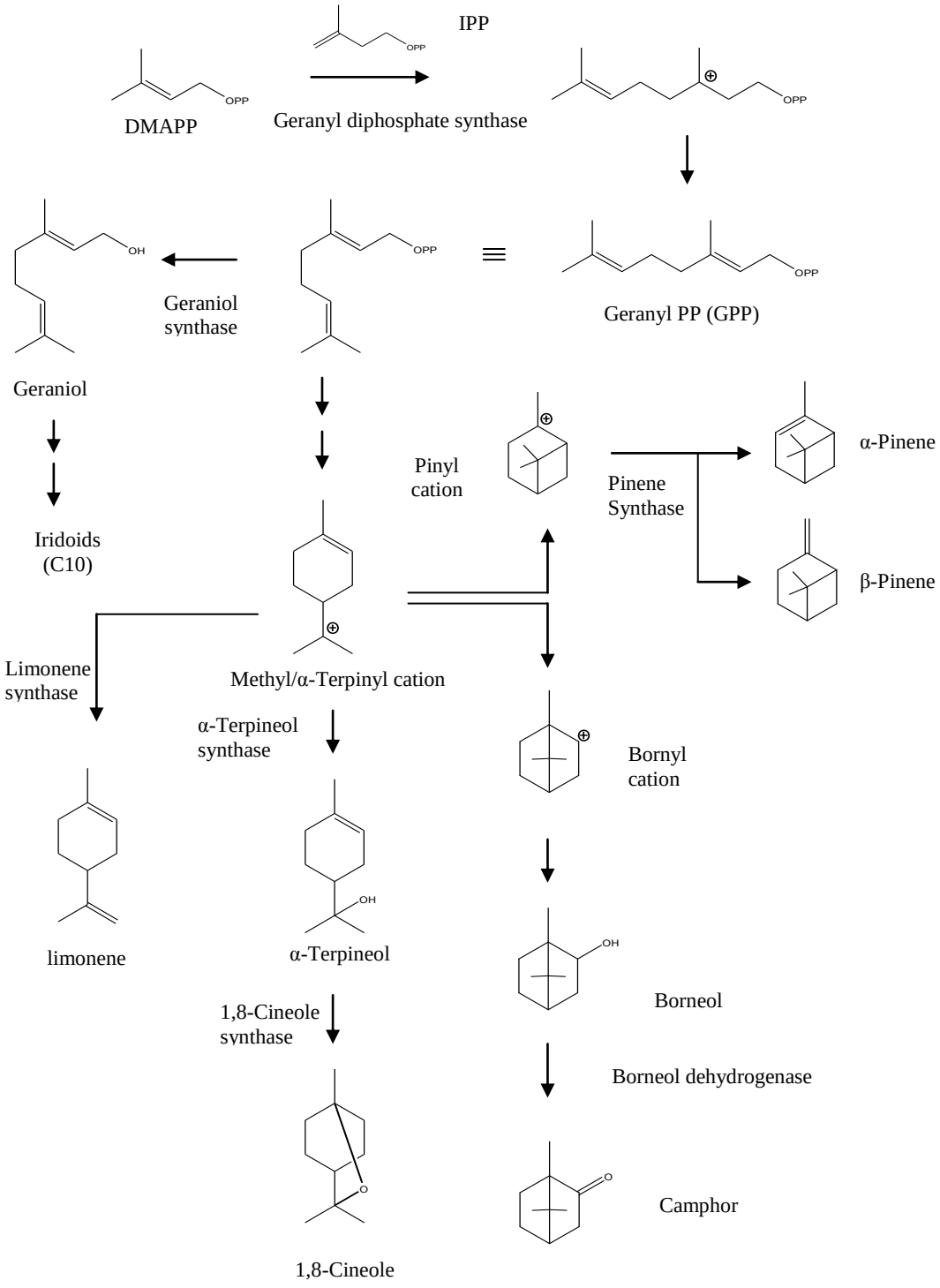

Figure 1.4 Biosynthesis pathways of common monoterpenoids (Dewick, 2009)

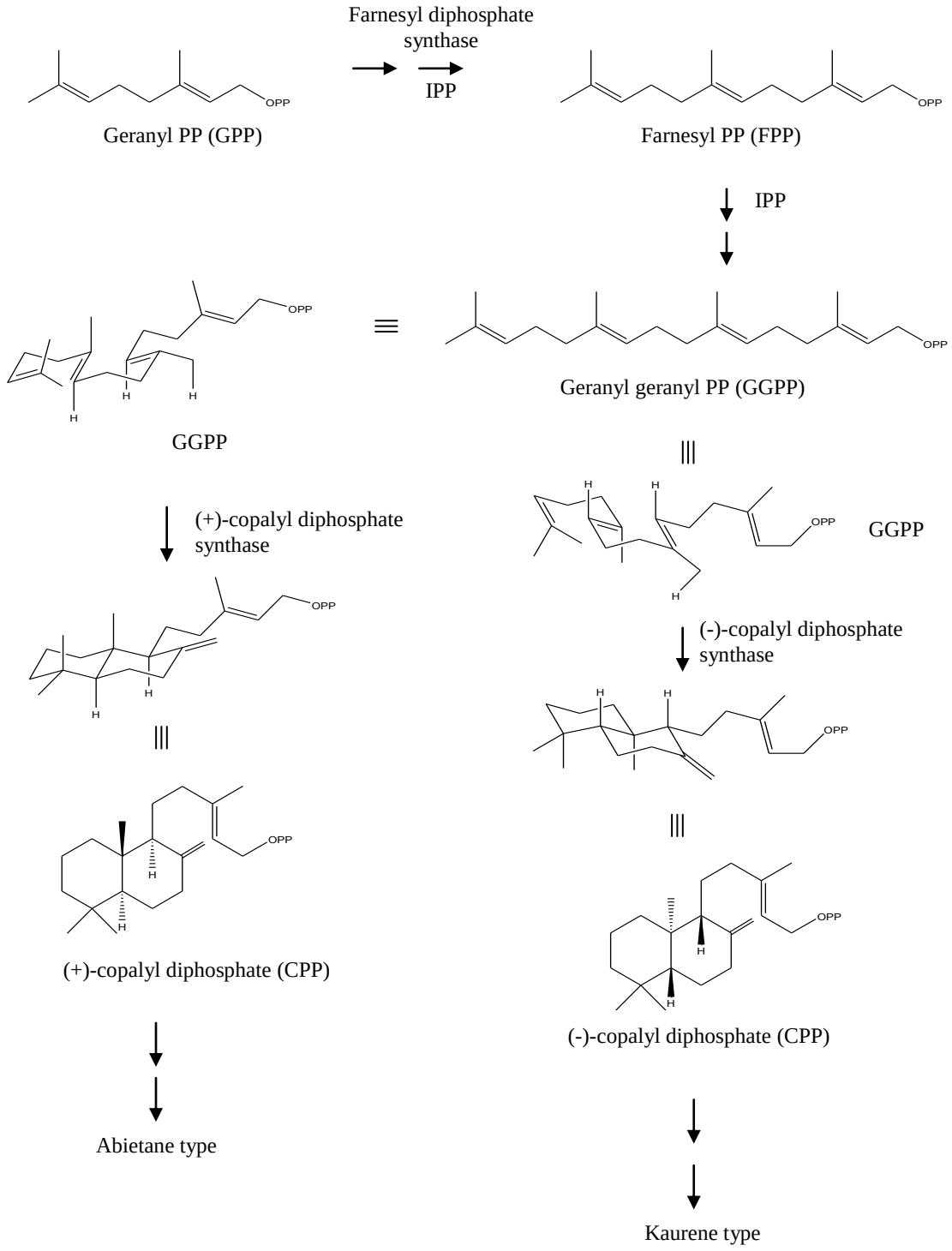

Figure 1.5 Biosynthesis pathways of diterpenoids (Dewick, 2009)

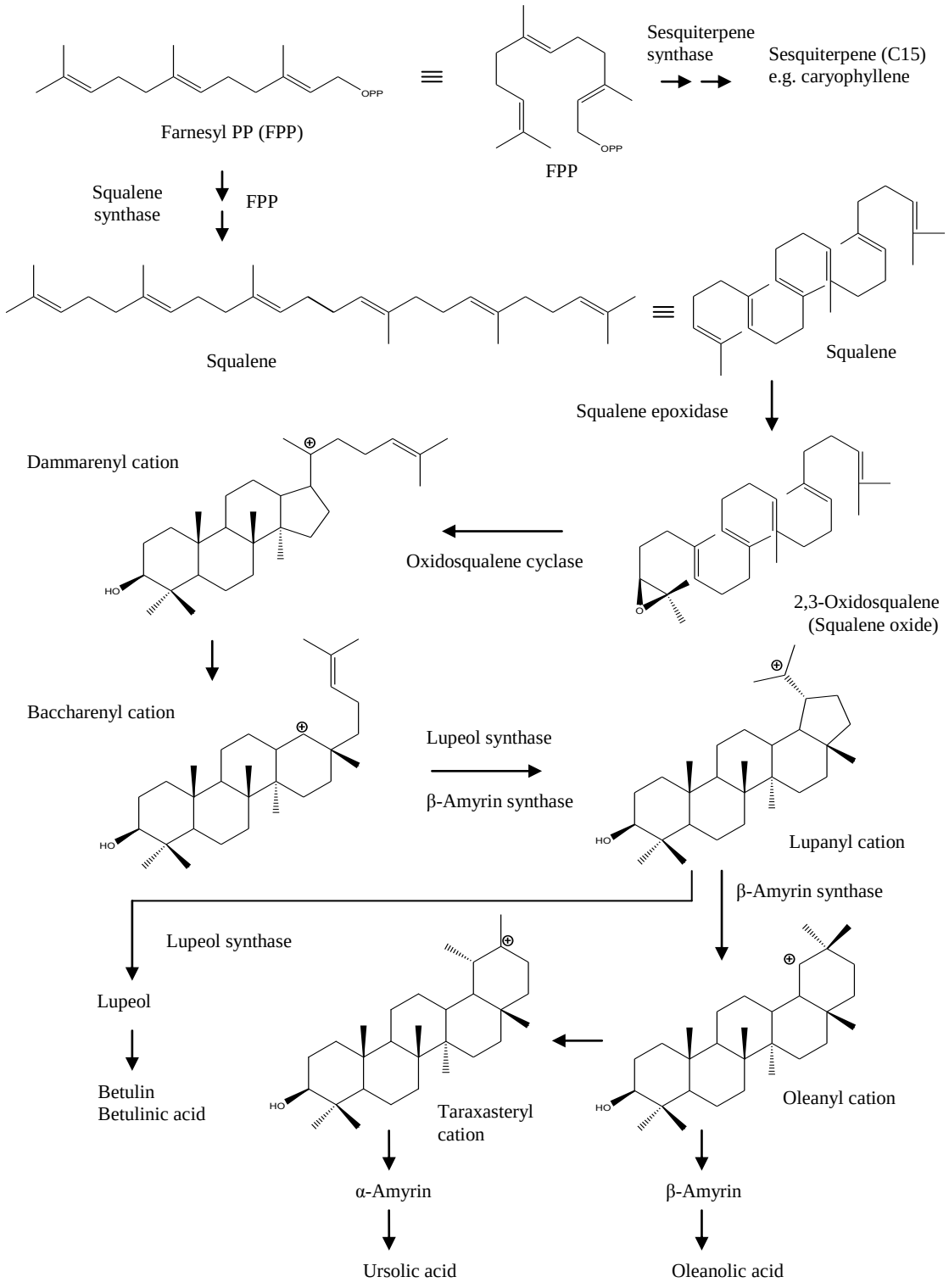

Figure 1.6 Biosynthesis pathways of sesquiterpenoid, and pentacyclic triterpenoids (Dewick, 2009)

1.1.1. Monoterpenoids (C10)

Monoterpenes comprise two isoprene units. As they are volatile with characteristic odours, they are common constituents in essential oils. Although essential oils are complex mixtures with various kinds of skeleton, 90% of them are monoterpene (Bakkali, et al., 2008). They can be classified according to functional group in the molecule, i.e., alcohols, aldehydes, ketone, esters, and ethers (Bakkali, et al., 2008), or by the arrangement of carbon atoms, i.e. menthane type, pinane type, camphane/bornane type, thujane type (Dewick, 2009). The most common monoterpenes from *Salvia* are pinenes, borneol, camphor, and 1,8-cineole, thujones as shown in Figure 1.7.

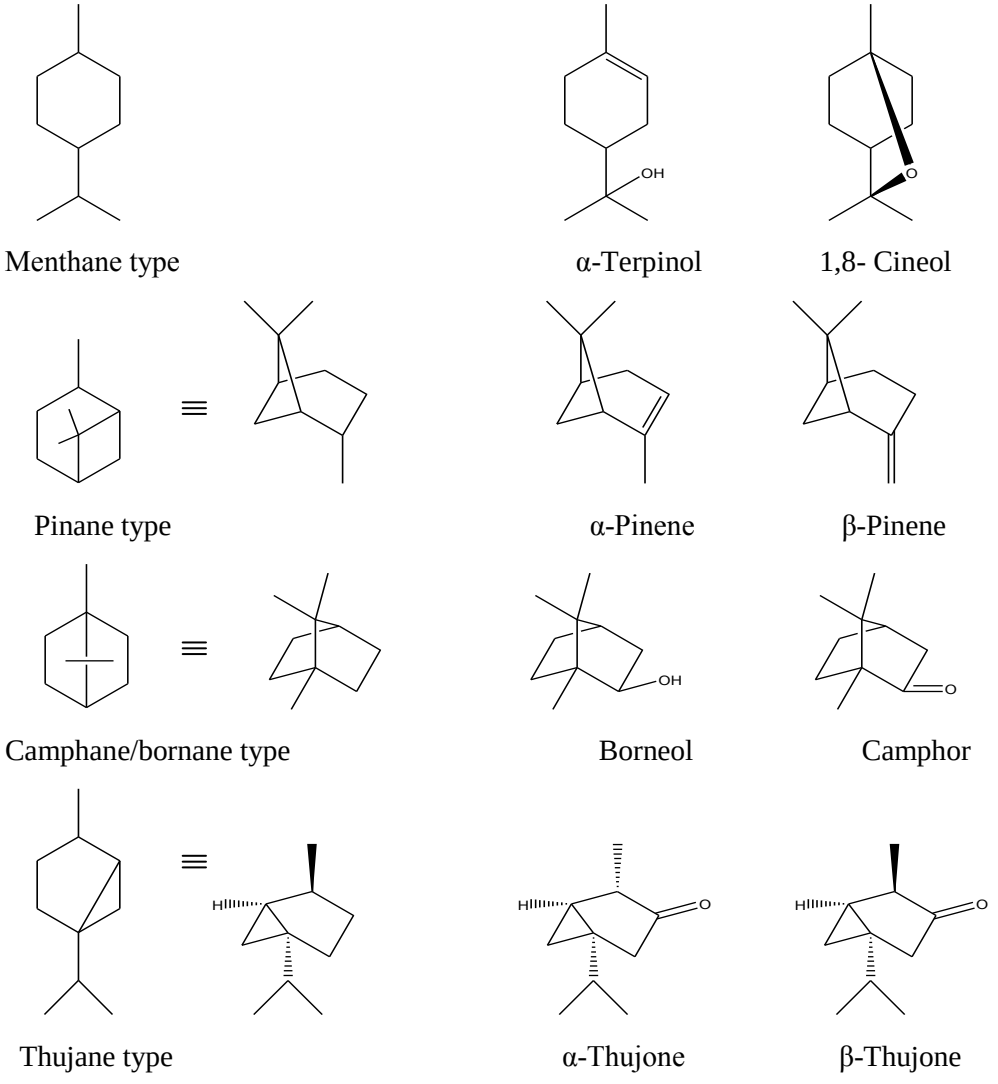

Figure 1.7 Common monoterpenoids in *Salvia* species

Aerial parts of certain *Salvia* spp. are rich in essential oils (Baser, 2002). The standard content of essential oil from *S. officinalis* L. should not less than 15 ml/kg for the whole drug while the minimal essential oil content of *S. fruticosa* Mill. is 18 ml/kg for the whole drug (British Pharmacopoeia, 2008). Environmental and genetic factors affect the production of the oil. Percentages of major essential oil components of *S. officinalis* L., *S. lavandulaefolia* Vahl., and *S. fruticosa* Mill. (Synonym *S. triloba* L.) varied as shown in Table 1.1. The essential oil of each species comprises more than 50 chemical components. Essential oil of *S. macrochlamys* Boiss et. Kotschy comprised 80 compounds mainly 1, 8-cineole (27%), borneol (13%), and camphor (11%) whereas essential oil of *S. recognita* Fisch. & Meyer comprised 82 compounds mainly camphor (42%), and 1, 8-cineol (12%) (Tabanca et al., 2006).

Sage oil is defined in the British Pharmacopoeia (2008) as the essential oil obtained by stream distillation from the fresh/dried flowering stems of *Salvia sclarea* L. The compositions of *S. sclarea* L. essential oil were mainly linalool, linalyl acetate, α-terpineol, geraniol, and sclareol (Giannouli and Kintzios, 2000; Pitarokili et al., 2002). British Pharmacopoeia (2008) states the standard percentage ranges of sage oil from *S. sclarea* L. as follows:

α/β Thujone: less than 0.2 %

Linalool: 6.5-24 %

Linalyl acetate: 56-78 %

α-Terpineol: less than 5 %

Germacrene D: 1-12 %

Sclareol: 0.4-2.6 %

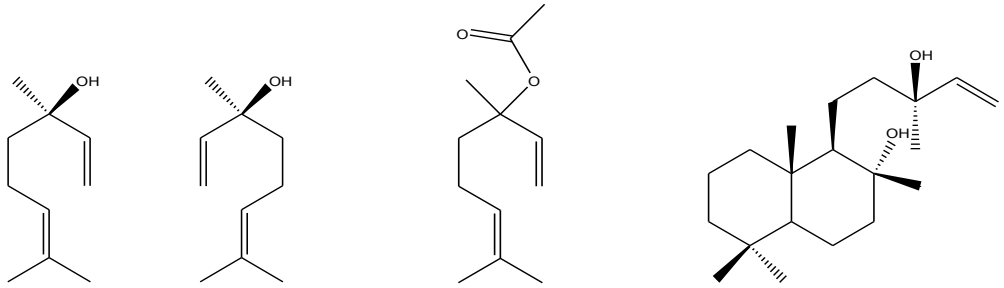

(+)-Linalool (-)-Linalool Linalyl acetate Sclareol

Figure 1.8 Terpenoids in sage oil from *S. sclarea* L.

Table 1.1 Percentages of the common essential oils in three *Salvia* species

% in oil	1,8-Cineol	Camphor	Pinenes		Thujones		Reference
			α	β	α	β	
S. officinalis L.	4	19	Less than 1		20	4	Bozin et al., 2007
	15	11	3	10	25	4	Delamare et al., 2007
	5	11	-	3	6		Savelev et al., 2004
	-	1-44	0.1-9	1-15	1-46	1-40	Giannouli and Kintzios, 2000
	5-16	1-14	1-5	2-19	15-53	2-13	Perry et al., 1999
Total range	**4-16**	**1-44**	**1-9**	**1-19**	**1-53**	**1-40**	
S. lavandulaefolia Vahl.	17	43	-	-	-	-	Savelev et al., 2004
	1-54	1-36	2-24	2-48	1-23	1-4	Giannouli and Kintzios, 2000
	17	27	5	12	-	-	Perry et al., 2000
Total range	**1-54**	**1-43**	**2-24**	**2-48**	**1-23**	**1-4**	
S. fruticosa Mill. (*S. triloba* L.)	16	13	1	4	20	5	Delamare et al., 2007
	20	49	2	2	-		Savelev et al., 2004
	17-54	1-16	2-7	2-9	1-8	1-9	Pitarokili et al., 2003
	48	9	5	5	4	8	Sivropoulou et al., 1997
Total range	**16-54**	**1-49**	**1-7**	**2-9**	**1-20**	**1-9**	

1.1.2. Sesquiterpenoids (C15)

Sesquiterpenoids are not common in the genus *Salvia*. Hydrocarbon and oxygenated sesquiterpenes have been generally isolated together with other monoterpenoids in essential oils. β-Caryophyllene, α-humulene and caryophyllene oxide were generally reported in range of 1-11% in essential oil of *S. officinalis* L. while germacrene D was mainly isolated from *S. sclarea* L. in range of 1-48% (Giannouli and Kintzios, 2000). Spathulenol was reported to form 39% of oil from *S. elegans* Vahl. (Mathew and Thoppil, 2011), and also a small percentage from *S. sclarea* L. (Ulubelen et al., 1994a; Giannouli and Kintzios, 2000). Viridiflorol was reported from *S. officinalis* L., *S. lavandulaefolia* Vahl., and *S. triloba* L. in

range of 1-18% in oil (Giannouli and Kintzios, 2000; Bozin et al., 2007; Delamare et al., 2007).

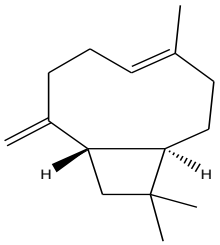

. β-Caryophyllene

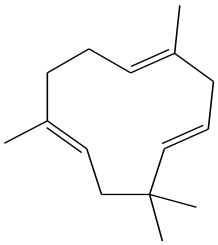

α-Humulene (α-Caryophyllene)

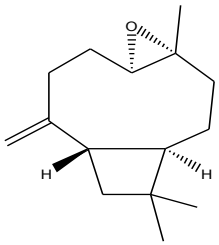

Caryophyllene oxide

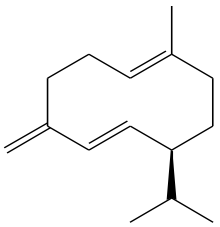

Germacrene D

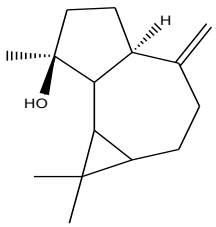

Spathulenol

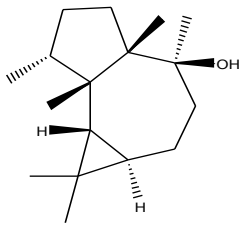

Viridiflorol

Figure 1.9 Sesquiterpenoids in *Salvia* species

1.1.3. Diterpenoids (C20)

Many and various diterpenoids have been found in the genus *Salvia*, many with interesting biological activity. Antibacterial, cytotoxic, and cardiovascular activities have been extensively reported (Topcu and Goren, 2007). Diterpenoids can be classified according to the ring number as acyclic, bicyclic, tricyclic, tetracyclic, macrocyclic, and miscellaneous (Hanson, 1998). Alvarenga et al. (2001) presented 91 diterpenoid skeletons from various genera in Lamiaceae by using a computer based system. From the total of 91 investigated *Salvia* species, there were 50 skeletons with 592 occurrences. The most common one was the abietane type (275 occurrences), and the others were clerodane, rearranged abietane, pimarane, icetexane, labdane, and kaurane as shown in Figure 1.10.

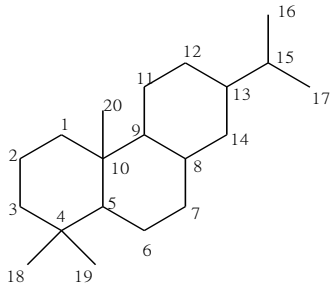

Abietane

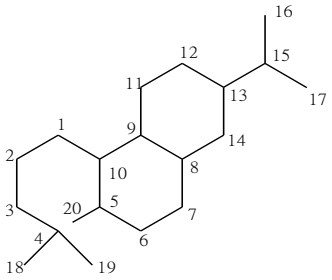

Rearranged abietane

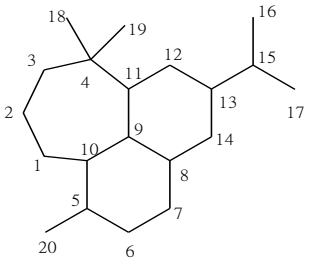

Rearranged abietane

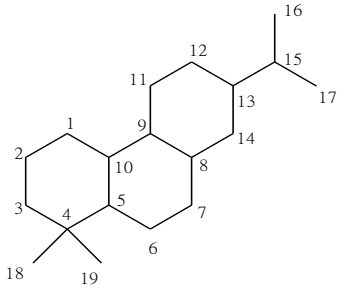

20-Norabietane

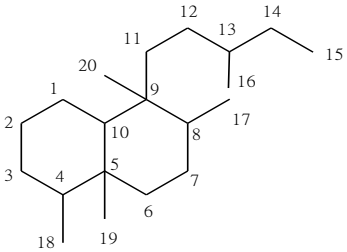

Clerodane

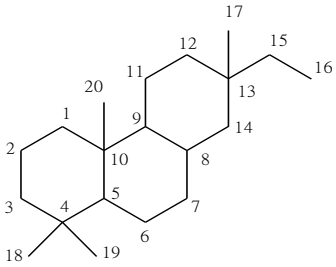

Pimarane

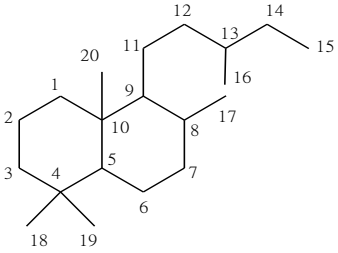

Labdane

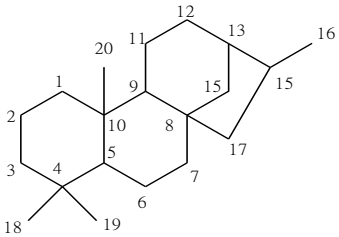

Kaurane

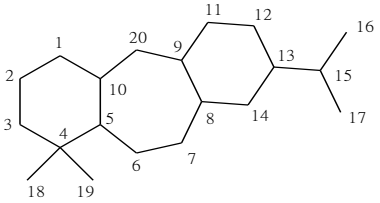

Icetexane

Figure 1.10 Common skeletons of diterpenoids in the genus *Salvia*

1.1.4. Triterpenoids

Triterpenoids have been isolated from 105 *Salvia* spp., 89 of 461 compounds were reported as new ones (Topcu, 2006; Mehmood et al., 2006; Ahmad et al., 2007; Rauter et al., 2007; Ahmad et al. 2008; Cioffi et al., 2008; Pan et al., 2010). There are more than 100 skeleton structure-types of triterpenoids (Mahato and Sen, 1997). These can be classified of according to the ring number, for example monocyclic, tricyclic, pentacyclic rings, and others with rearranged skeleton. Those found in *Salvia* spp. include the pentacyclic fused-ring types such as oleanane, ursane, lupane, and taraxastane as shown in Figure 1.11. The tetracyclic dammarane type and sterols have also been reported (Figure 1.12).

Ursolic and oleanolic acids are the most common triterpenoids in *Salvia* species (Topcu, 2006). The contents in dry weight of 37 investigated *Salvia* species were 0.02-1.84% for oleanolic acid, and 0.05-4% for ursolic acid (Janicsak et al., 2006). Lupeol, betulin and betulinic acid are representative of pentacyclic lupane-type (Figure 1.13).

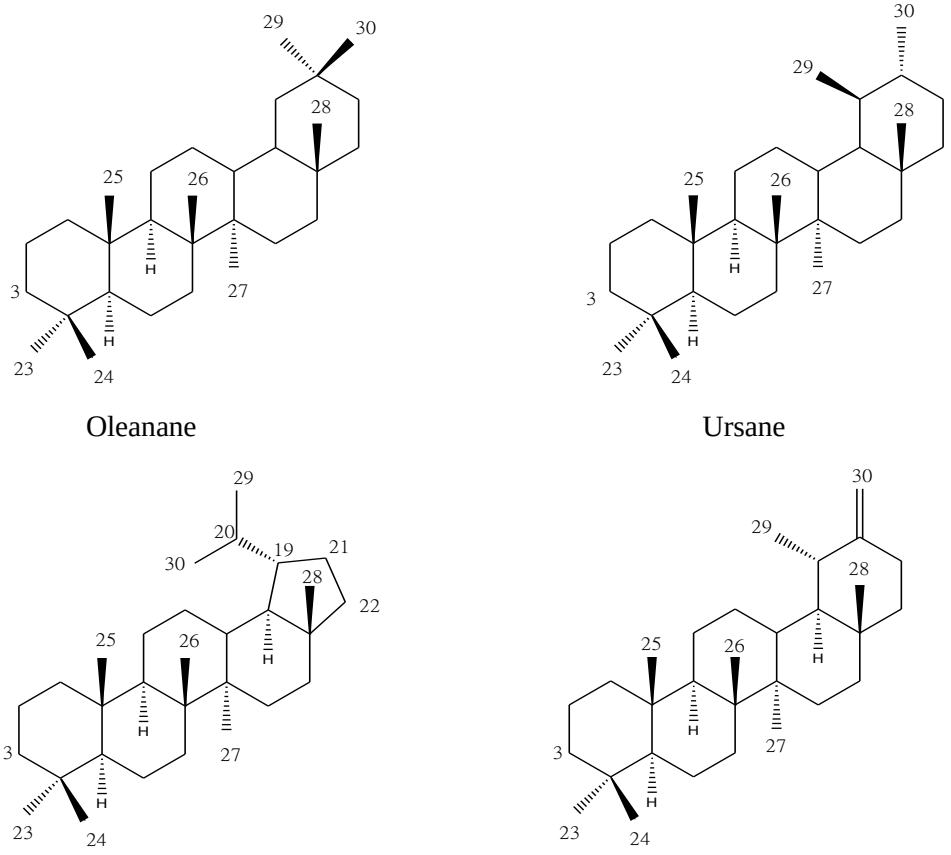

Figure 1.11 Common skeletons of pentacyclic triterpenoid in the genus *Salvia*

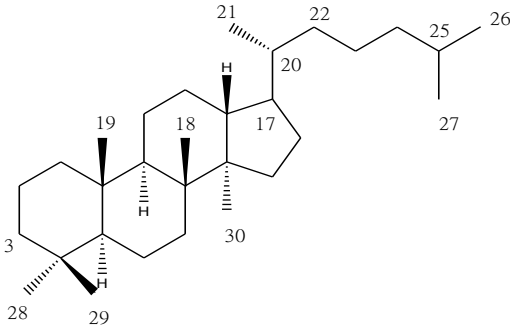

Dammarane

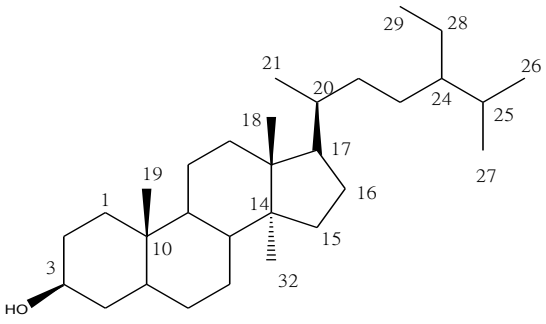

Sterol

Figure 1.12 Common skeletons of tetracyclic triterpenoid in the genus *Salvia*

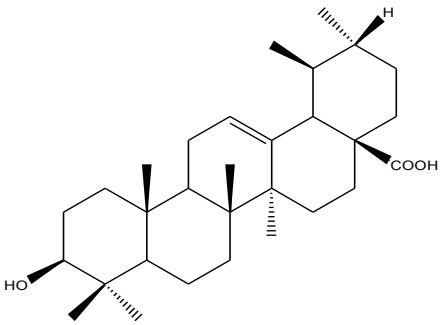

Ursolic acid

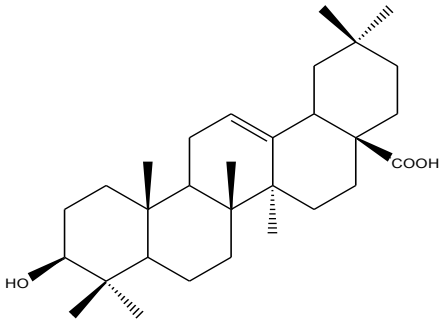

Oleanolic acid

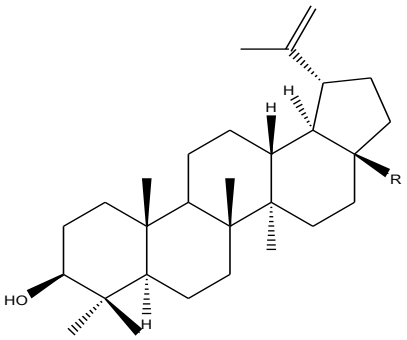

Lupeol R = CH_3

Betulin R = CH_2OH

Betulinic acid R = COOH

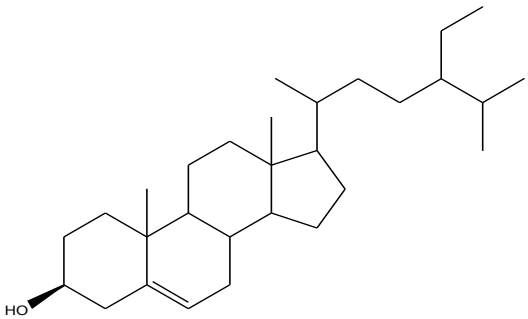

β-Sitosterol

Figure 1.13 Representative triterpenoids in the genus *Salvia*

1.2 Polyphenols in the genus *Salvia*

Polyphenolic compounds are abundant in plants and food. They have been reported to play a notable role in the prevention of degenerative diseases such as cancer and cardiovascular disease (Scalbert et al., 2005). Phenolic compounds in plants can be classified according to their basic skeleton, for example phenylpropanoids (C_6-C_3), and flavonoids (C_6-C_3-C_6). Flavonoids are found in many species of *Salvia*, particularly flavones, flavonols, anthocyanins and their glycosides (Lu and Foo, 2002). Lu and Foo (2001) reported the antioxidant activity of flavonoids, namely luteolin and apigenin glycosides from *Salvia officinalis* L., however, caffeic acid derivatives in this plant showed more potent activity. Caffeic acid derivatives which have been observed in this genus can be categorized into 5 classes depending on the number of caffeic acid units present, namely caffeic acid- monomer, dimers, trimers, tetramers, and a miscellaneous group (Lu and Foo, 2002; Jiang et al., 2005). They possess antioxidant, anti-thrombosis, anti-hypertension, antivirus, antitumor activities and protective effects against cerebral and heart ischemia-reperfusion (Jiang et al., 2005). These phenolic compounds are biosynthesized via the shikimate pathway which produces L-phenylalanine as a precursor for the other secondary metabolites. Figure 1.14 shows the C9 unit building block (*p*-coumaric acid) from which can be derived a variety of phenolic compounds (Winkel-Shirley, 2001; Dewick, 2009).

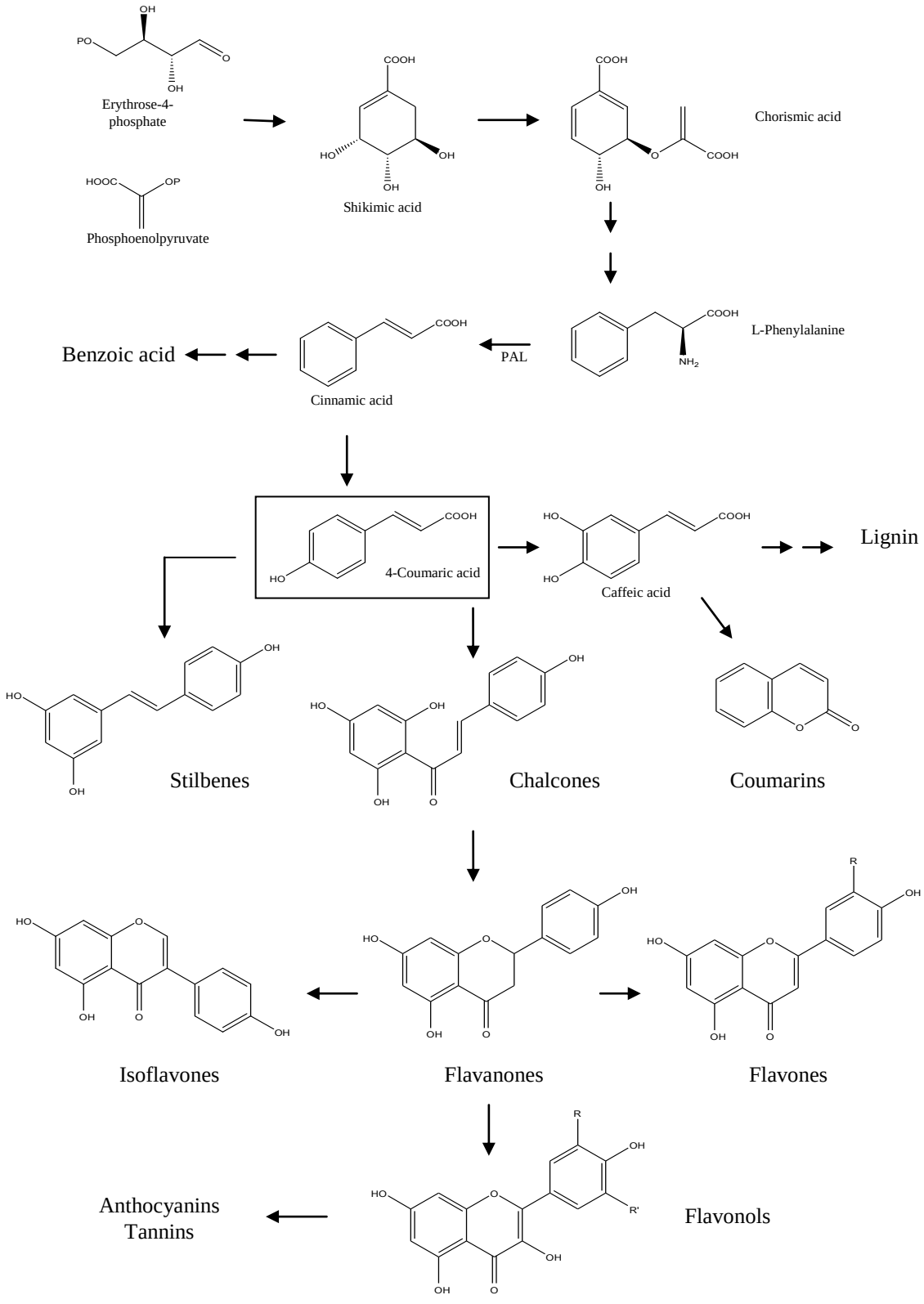

Figure 1.14 Biosynthesis of phenolic compounds via shikimate pathway (Winkel-Shirley, 2001; Dewick, 2009)

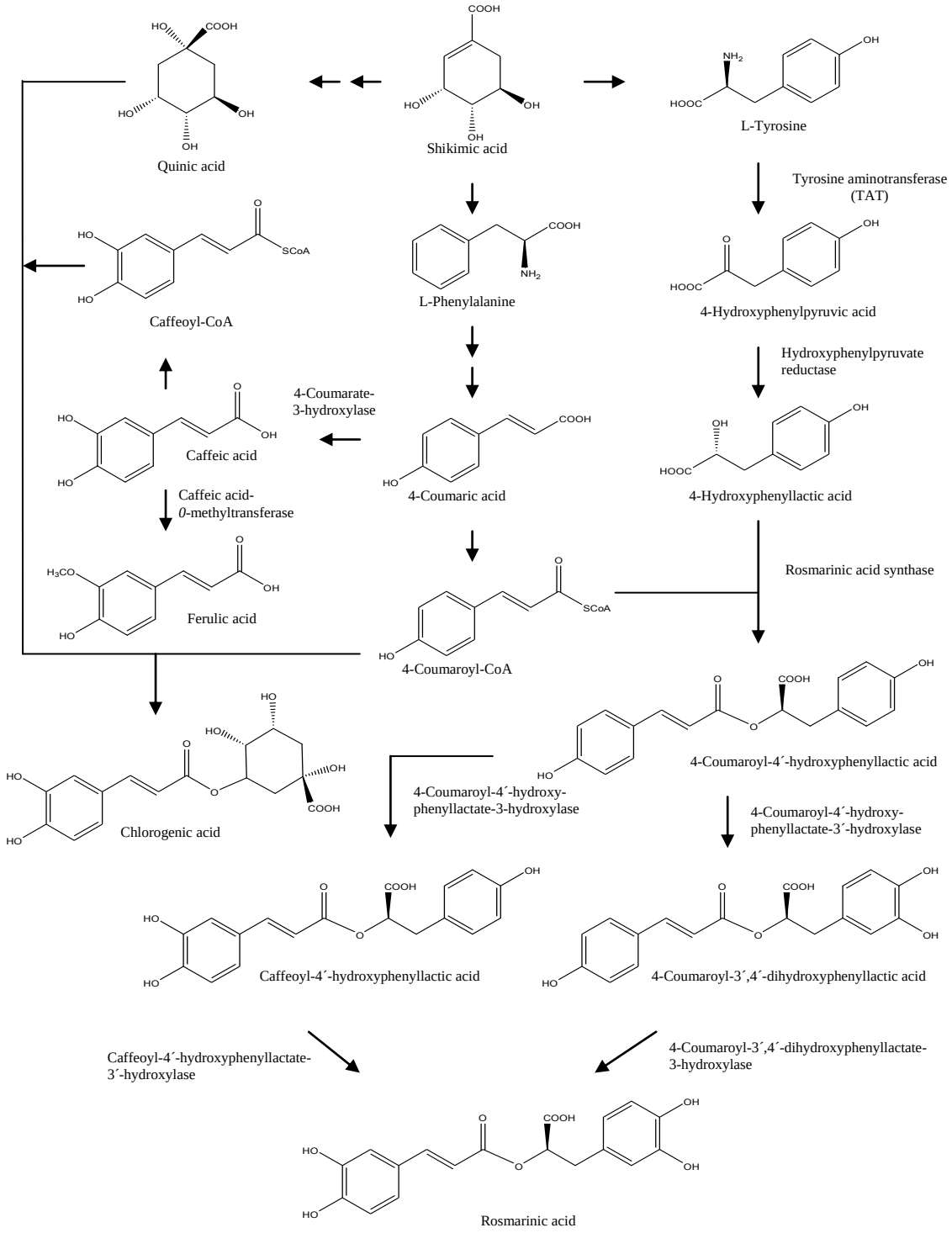

Figure 1.15 Biosynthesis pathways of caffeic acid derivatives (Dewick, 2009; Petersen et al., 2009)

1.2.1 Caffeic acid derivatives

In phenylpropranoid metabolism, the pathway starts from L-phenylalanine to cinnamic acid by the enzyme phenylalanine ammonia lyase (PAL), and then further hydroxylation to 4-coumaric acid (*p*-coumaric acid) as shown in Figure 1.15. Then, *p*-coumaric acid is converted into caffeic acid by enzyme *p*-coumarate-3-hydroxylase. Caffeic acid, or 3,4-dihydroxycinnamic acid, is found in various fruits and vegetables.

Other cinnamic derivatives, such as ferulic acid, sinapic acid, are further derived from caffeic acid by methylation and/or hydroxylation reactions. Besides caffeic acid, other mono-caffeic derivatives such as chlorogenic acid (5-caffeoylquinic acid), ferulic acid, and 3-(3,4-dihydroxyphenyl)lactic acid (danshenshu) have also been found in *Salvia* species (Figure 1.16). Chorogenic acid is an ester of caffeic acid, and quinic acid which can be generated from caffeoyl–CoA (Dewick, 2009), or 4-coumaroyl-CoA (Petersen et al., 2009) as shown in Figure 1.15.

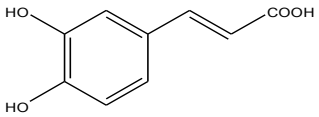

Caffeic acid

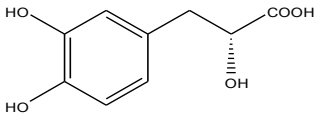

3-(3,4-Dihydroxyphenyl)lactic acid (Danshensu)

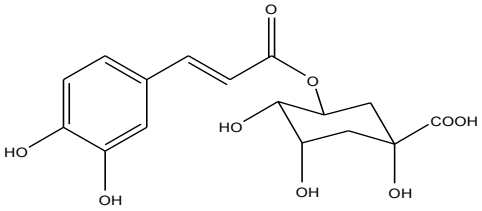

Chlorogenic acid

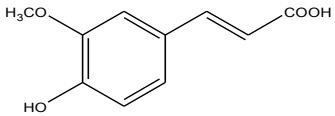

Ferulic acid

Figure 1.16 Caffeic acid derivatives

The caffeic acid dimer, rosmarinic acid, is found dominantly in *Salvia* species (Lu and Foo, 2002), and also distributed in other genera of Lamiaceae, Boraginaceae and Hydrophyllaceae (Petersen et al., 2009). It was firstly isolated from *Rosmarinus officinalis*

(Lamiaceae). Although rosmarinic acid is a caffeic acid dimer, each of the aromatic rings is derived from different aromatic amino acids (Dewick, 2009; Petersen et al., 2009) as shown in Figure 1.15. The caffeoyl residue is originally biosynthesized via the general pathway from L-phenylalanine, but the 3,4-dihydroxyphenyllactic acid residue arises from L-tyrosine. The two intermediate metabolites, 4-coumaroyl-CoA and 4-hydroxyphenyllactic acid are incorporated by the enzyme rosmarinic acid synthase (RAS), and the product is further hydroxylated at C-3, and C-3´ of each ring (Petersen et al., 2009).

Figures 1.17-1.18 shows caffeic acid trimers, salvianolic A and lithospermic acid, and also caffeic acid tetramers, salvianolic acid B, in Figure 1.19. They were isolated from danshen root, *S. miltiorrhiza* Bunge (Jiang et al., 2005), and other *Salvia* such as *S. cavaleriei* Lev. (Zhang and Li, 1994). Salvianolic B was reported in all samples in 18 species of Chinese *Salvia* together with lithospermic acid which was detected in 14 *Salvia* species (Li et al., 2008). Lithospermic acid was also found in certain plants in the genus *Lithospermum* and *Tournefortia* of the Boraginaceae family (Jiang et al., 2005).

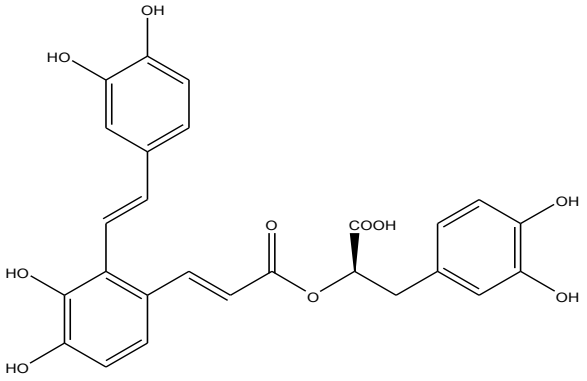

Figure 1.17 Salvianolic acid A

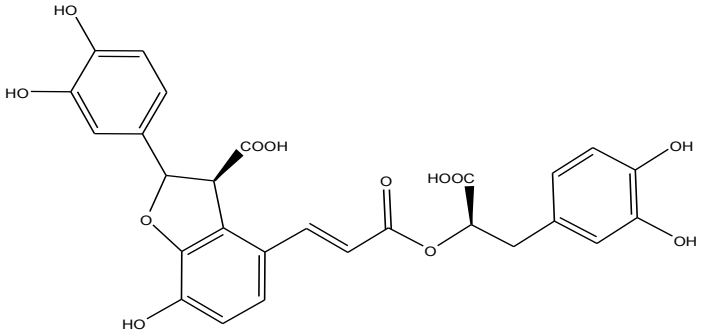

Figure 1.18 Lithospermic acid

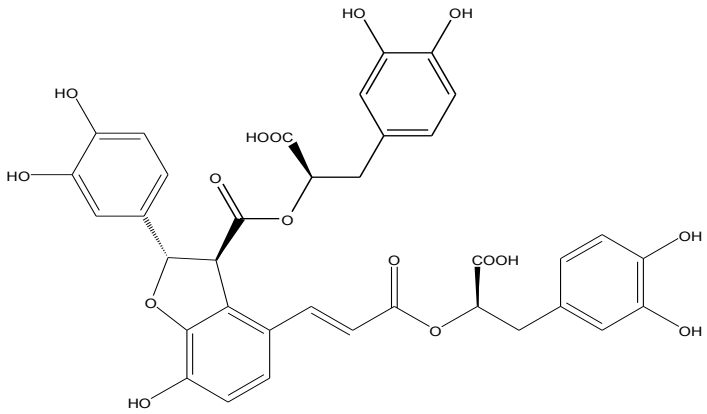

Figure 1.19 Salvianolic acid B (Lithospermic acid B)

1.2.2 Flavonoids

Flavonoids are a class of polyphenol that are biosynthesized via a combination of the shikimate and acetate pathways. They occur commonly in fruit, vegetables, nuts, seeds, stems and flowers (Cushnie and Lamb, 2005). They are mainly responsible for antioxidant, antimicrobial, photoreceptors, visual attractors, feeding repellants, and for light screening activities in plants (Pietta, 2000). Many findings have reported their activities as free radical scavenging or chelating agents which lead to protection from radical-induced cell damage.

The flavonoid skeleton comprises of 3 rings with C6-C3-C6; they can be classified into groups according to substitution of ring C as shown in Figure 1.20 (Pietta, 2000; Robards, 2003). Flavones, and flavonols are commonly isolated from *Salvia* spp. especially apigenin, luteolin, and their 6-hydroxylated derivatives (Lu and Foo, 2002). Nikolova et al. (2006) examined seven Bulgarian *Salvia* spp., *S. nemorosa* L., *S. glutinosa* L., *S. scabiosifolia* lam., *S. ringens* Sibth. Et Sm., *S. tomentosa* Mill., *S. argentea* L., and *S. officinalis* L. Flavones were detected in all species; there were derivatives of luteolin, and apigenin, 6-hydroxyluteolin, and 6-hydroxyapigenin. Luteolin was the most abundant while flavonols, derivatives of quercetin and kaempferol were present in low concentration from *S. glutinosa* L. and *S. ringens* Sibth. Et Sm. Flavonoid glycosides were also frequently found in this genus particularly the flavone-7-glycosides, apigenin-7-glucoside, and luteolin-7 glucoside (Lu and Foo, 2002).

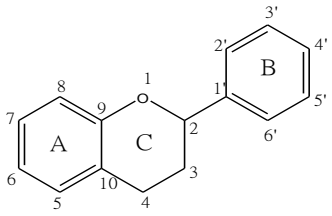

Basic structure

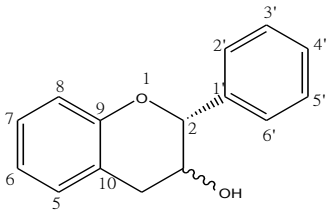

Flavanols

Catechin (2R, 3S) 5=7=3´=4´=OH

Epicatechin (2R, 3R) 5=7=3´=4´=OH

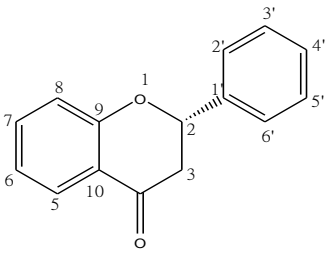

Flavanones

Naringenin 5=7=4´=OH

Naringin = naringenin-7-neohesperidoside

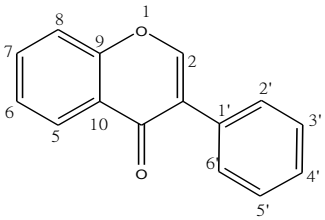

Isoflavones

Genistein 5=7=4´=OH

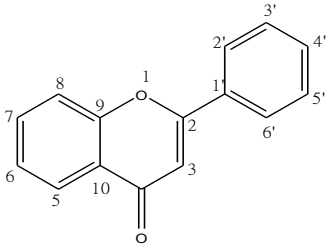

Flavones

Apigenin 5=7=4´=OH

Luteolin 5=7=3´=4´=OH

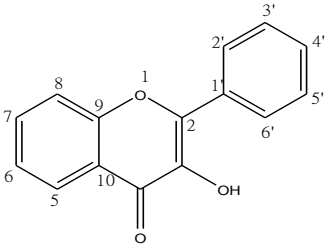

Flavonols

Kaempferol 5=7=4´=OH

Quercetin 5=7=3´=4´=OH

Rutin = quercetin-3-*O*-rutinoside

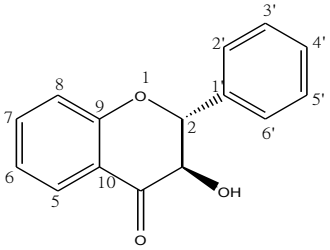

Flavanonols

Taxifolin 5=7=3´=4´=OH

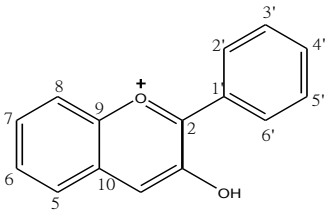

Anthocyanidins

Cyanidin 5=7=3´=4´=OH

Figure 1.20 Classifications of flavonoids (Pietta, 2000; Robards, 2003)

1.2.3 Anthocyanins

Anthocyanins are glycoside of anthocyanidins which may comprise of monosaccharide, disaccharides and trisaccharides. Anthocyanins are water soluble pigments, and responsible for conspicuous colours, orange, pink, red, violet, and blue, in fruits, and flowers of certain plants (Castaneda-Ovando et al., 2009). At least 26 anthocyanins have been identified from flowers of 49 species in the Lamiaceae including *Salvia* species (Saito and Harborne, 1992). Pigments based on pelargonidin glycoside and cyanidin glycoside were distributed in species with scarlet flowers such as *S. coccinea* Buchoz, and *S. greggii* A Gray, and red-purple flowers such as *S. lineate* Benth. While cyanidin, delphinidin, and malvidin types were found in species with purple-violet flowers such as *S. leucantha* Cav., violet flowers such as *S. viridis* L., and blue flowers such as *S. castanea* Diels.

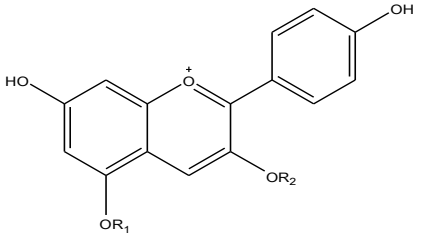

Pelargonidin

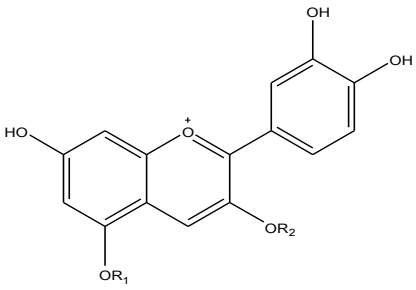

Cyanidin

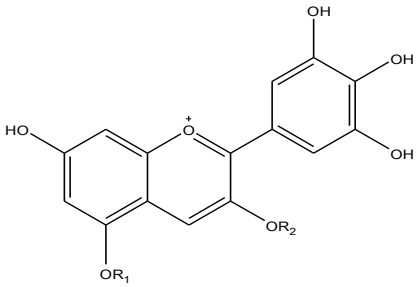

Delphinidin

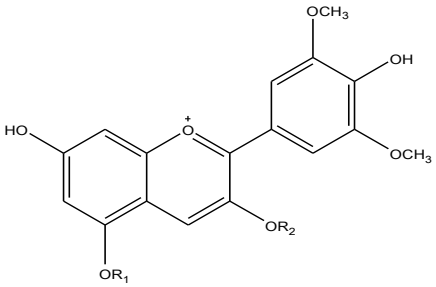

Malvidin

R_1 = glucoside with malonic acid acylation

R_2 = glucoside with caffeic acid or *p*-coumaric acid acylation

Figure 1.21 *Salvia* anthocyanins aglycone

1.3 Biological activities of compounds in the genus *Salvia*

1.3.1 Antibacterial activity

Essential oils of cultivated *S. officinalis* L., and *S. triloba* L. were tested against certain food borne bacteria strains (Delamare et al., 2007). Oils of *S. officinalis* L. not only inhibited the growth of *Aeromonas hydrophila, Klebsiella oxytoca*, *Bacillus megatherium, B. cereus, B. subtilis, Pseudomonas fluorescens* with MIC in range of 0.1-5 mg/ml but also showed bactericidal activity in the same range of concentration. The essential oil of *S. triloba* L. also showed both bacteriostatic and bactericidal against the same bacteria stains and *Salmonella typhimurium, Staphylococcus aureus*, and *Staphylococcus epidermidis* with MIC of this oil in range of 0.1-4 mg/ml. It also inhibited growth of *Escherichia coli* with MIC 5 mg/ml. The major content of *S. triloba* L. oils were α-thujone (20%), 1,8-cineol (16%), camphor (13%), β-caryophyllene (12%), α-humulene (8%), and viridiflorol (6%). However, the main constituents of *S. officinalis* L. oil were somewhat similar, namely α-thujone (25%), 1,8-cineol (15%), camphor (11%), β-pinene (10%) except those sesquiterpenoids which comprised 1-3% in oil.

Alim et al. (2009) reported 92 components from essential oils of *S. cedronella* Boiss mainly 1,8-cineol (13%), caryophyllene oxide (10%), α-pinene (10%), and sabinene (7%). This oil showed appreciable antibacterial activity against *Bacillus cereus*, *B. subtilis*, *Staphylococcus aureus*, *S. epidermidis* with MIC in range of 0.02-0.06 mg/ml. Essential oil of *S. ringens* Sibth. & Sm. showed antbacterial activity against *Pseudomanas aeruginosa*, *Enterobactor cloacae*, *Klebsiella pneumoniae*, and *Escherichia coli* with MIC in range of 2.8-3.8 mg/ml while its main isolated components, namely 1,8-cineol (48%), and α-pinene (11%) were active against those bacteria at MIC 2-3 mg/ml, and 2-15 mg/ml respectively (Tzakou et al., 2001).

The diterpenoid, salvipisone (Figure 1.22), from hairy roots of *S. sclarea* L. were reported as bacteriostatic, and bacteriocidal against *Staphyococcus aureus* (MIC 60 µM), and *Staphylococcus epidermidis* (MIC 30 µM) regarding its inhibition of bacterial adhesion and biofilm formation (Kuzma et al., 2007). Aethiopinone was also reported to possess antbacterial activity against *Staphylococcus epidermidis* and *Bacillus subtilis* with MIC 8.2 µM, and 4.1 µM respectively (Hernandez-Perez et al., 1999).

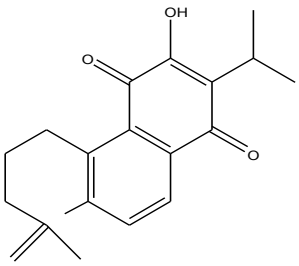

Salvipisone

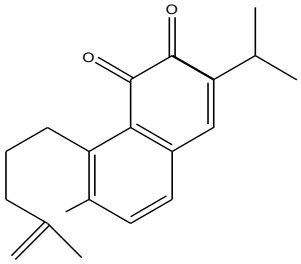

Aethiopinone

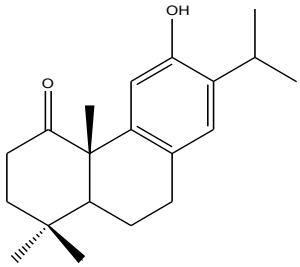

1-Oxoferruginol

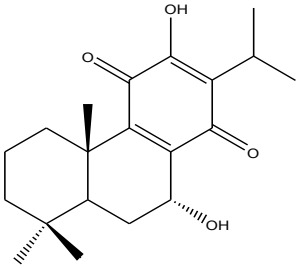

Horminone

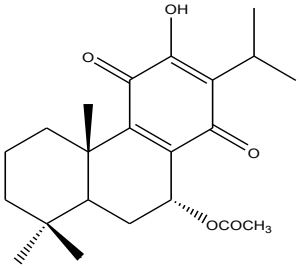

7-Acetylhorminone

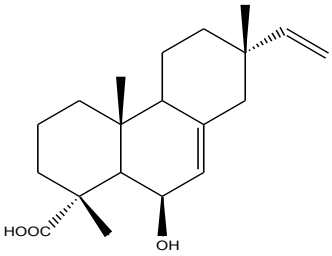

6β-Hydroxyisopimaric acid

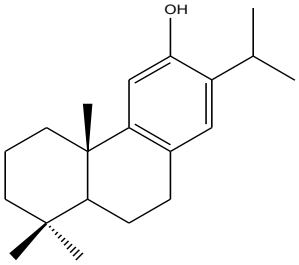

Ferruginol

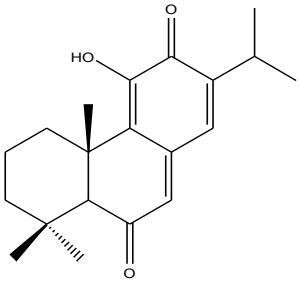

Taxodione

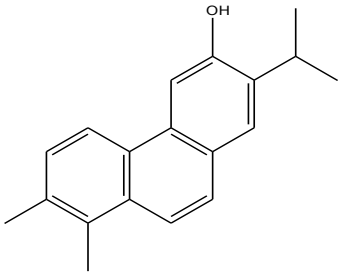

12-Demethylmulticauline

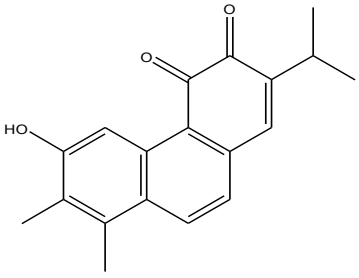

12-Demethylmultiorthoquinone

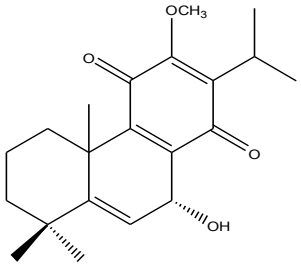

12-Methyl-5-dehydrohorminone

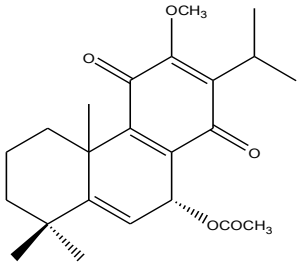

12-Methyl-5-dehydro--7-acetylhorminone

Figure 1.22 Diterpenoids with antibacterial activity

Other diterpenes from *Salvia* species with activity against certain bacteria were described by Ulubelen (2003). Horminone and 7-acetylhorminone (Figure 1.22) from *S. blepharochlaena* Hedge and Hub. Mor. were active against *Staphylococcus aureus* (ATCC 6538) with MIC at 19.5 µM and 26.7 µM respectively. 6-β-Hydroxyisopimaric acid (Figure 1.22) from *Salvia caespitosa* Montbret and Aucher ex. Bentham was active against *Staphylococcus aureus* (ATCC 6538) at MIC 28.3 µM comparable to antibiotic drugs activity, i.e. cefoperazone 24.8 µM and kanamycin 33.1 µM. Those three compounds, horminone, 7-acetylhorminone, and 6-β-hydroxyisopimaric acid, also showed antibacterial activity against *Staphylococcus epidermidis* (ATCC 12228) (MIC range 4.5-56.6 µM) and *Bacillus subtilis* (ATCC 6633) (MIC range 4.5-28.3 µM). Ferruginol, and taxodione (Figure 1.22) from *S. mellifera* Greene showed active activity against *Staphylococcus aureus* (ATCC 6538) at MIC 12.6 µM, and 9.6 µM respectively, and also *Bacillus subtilis* (CECT 39) at MIC 10.5 µM, and 9.6 µM respectively (Moujir et al., 1996).

Ulubelen et al. (1997) reported bioactive diterpenoids from *S. multicaulis* Vahl. against *Mycobacterium tuberculosis* H37Rv. The norditerpenoid, 12-demethylmulticaulin (Figure 1.22) showed the most potent activity with a MIC 1.7 µM while 12-methyl-5-dehydro-7-acetylhorminone, 12-methyl-5-dehydrohorminone, and 12-demethylmultiorthquinone (Figure 1.22) were appreciably active at MIC 2.3 µM, 3.5 µM, and 4.1 µM respectively.

Oleanolic acid (Figure 1.13) was described as a promising antibacterial agent against various strains of bacteria, *M. tuberculosis*, vancomycin-resistant enterococci, *Enterococcus faecalis*, *Bacillus subtilis*, and *Staphylococcus epidermidis*, with MIC less than 22 µM (Wolska et al., 2010). Both oleanolic and ursolic acids showed appreciable effect against *M. tuberculosis* H37Rv with MIC 5.5 µM (Bamuamba et al., 2008). Ursolic acid (Figure 1.13) was found to be active against vancomycin-resistant enterococci with low MIC at 8.8 µM while oleanolic was at MIC 17.6 µM (Horiuchi et al., 2007). Furthermore, ursolic acid exhibited its antibacterial activity against Methicillin-resistant *Staphylococcus aureus* (MRSA) with MIC 11 µM (Da Silva Filho et al., 2008), and *S. aureus* with MIC 17.5 µM (Fontanay et al., 2008). Szakiel et al. (2008) investigated oleanolic acid and its glycosides against Gram-positive, and Gram-negative bacteria and parasites. Oleanolic acid decreased cell growth and cell survival, and also increased cell autolysis including cell morphology alteration. The results suggested that the agycone part was vital for antibacterial activity while its C-3 glycosides, i.e. glucuronide showed greater antiparasitic effect against

Heligmosomoides polygyrus. As oleanolic acid showed more activity against Gram-positive than Gram-negative species the authors suggested that it may influence only the Gram-positive bacterial cell wall/envelope. Lupane triterpenoids, lupeol and betulinic acid (Figure 1.13), were inactive against *Staphylococcus aureus*, *Escherichia coli*, and *Pseudomanas aeroginosa,* however, betulinic acid inhibited *Enterococcus faecalis* with MIC 35 µM (Shai et al., 2008).

Apigenin and luteolin exhibited antibacterial activity against methicillin-resistant *Staphylococcus aureus* (Sato et al., 2000). Apigenin was active with MIC in range of 14-58 µM while luteolin showed weak inhibitory activity with MIC in range of 218-437 µM. In contrast, luteolin showed inhibitory activity against *Porphyromonas gingivalis* with MIC in range of 44-175 µM while apigenin was inactive (Yamamoto and Ogawa, 2002). The antibacterial activity of various flavonoids could be due to three inhibitory actions; namely nucleic acid synthesis, cytoplasmic membrane function and energy metabolism (Cushnie and Lamb, 2005).

1.3.2 Antiviral activity

S. fruticosa Mill. essential oil and isolated compounds, 1,8-cineol, camphor, isoborneol, and mixture of thujones were reported to possess activity against herpes simplex virus 1 (Sivropoulou et al., 1997; Armaka et al., 1999). 0.06% Isoborneol inactivated HSV-1 replication within 30 minutes of exposure. α-Pinene also showed HSV-1 inhibitory activity (Astani et al., 2010).

Akihisa et al. (2001) reported the inhibitory effect of various triterpenoids on HIV-1 reverse transcriptase. Among these, oleanolic acid and lupeol strongly inhibited this enzyme with IC_{50} 3.1 µM, and 3.8 µM respectively whereas ursolic acid, and betulinic acid showed the inhibitory effect at IC_{50} 6.4 µM, and 7.9 µM respectively.

There was also a study of lupane derivatives against influenza A and herpes simplex type 1 (HSV-1) virus in vitro (Baltina et al., 2003). Betulinic acid were fairly active against HSV-1 with EC_{50} 8.2 µM. Nevertheless, betulinic acid showed activity against influenza A with EC_{50} of more than 219 µM while a synthetic derivative of betulinic acid, betulonic acid, was active against influenza A and HSV-1 with EC_{50} 5.7 µM and 2.5 µM respectively.

Betulinic acid has been used as starting compounds for synthesizing more potent anti-viral agents. Betulinic acid derivatives, for instance 3-*O*-(3´, 3´-dimethylsuccinyl)-betulinic acid (DSB) is under clinical trials for treatment of HIV infection, and derivatives of DSB also showed strongly inhibitory effect against HIV-1 maturation in vitro (Gerrish et al., 2008).

Tewtrakul et al. (2003) reported antiviral activity against human immunodeficiency virus type 1 (HIV-1 IN) of rosmarinic acid and derivatives and luteolin and its glycoside in vitro. Among tested compounds, rosmarinic derivatives, namely salvianolic acid B, magnesium lithospermate, lithospermic acid, calcium rosmarinate and magnesium rosmarinate were the most potent with IC_{50} in range of 0.7-1.4 µM. While rosmarinic acid was active at IC_{50} 5 µM, its ester, rosmarinic methyl ester, exhibited lower IC_{50} value at 3 µM. Luteolin showed moderate inhibitory activity with IC_{50} 11 µM, however, it was the most potent among tested flavones (Figure 1.23). Luteolin-5-glucoside showed the weakest activity with IC_{50} 58 µM while luteolin-7-glucoronide was active with IC_{50} 20 µM. Methyl substitution showed superior inhibitory activity to sugar substitution at C-7 because luteolin-7-methyl ether was active at IC_{50}11 µM.

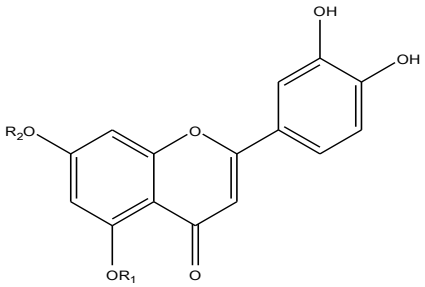

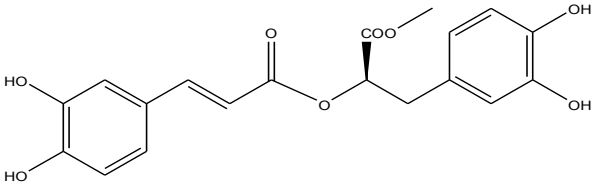

Luteolin R_1=R_2=H

Luteolin-5-glucoside R_1 = glucose, R_2=H

Luteolin-7-glucoronide R_1=H, R_2=Glucuronic acid

Luteolin-7-methyl ether R_1=H, R_2=CH_3

Rosmarinic methyl ester

Figure 1.23 Antiviral polyphenols

1.3.3 Antifungal activity

Essential oils of *Salvia cedronella* Boiss showed appreciable inhibitory activity against *Candida albicans* with MIC 0.06 mg/ml (Alim et al., 2009). Tzakou et al. (2001)

reported antifungal activity of essential oil from *S. ringens* Sibth. & Sm., and its main isolated components, namely 1,8-cineol, and α-pinene against *Candida albicans*, *Candida vaginalis* and *Torulopsis glabrata*. 1,8-Cineol showed lowest MIC at 0.25 mg/ml while the essential oils, and α-pinene were active against those pathogenic fungi at MIC of 0.75 mg/ml, and 2-4 mg/ml respectively.

Shai et al. (2008) reported antifungal activity of lupeol and betulinic acid. Both were active against *Sporothrix schenckii*, and *Microsporum canis* in the similar MIC range of 26-38 µM. Betulinic acid showed superior activity against *Aspergillus fumigatus*, *Candida albicans*, *Candida guilliermondi* with MIC in range of 35-53 µM while lupeol was inactive.

1.3.4 Antiparasite, insecticidal activity

Essential oils of *S. elegans* Vahl. and *S. splendens* Sell ex Roem. & Schult (Blue Ribbon) showed appreciable inhibitory effect against *Aedes albopictus* mosquito larvae with LC_{50} 46 ppm, and 59 ppm respectively. The oil compositions of *S. elegans* Vahl. were mainly sesquiterpene, namely spathulenol (39%), caryophyllene (10%) while the oil of *S. splendens* Sell ex Roem. & Schult (Blue Ribbon) comprised β-cubebene (23%), and caryophyllene (13%) (Mathew and Thoppil, 2011).

Lupeol and betulinic acid have been reported to possess antiprotozoal activity against *Plasmodium falciparum*. Lupeol was active in various findings with IC_{50} in range of 28-105 µM while betulinic acid showed higher sensitivity with IC_{50} in range of 14-57 µM (Gallo, and Sarachine, 2009). Semi-synthetic analogues of betulinic acid with substitution at C-28 such as methyl betulinate exhibited more potent activity with IC_{50} 7 µM (Ziegler et al., 2004).

In vitro antileishmanial activity of terpenoids from *S. cilicica* Boiss and Kotschy was detemined by Tan et al. (2002). Both oleanoic acid and ursolic acid showed strong activity against the intracellular amastigote forms of *Leishmania donovani* and *L. major* with IC_{50} values of 7-120 nM while they were moderately active against extracellular promastigote form of both *Leishmania* with IC_{50} in range of 51-137 nM.

1.3.5 Cytotoxic activity

Diterpenoids have been investigated for their cytotoxicity. Topcu et al. (2008) examined isolated compounds from *S. hypargeia* Fisch. Et Mey. against a human ovarian cancer cell line. Two diterpenoids, 6-hydroxysalvinolone, and demethylcryptojaponol (Figure 1.24) were active with IC_{50} values 11.8 µM and 3.8 µM respectively. 6-Hydroxysalvinolone also showed inhibitory activity against human breast cancer, colon cancer, and prostate cancer with IC_{50} in range of 12.1-14.2 µM (Ulubelen et al., 1999). Ulubelen et al. (1999) reported cytotoxic activity of diterpenoids from *S. hypargeia* Fisch. Et Mey against a variety of cancer cell lines. The most potent one was taxodione (Figure 1.22) which showed inhibitory effects against mouse lymphocytic leukemia, human breast cancer, colon cancer, prostate cancer with IC_{50} in range of 1-3.8 µM. Saprorthoquinone (Figure 1.24) was moderately active against mouse lymphocytic leukemia (IC_{50} 7.8 µM), and human colon cancer (IC_{50} 11.1 µM) while microstegiol was active against mouse lymphocytic leukemia with IC_{50} at 10.1 µM (Ulubelen et al., 1992).

Derivatives of saprorthoquinone from *S. prionitis* Hance also showed cytotoxic activities (Chen et al., 2002). 4-Hydroxysaprorthoquinone (Figure 1.24) appreciably inhibited topoisomerase I enzyme from Ehrlich carcinoma cells at IC_{50} value 0.8 µM while 3-keto-4-hydroxysaprorthoquinone (Figure 1.24) showed inhibitory activity against human leukemia and stomach cancer cell lines with IC_{50} values 4.6 µM, and 0.3 µM respectively. Chang et al. (2005) reported cytotoxic diterpenoids from the same species. Prionoid D (Figure 1.24) exhibited inhibitory activity against mouse lymphocytic leukemia with IC_{50} 0.4 µM whereas prionoid E (Figure 1.24) showed cytotoxic activity against human lung adenocarcinoma with IC_{50} 0.7 µM.

Guerrero et al. (2006) reported three diterpenoids with cytotoxic activity, carnosol, 20-deoxocarnosol, and 16-hydroxycarnosol (Figure 1.24) from *S. pachyphylla* Epling ex Munx, and *S. clevelandii* (Gray) Greene. They showed 50% growth inhibition in range of 3.6-5.4 µM against ovarian A2780, and breast HBL-100 cancer cell lines. Moreover, different kinds of breast cancer cell lines were examined. They inhibited breast cancer cells without estrogen-receptors (HBL-100) with lower concentration than those with estrogen receptors (T-47D). An abietane diterpenoid, carnosol, was reviewed for its anti-cancer activity. It promoted G_2 cell cycle arrest in prostate cancer cells decreasing cell viability. It also showed cytotoxicity against skin cancer, colon cancer, and leukemia (Johnson, 2011).

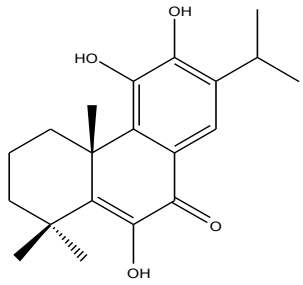

6-Hydroxysalvinolone

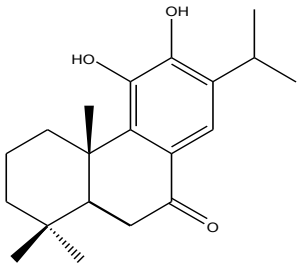

Demethylcryptojaponol

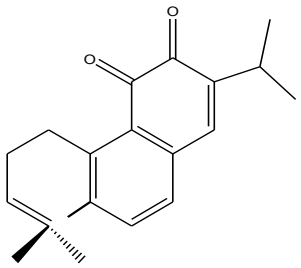

Saprorthoquinone

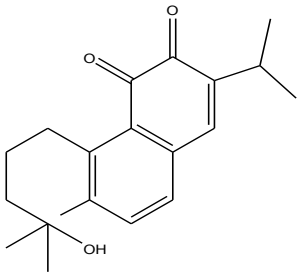

4-Hydroxysaprorthoquinone

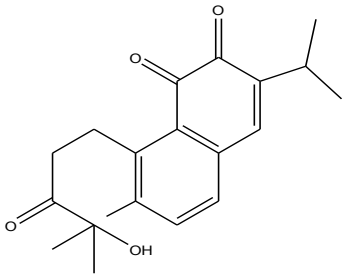

3-Keto-4-hydroxysaprorthoquinone

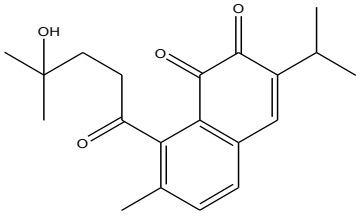

Prionoid D

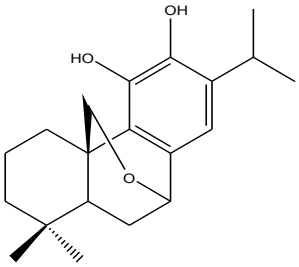

20-Deoxocarnosol

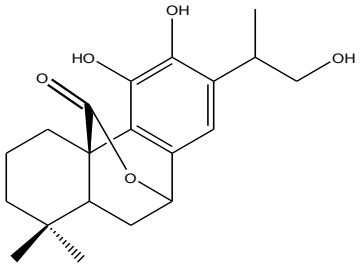

16-Hydroxycarnosol

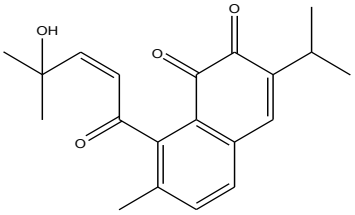

Prionoid E

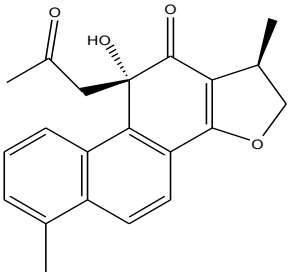

Danshenol A

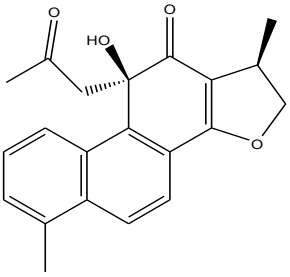

Danshenol C

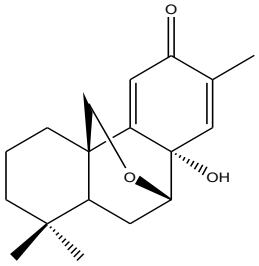

Yunnannin A

Figure 1.24 Diterpenoids with cytotoxic acitivity

Cytotoxicity against human cancer cell lines of three diterpenoids, danshenol A, C and yunnannin A (Figure 1.24), from *S. yunnanensis* C. H. Wright has been reported (Xu et al., 2006). Danshenol A showed an appreciable effect against chronic myelogenous leukemia cell line with IC_{50} at 1.6 μM while cisplatin was at 13.3 μM. It also inhibited growth of other cell lines, i.e. urinary carcinoma (IC_{50} at 23.6 μM), hepatocellular carcinoma (IC_{50} at 13.8 μM), cervix epidermoid carcinoma (IC_{50} at 20.5 μM) whilst a stereoisomer, danshenol C, was inactive. Yunnannin A was moderately active against cervix epidermoid carcinoma at IC_{50} 20.3 μM. Aethiopinone from *S. aethiopis* L. also showed cytotoxic activity against the KB human carcinoma cell line with IC_{50} value of 2 μM (Hernandez-Perez et al., 1999).

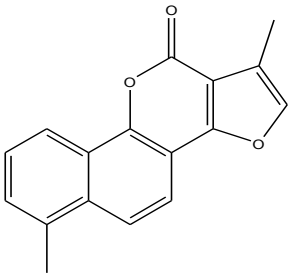

Neotanshinlactone

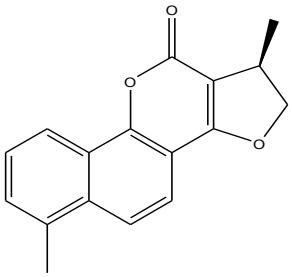

Dihydroneotanshinlactone

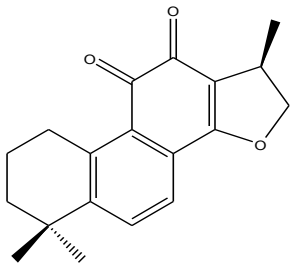

Cryptotanshinone

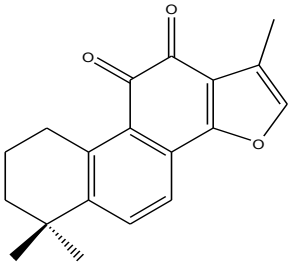

Tanshinone IIA

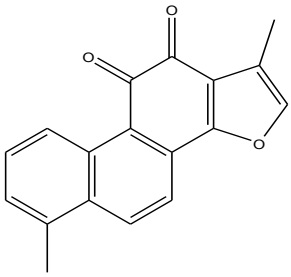

Tanshinone I

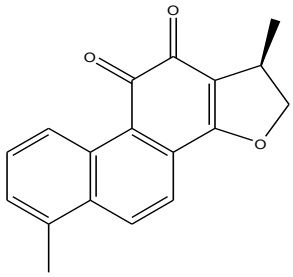

Dihydrotanshinone

Figure 1.25 Tanshinones with cytotoxic activity

Tanshinones from *S. digitaloides* Diels (Figure 1.25) were evaluated their cytotoxicity against five human cancer cell lines, i.e. acute leukemia, liver cancer, lung cancer, breast cancer, pancreatic cancer (Xu et al., 2010). Neotanshinlactone selectively inhibited only a breast cancer cell line with IC_{50} 4 μM while its derivative, dihydroneo-tanshinlactone, showed cytotoxicity against all cell lines with IC_{50} greater than 30 μM.

Orthoquinone tanshinones showed comparable cytotoxic activity with or without a double bond in the furan ring. Both tanshinone IIA, and cryptotanshinone inhibited a lung cancer and breast cancer cell lines with IC_{50} less than 6.4 µM. An aromatic ring A together with an orthoquinone in ring C increased cytotoxic activity against all five cancer cell lines. In comparison with cisplatin (IC_{50} 2-20 µM), tanshinone I was the most potent one with IC_{50} in range of 2.4-5.2 µM while IC_{50} of dihydrotanshinone was in range of 3.2-14 µM. However, taxol® was active in all cancer cell lines with IC_{50} value less than 0.2 µM.

A labdane diterpenoid, sclareol (Figure 1.8), was reported to possess cytotoxic activity against breast cancer cell lines by induction cell cycle arrest, and apoptosis (Dimas et al., 2006). It also showed a synergistic effect in vitro by increasing cytotoxicity of the chemotherapeutic agents, doxorubicin, etoposide, and cisplatin. The co-treatment of 50 µM sclareol and each of those chemotherapeutic agents were more active than single drug treatment. A liposome-incorporated sclareol formulation was prepared, and its activity evaluated against various cancer cell lines (Hatziantoniou et al., 2006). It showed cytotoxic activity against colon cancer, melanoma, prostate cancer, and leukemia cell lines with IC_{50} in range of 15-28 µM whereas empty liposome exhibited no cytotoxicity at the tested concentration. Nevertheless, the liposome-sclareol formulation was toxic against normal cell lines with IC_{50} more than 100 µM whilst the IC_{50} of free sclareol was at 34 µM. Furthermore, this formulation showed the reduction of the growth rate of human colon cancer tumors implanted in mice. Sclareol is found in the essential oil of *S. triloba* L. (Giannouli and Kintzios, 2000).

Several cell lines were employed to test the cytotoxic effect of isolated triterpenoids from *Salvia* spp. In comparison with cisplatin, hyptadienic acid (Figure 1.26) from *S. trijuga* Diels showed moderate toxicity against acute leukemia (IC_{50} 15.5 µM), liver cancer (IC_{50} 21 µM), lung cancer (IC_{50} 24.7 µM), and colon cancer (IC_{50} 10.9 µM) whereas IC_{50} of cisplatin to those cell lines were 0.8, 13, 15.2, and 12 µM respectively (Pan et al., 2010). For other cell lines, 1β,2α,3β,11α-tetrahydroxyurs-12-ene (Figure 1.26) from *S. kronenburgii* Rech. was reported as selectively active against renal, non-small cell lung, and breast cancer cell lines (Topcu et al., 2004). Wang et al. (2009a) isolated compounds from *S. chinensis* Bentham, and also determined the antiproliferative effects in human leukemia HL-60 cells. Pomolic acid (Figure 1.26) was found to be the most potent with IC_{50} 7.8 µM compared with 5-fluorourasil (IC_{50} 3 µM).

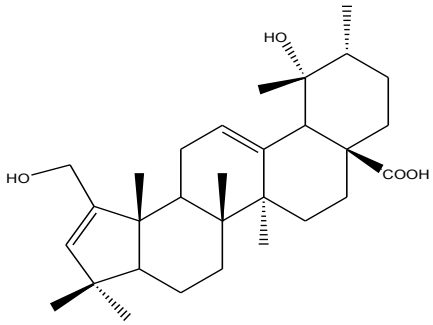

Hyptadienic acid

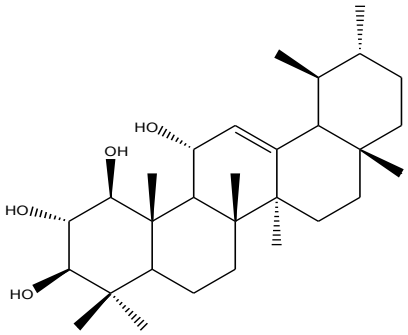

1β,2α,3β,11α-tetrahydroxyurs-12-ene

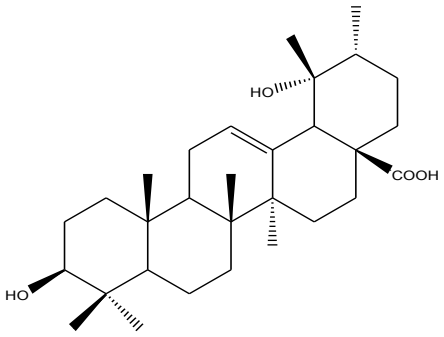

Pomolic acid

Figure 1.26 Triterpenoids with cytotoxic activity

Lupeol and betulinic acid were reviewed for their cytotoxicity by Gallo and Sarachine (2009). Lupeol exhibited inhibitory activity against human melanoma, leukemia, pancreatic adrenocarcinoma, neuroblastoma and prostate cancer cell lines with IC_{50} in the range of 17-38 µM. The mechanism of action was possibly due to inhibition of enzymes such as topoisomerase II, DNA polymerase β, and farnesyltransferase. Wada et al. (2001) reported inhibitory activity of lupeol against DNA topoisomerase II with IC_{50} value of 10.4 µM whilst betulin was moderately active with IC_{50} 38.6 µM. Besides lupeol, betulinic acid showed notable anticancer activity in various studies with a lower IC_{50} value than lupeol in certain type of cancer cell lines, namely melanoma (IC_{50} 2-11 µM), lung cancer (IC_{50} 7-27 µM), breast cancer (IC_{50} 11-36 µM), prostate cancer (IC_{50} 22-26 µM), cervical cancer (IC_{50} 5-31

μM), ovarian cancer (IC_{50} 6-25 μM), colon cancer (IC_{50} 20-29 μM), and colorectal cancer (IC_{50} 8-36 μM) (Gallo and Sarachine, 2009).

Ursolic and oleanolic acids have been extensively reviewed for their anticancer activity (Liu, 1995; Ikeda et al., 2008; Sultana and Ata, 2008). The suppression of the cancer promotion pathways are possibly due to the inhibition of inflammation produced by tumor promoters, the suppression of certain oncogene expression such as c-*jun* and c-*fos*, and the modulation of host immune system (Liu, 1995). Topical pharmaceutical products containing ursolic acid have been patented for skin cancer prevention in Japan (Ikeda et al., 2008). The possible mechanisms of anticancer activity in skin are through the inhibition of NF-κB causing down-regulation of the expression of certain oncogenes, and the induction of apoptosis (Ikeda et al., 2008).

The use of phytosterols as anticancer compounds was reviewed by Bradford and Awad (2007). Dietary phytosterols were examined for cytotoxicity against colon cancer, breast cancer, and prostate cancer. The authors suggested the mechanisms of anticancer action were due to the effects on the host and on the tumour itself. Serum phytosterols affected tumour cell cycle, apoptosis induction, tumor metastasis, and signal transduction, while they also influenced the host by boosting immune function.

The combination of β-caryophyllene (Figure 1.9) with α-humulene or paclitaxel showed potentiated cytotoxic effect against a human breast adenocarcinoma cell line (Legault and Pichette, 2007). The cytotoxicity activity of α-humulene alone was superior to β-caryophyllene alone. α-Humulene alone showed inhibitory activity by 50% at concentration of 0.16 mM, and increased to 75% inhibition when combined with 0.05 mM β-caryophyllene, while β-caryophyllene alone was inactive in all tested concentrations. The combination of 0.16 mM α-humulene, and 0.05 mM β-caryophyllene showed a similar inhibitory activity to 0.32 mM α-humulene alone. Moreover, 0.05 mM β-caryophyllene elevated 10 fold the cytotoxicity of paclitaxel against colon adenocarcinoma, and murine fibroblast cell lines in vitro compared to paclitaxel alone.

Luteolin showed cytotoxic acitivity against a lung cancer cell line with IC_{50} 33 μM (Zhao et al., 2011). It inhibited cancer cells by promoting cell arrest in G1 phase, and apoptosis. Brusselmans et al. (2005) reported the induction of cancer cell apoptosis by

flavonoids via inhibition of fatty acid synthase (FAS). At the same tested dose of 25 µM, luteolin and quercetin showed inhibitory activity against human prostate cancer cell lipogenesis with % inhibition more than 50%. Additionally, luteolin was also reported as a DNA topoisomerase I inhibitor in vitro (Chowdhury et al., 2002). Preincubation of luteolin for 4-10 minutes showed a lower IC_{50} of 0.66 µM while simultaneous addition together with substrate showed IC_{50} of 5 µM. At a dose of 40 µM, luteolin showed 100% inhibition.

1.3.6 Anti-cholinesterase activity

S. lavandulaefolia Vahl. was examined for anticholinesterase activity in vitro (Perry et al., 2000), and in vivo (Perry et al., 2002). They showed that certain essential oils, namely 1,8-cineole and α-pinene, were responsible for acetylcholinesterase inhibition by this species. This activity was also reported from essential oils of *S. leriifolia* Benth which comprised mainly camphor, 1,8-cineol, camphene, and α-pinene (Loizzo et al., 2009). Additionally, the essential oils of *S. lavandulaefolia* Vahl., and extracts of *S. officinalis* L. were reported to improve of cognitive function assessment in healthy volunteers, and in patients with mild to moderate symptoms of Alzheimer's disease (Houghton et al., 2006).

An ethanolic extract of *S. officinalis* L. was prepared in the form of a coated tablet, and orally administered to healthy elderly people (Scholey et al., 2008). Assessments included memory tests, accuracy of attention, speed of memory, and speed of attention at tested times, 1, 2.5, 4, and 6 hour after administration. A dose of 333 mg tablet showed a significant enhancement of memory performance compared to placebo. Other in vivo cognitive function test were performed in healthy adults by Kennedy et al. (2010). Essential oils of *S. lavandulaefolia* Vahl. was encapsulated in dose of 50 µl plus olive oil per capsule, and tested against placebo (olive oil). Results showed improvement of cognitive performance, mental fatigue reduction, and increased alertness at the 1, and 4 hour post-single dose. In vitro analysis of the essential oil showed a potent AChE inhibitory effect with IC_{50} value of 3 µg/ml. Monoterpenoids, camphor (37%), 1, 8-cineol (36.4%), camphene, α-pinene, limonene, and endo-borneol were reported from this oil.

Ren et al. (2004) examined the chemical constituents of *S. miltiorrhiza* Bunge root and determined the acetylcholinesterase inhibition activity of isolated compounds. Dihydrotanshinone, and cryptotanshinone (Figure 1.25) were reported as the most active

compounds among the other terpenes, namely tanshinone I, tanshinone IIA, argentatin A, 1,8-cineole, α-pinene.

In vitro tests for cholinesterase inhibition activity have been carried out in several *Salvia* species. For example, the acetone extracts of *S. sclareoides* Brot. demonstrated 100% inhibition of both acetylcholinesterase (AChE) and butyrylcholinesterase (BChE) at a concentration of 1 mg/ml (Rauter et al., 2007) while nonpolar extracts of *S. albimaculata* Hedge and Hub, and *S. cyanescens* Boiss and Bal. showed more than 80% inhibition of both enzymes at the same concentration (Orhan et al., 2007). A new triterpene, santolinoic acid (Figure 1.27) from *S. santolinifolia* Boiss. showed moderate inhibitory activity against the enzyme acetylcholinesterase with IC_{50} value 62.5 µM and butyrylcholinesterase with IC_{50} value 54.8 µM (Ahmad et al., 2007) while an other triterpene, salvin A (Figure 1.27) from the same plant displayed inhibitory activity only against butyrylcholinesterase with IC_{50} value 12.5 µM (Mehmood et al., 2006).

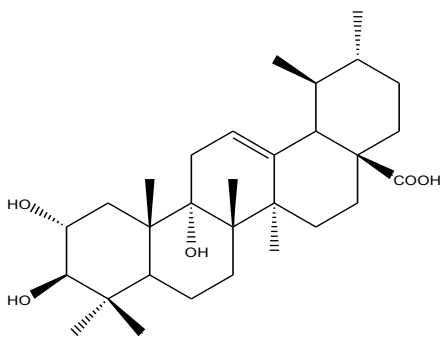

Santolinoic acid

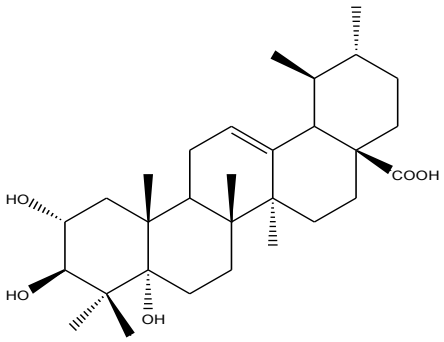

Salvin A

Figure 1.27 Tritepenoids with anti-cholinesterase activity

1.3.7 Cardiovascular activity

Various isolated terpenoids and steroids from three *Salvia* species, *S. syriaca* L., *S. amplexicaulis* Lam., and *S. eriphora* Boiss and Kotschy. were tested for cardioactive activity in Wistar Albino rats (Ulubelen, 2003). Arterial blood pressure and heart rate were evaluated in comparison with propranolol, and phentolamine. The diterpenoids, ferruginol, 7-oxo-abieta-9,12,14-triene,4,14-dihydroxysaprorthoquinone, aethiopinone, 4,12-dihydroxysapripa-

raquinone, and 6,7-dehydroroyleanone showed cardiovascular activity by reducing blood pressure significantly. Besides diterpenoids, the steroids, 3β-hydroxystigmast-5-en-7-one, and stigmast-4-en-3-one were also active as shown in Figure 1.28.

The cardiotonic and antidysrhythmic effects of oleanolic acid and ursolic acid has been evaluated in a rat model (Somova et al., 2004). Pretreatment by triterpenoids decreased the vasopressor and the tachicardic effects of the β-receptor agonist, isoproterenol. Oleanolic acid, 10 mg/kg, was claimed to show a similar effect to pretreatment with propranolol at dose of 2 mg/kg. Oleanolic acid and ursolic acid in a dose of 40mg/kg showed an antidysrhythmic effect on both calcium chloride-, and adrenaline-induced arrhythmias. They were suggested as β-adrenergic antagonists due to their ability to block the effects of adrenaline and isoprenaline in the same way as propranolol.

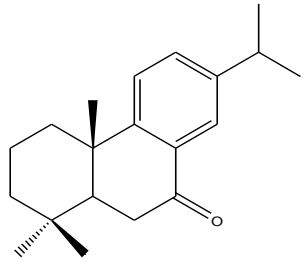

7-Oxo-abieta-9,12,14-triene

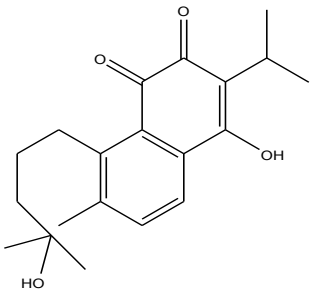

4,14-Dihydroxy-saprorthoquinone

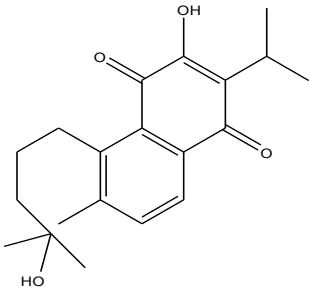

4,12-Dihydroxy sapriparaquinone

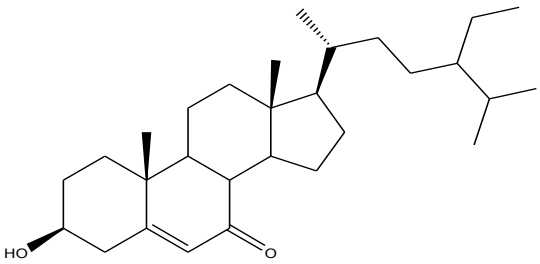

3β-Hydroxystigmast-5-en-7-one

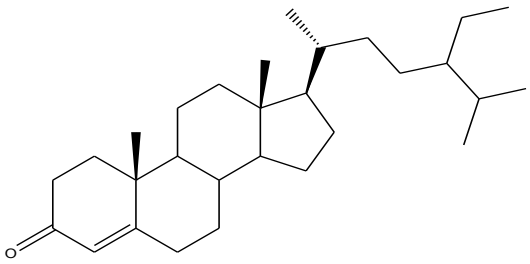

Stigmast-4-en-3-one

Figure 1.28 Diterpenoids and steroids with cardiovascular activity

Salvianolic acid A-F, and lithospermic acid were isolated from *Salvia miltiorrhiza* Bunge which has been traditionally used to treat various cardiovascular diseases (Jiang et al., 2005). Liu et al. (1992) studied the protective activity against peroxidation damage to biomembranes of phenolic compounds from this plant. The authors suggested that salvianolic acid A (Figure 1.17) possessed a potent activity against lipid peroxidation and erythrocyte hemolysis among other phenolic acids such as salvianolic acid B, danshenshu, rosmarinic acid, and caffeic acid.

Salvianolic acid B (lithospermic acid B, Figure 1.19) showed Angiotensin Converting Enzyme (ACE) inhibition activity with IC_{50} 120 μM in vitro (Kang et al., 2003a). Its effect on renal functional parameters in ischemia/reperfusion-induced acute renal failure (ARF) was further investigated in rats (Kang et al., 2004). Salvianolic acid B, at a dosage of 40 mg/kg/day for 4 days, alleviated renal functional defects and protected renal tissue from ischemia-induced ARF in rats. It also showed antioxidant activity against lipid peroxidation in rat kidney homogenates, red blood cells, superoxide, and hydroxyl scavenging activity over the dose range 70-278 μM. The authors suggested that Salvianolic acid B (lithospermic acid B) improved renal defects in rats with ischemia-reperfusion induced acute renal failure possibly due to its radical scavenging activity.

1.3.8 Central nervous system activity

S. divinorum Epling et Jativa leaves have been used by the Mazatec people in Mexico for religious purposes (Roth et al., 2002) and for the treatment of various ailments (Siebert, 1994). Salvinorin A (Figure 1.29), which is a main neoclerodane diterpene compound from leaves of *S. divinorum* Epling et Jativa, induced hallucinogenic symptoms after being inhaled in doses of 200-500 μg and these effects also depended on duration of absorption through oral mucosa after the fresh leaves were consumed (Siebert, 1994). Roth et al. (2002) evaluated radioligand-binding inhibitory activity of salvinorin A against many receptors, transporters, and ion channels. Salvinorin A inhibited only [^{3}H]-bremazocine-labeled κ opioid receptor (KOR), and showed insignificant binding inhibition to cloned human μ (MOR) or δ opioid (DOR) receptors. It was reported as a potent and selective κ opioid receptor (KOR) agonist, the first nonalkaloid one, and was the main component responsible for the psychomimetic effects.

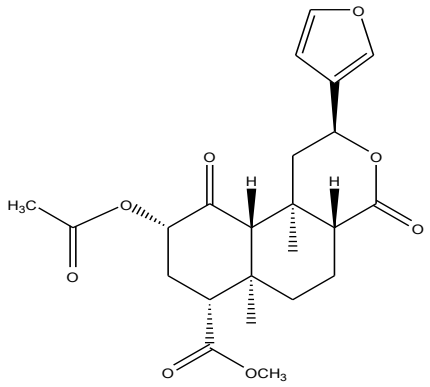

Figure 1.29 Salvinorin A (divinorin A)

Kavvadias et al. (2003) reported constituents from *S. officinalis* L. with in vitro affinity to human brain benzodiazepine receptor. This study aimed to find ligands which inhibited the binding of ^{3}H-flumazenil to benzodiazepine receptors. In comparison with diazepam, 7-methoxyrosmanol, and galdosol (Figure 1.30) showed the appreciable binding activity to the benzodiazepine receptor with IC_{50} 7.2 µM, and 0.8 µM while IC_{50} of diazepam was 0.05 µM.

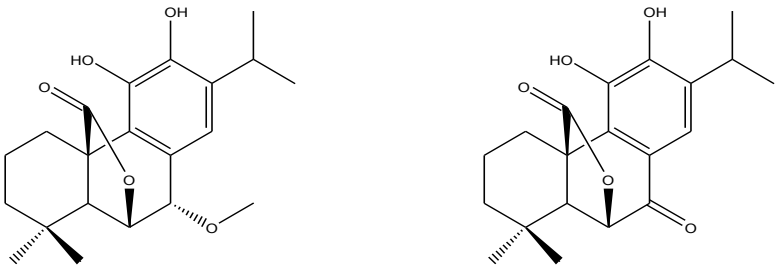

7-Methoxyrosmanol Galdosol

Figure 1.30 Diterpenoids with benzodiazepine receptor binding activity

1.3.9 Hepatoprotective activity

Rosmarinic acid was investigated for its hepatoprotective effect in a hepatic fibrosis cell line in vitro. It showed proliferation inhibitory activity against the rat hepatic stellate cells (HSC-T6) with IC_{50} value 20 µM, and also induced apoptosis (Zhang et al., 2011). The

phosphorylation of signal transducer and activator of transcription protein-3 (STAT3) also decreased; therefore, the authors suggested the activity was possibly due to the inhibition of phosphorylation in STAT3 which mediates growth promoting activity.

Salvianolic acid B (Figure 1.19) could reverse hepatic fibrosis in patients with chronic hepatitis B (Liu et al., 2002). Clinical efficacy of salvianolic acid B was evaluated in 60 patients having liver fibrosis with chronic hepatitis B, in a double blinded, randomized, controlled trial. Patients given tablets containing 30 mg/tablet salvianolic acid B orally administered, two tablets three times daily for six months were compared with patients receiving intramuscular injection of Interferon-γ (INF- γ) once daily for the first month, and then every other day in the following five months. Salvianolic acid B group showed appreciable reduction of serum fibrotic markers (HA, IV-C, and PIIIP) compared to the content before treatment. Reverse rate of fibrotic stage was 37% in salvianolic acid B group, and 30% in INF- γ group. However, the difference of efficacy between both salvianolic acid B and INF- γ groups were insignificant; INF-γ showed certain side effects (fever, and transient decrease of leucocytes) in some patients, while salvianolic acid B showed no change in any monitoring tests, namely EKG, renal function, blood, and urine analysis. There was also no significant change in hepatitis B antigen and antibody system in both groups.

The hepatoprotective effects of oleanolic acid, and ursolic acid were exhaustively reviewed by Liu (1995). Many findings reported protection against chemical damage such as carbon tetrachloride and acetaminophen induced liver damage. However, the mechanisms of hepatoprotection by both acids are not yet conclusive but may involve the inhibition of toxicant activation and the increase of the body defense systems (Liu, 1995).

1.3.10 Anti-inflammatory activity

Ursolic acid from the chloroform extracts of *S. officinalis* L. showed topical anti-inflammatory activity by evaluation of the inhibition of croton-oil-induced ear oedema in mice, and its effect was more potent than indomethacin (Baricevic et al., 2001). Using the same model in mice, Felice et al. (2006) reported that 2-deoxyasiatic acid, maslinic acid, and arjunolic acid (Figure 1.31) from *S. hierosolymitana* Boiss showed the same oedema reduction effect in comparison with indomethacin. For the same topical dose of 0.3 μmol/cm^2, asiatic acid (Figure 1.31) showed 2.8 fold less oedema reduction than 2-

deoxyasiatic acid. For the oleanane skeleton, a double bond at C-12(13) was advantageous because 2α,3β-Dihydroxyolean-28-oic acid (Figure 1.31) was 2.2 fold less active than maslinic acid. 24-Nor-2α,3β-dihydroxy-olean-4(23)-12-ene was 3.6 fold less active than maslinic acid. Moreover, the hydroxylation of C-23 in the oleanane type slightly increased the activity since arjunolic acid showed 60% of oedema reduction while maslinic acid showed 51% oedema reduction.

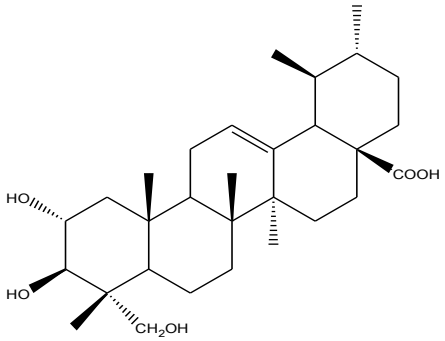

Asiatic acid

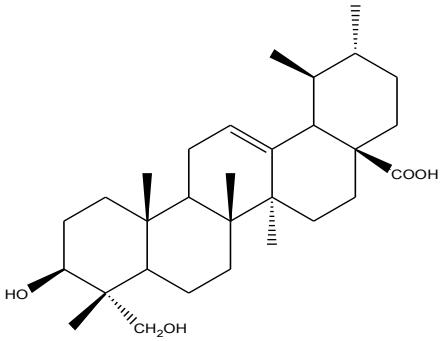

2-Deoxyasiatic acid

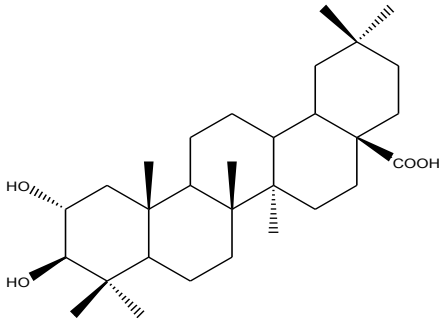

2α,3β-Dihydroxyolean-28-oic acid

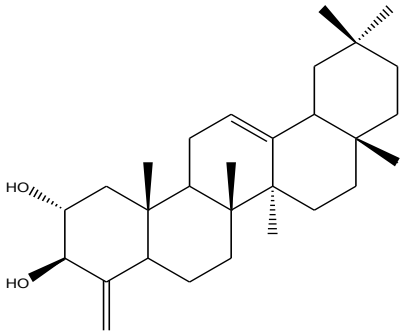

24-Nor-2α,3β-Dihydroxyolean-4(23)-12-ene

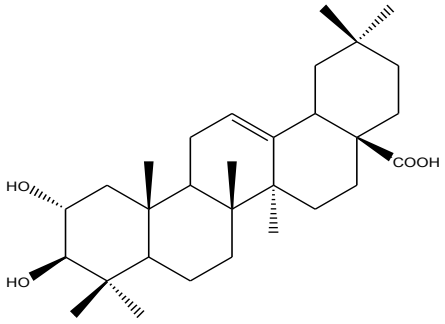

Maslinic acid

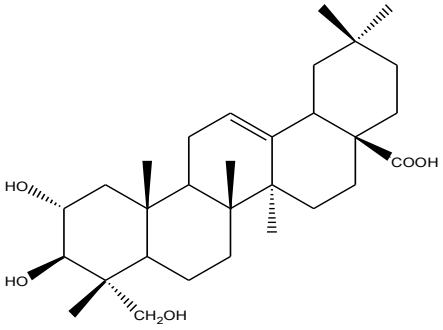

Arjunolic acid

Figure 1.31 Tritepenoids with anti-inflammatory activity

The determination of anti-inflammatory activity of lupeol and lupeol linoleate was carried out in rats by using a paw swelling model (Geetha and Varalakshmi, 2001). Lupeol and lupeol linoleate (50 mg/kg in 0.5 ml olive oil), and indomethacin (3 mg/kg in 0.5 ml saline) were administered to arthritic rats. They showed a paw thickness reduction in arthritic-induced rats as follows: lupeol 39%, lupeol linoleate 58%, and indomethacin 35%. Furthermore, rats orally administered with lupeol and lupeol linoleate (dose level of 100 and 200 mg/kg) did not show ulcerogenic activity in the stomach whereas it was found in indomethacin (20 mg/kg) treated rats.

The anti-inflammatory activity of triterpenic acids has been extensively reported for ursolic acid, oleanolic acid, lupeol, betulin, and betulinic acid (Liu, 1995; Ikeda et al. 2008; Sultana and Ata, 2008; Gallo and Sarachine, 2009).

The suppression of arachidonic acid metabolism and cytokine production in vitro by 1,8-cineol has been reported (Juergens et al., 1998). In vivo evaluation of 1,8-cineol anti-inflammatory activity was further carried out in a double-blinded, placebo-controlled trial on steroid-dependent bronchial asthma patients (Juergens et al., 2003). In a dose of 200 mg three times a day for 12 weeks, 1,8-cineol showed 36% daily prednisolone dosage reduction while the placebo group showed only 7% dose reduction.

Anti-inflammatory activity of linalool, and linalyl acetate were evaluated by using a model of carrageenin-induced edema in rats (Peana et al., 2002). Rats were pretreated with (-)-linalool, (±)-linaool, linalyl acetate via subcutaneous abdominal injection. After 30 minutes, paw edema was induced by carrageenan, and measured 1, 3, and 5 hours after induction. (-)-Linalool, at the dose of 25 mg/kg, showed strong inhibition of edema after 3, and 5 hours while the racemic compound showed the edema reduction only 1 hour after carrageenin administration without any effect after 3 and 5 hours. Linalyl acetate showed no effect at the same dose, however, it reduced inflammation only after 3 and 5 hour when the dose was increased to 64 mg/kg. The authors suggested the delayed effect of linalyl acetate was due to the biotransformation into the alcohol.

Luteolin was evaluated for anti-inflammatory activity in acute and chronic models in mice (Ziyan et al., 2007). Oral administration of luteolin in dose of 10 and 50 mg/kg significantly reduced paw edema in the acute carrageenan-induced model, and also reduced

the elevated level of 6-keto-$PGF_{1\alpha}$ in exudates. In a chronic inflammation model, luteolin showed the inhibition of cotton pellet-induced granuloma formation which led to the reduction of fibroblasts and synthesis of collagen and mucopolysaccharides. Apigenin also inhibited of fibroblast growth (Koganov et al., 1999). Fibroblasts play a role in tissue formation and interact with the immune system during inflammation which may cause a delay in wound healing (Harborne and Williams, 2000).

In addition, the human blood assay for cyclooxygenase (COX) activity was also carried out in vitro (Ziyan et al., 2007). Thromboxane B_2 (TXB_2), and prostacyclin (PGI_2) were measured as markers of COX-1, and COX-2 activities respectively. Luteolin showed selective potency by decreasing the concentration of PGI_2 (COX-2) while having no effect on TXB_2. The authors suggested that luteolin could be a selective inhibitor for cyclooxygenase-2 (COX-2).

1.3.11 Antioxidant activity

Tanshinone II-A (Figure 1.25) from *S. miltiorrhiza* Bunge showed inhibition of lipid peroxidation induced-DNA damage in liver cells (Cao et al., 1996). It was suggested to act as a lipid free radical scavenger and to inhibit the formation of malondialdehyde (MDA) and lipid-DNA adducts in a similar way to vitamin E and butylated hydroxyltoluene (BHT). Kabouche et al. (2007) reported a diterpene from the aerial part of from *S. barrelieri* Ettling, inuroyleanol (Figure 1.32) which also showed strong DPPH free radical scavenging activity, and the inhibition of lipid peroxidation in the β-carotene-linoleic acid system. Moreover, taxodione (Figure 1.22) from the root of the same species showed comparable antioxidant activity to the controls, BHT and vitamin E, in β-carotene bleaching, DPPH free radical scavenging activity, ABTS cation radical scavenging activity, and cupric reducing antioxidant capacity methods (Kolak et al., 2009).

Abreu et al. (2008) examined 60 species of *Salvia*. The result indicated that the antioxidant diterpenes, carnosic acid and carnosol (Figure 1.32) were found in 48 and 27 species respectively while α-tocopherol was detected in all species. Many findings have reported a promising antioxidant activity of carnosol, for example, inhibiting Cu^{2+} induced LDL oxidation and lipid free radicals in mouse microsomes, and enhancing glutathione-S-transferase (GST) activity in the rat liver (Johnson, 2011).

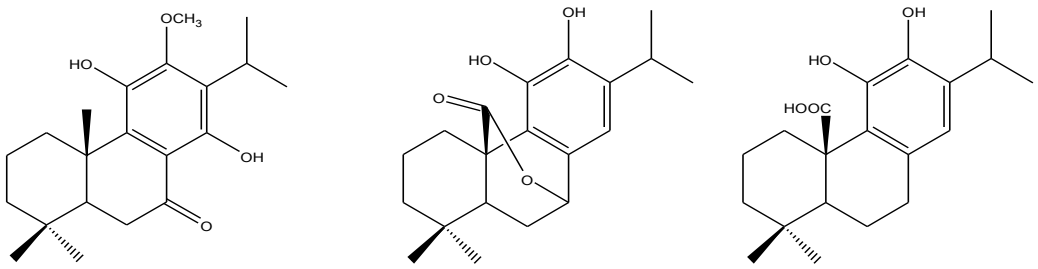

Inuroyleanol Carnosol Carnosic acid

Figure 1.32 Diterpenoids with antioxidant activity

The antioxidant activity of 42 flavonoids was determined against β-carotene oxidation inhibition, and DPPH scavenging activity (Burda and Oleszek, 2001). Among many classes of flavonoids, flavonols with a free hydroxyl group at the C-3 position exhibited high inhibitory activity against β-carotene oxidation. Kaempferol and quercetin showed comparable antioxidant activity, but kaempferol was slight higher. Moreover, the methylation or glycosylation substitution at C-3 showed a lower antioxidant activity than aglycone. In DPPH scavenging assay, the substitution at C-3 of flavonol showed no effect but ortho-dihydroxyl substitution at B ring (C-3', and C-4') with a hydroxyl group at C-3 and also a double bond (C-2 and C-3) are vital for radical scavenging activity. Kaempferol, rutin, quercetin and luteolin-7-glucoside showed comparable DPPH scavenging activity whereas apigenin-7-glucoside showed weak activity, and no activity for naringin and apigenin. The ortho-dihydroxy in the B ring stabilised the radical form while the conjugation of a double bond (C-2,3) and 4-oxo maintain electron delocalization in the aromatic nucleus (Rice-Evans et al., 1996).

S. officinalis L. infusion was evaluated for antioxidant activity in vivo in mice and rats (Lima et al., 2005). Both mice and rats were given sage tea (2 g dried plant/150 ml boiling water) as beverage compared with tap water for 14 days. Plasma transminase activities, alanine aminotransferase (ALT), aspartate aminotransferase (AST), and liver glutathione were measured from mouse blood samples. The sage tea drinking group showed no difference in plasma ALT and AST. However, the glutathione enzymes in liver, glutathione reductase (GR), and glutathione-S-transferase (GST), of the sage tea group were

10% higher than the water drinking group. Furthermore, isolated rat hepatocytes from sage tea feeding group were cultured and toxicity induced by tertiary-butyl hydroperoxide (t-BHP) in order to assess the protective effect of sage tea. t-BHP-induced lipid peroxidation effect between two groups were insignificant while the GSH level of sage tea group was higher than control after 4 h of culture. The authors suggested no toxicity to the liver of sage tea drinking in both mice and rats, but a positive effect on the antioxidant status of the liver. Sage tea contained the phenolic acid, rosmarinic acid (0.04%), luteolin-7-glucoside (0.01%), and volatile components (less than 0.01%) including 1,8-cineol, thujones, camphor, and borneol.

Zhao et al. (2008) reported that the radical scavenging activity against free hydroxyl radicals, superoxide anion radicals, DPPH, and ABTS, of danshenshu and salvianolic acid B were higher than vitamin C while salvianolic acid B was the most potent with IC_{50} value 0.1 mM. The protection effect against hydrogen peroxide induced human vein vascular endothelial cell damage corresponded to their antioxidant activity. 14 µM Salvianolic acid B exhibited the same % cell viability as untreated control culture.

1.3.12 Polyphenol and UV protection

In plants, flavonoids play a role as flavonoid pigment complexes in conspicuous flower colour, and also as UV filters in leaves due to their absorption in 280-320 nm region (Harborne and Williams, 2000). Flavone, and flavonol glycosides were commonly reported as the UVB protective flavonoids from various plant species, however, the ability to prevent damaging effect from UV radiation varied in plants ((Harborne and Williams, 2000).

Ultraviolet (UV) radiation exposure induces the generation of free radicals which could further react with DNA and cause biological damage (Svobodova et al., 2003). Rosmarinic acid showed photoprotection activity against UVA-induced oxidative stress (Psotova et al., 2006). 25 µM Rosmarinic acid pre-treatment led to increased cell viability of human keratinocytes after exposure to UVA (100 and 200 kJ/m^2). Caffeic acid, and ferulic acid also showed cytoprotection against UVB-induced erythema in vivo (Saija et al., 2000). The minimal erythema dose (MED) was firstly determined for each subject, and the irradiation dose corresponding to double the MED was used. After UVB exposure, 200 µl aqueous solution of caffeic acid, and ferulic acid were applied to the irradiated forearm skin area of six young healthy volunteers. Although both showed cytoprotection effect against

UVB, ferulic acid showed superior protection to caffeic acid with 1.8 fold higher percentage inhibition of UVB skin erythema. In addition, ferulic acid showed the better penetration through the stratum corneum in vitro which was possibly due to its greater lipophilicity. Hydroxycinnamic acids were previously reported by this research group to protect the phospholipid membrane from UV light by lipid peroxidation inhibition, and to react with nitrogen oxides.

Caffeic acid and its derivatives were evaluated for protection against UVA-induced reactive oxygen species in the skin of hairless mice (Yamada et al., 2006). Topical use of caffeic acid and rosmarinic acid suppressed reactive oxygen species (ROS) in mouse skin as determined by chemiluminescence (CL). The tested compounds were applied to the abdominal skin area 30 minutes before UVA exposure (180 kJ/m^2), and the CL light emission was measured. Caffeic acid showed better protection with IC_{50} 1.2 mM while rosmarinic acid was at 2.8 mM. However, they both suppressed UVA-induced ROS in the concentration of 5-10 mM. Furthermore, caffeic acid was given orally to the mice in dose of 200 mg/kg body weight for 3 consecutive days, and then followed by UVA exposure to the skin. The distribution of caffeic acid to the plasma and liver were detected after a single oral dose and to the skin after three consecutive days of oral administration. The ROS suppressive effect in skin exposed to UVA was also observed in the oral administration group. As caffeic acid can absorb certain wavelengths of UVA (320-400 nm), it possibly protected the skin by a sunscreen effect as well as ROS quenching activity.

Tong et al. (2007) evaluated the effect of apigenin against cyclooxygenase 2 (COX-2) enzyme expression which is induced by UVB exposure in vitro. Apigenin, at concentration of 50 µM, inhibited PGE_2 production in mouse keratinocytes through modulation of COX-2 gene. As carcinogenesis can cause COX-2 overexpression, the authors suggested the application of apigenin as alternative anticancer agent.

Luteolin was reported to protect skin from UVB-induced damage in vitro and in vivo (Wolfle et al., 2011). It inhibited the formation of ROS induced the production by UVB with EC_{50} 10.5 µM and by H_2O_2 with EC_{50} 36 µM in human keratinocytes. An in vivo study was also carried out using the UVB erythema test. Luteolin was applied to the backs of volunteers 30 minute before irradiation by UVB and the induced erythema was measured photometrically. 2.5% Luteolin showed a similar reduction of erythema as trolox (positive

control). Expression of COX-2 was also inhibited by luteolin which resulted in a reduction of PGE_2 in human keratinocytes cell culture supernatants. The authors suggested the protective effect of luteolin against UVB-induced damage was due to UV-adsorbtion, DNA-protection, antioxidant and anti-inflammatory properties.

1.3.13 Miscellaneous activities

A hydroalcoholic crude extract of *S. officinalis* L. was investigated for gastroprotective effect in a rat model (Mayer et al., 2009). In comparison with omeprazole, oral administration of the extract showed a decrease in ethanol-induced gastric lesions and acetic acid induced-gastric ulcer. It also inhibited H^+, K^+-ATPase activity in vitro which is comparable to omeprazole. Carnosol was suggested as an active component in the extract.

A new secoisopimarane diterpenoid, 3,4-secoisopimara-4(18),7,15-triene-3-oic acid (Figure 1.33), from *S. cinnabarina* M. Martens et Galeotti was tested in isolated guinea-pig ileum for antispasmodic activity (Romussi et al., 2001). This study employed histamine, acetylcholine, and barium chloride as agonists to induce contraction. The result showed a non-selective inhibitory effect of this compound and a comparable IC_{50} to papaverine against all tested agonists.

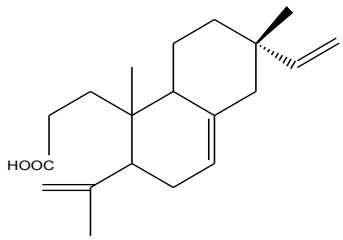

Figure 1.33 Antispasmodic diterpenoid

Oleanolic acid, ursolic acid, and lupeol were tested in an α-amylase assay (Ali et al., 2006). Among these compounds, ursolic acid showed the strongest inhibition property on α-amylase while lupeol was also active with the weakest inhibition. These findings suggested that the pentacyclic ring of the terpenoids may be responsible for this activity, however the structure activity relationship between cyclopentane E ring, and cyclohexane E ring was inconclusive.

Ninomiya et al. (2004) reported pancreatic lipase inhibitory activity of both carnosic acid and carnosol from leaves of *S. offinalis* L. Moreover, carnosic acid also showed decreased serum triglyceride elevation in olive oil-loaded mice including body weight and epidydimal fat reduction in high fat diet-fed mice.

Diterpenoid compounds from the root part of *S. miltiorrhiza* Bunge, tanshinone II-A, tanshinone I, cryptotanshinone, and 15,16-dihydrotanshinone, were reported to possess antiosterporotic effect in vitro. They showed appreciable inhibitory effects on osteoclast differentiation in the mouse osteoblast/bone marrow cell coculture system (Lee et al., 2005). Tanshinone II-A, danshenols A and B, dihydrotanshinone I, tanshinone I, cryptotanshinone, and danshexinkun A were also reported to show inhibitory activity against aldose reductase (Fuente and Manzanaro, 2003).

Luteolin-5-rutinoside from *S. lavandulifolia* Vahl. was evaluated for antidiabetic activity in streptozotocin (STZ)-induced diabetic rats (Zarzuelo et al., 1996). Oral administration of luteolin-5-rutinoside at dose of 2 mg/kg showed a 22% reduction of blood sugar with no effect on plasma insulin after a 20 day treatment in comparison with diabetic control. A combination of luteolin-5-rutinoside, and glibenclamide showed appreciable synergistic effects by 51% reduction of blood sugar, and 2.5 fold increase in blood insulin level. Moreover, body and pancreas weights of this group were higher than diabetic control.

1.4 Investigated plant: *Salvia viridis* L.

S. viridis L. (Synonym *S. horminum* L.), or Red Topped Sage, is a perennial, annual, or biennial herb with erect stems up to 50 cm, 4-8 flowers in axillary verticillasters with various coloured bracts (Hedge, 1972). In Flora Europaea (1972), it is placed along side *S. sclarea* L. In the wild, this species is distributed in Europe, particularly the Mediterranean region (Hedge, 1972) and has widely been cultivated in Britain as an ornamental plant (Walker, 2002). It has been used in traditional medicine, for example, an infusion of leaves as a gargle for sore gums, and has also been employed to increase the quality of liquor by putting leaves and seeds into the fermentation tank (Dweck, 2000).

Ulubelen and Brieskorn (1975) isolated ursolic, oleanolic and micromeric acids from the aerial part. Three triterpenic alcohols, i.e. lupeol, lup-(20)29-ene-2α,3β-diol, and olean-13(18)-ene-2β,3β-diol were additionally reported from the same plant part by Ulubelen et al. (1977). Kokkalou and Kapetanidis (1988) found phenolic acids and flavonoids including their glycosides, namely caffeic acid, chlorogenic acid, apigenin, luteolin, apigenin-7-glucoside, apigenin-7-rutinoside, luteolin-7-glucoside, and luteolin-7-rutinoside.

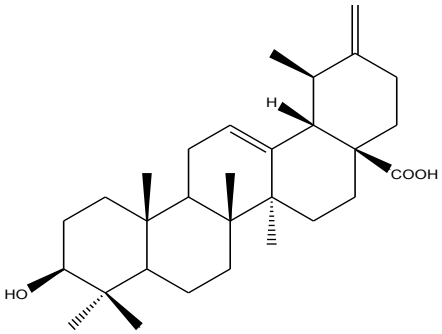

Micromeric acid

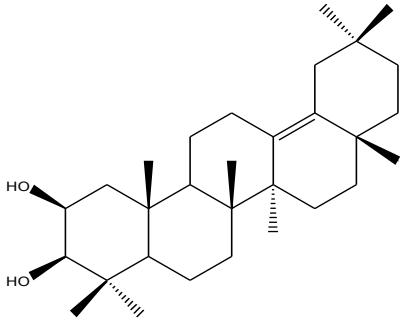

Olean-13(18)-ene-2β,3β-diol

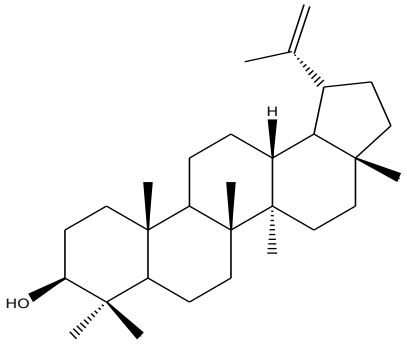

Lupeol

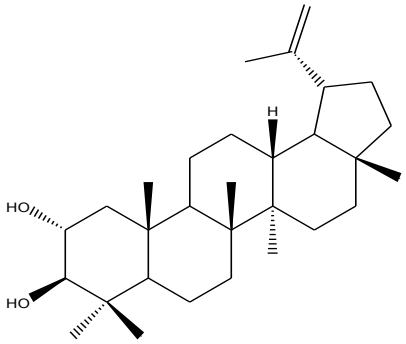

Lup-(20)29-ene-2α,3β-diol

Figure 1.34. Triterpenoids in aerial part of *Salvia viridis* L.

More recently, diterpenes, i.e. salviviridinol, viridinol, viridone, sugiol, 1-oxoferruginol, ferruginol, aethiopinone, and microstegiol were isolated from roots, and 1-oxoferruginol showed antibacterial activity against *Bacillus subtilis*, *Staphylococcus aureus* and *Staphylococcus epidermidis* (Ulubelen et al., 2000). Additionally, ferruginol, which was also isolated from *S. ceratophylla* L., *S. caespitosa* Montbret and Aucher ex. Bentham, and *S. blepharochlaena* Hedge and Hub. Mor., showed antihypertensive activity by reducing arterial blood pressure in rats (Ulubelen, 2003). Carnosic acid, carnosol, and α-tocopherol have also been reported in *S. viridis* L. (Abreu et al., 2008).

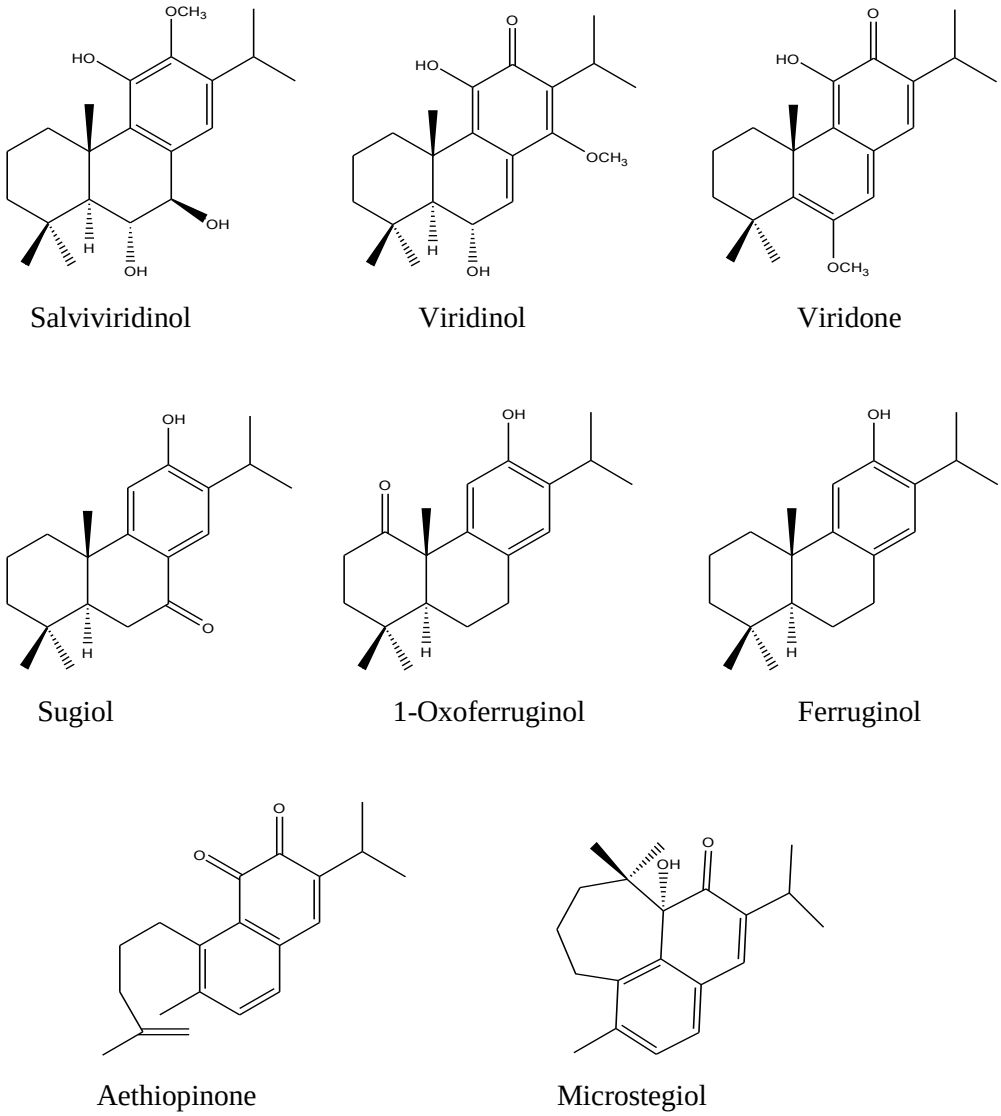

Figure 1.35. Diterpenoids in root part of *Salvia viridis* L.

Aims of this study

Previous phytochemical reports on *S. viridis* L. showed the presence of triterpenoids and flavonoids in the aerial part, and diterpenoids in the root part; several of which have been reported to possess interesting and varied biological activities. *S. viridis* L. cv. Blue Jeans is an ornamental cultivar selected for deep blue floral bracts (as opposed to violet, green, and pink) in the wild type. This is effectively, a chemical variant which might be expected to yield a generally novel chemistry when compared with the wild type.

Accordingly, the phytochemical aim of the project was to isolate and identify as many compounds as possible across a wide range of structural and biosynthetic types. Moreover, many different types of biological activity have been reported from the genus *Salvia*. Thus, a biological aim of the project was to utilize a series of TLC-based chemo- and bioautographic techniques to secure a biological activity profile of as many as possible of the isolated compounds. A final aim was to proceed to a more detailed in vitro biological study of compounds of interest identified in the previous steps.

Chapter 2
Experimental

2.1 Plant Materials

Salvia viridis L. cv. Blue Jeans (synonym: *S. horminum* L.) was grown in Bath from commercially available seed purchased from Thompson and Morgan, and harvested in September 2004. Roots and aerial parts were separated, air-dried at room temperature, ground and kept separately in airtight containers.

2.2 Material

2.2.1 Chemicals

All solvents, which were analytical or HPLC grade, ferric chloride, formic acid and silica gel 60 (35-70 µM, 60 A°) were supplied by Fisher. DPPH (2,2- Diphenyl-1-picryl-hydrazyl), *p*-iodonitrotetrazolium chloride (INT), caffeic acid, chlorogenic acid, rutin, 2-aminoethyl-diphenyl borinate, and polyethylene glycol 300 were purchased from Sigma. Deuterated-methanol, deuterated-chloroform, deuterated-DMSO, anisaldehyde, rosmarinic acid, and phosphomolybdic acid were purchased from Aldrich. Sulfuric acid and acetic acid were purchased from BDH chemical Ltd. Water was purified by Milli Q Plus PF.

2.2.2 Test organisms and media

The panel of test organisms consisted of the Gram-positive bacteria, *Staphylococcus aureus* (ATCC 6571), *Enterococcus faecalis* (ATCC 775), *Bacillus cereus* (ATCC 2599), and the Gram-negative bacteria, *Klebsiella pneumoniae* (ATCC 9633), *Proteus vulgaris* (ATCC 4636), and *Escherichia coli* (ATCC 86). Nutrient agar, Nutrient broth, ampicillin impregnated disc were supplied from Oxoid. Chloramphenical and ampicillin sodium, erythromycin powder were supplied from Sigma. All procedures were carried out under sterile conditions.

2.3. Thin layer chromatography (TLC)

TLC plates, aluminium-backed sheets coated with silica GF_{254} 60 in 0.25 mm thickness, were purchased from Merck. All crude extracts were dissolved in the appropriate

solvent, i.e. methanol and chloroform before being spotted on to the plate. The following standard compounds, naringin, rosmarinic acid, caffeic acid, chlorogenic acid, and rutin were applied side by side on the same plate. Two mobile phases were used to develop the TLC plates as follows: ethyl acetate: methanol:formic acid:water (50:3:3:6) and chloroform:methanol (9:1). The developed TLC plates were observed in visible light and under UV light at 254 nm and 365 nm, and then were sprayed with reagents as shown in Table 2.1.

Table 2.1 Spraying reagents (Reich and Schibli, 2007)

Reagent	Composition and Use	Examination	Type of compound
Anisaldehyde-Sulfuric acid	0.5% Anisaldehyde in solution of methanol:acetic acid:sulfuric acid (85:10:5) The plate was sprayed, and then heated at 100ºC for 2-5 minutes	Visible light, UV 366 nm	Terpenoids, saponin, sterols, iridoid, most lipophilic compounds
Iron (III) chloride	1% iron (III) chloride in ethanol The plate was sprayed then heated at 100ºC for 10 minutes	Visible light	Phenols, flavonoids, tannins, plant acids
Natural products/ polyethylene glycol (NP/PEG) spraying solutions	Solution A: 1% 2-aminoethyl-diphenyl borinate in methanol Solution B: 5% PEG in ethanol The plate was heated at 100ºC for 3 minutes then sprayed while still hot with solution A and B consecutively.	UV 366 nm	Flavonoids, carbohydrates, anthocyanins and plant acids
Phosphomolybdic acid	5% Phosphomolybdic acid in ethanol The plate was sprayed and then heated at 100ºC for 5 minutes.	Visible light	Fatty oils, reducing substances, steroids, essential oils

2.3.1 TLC-chemoautographic method: DPPH radical scavenging activity

This method was carried out as described by Cimpoiu (2006) and Tasdemir et al. (2004). Developed TLC plates were sprayed with 0.2 % DPPH solution in methanol, and left at room temperature for 30 minutes. Yellow spots or bands on a purple background were observed in visible light.

2.3.2 Antibacterial activity

2.3.2.1 TLC-bioautographic method; Agar overlay

This method was carried out as described by Raman et al. (1995) with slight modification. Nutrient agar (28 g/L) and nutrient broth (13 g/L) were dissolved in water as described by manufacturer, and sterilized by autoclave prior to use. Test organism was seeded in the Nutrient broth, and incubated in a shaking bath (Fisher Scientific DMS360) for 24 h at 37ºC. On the day of testing, a TLC plate was developed in the appropriate mobile phase, air-dried thoroughly, and placed in a sterile Petri dish. To 100 ml of Nutrient agar, 1 ml of the overnight broth cultures ($1x10^8$ CFU/ml) was added at 45ºC to make a final concentration of organism $1x10^6$ CFU/ml. Then, a developed TLC plate was carefully overlaid by the inoculated agar. Total volume of the inoculated agar was approximately 20 ml per 10x10 cm TLC plate. The agar overlaid plate was allowed to solidify at ambient temperature, further incubated for 24 h at 37º C, and then sprayed with an INT solution (2 mg/ml in water). The plate was further incubated for 30 min at 37ºC. Compounds with inhibitory activity were seen as clear or pale yellow zones against a purple background. Positive control of antibiotic, chloramphenicol, ampicillin, and erythromycin, were used by either spotting a solution or placing an impregnated disc on the developed plate.

2.3.2.2 Microorganism calibration

Viable bacteria counts were carried out by a serial dilution technique, and defined as the number of colony forming units/ml (CFU/ml) (Baker et al., 2011) as depicted in Figure 2.1. Test organism was seeded in the Nutrient broth, and incubated in a shaking bath (Fisher Scientific DMS360) for 24 h at 37ºC. To the first test tube containing 9 ml Nutrient broth, 1 ml the overnight inoculated broth was added, and mixed thoroughly. 0.1 ml of inoculated broth solution was seeded on an agar plate, and incubated 24 h at 37ºC. For the second serial dilution, 1 ml of the first inoculated broth was added to 9 ml of the fresh nutrient broth tube. The second one was also seeded in an agar plate, and further incubated 24 h at 37ºC. The inoculated nutrient broth was serially diluted to the appropriate tube at which it was possible

to count the number of colonies on an agar plate. Figure 2.1 demonstrates 5 dilutions from the overnight inoculated nutrient broth. Hundred colonies are counted in the fifth agar plate which referred to 1000 CFU/ml for this dilution. Therefore, the overnight inoculated nutrient broth would approximately be $1x10^8$ CFU/ml.

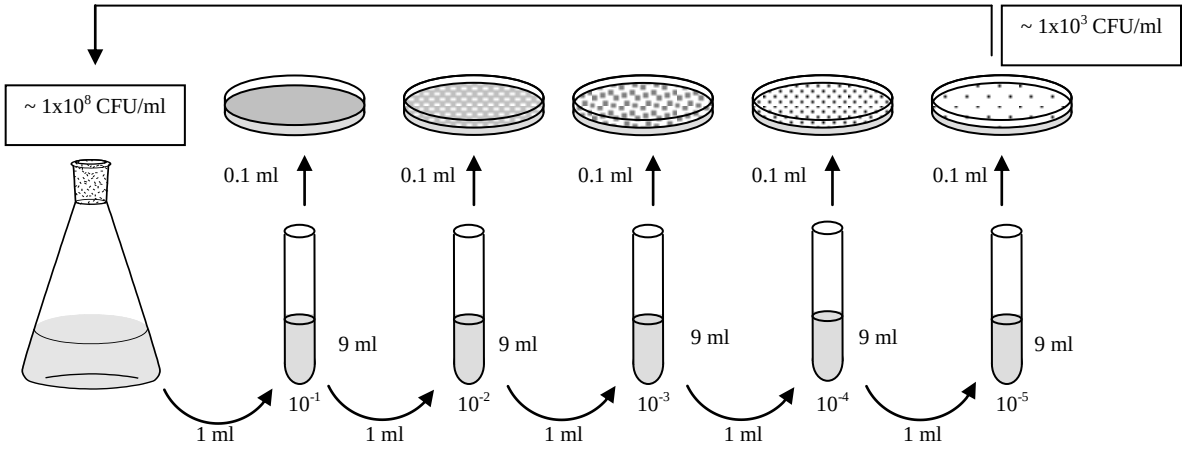

Figure 2.1 The serial dilution technique for calibration bacterial concentration

2.3.2.3 Minimum inhibitory concentration (MIC)

A 96 well microplate technique for MIC assay was based on Eloff (1998) with slight modification. Bacteria of choice, *Staphylococcus aureus* (ATCC 6571), *Enterococcus faecalis* (ATCC 775), *Bacillus cereus* (ATCC 2599), were seeded separately in the nutrient broth as described above. All crude fractions and isolated compounds were dissolved in DMSO to make stock solutions 200 mg/ml for crude fractions and 20 mM for isolated compounds, and further diluted in water to 2 mg/ml for crude fractions, and 200 µM for isolated compounds. Each crude fraction/compound was serially diluted to make two fold dilution for six wells. To each well was added 100 µl cell suspension ($1x10^5$ CFU/ml), and then 100 µl diluted crude fraction/compound was added, and mix thoroughly. The plate was incubated for 24 h at 37ºC on a microplate shaker. To visualize the bacterial growth, 50 µl INT solution (2 mg/ml in water) was added into each well, and further incubated for 30 min at 37ºC on a microplate shaker. A clear well was observed for the inhibitory activity of compounds/crude extracts while the presences of bacteria were seen as a purple colour. The MIC was reported as the minimum concentration of crude extracts/compounds that inhibited the growth of bacteria. The nutrient broth was used as blank, and the inoculated nutrient broth

was the negative control. Chloramphenical was employed as the positive control. The final concentration of DMSO was not more than 1% in each well of tested compounds. %Toxicity of DMSO was also evaluated starting from 10% with two fold dilution for six serial wells.

2.3.3 Acetylcholinesterase inhibitory activity

Acetylcholinesterase from electric eel (type VI-s, lyophilized powder, 1.17 mg solid/ 425.94 u/mg) was purchased from Sigma. To the lyophilized enzyme powder, 498 µl Tris buffer solution (50 mM Tris-HCl, pH 8) was added to make the stock solution of 1000 U/ml enzyme. The enzyme stock solution was prepared, and kept at -20ºC under dark condition. Further dilution of enzyme was made by mixing with solution of Tris buffer and 0.1% BSA. ACTI and DTNB were freshly prepared by dissolving in water, and Tris buffer solution respectively. Physostigmine was used as positive control.

2.3.3.1 TLC-bioautographic method

This AChE inhibitory activity assay was carried out as described by Rhee et al. (2003) with slight modification. The developed TLC plate was sprayed with 5 mM ACTI solution, and followed by 5 mM DTNB solution. The sprayed plate was allowed to dry for 15-20 min, and then further sprayed by 5 U/ml AChE enzyme solution. After 10 min, a white band/spot against a yellow background was observed as compound with enzyme inhibitory activity. The yellow background gradually faded, and disappeared within 30 min. Physostigmine (5 µl of 3.6 mM in methanol) was spotted as positive control.

2.3.3.2 Microplate assay

This AChE inhibitory activity assay was carried out as described by Rhee et al. (2003) with slight modification. To each well was added 125 µl of 3 mM DTNB, 25 µl of 15 mM ATCI, and 50 µl of Tris with 0.1% BSA. 25 µl Test sample solution (10 mg/ml in methanol) was finally added, and measured the absorbance by VERSAmaxTM (Molecular devices, California) at 405 nm every 10 seconds for five times. Enzyme solution (25 µl of 1 U/ml) was then added to each well, and the absorbance was read every 10 seconds for 3 minutes. The rates of reaction both before and after adding the enzyme were calculated by Microsoft Excel 2003. The reaction rate of spontaneous hydrolysis before adding the enzyme was subtracted from the rate after adding the enzyme. Enzyme activity of test samples was calculated compared to the blank (methanol). Percentage enzyme inhibitory activity was

reported by subtracting % enzyme activity from 100. Each experiment was carried out in triplicate. Physostigmine (1, 5 µl of 3.6 mM in methanol) was used as positive control.

2.4 High performance liquid chromatography (HPLC)

The HPLC instruments used were: Jasco PU-980 pump, Jasco UV-975 detector, Goerz Metrawatt Servogor 120 recorder, and commercial reversed-phase HPLC columns, i.e. Phenomenex Luna PFP 150x4.6 mm, and 250x10 mm. Detection wavelength at 330 nm was used for all crude samples. All mobile phase systems used HPLC grade solvents, filtered through a 0.45 µm nylon filter, and sonicated 30 minutes by a Decon ultrasonicater before being used. The sample was dissolved in methanol, and also filtered through 0.45 µm nylon Acrodisc prior to load into injection loop. For semi-preparative HPLC, sample was repeatedly injected, and eluent was collected separately according to each peak from a recorder. After being evaporated to dryness, the isolated compounds were submitted to Mass Spectrometry (MS) and Nuclear Magnetic Resonance spectroscopy (NMR).

2.5 Spectroscopic examinations

2.5.1 Mass Spectrometry (MS)

All mass spectra were performed on a Bruker micrOTOF mass spectrometer using electrospray ionization (ESI) at the Department of Chemistry, and Department of Pharmacy and Pharmacology, University of Bath. GC-CI-MS was analyzed by EPSRC National Mass Spectrometry Service Centre, School of Medicine, University of Swansea.

2.5.2 Nuclear Magnetic Resonance Spectroscopy (NMR)

NMR experiments were carried out by JEOL GX 270 (270 MHz for ^{1}H, and 67.8 MHz for ^{13}C) or Varian Mercury spectrometer (400 MHz for ^{1}H, and 100 MHz for ^{13}C) or Bruker spectrometer (500 MHz for ^{1}H, and 125 MHz for ^{13}C). Chemical shifts (δ) and coupling constant (*J*) were recorded in parts per million (ppm), and Hertz (Hz) respectively. Multiplicities were reported as singlet (s), doublet (d), doublet of doublet (dd), doublet of doublet of doublet (ddd), triplet (t), multiplet (m) and broad (br). All crude extracts or fractions or isolated compound were dissolved in appropriate solvents, i.e. deuterated-methanol (CD_3OD), deuterated-chloroform ($CDCl_3$), deuterated-water (D_2O) and deuterated-dimethyl sulfoxide (DMSO-d_6).

2.5.3 Ultraviolet Spectrometry (UV)

UV-visible spectra were carried out by UV/VIS spectrometer (Lambda EZ 201, Perkin Elmer) at the Department of Pharmacy and Pharmacology, University of Bath.

2.6 Extraction procedures of aerial part

Dried powdered aerial part of *Salvia viridis* L. cv. Blue Jeans (300 g) was extracted with 3 x 2.5 L acetone for one day each, and then with 3 x 2.5 L methanol for another three consecutive days. Both of filtrates were collected separately and evaporated under reduced pressure to dryness. Each of crude extracts, i.e. acetone and methanol was partitioned between petroleum ether (500 ml x 3) and methanol:water (9:1) (500 ml x 3). After evaporating each layer to dryness, the methanol fraction was subsequently partitioned between ethyl acetate (500 ml x 3) and water (500 ml x 3). Each fraction was evaporated to dryness and kept at 0-5 degree Celsius. The extraction procedures are shown in Scheme 2.1. The extraction procedure was carried out twice on a total weight 600 g dried plant material to yield totals of crude fractions AP (7.04 g), AE (7.75 g), AW (2.95 g), MP (1.04 g), ME (3.95 g), and MW (31.77 g). The fractions AW, and MW (water fractions from the original acetone and methanol extract respectively) were partitioned between 1-butanol (500 ml x 3), and water (500 ml x 3). Each layer was evaporated to dryness, and finally gave 4 fractions, i.e. AB (1.73 g), AWW (1.22 g), MB (6.37 g), and MWW (23.39 g). Fractions from these procedures were monitored by TLC, HPLC, and ^{1}H NMR spectroscopy. Subsequently, AE, and ME were further separated by open column chromatography while AB and MB were separated by semi-preparative HPLC. This method was selected for all subsequent extractions of plant material as shown in Scheme 2.2.

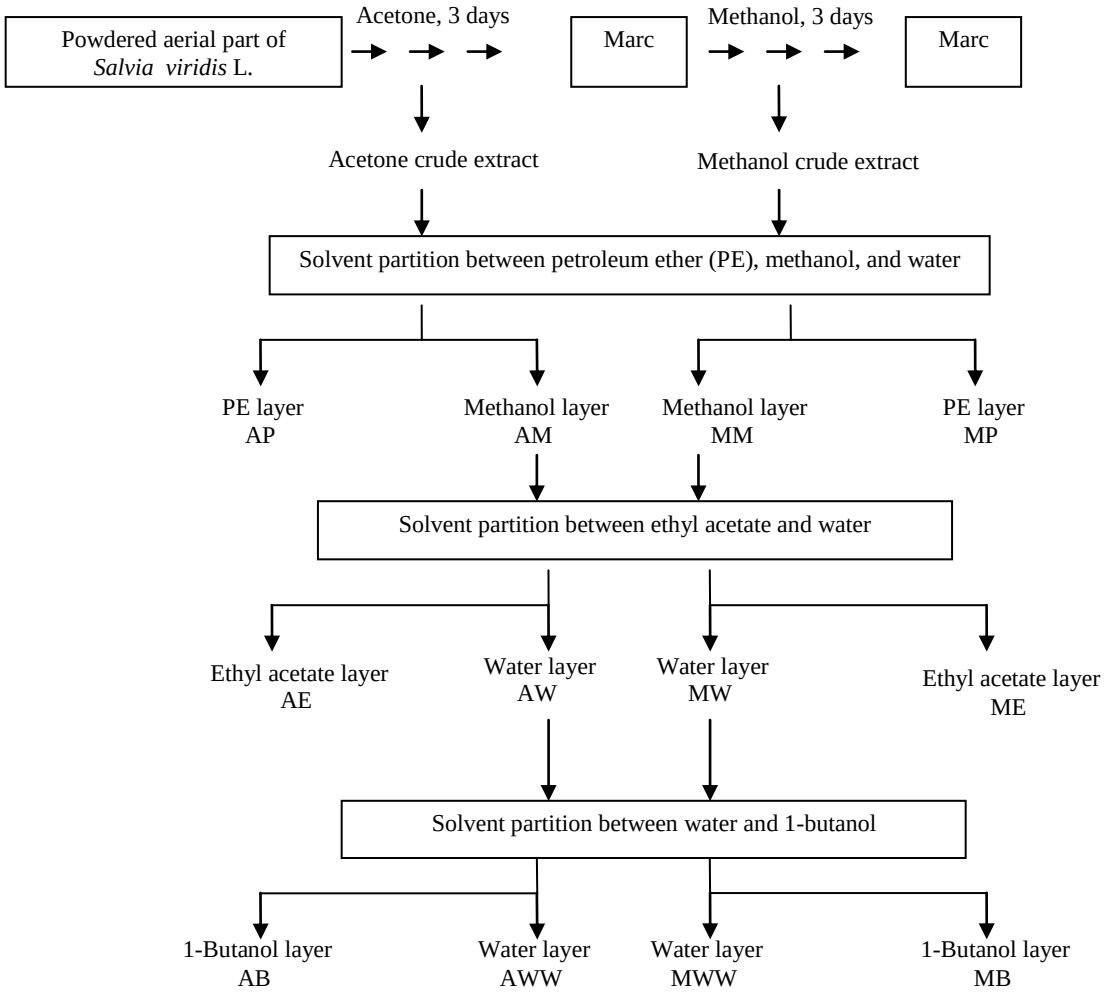

Scheme 2.1 Extraction procedures

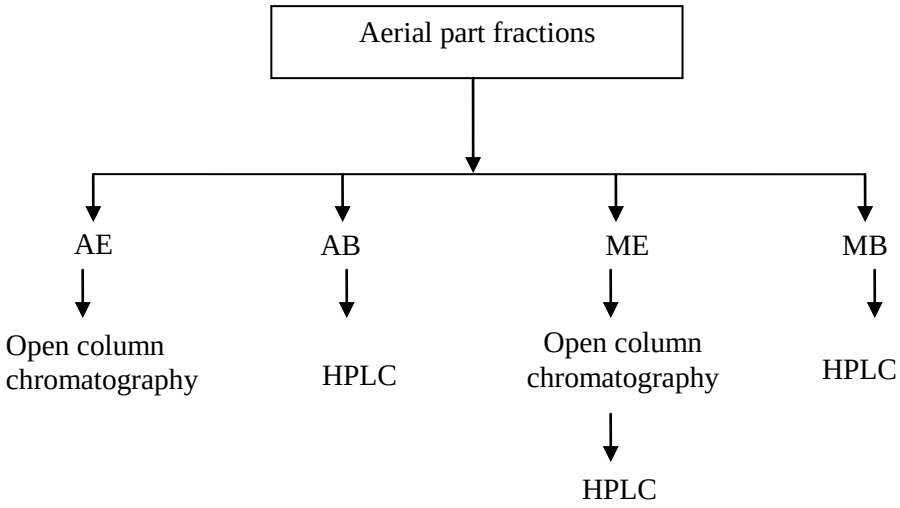

Scheme 2.2 Isolation steps

2.7 Chromatography of aerial part

2.7.1 Reversed-phase HPLC of the AB (Acetone-Butanol), and MB (Methanol-Butanol) fractions

A Phenomenex Luna PFP (250x10 mm) column was employed in separating fractions from AB (1.73 g), and MB (2.50 g) crude fraction. All crude fractions were dissolved in methanol, and then the solution (100 µl) was injected each time through column by using methanol:water (45:55) as mobile phase, flow rate 5 ml/min, and detection wavelength at 330 nm. HPLC chromatograms and TLC pattern of AB, and MB crude fractions were similar. A peak of each retention time represented the same compound in both fractions.

Sub-fractions and peaks were collected separately over the total retention time 45 min, i.e. peaks of retention time 2-7.5 min, 7.5-13.5 min, 14.5 min, 16.7 min, 18.3 min, and 19-45 min.

The sub-fraction from retention time 2-7.5 min was further chromatographed on the same column using 13% acetonitrile in water as mobile phase. Caffeic acid (14 mg), rosmarinic acid (3 mg), 6-caffeoyl-glucose (9 mg) were collected at retention time 6, 6.3 and 8.9 min respectively.

The sub-fraction from retention time 7.5-13.5 min was further purified by the same mobile phase, i.e., 45% methanol in water. Salidroside (4 mg) was isolated as a peak at retention time 8.2 min. The major peak at retention time 9.2 min was identified as verbascoside (or acteoside). The total weight of the MB crude fraction 2 g yielded 104 mg verbascoside (or acteoside). A peak at retention time 11.2 min was identified as a mixture of trans- and cis-verbascoside 15 mg.

Leucosceptocide A (10 mg) was collected from a peak at retention time 15.5 min by the same mobile phase, i.e., 45% methanol in water. The peak at retention time 16.7 min was identified as luteolin-7-*O*-rutinoside (9 mg) and luteolin-7-α-rhamnopyranosyl-(1→6)-β-galactopyranoside (compound 6; 4 mg). The peak at retention time 18.7 min was luteolin-7-*O*-glucoside (14 mg).

The sub-fraction from retention time 19-45 min was further separated by 25% acetonitrile in water on the same column. Peaks at retention time 5.1, 7.9, and 9.5 min were identified as luteolin-7-*O*-galactoside (5 mg), apigenin-7-*O*-glucoside (6 mg), and martynoside (6 mg) respectively.

2.7.2 Open column chromatography of the AE (Acetone-Ethyl acetate) fraction

2.7.2.1 Fractionation of AE crude fraction

An open glass column, diameter 4 cm with sintered disc, was packed by slurry of silica gel 60 (80 g) in solvent of choice. After the silica gel was stably packed, fine sand was carefully poured over silica gel to protect the smooth surface of silica gel. The separation of AE crude extract was carried out twice by different mobile systems. The first one was eluted by a mixture of chloroform and methanol while the other one was eluted by a mixture of toluene and ethyl acetate.

(a) AE crude fraction (1.5 g) was dissolved in chloroform, and loaded on to the silica gel packed column. The fraction was eluted by 1 L of 100% chloroform, and then with increasing polarity by adding methanol from 1-10%, 20%, 30%, 50%, and finally 100% methanol. Fractions (40 ml) were collected separately and monitored by TLC using the mobile phase chloroform:methanol (9:1). The developed plate was visulised by Anisaldehyde-Sulfuric acid Spraying Reagent and fractions with the same Rf value were combined. Fifteen fractions were collected and evaporated to dryness; two gave white powders. The fraction of 2% methanol in chloroform yielded a mixture of ursolic and oleanolic acids (15 mg), while the fractions of 5-6% methanol in chloroform gave β-sitosterol glucoside (10 mg). Trace amount of triterpenoids were observed in the 1% methanol in chloroform fraction.

(b) AE crude fraction (2.5 g) was dissolved in toluene, and then loaded on to the column. The column was eluted by 1 L of 100% toluene and followed by the mixture of toluene and ethyl acetate in order to increase polarity. The step gradients solvent system started from 1 to 10 %, and then 20%, 30%, 40%, 50%, 80% of ethyl acetate in toluene and finally 100% of ethyl acetate. Each solvent system was 1 L. Fractions (40 ml) were collected separately and evaporated to dryness. Thereafter, they were monitored by TLC using mobile phase toluene:ethyl acetate (7:3). The developed TLC plates were sprayed by Anisaldehyde-

Sulfuric acid Spraying Reagent in order to combine fractions with similar Rf values. Fourteen fractions were collected, i.e. AE1 (fractions 1-10), AE2 (fractions 11-45), AE3 (fractions 46-80), AE4 (fractions 85-109), AE5 (fractions 110-140), AE6 (fractions 141-160), AE7 (fractions 161-195), AE8 (fractions 196-220), AE9 (fractions 221-230), AE10 (fractions 231-250), AE11 (fractions 251-265), AE12 (fractions 266-290), AE13 (fractions 291-319), and AE14 (fractions 320-340). They were evaporated to dryness, kept at 0-5ºC, and then further separated by open column chromatography.

2.7.2.2 Isolation of compounds from AE subfractions

AE3 (fractions 46-84; 2-3% ethyl acetate in toluene) was repeatedly chromatographed over silica gel (80 g) eluting with 800 ml each of mobile phases as follows: 100% toluene, 1-5%, 10%, 20%, 30%, 50% of ethyl acetate in toluene and finally 100% ethyl acetate. Forty ml eluent was collected, evaporated to dryness, monitored by TLC using mobile phase toluene:ethyl acetate (7:3). Fractions 48-55 were combined to yield β-sitosterol (10 mg).

AE4 (fractions 85-109; 4-5% ethyl acetate in toluene) was rechromatographed over silica gel (80 g) eluting with 800 ml each of mobile phases as follows: 100% toluene, 1-5%, 10%, 20%, 30%, 50% of ethyl acetate in toluene and finally 100% ethyl acetate. Fifty ml eluent was collected, evaporated to dryness, monitored by TLC using mobile phase toluene:ethyl acetate (7:3). Nine fractions were collected, and one of those, subfractions 41-69 was further separated by column chromatography over silica gel (80 gm), and eluted with a step gradient of cyclohexane and ethyl acetate as follows: 5%, 10%, 15%, 20%, 50% of ethyl acetate in cyclohexane, and finally 100% ethyl acetate. Fractions 21-28 afforded compound 1 (6 mg) while fractions 34-45 were further rechromatographed over silica gel eluting with step gradient between chloroform and ethyl acetate, i.e. 10%, 20% of ethyl acetate in chloroform, and finally 100% ethyl acetate. Finally, this column afforded five fractions of which the fraction 31-35 gave compound 2 (5 mg).

AE6 (fractions 141-160; 7% ethyl acetate in toluene) was repeatedly chromatographed over silica gel (80 g) eluting with 800 ml each of mobile phases as follows: 100% chloroform, 5%, 10%, 15%, 20%, 50% of ethyl acetate in chloroform and finally 100% ethyl acetate. Forty ml eluent was collected, evaporated to dryness, monitored by TLC using

mobile phase chloroform:ethyl acetate (4:1). Fractions 60-65 yielded a compound identified as oleanolic acid (10 mg).

AE7 (fractions 161-195; 8% ethyl acetate in toluene) was repeatedly chromatographed over silica gel (80 g) eluting with 800 ml each of mobile phases as follows: 100% chloroform, 5%, 10%, 15%, 20%, 50% of ethyl acetate in chloroform and finally 100% ethyl acetate. Forty ml eluent was collected, evaporated to dryness, monitored by TLC using mobile phase chloroform:ethyl acetate (4:1). Fractions 104-112 yielded ursolic acid (12 mg). Fractions 120-130 afforded lup-(20)29-ene-2α, 3β-diol (6 mg).

AE11 (fractions 251-265; 30% ethyl acetate in toluene) was repeatedly chromatographed over silica gel (80 g) eluting with 800 ml each of mobile phases as follows: 100% chloroform, 10%, 20%, 50% of ethyl acetate in chloroform and finally 100% ethyl acetate. Forty ml eluent was collected, evaporated to dryness, monitored by TLC using mobile phase chloroform:ethyl acetate (4:1). Fractions 68-73 yielded ursolic acid (10 mg).

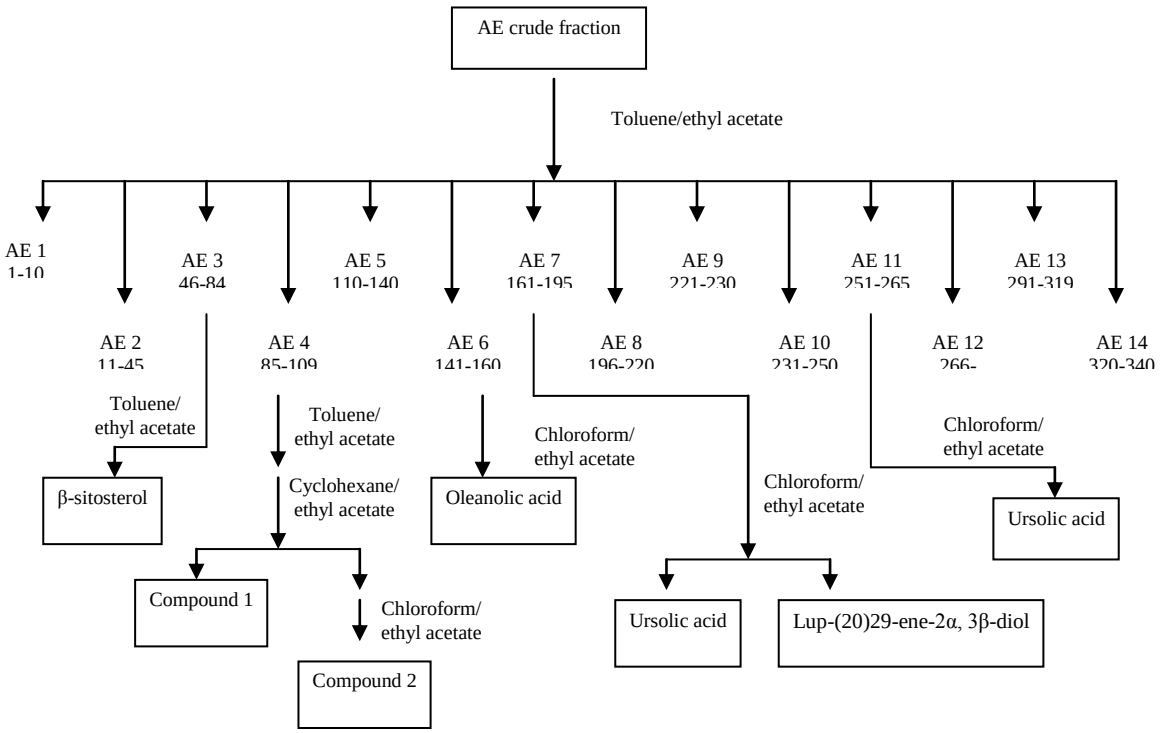

Scheme 2.3 Isolation of compounds from AE subfractions of aerial part by chromatography over silica gel 60

2.7.3. Open column chromatography of the ME (Methanol-Ethyl acetate) fraction

ME crude fraction (1 g) was dissolved in chloroform, and chromatographed over silica gel (60 g) eluting with 100% chloroform, and then the mixture of chloroform:methanol:water as follows: 80:20:2, 75:25:2.5, 70:30:3, 60:40:4, 50:50:5, and finally washed out with 100% methanol. Each solvent system was 600 ml, and 40 ml fractions were collected separately. They were evaporated to dryness, and monitored by TLC using solvent system ethyl acetate:formic acid:methanol:water (50:3:3:6). Developed TLC plates were sprayed by Natural Products Spraying Reagent. Fractions 60-65 (chloroform:methanol:water, 60:40:4) was further separated by reversed-phase HPLC using Phenomenex Luna PFP 250x10 mm, mobile phase 13% acetonitrile in water. A peak at retention time 6.3 min was identified as rosmarinic acid (10 mg) by MS and NMR spectroscopic data

2.8 Extraction procedures of root part

Dried powdered root (300 g) was extracted and partitioned by the same set of solvents as described in aerial part (Scheme 2.1). Eight crude fractions included: RAP (0.65 g), RAE (1 g), RAB (0.055 g), RAW (0.04 g), RMP (0.005 g), RME (0.87 g), RMB (0.63 g), and RMW (4.55 g). They were further separated by either open column chromatography (RAP and RAE) or reversed-phase HPLC (RAB) as described for the aerial parts.

2.9 Chromatography of root part

2.9.1 Acetone-ethyl acetate from root part (RAE)

Acetone-ethyl acetate from root part (RAE; 0.44 g) was chromatographed over 60 g silica gel by open glass column chromatography. The fraction was eluted by 100% toluene 600 ml, and then 600 ml each of the mixture of toluene and ethyl acetate with increasing polarity, i.e. 1-10%, 20%, 30%, 50% of ethyl acetate in toluene and finally 100% ethyl acetate. Fractions (40 ml) were collected separately and monitored by TLC using the mobile phase toluene:ethyl acetate (7:3). Fractions with the same Rf value were combined as shown in Scheme 2.4, and evaporated to dryness. RAE1-RAE17 were kept at 0-5°C.

The first fraction RAE1 (column fractions 1-7; 100% toluene) was further purified by column chromatography eluting by the mixture of cyclohexane and chloroform as follows: 100:0, 90:10, 80:20, 50:50, and 0:100. Fractions from 50% chloroform in cyclohexane gave ferruginol (4 mg).

Fraction RAE4 (column fractions 29-35; 1% ethyl acetate in toluene) was further separated over silica gel eluting with 100% cyclohexane followed by a mixture of cyclohexane and ethyl acetate was used as follows: 95:5, 90:10, 80:20, 50:50, and 0:100. Fractions from 10% ethyl acetate gave two compounds which were further purified by precipitation in methanol: 7α-acetoxy-14-hydroxy-8,13-abietadiene-11,12-dione (8 mg) and 7α,14-dihydroxy-8,13-abietadiene-11,12-dione (5 mg).

Fraction RAE5 (column fractions 36-42; 2% ethyl acetate in toluene) was further purified by precipitation in cyclohexane. The precipitate was an off-white diterpenoid compound; salvinolonyl-12-methyl ether (8 mg).

Fraction RAE6 (column fractions 43-49; 2% ethyl acetate in toluene) was repeatedly chromatograped over silica gel eluting with a mixture of cyclohexane and ethyl acetate as follows: 100:0, 95:5, 90:10, 85:15, 80:20, 50:50, and 0:100. Fractions from 20% ethyl acetate gave 9 mg β-sitosterol.

Fraction RAE7 (column fractions 50-70; 2-4% ethyl acetate in toluene) was further separated by open column chromatography. A mixture of cyclohexane and ethyl acetate was used as mobile phase as follows: 100:0, 95:5, 90:10, 85:15, 80:20, 50:50, and 0:100. Two fractions from 15% ethyl acetate in cyclohexane gave compound 3 (1-oxomicrostegiol; 6 mg), and compound 4 (viroxocane; 5 mg).

Fraction RAE11 (column fractions 124-139; 9% ethyl acetate in toluene) was precipitated in cyclohexane. The white precipitate was further identified as the mixture of oleanolic acid and ursolic acid (5 mg).

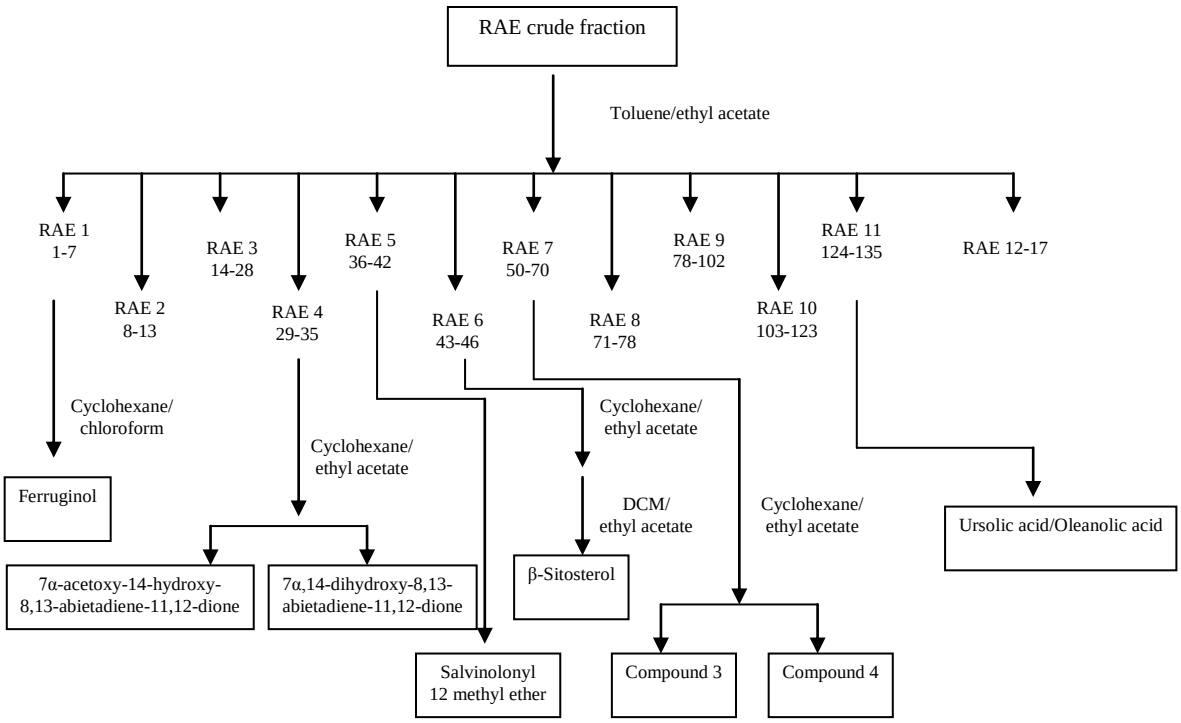

Scheme 2.4 Isolation of compounds from RAE subfractions of root part by chromatography over silica gel 60

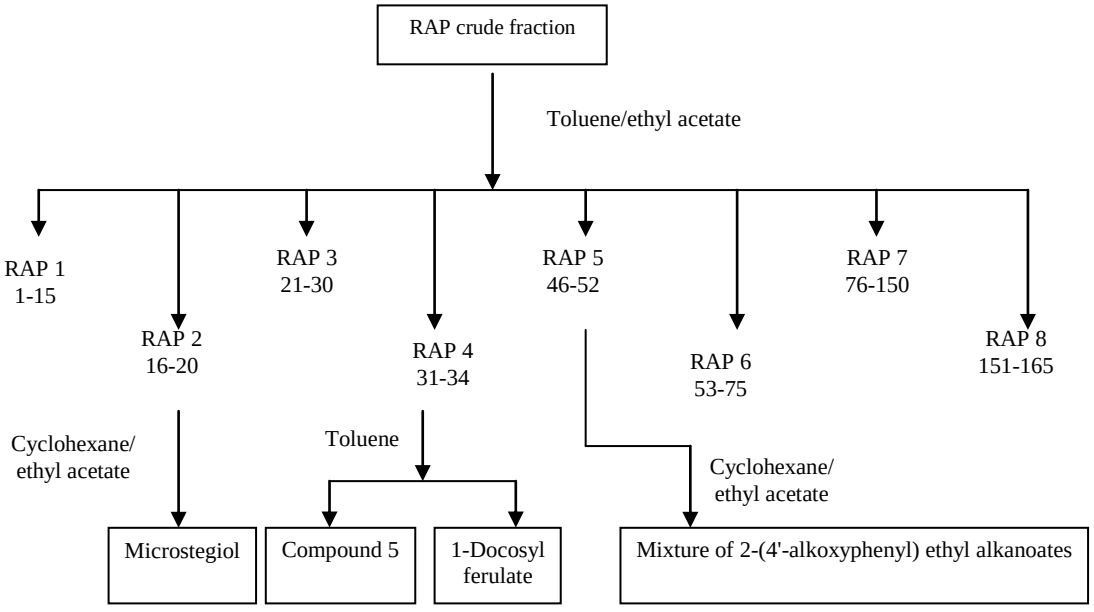

Scheme 2.5 Isolation of compounds from RAP subfractions of root part by chromatography over silica gel 60

2.9.2 Acetone-petroleum ether from root part (RAP)

RAP (0.55 g) was chromatographed over 60 g silica gel 60 through open glass column chromatography. The fraction was first eluted by 100% toluene 600 ml, and then 600 ml each of the mixture of toluene and ethyl acetate with increasing polarity, i.e. 1-10% and finally 100% ethyl acetate. Fractions (40 ml) were collected 40 ml separately and monitored by TLC using mobile phase toluene:ethyl acetate (7:3). Fractions with the same Rf value were combined, and evaporated to dryness. The dried fractions RAP1-RAP11 were kept at 0-5°C.

Fraction RAP2 (column fractions 16-20; 1% ethyl acetate in toluene) was further eluted over silica gel with 2% ethyl acetate in cyclohexane to yield microstegiol (7 mg).

Fraction RAP4 (column fractions 31-34; 2% ethyl acetate in toluene) was repeatedly chromatographed eluting with 100% toluene. Fractions 17-23 were comprised of two compounds. Methanol precipitation gave an off-white powder, 1-docosyl ferulate (5 mg), and a methanol soluble purple diterpenoid compound 5 (viridoquinone; 6 mg).

Fraction RAP5 (column fractions 46-52; 3% ethyl acetate in toluene) was further rechromatographed over silical gel eluting with the mixture of cyclohexane and ethyl acetate. The 10% ethyl acetate in cyclohexane fractions gave a mixture of 2-(4'-alkoxyphenyl) ethyl alkanoates (6 mg).

2.9.3 Methanol-ethyl acetate fraction from root part (RME)

RME (0.77 g) was chromatographed over 60 g silica gel 60 by open glass column chromatography. The fraction was first eluted by 100% chloroform 600 ml, and then 600 ml each of the mixture of chloroform and methanol with increasing polarity, i.e. 1-10%, 20%, 30%, 50% of methanol and finally 100% methanol. Fractions (40 ml) were collected separately and monitored by TLC using mobile phase chloroform:methanol (9:1). Fractions with the same Rf value were combined, evaporated to dryness and kept at 0-5°C.

Fractions 80-103 (5-6% methanol in chloroform) was rechromatographed over silica gel eluting by 100% dichloromethane, and adding methanol from 1-10%, and finally 100% methanol. Fraction of 4% methanol in dichloromethane was further purified by reversed-phase HPLC. The conditions and column were the same as described for the aerial parts. A

peak at retention time 6.7 min was eluted by 40% acetonitrile in water, and identified as 2", 3"-di-*O*-acetyl-martynoside (7 mg) by MS and NMR data.

2.9.4 Methanol-butanol fraction from root part (RMB)

RMB (0.57 g) was chromatographed over 60 g silica gel through open glass column chromatography eluting with 100% chloroform 600 ml, and then 600 ml each of the mixture of chloroform, methanol, and water with increasing polarity, i.e. 90:10:1, 80:20:2, 70:30:3, 60:40:4, 50:50:5, and 100% methanol. Fractions (40 ml) were collected separately and monitored by TLC using mobile phase ethyl acetate:methanol:formic acid:water (50:3:3:6). The developed TLC plate was visualized by UV 365 nm, and fractions with the same Rf value combined, and then evaporated to dryness and kept at 0-5°C.

Fractions of the mixture 60:40:4 was further purified by reversed-phase HPLC. The condition and column were the same as described in aerial part. A peak at retention time 3.7 min was eluted by 20% aqueous acetonitrile, and identified as rosmarinic acid (5 mg)

RMB crude fraction (0.5 g) was dissolved in methanol, and analysed by reversed-phase HPLC. The condition and column were the same as described for the aerial parts. Verbascoside was detected at retention time 9.2 min eluting with 45% methanol in water. HR-ESI-MS of this crude fraction showed two main constituents which were rosmarinic acid and verbascoside.

2.10 Spectroscopic data of isolated compounds from aerial part (see appendices for NMR spectra and section 3.6 for discussion of these data)

2.10.1. Caffeic acid

Caffeic acid ($C_9H_8O_4$; Figure 3.22) was obtained as light brown yellow amorphous powder. HR-ESI-MS (negative ion mode) showed a peak at *m/z* 179.0353; $C_9H_7O_4$ requires 179.0338. ^{1}H NMR data (500 MHz, CD_3OD): δ 7.51 (1H, d, *J* = 16 Hz, H-7), 7.03 (1H, d, *J* = 2 Hz, H-2), 6.93 (1H, dd, *J* = 8, 2 Hz, H-6), 6.77 (1H, d, *J* = 8 Hz, H-5), 6.20 (1H, d, *J* = 16 Hz, H-8). ^{13}C NMR data (125 MHz, CD_3OD): δ 171.1 (C-9), 149.4 (C-4), 146.9 (C-3), 146.8 (C-7), 127.8 (C-1), 122.8 (C-6), 116.5 (C-5), 115.7 (C-8), 115.1 (C-2).

2.10.2 Trans-verbascoside

Trans-verbascoside (acteoside; $C_{29}H_{36}O_{15}$; Figure 3.25) was obtained as yellow powder. HR-ESI-MS (positive ion mode) showed a peak at *m/z* 647.1921; $C_{29}H_{36}O_{15}Na$ requires 647.1943 while negative ion mode found *m/z* 623.1971; $C_{29}H_{35}O_{15}$ requires 623.1965. ^{1}H NMR data (400 MHz, CD_3OD): δ 7.60 (1H, d, *J* = 16 Hz, H-7'), 7.05 (1H, d, *J* = 2 Hz, H-2'), 6.95 (1H, dd, *J* = 8.2, 2 Hz, H-6'), 6.78 (1H, d, *J* = 8.2 Hz, H-5'), 6.69 (1H, d, *J* = 1.6 Hz, H-2), 6.68 (1H, d, *J* = 8 Hz, H-5), 6.56 (1H, dd, *J* = 8, 1.6 Hz, H-6), 6.29 (1H, d, *J* = 16 Hz, H-8'), 5.18 (1H, s, H-1r), 4.91 (1H, t, *J* = 9 Hz, H-4g), 4.38 (1H, d, *J* = 7.8 Hz, H-1g), 4.05 (1H, m, H-8), 3.91 (1H, d, *J* = 1.6 Hz, H-2r), 3.81 (1H, t, *J* = 9 Hz, H-3g), 3.70 (1H, m, H-8), 3.64 (1H, m, H-6g), 3.58 (1H, m, H-3r), 3.56 (1H, m, H-5r), 3.53 (1H, m, H-5g), 3.49 (1H, m, H-6g), 3.38 (1H, t, *J* = 9 Hz, H-2g), 3.29 (1H, t, *J* = 9.8 Hz, H-4r), 2.78 (2H, m, H-7), 1.09 (3H, d, *J* = 6.2 Hz, H-6r). ^{13}C NMR data (100 MHz, CD_3OD): δ 168.3 (C-9'), 149.7 (C-4'), 148.0 (C-7'), 146.8 (C-3'), 146.1 (C-3), 144.6 (C-4), 131.4 (C-1), 127.6 (C-1'), 123.2 (C-6'), 121.2 (C-6), 117.1 (C-2), 116.5 (C-5'), 116.3 (C-5), 115.2 (C-2'), 114.7 (C-8'), 104.2 (C-1g), 103.0 (C-1r), 81.6 (C-3g), 76.2 (C-2g), 76.0 (C-5g), 73.8 (C-4r), 72.3 (C-2r), 72.2 (C-8), 72.0 (C-3r), 70.5 (C-4g), 70.4 (C-5r), 60.9 (C-6g), 36.5 (C-7), 18.4 (C-6r).

2.10.3 Cis-verbascoside

Cis-verbascoside (acteoside; $C_{29}H_{36}O_{15}$; Figure 3.35) was obtained as yellow powder. HR-ESI-MS (positive ion mode) showed a peak at *m/z* 647.1926; $C_{29}H_{36}O_{15}Na$ requires 647.1943 while negative ion mode found *m/z* 623.1981; $C_{29}H_{35}O_{15}$ requires 623.1965. ^{1}H NMR data (400 MHz, CD_3OD): δ 7.52 (1H, d, *J* = 1.5 Hz, H-2'), 7.09 (1H, dd, *J* = 8.2, 2 Hz, H-6'), 6.86 (1H, d, *J* = 12.8 Hz, H-7'), 6.77 (1H, d, *J* = 8.2 Hz, H-5'), 6.73 (1H, d, *J* = 8.2 Hz, H-5), 6.69 (1H, d, *J* = 2 Hz, H-2), 6.55 (1H, dd, *J* = 8.2, 2 Hz, H-6), 5.75 (1H, d, *J* = 12.8 Hz, H-8'), 5.16 (1H, s, H-1r), 4.92 (1H, overlapped, H-4g), 4.34 (1H, d, *J* = 7.8 Hz, H-1g), 4.02 (1H, m, H-8), 3.92 (1H, br s, H-2r), 3.76 (1H, t, *J* = 9.4 Hz, H-3g), 3.70 (1H, m, H-8), 3.64 (1H, m, H-6g), 3.58 (1H, m, H-3r), 3.56 (1H, m, H-5r), 3.53 (1H, m, H-5g), 3.49 (1H, m, H-6g), 3.35 (1H, t, *J* = 8.2 Hz, H-2g), 3.32 (1H, overlapped, H-4r), 2.77 (2H, m, H-7), 1.16 (3H, d, *J* = 6.2 Hz, H-6r). ^{13}C NMR data (100 MHz, CD_3OD): δ 168.3 (C-9'), 149.4 (C-4'), 148.6 (C-7'), 146.8 (C-3'), 146.1 (C-3), 144.6 (C-4), 131.4 (C-1), 128.0 (C-1'), 125.9 (C-6'), 121.2 (C-6), 119.0 (C-2'), 116.5 (C-5), 116.3 (C-2), 115.2 (C-5'), 114.7 (C-8'), 104.1 (C-1g), 103.1 (C-1r), 81.9 (C-3g), 76.1 (C-2g), 76.0 (C-5g), 73.9 (C-4r), 73.9 (C-8), 72.3 (C-2r), 72.0 (C-3r), 70.6 (C-4g), 70.4 (C-5r), 62.3 (C-6g), 36.6 (C-7), 18.2 (C-6r).

2.10.4 Leucosceptoside A

Leucosceptoside A ($C_{30}H_{38}O_{15}$; Figure 3.39) was obtained as a brown-yellow amorphous powder. HR-ESI-MS (positive ion mode) showed a peak at *m/z* 661.2124; $C_{30}H_{38}O_{15}Na$ requires 661.2103 while the negative mode found *m/z* 637.2161; $C_{30}H_{37}O_{15}$ requires 637.2138. ^{1}H NMR data (500 MHz, CD_3OD): δ 7.64 (1H, d, *J* = 16 Hz, H-7'), 7.20 (1H, d, *J* = 2 Hz, H-2'), 7.07 (1H, dd, *J* = 8, 2 Hz, H-6'), 6.80 (1H, d, *J* = 8 Hz, H-5'), 6.69 (1H, d, *J* = 2 Hz, H-2), 6.66 (1H, d, *J* = 8 Hz, H-5), 6.56 (1H, dd, *J* = 8, 2.5 Hz, H-6), 6.35 (1H, d, *J* = 15.5 Hz, H-8'), 5.20 (1H, br s, *J* = 1.5 Hz, H-1r), 4.91 (1H, m, H-4g), 4.37 (1H, d, *J* = 8 Hz, H-1g), 4.05 (1H, m, H-8), 3.91 (1H, dd, *J* = 3.5, 2 Hz, H-2r), 3.89 (3H, s, H-3'-OCH_3), 3.82 (1H, t, *J* = 9 Hz, H-3g), 3.75 (1H, m, H-8), 3.64 (1H, m, H-6g), 3.59 (1H, m, H-5r), 3.56 (1H, m, H-3r), 3.54 (2H, m, H-5g and H-6g), 3.40 (1H, t, *J* = 9 Hz, H-2g), 3.30 (1H, m, H-4r), 2.78 (2H, m, H-7), 1.09 (3H, d, *J* = 6 Hz, H-6r). ^{13}C NMR data (125 MHz, CD_3OD): δ 168.2 (C-9'), 150.9 (C-4'), 149.5 (C-3'), 147.9 (C-7'), 146.2 (C-3), 144.5 (C-4), 131.5 (C-1), 127.7 (C-1'), 124.4 (C-6'), 121.3 (C-6), 117.1 (C-2), 116.5 (C-5'), 116.3 (C-5), 115.1 (C-8'), 111.8 (C-2'), 104.2 (C-1g), 103.0 (C-1r), 81.5 (C-3g), 76.2 (C-2g), 76.1 (C-5g), 73.8 (C-4r), 72.4 (C-2r), 72.3 (C-8), 72.1 (C-3r), 70.7 (C-4g), 70.4 (C-5r), 62.4 (C-6g), 56.5 (C-3'-OCH_3), 36.6 (C-7), 18.4 (C-6r).

2.10.5 Martynoside

Martynoside ($C_{31}H_{40}O_{15}$; Figure 3.42) was obtained as a brown-yellow amorphous powder. HR-ESI-MS (positive ion mode) showed a peak at *m/z* 675.2245; $C_{31}H_{40}O_{15}Na$ requires 675.2259 while the negative mode found *m/z* 651.2314; $C_{31}H_{39}O_{15}$ requires 651.2294. ^{1}H NMR data (500 MHz, CD_3OD): δ 7.64 (1H, d, *J* = 16 Hz, H-7'), 7.19 (1H, d, *J* = 2 Hz, H-2'), 7.07 (1H, dd, *J* = 8, 2 Hz, H-6'), 6.83 (1H, d, *J* = 7.5 Hz, H-5), 6.80 (1H, d, *J* = 8 Hz, H-5'), 6.74 (1H, d, *J* = 2 Hz, H-2), 6.68 (1H, dd, *J* = 8, 2.5 Hz, H-6), 6.35 (1H, d, *J* = 16 Hz, H-8'), 5.20 (1H, br s, *J* = 2 Hz, H-1r), 4.88 (1H, m, H-4g), 4.37 (1H, d, *J* = 8 Hz, H-1g), 4.08 (1H, m, H-8), 3.92 (1H, dd, *J* = 3, 1.5 Hz, H-2r), 3.89 (3H, s, H-3'-OCH_3), 3.84 (1H, m, H-3g), 3.81 (3H, s, H-4-OCH_3), 3.75 (1H, m, H-8), 3.64 (1H, m, H-6g), 3.59 (1H, m, H-5r), 3.56 (1H, m, H-3r), 3.53 (2H, m, H-5g and H-6g), 3.40 (1H, t, *J* = 9 Hz, H-2g), 3.29 (1H, m, H-4r), 2.82 (2H, m, H-7), 1.10 (3H, d, *J* = 6 Hz, H-6r). ^{13}C NMR data (125 MHz, CD_3OD): δ 168.2 (C-9'), 151.0 (C-4'), 149.4 (C-3'), 147.9 (C-7'), 147.6 (C-4), 147.4 (C-3), 132.9 (C-1), 127.6 (C-1'), 124.4 (C-6'), 121.1 (C-6), 117.1 (C-2), 116.5 (C-5'), 115.1 (C-8'), 112.9 (C-5), 111.8 (C-2'), 104.2 (C-1g), 103.0 (C-1r), 81.5 (C-3g), 76.2 (C-2g), 76.1 (C-5g), 73.8 (C-4r),

72.4 (C-2r), 72.1 (C-3r), 72.1 (C-8), 70.6 (C-5r), 70.4 (C-4g), 62.4 (C-6g), 56.5 (C-4-OCH_3), 56.4 (C-3'-OCH_3), 36.6 (C-7), 18.4 (C-6r).

2.10.6 Rosmarinic acid

Rosmarinic acid ($C_{18}H_{16}O_8$; Figure 3.45) was obtained as light brown yellow amorphous powder. HR-ESI-MS (negative ion mode) showed *m/z* 359.0784; $C_{18}H_{15}O_8$ requires 359.0767. ^{1}H NMR data (500 MHz, CD_3OD): δ 7.48 (1H, d, *J* = 16 Hz, H-7), 7.02 (1H, d, *J* = 2 Hz, H-2), 6.91 (1H, dd, *J* = 8, 2 Hz, H-6), 6.76 (1H, d, *J* = 2 Hz, H-2'), 6.75 (1H, d, *J* = 8 Hz, H-5), 6.65 (1H, d, *J* = 8 Hz, H-5'), 6.63 (1H, dd, *J* = 8, 2 Hz, H-6'), 6.25 (1H, d, *J* = 15.5 Hz, H-8), 5.07 (1H, dd, *J* = 10, 3 Hz, H-8'), 3.08 (1H, dd, *J* = 14, 3 Hz, H-7'), 2.92 (1H, dd, *J* = 14, 10 Hz, H-7'). ^{13}C NMR data (125 MHz, CD_3OD): δ 177.5 (C-9'), 169.1 (C-9), 149.3 (C-4), 146.7 (C-3), 146.5 (C-7), 146.0 (C-3'), 144.8 (C-4'), 131.3 (C-1'), 128.0 (C-1), 122.9 (C-6), 121.7 (C-6'), 117.5 (C-2'), 116.4 (C-5), 116.2 (C-5'), 115.8 (C-8), 115.1 (C-2), 77.8 (C-8'), 38.9 (C-7').

2.10.7 6-*O*-Caffeoyl-glucose

6-*O*-Caffeoyl-glucose ($C_{15}H_{18}O_9$; Figure 3.47) was obtained as light brown yellow amorphous powder. HR-ESI-MS (negative ion mode) showed *m/z* 341.0882; $C_{15}H_{17}O_9$ requires 341.0873. ^{1}H NMR data (500 MHz, CD_3OD): δ 7.55 (1H, d, *J* = 16 Hz, H-7), 7.04 (1H, d, *J* = 2 Hz, H-2), 6.94 (1H, d, *J* = 8, 2 Hz, H-6), 6.77 (1H, d, *J* = 8.5 Hz, H-5), 6.25 (1H, d, *J* = 16 Hz, H-8), 5.10 (1H, d, *J* = 4 Hz, H-1g-α), 4.50 (1H, d, *J* = 7.5 Hz, H-1g-β), 4.43 (1H, m, H-6g), 4.30 (1H, m, H-6g), 3.65 (1H, m, H-3g), 3.55 (1H, m, H-5g), 3.38 (1H, m, H-4g), 3.34 (1H, m, H-2g). ^{13}C NMR data (125 MHz, CD_3OD): δ 169.2 (C-9), 149.6 (C-4), 147.1 (C-7), 146.8 (C-3), 127.7 (C-1), 123.0 (C-6), 116.5 (C-5), 115.1 (C-2), 114.9 (C-8), 98.3 (C-1g-β), 94.0 (C-1g-α), 75.5 (C-5g), 74.8 (C-3g), 73.8 (C-4g), 71.8 (C-2g), 64.9 (C-6g).

2.10.8 Luteolin-7-*O*-β-glucopyranoside

Luteolin-7-*O*-β-glucopyranoside ($C_{21}H_{20}O_{11}$; Figure 3.49) was obtained as a yellow amorphous powder. HR-ESI-MS (negative ion mode) showed a peak at *m/z* 447.0955; $C_{21}H_{19}O_{11}$ requires 447.0927. ^{1}H NMR data (500 MHz, DMSO-d6): δ 7.47 (1H, dd, *J* = 8.5, 2, H-6'), 7.41 (1H, d, *J* = 2, H-2'), 6.89 (1H, d, *J* = 8, H-5'), 6.78 (1H, d, *J* = 2, H-8), 6.74 (1H, s, H-3), 6.44 (1H, d, *J* = 2, H-6), 5.06 (1H, d, *J* = 7.5, H-1g), 3.70 (1H, m, H-6g), 3.49 (1H, m, H-6g), 3.46 (1H, m, H-5g), 3.31 (1H, m, H-3g), 3.28 (1H, m, H-2g), 3.18 (1H, m, H-4g).

^{13}C NMR data (125 MHz, DMSO-d6): δ 181.9 (C-4), 164.5 (C-2), 163.0 (C-7), 161.1 (C-5), 157.0 (C-9), 150.0 (C-4'), 145.8 (C-3'), 121.3 (C-1'), 119.2 (C-6'), 116.0 (C-5'), 113.6 (C-2'), 105.3 (C-10), 103.1 (C-3), 99.9 (C-1g), 99.5 (C-6), 94.7 (C-8), 77.2 (C-5g), 76.4 (C-3g), 73.1 (C-2g), 69.6 (C-4g), 60.6 (C-6g).

2.10.9 Luteolin-7-*O* –β-galactopyranoside

Luteolin-7-*O*–β-galactopyranoside ($C_{21}H_{20}O_{11}$; Figure 3.52) was obtained as a yellow amorphous powder. HR-ESI-MS (negative ion mode) showed a peak at *m/z* 447.0934; $C_{21}H_{19}O_{11}$ 447.0927. ^{1}H NMR data (500 MHz, CD_3OD): δ 7.43 (1H, dd, *J* = 8.5, 2 Hz, H-5'), 7.40 (1H, d, *J* = 2 Hz, H-2'), 6.89 (1H, d, *J* = 8.5 Hz, H-6'), 6.79 (1H, d, *J* = 2 Hz, H-8), 6.60 (1H, s, H-3), 6.50 (1H, d, *J* = 2 Hz, H-6), 5.06 (1H, d, *J* = 7 Hz, H-1gal), 3.92 (1H, br d, *J* = 12 Hz, H-6gal), 3.71 (1H, dd, *J* = 12.5, 6 Hz, H-6gal), 3.54 (1H, m, H-5gal), 3.49 (2H, m, H-2gal and H-4gal), 3.40 (1H, d, *J* = 8.5 Hz, H-3gal). ^{13}C NMR data (125 MHz, CD_3OD): δ 184.0 (C-4), 166.9 (C-2), 164.8 (C-7), 162.9 (C-5), 159.0 (C-9), 151.9 (C-4'), 147.1 (C-3'), 123.4 (C-1'), 119.2 (C-5'), 116.8 (C-6'), 114.2 (C-2'), 107.1 (C-10), 104.1 (C-3), 101.7 (C-1gal), 101.1 (C-6), 96.0 (C-8), 78.4 (C-5gal), 77.9 (C-4gal), 74.7 (C-2gal), 71.3 (C-3gal), 62.4 (C-6gal).

2.10.10 Luteolin-7-*O*-rutinoside

Luteolin-7-*O*-rutinoside ($C_{27}H_{30}O_{15}$; Figure 3.55) was obtained as a yellow amorphous powder. HR-ESI-MS (negative ion mode) showed a peak at *m/z* 593.1554; $C_{27}H_{29}O_{15}$ requires 593.1506. ^{1}H NMR data (500 MHz, DMSO-d6): δ 7.44 (1H, dd, *J* = 8, 2 Hz, H-6'), 7.41 (1H, br s, H-2'), 6.90 (1H, d, *J* = 8.5 Hz, H-5'), 6.74 (2H, m, H-3 and H-8), 6.45 (1H, d, *J* = 2 Hz, H-6), 5.06 (1H, d, *J* = 7.5 Hz, H-1g), 4.54 (1H, br s, H-1r), 3.83 (1H, br d, *J* = 10.5 Hz, H-6g), 3.65 (1H, d, *J* = 2 Hz, H-2r), 3.59 (1H, t, *J* = 7.5 Hz, H-5g), 3.45 (1H, m, H-3r), 3.43 (1H, m, H-6g), 3.41 (1H, m, H-5r), 3.30 (1H, m, H-3g), 3.26 (1H, m, H-2g), 3.15 (1H, m, H-4g), 3.14 (1H, m, H-4r), 1.06 (3H, d, *J* = 6 Hz, H-6r). ^{13}C NMR data (125 MHz, DMSO-d6): δ 181.9 (C-4), 164.6 (C-2), 162.9 (C-7), 161.2 (C-5), 156.9 (C-9), 150.1 (C-4'), 145.8 (C-3'), 121.3 (C-1'), 119.2 (C-6'), 116.1 (C-5'), 113.5 (C-2'), 105.4 (C-10), 103.1 (C-3), 100.5 (C-1r), 99.9 (C-1g), 99.5 (C-6), 94.8 (C-8), 76.3 (C-3g), 75.6 (C-5g), 73.1 (C-2g), 72.1 (C-4r), 70.7 (C-3r), 70.3 (C-2r), 69.6 (C-4g), 68.3 (C-5r), 66.1 (C-6g), 17.8 (C-6r).

2.10.11 Luteolin-7-*O*-α-rhamnopyranosyl-(1→6)-β-galactopyranoside (compound 6)

Luteolin-7-*O*-α--rhamnopyranosyl-(1→6)-β-galactopyranoside ($C_{27}H_{30}O_{15}$; Figure 3.57) was obtained as a pale yellow amorphous powder. HR-ESI-MS (negative ion mode) showed a peak at *m/z* 593.1563; $C_{27}H_{29}O_{15}$ requires 593.1506. ^{1}H NMR data (500 MHz, CD_3OD): δ 7.42 (1H, m, H-6'), 7.41 (1H, br s, H-2'), 6.92 (1H, d, *J* = 9 Hz, H-5'), 6.75 (1H, d, *J* = 2 Hz, H-8), 6.61 (1H, s, H-3), 6.52 (1H, d, *J* = 2 Hz, H-6), 5.03 (1H, d, *J* = 7 Hz, H-1gal), 4.72 (1H, br s, H-1r), 4.05 (1H, br d, *J* = 9.5 Hz, H-6gal), 3.91 (1H, dd, *J* = 3.5, 1.5 Hz, H-2r), 3.72 (1H, dd, *J* = 9.5, 3.5 Hz, H-3r), 3.65 (1H, m, H-4gal), 3.64 (1H, m, H-5r), 3.63 (1H, m, H-6gal), 3.50 (1H, m, H-5gal), 3.49 (1H, m, H-2gal), 3.40 (1H, d, *J* = 9 Hz, H-3gal), 3.34 (1H, t, *J* = 10 Hz, H-4r), 1.18 (3H, d, *J* = 6.5 Hz, H-6r). ^{13}C NMR data (125 MHz, CD_3OD): δ 184.0 (C-4), 167.0 (C-2), 164.7 (C-7), 163.0 (C-5), 158.9 (C-9), 151.2 (C-4'), 147.0 (C-3'), 123.5 (C-1'), 120.6 (C-6'), 116.9 (C-5'), 114.3 (C-2'), 107.1 (C-10), 104.3 (C-3), 102.1 (C-1r), 101.6 (C-1gal), 101.1 (C-6), 96.1 (C-8), 77.8 (C-5gal), 77.2 (C-4gal), 74.7 (C-2gal), 74.1 (C-4r), 72.4 (C-3r), 72.1 (C-2r), 71.3 (C-3gal), 69.8 (C-5r), 67.5 (C-6gal), 17.9 (C-6r).

2.10.12 Apigenin-7-*O*-β-glucopyranoside

Apigenin-7-*O*-β-glucopyranoside ($C_{21}H_{20}O_{10}$; Figure 3.61) was obtained as a yellow amorphous powder. HR-ESI-MS (negative ion mode) showed a peak at *m/z* 431.0984; $C_{21}H_{19}O_{10}$ requires 431.0978. ^{1}H NMR data (500 MHz, CD_3OD): δ 7.88 (2H, d, *J* = 9 Hz, H-2' and H-6'), 6.92 (2H, d, *J* = 9 Hz, H-3' and H-5'), 6.82 (1H, d, *J* = 2 Hz, H-8), 6.66 (1H, s, H-3), 6.50 (1H, d, *J* = 2 Hz, H-6), 5.06 (1H, d, *J* = 9 Hz, H-1g), 3.92 (1H, m, H-6g), 3.70 (1H, m, H-6g), 3.50 (1H, m, H-5g), 3.45 (1H, m, H-3g), 3.44 (1H, m, H-2g), 3.40 (1H, m, H-4g). ^{13}C NMR data (125 MHz, CD_3OD): δ 184.1 (C-4), 166.8 (C-2), 164.9 (C-7), 162.9 (C-4'), 162.8 (C-9), 159.0 (C-5), 129.6 (C-2' and C-6'), 123.1 (C-1'), 117.2 (C-3' and C-5'), 107.1 (C-10), 104.1 (C-3), 101.7 (C-1g), 101.2 (C-6), 96.1 (C-8), 78.4 (C-5g), 77.9 (C-3g), 74.8 (C-2g), 71.3 (C-4g), 62.5 (C-6g).

2.10.13 Ursolic acid

Ursolic acid ($C_{30}H_{48}O_3$; Figure 3.63) was obtained as a white powder. HR-ESI-MS (positive ion mode) showed peak at m/z 479.3509; $C_{30}H_{48}NaO_3$ requires 479.3496. ^{1}H NMR data (500 MHz, a mixture of CD_3OD and $CDCl_3$): δ 5.21 (1H, t, *J* = 3.5 Hz, H-12), 3.14 (1H, dd, *J* = 11, 5 Hz, H-3-α), 2.16 (1H, d, *J* = 11 Hz, H-18), 1.98 (1H, m, H-16), 1.89 (1H, m, H-11), 1.88 (1H, m, H-15), 1.67 (2H, m, H-22), 1.63 (2H, m, H-1 and H-19), 1.62 (1H, m, H-16), 1.54 (2H, m, H-2), 1.53 (2H, m, H-9 and H-6), 1.52 (1H, m, H-7), 1.51 (2H, m, H-21),

1.37 (1H, m, H-6-α), 1.36 (1H, m, H-20), 1.35 (1H, m, H-7), 1.09 (3H, s, H-27-α), 1.09 (1H, overlapped, H-11), 1.05 (1H, m, H-15), 0.93 (3H, s, H-23-α), 0.93 (1H, overlapped, H-1), 0.92 (3H, d, *J* = 6.5 Hz, H-30-α), 0.91 (3H, s, H-25-β), 0.84 (3H, d, *J* = 6.5 Hz, H-29-β), 0.82 (3H, s, H-26-β), 0.76 (3H, s, H-24-β), 0.73 (1H, d, *J* = 11.5 Hz, H-5-α). ^{13}C NMR data (125 MHz, a mixture of CD_3OD and $CDCl_3$): δ 181.3 (C-28), 139.1 (C-13), 126.4 (C-12), 79.3 (C-3), 56.2 (C-5), 53.8 (C-18), 48.5 (C-17), 48.2 (C-9), 42.8 (C-14), 40.3 (C-8), 39.9 (C-20), 39.8 (C-19), 39.6 (C-1), 39.4 (C-4), 37.7 (C-22), 37.6 (C-10), 33.9 (C-7), 31.4 (C-21), 28.8 (C-15), 28.6 (C-23), 27.4 (C-2), 24.9 (C-16), 24.0 (C-11), 24.0 (C-27), 21.5 (C-30), 19.1 (C-6), 17.5 (C-26), 17.1 (C-29), 16.1 (C-24), 15.9 (C-25).

2.10.14 Oleanolic acid

Oleanolic acid ($C_{30}H_{48}O_3$; Figure 3.70) was obtained as a white powder. Judging from the NMR spectra, this material was about 70% pure, with ursolic acid as the major impurity. HR-ESI-MS (positive ion mode) showed peak at m/z 479.3493; $C_{30}H_{48}NaO_3$ requires 479.3496. ^{1}H NMR data (500 MHz, a mixture of CD_3OD and $CDCl_3$): δ 5.23 (1H, t, *J* = 3 Hz, H-12), 3.14 (1H, dd, *J* = 10.5, 5 Hz, H-3), 2.80 (1H, dd, *J* = 13.5, 4 Hz, H-18-β), 1.96 (1H, m, H-16), 1.84 (1H, m, H-11), 1.71 (2H, m, H-15 and H-22), 1.63 (1H, m, H-19), 1.60 (1H, m, H-1), 1.58 (1H, m, H-16), 1.56 (2H, m, H-2), 1.54 (1H, m, H-9), 1.53 (1H, m, H-6), 1.52 (1H, m, H-22), 1.46 (1H, m, H-7), 1.37 (1H, m, H-6), 1.33 (1H, m, H-21), 1.29 (1H, m, H-7), 1.18 (1H, m, H-21), 1.11 (3H, s, H-27-α), 1.10 (1H, m, H-19), 1.07 (1H, m, H-11), 1.04 (1H, m, H-15), 0.94 (3H, s, H-23-α), 0.94 (1H, m, H-1), 0.90 (3H, s, H-30-β), 0.89 (3H, s, H-25-β), 0.87 (3H, s, H-29-α), 0.77 (3H, s, H-26-β), 0.74 (3H, s, H-24-β), 0.70 (1H, d, *J* =10 Hz, H-5-α). ^{13}C NMR data (125 MHz, a mixture of CD_3OD and $CDCl_3$): δ 181.4 (C-28), 144.5 (C-13), 123.0 (C-12), 79.2 (C-3), 56.0 (C-5), 49.0 (C-9), 47.0 (C-17), 46.6 (C-19), 42.3 (C-14), 41.9 (C-18), 39.9 (C-8), 39.3 (C-1), 39.2 (C-4), 37.6 (C-10), 34.4 (C-21), 33.7 (C-7), 33.4 (C-29), 33.2 (C-22), 31.2 (C-20), 28.4 (C-23), 28.3 (C-15), 27.2 (C-2), 26.3 (C-27), 24.0 (C-11), 23.9 (C-30), 23.6 (C-16), 18.9 (C-6), 17.3 (C-26), 16.0 (C-24), 15.7 (C-25).

2.10.15 Lup-(20)29-ene-2α, 3β-diol

Lup-(20)29-ene-2α, 3β-diol ($C_{30}H_{50}O_2$; Figure 3.73) was obtained as a white powder. HR-ESI-MS (positive ion mode) showed a peak at m/z 465.3690; $C_{30}H_{50}O_2Na$ requires 465.3703. ^{1}H NMR data (500 MHz, $CDCl_3$): δ 4.69 (1H, d, *J* = 2 Hz, H-29), 4.57 (1H, d, *J* = 2 Hz, H-29), 3.67 (1H, ddd, *J* = 10, 9.5, 4.5 Hz, H-2-β), 2.97 (1H, d, *J* = 9.5 Hz, H-3-α), 2.36 (1H, ddd, *J* = 11, 11, 6 Hz, H-19), 2.03 (1H, dd, *J* = 12, 4 Hz, H-1-β), 1.92 (1H, m, H-21),

1.74 (1H, m, H-15), 1.67 (3H, s, H-30), 1.67 (1H, overlapped, H-12), 1.65 (1H, m, H-13), 1.52 (1H, m, H-6), 1.47 (1H, m, H-16), 1.45 (1H, m, H-11), 1.40 (1H, m, H-6), 1.39 (2H, m, H-7), 1.38 (2H, m, H-16 and H-22), 1.35 (1H, m, H-18), 1.32 (2H, m, H-9 and H-21), 1.26 (1H, m, H-11), 1.20 (1H, m, H-22), 1.08 (1H, m, H-12), 1.05 (1H, m, H-15), 1.02 (3H, s, H-26-β), 1.01 (3H, s, H-23-α), 0.94 (3H, s, H-27-α), 0.90 (3H, s, H-25-β), 0.83 (1H, dd, *J* = 12, 7 Hz, H-1-α), 0.80 (3H, s, H-24-β), 0.79 (1H, overlapped, H-5), 0.78 (3H, s, H-28-β). ^{13}C NMR data (125 MHz, $CDCl_3$): δ 150.9 (C-20), 109.4 (C-29), 83.9 (C-3), 69.3 (C-2), 55.4 (C-5), 50.4 (C-9), 48.3 (C-18), 48.0 (C-19), 46.7 (C-1), 43.0 (C-17), 42.9 (C-14), 40.9 (C-8), 40.0 (C-22), 39.2 (C-10), 38.6 (C-4), 38.0 (C-13), 35.6 (C-16), 34.2 (C-7), 29.8 (C-21), 28.5 (C-23), 27.4 (C-15), 25.0 (C-12), 21.0 (C-11), 19.3 (C-30), 18.3 (C-6), 18.0 (C-28), 17.4 (C-25), 16.5 (C-24), 16.0 (C-26), 14.5 (C-27).

2.10.16 Compound 1 (lup-(20)29-ene-2α-acetate-3β-ol)

Compound 1 ($C_{32}H_{52}O_3$; Figure 3.80) was obtained as white powder. HR-ESI-MS (positive ion mode) showed a peak at m/z 507.3784; $C_{32}H_{52}O_3Na$ requires 507.3809. ^{1}H NMR data (500 MHz, $CDCl_3$): δ 4.86 (1H, ddd, J = 10, 10, 5 Hz, H-2-β), 4.67 (1H, d, *J* = 2 Hz, H-29), 4.55 (1H, d, *J* = 2 Hz, H-29), 3.15 (1H, d, *J* =10 Hz, H-3-α), 2.37 (1H, ddd, *J* = 11, 11, 6 Hz, H-19-β), 2.05 (3H, s, H-OCOC<u>H</u>$_3$), 2.04 (1H, m, H-1), 1.92 (1H, m, H-21), 1.66 (2H, m, H-12 and H-15), 1.65 (3H, s, H-30), 1.64 (1H, m, H-13-β), 1.53 (1H, m, H-6), 1.47 (1H, m, H-16), 1.43 (2H, m, H-7), 1.40 (1H, m, H-6), 1.38 (2H, m, H-11 and H-21), 1.38 (1H, m, H-22), 1.37 (1H, m, H-16), 1.34 (1H, overlapped, H-18-α), 1.31 (1H, m, H-9), 1.25 (1H, m, H-11), 1.19 (1H, m, H-22), 1.07 (1H, m, H-12), 1.03 (3H, s, H-23-α), 1.02 (3H, s, H-26-β), 0.98 (1H, m, H-15), 0.94 (3H, s, H-25-β), 0.93 (3H, s, H-27-α), 0.90 (1H, m, H-1), 0.84 (3H, s, H-24-β), 0.78 (3H, s, H-28-β), 0.76 (1H, overlapped, H-5). ^{13}C NMR data (125 MHz, $CDCl_3$): δ 171.6 (C-O<u>C</u>OCH$_3$), 150.8 (C-20), 109.4 (C-29), 80.9 (C-3), 73.6 (C-2), 55.2 (C-5), 50.4 (C-9), 48.3 (C-18), 47.9 (C-19), 44.0 (C-1), 43.0 (C-17), 42.9 (C-14), 40.9 (C-8), 40.0 (C-22), 39.8 (C-4), 38.5 (C-10), 38.0 (C-13), 35.6 (C-16), 34.1 (C-7), 29.7 (C-21), 28.4 (C-23), 27.4 (C-15), 25.0 (C-12), 21.3 (C-OCO<u>C</u>H$_3$), 21.1 (C-11), 19.3 (C-30), 18.2 (C-6), 18.0 (C-28), 17.1 (C-25), 16.4 (C-24), 16.0 (C-26), 14.5 (C-27).

2.10.17 Compound 2 (lup-(20)29-ene-2α-ol-3β-acetate)

Compound 2 ($C_{32}H_{52}O_3$; Figure 3.85) was obtained as white powder. HR-ESI-MS (positive ion mode) showed a peak at m/z 507.3794; $C_{32}H_{52}O_3Na$ requires 507.3809 while negative ion mode found at m/z 483.3462; $C_{32}H_{51}O_3$ requires 483.3480. ^{1}H NMR data (500

MHz, $CDCl_3$): δ 4.68 (1H, d, *J* = 2.5 Hz, H-29), 4.57 (1H, d, *J* = 2.5 Hz, H-29), 4.46 (1H, d, *J* = 10 Hz, H-3-α), 3.77 (1H, ddd, *J* = 10, 10, 5 Hz, H-2-β). 2.37 (1H, ddd, *J* = 11, 11, 6 Hz, H-19-β), 2.13 (3H, s, H-OCOC$\underline{H}_3$), 2.09 (1H, m, H-1), 1.90 (1H, m, H-21), 1.68 (3H, s, H-30), 1.68 (2H, overlapped, H-12 and H-15), 1.65 (1H, m, H-13), 1.50 (1H, m, H-6), 1.46 (1H, m, H-16), 1.43 (1H, m, H-11), 1.40 (4H, m, H-6 and H-7 and H-22), 1.38 (1H, m, H-16), 1.36 (1H, m, H-18-α), 1.34 (1H, m, H-9), 1.32 (1H, m, H-21), 1.26 (1H, m, H-11), 1.20 (1H, m, H-22), 1.08 (1H, m, H-12), 1.02 (3H, s, H-26-β), 0.98 (1H, m, H-15), 0.94 (3H, s, H-27-α), 0.91 (3H, s, H-25-β), 0.90 (1H, m, H-1), 0.88 (1H, m, H-5), 0.87 (3H, s, H-23-α), 0.85 (3H, s, H-24-β), 0.78 (3H, s, H-28-β). ^{13}C NMR data (125 MHz, $CDCl_3$): δ 172.4 (C-O$\underline{C}$OCH$_3$), 150.8 (C-20), 109.4 (C-29), 85.0 (C-3), 67.8 (C-2), 55.3 (C-5), 50.3 (C-9), 48.2 (C-18), 48.1 (C-1), 48.0 (C-19), 43.0 (C-17), 42.9 (C-14), 40.9 (C-8), 40.0 (C-22), 39.3 (C-4), 38.4 (C-10), 37.9 (C-13), 35.5 (C-16), 34.1 (C-7), 29.8 (C-21), 28.4 (C-23), 27.4 (C-15), 25.0 (C-12), 21.1 (C-11), 21.0 (C-OCO$\underline{C}$H$_3$), 19.3 (C-30), 18.3 (C-6), 18.0 (C-28), 17.4 (C-24), 17.3 (C-25), 16.0 (C-26), 14.5 (C-27).

2.10.18 β-Sitosterol

β-Sitosterol ($C_{29}H_{50}O$; Figure 3.90) was obtained as a white amorphous powder. HR-ESI-MS (positive ion mode) showed a peak at *m/z* 437.3797; $C_{29}H_{50}ONa$ requires 437.3759. ^{1}H NMR data (500 MHz, $CDCl_3$): δ 5.35 (1H, d, *J* = 5.5 Hz, H-6), 3.52 (1H, m, *J* = 11, 4.5 Hz, H-3-α), 2.29 (1H, m, H-4), 2.23 (1H, m, H-4), 1.99 (1H, m, H-12), 1.96 (2H, m, H-7), 1.86 (1H, m, H-1), 1.84 (3H, m, H-2 and H-16), 1.55 (1H, m, H-15), 1.50 (1H, m, H-11), 1.49 (1H, m, H-2), 1.43 (1H, m, H-8), 1.34 (2H, m, H-20 and H-22), 1.28 (1H, m, H-28), 1.25 (1H, m, H-25), 1.16 (3H, m, H-12 and H-23), 1.08 (3H, m, H-15, H-17 and H-28), 1.05 (3H, m, H-1, H-11 and H-22), 1.03 (3H, s, H-19), 0.99 (1H, m, H-14), 0.92 (2H, m, H-9 and H-24), 0.90 (3H, m, H-21), 0.84 (3H, s, H-29), 0.83 (3H, d, *J* = 7 Hz, H-26), 0.81 (3H, d, *J* = 7 Hz, H-27), 0.68 (3H, s, H-18). ^{13}C NMR data (125 MHz, $CDCl_3$): δ 140.8 (C-5), 121.7 (C-6), 71.8 (C-3), 56.8 (C-14), 56.1 (C-17), 50.1 (C-9), 45.8 (C-24), 42.3 (C-4 and C-13), 39.8 (C-12), 37.2 (C-1), 36.5 (C-10), 36.1 (C-20), 33.9 (C-22), 31.9 (C-7 and C-8), 31.7 (C-2), 29.1 (C-25), 28.2 (C-16), 26.1 (C-23), 24.3 (C-15), 23.1 (C-28), 21.1 (C-11), 19.8 (C-26), 19.4 (C-19), 19.0 (C-27), 18.7 (C-21), 12.0 (C-29), 11.9 (C-18).

2.10.19 β-Sitosterol-3-*O*-β-glucoside

β-Sitosterol-3-*O*-β-glucoside ($C_{35}H_{60}O_6$; Figure 3.94) was obtained as a white amorphous powder. HR-ESI-MS (positive ion mode) showed a peak at *m/z* 599.4258;

$C_{35}H_{60}O_6Na$ requires 599.4282 while negative ion mode found at 575.4335; $C_{35}H_{59}O_6$ requires 575.4367. ^{1}H NMR data (500 MHz, a mixture of CD_3OD and $CDCl_3$): δ 5.35 (1H, d, *J* = 5.5, 2.5 Hz, H-6), 4.37 (1H, d, *J* = 8 Hz, H-1g), 3.82 (1H, dd, *J* = 12, 3 Hz, H-6g), 3.72 (1H, dd, *J* = 12, 4.5 Hz, H-6g), 3.56 (1H, m, *J* = 9.5, 5 Hz, H-3-α), 3.39 (2H, overlapped, H-3g and H-4g), 3.25 (1H, m, H-5g), 3.20 (1H, t, *J* = 9.5 Hz, H-2g), 2.36 (1H, m, H-4), 2.23 (1H, m, H-4), 1.99 (1H, m, H-12), 1.92 (1H, m, H-7), 1.87 (1H, m, H-2), 1.83 (1H, m, H-1), 1.63 (1H, m, H-25), 1.56 (1H, m, H-2), 1.53 (1H, m, H-15), 1.49 (1H, m, H-7), 1.46 (2H, m, H-11), 1.41 (1H, m, H-8), 1.32 (1H, m, H-20), 1.29 (1H, m, H-22), 1.23 (1H, m, H-16), 1.22 (2H, m, H-28), 1.18 (1H, m, H-16), 1.12 (3H, m, H-12 and H-23), 1.08 (1H, m, H-17), 1.03 (2H, m, H-1 and H-15), 0.99 (1H, m, H-22), 0.97 (3H, s, H-19), 0.96 (1H, m, H-14), 0.90 (1H, m, H-9), 0.89 (1H, m, H-24), 0.87 (3H, overlapped, H-21), 0.80 (3H, s, H-29), 0.78 (3H, d, *J* = 7 Hz, H-26), 0.76 (3H, d, *J* = 7 Hz, H-27), 0.64 (3H, s, H-18). ^{13}C NMR data (125 MHz, a mixture of CD_3OD and $CDCl_3$): δ 140.6 (C-5), 122.4 (C-6), 101.4 (C-1g), 79.4 (C-3), 76.8 (C-4g), 76.2 (C-5g), 73.9 (C-2g), 70.5 (C-3g), 62.1 (C-6g), 57.1 (C-14), 56.4 (C-17), 50.5 (C-9), 46.2 (C-24), 42.6 (C-13), 40.1 (C-12), 38.9 (C-4), 37.6 (C-1), 37.0 (C-10), 36.4 (C-20), 34.2 (C-22), 32.2 (C-7 and C-8), 29.9 (C-2), 29.4 (C-25), 28.5 (C-16), 26.3 (C-23), 24.5 (C-15), 23.3 (C-28), 21.3 (C-11), 19.9 (C-26), 19.5 (C-19), 19.2 (C-27), 19.0 (C-21), 12.1 (C-29), 12.0 (C-18).

2.10.20 Salidroside

Salidroside (2-(4'-hydroxyphenyl) ethyl β-glucopyranoside) ($C_{14}H_{20}O_7$; Figure 3.96) was obtained as a brown-yellow amorphous powder. HR-ESI-MS (positive ion mode) showed a peak at *m/z* 323.1132; $C_{14}H_{20}O_7Na$ requires 323.1107. ^{1}H NMR data (500 MHz, CD_3OD): δ 7.06 (2H, d, *J* = 8 Hz, H-3 and H-5), 6.68 (2H, d, *J* = 8.5 Hz, H-2 and H-6), 4.28 (1H, d, *J* = 8 Hz, H-1g), 4.04 (1H, m, H-8), 3.86 (1H, m, H-6g), 3.70 (1H, m, H-8), 3.68 (1H, m, H-6g), 3.34 (1H, m, H-4g), 3.26 (1H, m, H-3g), 3.25 (1H, m, H-5g), 3.18 (1H, t, *J* = 8 Hz, H-2g), 2.81 (2H, m, H-7). ^{13}C NMR data (125 MHz, CD_3OD): δ 156.8 (C-4), 130.9 (C-3 and C-5), 130.7 (C-1), 116.1 (C-2 and C-6), 104.2 (C-1g), 78.1 (C-4g), 77.9 (C-5g), 75.1 (C-2g), 72.1 (C-8), 71.6 (C-3g), 62.7 (C-6g), 36.4 (C-7).

2.11 Spectroscopic data of isolated compounds from root part (see appendices for NMR spectra and section 3.8 for discussion of these data)

2.11.1 2'',3''-Di-*O*-acetyl-martynoside

2",3"-Di-*O*-acetyl-martynoside ($C_{35}H_{44}O_{17}$; Figure 3.99) was obtained as a brown-yellow amorphous powder. HR-ESI-MS in the negative ion mode found *m/z* 735.2495; $C_{35}H_{43}O_{17}$ requires 735.2506 while the positive mode showed a peak at *m/z* 759.2416; $C_{35}H_{44}O_{17}Na$ requires 759.2471. ^{1}H NMR data (500 MHz, $CDCl_3$): δ 7.67 (1H, d, *J* = 15.5 Hz, H-7'), 7.07 (1H, dd, *J* = 8, 2 Hz, H-6'), 7.02 (1H, d, *J* = 2 Hz, H-2'), 6.90 (1H, d, *J* = 8.5 Hz, H-5'), 6.80 (1H, d, *J* = 2 Hz, H-2), 6.77 (1H, d, *J* = 8 Hz, H-5), 6.67 (1H, dd, *J* = 8.5, 2 Hz, H-6), 6.26 (1H, d, *J* = 15.5 Hz, H-8'), 5.89 (1H, s, 4'-OH), 5.62 (1H, s, 3-OH), 5.29 (1H, dd, *J* = 3.5, 1.5 Hz, H-2r), 5.19 (1H, br s, *J* = 1.5 Hz, H-1r), 5.04 (1H, t, *J* = 10 Hz, H-4g), 5.01 (1H, dd, *J* = 10, 3.5 Hz, H-3r), 4.28 (1H, d, *J* = 8 Hz, H-1g), 4.13 (1H, m, H-8), 3.92 (3H, s, H-3'-OC$\underline{H}_3$), 3.86 (3H, s, H-4-OC$\underline{H}_3$), 3.86 (1H, overlapped, H-3g), 3.77 (1H, m, H-4r), 3.74 (1H, m, H-6g), 3.70 (1H, m, H-8), 3.62 (1H, m, H-6g), 3.60 (1H, m, H-2g), 3.50 (1H, m, H-5r), 3.48 (1H, m, H-5g), 2.83 (2H, m, H-7), 2.12 (3H, s, H-2"-OCOC$\underline{H}_3$), 2.03 (3H, s, H-3"-OCOC$\underline{H}_3$), 1.22 (3H, d, *J* = 6.5 Hz, H-6r). ^{13}C NMR data (125 MHz, $CDCl_3$): δ 171.3 (C-2"-O$\underline{C}$OCH$_3$), 170.0 (C-3"-O$\underline{C}$OCH$_3$), 167.0 (C-9'), 148.4 (C-4'), 147.1 (C-7'), 147.0 (C-3'), 145.5 (C-4), 145.2 (C-3), 131.5 (C-1), 126.5 (C-1'), 123.4 (C-6'), 120.3 (C-6), 115.0 (C-2), 114.8 (C-5'), 113.8 (C-'), 110.7 (C-5), 109.6 (C-2'), 102.7 (C-1g), 98.3 (C-1r), 79.0 (C-3g), 74.8 (C-2g), 74.5 (C-5g), 72.1 (C-3r), 71.3 (C-5r), 70.9 (C-8), 70.1 (C-2r), 69.1 (C-4r), 68.9 (C-4g), 61.4 (C-6g), 56.0 (C-4-O$\underline{C}$H$_3$), 55.9 (C-3'-O$\underline{C}$H$_3$), 35.4 (C-7), 20.9 (C-2"-OCO$\underline{C}$H$_3$ and C-3"-OCO$\underline{C}$H$_3$), 17.7 (C-6r).

2.11.2 1-Docosyl ferulate

1-Docosyl ferulate ($C_{32}H_{54}O_4$; Figure 3.101) was obtained as a white powder. HR-ESI-MS (negative ion mode) showed a peak at *m/z* 501.3942; $C_{32}H_{53}O_4$ requires 501.3949. ^{1}H NMR data (500 MHz, $CDCl_3$): δ 7.58 (1H, d, *J* = 16 Hz, H-7'), 7.06 (1H, d, *J* = 8, 2 Hz, H-6'), 7.03 (1H, d, *J* = 2 Hz, H-2'), 6.90 (1H, d, *J* = 8 Hz, H-5'), 6.27 (1H, d, *J* = 16 Hz, H-8'), 5.82 (1H, s, 4'-OH), 4.18 (2H, t, *J* = 7 Hz, H-1), 3.92 (3H, s, H-3'-OC$\underline{H}_3$), 1.67 (2H, quintet, *J* = 8 Hz, H-2), 1.38 (2H, m, H-3), 1.25 (36H, m, H-4 to H-21), 0.86 (3H, t, *J* = 7 Hz, H-22). ^{13}C NMR data (125 MHz, $CDCl_3$): δ 167.4 (C-9'), 147.9 (C-4'), 146.7 (C-3'), 144.6 (C-7'), 127.1 (C-1'), 123.0 (C-6'), 115.7 (C-8'), 114.7 (C-5'), 109.3 (C-2'), 64.6 (C-1), 55.9 (C-3'-O$\underline{C}$H$_3$), 29.3-31.9 (C-4 to C-20), 28.8 (C-2), 26.0 (C-3), 22.7 (C-21), 14.1 (C-22).

2.11.3 Ferruginol

Ferruginol ($C_{20}H_{30}O$; Figure 3.104) was obtained as yellow powder. HR-ESI-MS (negative ion mode) showed a peak at m/z 285.2221; $C_{20}H_{29}O$ requires 285.2224. ^{1}H NMR data (500 MHz, $CDCl_3$): δ 6.82 (1H, s, H-14), 6.62 (1H, s, H-11), 4.46 (1H, s, 12-OH), 3.10 (1H, septet, *J* = 7 Hz, H-15), 2.83 (1H, ddd, *J* = 17, 6, 1.5 Hz, H-7-β), 2.76 (1H, ddd, *J* = 17, 11, 7.5 Hz, H-7-α), 2.15 (1H, dt, *J* = 12.5, 4, 1 Hz, H-1-β), 1.85 (1H, dddd, *J* = 17, 6, 3.5, 2 Hz, H-6-α), 1.73 (1H, ddd, *J* = 13.5, 6.5, 3 Hz, H-2-α), 1.65 (1H, m, H-6-β), 1.59 (1H, ddd, *J* = 14, 10, 3.5 Hz, H-2-β), 1.46 (1H, ddd, *J* = 13.5, 3.5, 1.5 Hz, H-3-β), 1.37 (1H, m, H-1-α), 1.31 (1H, dd, *J* = 12.5, 2 Hz, H-5-α), 1.23 (3H, d, *J* = 7 Hz, H-16), 1.21 (3H, d, *J* = 7 Hz, H-17), 1.19 (1H, m, H-3-α), 1.16 (3H, s, H-20-β), 0.93 (3H, s, H-18-α), 0.91 (3H, s, H-19-β). ^{13}C NMR data (125 MHz, $CDCl_3$): δ 150.6 (C-12), 148.7 (C-9), 130.9 (C-13), 127.3 (C-8), 126.6 (C-14), 110.9 (C-11), 50.3 (C-5), 41.7 (C-3), 38.8 (C-1), 37.5 (C-10), 33.4 (C-4), 33.3 (C-18), 29.7 (C-7), 26.8 (C-15), 24.8 (C-20), 22.7 (C-16), 22.5 (C-17), 21.6 (C-19), 19.3 (C-2), 19.2 (C-6).

2.11.4 Salvinolonyl 12-methyl ether

Salvinolonyl 12-methyl ether ($C_{21}H_{28}O_3$; Figure 3.109) was obtained as off white powder. HR-ESI-MS (positive ion mode) showed a peak at m/z 351.1919; $C_{21}H_{28}O_3Na$ requires 351.1931. ^{1}H NMR data (500 MHz, $CDCl_3$): δ 7.73 (1H, s, H-14), 6.47 (1H, s, H-6), 6.25 (1H, s, 11-OH), 3.83 (3H, s, H-OC$\underline{H}_3$), 3.27 (1H, ddd, *J* = 14, 4, 2 Hz, H-1-β), 3.25 (1H, septet, *J* = 7 Hz, H-15), 1.97 (1H, m, H-2), 1.73 (1H, ddd, *J* = 13, 7, 2 Hz, H-3-β), 1.65 (3H, s, H-20-β), 1.62 (1H, m, H-2), 1.43 (2H, ddd, *J* = 14, 12, 4 Hz, H-1-α and H-3-α), 1.36 (3H, s, H-19-β), 1.28 (3H, d, *J* = 7 Hz, H-16), 1.27 (3H, s, H-18-α), 1.26 (3H, d, *J* = 7 Hz, H-17). ^{13}C NMR data (125 MHz, $CDCl_3$): δ 185.4 (C-7), 175.3 (C-5), 148.2 (C-12), 145.8 (C-11), 139.7 (C-13), 136.7 (C-9), 127.4 (C-8), 123.6 (C-6), 115.9 (C-14), 61.9 (C-O$\underline{C}H_3$), 42.2 (C-10), 40.4 (C-3), 38.1 (C-4), 34.2 (C-1), 33.1 (C-18), 29.3 (C-19), 26.8 (C-15), 24.8 (C-20), 23.6 (C-16), 23.5 (C-17), 18.7 (C-2)

2.11.5 7α-Acetoxy-14-hydroxy-8,13-abietadiene-11,12-dione

7α-Acetoxy-14-hydroxy-8,13-abietadiene-11,12-dione ($C_{22}H_{30}O_5$; Figure 3.113) was obtained as yellow powder. HR-ESI-MS (positive ion mode) showed a peak at m/z 397.1974; $C_{22}H_{30}O_5Na$ requires 397.1985 while the negative ion mode found at m/z 373.2004; $C_{22}H_{29}O_5$ requires 373.2020. ^{1}H NMR data (500 MHz, $CDCl_3$): δ 7.12 (1H, s, 14-OH), 5.92 (1H, dd, *J* = 4, 1.5 Hz, H-7-β), 3.15 (1H, septet, *J* = 7 Hz, H-15), 2.71(1H, ddd, *J* = 13, 4, 1 Hz, H-1-β),

2.03 (3H, s, H-OCOC$\underline{H}_3$), 1.92 (1H, br d, *J* = 15 Hz, H-6-β), 1.72 (1H, dddd, *J* = 13, 6, 2 Hz, H-2-α), 1.59 (1H, ddd, *J* = 15, 11, 1.5 Hz, H-6-α), 1.57 (1H, m, H-2-β), 1.49 (2H, br d, *J* = 13, 1 Hz, H-3-α and H-5-α), 1.22 (3H, s, H-20-β), 1.20 (3H, d, *J* = 7 Hz, H-16), 1.20 (2H, overlapped, H-1-α and H-3-β), 1.18 (3H, d, *J* = 7 Hz, H-17), 0.88 (3H, s, H-18-α), 0.87 (3H, s, H-19-β). ^{13}C NMR data (125 MHz, $CDCl_3$): δ 185.4 (C-11), 183.7 (C-12), 169.4 (C-O$\underline{C}$OCH$_3$), 150.7 (C-14), 149.9 (C-9), 139.4 (C-8), 124.6 (C-13), 64.5 (C-7), 46.1 (C-5), 41.0 (C-3), 39.0 (C-10), 35.8 (C-1), 32.9 (C-4 and C-18), 24.6 (C-6), 24.1 (C-15), 21.6 (C-19), 21.1 (C-OCO$\underline{C}$H$_3$), 19.8 (C-16), 19.7 (C-17) 18.8 (C-2), 18.5 (C-20).

2.11.6 7α,14-Dihydroxy-8,13-abietadiene-11,12-dione

7α,14-Dihydroxy-8,13-abietadiene-11,12-dione ($C_{20}H_{28}O_4$; Figure 3.116) was obtained as yellow powder HR-ESI-MS (positive ion mode) showed a peak at m/z 355.1880; $C_{20}H_{28}O_4Na$ requires 355.1880 while the negative ion mode showed a peak at m/z 331.1898; $C_{20}H_{27}O_4$ requires 331.1915. ^{1}H NMR data (500 MHz, $CDCl_3$): δ 7.20 (1H, s, 14-OH), 4.72 (1H, dd, *J* = 3.5, 2 Hz, H-7-β), 3.15 (1H, septet, H-15), 3.00 (1H, s, 4-OH-α), 2.70 (1H, dt, *J* = 13.5, 2.5 Hz, H-1-β), 1.94 (1H, ddd, *J* = 15 Hz, H-6-β), 1.70 (1H, m, H-2), 1.60 (1H, m, H-6-α), 1.53 (1H, m, H-2), 1.49 (1H, br d, *J* = 10.5 Hz, H-5-α), 1.46 (1H, m, H-3), 1.25 (1H, m, H-3), 1.22 (3H, s, H-20-β), 1.20 (6H, *J* = 7 Hz, H-16 and H-17), 1.18 (1H, m, H-1-α), 0.98 (3H, s, H-18-β), 0.90 (3H, s, H-19-β). ^{13}C NMR data (125 MHz, $CDCl_3$): δ 189.1 (C-12), 185.0 (C-11), 151.0 (C-14), 147.8 (C-9), 143.2 (C-8), 124.2 (C-13), 63.2 (C-7), 45.7 (C-5), 41.0 (C-3), 39.1 (C-10), 35.8 (C-1), 33.1 (C-18), 32.9 (C-4), 25.8 (C-6), 24.0 (C-15), 21.7 (C-19), 19.9 (C-16), 19.8 (C-17), 18.8 (C-2), 18.4 (C-20).

2.11.7 Microstegiol

Microstegiol ($C_{20}H_{26}O_2$; Figure 3.119) was obtained as yellow powder. HR-ESI-MS (positive ion mode) showed a peak at m/z 321.1820; $C_{20}H_{26}O_2Na$ requires 321.1825. ^{1}H NMR data (500 MHz, $CDCl_3$): δ 7.05 (1H, d, *J* = 7.5 Hz, H-6), 6.95 (1H, s, H-14), 6.88 (1H, d, *J* = 7.5 Hz, H-7), 4.50 (1H, s, 11-OH), 3.59 (1H, ddd, *J* = 14, 12, 2 Hz, H-1-β), 3.00 (1H, septet, *J* = 6 Hz, H-15), 2.79 (1H, ddd, *J* = 14, 6, 2.5 Hz, H-1-α), 2.35 (1H, m, H-3), 2.31 (3H, s, H-20), 1.78 (1H, m, H-2-β), 1.41 (1H, m, H-2-α), 1.24 (1H, m, H-3), 1.19 (3H, d, *J* = 7 Hz, H-17), 1.14 (3H, d, *J* = 7 Hz, H-16), 0.79 (3H, s, H-18-α), 0.78 (3H, s, H-19-β). ^{13}C NMR data (125 MHz, $CDCl_3$): δ 206.1 (C-12), 143.3 (C-10), 141.0 (C-13), 140.9 (C-14), 139.3 (C-9), 137.4 (C-5), 130.1 (C-6), 129.0 (C-8), 126.7 (C-7), 84.4 (C-11), 42.9 (C-3), 39.0

(C-4), 28.0 (C-19), 27.0 (C-1), 26.8 (C-15), 23.5 (C-2), 22.1 (C-16), 21.4 (C-18 and C-20), 21.1 (C-17).

2.11.8 Compound 3 (1-oxomicrostegiol; 10aS-8,9,10,10a-tetrahydro-10a-hydroxy-6,10,10-trimethyl-2-(1-methylethyl)-cyclohepta[de]naphthalene-1,7-dione)

Compound 3 ($C_{20}H_{24}O_3$; Figure 3.123) was obtained as brown-yellow powder. HR-ESI-MS (positive ion mode) showed a peak at m/z 335.1610; $C_{20}H_{24}O_3Na$ requires 335.1618. UV (MeOH): λ_{max} (log ε) = 312 (3.87), 278 (3.71), 253 (4.17), 236 (4.11). ^{1}H NMR data (500 MHz, $CDCl_3$): δ 7.22 (1H, d, *J* = 7.5 Hz, H-6), 7.20 (1H, d, *J* = 7.5 Hz, H-7), 7.07 (1H, s, H-14), 3.88 (1H, s, 11-OH), 3.11 (1H, ddd, *J* = 14, 11.5, 2.5 Hz, H-2-α), 2.98 (1H, septet, *J* = 7 Hz, H-15), 2.34 (3H, s, H-20), 2.30 (1H, ddd, *J* = 14, 5, 3 Hz, H-2-β), 1.54 (1H, dd, *J* = 14, 3 Hz, H-3-β), 1.42 (1H, ddd, *J* = 14, 5, 3 Hz, H-3-α), 1.18 (3H, d, *J* = 7 Hz, H-17), 1.16 (3H, d, *J* = 7 Hz, H-16), 1.05 (3H, s, H-18-α), 0.80 (3H, s, H-19-β). ^{13}C NMR data (125 MHz, $CDCl_3$): δ 207.2 (C-1), 203.5 (C-12), 141.5 (C-13), 139.1 (C-14), 138.1 (C-9), 137.6 (C-10), 136.9 (C-5), 131.2 (C-6), 129.6 (C-7), 127.6 (C-8), 81.5 (C-11), 40.9 (C-4), 38.2 (C-2), 37.5 (C-3), 26.9 (C-15), 26.9 (C-19), 21.9 (C-16), 21.5 (C-17), 19.9 (C-20), 17.4 (C-18).

2.11.9 Compound 4 (viroxocane; 3,4-dihydro-11-hydroxy-10-(1-methylethyl)-2,2,6-trimethyl-naphtha[1,8-bc]oxocin-5(2H)-one)

Compound 4 ($C_{20}H_{24}O_3$; Figure 3.127) was obtained as brown-yellow powder. HR-ESI-MS (positive ion mode) showed a peak at m/z 335.1628; $C_{20}H_{24}O_3Na$ requires 335.1618 while the negative mode showed a peak at m/z 311.1642; $C_{20}H_{23}O_3$ requires 311.1653. UV (MeOH): λ_{max} (log ε) = 337 (3.56), 294 (3.72), 237 (4.45). ^{1}H NMR data (500 MHz, $CDCl_3$): δ 7.61 (1H, d, *J* = 8 Hz, H-7), 7.41 (1H, s, H-14), 7.11 (1H, d, *J* = 8 Hz, H-6), 5.90 (1H, s, 12-OH), 3.34 (1H, septet, *J* = 7 Hz, H-15), 3.02 (1H, ddd, *J* = 14, 10.5, 3.5 Hz, H-2-α), 2.60 (1H, ddd, *J* = 14, 4, 4 Hz, H-2-β), 2.33 (3H, s, H-20), 2.17 (1H, ddd, *J* = 14, 10.8, 4 Hz, H-3-β), 1.62 (3H, s, H-19-β), 1.60 (1H, m, H-3-α), 1.33 (3H, d, *J* = 7 Hz, H-16), 1.28 (3H, d, *J* = 7 Hz, H-17), 1.23 (3H, s, H-18-α). ^{13}C NMR data (125 MHz, $CDCl_3$): δ 210.85 (C-1), 147.38 (C-12), 136.58 (C-13), 132.20 (C-10), 132.08 (C-11), 130.37 (C-5), 128.15 (C-7), 126.96 (C-9), 126.77 (C-8), 126.27 (C-6), 121.16 (C-14), 84.27 (C-4), 41.20 (C-2), 35.10 (C-3), 27.82 (C-15), 26.24 (C-19), 26.02 (C-18), 22.33 (C-16), 22.29 (C-17), 18.89 (C-20).

2.11.10 Compound 5 (viridoquinone; 5-methyl-20-nor-abieta-1(10),6,8,13-tetraen-11,12-dione)

Compound 5 ($C_{20}H_{24}O_2$; Figure 3.131) was obtained as purple powder. HR-ESI-MS (positive ion mode) showed a peak at m/z 319.1662; $C_{20}H_{24}O_2Na$ requires 319.1669. UV (MeOH): λ_{max} (log ε) = 460 (2.42), 325 (3.86), 285 (3.99), 246 (4.32). ^{1}H NMR data (500 MHz, $CDCl_3$): δ 6.72 (1H, t, *J* = 4.5 Hz, H-1), 6.58 (1H, s, H-14), 6.46 (1H, d, *J* = 9.5 Hz, H-6), 5.97 (1H, d, *J* = 9.5 Hz, H-7), 2.95 (1H, septet, *J* = 6 Hz, H-15), 2.30 (2H, m, H-2), 1.86 (1H, ddd, *J* = 14, 10, 5 Hz, H-3-β), 1.26 (1H, m, H-3-α), 1.12 (3H, d, *J* = 7 Hz, H-16), 1.10 (3H, d, *J* = 7 Hz, H-17), 1.08 (3H, s, H-20-β), 1.02 (3H, s, H-19-β), 0.91 (3H, s, H-18-α). ^{13}C NMR data (125 MHz, $CDCl_3$): δ 180.53 (C-11), 180.48 (C-12), 146.90 (C-13), 146.57 (C-6), 137.17 (C-8), 137.01 (C-14), 134.35 (C-1), 132.44 (C-10), 125.41 (C-9), 123.90 (C-7), 43.37 (C-5), 33.10 (C-4), 31.83 (C-3), 27.18 (C-15), 25.74 (C-18), 24.51 (C-19), 23.84 (C-2), 23.44 (C-20), 21.55 (C-16), 21.41 (C-17).

2.11.11 A mixture of 2-(4'-alkoxyphenyl) ethyl alkanoates

A mixture of 2-(4'-alkoxyphenyl) ethyl alkanoate (Figure 3.135) was obtained as white powder. CIMS and GC-CI-MS carried out using NH_3 as reagent gas at the EPSRC National Mass Spectrometry Service Centre, School of Medicine, University of Swansea. The GC-CI-MS data (positive ion mode) showed three main components at *m/z* 478.4245; $C_{30}H_{52}O_3NH_4$ requires 478.4255, 506.4557; $C_{32}H_{56}O_3NH_4$ requires 506.4593 and 534.4869; $C_{34}H_{60}O_3NH_4$ requires 534.4881. ^{1}H NMR data (500 MHz, $CDCl_3$): δ 7.07 (2H, d, *J* = 8.5 Hz, H-2' and H-6'), 6.75 (2H, d, *J* = 8.5 Hz, H-3' and H-5'), 4.23 (2H, t, *J* = 7 Hz, H-2), 3.64 (2H, t, *J* = 6.5 Hz, H-α-alkoxy), 2.85 (2H, t, *J* = 7 Hz, H-1), 2.27 (2H, t, *J* = 7.5 Hz, H-β-alkanoate), 1.25-1.56 (-C<u>H</u>$_2$-), 0.88 (6H, t, *J* = 7 Hz, -C<u>H</u>$_3$ of alkoxy and alkanoate). ^{13}C NMR data (125 MHz, $CDCl_3$): δ 173.85 (C-α-alkanoate), 154.16 (C-4'), 130.04 (C-1', C-2' and C-6'), 115.28 (C-3' and C-5'), 64.89 (C-2), 63.12 (C-α-alkoxy), 34.34 (C-1), 34.26 (C-β-alkanoate), 32.80 (C-β-alkoxy), 22.68-29.45 (-<u>C</u>H$_2$-), 14.11 (<u>C</u>H$_3$ of alkoxy and alkanoate).

Chapter 3
Results and discussions

3.1 TLC patterns of crude fractions and their detection

The developed TLC plates were sprayed by different reagents according to Table 2.1 in order to screen their type of chemical compounds. Figures 3.1-3.2 show the various TLC patterns from two mobile phases with different detection methods. The Rf values of the standards and extract fractions are shown in Table 3.1.

It can be seen in Figure 3.1A-B that various compounds were detected under UV at 254 nm and 366 nm in four polar fractions from the aerial parts, i.e. AWW, AB, MWW, and MB by using mobile phase: ethyl acetate:methanol:formic acid:water (50:3:3:6). Fluorescence of those compounds was enhanced under UV at 366 nm after a plate was sprayed by Natural Products Reagent (Figure 3.1C). Water and 1-butanol fractions (tracks 6-7, 10-11) may contain flavonoids, and polyphenolic compounds such as cinnamic acid derivatives. The plate sprayed with Iron (III) chloride Reagent indicated phenol group containing compounds as shown in Figure 3.1D. The other two reagents were sprayed on a less polar mobile phase (chloroform:methanol, 9:1). Many lipophilic compounds which might be terpenoids, and steroids in both AE (Figure 3.2, track 5), and ME (Figure 3.2, track 9) (ethyl acetate fractions from acetone, and methanol extracts respectively) gave various colours in visible light after being sprayed with Anisaldehyde-Sulfuric acid Reagent and Phosphomolybdic acid Reagent.

The similar patterns of track 6, 7, 10, and 11 (Figures 3.1-3.3), which are polar fractions from acetone, and methanol, indicated the comparable solubility of those compounds in both solvents. TLC of root part crude fraction exhibited a similar pattern as aerial part as shown in Figure 3.4. However, the bands of compounds in polar crude fractions (tracks 13-14 and 17-18) were relatively less intense than in aerial crude fractions (tracks 3-4 and 7-8).

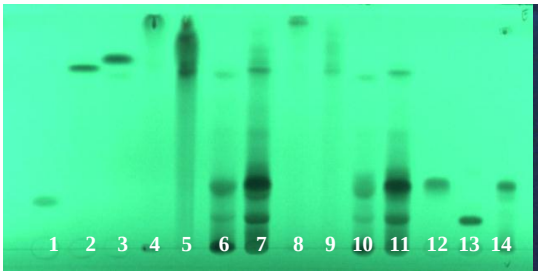

A. Under UV at 254 nm

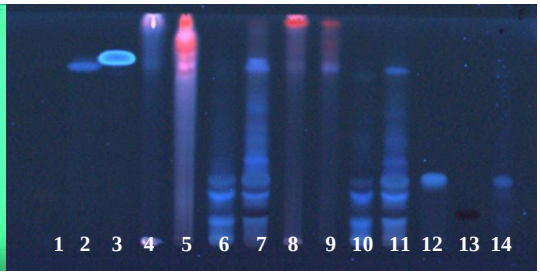

B. Under UV at 366 nm

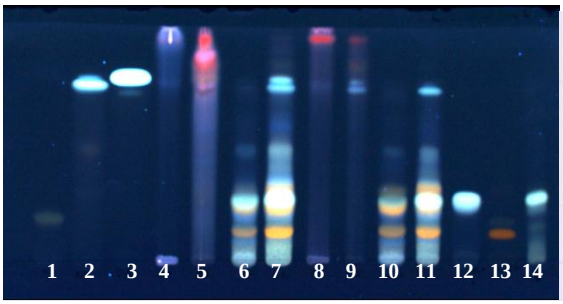

C. Natural Products Reagent, under UV at 366 nm

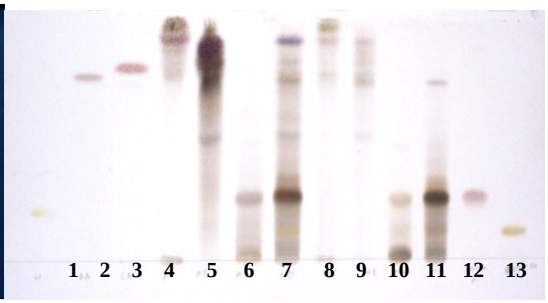

D. Iron (III) chloride Reagent, white light

Figure 3.1 A-D Separation of *Salvia viridis* L. cv. Blue Jeans aerial part crude fractions. Mobile phase: ethyl acetate:methanol:formic acid:water (50:3:3:6).

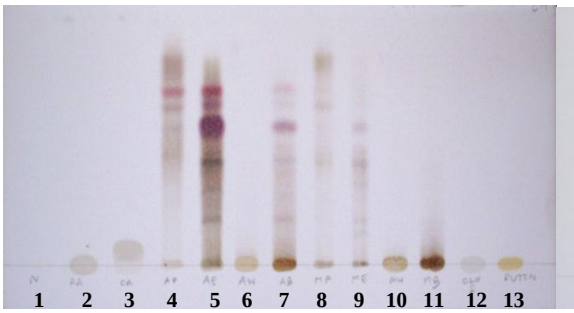

A. Anisaldehyde-Sulfuric acid Reagent, white light

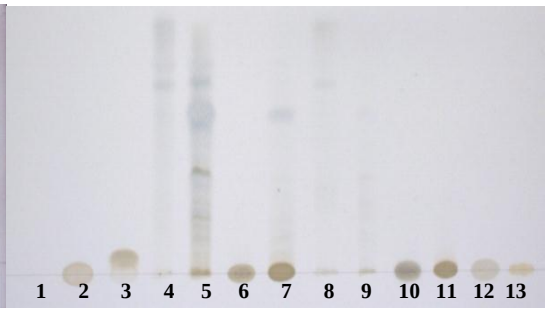

B. Phosphomolybdic acid Reagent, white light

Figure 3.2 A-B Separation of *Salvia viridis* L. cv. Blue Jeans aerial part crude fractions. Mobile phase: chloroform:methanol (9:1)

Figure 3.3 DPPH stained plate of aerial part, white light. Mobile phase: ethyl acetate, methanol, formic acid, water (50:3:3:6).

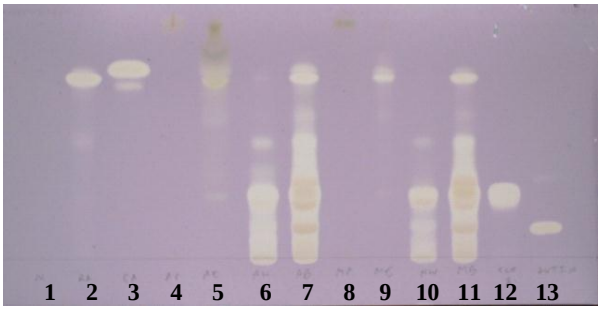

Table 3.1 Rf values of all aerial part extract fractions and standard

Track	Name	Rf values of compounds	
		Mobile phase: ethyl acetate:methanol: formic acid:water (50:3:3:6).	Mobile phase: chloroform:methanol (9:1)
1	Naringin	0.20	-
2	Rosmarinic acid	0.70	-
3	Caffeic acid	0.75	0.05
4	AP (Acetone-PE)	-	0.25, 0.45, 0.55, 0.63, 0.73
5	AE (Acetone-Ethyl acetate)	-	0.18, 0.23, 0.30, 0.35, 0.45, 0.55, 0.60, 0.63, 0.73
6	AW (Acetone-Water)	0.08, 0.13, 0.23, 0.25, 0.43	-
7	AB (Acetone-1-Butanol)	0.08, 0.13, 0.23, 0.25, 0.27, 0.43, 0.70, 0.75	0.25, 0.45, 0.55, 0.63, 0.73
8	MP (Methanol-PE)	-	0.18, 0.23, 0.40, 0.63, 0.73
9	ME (Methanol-Ethyl acetate)	0.70, 0.75	0.18, 0.23, 0.30, 0.35, 0.45, 0.55, 0.60, 0.63, 0.73
10	MW (Methanol-Water)	0.08, 0.13, 0.23, 0.25, 0.43	-
11	MB (Methanol-1-Butanol)	0.08, 0.13, 0.23, 0.25, 0.27, 0.43, 0.70	0.18
12	Chlorogenic acid	0.25	-
13	Rutin	0.13	-
14	Verbascoside	0.25	-

TLC of crude fraction from the root extracts exhibited a similar broad pattern to the aerial part as shown in Figure 3.4. However, the root extracts showed a greater preponderance of non-polar constituents.

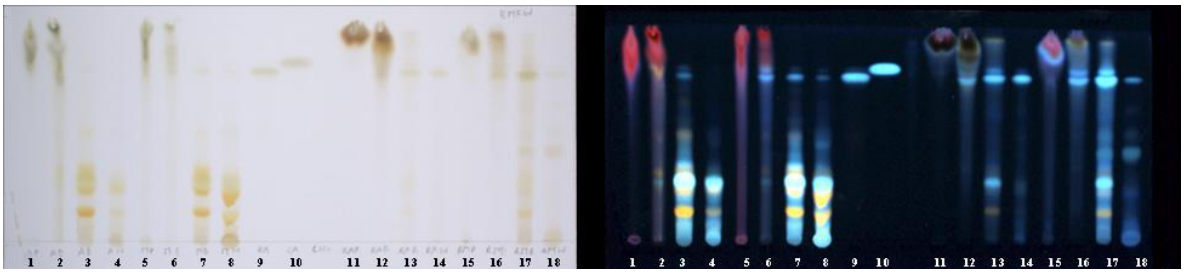

A. White light B. Natural Product Reagent, under UV at 366 nm

Figure 3.4 A-B Separation of *Salvia viridis* L. cv. Blue Jeans root part crude fractions (tracks 11-18). Mobile phase: ethyl acetate, methanol, formic acid, water (50:3:3:6). Labeling of each track is given in Table 3.2.

Table 3.2 Crude fractions abbreviations and track labeling

Track	Part	Crude fraction	
1	Aerial	AP	Acetone-Petroluem ether crude fraction
2	Aerial	AE	Acetone-Ethyl acetate crude fraction
3	Aerial	AB	Acetone-1-Butanol crude fraction
4	Aerial	AW	Acetone-Water crude fraction
5	Aerial	MP	Methanol-Petroleum ether crude fraction
6	Aerial	ME	Methanol-Ethyl acetate crude fraction
7	Aerial	MB	Methanol-1-Butanol crude fraction
8	Aerial	MW	Methanol-Water crude fraction
9	Standard	RA	Rosmarinic acid
10	Standard	CA	Caffeic acid
11	Root	RAP	Acetone-Petroluem ether crude fraction
12	Root	RAE	Acetone-Ethyl acetate crude fraction
13	Root	RAB	Acetone-1-Butanol crude fraction
14	Root	RAW	Acetone-Water crude fraction
15	Root	RMP	Methanol-Petroleum ether crude fraction
16	Root	RME	Methanol-Ethyl acetate crude fraction
17	Root	RMB	Methanol-1-Butanol crude fraction
18	Root	RMW	Methanol-Water crude fraction

For preliminary screening, the detecting reagents are a useful guide to compound type, and also to aid the isolation. Under UV 366 nm, compounds are commonly seen as blue or red fluorescent spots, Natural Product Reagent can differentiate compounds by enhancing fluorescence intensity and colour. Natural Product Reagent contains 2-aminoethyl-diphenyl borinate (or diphenylboric acid-2-aminoethyl ester) which possibly forms a complex with certain substances, for example, flavonoids, and results in a bathochromic shift of the complex. PEG (Polyethylene glycol) in solution B was sprayed on the TLC plate in order to increase and stabilize the fluorescence (Jork et al., 1990).

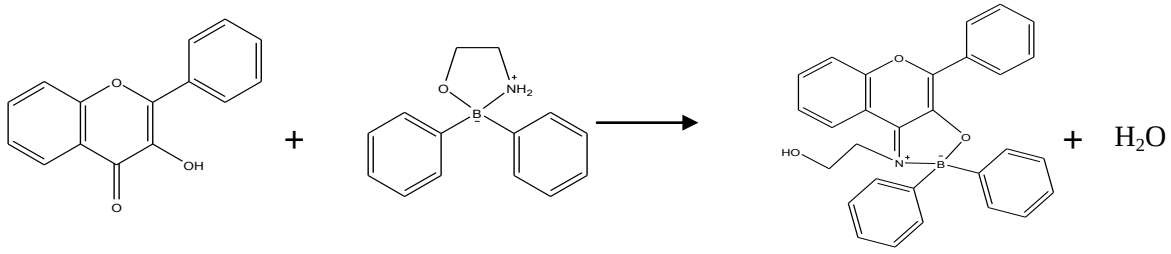

Flavonol Diphenylboric acid-2-aminoethyl ester

Figure 3.5 Reaction of flavonol and diphenylboric acid-2-aminoethyl ester (Jork et al., 1990)

Iron (III) chloride Reagent is widely used to detect phenols, flavonoids, and plant acids. A range of colours with polyphenols (deep violet to orange) are detected in visible light due to the d-d transitions in the octahedral complex between iron (III) ion and hydroxyl groups of phenols.

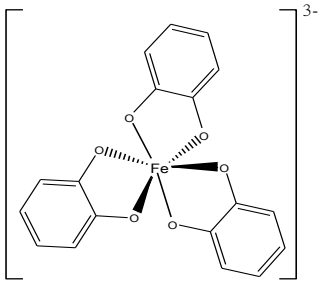

Figure 3.6 Proposed complex between iron (III) ion and catechols

There is no specific reaction of Anisaldehyde-Sulfuric acid Reagent with various compounds. However, colour changes were observed after the TLC plate was heated possibly due to condensation of anisaldehyde with certain functional groups of compounds. Reactive

aldehyde can react with nucleophiles to add a substituted styrene group to the analyte. In addition, sulfuric acid can dehydrate analyte molecules to generate double bond systems to give conjugated chromophores.

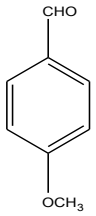

Figure 3.7 Anisaldehyde

Phosphomolybdic acid reagent was sprayed to detect terpenoids, fatty oils, and reducing substances. Blue bands were observed on a yellow background. The mechanism of reaction is due to the reduction of Molybdenum. Mo (VI) is reduced to Mo (IV), which forms blue-grey mixed oxides with the remaining Mo (VI) (Jork et al., 1990).

$$2MoO_3 \longrightarrow MoO_2 \bullet MoO_3$$

Figure 3.8 Reaction of Phosphomolybdic acid reagent

3.2 TLC-chemoautographic method (DPPH radical scavenging activity)

As a preliminary test for biological antioxidant activity, a TLC-chemoautographic method was introduced to monitor antioxidant activity in the fractions (Cimpoiu, 2006; Tasdemir et al., 2004). This method offers a simple activity test and the result is also used as a guideline for isolating active compounds. 2, 2- Diphenyl-1-picrylhydrazyl (DPPH) is a relatively stable free radical that is frequently used to detect free radical scavengers. The radical form of DPPH absorbs at 515 nm as seen in purple colour. When its electron is paired off because of either an antioxidant or a radical species, the absorption disappears. As can be seen in Figure 3.9, the equations II, and III are considered to be termination reactions but equation II is very slow because of steric hindrance. The rate of reaction in equation III depends on the molecular structure of the phenol, and aromatic substituent volumes

(Cimpoiu, 2006). The dimerization between two phenoxyl radicals depends on a free ortho, or para position (Brand-Williams et al., 1995).

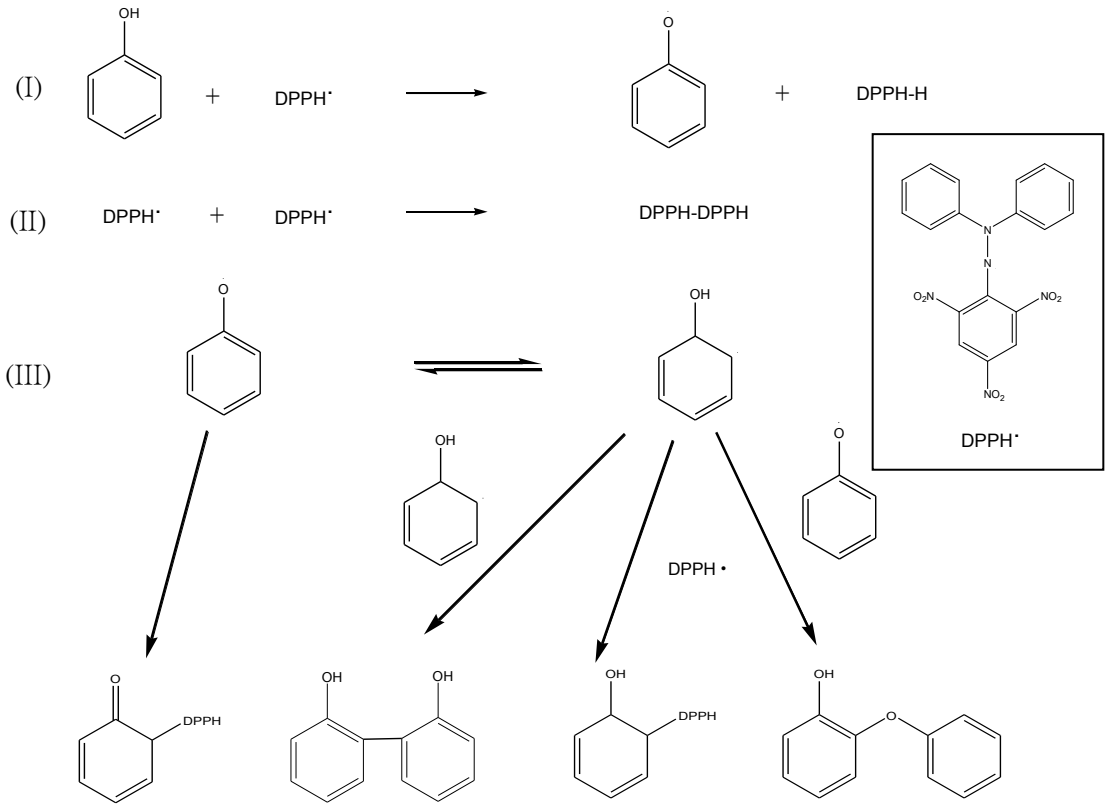

Figure 3.9 Proposed reaction of DPPH· with phenol

Compounds that possess this activity were seen as yellow bands or spots on a purple background in visible light shortly after a developed TLC plate was sprayed with DPPH solution as shown in Figure 3.3. All crude fractions indicate compounds which possess this activity except the petroleum ether fraction from both acetone and methanol extracts. The 1-butanol fractions that contained many radical scavengers were, therefore, further separated by HPLC.

The isolated compounds from HPLC revealed that the yellow bands of DPPH scavenging activity belonged to phenylpropanoids and flavonoids. The Rf values of each compounds were given in Table 3.5. Previously reported DPPH scavenging activity in regard

to IC_{50} and percentage of DPPH inhibition are given in Table 3.3. Structure activity relationships of DPPH scavenging activity suggests that ortho-dihydroxyl substitution at the aromatic ring yields high activity. Among these isolated compounds, verbascoside would be the most potent one against DPPH according to those finding.

Table 3.3 Review of DPPH scavenging activity of main isolated compounds

Compound	IC_{50} (μM)	% DPPH inhibition	Reference
Verbascoside	9[a],12[b], 15[c]	-	[a]Ono et al., 2008
Leucosceptoside A	26[a]	-	[b]Galvez et al., 2005
Martynoside	23[a]	-	[c]Gao et al., 1999
Rosmarinic acid	9[d]	88[e] (20 μM)	[d]Gu et al., 2009
Caffeic acid	16[a]	-	[e]Wang et al., 1998
Luteolin-7-*O*-glucoside	28[f]	62[e] (20 μM)	[f] Seyoum et al., 2006
6-*O*-caffeoyl-glucose	>30[c]	-	

IC_{50} is defined as the concentration of tested sample to inhibit 50% DPPH radical.
%DPPH inhibition is percentage of scavenging activity at the certain concentration (in parenthesis).

3.3 Antibacterial activity

3.3.1 TLC-bioautographic method; agar overlay technique

In order to determine the antibacterial activity, all crude fractions were tested against certain bacteria by using the TLC-bioautographic assay. The agar-overlay technique offered the direct and localized detection of antibacterial activity over the developed TLC plate (Hamburger and Cordell, 1987). The panel of test organisms consisted of both the Gram-positive cocci, *Staphylococcus aureus* (ATCC 6571) and *Enterococcus faecalis* (ATCC 775), the spore-forming Gram-positive rod *Bacillus cereus* (ATCC 2599), and the three Gram-negative bacteria, *Escherichia coli* (ATCC 86), *Klebsiella pnueminiae* (ATCC 9633) and *Proteus vulgaris* (ATCC 4636).

. Results of the TLC-bioautographic method against three bacteria are shown in Figures 3.10-3.12. For the Gram-positive bacteria, the non-polar crude fractions exhibited the inhibition zone encircling the spots particularly acetone crude fraction from root part (RAP and RAE) as shown in Figures 3.10-3.12 (plate A). Acetone crude fraction (AE) from aerial part also showed clear zone against those three bacteria (Figures 3.10-3.12, plate B). According to the Rf values, compounds with antibacterial activity were identified as triterpenoids and diterpenoids. The MIC values of compounds isolated from the fractions (AE, RAP and RAE) against the three Gram-positive bacteria were measured by a 96 well microplate assay. On the other hand, the polar crude fractions (AB, AW, MB and MW) showed little activity in comparison with the positive control. However, an ambiguous yellow zone was observed at these polyphenol fractions as shown in Figures 3.10-3.12 (plate C). Compounds such as verbascoside and luteolin-7-glucoside could possibly show only bacteriostatic effect. As they are water miscible compounds, the overlaid agar which consisted of water could partly dissolve those particular components in the crude fraction and caused the yellow zone. To determine their activity, the MIC values of the crude fraction (MB) and the main isolated compound, verbascoside, were determined by 96 well microplate assay.

All crude fractions failed to show antibacterial activity against the three Gram-negative bacteria. The agar-overlaid TLC plates were completely seen as a purple colour except the clear zone of positive control. These results corresponded to previously published findings. Diterpenoids and triterpenoids isolated from various *Salvia* species which were either inactive or active with MIC greater than 200 µM against Gram-negative bacteria (Moujir et al., 1996; Ulubelen, 2003; Kuzma et al., 2007; Shai et al., 2008; Wolska et al., 2010).

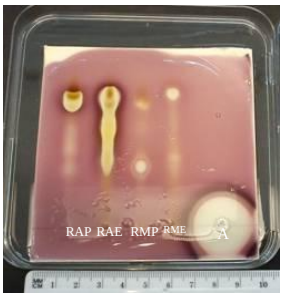

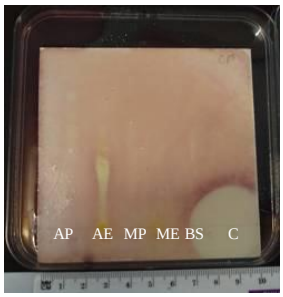

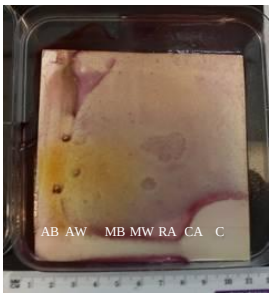

A. Root part B. Aerial part C. Aerial part

Figure 3.10A-C TLC-bioautographic method* against *Staphylococcus aureus* (ATCC 6571)

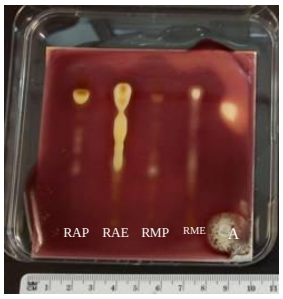

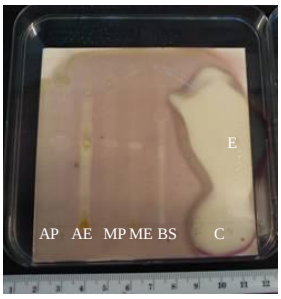

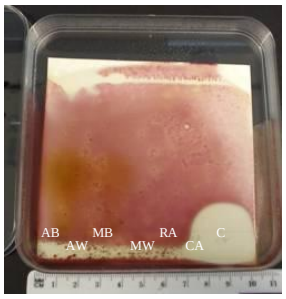

A. Root part B. Aerial part C. Aerial part

Figure 3.11A-C TLC-bioautographic method* against *Bacillus cereus* (ATCC 2599)

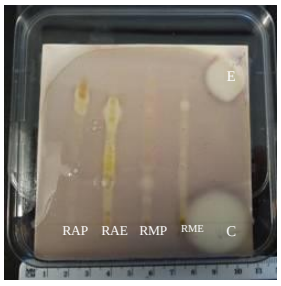

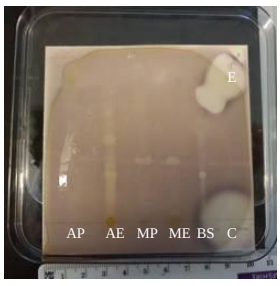

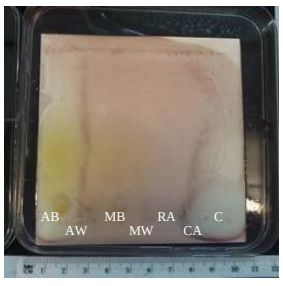

A. Root part B. Aerial part C. Aerial part

Figure 3.12A-C TLC-bioautographic method* against *Enterococcus faecalis* (ATCC 775)

*Conditions: (a) Crude fractions: 10 µl of 10 mg/ml in either methanol (AB, AW, MB, MW, RAB, RAW, RMB, RMW), or chloroform (AP, AE, MP, ME, RAP, RAE, RMP, RME). Crude fractions abbreviations see Table 3.2. (b) Standard: 10 µl caffeic acid (CA) solution (10 mg/ml in methanol), 10µl rosmarinic acid (RA) solution (10 mg/ml in methanol), and 10 µl β-sitosterol (BS) solution (10 mg/ml in chloroform). (c) Positive control: Inpregnated ampicillin disc (Oxoid), 5 µl Chloramphenicol (C) solution (50 mg/ml in methanol), and 5 µl Erythomycin (E) solution (50 mg/ml in methanol). (d) Mobile phase: chloroform, methanol (9:1) for plates A and B, and ethyl acetate, methanol, formic acid, water (50:3:3:6) for plate C.

3.3.2 Minimum inhibitory concentration (MIC)

MIC of crude fractions and isolated compounds were determined by the 96 well microplate dilution technique. Results are presented in Figures 3.14-3.16 and Table 3.4. Three crude fractions, AE (aerial part), RAE (root part), and RAP (root part), exhibited notable inhibition zones against three Gram-positive bacteria on the TLC-bioautographic method (Figures 3.10-3.12, plates A and B). MIC of these crude fractions corroborated the preliminary screening technique, particularly the two fractions from root parts. RAE and RAP showed MIC against *Enterococcus faecalis* (ATCC 775) at 62.5 µg/ml and 125 µg/ml respectively. Both fractions also inhibited the growth of the other two bacteria with MIC values at 250 µg/ml against *Staphylococcus aureus* (ATCC 6571) and 125 µg/ml against *Bacillus cereus* (ATCC 2599) as shown in Table 3.4. On the other hand, the aerial part crude fraction AE showed a less potent MIC of 500 µg/ml against *Enterococcus faecalis* (ATCC 775) and 1000 µg/ml against both *Staphylococcus aureus* (ATCC 6571) and *Bacillus cereus* (ATCC 2599). The polar crude fraction MB showed poor antibacterial activity with MIC value 2000 µg/ml which corresponded to results of the agar overlaid TLC assay.

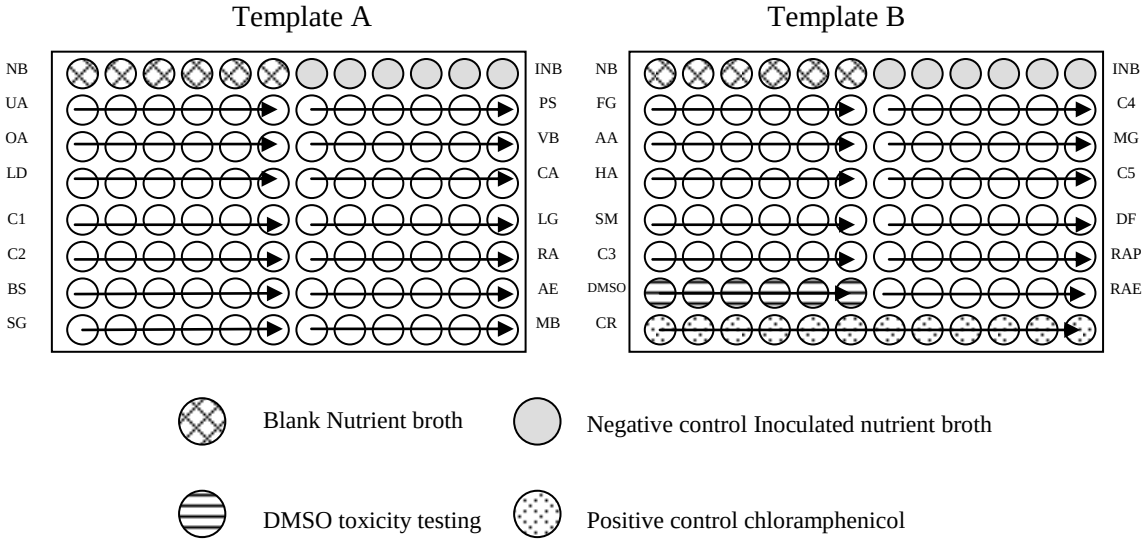

Figure 3.13 Templates of MIC 96 well microplate assay

A. B.

Figure 3.14A-B MIC microplate assay against *Staphylococcus aureus* (ATCC 6571)

A. B.

Figure 3.15A-B MIC microplate assay against *Bacillus cereus* (ATCC 2599)

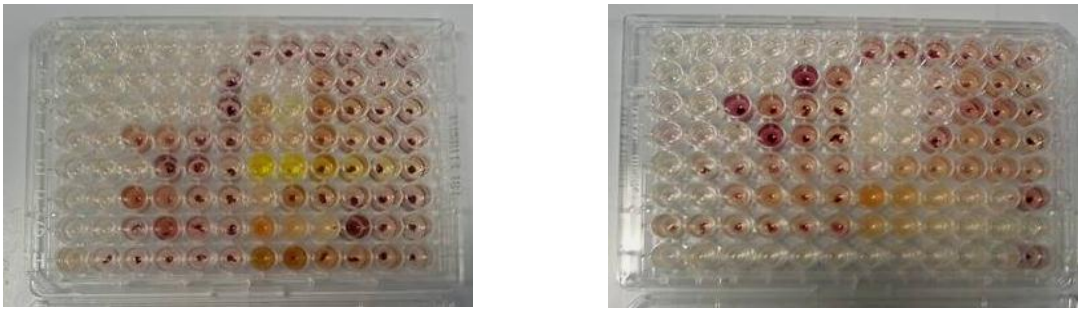

A. B.

Figure 3.16A-B MIC microplate assay against *Enterococcus faecalis* (ATCC 775)

Table 3.4. MIC of crude fractions and isolated compounds from *S. viridis* L. cv. Blue Jeans

Sample[a]		Rf value[b]	*Staphylococcus aureus* (ATCC 6571)	*Bacillus cereus* (ATCC 2599)	*Enterococcus faecalis* (ATCC 775)
AE crude fraction		-	1000	1000	500
UA	Ursolic acid	0.48	25	50	12.5
OA	Oleanolic acid	0.48	50	12.5	12.5
LD	Lup-20(29)-ene-2α-3β-diol	0.43	100	100	100
C1	Compound 1	0.63	100	100	50
C2	Compound 2	0.63	100	100	100
BS	β-Sitosterol	0.60	100	50	100
SG	β-Sitosterol glucoside	0.23	>200	100	>200
PS	A mixture of phytosterols	0.60	100	100	100
MB crude fraction		-	>2000	2000	2000
VB	Verbascoside	0.25	100	100	100
CA	Caffeic acid	0.80	100	100	100
LG	Luteolin-7-*O*-glucoside	0.25	100	100	200
RA	Rosmarinic acid	0.78	200	100	200
RAE crude fraction		-	250	125	62.5
FG	Ferruginol	0.84	25	50	25
AA	7α-Acetoxy-14-hydroxy-8,13-abietadiene-11,12-dione	0.79	100	200	100
HA	7α,14-dihydroxy-8,13-abietadiene-11,12-dione	0.79	100	100	50
SM	Salvinolonyl-12-methyl-ether	0.80	200	200	200
C3	Compound 3	0.75	200	200	100
C4	Compound 4	0.75	100	200	100
RAP crude fraction		-	250	125	125
MG	Microstegiol	0.80	50	100	100
C5	Compound 5	0.80	100	100	100
DF	1-Docasyl ferulate	0.80	200	200	>200
Chloramphenicol (μM)		-	7.8	1	2
DMSO (%)		-	>10	10	>10

[a]MIC of crude fractions (μg/ml), isolated compounds (μM). [b]mobile phases: ethyl acetate, methanol, formic acid, water (50:3:3:6) for MB, and chloroform, methanol (9:1) for AE, RAE, RAP.

The fractionation of these four crude fractions led to the isolation of terpenoids from aerial part (AE crude fraction), and diterpenoids from root part (RAE and RAP crude fractions). A novel terpenoid compound, compound 1, exhibited antibacterial activity against *Enterococcus faecalis* (ATCC 775) with MIC value of 50 µM. 7α,14-Dihydroxy-8,13-abietadiene-11,12-dione was also active against *Enterococcus faecalis* (ATCC 775) with MIC 50 µM. A diterpenoid from root part, ferruginol, also inhibited *Staphylococcus aureus* (ATCC 6571) and *Enterococcus faecalis* (ATCC 775) with MIC value of 25 µM and a higher MIC value of 50 µM against *Bacillus cereus* (ATCC 2599). Oleanolic acid inhibited those Gram-positive bacteria with MIC 12.5 µM against both *Bacillus cereus* (ATCC 2599) and *Enterococcus faecalis* (ATCC 775), and 50 µM against *Staphylococcus aureus* (ATCC 6571). Ursolic acid was also active with MIC 12.5-50 µM against the three tested bacteria. Verbascoside, and caffeic acid from the polar crude fraction were moderately active with MIC value at 100 µM against those three bacteria (Table 3.4). In addition, the solvent DMSO exhibited the toxicity at a concentration 10%.

INT (*p*-iodonitrotetrazolium chloride) solution was employed to detect the presence of bacteria on the agar overlaid TLC plates and also in the MIC microplate assay. INT was converted into formazan product by viable bacteria as shown in Figure 3.17. Besides INT, other tetrazolium salts such as MTT (thiazolyl blue) can also be used in this assay (Hamburger and Cordell, 1987; Eloff, 1998). However INT was preferred because it gave a pale yellow solution which facilitated the observation (Hamburger and Cordell, 1987) and also no colour change in the absence of bacteria (Eloff, 1998). The concentration of INT solution also influenced the shade of the purple colour. The optimum concentration of INT solution was 2 mg/ml to observe the purple colour within 30 minutes incubation period. Nevertheless, the more incubation time, the deeper violet was developed.

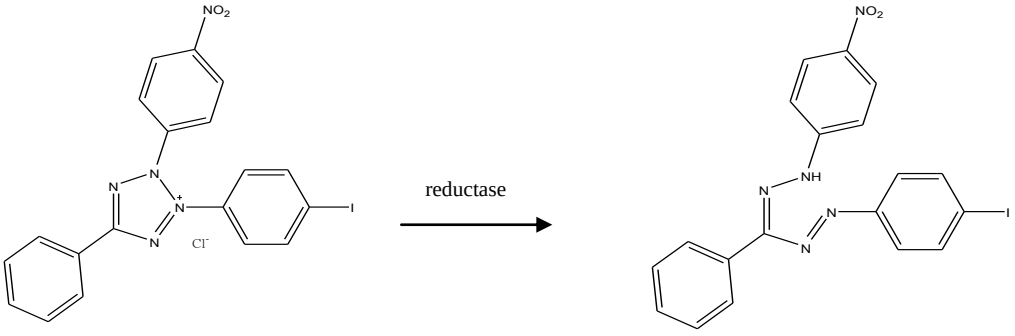

INT Formazan

Figure 3.17 The formation of deep purple formazan product from INT

3.4 Acetylcholinesterase inhibitory activity

Based on Ellman's method (Ellman et al., 1961), the enzyme (AChE) reacts with substrate (ACTI), and produces thiocholine and acetate. Then, the thiocholine rapidly reacts with the reagent DTNB to yield a yellow product as shown in Figure 3.18. The enzyme activity can be determined by measuring the increase of the absorbance at 405 nm.

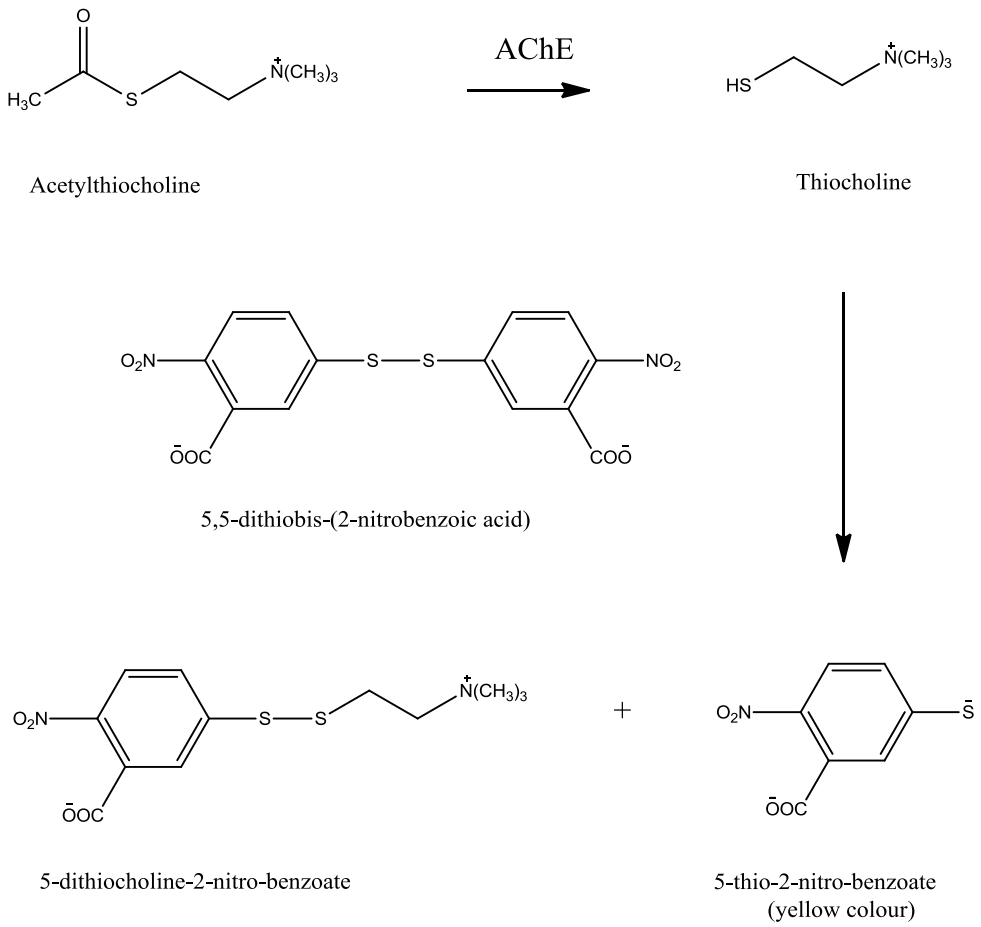

Figure 3.18 Reactions of colorimetric assay of Acetylcholinesterase activity (Ellman et al., 1961).

TLC-bioautographic methods exhibited the presence of yellow colour product (5-thio-2-nitro-benzoate) of the reaction on the plate background as shown in Figure 3.19. Physostigmine showed a white zone which denoted the inhibitory activity of the enzyme. Polar crude fractions showed no activity (Figure 3.19, plate B). In addition, polar compounds at certain Rf values partly dissolved in the process of spraying. However, no white spot was observed in the Rf value of the main constituent, verbascoside. On the other hand, white

spots/bands were seen in AE, RAP, RAE, RMP crude fractions including β-sitosterol (BS), ursolic acid (UA), and oleanolic acid (OA) as shown in Figure 3.19 (Plate A). These white spots were likely to be due to the deposit of lipophilic compounds on the plate as seen in AE crude fraction. To determine their activity, these fractions were further tested in a microplate assay.

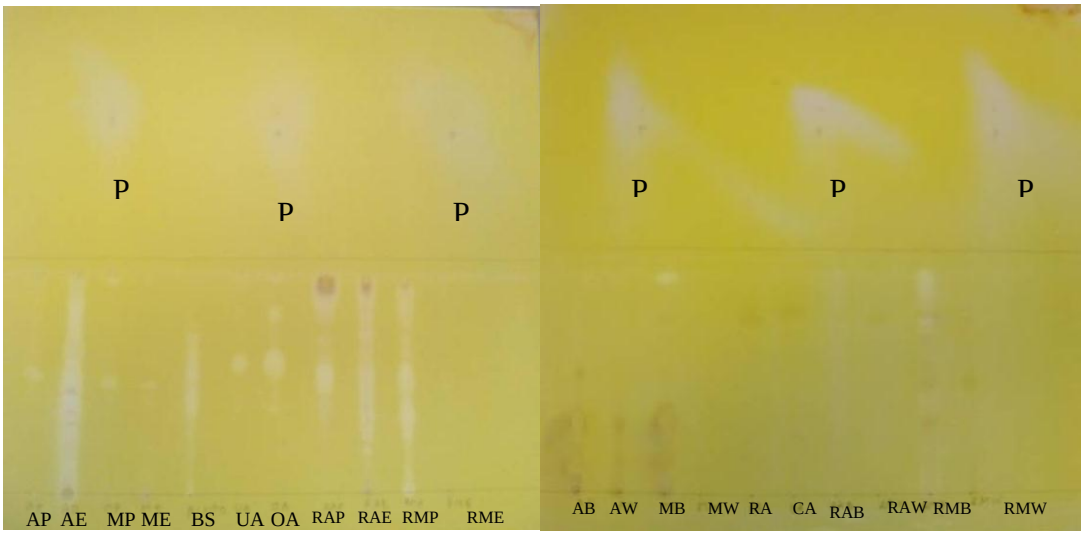

A. B.

Figure 3.19A-B TLC-bioautographic method of Acetylcholinesterase inhibitory activity.
Plate A mobile phase: chloroform:methanol (9:1); Plate B mobile phase: ethyl acetate:methanol:formic acid:water (50:3:3:6). Plate was developed by corresponded mobile phase for 10 cm, and physostigmine (P) was spotted before spraying. Crude fractions abbreviations are given in Table 3.2.

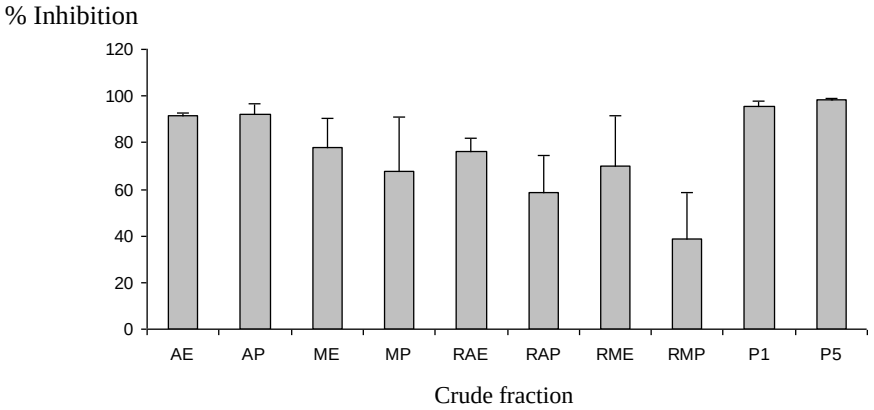

Figure 3.20 % AChE inhibitory activity of crude fractions. Data were reported as mean ± SD (n = 3). Physostigmine was used as a positive control at concentration of 1 µl (P1) and 5 µl (P5) of 3.6 mM.

As can be seen from Figure 3.20, AE and AP crude fractions showed % inhibitory more than 90% compare to 96% of physostigmine (14.4 µM, P1 1 µl of 3.6 mM). The others showed % inhibition more than 50% but RMP at 39%. However, these crude fractions were precipitated in the water based testing solvent which can cause inaccuracies in absorbance measurement.

3.5 Separation compounds from aerial part

The dried aerial part was macerated by two steps of solvents, acetone and methanol, in order to extract as many compounds as possible. Each of those crude extracts was further separated by liquid-liquid partition to achieve a preliminary fractionation. ^{1}H NMR spectra at 270 MHz of crude fractions were examined. Spectra of petroleum ether fractions (AP and MP) and ethyl acetate fractions (AE and ME) showed mainly aliphatic proton peaks. Compounds of petroleum ether fractions were certainly fats while ethyl acetate fractions were possibly comprised of fats and terpenoids. There were aromatic proton peaks in the water, and 1-butanol extract from both acetone and methanol fractions. Thus, this water fraction was further partitioned with 1-butanol. All aromatic compounds were successfully extracted from the water fraction (AW, MW) to 1-butanol fraction (AB, MB). NMR spectra of water fractions (after partitioned with 1-butanol) contained mainly sugar peaks while spectra of 1-butanol fractions showed aromatic glycoside peaks. According to the partition process, it can be concluded that 1-butanol was the suitable solvent for screening those polyphenol compounds from water fraction prior to the isolation process.

3.5.1 HPLC of aerial part crude fractions

Figure 3.21 shows HPLC chromatograms of MB and AB crude fractions. All the peaks were isolated using repeated semi-preparative HPLC; the main peak at retention time 9.2 min was identified as verbascoside (also known as acteoside). The chemical structures of all peaks were determined by MS and NMR as described below in structure elucidation section. Table 3.5 shows all identified compounds from MB of aerial part of *S. viridis* L. cv. Blue Jeans. Comparison between AB (Acetone-Butanol fraction) and MB (Methanol-Butanol fraction), as seen in Figure 3.21 shows a very similar pattern of compounds. However, the dried weight of AB (1.73 gm; 0.29% of dried aerial part) was 3.7 fold less than MB (6.37 gm; 1.06% of dried aerial part).

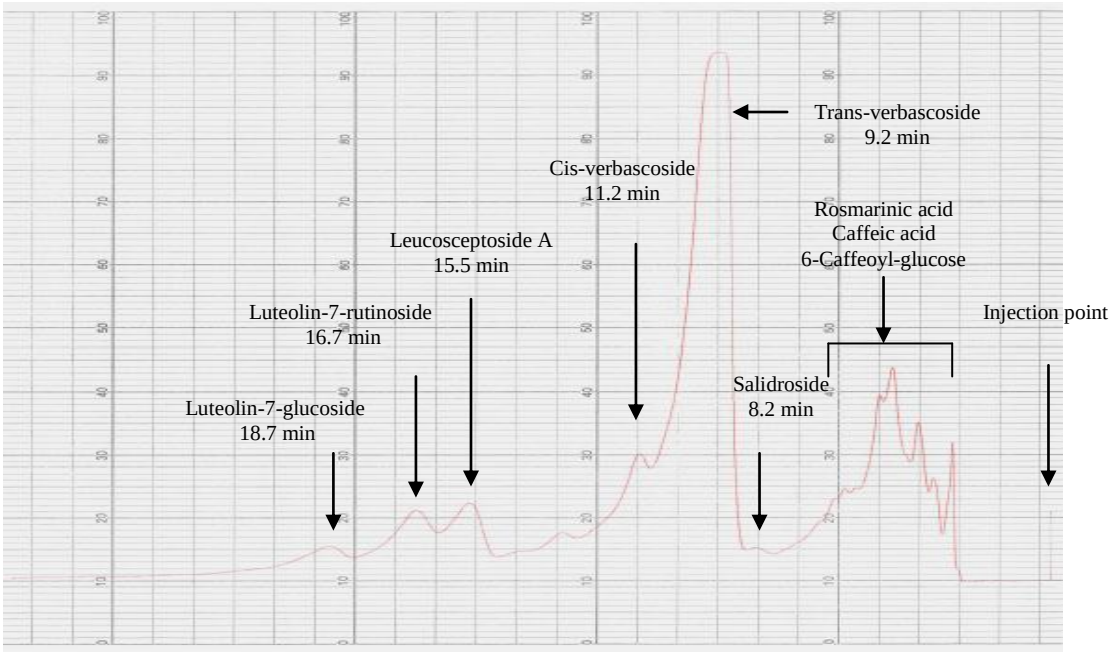

A. MB crude fraction

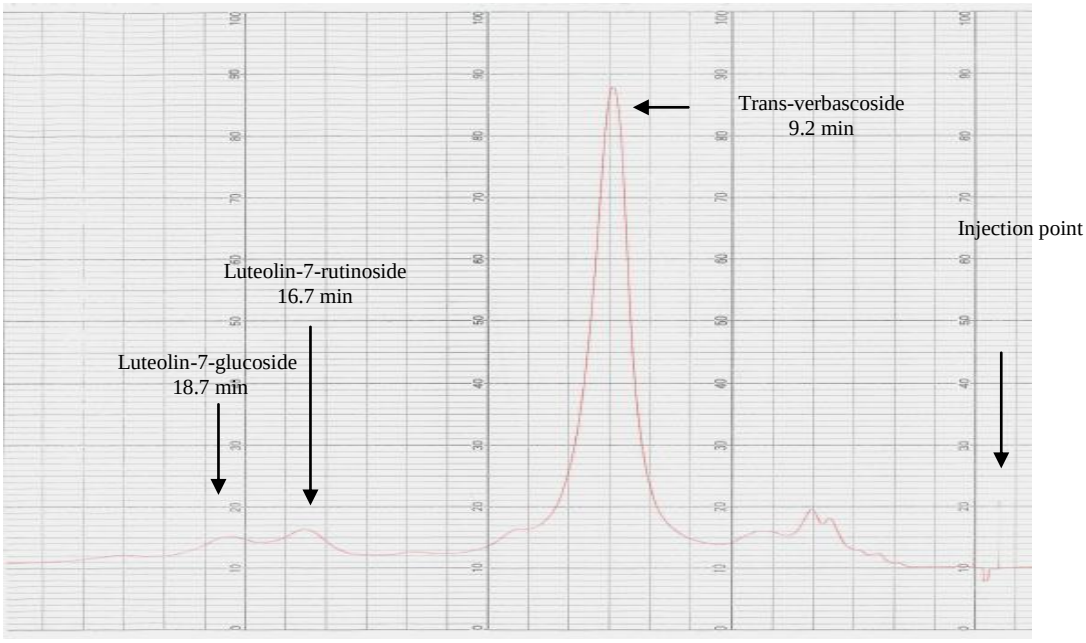

B. AB crude fraction

Figure 3.21A-B Chromatograms of MB and AB crude fractions from retention time 0-25 minutes. Condition: Phenomenex Luna PFP 250x10mm, injection volume 20 µl of 10 mg/ml, mobile phase methanol:water (45:55), flow rate 5 ml/min, wavelength at 330 nm.

Table 3.5 Isolated compounds from methanol-1-butanol (MB) crude fraction of aerial part

Retention time[a] (minute)	Identification	Formula	MW	Rf value[b]
4.6	Caffeic acid	$C_9H_8O_4$	180	0.75
4.5	Rosmarinic acid	$C_{18}H_{16}O_8$	360	0.78
5.7	6-*O*-Caffeoyl-glucose	$C_{15}H_{18}O_9$	342	0.25
8.2	Salidroside	$C_{14}H_{20}O_7$	300	0.25
9.2	Trans-verbascoside	$C_{29}H_{36}O_{15}$	624	0.25
11.2	Cis-verbascoside	$C_{29}H_{36}O_{15}$	624	0.25
15.5	Leucosceptoside A	$C_{30}H_{38}O_{15}$	638	0.25
16.7	Luteolin-7-*O*-rutinoside	$C_{27}H_{30}O_{15}$	594	0.13
16.7	Luteolin-7-*O*-α-rhamnosyl (1→6)-β-galactopyranoside	$C_{27}H_{30}O_{15}$	594	0.13
18.7	Luteolin-7-*O*-glucoside	$C_{21}H_{20}O_{11}$	448	0.23
19.5	Luteolin-7-*O*-galactoside	$C_{21}H_{20}O_{11}$	448	0.27
34.7	Apigenin-7-*O*-glucoside	$C_{21}H_{20}O_{10}$	432	0.25
39.5	Martynoside	$C_{31}H_{40}O_{15}$	652	0.25

[a]Mobile phase: methanol:water (45:50); column Phenomenex Luna PFP 250x10mm

[b]Mobile phase: ethyl acetate:methanol:formic acid:water (50:3:3:6); silica gel GF_{254}

3.5.2 Open column chromatography of aerial part crude fractions

Terpenoids were isolated from the AE fraction of aerial part including ursolic acid, oleanolic acid, lup-(20)29-ene-2α,3β-diol, two new triterpenoids, β-sitosterol, and β-sitosterol glucoside as shown in Table 3.6. A main spot at Rf 0.45 using chloroform:methanol (9:1) constituted a mixture of ursolic acid and oleanolic acid while the other one at Rf 0.60 was plant sterol, β-sitosterol (Figure 3.2A, track 5). Their structures are described below in section 3.6.

Table 3.6 Isolated compounds from acetone-ethyl acetate (AE) crude fraction of aerial part

Identification	Formula	MW	Rf value[a]
Compound 1	$C_{32}H_{52}O_3$	484	0.63
Compound 2	$C_{32}H_{52}O_3$	484	0.63
β-Sitosterol	$C_{29}H_{50}O$	414	0.60
Oleanolic acid	$C_{30}H_{48}O_3$	456	0.45
Ursolic acid	$C_{30}H_{48}O_3$	456	0.45
Lup-(20)29-ene-2α, 3β-diol	$C_{30}H_{50}O_2$	442	0.43
β-Sitosterol glucoside	$C_{35}H_{60}O_6$	576	0.23

[a]Mobile phase: chloroform:methanol (9:1); silica gel GF_{254}

3.6. Structure elucidations of isolated compounds from aerial part

3.6.1 Caffeic acid derivatives

The polar fractions, MB and AB contained a series of compounds of varied molecular weight with NMR signals in the aromatic region that were characteristic of caffeic acid.

3.6.1.1 Caffeic acid

Caffic acid ($C_9H_8O_4$; Figure 3.22) was identified by comparison of its NMR spectra with literatures values and an authentic sample. ^1H and ^{13}C NMR data of the isolated compound are shown in Table 3.7 and NMR spectra are shown in Appendix 1.

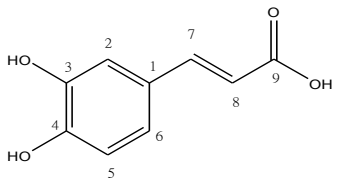

Figure 3.22 Caffeic acid

^{13}C NMR displayed 9 signals with 4 quaternary carbon and 5 methine groups from DEPT-135. ^1H NMR displayed 5 signals in the aromatic and alkene region with two noticeable signals of trans configuration, δ 6.20 ppm (H-8) and 7.51 ppm (H-7) with a

coupling constant of 16 Hz. Figure 3.24 shows the coupling pattern of a 3, 4-disubstituted phenyl ring with related coupling constants. H-5 (δ 6.77 ppm) and H-6 (δ 6.93 ppm) were coupled to each other with ^{3}J value 8 Hz. While H-2 (δ 7.03 ppm) displayed meta coupling to H-6 (δ 6.93 ppm) with ^{4}J value 2 Hz as a doublet, H-6 exhibited a doublets of doublet (J value = 8, 2 Hz) signal due to being coupled to both H-5, and H-2. COSY, NOESY and HMBC correlations are shown in Figure 3.23.

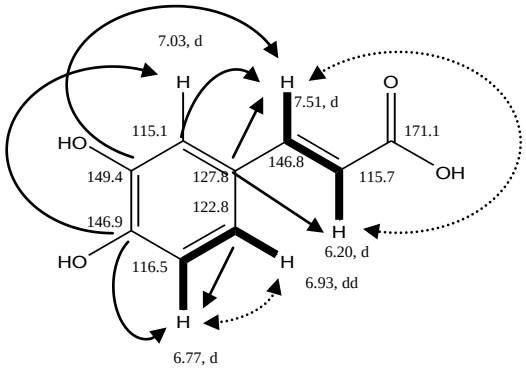

Figure 3.23 Salient signals of caffeic acid
COSY (bold line), NOESY (dot arrow), and HMBC (arrow)

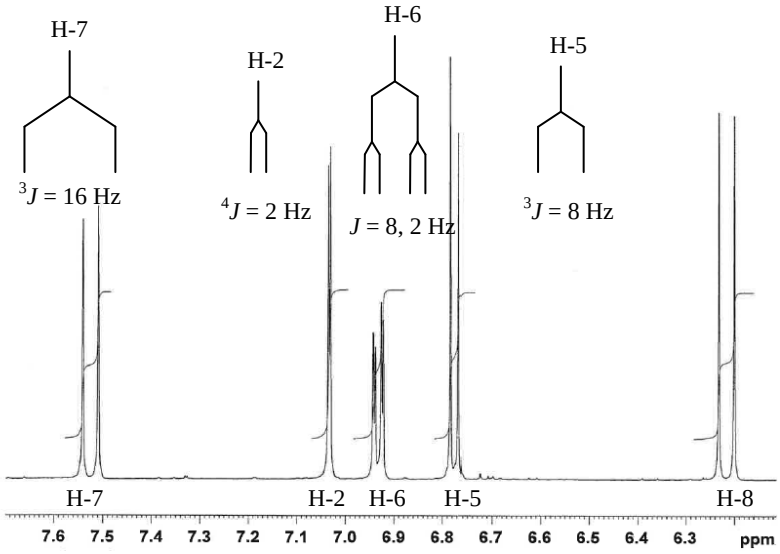

Figure 3.24 Coupling patterns of a 3, 4-disubstituted phenyl ring (^{1}H NMR, 500 MHz; in CD_3OD)

Caffeic acid has previously been reported in *S. viridis* L. (Kokkalou and Kapetanidis, 1988). It has commonly been found in other *Salvia* species (Lu and Foo, 2002), and in dietary sources such as orange, grape, berry, kiwi, and olives (Robbins, 2003).

Table 3.7 1D and 2D NMR data of caffeic acid (^{1}H, 500 MHz; ^{13}C, 125 MHz; in CD_3OD; δ in ppm; *J* in Hz)

Position	^{13}C	^{1}H	COSY	NOESY	HMBC
1	127.8	-	-	-	6.20 6.77 7.51
2	115.1	7.03 (d, *J* = 2)	-	6.20 7.51	6.93 7.51
3	146.9[§]	-	-	-	6.77 6.93 7.03
4	149.4[§]	-	-	-	6.20 7.51
5	116.5	6.77 (d, *J* = 8)	6.93	6.93	6.93
6	122.8	6.93 (dd, *J* = 8, 2)	6.77	6.20 6.77 7.51	6.77 7.03 7.51
7	146.8	7.51 (d, *J* = 16)	6.20	6.20	6.77 6.93 7.03
8	115.7	6.20 (d, *J* = 16)	7.51	7.51	6.93 7.51
9	171.1	-	-	-	-

[§]Interchangeable

3.6.1.2 Trans-verbascoside

Verbascoside or acteoside (Figure 3.25) was identified by 1D and 2D NMR spectra and by comparing its NMR spectra to previous reports (Andary et al., 1982; Owen et al., 2003; Li et al., 2005). The structure of verbascoside (or acteoside) is comprised of caffeic acid, a dihydroxy-phenylethyl part, and saccharides i.e., glucose and rhamnose. All 1D and 2D NMR data are given in Table 3.8.

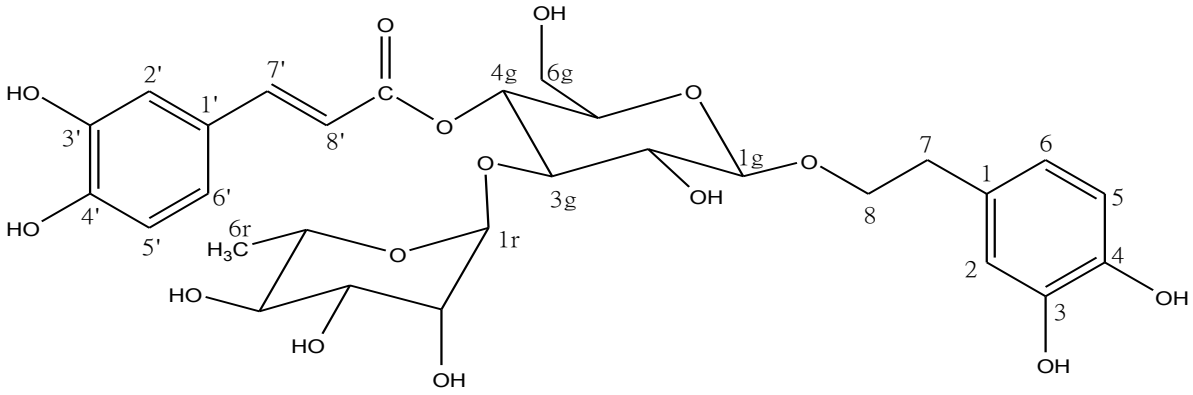

Figure 3.25 Verbascoside (or acteoside)

Aromatic protons from the caffeic acid and dihydroxyphenylethyl parts resonated at 6-8 ppm as seen in Figure 3.26. Signals of H-2 and H-5 showed splitting pattern as doublet with coupling constant 1.6 and 8 Hz respectively while signal of H-6 was doublet of doublet with coupling constant 8 and 1.6 Hz. Although the splitting patterns of aromatic protons from the caffeic acid and the dihydroxyphenylethyl part were similar, the aromatic protons of caffeic acid resonated slightly more downfield due to the conjugated double bond of the side chain. According to H-H COSY spectrum (Appendix 2.2), there were correlations between H-7' and H-8' of the caffeic acid moiety, and they were coupled to each other with J_{trans} 16 Hz.

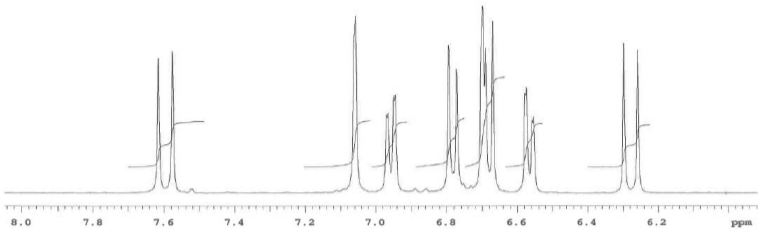

Figure 3.26 ^{1}H NMR expansion of verbascoside (400 MHz; CD_3OD)

Table 3.8 1D and 2D NMR data of trans-verbascoside (^{1}H 400 MHz; ^{13}C 100 MHz in CD_3OD; δ in ppm; *J* in Hz)

Position	^{13}C	^{1}H	COSY	NOESY	HMBC
1	131.4	-	-	-	2.78 3.70 4.05 6.68
2	117.1	6.69 (d, *J* = 1.6)	6.56	-	2.78 6.56
3	146.1[§]	-	-	-	6.68
4	144.6[§]	-	-	-	6.56 6.69
5	116.3	6.68 (d, *J* = 8)	6.56	-	-
6	121.2	6.56 (dd, *J* = 8, 1.6)	6.68 6.69	-	2.78 6.68 6.69
7	36.5	2.78 (2H, m)	3.70 4.05	3.70 4.05 6.56 6.69*	6.56 6.69
8	72.2	3.70 (m)	2.78 4.05	2.78	2.78 4.38
		4.05 (m)	2.78 3.70	2.78	
1'	127.6	-	-	-	6.29 6.78 7.60
2'	115.2	7.05 (d, *J* = 2)	6.95	-	6.95 7.60
3'	146.8[¶]	-	-	-	6.78 7.05
4'	149.7[¶]	-	-	-	6.78 6.95 7.05

Table 3.8 (continued)

Position	^{13}C	^{1}H	COSY	NOESY	HMBC
5'	116.5	6.78 (d, *J* = 8.2)	6.95	-	6.95 7.60
6'	123.2	6.95 (dd, *J* = 8.2, 2)	7.05 6.78	-	6.78 7.05 7.60
7'	148.0	7.60 (d, *J* = 16)	6.29	6.29†	6.95 7.05
8'	114.7	6.29 (d, *J* = 16)	7.60	7.60†	7.60
9'	168.3	-	-	-	4.91 6.29 7.60
1g	104.2	4.38 (d, *J* = 7.8)	3.38	-	3.38 3.70
2g	76.2	3.38 (t, *J* = 9)	4.38 3.81	-	3.53* 3.81
3g	81.6	3.81 (t, *J* = 9)	4.91 3.38	5.18	3.38 5.18
4g	70.5	4.91 (t, *J* = 9)	3.81* 3.53*	-	3.53* 3.81 5.18
5g	76.0	3.53* (m)	4.91 3.64* 3.56*	-	3.81
6g	60.9	3.49 (m) 3.64 (m)	3.53*	-	-
1r	103.0	5.18 (s)	3.91	3.91 3.81	3.81
2r	72.3	3.91 (d, *J* = 1.6)	5.18	5.18	3.29* 5.18
3r	72.0	3.58* (m)	3.56* 3.29	-	3.29* 5.18

Table 3.8 (continued)

Position	^{13}C	^{1}H	COSY	NOESY	HMBC
4r	73.8	3.29* (m)	3.58* 3.56*	1.09	1.09 3.91
5r	70.4	3.56* (m)	3.29* 1.09*	1.09	1.09 5.18
6r	18.4	1.09 (3H, d, *J* = 6.2)	3.56*	3.56* 3.29	3.29*

* Overlapped signal; § ¶ Interchangeable

† Coupling constant shows that these protons are trans with respect to each other. NOESY interaction may be an artefact.

g-glucose; r-rhamnose

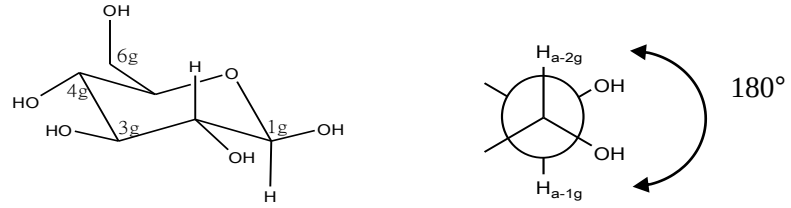

A. β-Glucose

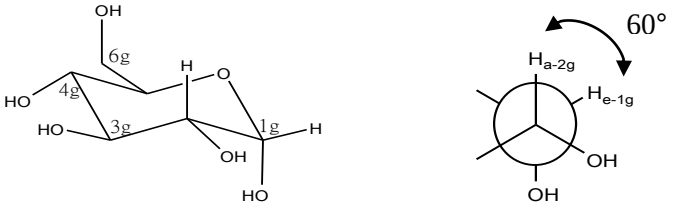

B. α-Glucose

Figure 3.27 β- and α-Configurations of D-glucose*

*Optical rotation and chiral NMR were not obtained, D-glucose commonly occurs (Dewick, 2009).

A downfield shift of glucose proton of H-4g, a triplet signal with coupling constant 9.3 Hz at δ 4.91 ppm was due to caffeic acid substitution. The anomeric glucose proton gave a doublet signal at δ 4.38 ppm with vicinal coupling 7.8 Hz that indicated axial, axial bond angle 180º between H-1g and H-2g as shown in Figure 3.27A. Therefore, the configuration of glucose is the β-anomer.

The methyl protons of rhamnose showed a conspicuous signal in the alkane region at δ 1.09 ppm as a doublet while the anomeric proton (H-1r) resonated at δ 5.18 ppm as a broad singlet. Many findings have reported the splitting pattern of the anomeric rhamnose proton as a doublet with a small coupling constant (1-1.8 Hz) (Andary et al., 1982; Owen et al., 2003; Li et al., 2005). According to the Karplus equation, a small vicinal coupling constant of H-1r and H-2r indicated a dihedral angle about 60º between them. Both α-, and β-anomers of rhamnose would give a small coupling constant as shown in Figure 3.28. However, NOESY showed that the anomeric rhamnose proton was close in space to both H-3g and H-2r, and examination of models suggested that rhamnose was present as the α-anomer (Figure 3.28A, and 3.29).

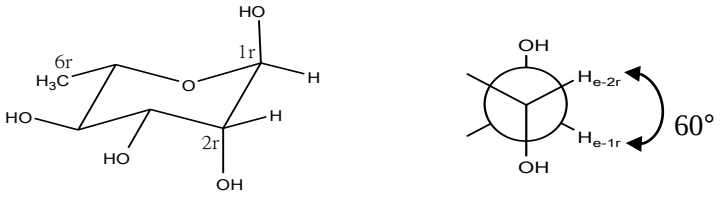

A. α-Rhamnose

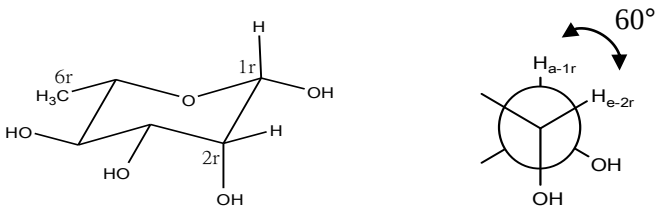

B. β-Rhamnose

Figure 3.28 α- and β-Configurations of L-rhamnose*

*Optical rotation and chiral NMR were not obtained, L-rhamnose commonly occurs (Dewick, 2009).

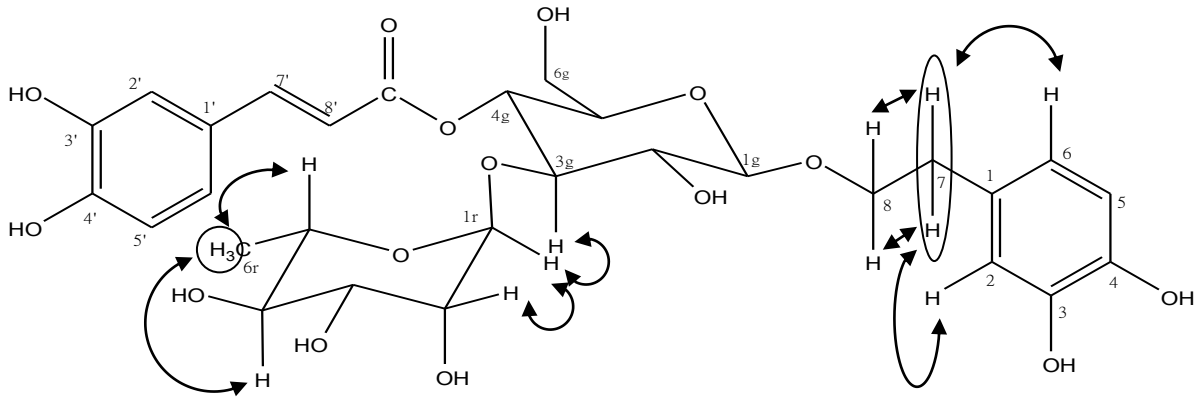

Figure 3.29 Selected NOESY correlations

The coupling pattern of H-2r and H-3r were characteristic of rhamnose besides the doublet of methyl proton. H-2r is β-equatorial orientation; therefore, its coupling constants between H-1r (J_{ee}), and H-3r (J_{ea}), would be small around 2-5 Hz (Williams and Fleming, 2008). The observed coupling constants of H-2r were 3, and 1.6 Hz which should result in the dd pattern but it could likely be seen as broad singlet as shown in Figures 3.31. On the other hand, the coupling pattern of H-3r with β-axial orientation would be dd because it was coupled to H-4r, and H-2r with $^3J_{aa}$, and $^3J_{ae}$ respectively. The expected coupling constant should be around 9-13 Hz (H-3r and H-4r, J_{aa}) and 2-5 HZ (H-3r and H-2r, J_{ae}) (Williams and Fleming, 2008), but H-3r of verbascoside was overlapped by other sugar peaks as shown in Figure 3.31. H-2g is typically a triplet with ^3J value 9 Hz in the β-anomer configuration from glucose.

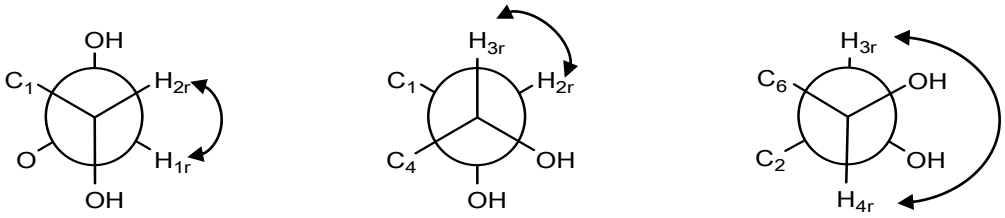

$^3J_{ee}$ ~ 2-5 Hz $^3J_{ae}$ ~ 2-5 Hz $^3J_{aa}$ ~ 9-13 Hz

Figure 3.30 Coupling constants of H-2r and H-3r

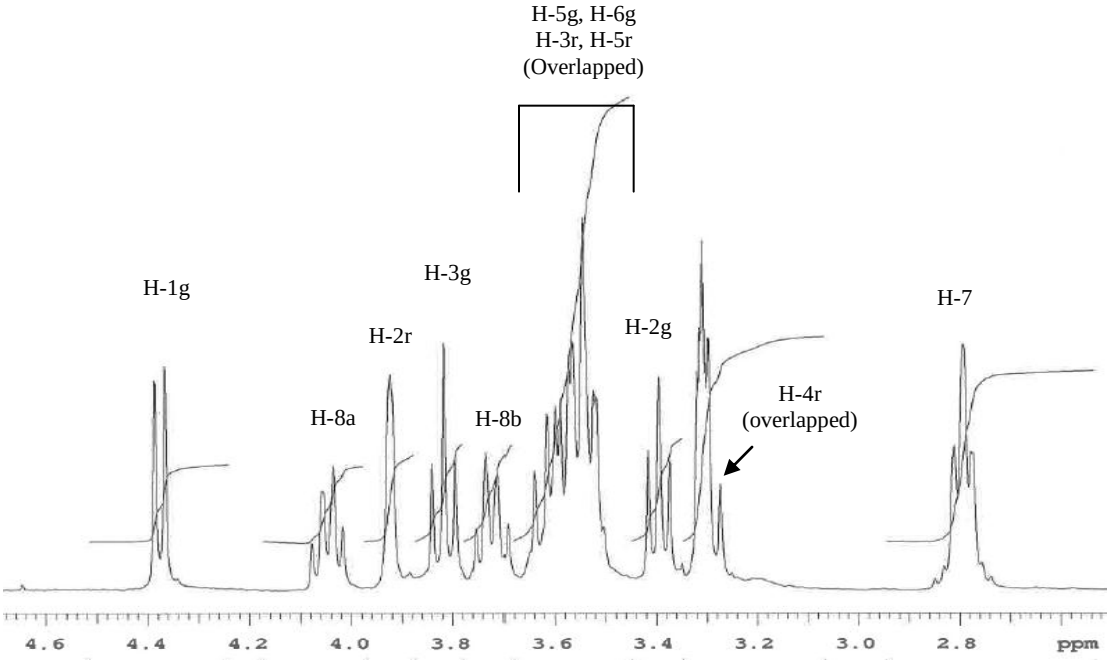

Figure 3.31 ^{1}H NMR expansion in sugar region of verbascoside (400 MHz; CD_3OD)

A cross peak of the anomeric rhamnose proton from H-H COSY (Figure 3.32) indicated a signal of H-2r at δ 3.91 ppm. The anomeric glucose proton was correlated to peak at δ 3.38 ppm which was a signal of H-2g. H-4g was correlated to two peaks at δ 3.81 ppm and δ 3.53 ppm, and the former had a cross peak with H-2g. Therefore, this triplet peak at δ 3.81 ppm must be H-3g. The signal of H-7 at δ 2.78 ppm related to two signals of H-8 at δ 3.70 ppm, and δ 4.05 ppm. These two proton of H-8 were correlated to each other as seen in H-H COSY (Figure 3.32). Moreover, HMQC indicated one signal of C at δ 72.2 ppm that matched those two signals of H-8 at δ 3.70 ppm, and 4.05 ppm. HMQC also showed the two protons with different chemical shifts of methylene group at glucose H-6g attached to one carbon at 60.9 ppm.

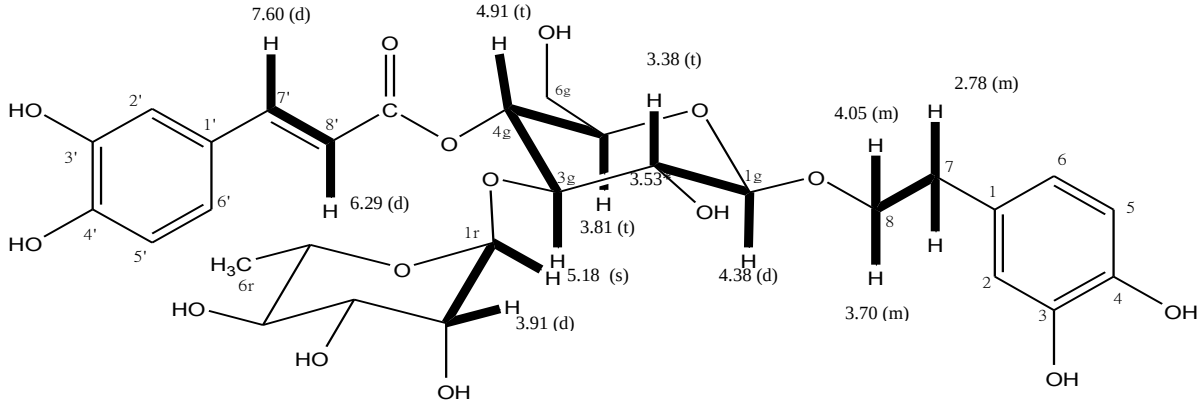

Figure 3.32 Selected H-H COSY correlations

Chemical shifts of carbon can be assigned by HMQC and HMBC. ^{13}C spectra (Appendix 2.3) indicated 29 signals of carbon with three signals of CH_2 and seven signals of quarternary carbon. Three quaternary carbon atoms belonged to the dihydroxyphenylethyl moiety, namely C-1, C-3, and C-4, and can be assigned by HMBC. There were three signals at δ 131.4 ppm, 144.6 ppm, and 146.1 ppm that were correlated to other protons in this moiety. The HMBC of H-7 involved four signals at δ 131.4 ppm, 121.2 ppm, 117.1 ppm, and 72.2 ppm, therefore, quaternary carbon C-1 must be a signal at δ 131.4 ppm. C-3 resonated at δ 146.1 ppm because of a weak correlation in HMBC between this signal and proton at H-6. Accordingly, C-4 was a signal at δ 144.6 ppm, however, these two signals of C-3 and C-4 may be interchangeable.

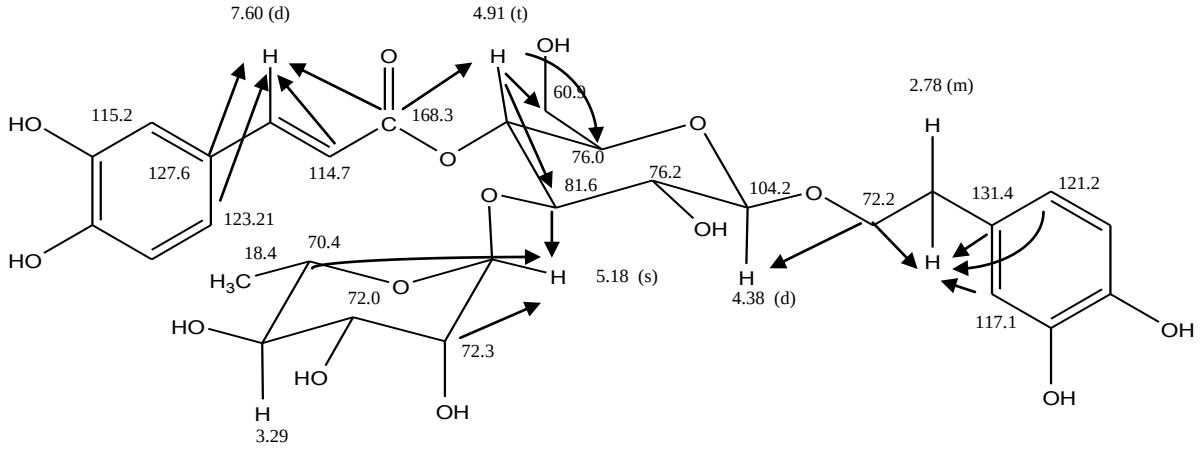

(A)

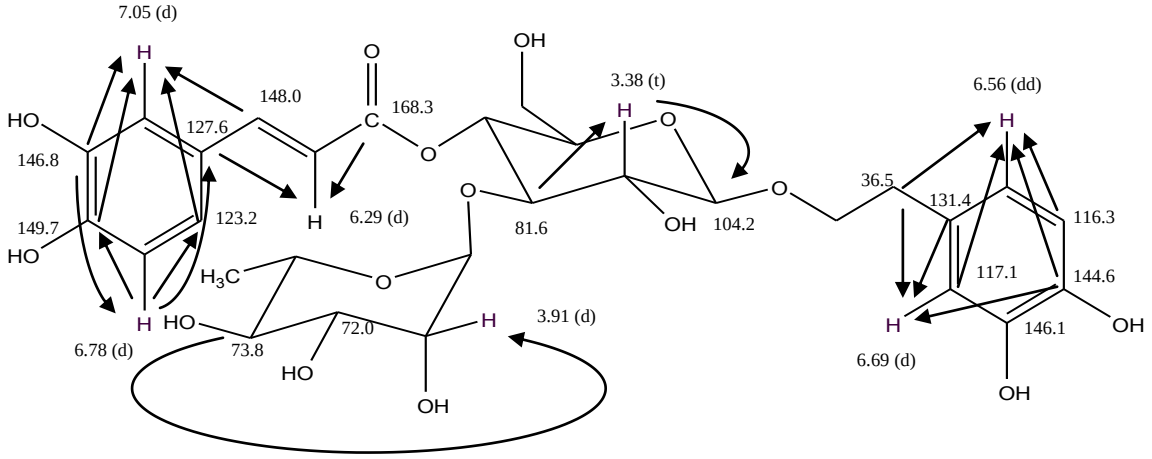

(B)

Figure 3.33A-B Selected HMBC correlations

The other quaternary carbon signals were at δ 127.6 ppm, 146.8 ppm, 149.7 ppm, and 168.3 ppm and belonged to the caffeic acid group. HMBC correlated a signal at δ 168.3 ppm to three proton of H-7', H-8', and H-4g, consequently, this was a downfield signal of carbonyl carbon. A signals of C-1' at δ 127.6 ppm had a strong correlation to H-7', H-8', H-5' while a weak HMBC correlation between a signal at δ 146.8 ppm and H-6' indicated C-3', and then C-4' resonated at δ 149.7 ppm. However, the signals of C-3' and C-4' may be interchangeable.

Verbascoside can be classified according to its structure as a phenylethanoid glycoside (Jimenez and Riguera, 1994) or as a phenylpropanoid (Kurkin, 2003). Ellis (1983) reported that phenylalanine was the main precursor of the caffeic acid moiety while the

dihydroxyphenylethanol moiety was derived from either tyrosine or tyramine in cell cultures of *Syringa vulgaris* L. provided with various radioactive precursors as a starter to synthesize verbascoside.

Verbascoside is widely distributed in plants from a variety of families such as Lamiaceae, Plantaginaceae, Oleaceae. This is however, the first report of its occurrence in the genus *Salvia*. Its bioactivities have been extensively studied as shown in Table 3.9. As can be seen, many and various activities have been assigned to this compound including radical scavenging and metal chelating activities. For example, the Fenton reaction was used to induce DNA damage by generating hydroxyl radical (OH·) from hydrogen peroxide and metal ion (either Fe(II), or Fe(III)) In the presence of verbascoside, DNA damage was inhibited, possibly due to the complex between verbacoside and metal ion (Zhao et al., 2005). Besides Fe(II) or Fe(III), Kang et al. (2003b) suggested that verbascoside might chelate the zinc ion of Angiotensin Converting Enzyme (ACE), resulting in an inhibitory effect.

A comparison of cytotoxic activity of phenylpropanoid glycosides against cancer cell lines was reported by Saracoglu et al. (1995). The authors suggested the ortho-dihydroxy aromatic systems were responsible for the cytotoxic and cytostatic activities because leucosceptoside A, and martynoside were inactive against all tested cell lines. Verbascoside showed appreciable IC_{50} values of 0.99 µM and 0.47 µM against rat hepatoma, and sarcoma respectively. It also inhibited human epithelial carcinoma cell growth with IC_{50} 0.13 µM.

Table 3.9 Biological activities of verbascoside

Activity	Source of verbascoside	Reference
Cytoprotective against UV-C induced necrosis	*Syringa vulgaris* L., Oleaceae	Kostyuk et al., 2008; Pastore et al., 2009
Antioxidant	*Orobanche caerulescens* Steph., Orobanchaceae	Chiou et al., 2004
	Plantago bellardii All., Plantaginaceae	Galvez et al., 2005
	Caryopteris incana (Thunb.) Miq., Verbenaceae	Gao et al., 1999
Antibacterial activity	*Verbascum sinuatum* L., Scrophulariaceae	Senatore et al., 2007
	Buddleja cordata Kunth, Loganiaceae	Avila et al., 1999
Protection of DNA damage by radicals from Fenton reaction	*Pedicularis striata* Pall, Scrophulariaceae	Zhao et al., 2005
Anti-inflammatory activity	*Scrophularia scorodonia* L., Scrophulariaceae	Diaz et al., 2004
	Plantago lanceolata L., Plantaginaceae	Murai et al., 1995
	Forsythia viridissima Lindley, Oleaceae	Kimura et al., 1987
Anti-hepatotoxic activity against carbon tetrachloride	*Buddleia officinalis* Maxim., Loganiaceae	Lee et al., 2004
	Cistanche deserticola Y.C. Ma, Orobanchaceae	Xiong et al., 1998
Angiotensin converting enzyme (ACE) inhibition	*Clerodendron trichotomum* Thunb., Verbenaceae	Kang et al., 2003b

Table 3.9 (Continued)

Activity	Source of verbascoside	Reference
Cardioactivity	*Eremophila alternifolia* R. Br., Myoporaceae	Pennacchio et al., 1999
Inhibitor of protein kinase C	*Lantana Camara* L., Verbenaceae	Herbert et al., 1991
Cytotoxic	*Phlomis armeniaca* Willd, and *Scutellaria salviifolia* Bentham, Labiatae	Saracoglu et al., 1995; Inoue et al., 1998
	Castilleja linariaefolia Benth., Scrophulariaceae	Pettit et al., 1990
Inhibition of oxidative hemolysis of erythrocytes	*Pedicularis striata* Pall, Scrophulariaceae	Ji et al., 1993
Aldose reductase inhibition	*Plantago asiatica* L., Plataginaceae	Ravn et al., 1990
Phytoalexin and antibacterial activity	*Rehmannia glutinosa* var. *purpurea* Makino, Phrymaceae	Shoyama et al., 1987

3.6.1.3 Cis-verbascoside

The HPLC chromatogram in Figure 3.21 shows a shoulder on the peak of trans-verbascoside at retention time 11.2 min. This was separately collected and further identified as a mixture of trans- and cis-verbascoside by NMR and HR-ESI-MS spectroscopic data, and also by comparison with previous published literature (Nishimura et. al, 1991). NMR spectra exhibited 2 sets of signals, however, certain dissimilar signals were observed. Two pairs of doublets were individually coupled to each other with coupling constant 16 Hz, and 12.8 Hz. The first pair, δ 6.29 and 7.60 ppm, showed ^{3}J value 16 Hz and also correlated to aromatic signals of the caffeic acid moiety as described in trans-verbascoside. The second pair, δ 5.75 ppm and 6.86 ppm, exhibited ^{3}J value 12.8 Hz, and showed the same correlation pattern to certain aromatic signals as the trans-isomer. The dihedral angle of vicinal trans protons is 180°, and the cis protons was 0° as shown in Figure 3.34.

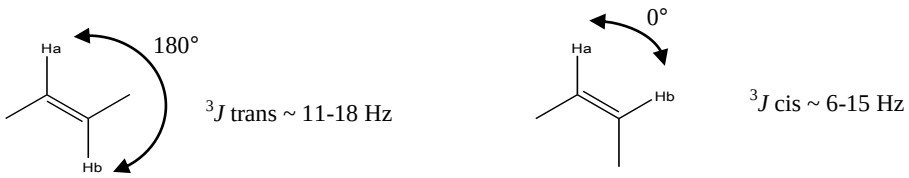

Figure 3.34 Vicinal coupling constant of trans- and cis isomer

The coupling constant of 180° dihedral angle is normally around 11-18 Hz while the coupling constant of 0° dihedral angle is approximately 6-15 Hz (Pavia et al., 2009). The observed coupling constant of cis- isomer at 12.8 Hz accorded with previous findings for cis-verbascoside (Nishimura et al., 1991; Budzianowski and Skrzypczak, 1995).

The cis double bond affected the chemical shifts of protons in caffeic acid moiety particularly H-2'. It was deshieled at δ 7.52 ppm in cis isomer while it was at δ 7.05 ppm in trans. The arrangement of cis-configuration may cause the downfield chemical shift of H-2' by an anisotropic effect of the carbonyl group as shown in Figure 3.35. In addition to the change of coupling constant, the cis isomer showed a substantial upfield shift of both alkene protons to values more closely resembling the alkene in a non-aromatic system. This may be because steric hindrance of the bulky sugar moieties forces the aromatic group out of a conformation in which the whole cinnamoyl group can be coplanar. All HMBC, COSY, and NOESY correlations were the same as trans-verbascoside as described above. NMR data comparison between trans- and cis-isomers are given in Table 3.10. NMR spectra of cis-isomer are presented in Appendix 3.

Table 3.10 NMR data of trans- and cis-verbascoside (^{1}H, 400 MHz; ^{13}C, 100 MHz; in CD_3OD; δ in ppm; *J* in Hz)

Moiety	Position	Trans-verbascoside		Cis-verbascoside	
		δ_C	δ_H	δ_C	δ_H
Dihydroxyphenyl ethyl	1	131.4	-	131.4	-
	2	117.1	6.69 (d, 1.6)	116.3	6.69 (d, 2)
	3	146.1[a]	-	146.1[c]	-
	4	144.6[a]	-	144.6[c]	-
	5	116.3	6.68 (d, 8)	116.5	6.73 (d, 8.2)
	6	121.2	6.56 (dd, 8, 1.6)	121.2	6.55 (dd, 8.2, 2)
	7	36.5	2.78 (2H, m)	36.6	2.77 (2H, m)
	8	72.2	3.70 (m)	73.9	3.70 (m)
			4.05 (m)		4.02 (m)
Caffeic acid	1'	127.6	-	128.0	-
	2'	115.2	7.05 (d, 2)	119.0	7.52 (d, 1.5)
	3'	146.8[b]	-	146.8[d]	-
	4'	149.7[b]	-	149.7[d]	-
	5'	116.5	6.78 (d, 8.2)	115.2	6.77 (d 8.2)
	6'	123.2	6.95 (dd, 8.2, 2)	125.9	7.09 (dd, 8.2, 2)
	7'	148.0	7.60 (d, 16)	148.6	6.86 (d, 12.8)
	8'	114.7	6.29 (d, 16)	114.7	5.75 (d, 12.8)
	9'	168.3	-	168.3	-
Glucose	1g	104.2	4.38 (d, 7.8)	104.1	4.34 (d, 7.8)
	2g	76.2	3.38 (t, 9)	76.1	3.35 (t, 8.2)
	3g	81.6	3.81 (t, 9)	81.9	3.76 (t, 9.4)
	4g	70.5	4.91 (t, 9)	70.6	4.92*
	5g	76.0	3.53*	76.0	3.53*
	6g	60.9	3.49*	62.3	3.49*
			3.64*		3.64*
Rhamnose	1r	103.0	5.18 (s)	103.1	5.16 (s)
	2r	72.3	3.91 (d, 1.6)	72.3	3.92 (br s)
	3r	72.0	3.58*	72.0	3.58*
	4r	73.8	3.29* (m)	73.9	3.32* (m)
	5r	70.4	3.56*	70.4	3.56*
	6r	18.4	1.09 (3H, d, 6.2)	18.2	1.16 (3H, d, 6.2)

*Overlapped signal; [a, b, c, d] Interchangeable

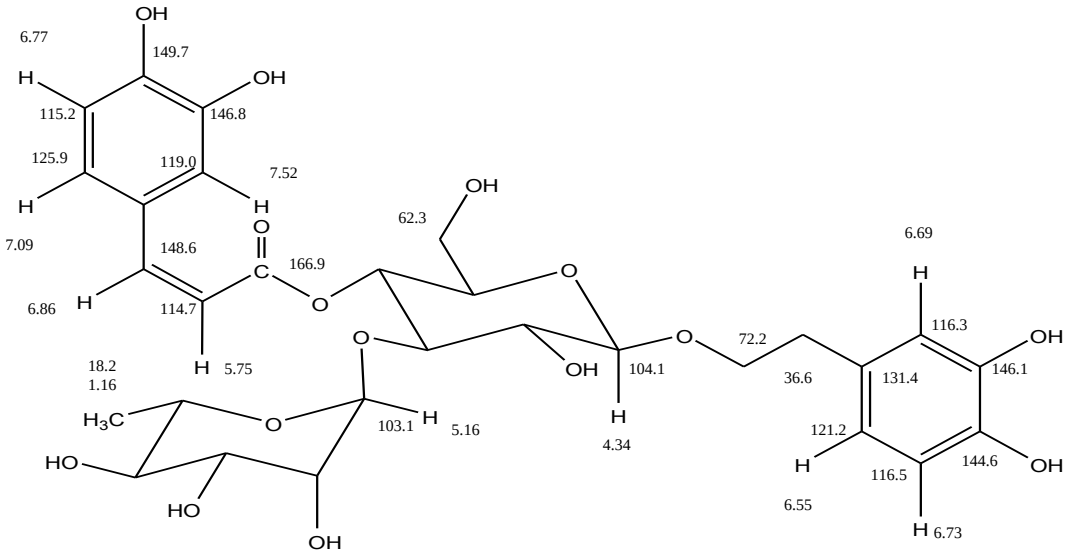

Figure 3.35 Salient chemical shifts of cis-verbascoside

On the basis of the integrals of the alkene protons, the cis isomer comprised about 67% of the mixture (^{1}H NMR spectra ratio cis:trans, 2:1; Appendix 3.1). Previous published literature reported the ratio of cis:trans content as 1:9 (Nishimura et al., 1991), and 1:6 (Budzianowski and Skrzypczak, 1995). Cis-isomer was suggested to be converted to trans-isomer in daylight (Nishimura et al., 1991).

In the present study, the conversion of trans- to cis-isomer was observed under UVA (wavelength 350-400 nm) light at 500 kJ/m^2. This UVA intensity is equivalent to the amount on a cloudless summer day around noon at a northern latitude of 30-35^o (Frederick and Lubin, 1988). Result showed trans-isomer was able to convert to cis-isomer at amount of approximately 30% under this condition as shown in Figures 3.37-3.38. UVA can cause the transition of an electron from the ground state to the excited state of the olefinic bond and initiate the radicals as shown in Figure 3.36. Then, the rotation of this single bond followed by reformation of the double bond results in the cis-configuration.

Whist it is clearly possible that cis-derivatives may arise by photoisomerisation, recent studies have demonstrated that in the biosynthesis of coumarins in Cassava, trans→cis isomerisation of cinnamic acid intermediate involves a non-light dependent, enzymic process (Bayoumi et al., 2008). Therefore, cis-verbascoside may not be an artifact of the isolation process.

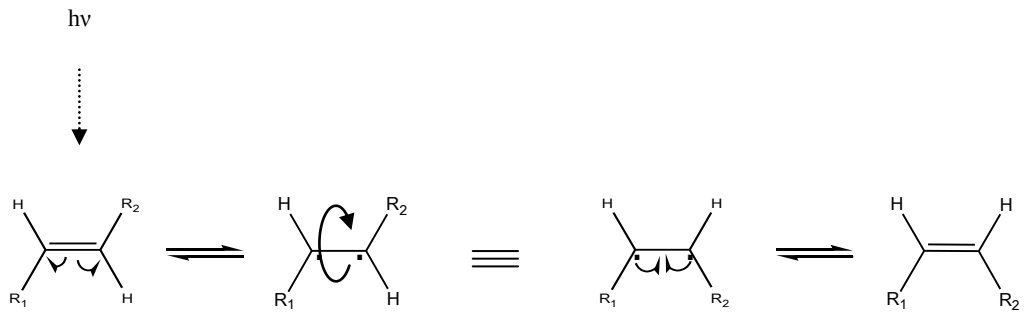

Figure 3.36 The conversion of trans- to cis-isomer by UVA

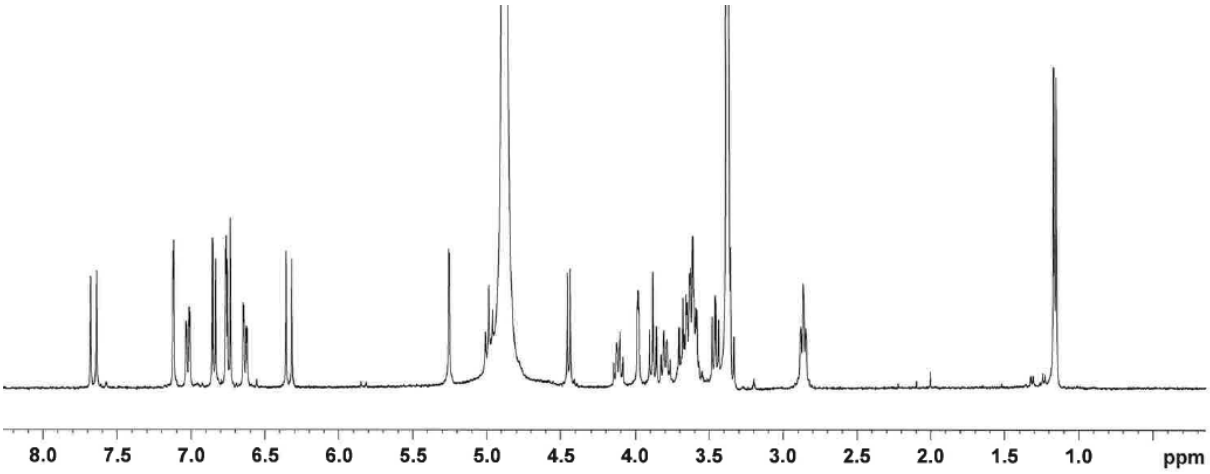

Figure 3.37 ^{1}H NMR spectra of trans-verbascoside (400 MHz; CD_3OD) before irradiation

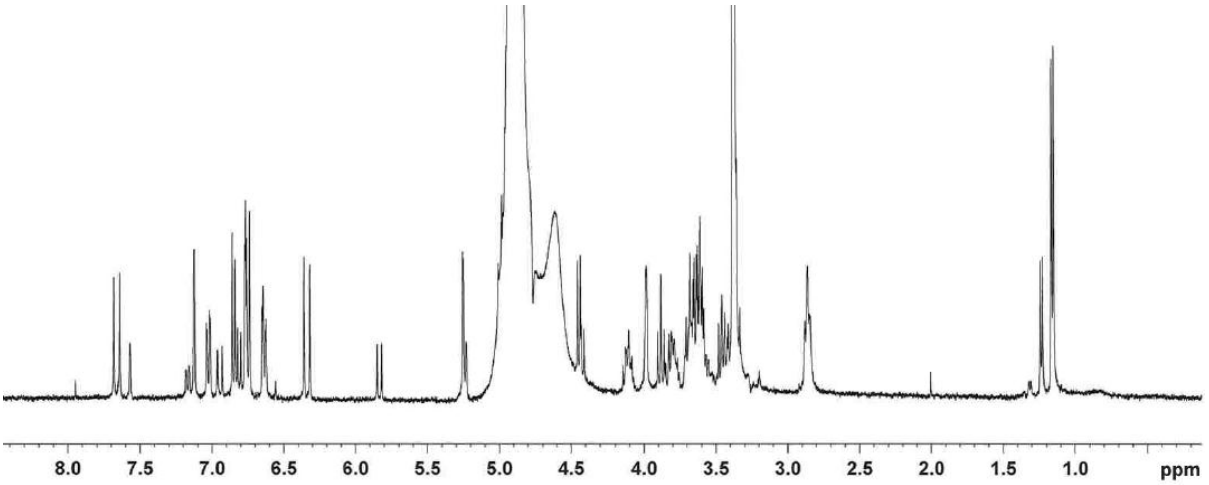

Figure 3.38 ^{1}H NMR spectra of a mixture of trans- and cis-verbascoside (400 MHz; CD_3OD) after irradiation by UVA light.

3.6.1.4 Leucosceptoside A

The MS of leucosceptoside A ($C_{30}H_{38}O_{15}$; Figure 3.39) showed a molecular mass 14 mass units greater than verbascoside ^{1}H and ^{13}C NMR data are shown in Table 3.11 and NMR data are given in Appendix 4.

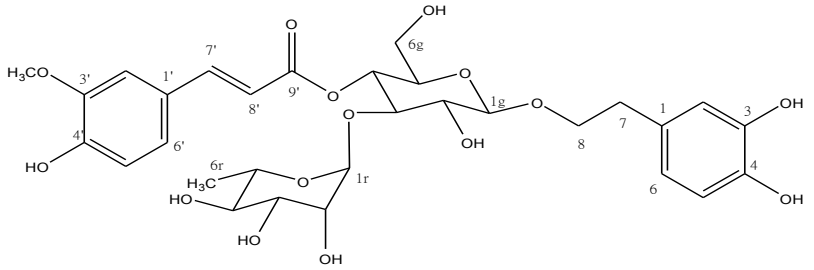

Figure 3.39 Leucosceptoside A

Both ^{1}H and ^{13}C signals resonated in the same pattern as verbascoside but this compound showed an additional 3H singlet at δ 3.89 ppm in the ^{1}H NMR spectrum (Appendix 4.1), and an extra carbon signal at δ 56.5 ppm in the ^{13}C spectrum (Appendix 4.3). This singlet exhibited a NOESY correlation to H-2' at δ 7.20 ppm, and also a HMBC cross peak to C-3' at δ 149.5 ppm of acyl moiety as shown in Figure 3.40. Therefore, the methoxyl group was likely substituted at C-3' which referred to a ferulic acid acyl group instead of caffeic acid. Verbascoside with a feruloyl moiety is known as leucosceptoside A. The configurations of glucose and rhamnose moieties were the same as verbascoside as described above.

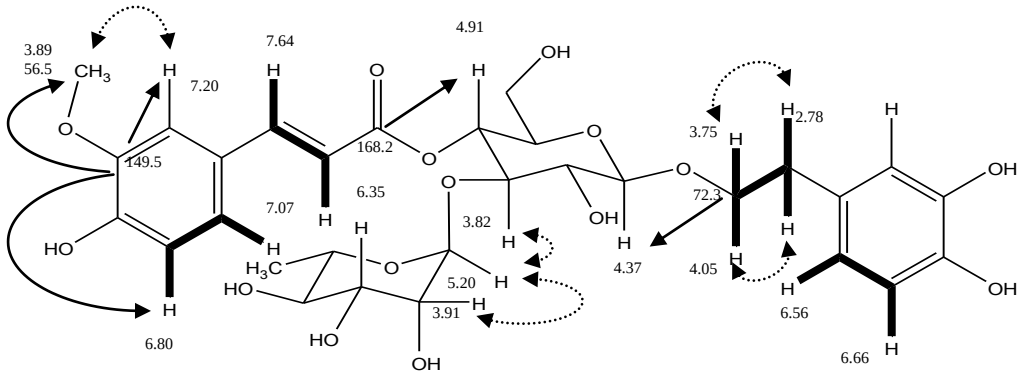

Figure 3.40 Certain salient signals of leucosceptoside A
H-H COSY (bold line), NOESY (dot arrow), HMBC (arrow)

Table 3.11 1D and 2D NMR data of leucosceptoside A (^{1}H, 500 MHz; ^{13}C, 125 MHz; in CD_3OD; δ in ppm; *J* in Hz)

Position	^{13}C	^{1}H	COSY	NOESY	HMBC
1	131.5	-	-	-	2.82 6.66 6.69
2	117.1	6.69 (d, *J* = 2)	-	-	2.78 6.56
3	146.2	-	-	-	6.66 6.69
4	144.5	-	-	-	6.56 6.69
5	116.3	6.66 (d, *J* = 8)	6.56	6.56	6.56
6	121.3	6.56 (dd, *J* = 8, 2.5)	6.66	6.66	2.78 6.69
7	36.6	2.78 (2H, m)	3.75* 4.05	3.75* 4.05	6.56 6.69
8	72.3	3.75* (m)	2.78 4.05	2.78	2.78 4.37
		4.05 (m)	2.78 3.75*	2.78 3.75*	
1'	127.7	-	-	-	6.35 6.80
2'	111.8	7.20 (d, *J* = 2)	-	3.89	7.07 7.64
3'	149.5	-	-	-	3.89 6.80 7.20
4'	150.9	-	-	-	6.80 7.07 7.20
5'	116.5	6.80 (d, *J* = 8)	7.07	7.07	-
6'	124.4	7.07 (dd, *J* = 8, 2)	6.80	6.80	7.20 7.64

Table 3.11 (continued)

Position	^{13}C	^{1}H	COSY	NOESY	HMBC
7'	147.9	7.64 (d, *J* = 16)	6.35	6.35	7.07 7.20
8'	115.1	6.35 (d, *J* = 15.5)	7.64	7.64	7.64
9'	168.2	-	-	-	4.91 6.35 7.64
1g	104.2	4.37 (d, *J* = 8)	3.40	-	3.40
2g	76.2	3.40 (t, *J* = 9)	4.37	-	3.82 4.91*
3g	81.5	3.82* (t, *J* = 9)	3.40 4.91*	-	3.40 4.91* 5.20
4g	70.7	4.91*	3.54* 3.82*	3.54*	3.54* 3.82* 5.20
5g	76.1	3.54* (m)	-	-	4.91*
6g	62.4	3.64* (m)	3.54*	*	4.91*
		3.54* (m)	3.64*	*	
1r	103.0	5.20 (br s, *J* = 1.5)	3.91	3.82* 3.91	3.82*
2r	72.4	3.91 (dd, *J* = 3.5, 2)	5.20	5.20	5.20
3r	72.1	3.56* (m)	-	-	5.20
4r	73.8	3.30* (m)	-	-	1.09 3.59*
5r	70.4	3.59* (m)	-	-	1.10
6r	18.4	1.09 (d, *J* = 6)	3.59*	3.59*	3.30*
3'-OCH_3	56.5	3.89 (3H, s)	-	7.20	-

*Overlapped signal; g- glucose; r-rhamnose

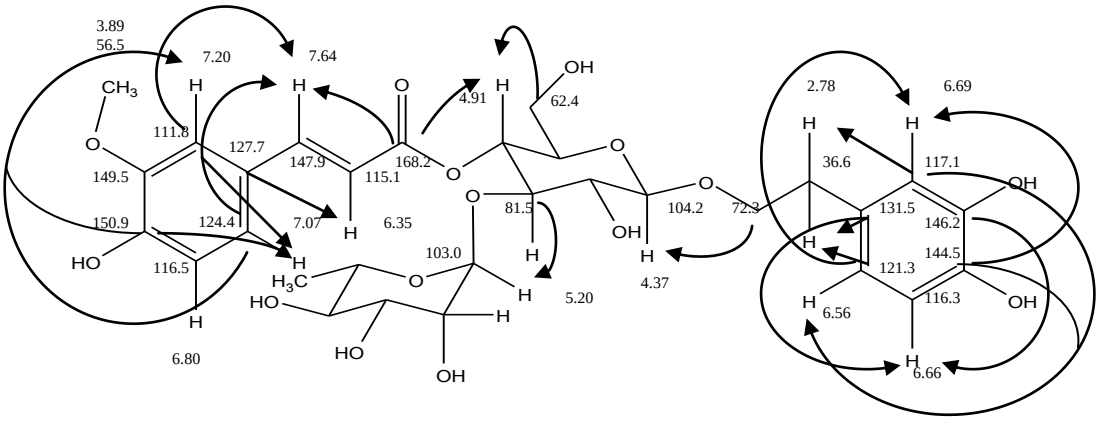

Figure 3.41 Selected HMBC correlations of leucosceptoside A

Leucosceptoside A has not been reported from the genus *Salvia* before. It was reported together with verbascoside and/or martynoside in *Clerodendron trichotomum* Thunb. (Kim et al., 2001). *Leucosceptrum japonicum* (Miq.) Kitamura et Murata (Miyase et al., 1982), *Sideritis perfoliata* L. subsp. *perfoliata* (Charami et al., 2008), *Lippia canescens* Kunth (Abe et al., 2002), and *Plantago asiatica* L. (Miyase et al., 1991).

3.6.1.5 Martynoside

The MS of martynoside ($C_{31}H_{40}O_{15}$; Figure 3.42) showed a molecular mass 14 mass units greater than leucosceptoside A. ^{1}H and ^{13}C NMR data are shown in Table 3.12 and NMR spectra are given in Appendix 5.

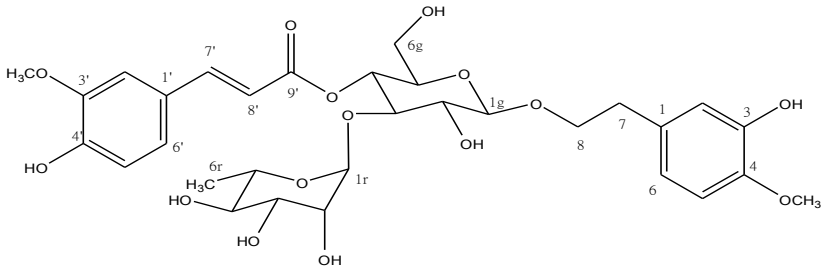

Figure 3.42 Martynoside

Table 3.12 1D and 2D NMR data of martynoside (^{1}H, 500 MHz; ^{13}C, 125 MHz; in CD_3OD; δ in ppm; *J* in Hz)

Position	^{13}C	^{1}H	COSY	NOESY	HMBC
1	132.9	-	-	-	2.82 6.83
2	117.1	6.74 (d, *J* = 2)	-	-	2.82
3	147.4	-	-	-	3.81 6.68 6.74 6.83
4	147.6	-	-	-	3.81 6.68 6.74 6.83
5	112.9	6.83 (d, *J* = 7.5)	6.68	3.81 6.68	-
6	121.1	6.68 (dd, *J* = 8, 2.5)	6.83	6.83	2.82 6.74 6.83
7	36.6	2.82 (2H, m)	3.75 4.08	3.75 4.08	6.74
8	72.1	3.75 (m)	2.82	2.82	2.82 4.37
		4.08 (m)	2.82 3.75	2.82 3.75	
1'	127.6	-	-	-	6.35 6.80
2'	111.8	7.19 (d, *J* = 2)	-	3.89	7.07 7.64
3'	149.4	-	-	-	3.89 6.80 7.19
4'	151.0	-	-	-	6.80 7.07 7.19

Table 3.12 (continued)

Position	^{13}C	^{1}H	COSY	NOESY	HMBC
5'	116.5	6.80 (d, *J* = 8)	7.07	7.07	-
6'	124.4	7.07 (dd, *J* = 8, 2)	6.80	6.80	7.19 7.64
7'	147.9	7.64 (d, *J* = 16)	6.35	6.35	7.07 7.20
8'	115.1	6.35 (d, *J* = 16)	7.64	7.64	-
9'	168.2	-	-	-	4.88 6.35 7.64
1g	104.2	4.37 (d, *J* = 8)	3.40	-	3.40
2g	76.2	3.40 (t, *J* = 9)	4.37	-	3.84 4.88*
3g	81.5	3.84* (t, *J* = 6)	4.88*	-	3.40 5.20
4g	70.4	4.88*	3.84*	-	3.84 5.20
5g	76.1	3.53* (m)	-	-	3.84* 4.88*
6g	62.4	3.64* (m)	3.53*	*	4.88*
		3.53* (m)	3.64*	*	
1r	103.0	5.20 (br s, *J* = 2)	3.92	3.84* 3.92	3.84*
2r	72.4	3.92 (dd, *J* = 3, 1.5)	5.20	5.20	5.20
3r	72.1	3.56* (m)	-	-	5.20
4r	73.8	3.29* (m)	-	-	1.10
5r	70.6	3.59* (m)	-	-	1.10
6r	18.4	1.10 (d, *J* = 6)	3.59*	3.59*	3.29*
4-OCH_3	56.5	3.81 (3H, s)	-	6.83	
3'-OCH_3	56.4	3.89 (3H, s)	-	7.19	

*Overlapped signal; g-glucose; r-rhamnose

^{1}H and ^{13}C NMR spectra of martynoside show similar signals to verbascoside except two ^{1}H singlet signals at δ 3.81 ppm and 3.89 ppm each integration to three protons. HMQC correlated these two singlets to ^{13}C signals at δ 56.5 ppm and 56.4 ppm respectively. Therefore, this compound was likely to be a verbascoside derivative substituted with two methoxyl groups.

There was no HMBC or NOESY correlation between these two methoxyl groups which suggests the substitution of different aromatic rings. Figures 3.43-3.44 show salient correlations of martynoside. HMBC correlated a singlet at δ 3.81 ppm to ^{13}C at 147.4 ppm (C-3), and 147.6 ppm (C-4), and also had a NOESY correlation to a doublet signal at δ 6.83 ppm (H-5). While the other singlet at δ 3.89 ppm had a NOESY cross peak to ^{1}H signal at δ 7.19 ppm (H-2') of the caffeoyl moiety. Due to the methoxyl substitution, both C-5 (dihydroxyphenylethyl moiety), and C-2' (caffeoyl moiety) resonated more upfield at δ 112.9 ppm, and 111.8 ppm respectively in comparison with verbascoside at δ 116.3 ppm (C-5), and 115.2 ppm (C-2'). This compound was thus assigned as martynoside. Structure elucidation of martynoside, e.g. sugar configulations and coupling patterns, was similar to verbascoside as described above.

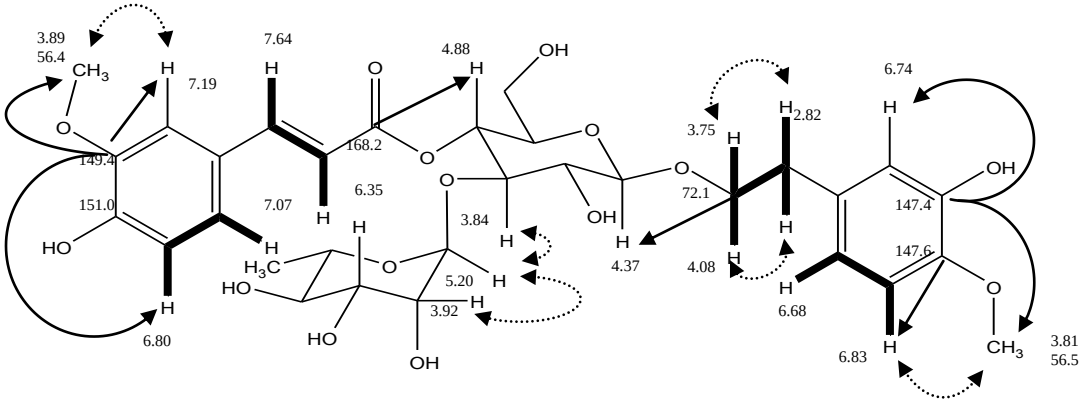

Figure 3.43 Salient signals of martynoside
COSY (bold line), NOESY (dot arrow), and HMBC (arrow)

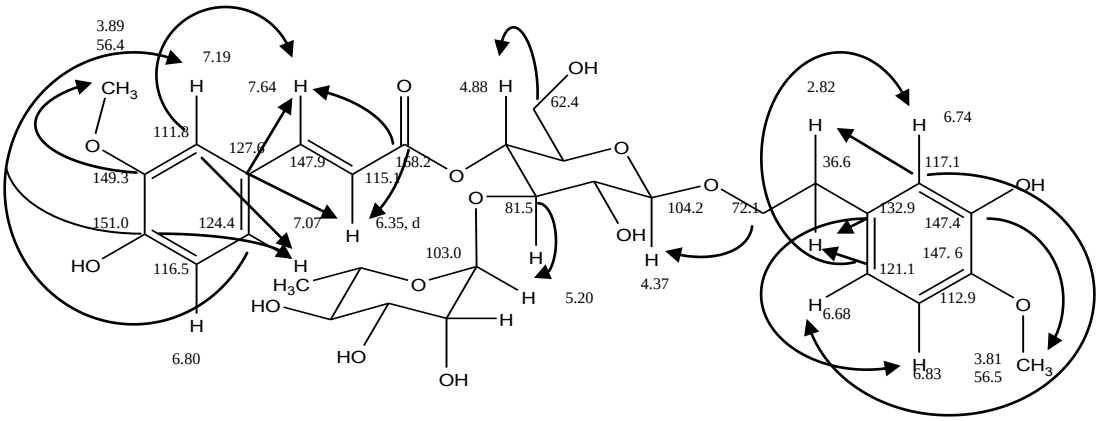

Figure 3.44 Selected HMBC correlations of martynoside

Martynoside has not been reported in the genus *Salvia* before but it was previously isolated from other genera in the family Lamiaceae, for example *Leucosceptrum japonicum* (Miq.) Kitamura et Murata (Miyase et al., 1982), *Ballota nigra* L. (Toth et al., 2007), and *Sideritis perfoliata* L. subsp. *perfoliata* (Charami et al., 2008) and from Verbenaceae family, *Lippia dulcis* Trev. (Abe et al., 2002), *Clerodendron trichotomum* Thunb. (Kim et al., 2001), and also from Plantaginaceae, *Plantago asiatica* L. (Miyase et al., 1991). Its spectroscopic data are comparable to those described in the literature.

3.6.1.6 Rosmarinic acid

Rosmarinic acid ($C_{18}H_{16}O_8$; Figure 3.45) was identified by comparison of its NMR spectra with literature values and an authentic sample. ^{1}H and ^{13}C NMR data are given in Table 3.13 and NMR spectra are shown in Appendix 6.

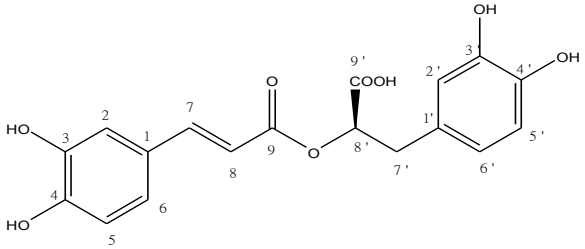

Figure 3.45 Rosmarinic acid

Table 3.13 1D and 2D NMR data of rosmarinic acid (^{1}H, 500 MHz; ^{13}C, 125 MHz; in CD_3OD; δ in ppm; *J* in Hz)

Position	^{13}C	^{1}H	COSY	NOESY	HMBC
1	128.0	-	-	-	6.25 6.75
2	115.1	7.02 (d, *J* = 2)	-	6.25 7.48	6.91 7.48
3	146.7	-	-	-	6.75 6.91 7.02
4	149.3	-	-	-	6.75 6.91 7.02
5	116.4	6.75 (d, *J* = 8)	6.91	6.91	6.91
6	122.9	6.91 (dd, *J* = 8, 2)	6.75	6.25 6.75 7.48	6.75 7.02 7.48
7	146.5	7.48 (d, *J* = 16)	6.25	6.25 6.91 7.02	6.75 7.02
8	115.8	6.25 (d, *J* = 15.5)	7.48	6.91 7.02 7.48	6.91
9	169.1	-	-	-	5.07 6.25 7.48
1'	131.3	-	-	-	2.92 3.08 5.07 6.65
2'	117.5	6.76 (d, *J* = 2)	-	5.07	2.92 3.08 6.63

Table 3.13 (continued)

Position	^{13}C	^{1}H	COSY	NOESY	HMBC
3'	146.0	-	-	-	6.65
4'	144.8	-	-	-	6.63 6.76
5'	116.2	6.65 (d, *J* = 8)	*	*	-
6'	121.7	6.63 (dd, *J* = 8, 2)	*	*	2.92 3.08 6.76
7'	38.9	2.92 (dd, *J* = 14, 10)	3.08	3.08 5.07	6.63 6.76
		3.08 (dd, *J* = 14, 3)	2.92	2.92 5.07	
8'	77.8	5.07 (dd, *J* = 10, 3)	2.92 3.08	2.92 3.08	2.92
9'	177.5	-	-	-	2.92 5.07

* Overlapped signal

There were 18 signals of ^{13}C NMR which distributed to nine methine groups, eight quaternary carbon atoms, and only one methylene group. ^{1}H displayed 11 signals of alkane and aromatic protons. Two of them, δ 6.25 ppm and 7.48 ppm, exhibited the coupling patterns of the trans configuration protons with ^{3}J value 16 Hz. Two sets of six signals were shown as 3,4-disubstituted coupling patterns the same as caffeic acid (Figure 3.24). There were three signals, δ 2.92 ppm, 3.08 ppm, and 5.07 ppm, which coupled to each other, and ^{13}C showed two corresponding signals of those three protons at δ 38.9 ppm (CH_2), and 77.8 ppm (CH). The downfield methylene atoms implied the attachment of an aromatic ring or an electronegative group. In addition, these methylene atoms had HMBC correlation to signals of aromatic protons at δ 6.63 ppm and 6.76 ppm. The molecular formula $C_{18}H_{16}O_8$ was twice of caffeic acid plus the coupling patterns; therefore, this compound was identified as rosmarinic acid. Salient two dimensional correlations are shown in Figure 3.46.

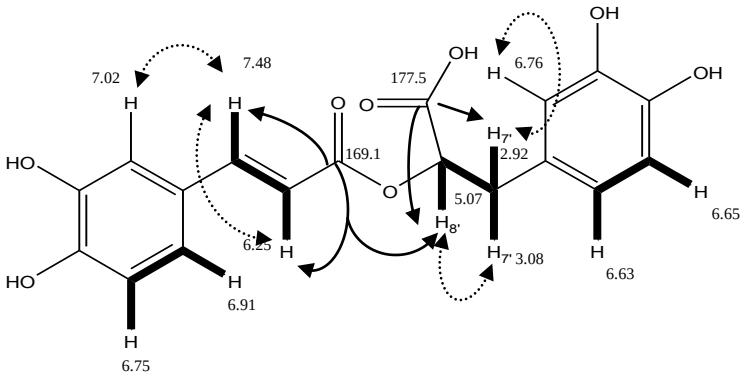

Figure 3.46 Salient correlations of rosmarinic acid
COSY (bold line), NOESY (dot arrow), and HMBC (arrow)

Rosmarinic has never been reported in *S. viridis* L. before but it has been reported in other *Salvia* species, for example *S. officinalis* L. (Wang et al., 1998). It has also been found in families Boraginaceae, Cucurbitaceae, Rubiaceae, Araliaceae, and Plantaginaceae (Petersen and Simmonds, 2003).

3.6.1.7 6-*O*-Caffeoyl-glucose

The HR-ESI-MS of 6-*O*-caffeoyl-glucose (Figure 3.47) gave a molecular mass of 342, consistent with the molecular formula $C_{15}H_{18}O_9$. ^{1}H and ^{13}C NMR data are shown in Table 3.14 and NMR spectra are shown in Appendix 7.

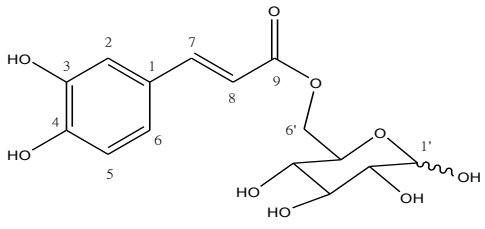

Figure 3.47 6-*O*-Caffeoyl-glucose

Table 3.14 1D and 2D NMR data of 6-*O*-caffeoyl-glucose (^{1}H, 500 MHz; ^{13}C, 125 MHz; CD_3OD; δ in ppm; *J* in Hz)

Position	^{13}C	^{1}H	COSY	NOESY	HMBC
1	127.7	-	-	-	6.25 7.55
2	115.1	7.04 (d, *J* = 2)	-	6.25 7.55	6.77 6.94 7.55
3	146.8	-	-	-	6.77 6.94 7.04
4	149.6	-	-	-	6.77 6.94 7.04
5	116.5	6.77 (d, *J* = 8.5)	6.94	6.94	6.94
6	123.0	6.94 (dd, *J* = 8, 2)	6.77	6.25 6.77 7.55	6.77 7.04 7.55
7	147.1	7.55 (d, *J* = 16)	6.25	6.25 6.94	6.77 6.94 7.04
8	114.9	6.25 (d, *J* = 16)	7.55	6.94 7.04 7.55	6.94 7.55
9	169.2	-	-	-	4.30* 4.43* 6.25 7.55
1'	98.3[§]	1β 4.50 (d, *J* = 7.5)	-	3.34* 3.55*	-
	94.0[§]	1α 5.10 (d, *J* = 4)	3.34*	3.34*	-
2'	71.8	3.34* (m)	5.10	4.50 5.10	3.55*

Table 3.14 (continued)

Position	^{13}C	^{1}H	COSY	NOESY	HMBC
3'	74.8	3.65* (m)	*	*	3.34* 5.10
4'	73.8	3.38*	*	4.43*	3.55*
5'	75.5	3.55* (m)	-	4.30* 4.50	4.30*
6'	64.9	4.30* (m)	4.43	-	3.38*
		4.43* (m)	4.30*	-	

*Overlapped signal; [§]Interchangeable

^{1}H NMR showed the aromatic signals of caffeic acid plus signals in the sugar region which from the molecular formula was likely to be a hexose unit. Two signals of anomeric protons were observed at δ 4.50 ppm (*J* value 7.5 Hz) and 5.10 ppm (*J* value 4 Hz). The only methylene carbon at δ 64.9 ppm correlated to two protons at δ 4.30 and 4.43 ppm which was somewhat deshielded compared to C-6 of a glucose unit of verbascoside at 60.9 ppm and 3.49/3.64 ppm. In addition, HMBC correlated a carbonyl carbon signal at δ 169.2 ppm to these methylene protons. Therefore, this compound was identified 6-*O*-caffeoyl-glucose with the free configuration of the anomeric proton. The free interconversion of the anomeric centre contributed to a highly complex spectrum for the sugar part of the molecule. All NMR data were similar to a previous finding (Gao et al., 1999). Selected salient signals are given in Figure 3.48. 6-*O*-Caffeoyl-glucose was reported from the whole plants of *Caryopteris incana* (Thunb.) Miq., family Verbenaceae (Gao et al., 1999).

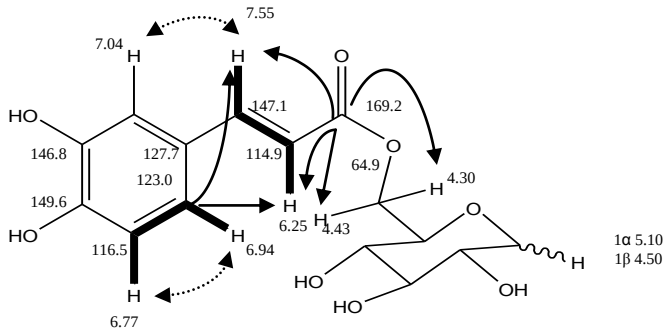

Figure 3.48 Selected correlations of 6-*O*-caffeoyl-glucose
COSY (bold line), NOESY (dot arrow), and HMBC (arrow)

3.6.2 Flavonoid glycosides

The polar fractions also included a series of compounds with ^{1}H NMR signals characteristic of flavone including a singlet for H-3 and finely coupled doublets for H-6 and H-8 in the aromatic/alkene region of the spectrum together with signals for a second aromatic ring. MS showed that these compounds fell into two molecular weight classes consistent with mono- and di-glycosides. All the diglycoside compounds showed NMR signals characteristic of the deoxyhexose, rhamnose.

3.6.2.1 Luteolin-7-*O*-β-glucopyranoside

The MS data of luteolin-7-*O*-β-glucopyranoside (Figure 3.49) gave a molecular mass of 448 and a molecular formula of $C_{21}H_{20}O_{11}$. It was identified as luteolin-7-*O*-β-D-glucopyranoside by comparison of its NMR data with an authentic standard. ^{1}H and ^{13}C NMR data are shown in Table 3.15 and NMR spectra are given in Appendix 8.

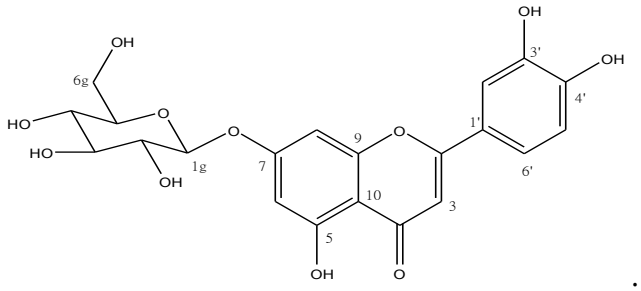

Figure 3.49 Luteolin-7-*O*-β-glucopyranoside

^{1}H NMR showed six signals in aromatic proton region with the ordinary doublet signal of the β-anomeric glucose proton at δ 5.06 ppm. ^{13}C and DEPT-135 NMR displayed 21 signals with nine signals of quaternary carbon, and only one methylene signal. The COSY, NOESY and HMBC correlations indicated two sets of aromatic protons in separate ring system typical of the flavone skeleton. Three of proton signals, δ 6.89 ppm (d), 7.41 ppm (br s), 7.47 ppm (dd), were observed in the same ring system by the HMBC, COSY, and NOESY correlations. The patterns of splitting indicated a 3, 4-disubstituted aromatic ring B of flavonoid. A finely coupled doublet at δ 6.44 ppm (J = 2 Hz) showed COSY cross correlation to a doublet signal at δ 6.78 ppm (J = 2 Hz). This correlation suggested two protons of H-6 and H-8 respectively. A singlet proton signal at δ 6.74 ppm had HMBC correlations to ^{13}C signals at δ 164.5 ppm and 181.9 ppm suggested the proton H-3 of flavone skeleton.

Table 3.15 1D and 2D NMR data of luteolin-7-*O*-β-glucopyranoside (^{1}H, 500 MHz; ^{13}C, 125 Mz; DMSO-d6; δ in ppm; *J* in Hz)

Position	^{13}C	^{1}H	COSY	NOESY	HMBC
1	-	-	-	-	-
2	164.5	-	-	-	6.74 7.47
3	103.1	6.74 (s)	-	7.41 7.47	-
4	181.9	-	-	-	6.74
5	161.1	-	-	-	6.44
6	99.5	6.44 (d, *J* = 2)	6.78	5.06	6.78
7	163.0	-	-	-	6.44 6.78
8	94.7	6.78 (d, *J* = 2)	6.44	5.06	6.44
9	157.0	-	-	-	6.78
10	105.3	-	-	-	6.44 6.74 6.78
1'	121.3	-	-	-	6.89
2'	113.6	7.41 (d, *J* = 2)	-	6.74	7.47
3'	145.8	-	-	-	6.89 7.41
4'	150.0	-	-	-	6.89 7.41 7.47
5'	116.0	6.89 (d, *J* = 8)	7.47	7.43	-
6'	119.2	7.47 (dd, *J* = 8.5, 2)	6.89	6.74 6.89	7.41
1g	99.9	5.06 (d, *J* = 7.5)	3.28*	6.44 6.78	3.28* 6.78
2g	73.1	3.28*	*	*	3.31*

Table 3.15 (continued)

Position	^{13}C	^{1}H	COSY	NOESY	HMBC
3g	76.4	3.31*	*	*	3.28*
4g	69.6	3.18*	*	*	3.31* 3.70
5g	77.2	3.46*	*	*	3.49*
6g	60.6	3.49*	3.70*	*	3.18*
		3.70	3.49*		

*Overlapped signal; g-glucose

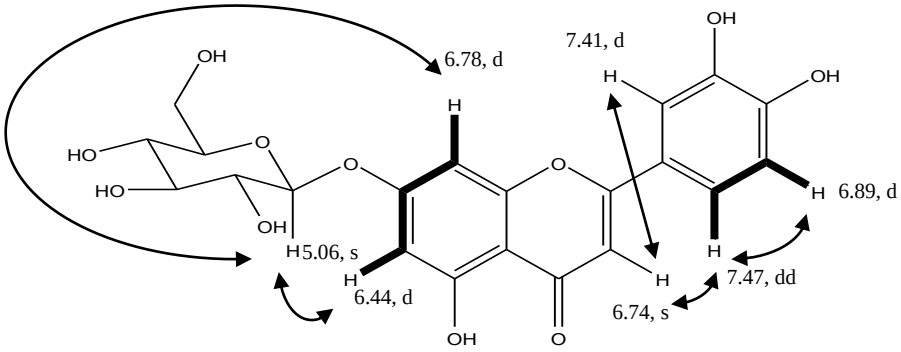

Figure 3.50 Selected COSY (bold line), and NOESY (arrow) of luteolin-7-*O*-β-glucopyrano-side

The broad overlapped signals at 3-4 ppm may be cause by the hydroxyl groups of the sugar which are observed when using DMSO-d6 as solvent. The anomeric proton signal and one methylene group suggested a glucose containing compound. The β-anomeric glucose signal correlated to two proton signals at 6.44 ppm, and 6.78 ppm in NOESY revealing the attachment of glucose to the aglycone at C-7. All assignments were compared to previous literature (Siciliano et al., 2004).

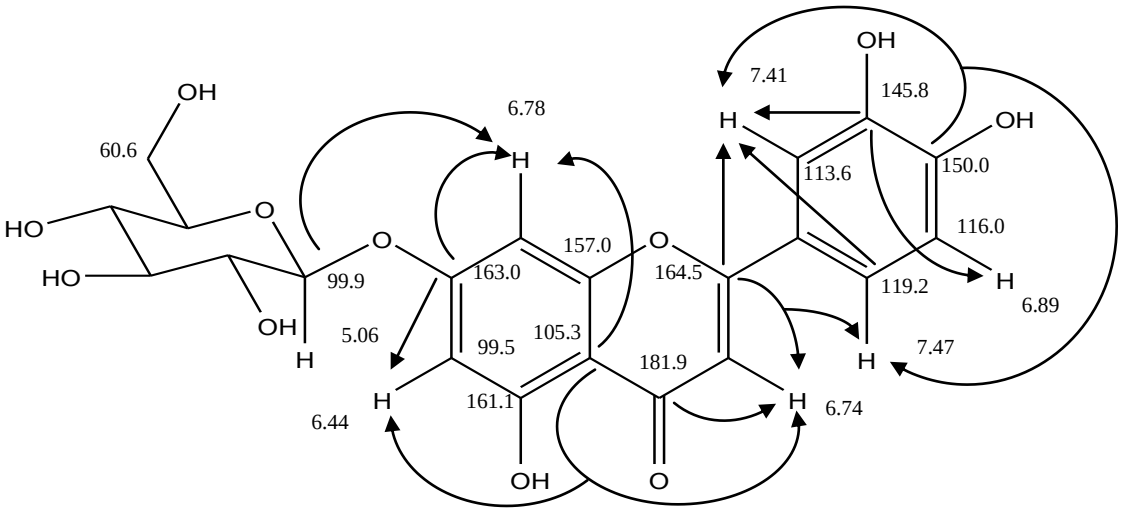

Figure 3.51 HMBC correlation of luteolin-7-*O*-β-glucopyranoside

This compound was previously reported in this plant (Kokkalou and Kapetanidis, 1988), and also from many *Salvia* species (Lu and Foo, 2002).

3.6.2.2 Luteolin-7-*O*-β-galactopyranoside

The MS data of luteolin-7-*O*-β-galactopyranoside (Figure 3.52) gave a molecular mass of 448 and a molecular formula $C_{21}H_{20}O_{11.}$ ^{1}H and ^{13}C NMR data are shown in Table 3.16 and NMR spectra are shown in Appendix 9.

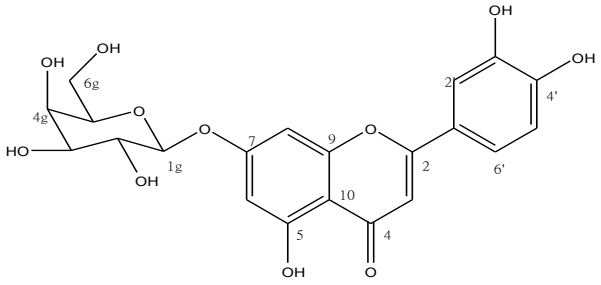

Figure 3.52 Luteolin-7-*O*-β-galactopyranoside

This compound exhibited the same aromatic proton NMR signals as its isomer luteolin-7-glucoside. Unlike luteolin-7-glucoside, this compound dissolved in deuterated-methanol; therefore, all sugar signals were clearly seen in ^{1}H NMR.

Table 3.16 1D and 2D NMR data of luteolin-7-*O*-β-galactopyranoside (^{1}H, 500 MHz; ^{13}C, 125 Mz; CD_3OD; δ in ppm; *J* in Hz)

Position	^{13}C	^{1}H	COSY	NOESY	HMBC
1	-	-	-	-	-
2	166.9	-	-	-	6.60 7.40 7.42
3	104.1	6.60 (s)	-	7.40 7.42	-
4	184.0	-	-	-	6.60
5	162.9	-	-	-	6.50
6	101.1	6.50 (d, *J* = 2)	6.79	5.06	6.79
7	164.8	-	-	-	5.06 6.50 6.79
8	96.0	6.79 (d, *J* = 2)	6.50	5.06	6.50
9	159.0	-	-	-	6.79
10	107.1	-		-	6.50 6.60 6.79
1'	123.4	-	-	-	6.60 6.89
2'	114.2	7.40 (d, *J* = 2)	6.89	6.89	7.42
3'	147.1	-	-	-	6.89 7.40
4'	151.9	-	-	-	6.89 7.40 7.42
5'	119.2	7.43 (dd, *J* = 8.5, 2)	6.89	6.74 6.89	7.41
6'	116.8	6.89 (d, *J* = 8.5)	7.40 7.42	7.40 7.42	-

Table 3.16 (continued)

Position	^{13}C	^{1}H	COSY	NOESY	HMBC
1gal	101.7	5.06 (d, *J* = 7)	3.49*	3.54 6.50 6.79	-
2gal	74.7[§]	3.49*	3.40	*	-
3gal	71.3	3.40 (d, *J* = 8.5)	3.40 3.49	*	-
4gal	77.9[§]	3.49*	3.40	*	3.40 3.49*
5gal	78.4	3.54 (m)	3.71	5.06	-
6gal	62.4	3.71 (dd, *J* = 12.5, 6)	3.54 3.92	*	-
		3.92 (d, *J* = 12)	3.71		

*Overlapped signal; [§] Interchangeable; gal-galactose

The doublet signal at δ 5.06 ppm indicated the anomeric sugar proton attachment to aglycone luteolin. NOESY correlated this anomeric proton to two signals at δ 6.50 ppm (H-6) and 6.79 ppm (H-8) which implied the substitution at C-7. A methylene proton of the sugar had a COSY correlation to a signal at δ 3.54 ppm which implied H-5gal. In addition, a NOESY cross-peak of this signal at δ 3.54 ppm (H-5gal) to the anomeric proton was also observed. COSY correlated the anomeric signal to H-2gal at δ 3.49 ppm, and H-2 further had a COSY correlation to H-3gal at δ 3.40 ppm.

In comparison with verbascoside (Figure 3.31), the peak shapes of sugar proton did not appear as ordinary triplets of axial-axial orientation. As glucose protons of position 2-5 resonated as triplet signal with ^{3}J value around 9-10 Hz, a signal at δ 3.40 ppm (H-3gal) exhibited a broad doublet (^{3}J = 9 Hz) due to smaller coupling constant of axial-equatorial orientation (^{3}J between H-3gal and H-4gal) (Figure 3.53). This compound was likely to be a galactose substitution. Certain salient correlations are given in Figure 3.54.

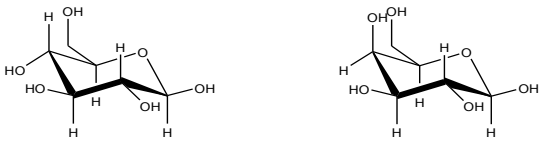

β-glucose β-galactose

Figure 3.53 Pyranose rings of glucose and galactose

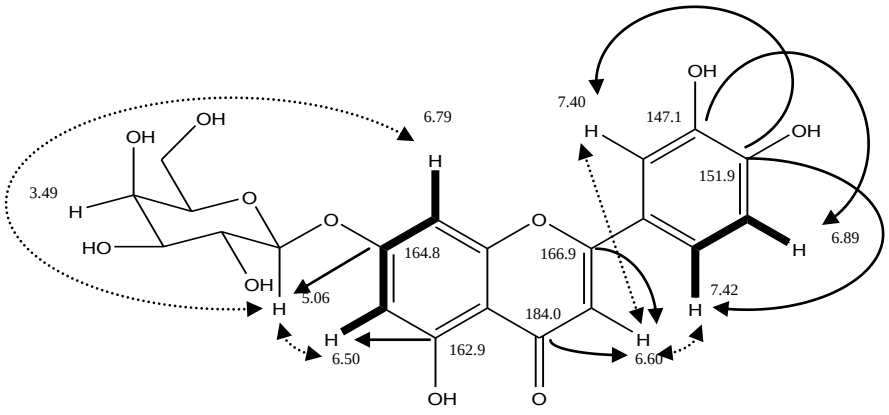

Figure 3.54 Certain salient correlations of luteolin-7-*O*-β-galactopyranoside H-H COSY (bold line), NOESY (dot arrow), HMBC (arrow)

Luteolin-7-*O*-β-galactoside was reported in *Verbena officinalis* L. and *V. supina* L., family Verbenaceae (Kawashty and El-Garf, 2000) and also in *Cynara scolimus* L., family Asteraceae (Sanchez-Rabaneda et al., 2003).

3.6.2.3 Luteolin-7-*O*-rutinoside

The MS data of luteolin-7-*O*-rutinoside (luteolin-7-*O*-α-rhamnopyranosyl-(1→6)-β-glucopyranoside, Figure 3.55) gave a molecular mass of 594, consistent with a flavonoid glycoside with two monosaccharides units. ^{1}H and ^{13}C NMR data are shown in Table 3.17 and NMR spectra are given in Appendix 10.

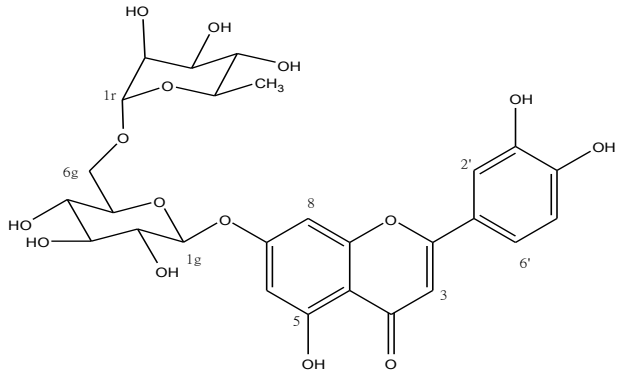

Figure 3.55 Luteolin-7-*O*-rutinoside

^{1}H NMR showed the five signals of protons in the aromatic and alkene region of the spectrum. Three of them, δ 6.90 ppm (d), 7.41 ppm (s), 7.44 ppm (dd), were observed to be in the same ring system by the HMBC, COSY, and NOESY correlations. The patterns of splitting indicated a 3,4-disubstituted aromatic ring B of flavonoid. A coupled doublet at δ 6.45 ppm (J = 2 Hz) showed COSY cross correlation to a broad, two proton, singlet at δ 6.74 ppm. This latter signal was cross correlated by HMBC to two separate carbon signals at δ 94.8 ppm and 103.1 ppm. Thus, the proton at δ 6.45 ppm was assigned to H-6 of the flavonoid A ring, and the two protons at δ 6.74 ppm to H-8 of A ring and H-3 of flavone skeleton.

^{13}C and ^{1}H spectra showed signals corresponding to the methylene group of glucose and a methyl group of rhamnose, also two anomeric proton signals at δ 4.54 ppm (s) of rhamnose, and 5.06 ppm (d, J = 7.5 Hz) of glucose as described in verbascoside structure elucidation (Figures 3.27-3.28). The attachment of glucose to rhamnose was at C-6g which was shifted downfield to δ 66.1 ppm (C-6g) when compared with C-6g in verbascoside at δ 60.9 ppm. There was also a HMBC correlation from C-6g to the anomeric proton of rhamnose at δ 4.54 ppm (H-1r). On the other hand, the attachment of anomeric glucose at δ 5.06 ppm (H-1g) to luteolin was at δ 162.9 ppm (C-7) due to a HMBC correlation between them. In addition, NOESY correlated this anomeric glucose to two proton signals at δ 6.45 ppm (H-6), and δ 6.74 ppm (H-8).

Table 3.17 1D and 2D NMR data of luteolin-7-*O*-rutinoside (^{1}H, 500 MHz; ^{13}C, 125 MHz; DMSO-d_6; δ in ppm; *J* in Hz)

Position	^{13}C	^{1}H	COSY	NOESY	HMBC
1	-	-	-	-	-
2	164.6	-	-	-	6.74 7.44
3	103.1	6.74* (s)	-	5.06 7.41 7.44	-
4	181.9	-	-	-	6.74
5	161.2	-	-	-	6.45
6	99.5	6.45 (d, *J* = 2)	6.74	5.06	6.74
7	162.9	-	-	-	5.06 6.45 6.74
8	94.8	6.74* (s)	6.45	5.06	6.45
9	156.9	-	-	-	6.74
10	105.4	-	-	-	6.45 6.74
1'	121.3	-	-	-	6.74 6.90
2'	113.5	7.41 (br s)	-	6.74	7.44
3'	145.8	-	-	-	6.90 7.41
4'	150.1	-	-	-	7.41 7.44
5'	116.1	6.90 (d, *J* = 8.5)	7.44	7.44	7.44$^{\Phi}$
6'	119.2	7.44 (dd, *J* = 8, 2)	6.90	6.90	6.90$^{\Phi}$ 7.41
1g	99.9	5.06 (d, *J* = 7.5)	3.26*	3.59 6.45 6.74	3.26$^{\Phi}$

Table 3.17 (continued)

Position	^{13}C	^{1}H	COSY	NOESY	HMBC
2g	73.1	3.26*	5.06	-	3.30* 5.06 $^{\Phi}$
3g	76.3	3.30*	-	-	3.26*
4g	69.6	3.15*	*	-	3.59 $^{\Phi}$
5g	75.6	3.59 (t, *J* = 7.5)	3.15* 3.83	5.06	3.15* $^{\Phi}$
6g	66.1	3.43*	3.83	-	4.54
		3.83 (d, *J* = 10.5)	3.43*		
1r	100.5	4.54 (br s)	3.65	3.65	-
2r	70.3	3.65 (d, *J* = 2)	4.54	4.54	-
3r	70.7	3.45*	-	-	3.14* $^{\Phi}$ 4.54
4r	72.1	3.14*	-	-	3.65
5r	68.3	3.41*	-	-	3.14* $^{\Phi}$
6r	17.8	1.06 (3H, d, *J* = 6)	-	-	3.14* 3.41* $^{\Phi}$

*Overlapped signal; $^{\Phi}$ H2BC; g-glucose; r-rhamnose

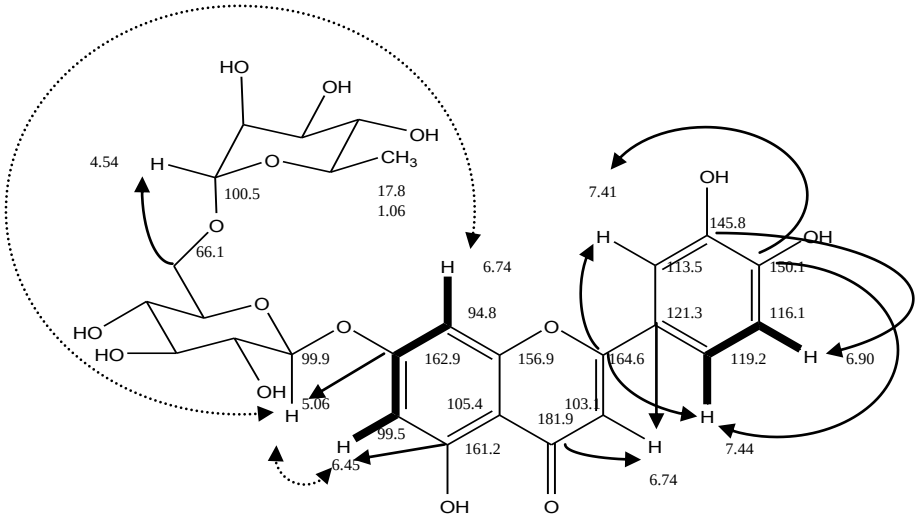

Figure 3.56 Selected salient correlations of luteolin-7-*O*-rutinoside
H-H COSY (bold line), NOESY (dot arrow), HMBC (arrow)

Though DMSO-d_6 overlapped peaks extensively within the sugar region as shown in Appendix 10.1, the chemical shifts of sugar could be assigned by HMBC, NOSY, and COSY correlations. In brief, the anomeric rhamnose proton at δ 4.54 ppm (H-1r) had a NOESY cross peak to H-2r at δ 3.65 ppm. H-2r was further correlated to C-4r at δ 72.1 ppm by HMBC. H-4r had HMBC correlations to C-3r, C-5r, and C-6r. For glucose, H-1g at δ 5.06 ppm had a COSY correlation to H-2g at δ 3.26 ppm, and also a NOESY correlation to H-5g at δ 3.59 ppm. H-5g showed a COSY cross-peak to H-6g, and further correlated to C-4g.

All NMR data were identical to a published literature (Siciliano et al. 2004). Therefore, this compound was identified as luteolin-7-*O*-rutinoside. Certain salient correlations are shown in Figure 3.56. Luteolin-7-*O*-rutinoside was previously reported in this species (Kokkalou and Kapetanidis, 1988).

3.6.2.4 Luteolin-7-*O*-α-rhamnopyranosyl-(1→6)-β-galactopyranoside

This compound was eluted together with luteolin-7-rutinoside at retention time 16.7 minutes but it precipitated out from the eluent in 20% aqueous acetonitrile. The solubility in deuterated solvent of luteolin-7-rutinoside and this compound also differed. This powder dissolved in deuterated-methanol while luteolin-7-rutinoside dissolved only in deuterated-DMSO and D_2O. Accordingly, all ^1H signals of sugar were clearly seen in deuterated methanol (Appendix 11.1) compared to signals of luteolin-7-*O*-rutinoside in deuterated-DMSO (Appendix 10.1).

MS showed a molecular mass of 594 as in luteolin-7-*O*-rutinoside. ^1H and ^{13}C NMR data are shown in Table 3.18, and NMR spectra are given in Appendix 11.

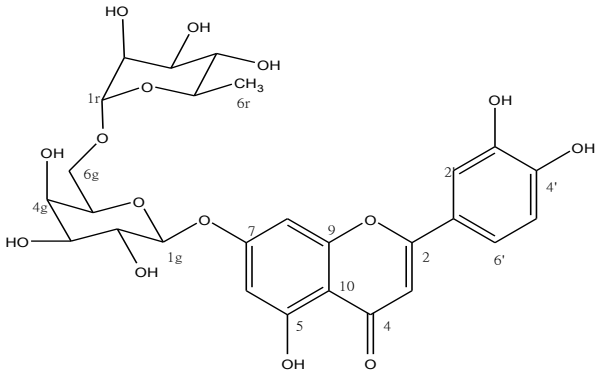

Figure 3.57 Luteolin-7-*O*-α-rhamnopyranosyl-(1→6)-β-galactopyranoside

Table 3.18 1D and 2D NMR data of luteolin-7-*O*-α-rhamnopyranosyl-(1→6)-β-galacto-pyranoside (^{1}H, 500 MHz; ^{13}C, 125 MHz; CD_3OD; δ in ppm; *J* in Hz)

Position	^{13}C	^{1}H	COSY	NOESY	HMBC
1	-	-	-	-	-
2	167.0	-	-	-	6.61
3	104.3	6.61 (s)	-	7.41* 7.42*	-
4	184.0	-	-	-	6.61
5	163.0	-	-	-	6.52
6	101.1	6.52 (d, *J* = 2)	6.75	5.03 6.75	6.75
7	164.7	-	-	-	5.03 6.52 6.75
8	96.1	6.75 (d, *J* = 2)	6.52	5.03	6.52
9	158.9	-	-	-	6.75
10	107.1	-	-	-	6.52 6.61 6.75
1'	123.5	-	-	-	6.61 6.92
2'	114.3	7.41* (br s)	-	6.61	7.42
3'	147.0	-	-	-	6.92 7.41
4'	151.2	-	-	-	7.41 7.42
5'	116.9	6.92 (d, *J* = 9)	7.42	7.42	7.42Φ
6'	120.6	7.42*	6.92	6.92	6.92 Φ 7.41 7.42

Table 3.18 (continued)

Position	^{13}C	^{1}H	COSY	NOESY	HMBC
1gal	101.6	5.03 (d, *J* = 7)	3.49	3.49* 3.50* 3.65 6.52 6.75	-
2gal	74.7	3.49*	3.40 5.03	-	3.50* 5.03$^{\Phi}$
3gal	71.3	3.40 (d, *J* = 9)	3.49* 3.65	-	3.49* 3.65*
4gal	77.2	3.65*	3.49*	-	3.40$^{\Phi}$ 3.63*
5gal	77.8	3.50*	-	5.03*	3.40 3.49
6gal	67.5	3.63*	4.05	-	4.72
		4.05 (d, *J* = 9.5)	3.63*	3.63* 4.05 4.72	
1r	102.1	4.72 (br s)	3.91	3.63* 3.91 4.05	4.05
2r	72.1	3.91 (dd, *J* = 3.5, 1.5)	4.72	4.72	3.34 4.72
3r	72.4	3.72 (dd, *J* = 9.5, 3.5)	-	1.18 3.91	4.72
4r	74.1	3.34 (t, *J* = 10)	*	*	1.18 3.72$^{\Phi}$ 3.91
5r	69.8	3.64*	-	-	1.18$^{\Phi}$ 3.34 4.72
6r	17.9	1.18 (3H, d, *J* = 6.5)	3.64*	3.72	3.34 3.64*$^{\Phi}$

*Overlapped signal; $^{\Phi}$ H2BC; gal- galactose; r- rhamnose

^{1}H and ^{13}C signals of this compound were very similar to luteolin-7-*O*-rutinoside but chemical shifts differences due to the different solvents were observed. In general, the chemical shifts of a compound in CD_3OD were a few ppm higher than one in DMSO-d6. For example, the only carbonyl carbon of luteolin-7-rutinoside resonated at δ 181.9 ppm in DMSO-d6 while C-4 of this compound was at δ 184.0 ppm in CD_3OD. Higher chemical shifts of aromatic ^{1}H were also observed. All COSY, HMBC, NOESY correlations were matched to luteolin-7-*O*-rutinoside, for instance the NOESY correlation of the anomeric proton of galactose at δ 5.03 ppm to two aromatic protons at δ 6.52 ppm (H-6) and 6.75 ppm (H-8) which confirmed the substitution of sugar at C-7. Also, the attachment of rhamnose was verified by a HMBC cross-peak between the anomeric proton of rhamnose at δ 4.72 ppm and C-6gal at δ 67.48 ppm. Selected correlations are shown in Figures 3.59-3.60.

NOESY correlated the anomeric proton of galactose at δ 5.03 ppm to a signal at δ 3.50 ppm (H-5gal). The anomeric proton had a COSY correlation to H-2gal (δ 3.49 ppm). Then, H-2gal had a COSY correlation to H-3gal at δ 3.40 ppm which further correlated to H-4gal at δ 3.65 ppm as shown in Figure 3.58. For rhamnose assignments, the pattern of H-2r and H-3r splitting were clearly identified as described in verbascoside.

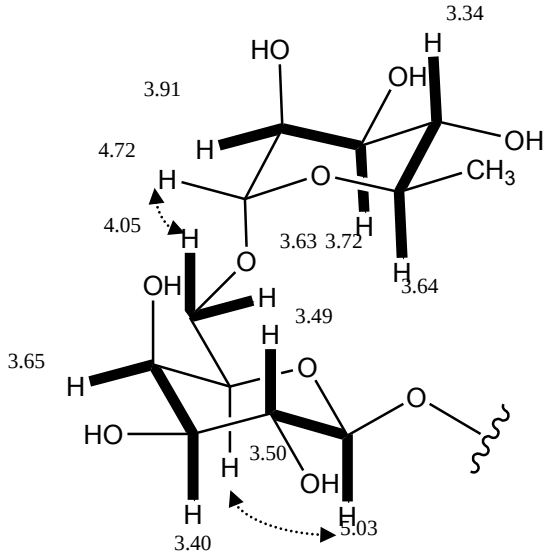

Figure 3.58 H-H COSY (bold line) and NOESY (dot arrow) correlations of disaccharide of luteolin-7-*O*-α-rhamnopyranosyl-(1→6)-β-galactopyranoside.

H-2r was a dd with two small coupling constants (3.5 Hz and 1.5 Hz) and can be seen as broad singlet while H-3r was a dd with ^{3}J values 9.5 and 3.5 Hz. H-2r also had a NOESY

correlation to the anomeric rhamnose proton. C-5r at δ 69.8 ppm and C-4r at δ 74.1 ppm had HMBC correlation to the only methyl doublet signal at δ 1.18 ppm. A cross peak of C-5r at δ 69.8 ppm to the doublet of H-6r was observed in two bond correlation.

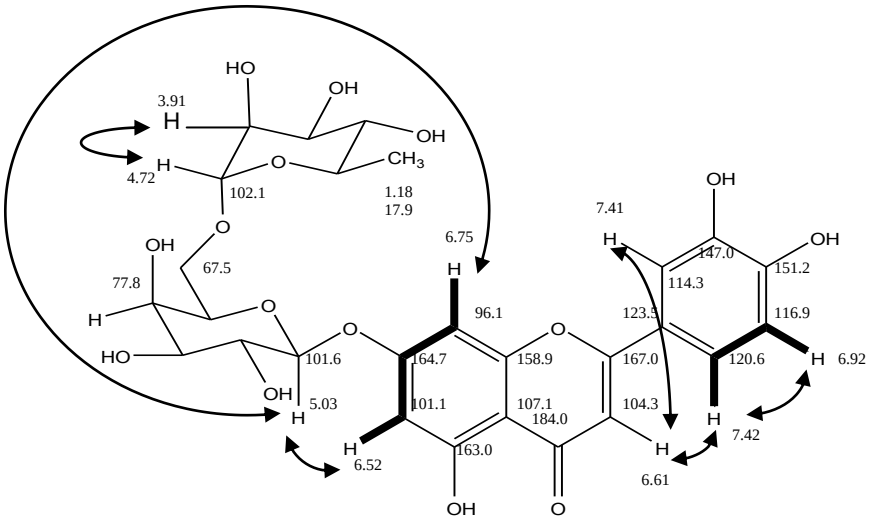

Figure 3.59 Selected salient correlations of luteolin-7-*O*-α-rhamnopyranosyl-(1→6)-β-galactopyranoside. H-H COSY (bold line), NOESY (arrow)

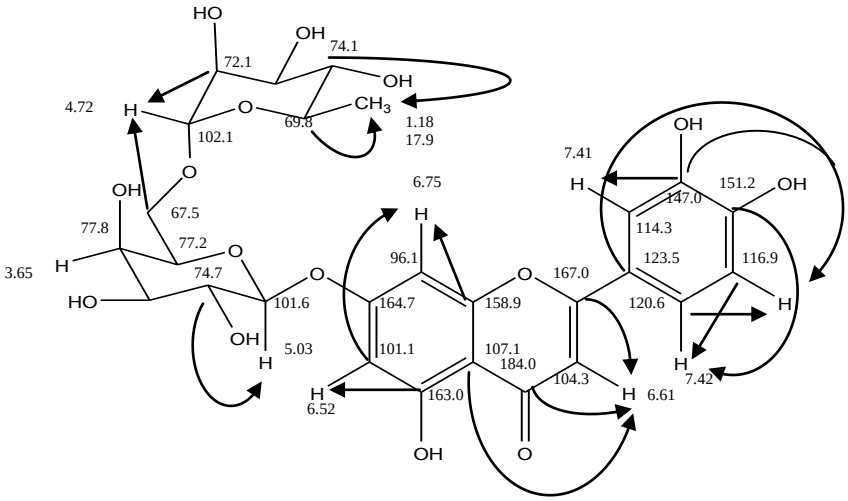

Figure 3.60 Partial HMBC correlations of luteolin-7-*O*-α-rhamnopyranosyl-(1→6)-β-galacto-pyranoside

As many of the sugar signals of luteolin-7-*O*-rutinoside were overlapped by hydroxyl signals stabilized by DMSO-d6, it proved difficult to make a direct comparison between luteolin-7-rutinoside and luteolin-7-*O*-α-rhamnopyranosyl-(1→6)-β-galactopyranoside.

However, this compound displays the different triplet signal of H-3gal. H-3gal (δ 3.40 ppm) exhibited a broad doublet (^3J = 9 Hz) due to smaller coupling constant of axial-equatorial orientation (^3J between H-3gal and H-4gal) as shown in Figure 3.53.

Therefore, this compound was identified luteolin-7-*O*-α-rhamnopyranosyl-(1→6)-β-galactopyranoside. To the best of literature searching, this compound appears to be a new flavonoid glycoside.

3.6.2.5 Apigenin-7-*O*-β-glucopyranoside

The MS data of apigenin-7-*O*-β-glucopyranoside (Figure 3.61) suggested a molecular mass of 432 and the molecular formula $C_{21}H_{20}O_{10.}$ ^{1}H and ^{13}C NMR data are shown in Table 3.19 and NMR spectra are given in Appendix 12.

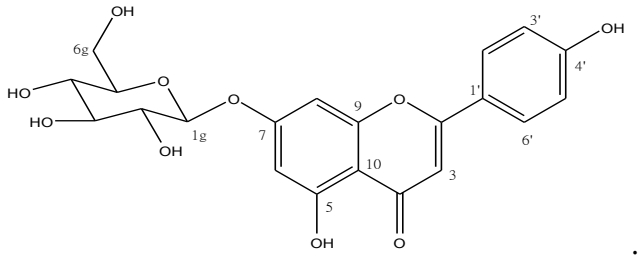

Figure 3.61 Apigenin-7-*O*-β-glucopyranoside

^{1}H NMR showed a similar overall pattern to luteolin-7-*O*-β-glucopyranoside which comprised a group of monosaccharide signals and certain signals in aromatic region. Two pairs of doublets were coupled to each other with coupling constants 9 Hz and 2 Hz. HMBC correlations exhibited the same patterns as luteolin-7-*O*-β-glucopyranoside except there were only two doublet signals instead of three signals in ring B. The MW of 432 suggested one oxygen atom less than luteolin-7-*O*-β-glucopyranoside. ^{13}C NMR showed 19 signals including two strong signals at δ 117.1 ppm (C-3' and C-5') and 129.7 ppm (C-2' and C-6'). This compound was thus identified apigenin-7-*O*-β-glucopyranoside.

Table 3.19 1D and 2D NMR data of apigenin-7-*O*-β-glucopyranoside (^{1}H, 500 MHz; ^{13}C, 125 Mz; CD_3OD; δ ppm; *J*, Hz)

Position	^{13}C	^{1}H	COSY	NOESY	HMBC
1	-	-	-	-	-
2	166.8	-	-	-	7.88
3	104.1	6.66 (s)	-	7.88	-
4	184.1	-	-	-	-
5	159.0	-	-	-	-
6	101.2	6.50 (d, *J* = 2)	6.82	5.06	-
7	164.9	-	-	-	6.50
8	96.1	6.82 (d, *J* = 2)	6.50	5.06	6.50
9	162.8	-	-	-	6.50
10	107.1	-	-	-	6.50 6.66
1'	123.1	-	-	-	6.66 6.92
2', 6'	129.6	7.88 (d, *J* = 9)	6.92	6.66 6.92	-
3', 5'	117.2	6.92 (d, *J* = 9)	7.88	7.88	-
4'	162.9	-	-	-	6.92 7.88
1g	101.7	5.06 (d, *J* = 7.5)	3.44 3.45	3.44 3.45	-
2g	74.8	3.44	*	*	-
3g	77.9	3.45	*	*	-
4g	71.3	3.40	*	*	-
5g	78.4	3.50	*	*	-
6g	62.5	3.70 (m)	3.92	3.92	-
		3.92 (m)	3.70	3.70	

*Overlapped signal; g-glucose

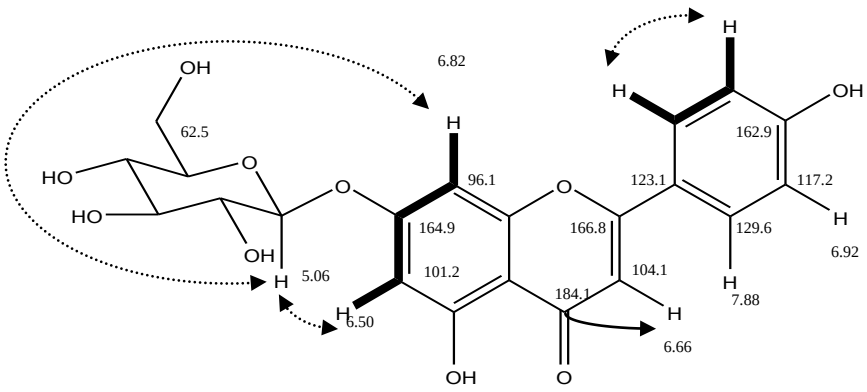

Figure 3.62 Selected correlations of apigenin-7-*O*-β-glucopyranoside
COSY (bold line), NOESY (dotted arrow), HMBC (arrow)

The NOESY correlations of anomeric proton at δ 5.06 ppm to two signals at δ 6.50 ppm (H-6) and δ 6.82 ppm (H-8) were observed the same as previous described in luteolin glycoside which verified the attachment of the anomeric position to C-7 of the aglycone apigenin.

Apigenin-7-*O*-β-glucopyranoside was previously reported in *S. viridis* L. (Kokkalou and Kapetanidis, 1988), and also is commonly found in other species (Lu and Foo, 2002).

3.6.3 Triterpenoids and steroids

The non-polar fractions of the aerial parts (AE) contained a series of relatively high molecular weight compounds with molecular formula and NMR spectra consistent with triterpenoids.

3.6.3.1 Ursolic acid

Ursolic acid (Figure 3.63) was obtained as a white powder by silica column chromatography. Mass spectral data showed a molecular mass of 456 and a molecular formula of $C_{30}H_{48}O_3$. ^1H and ^{13}C NMR data are shown in Table 3.20 and NMR spectra are presented in Appendix 13.

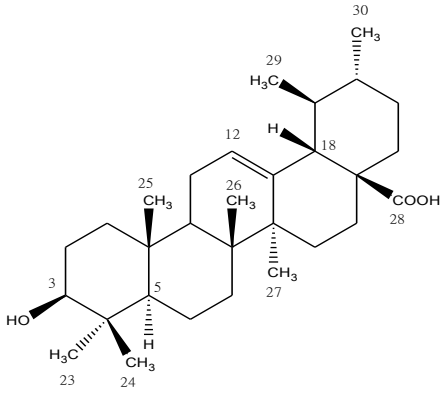

Figure 3.63 Ursolic acid

The formula $C_{30}H_{48}O_3$ indicated seven double bond equivalent (DBE). ^{13}C NMR and DEPT-135 also corresponded to the formula $C_{30}H_{48}O_3$ with 30 signals of carbon atoms, and nine negative signals of methylene groups with seven signals of quaternary carbon atoms at δ 181.3, 139.1, 48.5, 42.8, 40.3, 39.4, and 37.6 ppm. The two conspicuous proton signals (Figure 3.64) at δ 5.21 ppm and 3.14 ppm implied the deshielded protons of a trisubstituted double bond (H-12), and hydroxyl group substitution (H-3) respectively. The proton NMR spectrum showed five, three proton singlets and two, three proton doublets indicative of five methyl group attached at quaternary centre and two attached to methine carbon atoms. Therefore, the structure of this formula is likely to be an ursane type triterpenoid, ursolic acid.

Table 3.20 1D and 2D NMR data of ursolic acid (^{1}H, 500 MHz; ^{13}C, 125 MHz in a mixture of CD_3OD and $CDCl_3$, δ in ppm; *J* in Hz)

Position	^{13}C	^{1}H	COSY	NOESY	HMBC
1	39.6	0.93*	-	-	0.73 0.76 0.91
		1.63*	3.14	-	0.93
2	27.4	1.54*	3.14	-	0.76
3	79.3	α3.14 (dd, *J* = 11, 5)	1.63 1.54	1.54* 0.91 0.73	0.73 0.76 0.91 0.93 1.54* 1.63*
4	39.4	-	-	-	0.76 0.93
5	56.2	α0.73 (d, *J* = 11.5)	-	1.53*	0.76 0.91 0.93 1.52 1.63*
6	19.1	α1.37	-	1.53*	0.73
		β1.53*	-	1.35*	
7	33.9	1.35	-	-	0.76
		1.52*	-	-	0.82
8	40.3	-	-	-	0.82 1.09 1.53*
9	48.2	1.53*	-	-	0.82 0.91 2.16

Table 3.20 (continued)

Position	^{13}C	^{1}H	COSY	NOESY	HMBC
10	37.6	-	-	-	0.73 0.91 1.53* 1.63*
11	24.0	1.09*	-	-	0.84
		1.89*	-	5.21	5.21
12	126.4	5.21 (t, *J* = 3.5)	1.89*	1.09 1.89 2.16	1.89* 2.16
13	139.1	-	-	-	1.09 1.89* 2.16
14	42.8	-	-	-	0.82 1.09 1.52* 1.89* 2.16 5.21
15	28.8	1.05*	-	-	1.09
		1.88*	1.98	-	1.98
16	24.9	1.62	-	-	1.89*
		1.98	1.88*	-	2.16
17	48.5	-	-	-	2.16
18	53.8	2.16 (d, *J* = 11)	1.36*	5.21	0.84 5.21
19	39.8	1.63*	-	-	0.84 0.92 2.16
20	39.9	1.36*	0.84 2.16	-	0.84 0.92 2.16
21	31.4	1.51	-	-	0.84 0.92

Table 3.20 (continued)

Position	^{13}C	^{1}H	COSY	NOESY	HMBC
22	37.7	1.67	-	-	0.84 1.51*
23	28.6	α0.93* (3H, s)	0.76	-	0.73 0.76 3.14
24	16.1	β0.76 (3H, s)	0.93	-	0.73 0.91 0.93 1.54*
25	15.9	β0.91 (3H, s)	-	-	0.73 0.91 0.93 1.54*
26	17.5	β0.82 (3H, s)	-	-	1.52* 1.53*
27	24.0	α1.09* (3H, s)	-	-	1.05* 1.62* 1.89* 2.16
28	181.3	-	-	-	1.98 2.16
29	17.1	β0.84 (3H, d, *J* = 6.5)	1.36*	-	1.51* 2.16
30	21.5	α0.92 (3H, d, *J* = 6.5)	-	-	1.36*

*Overlapped signal

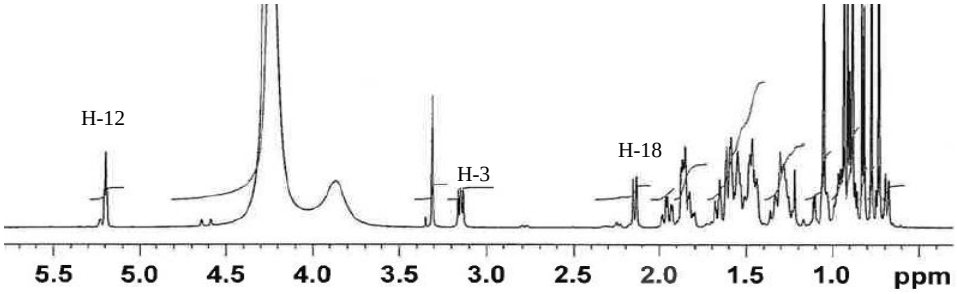

Figure 3.64 ^{1}H NMR of ursolic acid (500 MHz; a mixture of CD_3OD and $CDCl_3$)

The configuration of proton at positions 3, 5, and 18 were assigned by their coupling constant values. The proton H-3 resonated at δ 3.14 ppm as a doublet of doublets with coupling constants 11, and 5 Hz indicating β-hydroxyl group (equatorial) substitution at position C-3 as shown in Figure 3.65A.

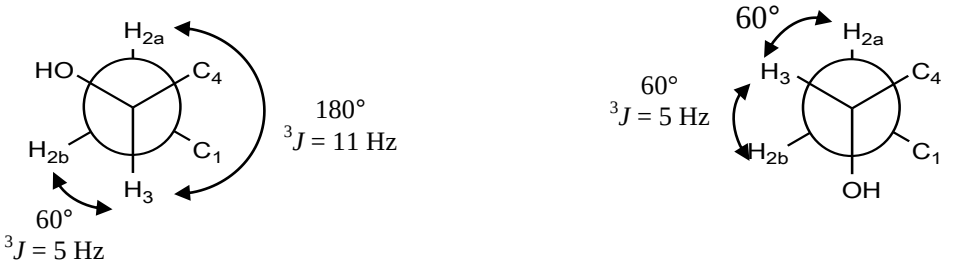

A. β-Hydroxyl group substitution B. α-Hydroxyl group substitution

Figure 3.65 Newman projections of C-2, and C-3 of ursolic acid

The other noticeable signal of the ursane type triterpenoid is one proton doublet at H-18 (Figure 3.64). It was deshielded at δ 2.16 ppm because of double bond at position 12-13. Its coupling constant to H-19 is 11 Hz (di-axial) which indicates the β-substitution (equatorial) of the methyl group at C-19.

Proton H-5 of the triterpenic acids with geminal methyl groups at C-4 was obviously seen in ^{1}H NMR as the first low-field broad doublet signal at δ 0.73 with coupling constant 11 Hz, and it had a HMQC correlation to carbon at δ 56.2 ppm (Figure 3.67). A large vicinal coupling constant denoted 180° dihedral angle, and thus the H-5 is likely to be an axial proton as shown in Figure 3.66. Figures 3.68-3.69 illustrate the chemical shift assignments of carbon and proton by using HMBC, COSY, and NOESY correlations.

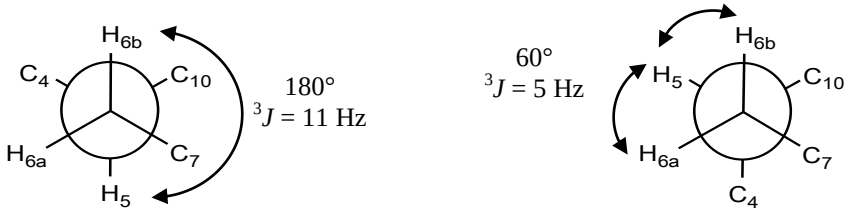

A. H-5 axial B. H-5 equatorial

Figure 3.66 Newman projections of C-5, and C-6 of ursolic acid

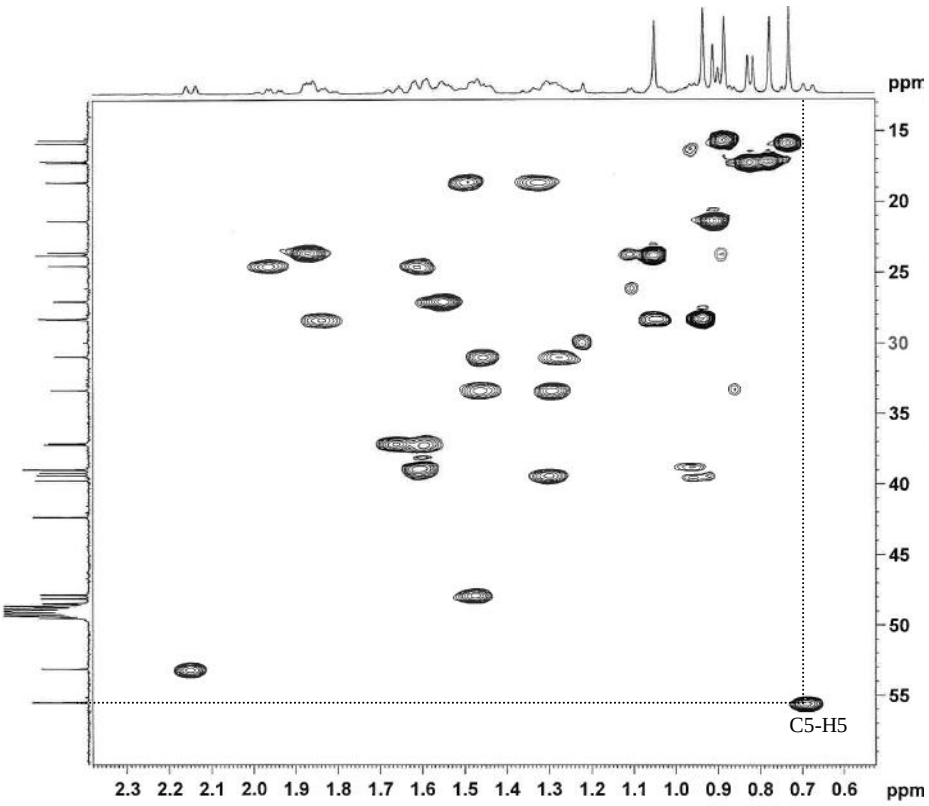

Figure 3.67 HMQC expansion of ursolic acid (^{1}H, 500 MHz; ^{13}C, 125 MHz in mixture of CD_3OD and $CDCl_3$)

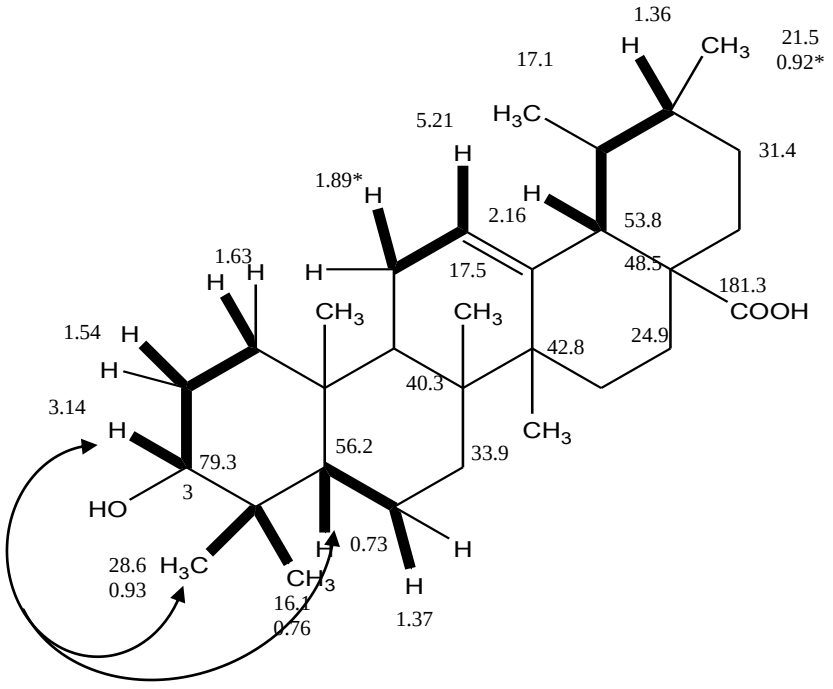

Figure 3.68 Selected COSY (bold line) and NOESY (arrow) correlations of ursolic acid

A.

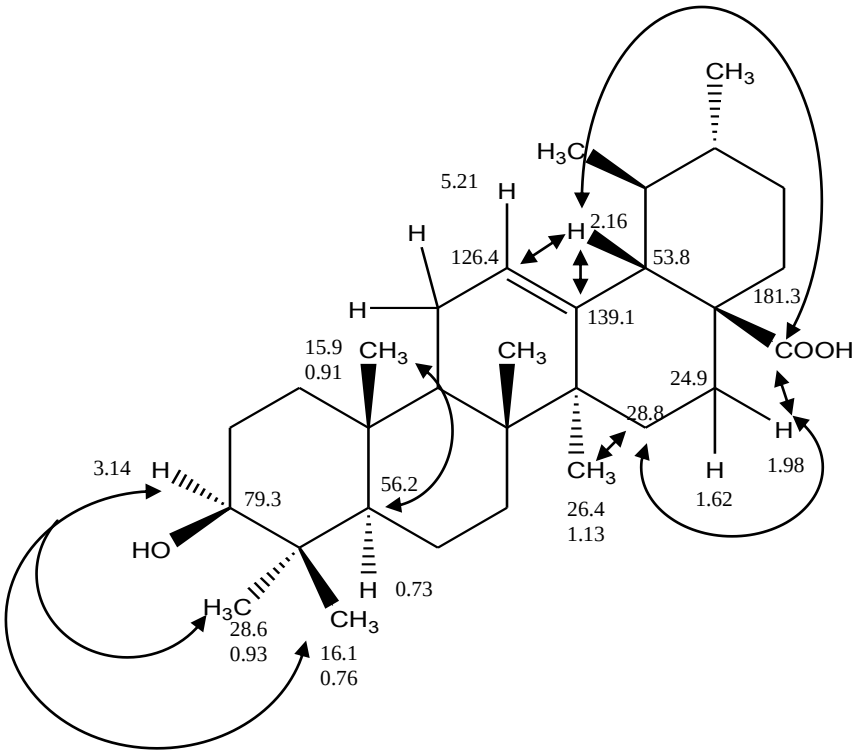

B.

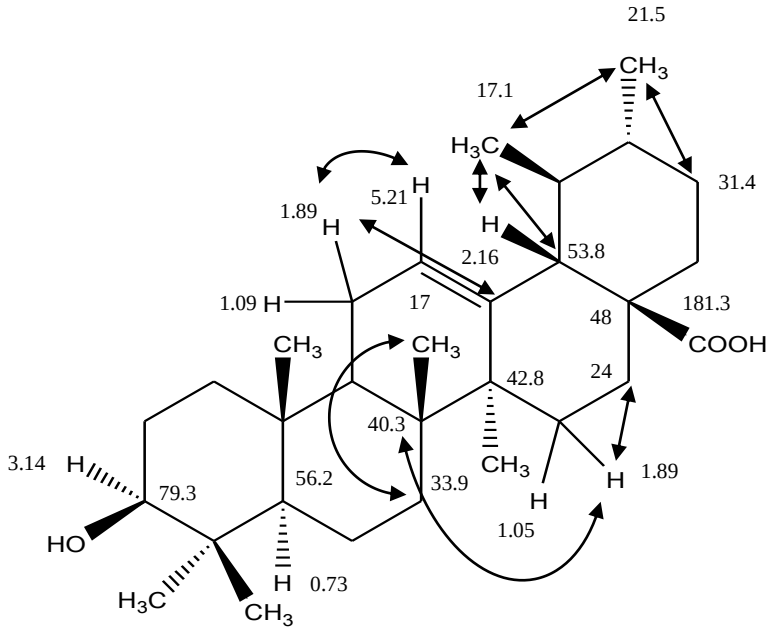

Figure 3.69A-B Selected HMBC correlations of ursolic acid

3.6.3.2 Oleanolic acid

Oleanolic acid (Figure 3.70) was obtained as a white powder by silica column chromatography. Judging from the NMR spectra, this material was about 70% pure, with ursolic acid as the major impurity. MS data gave a molecular mass of 456, corresponding to a molecular formula of $C_{30}H_{48}O_3$. ^1H and ^{13}C NMR data are shown in Table 3.21 and NMR spectra are given Appendix 14.

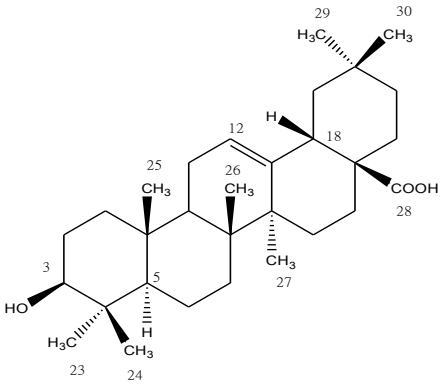

Figure 3.70 Oleanolic acid

The formula $C_{30}H_{48}O_3$ indicated seven double bond equivalent (DBE). ^{13}C NMR and DEPT-135 also corresponded to the formula $C_{30}H_{48}O_3$ with 30 signals of carbon atoms, and 10 negative signals of methylene groups and eight signals of quaternary carbon atoms at δ 181.4, 144.5, 47.0, 42.3, 39.9, 39.2, 37.6, and 31.2 ppm. The two conspicuous protons at δ 5.23, and 3.13 ppm, pointed to deshielded protons of a trisubstitutd double bond (position 12), and hydroxyl group substitution (position 3) respectively. A doublet of doublet at δ 2.80 ppm indicated H-18 with two protons nearby whereas the H-18 of ursane triterpenoid has only one proton adjacent and resonated as a doublet. Moreover, in the ^1H NMR spectrum all the methyl groups were three proton singlets, indicating that all were attached at quaternary centres. Therefore, the structure of this formula is likely to be an oleanane type triterpenoid, oleanolic acid.

Table 3.21 1D and 2D NMR data of oleanolic acid (^{1}H, 500 MHz; ^{13}C, 125 MHz in a mixture of CD_3OD and $CDCl_3$, δ in ppm; *J* in Hz)

Position	^{13}C	^{1}H	COSY	NOESY	HMBC
1	39.3	0.94*	-	-	0.70
		1.60	-	-	0.74
					0.89
					0.94
2	27.2	1.56*	3.14	3.14	-
3	79.2	3.14 (dd, *J* = 10.5, 5)	1.56	0.70	0.74
				0.94	0.94
				1.56	1.60
4	39.2	-	-	-	0.70
					0.74
					0.89
					0.94
5	56.0	α0.70 (d, *J* = 10)	1.37	3.14	0.74
					0.89
					0.94
6	18.9	1.37	0.70	-	0.70
		1.53*		-	
7	33.7	1.29	-	-	0.77
		1.46	-	-	
8	39.9	-	-	-	0.77
					1.11
					1.54*
9	49.0	1.54*	1.84	-	0.77
					0.89
10	37.6	-	-	-	0.70
					0.89
					1.54*
					1.56*
11	24.0	1.07	5.23	-	1.54*
					1.60*
		1.84	1.54	5.23	

Table 3.21 (continued)

Position	^{13}C	^{1}H	COSY	NOESY	HMBC
12	123.0	5.23 (t, *J* = 3)	1.84	1.84 2.80	1.84 2.80
13	144.5	-	-	-	1.11 1.84 2.80
14	42.3	-	-	-	0.77 1.11 1.71
15	28.3	1.04	1.96	-	1.11
		1.71*	1.04	-	
16	23.6	1.58	-	-	1.58
		1.96	1.04	-	1.71
17	47.0	-	-	-	1.11 1.71 1.96
18	41.9	2.80 (dd, *J* = 13.5, 4)	1.10 1.63	0.90 5.23	1.11 1.63*
19	46.6	1.10	2.80	-	0.87
		1.63*			0.90
20	31.2	-	-	-	0.87 0.90 1.33 1.63*
21	34.4	1.18	-	-	0.87
		1.33	-	-	1.71*
22	33.2	1.52*	-	-	1.33
		1.71*	-	-	
23	28.4	α0.94 (3H, s)	0.74	-	0.74
24	16.0	β0.74 (3H, s)	0.94	-	0.70 0.94

Table 3.21 (continued)

Position	^{13}C	^{1}H	COSY	NOESY	HMBC
25	15.7	β0.89 (3H, s)	-	-	0.70 0.94 1.53*
26	17.3	β0.77 (3H, s)	-	-	0.89 1.54*
27	26.3	α1.11 (3H, s)	-	-	-
28	181.4	-	-	-	1.71 1.96
29	33.4	α 0.87 (3H, s)	-	-	0.90 1.33
30	23.9	β0.90 (3H, s)	-	2.80	0.87 1.63*

*Overlapped signal

The configurations of protons at position 3, 5, and 18 were assigned by coupling constant values as described in ursolic acid. The H-3 resonated at δ 3.14 ppm as doublets of doublets with coupling constant 10.5, and 5 Hz indicating the β-hydroxyl group (equatorial) substitution at position C-3. The other noticeable signal of the oleanane type triterpenoid is a doublet of doublet of proton H-18. It was deshielded at δ 2.80 ppm because of double bond at position 12-13. Its coupling constants are 13.5, and 4 Hz which indicates its axial (β) configuration and the fact that it is adjacent to a methylene group. H-5 of oleanolic acid is also seen in ^{1}H NMR as the first low-field doublet signal at δ 0.70 with coupling constant 10 Hz. The configuration of H-5 was similar to ursolic acid as described above.

Figures 3.71-3.72 illustrates the chemical shift assignment of carbon and proton by using HMBC, COSY, and NOESY correlations.

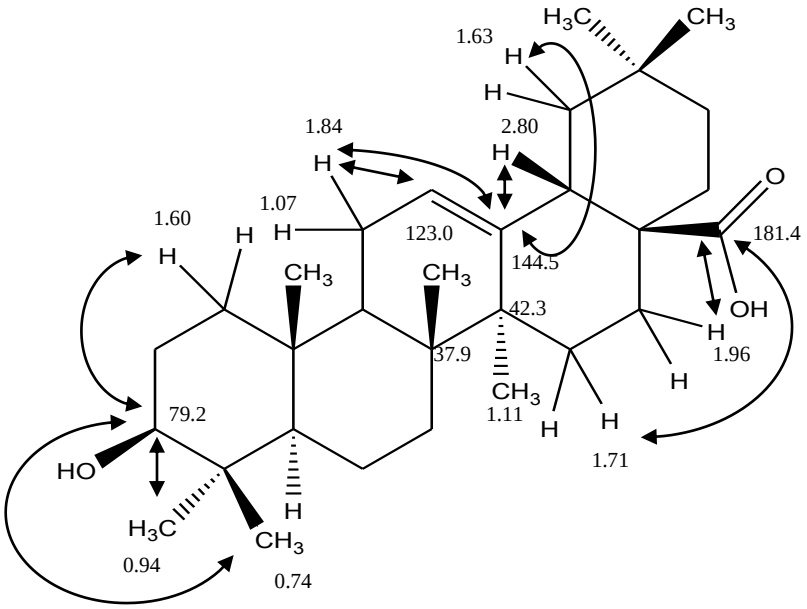

A.

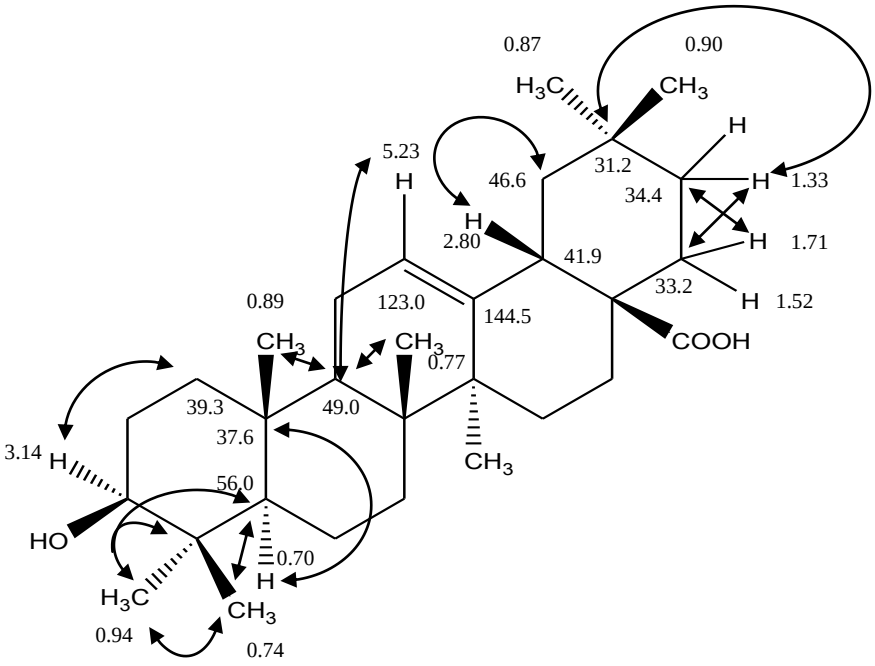

B.

Figure 3.71A-B Selected HMBC correlations of oleanolic acid

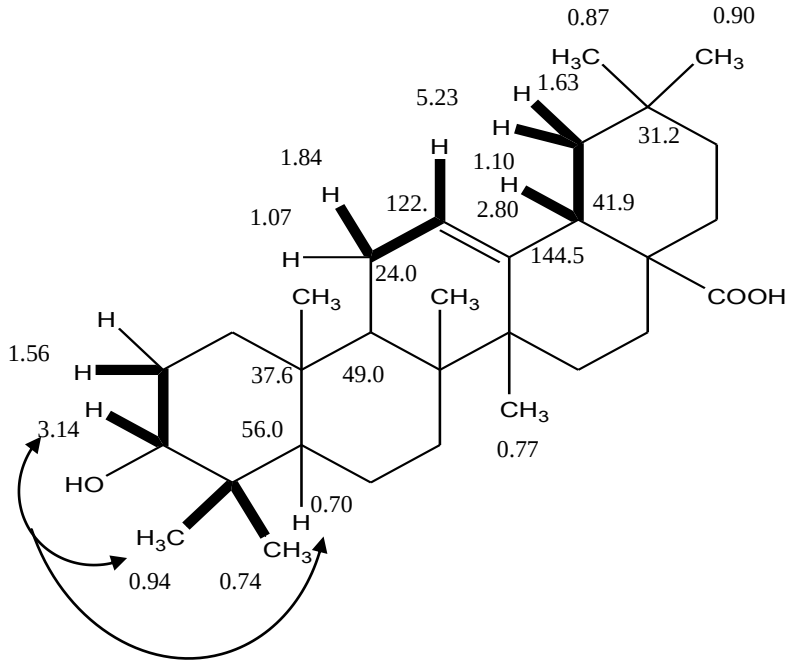

Figure 3.72 Selected COSY (bold line) and NOESY (arrow) correlations of oleanolic acid

Both ursolic and oleanolic acids have been previously reported in *S. viridis* L. (Ulubelen and Brieskorn, 1975), and are also common in other *Salvia* species (Topcu, 2006).

3.6.3.3 Lup-(20)29-ene-2α,3β-diol

The MS data of lup-(20)29-ene-2α,3β-diol (Figure 3.73) gave a molecular mass of 442 and a molecular formula of $C_{30}H_{50}O_2$. ^1H and ^{13}C NMR data are shown in Table 3.22, and the NMR spectra are given in Appendix 15.

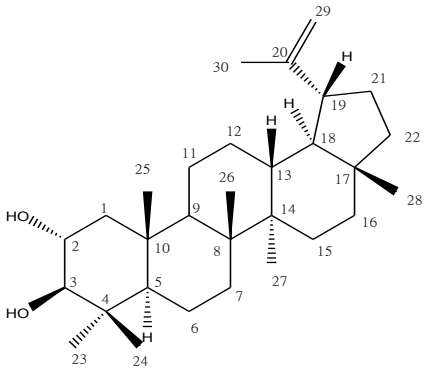

Figure 3.73 Lup-(20)29-ene-2α,3β-diol

Table 3.22 1D and 2D NMR data of lup-(20)29-ene-2α,3β-diol (^{1}H, 500 MHz; ^{13}C, 125 MHz in $CDCl_3$; δ in ppm; *J* in Hz)

Position	^{13}C	^{1}H	COSY	NOESY	HMBC
1	46.7	α0.83 (dd, *J* = 12, 7)	2.03	2.03	0.90
		β2.03 (dd, *J* = 12, 4)	0.83	0.83	
			3.67	3.67	
2	69.3	β3.67	0.83	0.80	0.80
		(ddd, *J* = 10, 9.5, 4.5)	2.03	0.90	0.83
			2.97	2.03	1.26*
				2.97	2.03
					2.97
3	83.9	α2.97 (d, *J* = 9.5)	3.67	0.80	0.80
				0.83	0.83
				1.01	1.01
				3.67	2.03
4	38.6	-	-	-	1.52
					2.03
5	55.4	0.79*	*	*	0.80
					0.90
					1.01
					2.03
6	18.3	1.40*	-	-	1.40*
		1.52	0.79*	0.80	
				1.01	
7	34.2	1.39	*	*	1.02
8	40.9	-	-	-	0.94
					1.02
9	50.4	1.32*	-	-	0.90
					1.02
10	39.2	-	-	-	0.80
					0.90
					1.01
					1.02
					2.97

Table 3.22 (continued)

Position	^{13}C	^{1}H	COSY	NOESY	HMBC
11	21.0	1.26*	*	*	1.32
		1.45*			
12	25.0	1.08	1.26*	-	0.94
		1.67*	*	1.02	
13	38.0	1.65*	1.35*	-	0.94
					1.02
					1.35*
					2.36
14	42.9[§]	-	-	-	0.78
					0.94
					1.02
15	27.4	1.74*	-	-	-
16	35.6	1.38*	*	*	0.78
		1.47*			1.35*
17	43.0[§]	-	-	-	0.78
					0.94
					1.02
18	48.3	1.35*	*	*	0.78
					1.39
					1.67
					2.36
					4.57
					4.69
19	48.0	2.36	1.39	0.78	0.78
		(ddd, J = 11, 11, 6)	1.92	1.67	1.39
				1.92	1.67
					2.36
					4.57
					4.69
20	150.9	-	-	-	1.35*
					1.67
					2.36

Table 3.22 (continued)

Position	^{13}C	^{1}H	COSY	NOESY	HMBC
21	29.8	1.32*	*	*	2.36
		1.92	1.39*	0.78 1.20 2.36	
22	40.0	1.20	*	*	0.78
		1.38*			
23	28.5	α1.01 (3H, s)	0.80	*	0.80 0.90 2.97
24	16.5	β0.80 (3H, s)	1.01	*	1.01 2.97
25	17.4	β0.90 (3H, s)	-	2.03 3.67	2.03
26	16.0	β1.02 (3H, s)	-	-	1.39
27	14.5	α0.94 (3H, s)	-	-	1.65
28	18.0	β0.78 (3H, s)	1.20	2.36	-
29	109.4	4.57 (d, *J* = 2)	1.67 4.69	1.67 4.69	1.67 2.36
		4.69 (d, *J* = 2)	1.67 4.57	1.67 2.36 4.57	
30	19.3	1.67* (3H, s)	4.57 4.69	4.57 4.69	2.36 4.57 4.69

*Overlapped signal; [§] Interchangeable

The NMR spectra indicated a lupane type triterpenoid due to certain typical signals, i.e., exo-methylene protons (H-29) at δ 4.57 ppm, and 4.69 ppm, carbon signals at δ 109.4 ppm (C-29) and 150.9 ppm (C-20), and the carbon atom at position 3 with hydroxyl group substitution δ 83.4 ppm (Mahato and Kundu, 1994). ^{1}H NMR spectrum showed seven, three proton methyl singlets, one of which was deshielded at δ 1.67 ppm (H-30).

An additional deshielded carbon signal at δ 69.3 ppm together with the extra oxygen atom in the molecular formula pointed to a second hydroxyl group substitution to the lupeol skeleton. A doublet proton signal at δ 2.97 ppm with coupling constant 9.5 Hz revealed only one adjacent proton with di-axial coupling. Moreover, there is a COSY correlation between the signal at δ 2.97 ppm, and 3.67 ppm. Thus, these signals were assigned to H-3 and H-2 respectively and the compound was identified as a lupene diol with 2α-OH, and 3β-OH substitutions. Configurations of each chiral carbon were assigned according to coupling constants, and NOESY correlations.

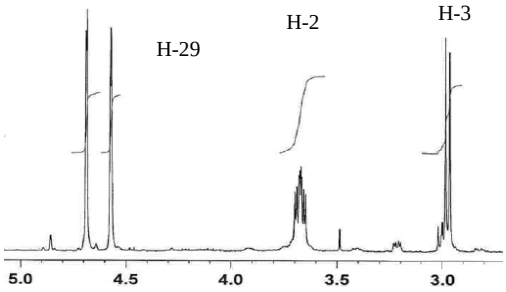

Figure 3.74 ^{1}H expansion of lup-(20)29-ene-2α,3β-diol (500 MHz; $CDCl_3$; δ in ppm)

Figure 3.75 illustrates the configurations of 2-OH, and 3-OH subsititution by using Newman projection. The doublet of H-3 had a coupling constant 9.5 Hz, and the ddd of H-2 had three coupling constant values, 10, 9.5 and 4.5 Hz. These indicated the large dihedral angle between them, thus the substitution must be 2α-OH, and 3β-OH (Figure 3.75A).

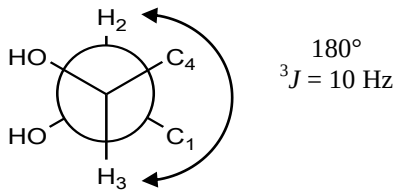

A. 2α-OH, and 3β-OH

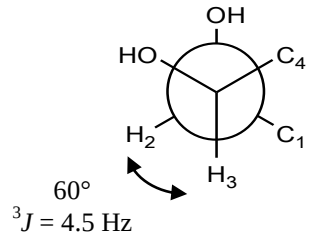

B. 2β-OH, and 3β-OH

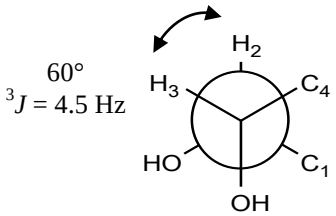

C. 2α-OH, and 3α-OH

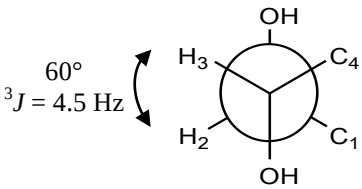

D. 2β-OH, and 3α-OH

Figure 3.75 Newman projections of C-2, and C-3 of lup-(20)29-ene-2α,3β-diol

The other salient configuration is H-19 at δ 2.36 ppm. It was coupled to the H-18, and H-21a, 21b nearby with coupling constant 11, 11 and 6 Hz. As the large coupling constant, H-19, and H-18 must be an axial-axial as shown in Figure 3.76.

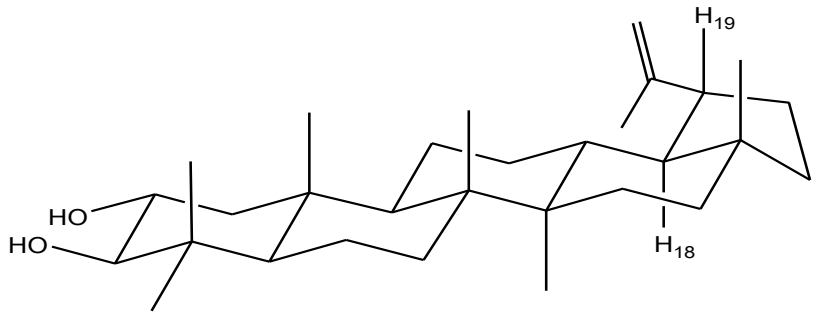

Figure 3.76 Chair conformation of lup-(20)29-ene-2α,3β-diol

Figures 3.77-3.79 show chemical shifts of protons and carbon atoms at salient positions assigned by using HMBC, COSY, and NOESY. HMBC correlated the exo-methylene protons to signals at δ 19.3 ppm (C-30), and 48.0 ppm (C-19). Accordingly, H-19 was correlated to C-21 at δ 29.8 ppm, and a singlet signal of methyl group at δ 0.78 ppm (C-28; δ 18.0 ppm) by NOESY. HMBC showed correlations between the doublet signal of H-3 at δ 2.97 ppm to signals, at δ 28.5 ppm (C-23), 16.5 ppm (C-24), 39.2 ppm (C-10), and 69.3 ppm (C-2). In addition, there is a COSY correlation between 2 singlet signals, 1.01 ppm (H-23), and 0.80 ppm (H-24). H-23, and H-24 were assigned by NOESY as shown in Figure 3.79.

Lup-(20)29-ene-2α,3β-diol was first isolated from *Pterocarpus santalinus* L. f., family Leguminosae (Kumar and Seshadri, 1976) and also reported in *S. viridis* L. (Ulubelen et al., 1977).

A.

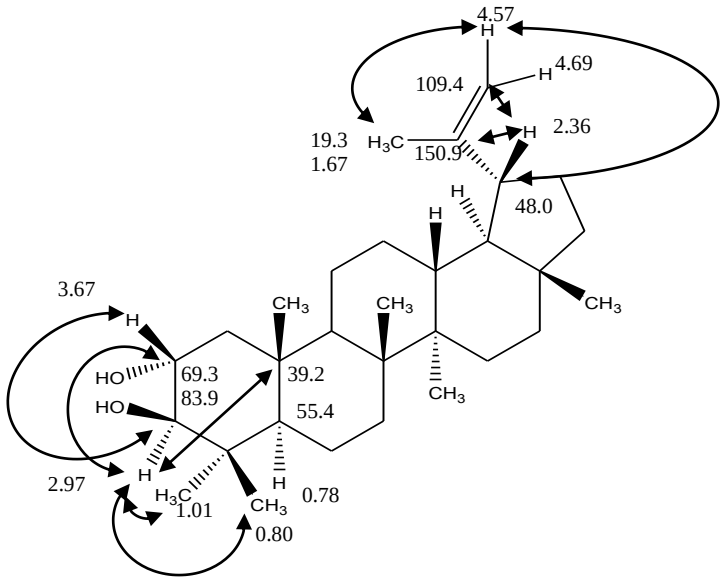

B.

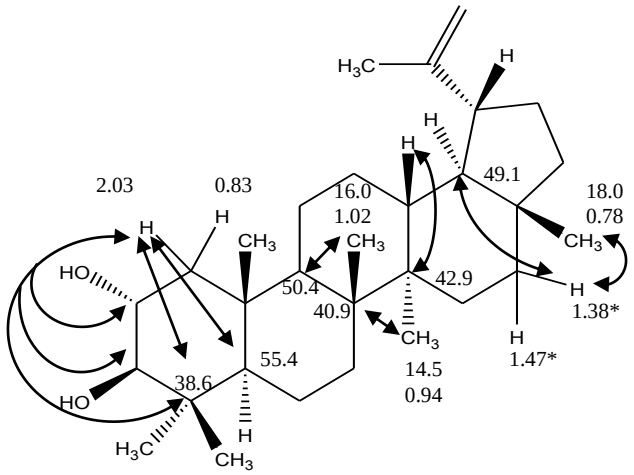

Figure 3.77A-B Selected HMBC correlations of lup-(20)29-ene-2α,3β-diol

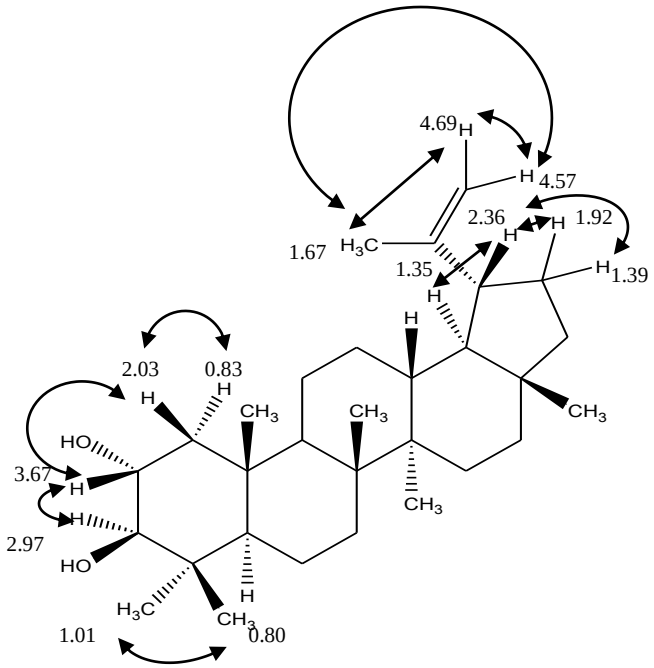

Figure 3.78 Selected COSY correlations of lup-(20)29-ene-2α,3β-diol

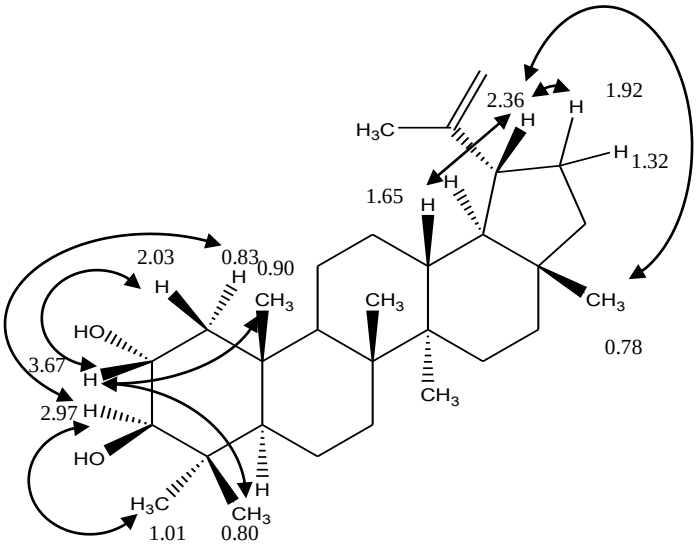

Figure 3.79 Selected NOESY correlations of lup-(20)29-ene-2α,3β-diol

3.6.3.4 Compound 1 (lup-(20)29-ene-2α-acetate-3β-ol)

The MS data of compound 1 (Figure 3.80) gave a molecular mass of 484 and a molecular formula of $C_{32}H_{52}O_3$. ^1H and ^{13}C NMR data are shown in Table 3.23 and NMR spectra are given in Appendix 16.

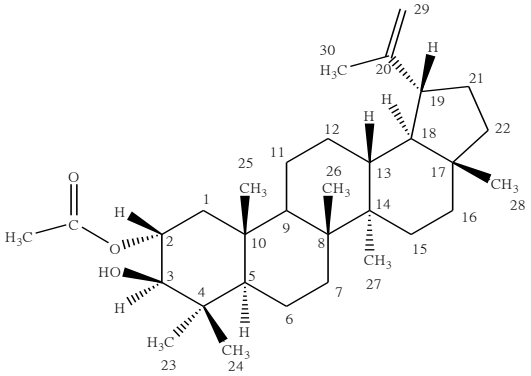

Figure 3.80 Compound 1 (lup-(20)29-ene-2α-acetate-3β-ol)

Both ^1H and ^{13}C NMR spectrum corresponded to the lupane type triterpenoid as described for the previous compound. A doublet signal at δ 3.15 ppm had a COSY correlation to a downfield methine signal at δ 4.86 ppm. Therefore, this $C_{32}H_{52}O_3$ is likely to be a lupane skeleton with 2 oxygen functions at C-2, and C-3; the additional deshielding of δ 4.86 ppm.suggested acetylation. All salient signals were assigned as shown in Figure 3.81.

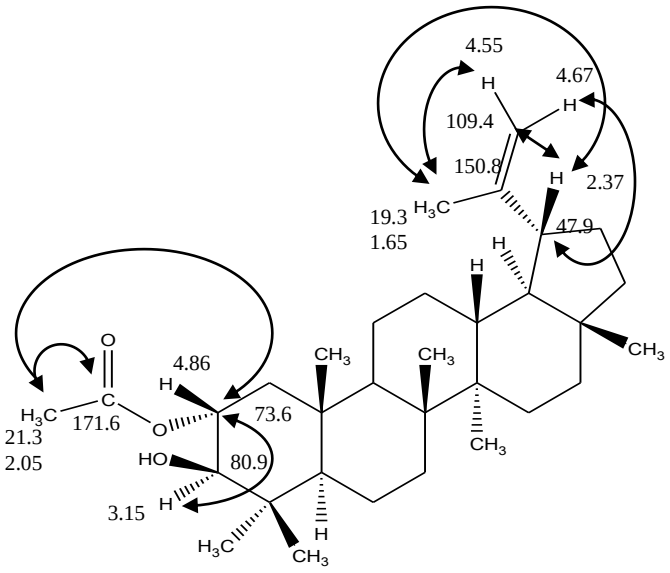

Figure 3.81 Salient HMBC signals of compound 1 (lup-(20)29-ene-2α-acetate-3β-ol)

Table 3.23 1D and 2D NMR data of compound 1 (lup-(20)29-ene-2α-acetate-3β-ol) (^{1}H, 500 MHz; ^{13}C, 125 MHz; $CDCl_3$; δ in ppm; *J* in Hz)

Position	^{13}C	^{1}H	COSY	NOESY	HMBC
1	44.0	2.04*	-	-	0.94
		0.90	4.86	2.05	
2	73.6	4.86	0.90*	0.84	0.90
		(ddd, *J* = 10, 10, 5)	2.05	0.94	2.05
			3.15	2.05	3.15
3	80.9	3.15 (d, *J* = 10)	4.86	0.76*	0.84
				0.90	1.03
				1.03	2.04*
					2.05
4	39.8	-	-	-	0.94
					1.03
					3.15
5	55.2	0.76*	1.53	-	0.84
					0.94
					1.03
					2.04*
6	18.2	1.40	-	-	-
		1.53	0.76*	-	
7	34.1	1.43* (2H)	-	-	1.02
8	40.9	-	-	-	0.93
					0.94
					1.02
9	50.4	1.31	-	-	0.93
					0.94
					1.02
10	38.5	-	-	-	0.93
					0.94
					1.38*
					2.05

Table 3.23 (continued)

Position	^{13}C	^{1}H	COSY	NOESY	HMBC
11	21.1	1.25*	-	-	-
		1.38*	-	-	
12	25.0	1.07	-	-	-
		1.66*	-	1.02	
13	38.0	1.64*	-	1.02	0.93 1.38*
14	42.9[§]	-	-	-	0.78 0.93 1.02 1.38*
15	27.4	0.98*	-	-	0.93
		1.66*	-	-	1.19
16	35.6	1.37*	-	-	0.78
		1.47	-	-	
17	43.0[§]	-	-	-	0.78 0.93 1.02 1.38*
18	48.3	1.34*	-	-	1.38* 2.37 4.55 4.67
19	47.9	2.37 (ddd, *J* = 11, 11, 6)	1.38* 1.92	0.78 1.65 1.92	0.78 1.38* 1.65 4.55 4.67
20	150.8	-	-	-	1.34* 1.65 2.37

Table 3.23 (continued)

Position	^{13}C	^{1}H	COSY	NOESY	HMBC
21	29.7	1.38*	1.92 2.37	-	2.37
		1.92	1.38* 2.37	-	
22	40.0	1.19	-	-	-
		1.38*	-	-	
23	28.4	α1.03 (3H, s)	0.84	3.15	0.84 3.15
24	16.4	β0.84 (3H, s)	1.03	4.86	0.76* 1.03 3.15
25	17.1	β0.94 (3H, s)	-	-	0.90* 2.04*
26	16.0	β1.02 (3H, s)	-	-	1.40*
27	14.5	α0.93 (3H, s)	-	-	1.64*
28	18.0	β0.78 (3H, s)	-	2.37	1.19 1.38*
29	109.4	4.55 (d, *J* = 2)	1.65 4.67	1.65 4.67	1.34* 2.37
		4.67 (d, *J* = 2)	1.65 4.55	1.38 1.65 2.37 4.55	
30	19.3	1.65 (3H, s)	1.34* 1.38* 4.55 4.67	2.37 4.55 4.67	2.37 4.55 4.67
Acetyl group	21.3	2.05 (3H, s)	0.90* 4.86	0.90	-
	171.6	-	-	-	2.05

* Overlapped peak; § Interchangeable

.

^{13}C NMR showed 32 signals with seven quaternary carbon atoms, and ten methylene groups from DEPT-135. An extra carbonyl carbon signal at δ 171.6 ppm had a HMBC correlation to a ^{1}H singlet signal at δ 2.05 ppm. Moreover, this singlet showed NOESY and HMBC correlations to the proton at δ 4.86 ppm and the carbon at δ 73.6 ppm respectively. Thus, these signals are assigned to an acetate ester attached to the lupane pentacyclic ring at C-2. All configurations of compound 1 were assigned as described above in structure elucidation of lup-(20)29-ene-2α,3β-diol. The other chemical shift of protons and carbons were assigned by using HMBC, COSY, and NOESY as shown in Figures 3.82-3.84.

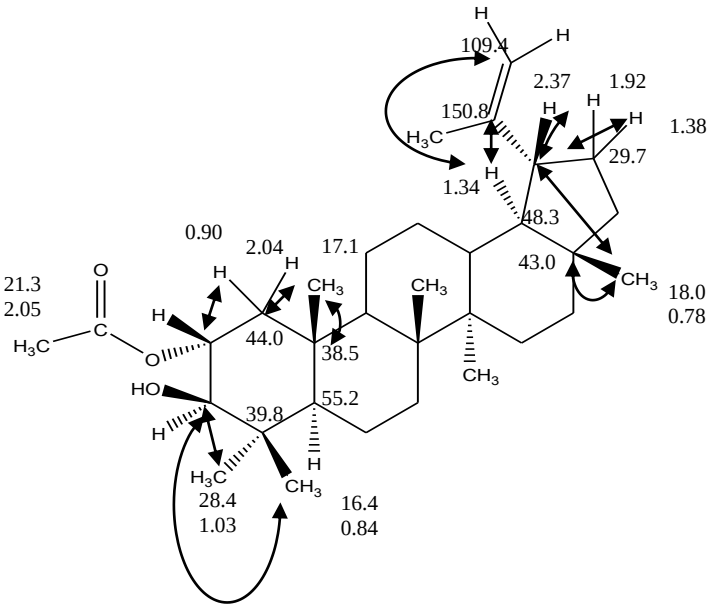

A.

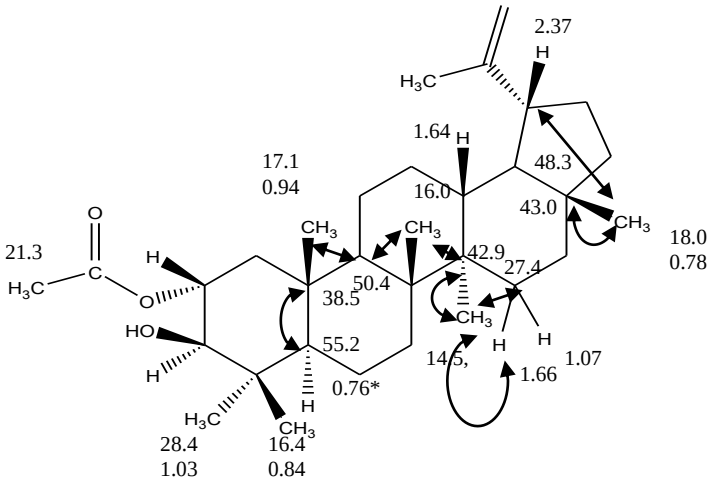

B.

Figure 3.82A-B Selected HMBC correlations of compound 1 (lup-(20)29-ene-2α-acetate-3β-ol)

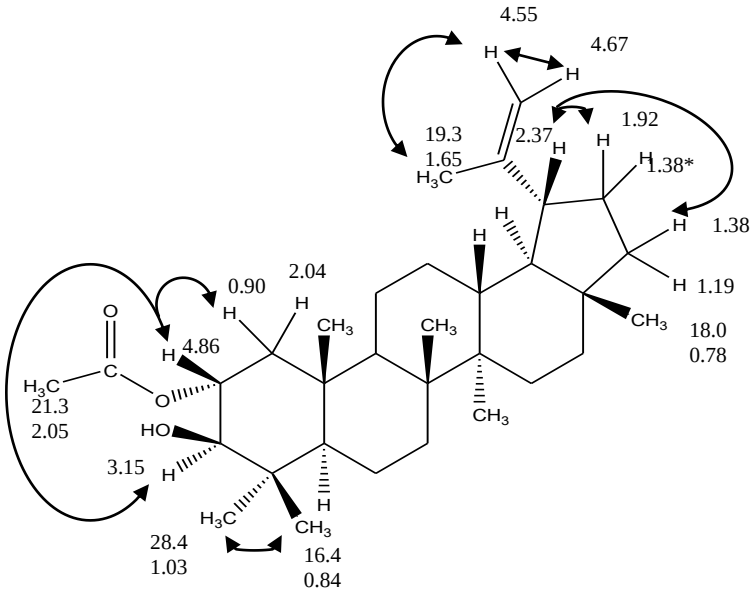

Figure 3.83 Selected COSY correlations of compound 1 (lup-(20)29-ene-2α-acetate-3β-ol)

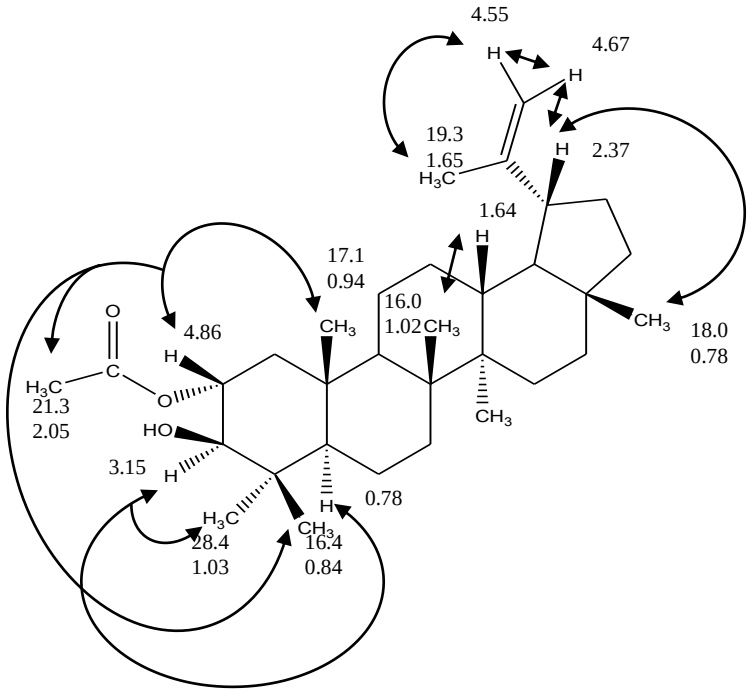

Figure 3.84 Selected NOESY correlations of compound 1 (lup-(20)29-ene-2α-acetate-3β-ol)

Therefore, compound 1 was identified as lup-(20)29-ene-2α-acetate-3β-ol established by its molecular formula $C_{32}H_{52}O_3$ (MW 484) and NMR spectroscopic data. This compound is now reported here for the first time.

3.6.3.5 Compound 2 (lup-(20)29-ene-2α-ol-3β-acetate)

The MS data showed compound 2 (Figure 3.85) to be an isomer of compound 1 with a molecular mass of 484 and a molecular formula of $C_{32}H_{52}O_3$. ^1H and ^{13}C NMR data are shown in Table 3.24 and NMR spectra are given in Appendix 17.

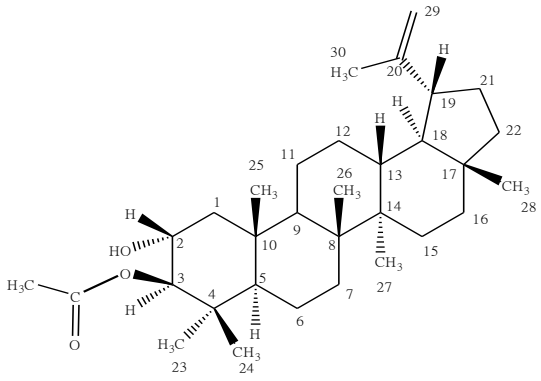

Figure 3.85 Compound 2 (lup-(20)29-ene-2α-ol,3β-acetate)

All NMR data were similar to compound 1 (lup-(20)29-ene-2α-acetate-3β-ol) except two methine proton signals; the downfield doublet at δ 4.46 ppm, and the ddd at δ 3.77 ppm. The doublet indicated that there was only one vicinal proton, and it had a COSY correlation to the methine signal at δ 3.77 ppm, and also HMBC correlations to the carbonyl carbon signal at δ 172.4 ppm, and to one methyl group at δ 21.04 ppm. These pointed to an acetate ester group attached to the C-3 hydroxyl group of lup-(20)29-ene-2α,3β-diol and thus, this structure is an isomer of compound 1. The configurations at each position were the same as compound 1. Selected HMBC, NOESY and COSY correlations are presented in Figures 3.87-3.89.

Table 3.24 1D and 2D NMR data of compound 2 (lup-(20)29-ene-2α-ol-3β-acetate) (^{1}H, 500 MHz; ^{13}C, 125 MHz in $CDCl_3$; δ in ppm; *J* in Hz)

Position	^{13}C	^{1}H	COSY	NOESY	HMBC
1	48.1	2.09	-	0.91 3.77	0.91 4.46
		0.90*	-	2.13	
2	67.8	3.77 (ddd, *J* = 10, 10, 5)	0.90* 2.09 4.46	0.85 2.09 2.13 4.46	0.91 2.09* 2.13 4.46
3	85.0	4.46 (d, *J* = 10)	3.77	0.87 3.77	0.85 0.87 2.09* 2.13 3.77
4	39.3	-	-	-	0.85 0.87 4.46
5	55.3	0.88*	1.40* 1.50*	1.50	0.85 0.87 0.91 1.02 2.09* 2.13
6	18.3	1.40*	0.88*	-	1.34
		1.50*	0.88*	-	1.40*
7	34.1	1.40* (2H)	0.88*	-	1.02
8	40.9	-	-	-	0.94 1.02
9	50.3	1.34	-	-	0.91 1.02
10	38.4	-	-	-	0.91 1.34* 2.09*

Table 3.24 (continued)

Position	^{13}C	^{1}H	COSY	NOESY	HMBC
11	21.1	1.26	1.43	-	-
		1.43	-	-	
12	25.0	1.08	1.68*		-
		1.68*	1.02 1.08	-	
13	37.9	1.65*	-	-	0.94 1.08 1.36* 2.37
14	42.9[§]	-	-	-	0.78 0.94 1.02 1.20 1.40* 1.65*
15	27.4	0.98*	-	-	0.94
		1.68*	-	-	
16	35.5	1.38*	-	-	0.78
		1.46	-	-	
17	43.0[§]	-	-	-	0.78 0.94 1.02 1.20 1.40* 1.65*
18	48.2	1.36	-	-	0.78 1.38* 1.40* 1.68* 4.57 4.68

Table 3.24 (continued)

Position	^{13}C	^{1}H	COSY	NOESY	HMBC
19	48.0	β2.37 (ddd, *J* = 11, 11, 6)	0.78 1.40* 1.90	0.78 1.68 4.68	0.78 1.38* 1.40* 1.68* 4.57 4.68
20	150.8	-	-	-	1.36* 1.40* 1.68 2.37
21	29.8	1.32*	-	-	2.37
		1.90	1.20 1.32*	-	
22	40.0	1.20	0.78	-	0.78
		1.40*	-	-	
23	28.4	α0.87 (3H, s)	-	1.50	0.85 4.46
24	17.4	β0.85 (3H, s)	-	-	0.87 0.88* 0.91 2.09* 2.13 4.46
25	17.3	β0.91 (3H, s)	-	2.09	0.87 0.88* 0.91 2.09* 2.13
26	16.0	β1.02 (3H, s)	-	-	1.34* 1.40*
27	14.5	α0.94 (3H, s)	-	-	1.65*

Table 3.24 (continued)

Position	^{13}C	^{1}H	COSY	NOESY	HMBC
28	18.0	β0.78 (3H, s)	-	1.46* 1.65* 1.90 2.37	1.20 1.38* 1.40*
29	109.4	4.57 (d, *J* = 2.5)	1.68 4.68	1.68 4.68	1.68 2.37
		4.68 (d, *J* = 2.5)	1.68 4.57	1.36* 2.37 4.57	
30	19.3	1.68* (3H, s)	4.57 4.68	2.37 4.57 4.68	2.37 4.57 4.68
Acetyl group	21.0	2.13 (3H, s)	0.88* 3.77	2.09 2.13 3.77	-
	172.4	-	-	-	2.13 4.46

* Overlapped signal; § Interchangeable

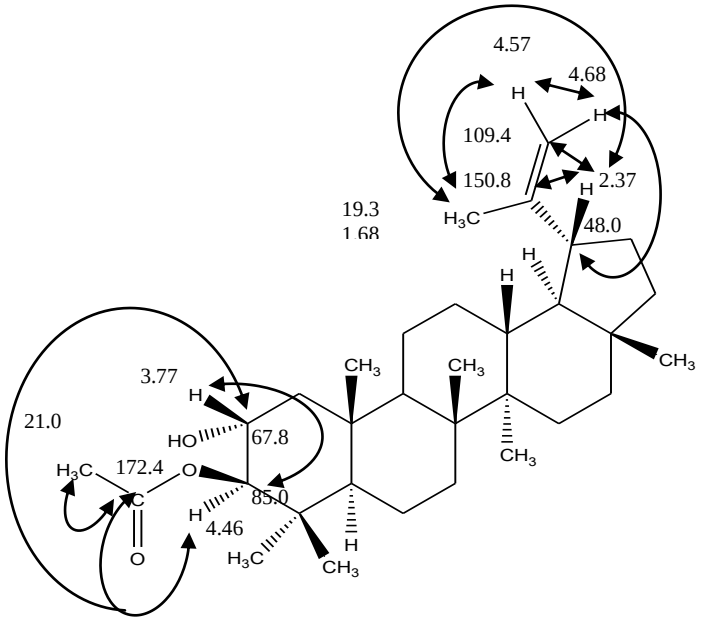

Figure 3.86 Salient HMBC signals of compound 2 (lup-(20)29-ene-2α-ol-3β-acetate)

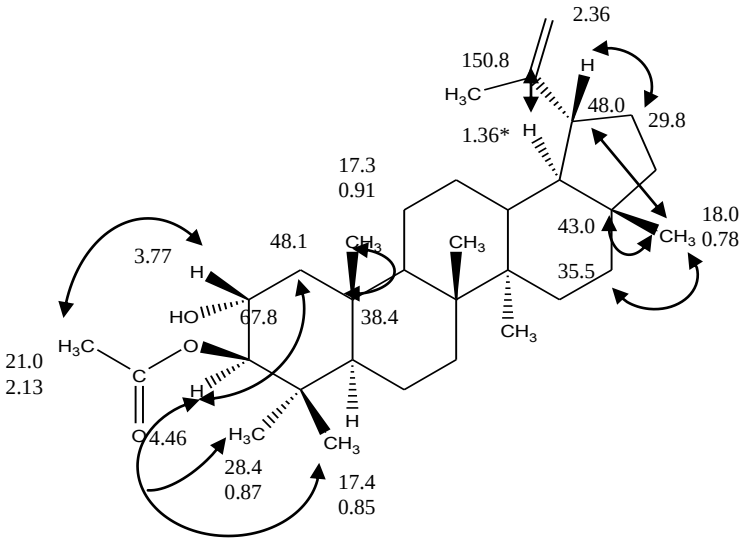

A.

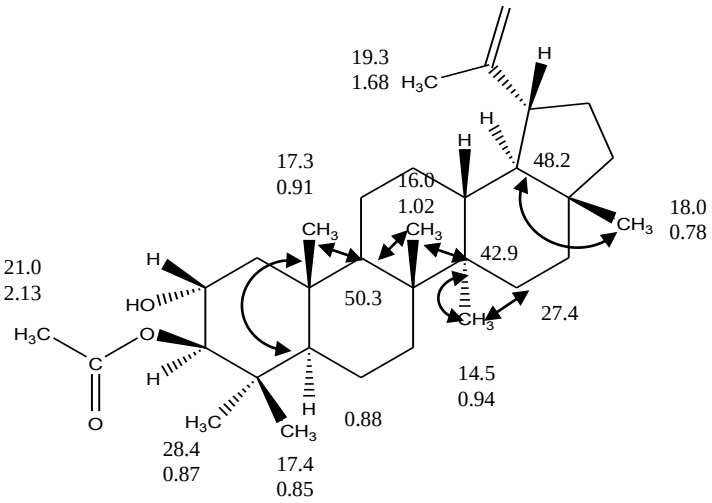

B.

Figure 3.87A-B Selected HMBC correlations of compound 2 (lup-(20)29-ene-2α-ol-3β-acetate)

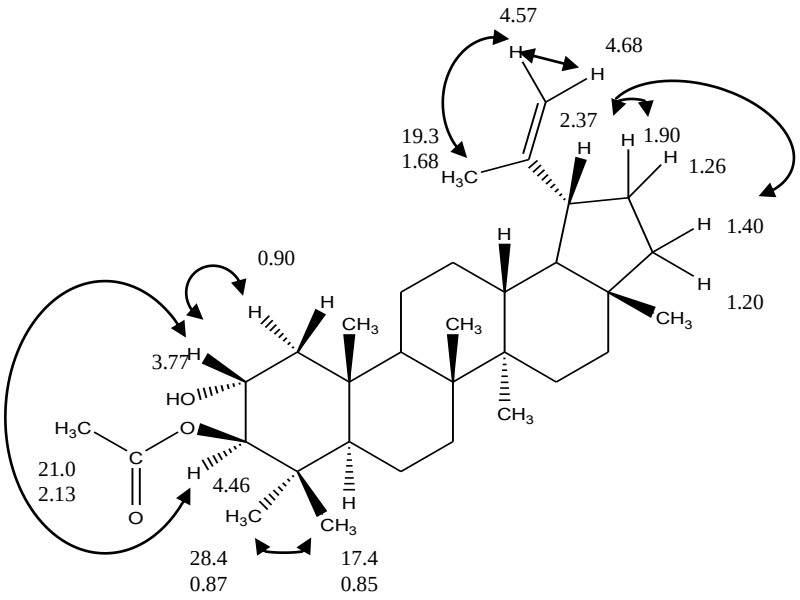

Figure 3.88 Selected COSY correlations of compound 2 (lup-(20)29-ene-2α-ol-3β-acetate)

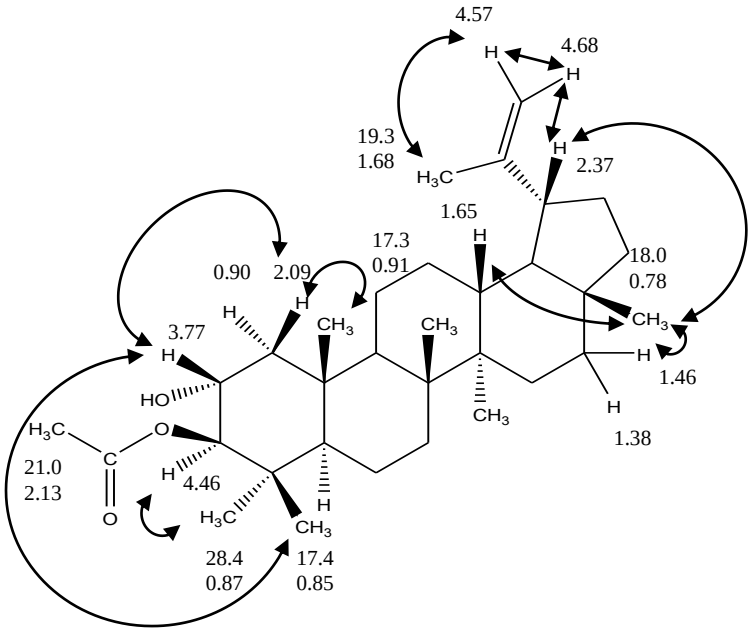

Figure 3.89 Selected NOESY correlations of compound 2 (lup-(20)29-ene-2α-ol-3β-acetate)

Therefore, compound 2 was identified as lup-(20)29-ene-2α-ol-3β-acetate established by its molecular formula $C_{32}H_{52}O_3$ (MW 484) and NMR spectroscopic data. It is now reported here for the first time.

Table 3.25 shows the comparison data of three isolated lupane triterpenoids. Lup-(20)29-ene-2α,3β-diol has been previously reported in *S. viridis* L. (Ulubelen et al., 1977). The two acetate esters described here have not previously been reported. As can be seen, the acetyl substitution caused the deshielding of the chemical shifts of both ^{1}H and ^{13}C at the position of substitution.

An isomer of compound 2, lup-(20)29-ene-2α-ol-3α-acetate, was recently found in *S. trijuga* Diels as shown in Table 3.25 (Pan et al., 2010).

Table 3.25 ^{1}H, and ^{13}C NMR comparison of two novel lupane triterpenoids (^{1}H, 500 MHz; ^{13}C, 125 MHz in $CDCl_3$; δ in ppm; *J* in Hz)

Position	Lup-(20)29-2n2-2α, 3β-diol		Compound 1 Lup-(20)29-ene-2α-acetate-3β-ol		Compound 2 Lup-(20)29-ene-2α-ol-3β-acetate		Lup-(20)29-ene-2α-ol-3α-acetate (Pan et al., 2010)	
	δ_C	δ_H	δ_C	δ_H	δ_C	δ_H	δ_C	δ_H
1	46.7	0.83* 2.03	44.0	0.90 2.04*	48.1	0.90* 2.09	42.3	1.09* 1.76
2	69.3	3.67 (ddd, 10, 10, 4.5)	73.6	4.86 (ddd, 10, 10, 5)	67.8	3.77 (ddd, 10, 10, 5)	65.8	4.08 (td, 15, 5)
3	83.9	2.97 (d, 9.5)	80.9	3.15 (d, 10)	85.0	4.46 (d, 10)	80.6	4.87 (d, 3)
4	38.6	-	39.8	-	39.3	-	38.2	-
5	55.4	0.79*	55.2	0.76*	55.3	0.88*	49.6	1.09*
6	18.3	1.40* 1.52	18.2	1.40 1.53	18.3	1.40* 1.50*	17.8	1.35* 1.40*
7	34.2	1.39*	34.1	1.43*	34.1	1.40*	33.9	1.40*
8	40.9	-	40.9	-	40.9	-	40.9	-
9	50.4	1.32*	50.4	1.31	50.3	1.34	50.1	1.41*
10	39.2	-	38.5	-	38.4	-	38.5	-

Table 3.25 (continued)

Position	Lup-(20)29-2n2-2α, 3β-diol		Compound 1 Lup-(20)29-ene-2α-acetate-3β-ol		Compound 2 Lup-(20)29-ene-2α-ol-3β-acetate		Lup-(20)29-ene-2α-ol-3α-acetate (Pan et al., 2010)	
	δ_C	δ_H	δ_C	δ_H	δ_C	δ_H	δ_C	δ_H
11	21.0	1.26*	21.1	1.25*	21.1	1.26	21.1	1.26*
		1.45*		1.38*		1.43		1.44*
12	25.0	1.08	25.0	1.07	25.0	1.08	24.9	1.08*
		1.67*		1.66*		1.68*		1.68*
13	38.0	1.65*	38.0	1.64*	37.9	1.65*	37.9	1.65*
14	42.9	-	42.9	-	42.9	-	42.9	-
15	27.4	1.05	27.4	0.98*	27.4	0.98*	27.4	1.00*
		1.74		1.66*		1.68*		1.69*
16	35.6	1.38*	35.6	1.37	35.5	1.38	35.5	1.38*
		1.47*		1.47		1.46		1.48*
17	43.0	-	43.0	-	43.0	-	42.9	-
18	48.3	1.35*	48.3	1.34	48.2	1.36	48.2	1.35*
19	48.0	2.36 (ddd, 11, 11, 6)	47.9	2.37 (ddd, 11, 11, 6)	47.9	2.37 (ddd, 11, 11, 6)	47.9	2.37 (td, 13.5, 7.5)
20	150.9	-	150.8	-	150.8	-	150.7	-
21	29.8	1.32	29.7	1.38*	29.8	1.32*	29.8	1.32*
		1.92		1.92		1.90		1.91
22	40.0	1.20	40.0	1.19	40.0	1.20	39.9	1.20*
		1.38*		1.38*		1.40*		1.38*
23	28.5	1.01 (s)	28.4	1.03 (s)	28.4	0.87 (s)	27.9	0.86 (s)
24	16.5	0.80 (s)	16.4	0.84 (s)	17.4	0.85 (s)	21.6	0.91 (s)
25	17.4	0.90 (s)	17.1	0.94 (s)	17.3	0.91 (s)	17.0	0.88 (s)
26	16.0	1.02 (s)	16.0	1.02 (s)	16.0	1.02 (s)	16.0	1.02 (s)
27	14.5	0.94 (s)	14.5	0.93 (s)	14.5	0.94 (s)	14.7	0.98 (s)
28	18.0	0.78 (s)	18.0	0.78 (s)	18.0	0.78 (s)	17.9	0.78 (s)
29	109.4	4.57	109.4	4.55	109.4	4.57	109.3	4.57
		4.69		4.67		4.68		4.69
30	19.3	1.67 (s)	19.3	1.65 (s)	19.3	1.68 (s)	19.2	1.67 (s)
Acetyl group	-	-	21.3	2.05 (s)	21.0	2.13 (s)	20.8	2.14 (s)
	-	-	171.6	-	172.4	-	172.0	

*Overlapped signal

3.6.3.6 β-Sitosterol

β-Sitosterol ($C_{29}H_{50}O$; Figure 3.90) was identified by NMR data with those of an authentic specimen. NMR data are shown in Table 3.26 and NMR spectra are given in Appendix 18.

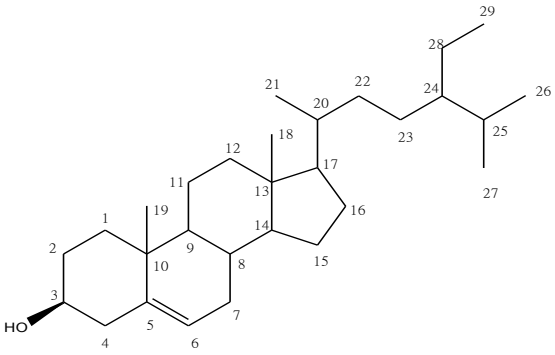

Figure 3.90 β-Sitosterol

^{13}C NMR showed 29 signals which comprised six methyl signals, 11 methylene signals, nine methine signals and three quaternary carbon atoms from DEPT-90 and DEPT-135. The ^{1}H spectrum displayed two recognized signals of sterols at δ 3.52 ppm and δ 5.35 ppm which belonged to hydroxyl substitution proton (H-3) and the alkene proton (H-6) respectively. This compound was thus identified as β-sitosterol. Its spectra were identical to the commercial standard, and to previous published data (Kojima et al., 1990).

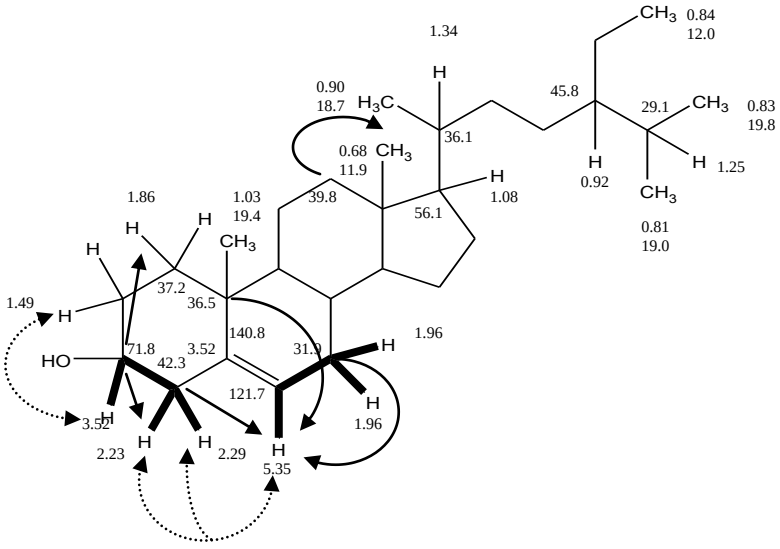

Figure 3.91 Selected signals of β-sitosterol
COSY (bold line), NOESY (dot arrow), and HMBC (arrow)

Table 3.26 1D and 2D NMR data of β-sitosterol (^{1}H, 500 MHz; ^{13}C, 125 MHz; $CDCl_3$; δ in ppm; *J* in Hz)

Position	^{13}C	^{1}H	COSY	NOESY	HMBC
1	37.2	1.05*	1.86*	-	1.49*
		1.86*	1.05*		
2	31.7	1.49*	3.52		1.84*
		1.84*	3.52		1.86*
					2.23
					2.29
3	71.8	3.52 (m, *J* = 11, 4.5)	2.23	-	1.05*
			2.29		1.49*
					1.84*
					1.86*
					2.23*
					2.29*
4	42.3	2.23 (m)	-	-	0.68
		2.29 (m)			1.08*
					1.16*
					1.50*
					1.84*
					1.99*
5	140.8	-	-	-	1.03*
					1.84*
					1.86*
					2.23
					2.29
6	121.7	5.35 (d, *J* = 5.5)	1.96*	1.96*	2.23
				2.23	2.29
				2.29	
7	31.9	1.96* (2H)	1.43*	1.43*	0.92*
					0.99*
					1.03*
					1.08*
					1.43*

Table 3.26 (continued)

Position	^{13}C	^{1}H	COSY	NOESY	HMBC
8	31.9	1.43*	1.96*	1.96*	0.92* 0.99* 1.03* 1.08* 1.43*
9	50.1	0.92*	*	*	1.43* 1.50* 1.96* 1.99*
10	36.5	-	-	-	0.92* 1.03* 1.05* 1.86* 2.23 2.29 5.35
11	21.1	1.05* 1.50*	*	*	0.92* 1.16*
12	39.8	1.16* 1.99*	*	*	0.68 1.05* 1.50*
13	42.3	-	-	-	0.68 1.08* 1.16* 1.50* 1.84* 1.99*
14	56.8	0.99*	*	*	0.68 0.90 1.08* 1.43* 1.55* 1.96*

Table 3.26 (continued)

Position	^{13}C	^{1}H	COSY	NOESY	HMBC
15	24.3	1.08* 1.55*	*	*	0.99*
16	28.2	1.84* (2H)	*	*	1.08*
17	56.1	1.08*	*	*	0.68 0.90 1.05*
18	11.9	0.68 (3H, s)	-	-	0.90 0.99 1.08* 1.16*
19	19.4	1.03 (3H, s)	-	-	0.92* 1.05* 1.86*
20	36.1	1.34*	-	-	0.90* 1.05* 1.08* 1.84*
21	18.7	0.90* (3H)	*	-	1.05* 1.16*
22	33.9	1.05* 1.34*	*	*	0.90* 1.05* 1.08*
23	26.1	1.16* (2H)	*	-	0.90* 1.25*
24	45.8	0.92*	*	*	0.81 0.83 0.84 1.25*
25	29.1	1.25*	*	*	0.81 0.83 0.84
26	19.8[§]	0.83 (3H, d, J = 7)	-	-	0.92* 1.08*

Table 3.26 (continued)

Position	^{13}C	^{1}H	COSY	NOESY	HMBC
27	19.0[§]	0.81 (3H) (d, *J* = 7)	-	-	0.92* 1.08*
28	23.1	1.08* 1.28*	*	*	0.81 0.83 0.84
29	12.0	0.84 (3H, s)	*	-	0.92* 1.08* 1.25*

[*] Overlapped signal; [§] Interchangeable

Figure 3.91 shows the salient correlations of β-sitosterol. The peak at δ 3.52 ppm (H-3) was correlated to a carbon at δ 71.8 ppm (C-3) by HMQC, and also had COSY correlations to two protons of H-4 at δ 2.23 ppm, and 2.29 ppm. The coupling constants of H-3 were 11 and 4.5 Hz which implied the α-axial orientation. HMBC correlated C-3 to H-1 and H-2, consequently, C-1, and C-2 were assigned at δ 37.2 ppm and 31.7 ppm. The other conspicuous signal at δ 5.35 ppm (H-6) was correlated to protons of H-4, and also two protons of H-7 at δ 1.96 ppm; accordingly C-7 was at δ 31.9 ppm.

The β-sitosterol was only partially resolved from other plant sterols. In a mixed sterol fraction, campesterol ($C_{28}H_{48}O$) was tentatively identified in ^{13}C NMR spectra concomitant with β-sitosterol ($C_{29}H_{50}O$). In the ^{1}H NMR spectrum, the characteristic of signals of a Δ^{22} double bond could be seen as illustrated in Figure 3.92. This amounted to about 12% of the total sterol in the fraction and was possibly due to stigmasterol (Figure 3.93).

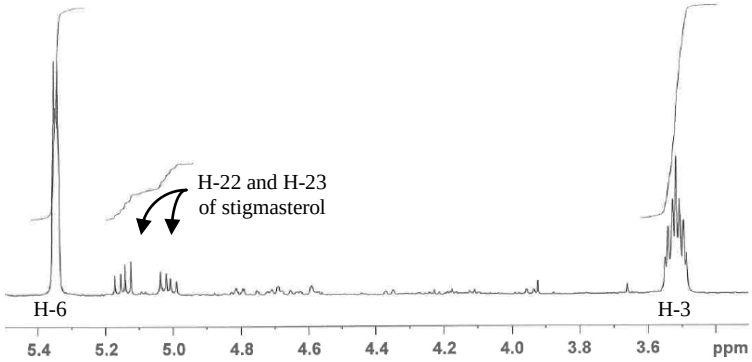

Figure 3.92 ^{1}H NMR expansion of the sterols sample (500 MHz; $CDCl_3$)

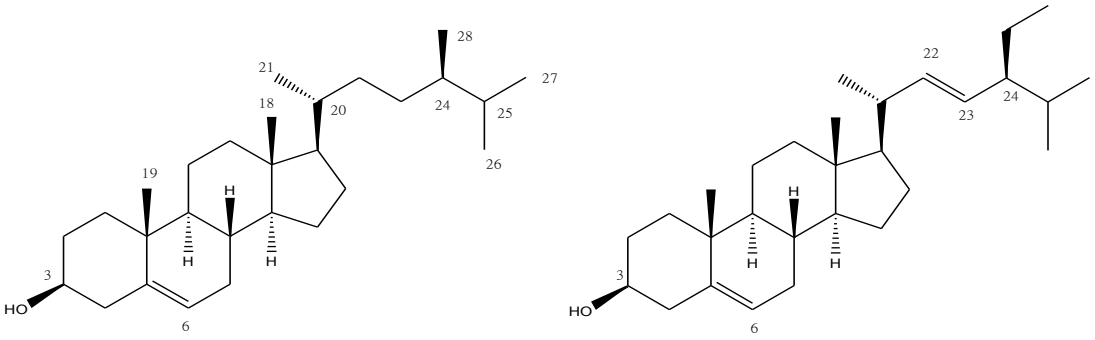

Campesterol Stigmasterol

Figure 3.93 Plant sterols

3.6.3.7 β-Sitosterol glucoside

The MS data of β-sitosterol glucoside (Figure 3.94) gave a molecular mass of 576 and a molecular formula of $C_{35}H_{60}O_6$. NMR data are shown in Table 3.27 and NMR spectra are given in Appendix 19.

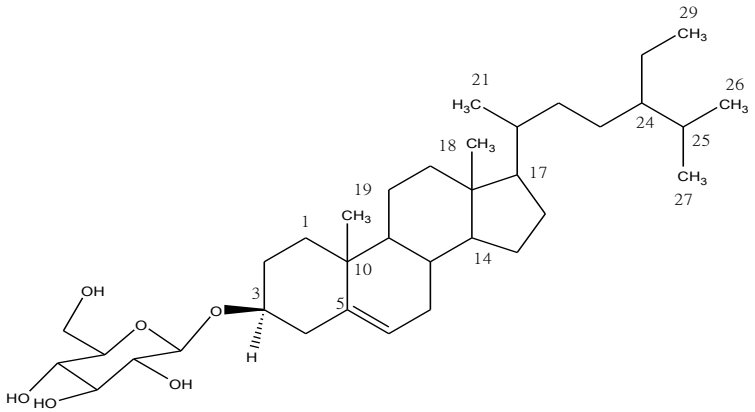

Figure 3.94 β-sitosterol-3-*O*-glycoside (daucosterol)

This agrees with that of β-sitosterol with glucose substitution. This is supported by ^{1}H NMR and ^{13}C NMR. ^{13}C NMR displayed 6 signals more than β-sitosterol while resonated in the sugar region at δ 62-101 ppm. ^{1}H NMR exhibited the signals of glucose at δ 3.2-3.8 ppm with the anomeric proton at δ 4.37 ppm (d, J = 8 Hz). The chemical shifts of glucose were assigned by HMBC, COSY, and NOESY correlations.

Table 3.27 1D and 2D NMR data of β-sitosterol glucoside (^{1}H, 500 MHz; ^{13}C, 125 MHz; in a mixture of CD_3OD and $CDCl_3$; δ in ppm; *J* in Hz)

Position	^{13}C	^{1}H	COSY	NOESY	HMBC
1	37.6	1.03*	*	1.83*	0.90
		1.83*	-	1.03*	
2	29.9	1.56*	1.87*	-	2.36
		1.87*	1.56*		
3	79.4	3.56 (m, *J* = 9.5, 5)	1.56 2.23 2.36	4.37	1.87* 2.23 2.36 4.37
4	38.9	2.23 (m)	2.36	2.36	0.97
		2.36 (m)	2.23	2.23 5.35	5.35
5	140.6	-	-	-	0.97 1.49* 1.83* 2.36
6	122.4	5.35 (d, *J* = 5.5)	1.92*	2.36	1.49* 2.36
7	32.2	1.92*	5.35	-	0.89* 1.41*
		1.49*	*		5.35
8	32.2	1.41*	*	*	0.89* 1.49* 5.35
9	50.5	0.90*	*	*	0.97 1.49* 1.99*
10	37.0	-	-	-	0.97 2.36 5.35

Table 3.27 (continued)

Position	^{13}C	^{1}H	COSY	NOESY	HMBC
11	21.3	1.46* (2H)	-	*	1.12
12	40.1	1.12* 1.99*	-	*	0.64 0.97 1.03
13	42.6	-	-	-	0.64 1.03* 1.99*
14	57.1	0.96	*	*	0.64 0.87
15	24.5	1.03* 1.53*	*	*	0.87
16	28.5	1.18 1.23	-	*	0.87
17	56.4	1.08*	-	*	0.64 0.87
18	12.0	0.64 (3H, s)	-	-	0.87 1.12* 1.32*
19	19.5	0.97 (3H, s)	-	-	0.90 1.83
20	36.4	1.32*	-	-	0.87* 0.99*
21	19.0	0.87 (3H)	*	-	1.08 1.63*
22	34.2	0.99 1.29	*	*	0.87 0.89 0.99* 1.12*
23	26.3	1.12 (2H)	-	-	1.22 1.63

Table 3.27 (continued)

Position	^{13}C	^{1}H	COSY	NOESY	HMBC
24	46.2	0.89	*	*	0.76 0.78 0.80 0.87 1.22* 1.29* 1.63
25	29.4	1.63*	*	*	0.76 0.78
26	19.9[§]	0.78 (3H, d, *J* = 7)	*	-	0.76* 0.80* 1.12* 1.63
27	19.2[§]	0.76 (3H, d, *J* = 7)	*	-	0.76* 0.80* 1.12* 1.63
28	23.3	1.22* (2H)	*	*	0.76* 0.78* 0.89* 1.12* 1.63
29	12.1	0.80 (3H, s)	*	-	0.89* 1.12* 1.22
1'	101.4	4.37 (d, *J* = 8)	3.20	2.36 3.25 3.36 3.56	3.20 3.56
2'	73.9	3.20 (t, *J* = 9.5)	3.39 4.37	-	3.39*

Table 3.27 (continued)

Position	^{13}C	^{1}H	COSY	NOESY	HMBC
3'	70.5¤	3.39*	3.20 3.25	3.72 4.37	3.25 3.39* 3.72 3.82
4'	76.8¤	3.39*	3.20 3.25	3.72 4.37	3.20 3.25 3.39 4.37
5'	76.2	3.25	3.39	3.72 3.82 4.37	3.72 3.39 4.37
6'	62.1	3.72 (dd, *J* = 12, 4.5)	3.82	3.82	3.39
		3.82 (dd, *J* = 12, 3)	3.72	3.72	

* Overlapped signal; §, ¤ Interchangeable

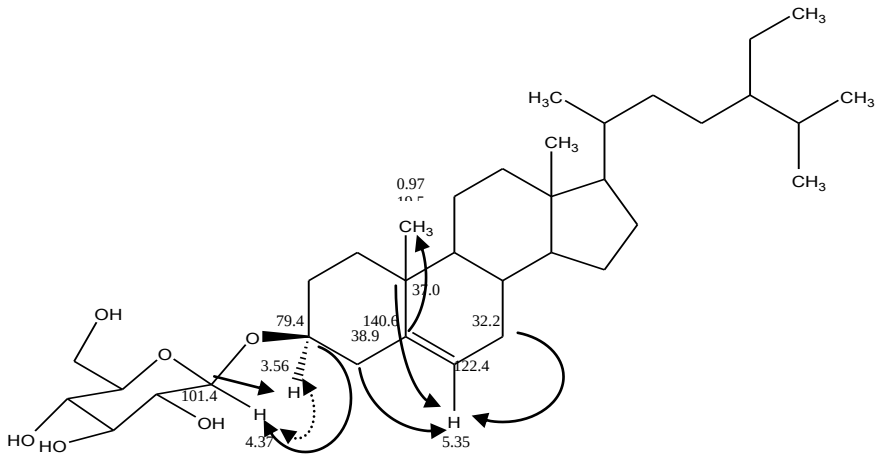

Figure 3.95 Selected correlations of β-sitosterol-3-*O*-glucoside
NOESY (dot arrow), and HMBC (arrow)

HMBC correlated C-3 to the anomeric proton of glucose (δ 4.37 ppm) and also C-1' to H-3. The large coupling constant of the anomeric proton of glucose with ^{3}J = 8 Hz, indicated the β-configuration of glucose. The hydroxyl substitution was β-equatorial orientation because the coupling constants of H-3 were 9.5 and 5 Hz. A NOESY cross-peak of H-3α at δ 3.56 ppm to the anomeric H-1' was also observed.

This compound was thus identified as β-sitosterol-3-*O*-glycoside. It is also known as daucosterol isolated from *Daucus carota* L., family Apiaceae (Fu et al., 2010). Its spectra were compared to previous published data (Kojima et al., 1990). β-Sitosterol and its glycoside have commonly been found in plants particularly high lipid content ones such as nuts and legumes (Kojima et al., 1990; Bradford and Awad, 2007).

3.6.4 Miscellaneous

3.6.4.1 Salidroside

The MS data of salidroside (2-(4'-hydroxyphenyl) ethyl β-glucopyranoside) (Figure 3.96) was consistent with a molecular mass of 300 mass units and a molecular formula of $C_{14}H_{20}O_7$. ^1H and ^{13}C NMR data are shown in Table 3.28 and NMR spectra are given in Appendix 20.

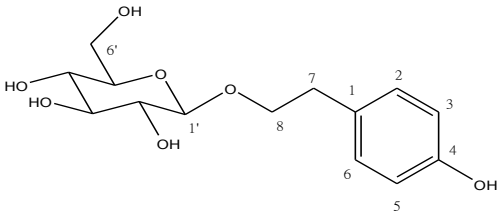

Figure 3.96 Salidroside

^1H NMR showed the characteristics of glucose substitution, an anomeric proton at δ 4.28 ppm (J = 8 Hz), and many signals in δ 3-4 ppm, and also two noticeable methylene signals of phenylethanol at δ 2.81 ppm (H-7), and 4.04 ppm ($H8_a$). Two doublets were shown in aromatic region, δ 6.68 ppm and 7.06 ppm, which represented a para-disubstituted coupling pattern. These two signals were correlated to a downfield carbon atom at δ 156.8 ppm (C-4). Figure 3.97 shows the assignment of δ 6.68 ppm (H-3, 5) and 7.06 ppm (H-2, 6) because there was a NOESY cross peak between a methylene signal at δ 2.81 ppm (H-7) to a ^1H signal at δ 7.06 ppm (H-2, 6). The attachment of glucose to aglycone part was indicated by HMBC correlation of the anomeric carbon at δ 104.2 ppm to H-8. The glucose assignments were based on HMBC, COSY, and NOESY correlations. Certain overlapping correlations are compared to one in the verbascoside.

Table 3.28 1D and 2D NMR data of salidroside (^{1}H, 500 MHz; ^{13}C, 125 MHz; CD_3OD; δ in ppm; *J* in Hz)

Position	^{13}C	^{1}H	COSY	NOESY	HMBC
1	130.7	-	-	-	2.81 3.70* 4.04 6.68 7.06
2, 6	116.1	6.68 (d, *J* = 8.5)	7.06	7.06	6.68 7.06
3, 5	130.9	7.06 (d, *J* = 8)	6.68	6.68	2.81 3.70* 4.04 6.68 7.06
4	156.8	-	-	-	6.68 7.06
7	36.4	2.81 (2H, m)	3.70* 4.04	3.70* 4.04	3.70* 4.04 7.06
8	72.1	3.70* (m)	4.04	2.83 3.70*	2.83 4.28
		4.04 (m)	3.70* 4.28	3.70* 4.28	
1'	104.2	4.28 (d, *J* = 8)	3.18 4.04	3.25*	3.18 3.70* 4.04
2'	75.1	3.18 (t, *J* = 8)	4.28	-	3.34*
3'	71.6	3.26* (m)	*	4.28	3.34* 3.86* 4.28

Table 3.28 (continued)

Position	^{13}C	^{1}H	COSY	NOESY	HMBC
4'	78.1	3.34* (m)	*	-	3.18 3.25* 3.26* 3.68*
5'	77.9	3.25* (m)	*	-	3.68* 4.28
6'	62.7	3.86* (m)	*	-	3.25*
		3.68* (m)	*	-	3.26*

* Overlapped signal

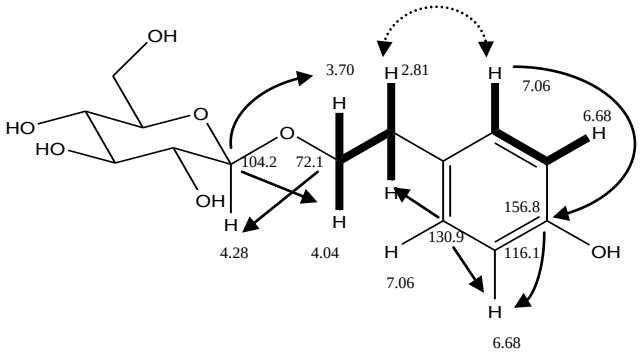

Figure 3.97 Salient signals of salidroside
COSY (bold line), NOESY (dot arrow), and HMBC (arrow)

Salidroside was reported in many *Rhodiola* species (family Crassulaceae), for example, *R. sacra* (Prain ex. Hamet) S. H. Fu, *R. yunnanensis* (Franch.) S. H. Fu and *R. coccinea* (Royle) Borrisour (Chen et al., 2008) and also in *Cistanche deserticola* Y. C. Ma. (family Orobanchaceae) (Yu et al., 2007). Certain biological activities have been noted such as antiviral (Wang et al., 2009b), and antioxidant effects (Yu et al., 2007). Its spectroscopic data are comparable to a published literature (Yu et al., 2007).

3.7 Separation compounds from root part

Dried root of this plant was also macerated by two steps of solvents, acetone and methanol, and partitioned by the same set of solvents as the aerial part (Scheme 2.1). Eight crude fractions were RAP (Acetone-Petroleum ether fraction; 0.65 gm), RAE (Acetone-Ethyl acetate fraction; 1 gm), RAB (Acetone-1-Butanol fraction; 0.055 gm), RAW (Acetone-Water fraction; 0.04 gm), RMP (Methanol-Petroleum ether fraction; 0.005 gm), RME (Methanol-Ethyl acetate fraction; 0.87 gm), RMB (Methanol-1-Butanol fraction; 0.63 gm), and RMW (Methanol-Water fraction; 4.55 gm). Terpenoids and fatty acid ester were isolated from RAP and RAE over silica gel by open column chromatography while certain polyphenols were detected in RME and RMB crude fractions.

3.7.1 Open column chromatography and HPLC of root part crude fractions

3.7.1.1 RME crude fraction

RME (ethyl acetate fraction from methanol fraction) was first separated by open column chromatography, and then further purified by reversed phase HPLC. A phenylpropanoid compound was isolated from RME identified as 2", 3"-di-*O*-acetyl-martynoside. This compound was not detected in aerial part of this plant.

3.7.1.2 RMB crude fraction

Figure 3.98 shows a HPLC chromatogram of RMB (1-butanol fraction from methanol fraction). MS spectra indicated two main compounds in this crude extract, verbascoside and rosmarinic acid, which corresponded to the two main peaks at retention time 9.2 min, and a broad peak at 3-5 min respectively. Separation of this crude fraction by open column chromatography and reversed phased HPLC afforded rosmarinic acid, and a trace amount of verbascoside.

Table 3.29 Isolated compounds from RME and RMB root part crude fractions

Identification	Formula	MW	Rf value[a]
2", 3"-Di-*O*-acetyl-martynoside	$C_{35}H_{44}O_{17}$	736	0.75
Rosmarinic acid	$C_{18}H_{16}O_8$	360	0.70
Verbascoside	$C_{29}H_{36}O_{15}$	624	0.25

[a]Mobile phase: ethyl acetate:methanol:formic acid:water (50:3:3:6); silica gel GF_{254}

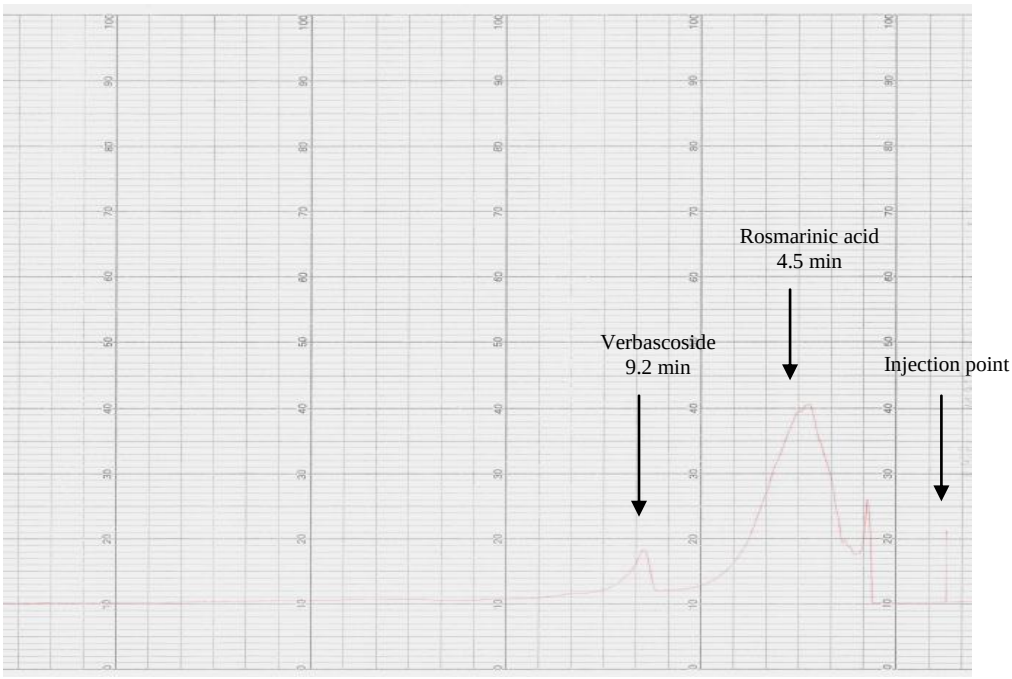

Figure 3.98 A chromatogram of RMB crude fraction from retention time 0-24 minutes. Condition: Phenomenex Luna PFP 250x10mm, injection volume 20 µl of 10 mg/ml, mobile phase methanol:water (45:55), flow rate 5 ml/min, wavelength at 330 nm.

Table 3.30 Isolated compounds from RAE and RAP root part crude fractions

Identification	Formula	MW	Rf value[a]
Ferruginol	$C_{20}H_{30}O$	286	0.78
7α-Acetoxy-14-hydroxy-8,13-abietadiene-11,12-dione	$C_{22}H_{30}O_5$	374	0.71
7α,14-Dihydroxy-8,13-abietadiene-11,12-dione	$C_{20}H_{28}O_4$	332	0.71
Salvinolonyl-12 methyl ether	$C_{21}H_{28}O_3$	328	0.64
Compound 3 (1-oxomicrostegiol)	$C_{20}H_{24}O_3$	312	0.59
Compound 4 (viroxocane)	$C_{20}H_{24}O_3$	312	0.58
Microstegiol	$C_{20}H_{26}O_2$	298	0.75
Compound 5 (viridoquinone)	$C_{20}H_{24}O_2$	296	0.71
1-Docosyl ferulate	$C_{32}H_{54}O_4$	502	0.65
A mixture of 2-(4'-alkoxyphenyl) ethyl alkanoates	-	-	0.76
A mixture of oleanolic acid and ursolic acid	$C_{30}H_{48}O_3$	456	0.45
β-Sitosterol	$C_{29}H_{50}O$	414	0.60

[a]Mobile phase: chloroform:methanol (9:1); silica gel GF_{254}

3.7.2 Open column chromatography of root part crude fractions

Three new diterpenoids were isolated from RAE and RAP crude fractions plus five known, ferruginol, salvinoloyl-12-methyl-ether, 7α-Acetoxy-14-hydroxy-8,13-abietadiene-11,12-dione, 7α,14-dihydroxy-8,13-abietadiene-11,12-dione and microstegiol. β-Sitosterol and a mixture of ursolic acid and oleanolic acid were also found in the root part (Table 3.30). Their structures are given and elucidated in section 3.8.

3.8 Structure elucidations of compounds from root part

3.8.1 Caffeic acid derivatives

In addition to verbascoside and rosmarinic acid also isolated from aerial part and discussed in section 3.6, the roots also yield two caffeic acid derivatives not found in aerial part.

3.8.1.1 2'',3''-Di-*O*-acetyl-martynoside

The MS data of 2",3"-di-*O*-acetyl-martynoside (Figure 3.99) gave a molecular mass of 736 and a molecular formula of $C_{35}H_{44}O_{17.}$ ^{1}H and ^{13}C NMR data are shown in Table 3.31 and NMR spectra give in Appendix 21.

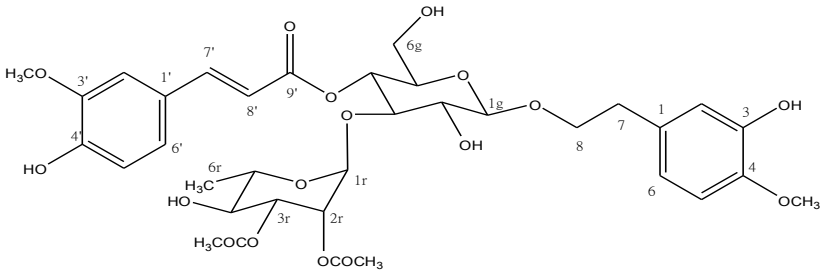

Figure 3.99 2",3"-Di-*O*-acetyl-martynoside

^{1}H and ^{13}C NMR spectra of this compound show similar signals to martynoside plus two ^{1}H singlet signals at δ 2.03 ppm, 2.12 ppm, each integrating to three protons and also carbonyl carbon signals at δ 170.0 ppm, and 171.3 ppm. The signals at δ 2.03 ppm, and 2.12 ppm had HMBC correlation to these carbonyl ^{13}C signals at δ 170.0 ppm, and 171.3 ppm respectively. The MW at 736 was consistent with a diacetylated martynoside.

Table 3.31 1D and 2D NMR data of 2",3"-di-*O*-acetyl-martynoside (^{1}H, 500 MHz; ^{13}C, 125 MHz; $CDCl_3$; δ in ppm; *J* in Hz)

Position	^{13}C	^{1}H	COSY	NOESY	HMBC
1	131.5	-	-	-	2.83 6.77
2	115.0	6.80 (d, *J* = 2)	-	-	2.83 5.62
3	145.2[§]	5.62 (OH, s)	-	-	3.86 5.62 6.67 6.77 6.80
4	145.5[§]	-	-	-	3.86 5.62 6.67 6.77 6.80
5	110.7	6.77 (d, *J* = 8)	6.67	3.86	-
6	120.3	6.67 (dd, *J* = 8.5, 2)	6.77	6.77	2.83 6.80
7	35.4	2.83 (2H, m)	3.70* 4.13	3.70* 4.13	-
8	70.9	3.70* (m)	2.83	2.83	2.83 4.28
		4.13 (m)	2.83 3.70*	2.83 3.70*	
1'	126.5	-	-	-	6.26 6.90
2'	109.6	7.02 (d, *J* = 2)	-	3.92	7.07 7.67
3'	147.0	-	-	-	3.92 5.89 6.90 7.02 7.07

Table 3.31 (continued)

Position	^{13}C	^{1}H	COSY	NOESY	HMBC
4'	148.4	5.89 (OH, s)	-	-	5.89 7.02 7.07
5'	114.8	6.90 (d, *J* = 8.5)	7.07	7.07	5.89
6'	123.4	7.07 (dd, *J* = 8, 2)	6.90	6.90	7.02 7.67
7'	147.1	7.67 (d, *J* = 15.5)	6.26	6.26	6.90 7.02 7.07
8'	113.8	6.26 (d, *J* = 15.5)	7.67	7.67	-
9'	167.0	-	-	-	5.04 6.26 7.67
1g	102.7	4.28 (d, *J* = 8)	3.60*	3.48	3.70*
2g	74.8	3.60* (m)	4.28	-	3.86* 4.88*
3g	79.0	3.86*	-	5.19	5.19
4g	68.9	5.04 (t, *J* = 10)	3.48	-	3.86* 5.19
5g	74.5	3.48 (m)	5.04	-	5.04
6g	61.4	3.62* (m)	3.74*	-	-
		3.74* (m)	3.62*	-	
1r	98.3	5.19 (br s, *J* = 1.5)	-	3.86*	3.86*
2r	70.1	5.29 (dd, *J* = 3.5, 1.5)	5.01	-	1.22
3r	72.1	5.01 (dd, *J* = 10, 3.5)	5.29	3.50*	5.19
4r	69.1	3.77* (m)	1.22	1.22	1.22 5.19
5r	71.3	3.50* (m)	-	-	1.22
6r	17.7	1.22 (d, *J* = 6.5)	3.50*	3.50*	-
4-OCH_3	56.0	3.86 (3H, s)	-	6.77	-
3'-OCH_3	55.9	3.92 (3H, s)	-	7.02	-

Table 3.31 (continued)

Position	^{13}C	^{1}H	COSY	NOESY	HMBC
2" (2r)-Acetyl	171.3	-	-	-	2.03
	20.9*	2.03 (3H, s)	-	-	-
3" (3r)-Acetyl	170.0	-	-	-	2.12
	20.9*	2.12 (3H, s)	-	-	-

* Overlapped signal; g-glucose; r-rhamnose

The ^{1}H spectrum of this compound in deuterated-chloroform exhibited four singlets of methyl groups and anomeric protons of glucose (H-1g) and rhamnose (H-1r) at δ 4.28 ppm (d, ^{3}J = 8 Hz), and 5.19 ppm (br s, ^{3}J = 1.5 Hz) respectively, and also an upfield doublet at δ 1.22 ppm (rhamnose H-6). Deuterium exchange indicated 2 hydroxyl groups at δ 5.62 ppm (s), and 5.89 ppm (s). The downfield triplet peak at δ 5.04 ppm (^{3}J = 10 Hz) was assigned as H-4g due to a HMBC correlation to a carbonyl at δ 167.0 ppm (C-9') of the feruloyl moiety. This H-4g peak was partly masked in the verbascoside spectrum because there was an overlapping -OH peak caused by deuterated methanol.

The other ^{1}H signals at δ 5.01 ppm and 5.29 ppm resonated as doublets of doublet with two sets of vicinal coupling constant, i.e. 10 and 3.5 Hz, and 3.5 and 1.5 Hz respectively. The ^{3}J values indicated the coupling patterns of H-3r (axial orientation), and H-2r (equatorial orientation) as previous structure elucidation of verbascoside (Figure 3.30). In addition, there was a COSY cross peak between these two signals at δ 5.01 ppm and 5.29 ppm. There was also HMBC correlation between C-3r to the anomeric proton of rhamnose (H-1r). The downfield chemical shifts were likely due to the substitution of acetyl groups. Therefore, this compound was assigned as diacetylmartynoside with 2r- and 3r-acetyl substitution. Sugar configurations and coupling patterns were similar to verbascoside, martynoside, and leucosceptoside A as described above.

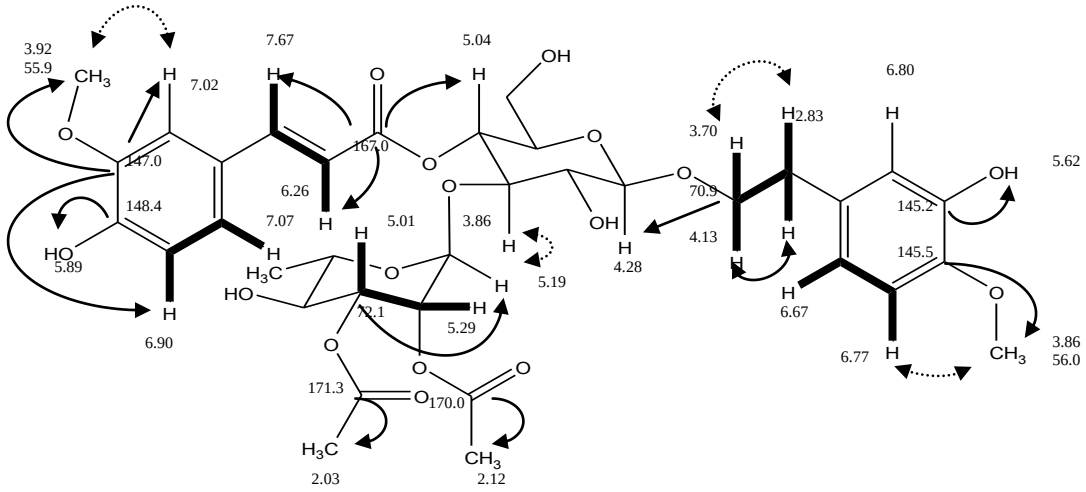

Figure 3.100 Salient signals of 2",3"-Di-*O*-acetyl-martynoside
COSY (bold line), NOESY (dot arrow), and HMBC (arrow)

2",3"-Di-*O*-acetyl martynoside has not been reported in the genus *Salvia* before but it was first isolated from *Lippia dulcis* Trev. in family Verbenaceae (Abe et al., 2002).

3.8.1.2 1-Docosyl ferulate

The MS data of 1-docosyl ferulate (Figure 3.101) gave a molecular mass of 502 and a molecular formula of $C_{32}H_{54}O_4$. ^1H and ^{13}C NMR data are shown in Table 3.32 and NMR spectra are given in Appendix 22.

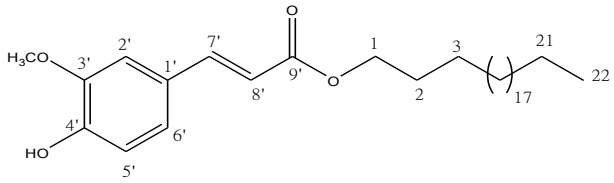

Figure 3.101 1-Docosyl ferulate

^1H NMR exhibited six signals in aromatic and alkene region, a triplet at δ 4.18 ppm, a three protons singlet at δ 3.92 ppm and a strong broad -CH_2- signal in the alkane region (Appendix 22.1). The typical signals of the ferulic acid trans protons were observed at δ 6.27 ppm and 7.58 ppm with coupling constant 16 Hz. Three signals, at δ 6.90 (d), 7.03 (d), 7.06 (dd) ppm, were noticeable as the 3, 4-disubstitued coupling pattern which was similar to

caffeic acid (Figure 3.24). There was also a NOESY cross-peak between δ 7.03 ppm and a singlet signal at δ 3.92 ppm which implied the ferulic acid moiety. In addition, a singlet signal at δ 5.82 ppm was exchangeable with D_2O which implied hydroxyl group substitution.

^{13}C NMR showed 16 signals include strong methylene signals around δ 29.3 ppm which clearly corresponded to several carbon atoms. These methylene protons also correlated by HMBC to a triplet signal at δ 0.86 ppm (H-22) which implied the long chain alkane moiety. The other deshielded triplet at δ 4.18 ppm had COSY, NOESY, HMBC correlations to a quintet signal at 1.67 ppm. The deshielded triplet at 4.18 ppm was thus assigned H-1 while the quintet was H-2. These data all suggested a ferulic acid moiety esterified to a n-alkanol which, from the molecular weight, was deduced to be docosanol. Salient COSY, NOESY and HMBC correlations are presented in Figures 3.102-3.103.

1-Docosyl ferulate was previously reported from the stem bark of *Pavetta owariensis* P. Beauv., family Rubiaceae (Balde et al., 1991), and the whole plant of *Teucrium divaricatum* subsp. *villosum* (Celak) Rech. fil., family Lamiaceae (Ulubelen et al., 1994b).

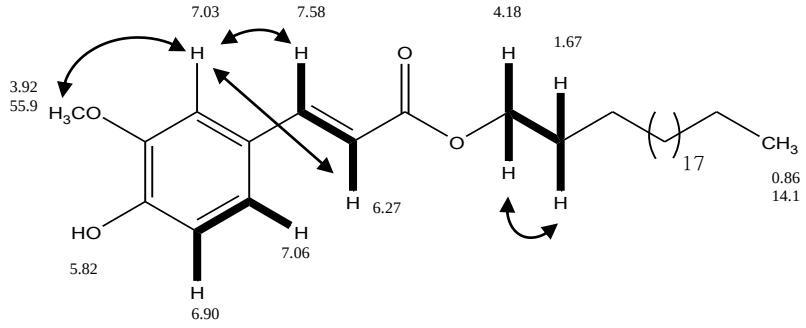

Figure 3.102 H-H COSY (bold line) and NOESY (arrow) correlations of 1-docosyl ferulate

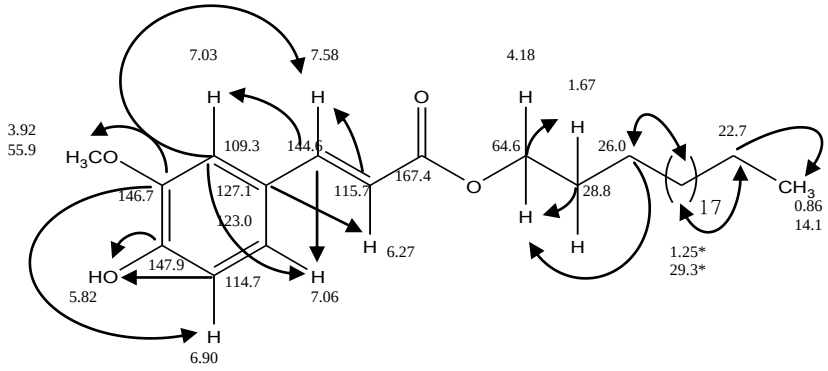

Figure 3.103 HMBC correlations of 1-docosyl ferulate (* overlapped signal)

Table 3.32 1D and 2D NMR data of 1-docosyl ferulate (^{1}H, 500 MHz; ^{13}C, 125 MHz; in $CDCl_3$; δ in ppm; *J* in Hz)

Position	^{13}C	^{1}H	COSY	NOESY	HMBC
1	64.6	4.18 (2H, t, *J* = 7)	1.67	1.67	1.67[Φ]
2	28.8	1.67 (2H, quintet, *J* = 8)	4.18	4.18	1.25* 4.18[Φ]
3	26.0	1.38 (2H, m)	1.67	-	1.67 4.18
4-20	29.3-31.9	1.25* (34H)	*	*	* 1.38
21	22.7	1.25* (2H)	0.86	-	0.86[Φ] 1.25*
22	14.1	0.86 (3H, t, *J* = 7)	1.25*	-	1.25*
1'	127.1	-	-	-	6.27 6.90
2'	109.3	7.03 (d, *J* = 2)	-	3.92 6.27	6.27 7.06 7.58
3'	146.7[§]	-	-	-	3.92 5.82 6.90 7.03
4'	147.9[§]	5.82 (OH, s)	-	-	5.82 7.03 7.06
5'	114.7	6.90 (d, *J* = 8)	7.06	7.06	5.82 7.06[Φ]
6'	123.0	7.06 (dd, *J* = 8, 2)	6.90	6.90	6.90[Φ] 7.03 7.58
7'	144.6	7.58 (d, *J* = 16)	6.27	6.27 7.03	6.27[Φ] 7.03 7.06

Table 3.32 (continued)

Position	^{13}C	^{1}H	COSY	NOESY	HMBC
8'	115.7	6.27 (d, *J* = 16)	7.58	7.03 7.58	7.58 $^{\Phi}$
9'	167.4	-	-	-	-
Methoxyl group	55.9	3.92 (3H, s)	-	7.03	-

*Overlapped signal; $^{\Phi}$ H2BC; § Interchangeable

3.8.2 Diterpenoids

The main components in the less polar fractions from the roots (RAP and RAE crude fractions) were a series of diterpenoids. ^{1}H NMR of all these compounds showed a one proton septet coupled to two methyl doublets typical of the isopropyl side chain of the abietane or rearranged abietane skeleton.

3.8.2.1 Ferruginol

The MS data of ferruginol (Figure 3.104) gave a molecular mass of 286 and a molecular formula of $C_{20}H_{30}O$. ^{1}H and ^{13}C NMR data are shown in Table 3.33 and NMR spectra are given in Appendix 23.

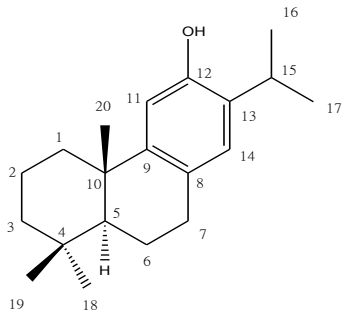

Figure 3.104 Ferruginol

Table 3.33 1D and 2D-NMR data of ferruginol (^{1}H, 500 MHz; ^{13}C, 125 MHz; $CDCl_3$; δ in ppm; *J* in Hz)

Position	^{13}C	^{1}H	COSY	NOESY	HMBC
1	38.8	α1.37* (m)	0.93 2.15	2.15 6.62	0.91 0.93 1.16
		β2.15 (dt, *J* = 12.5, 4, 1)	1.37	1.16 1.37 6.62	
2	19.3	α1.73 (ddd, *J* = 13.5, 6.5, 3)	-	-	0.93
		β1.59 (ddd, *J* = 14, 10, 3.5)	-	-	
3	41.7	1.19* (m)	1.46	-	0.91 0.93
		β1.46 (ddd, *J* = 13.5, 3.5, 1.5)	1.19*	-	
4	33.4	-	-	-	0.91 0.93
5	50.3	α1.31* (dd, *J* = 12.5, 2)	1.59	-	0.91 0.93 1.16 1.65 2.83
6	19.2	α1.85 (dddd, *J* = 17, 6, 3.5,2)	1.31* 1.65 2.76	-	0.93 1.31* 2.76 2.83
		β1.65 (m)	1.85 2.76	-	
7	29.7	α2.76 (ddd, *J* = 17, 11, 7.5)	1.65 1.85 2.83	1.85 6.82	1.31* 6.82
		β2.83 (ddd, *J* = 17, 6, 1.5)	2.76	6.82	
8	127.3	-	-	-	1.85 2.76 2.83

Table 3.33 (continued)

Position	^{13}C	^{1}H	COSY	NOESY	HMBC
9	148.7	-	-	-	1.16 2.76 2.83 6.82
10	37.5	-	-	-	1.85 1.16
11	110.9	6.62 (s)	-	1.16 2.15 4.46	4.46
12	150.6	4.46 (OH, s)	-	6.62	3.10 4.46 6.62 6.82
13	130.9	-	-	-	1.21 1.23 3.10 4.46 6.62
14	126.6	6.82 (s)	-	1.21 1.23	2.76 2.83 3.10 6.62
15	26.8	3.10 (septet, *J* = 7)	1.21 1.23	1.21 1.23	1.21 1.23
16	22.7[§]	1.23 (3H, d, *J* = 7)	3.10	3.10	1.21 3.10
17	22.5[§]	1.21 (3H, d, *J* = 7)	3.10	3.10	1.23 3.10
18	33.3	α0.93 (3H, s)	1.37	-	0.91
19	21.6	β0.91 (3H, s)	1.37	-	0.93 1.31*
20	24.8	β1.16 (3H, s)	1.73	6.62	1.37

*Overlapped signal; [§] Interchangeable

^{13}C NMR displayed 20 signals which comprised five methylene groups, six quaternary carbon atoms, and nine positive signals of methyl and methine groups from DEPT-135. In the ^{1}H NMR spectrum, COSY and NOESY correlations of the septet signal, δ 3.10 ppm, and pair of three proton doublets, δ 1.21 ppm and 1.23 ppm, implied the isopropyl group in this structure. There were also three singlet signals of one hydrogen atom in the low field at δ 4.46 ppm, 6.62 ppm, and 6.82 ppm. While HMQC correlated the two signals of δ 6.62 ppm, and 6.82 ppm to two aromatic carbons at δ 110.9 ppm, and 126.6 ppm respectively, there was no correlation of signal δ 4.46 ppm to any carbon atom. This signal, δ 4.46 ppm, was exchanged by D_2O which indicated that it was the hydroxyl-OH. In addition, HMQC correlated a carbon signal at δ 50.3 ppm to a proton at δ 1.31 ppm which inferred the methine proton of C-5. The presence of three singlet signals and two doublet signals of methyl groups plus the septet signal in ^{1}H NMR indicated an abietane diterpenoid. The double-bond equivalent (DBE) of $C_{20}H_{30}O$ is six, therefore, the structure is likely comprised of one aromatic and two aliphatic rings.

An aromatic proton signal at δ 6.62 ppm (H-11) had NOESY correlations to the hydroxyl signal at δ 4.46 ppm, and also to a methylene signal at δ 2.15ppm (H-1) and methyl protons δ 1.16 ppm (H-20) as shown in Figure 3.105. The other aromatic proton at δ 6.82 ppm (H-14) showed NOESY correlation to a pair of isopropyl side chain (H-16 and H-17). COSY also correlated H-7 at δ 2.76 ppm and 2.83 ppm to H-6 at δ 1.65 ppm, and 1.85 ppm.

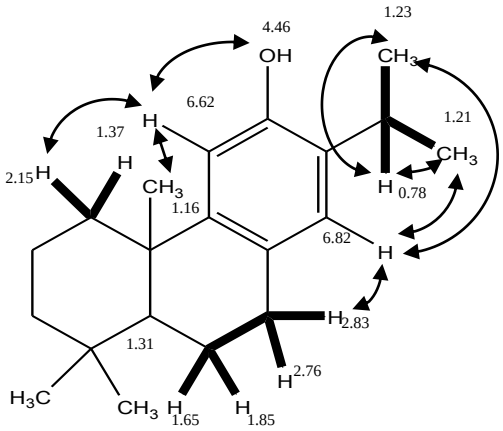

Figure 3.105 H-H COSY (bold line), and NOESY (arrow) of salient signals of ferruginol

The carbon signal at δ 50.3 ppm (C-5) had HMBC correlations to H-7 (δ 2.83 ppm), and H-20. Additionally, the coupling pattern with large *J* value (12.5 Hz) revealed the α-axial

orientation of H-5 due to 180° vicinal dihedral angle to a proton of H-6β. H-7β at δ 2.83 ppm has a coupling pattern as ddd with *J* values 17, 6, and 1.5 Hz which indicated an equatorial orientation. On the other hand, H-7α with axial orientation showed a large vicinal coupling constant at 11, and 7.5 Hz. The coupling constant of axial-equatorial (H-7α and H-6α; 7.5 Hz or H-7β and H-6β; 6 Hz) was larger than equatorial-equatorial (H-7β and H-6α; 1.5 Hz) as can be seen from Figure 3.106; usually there is not much difference. The geminal coupling constant (^2J) between $H_{7\alpha}$ and $H_{7\beta}$ was 17 Hz.

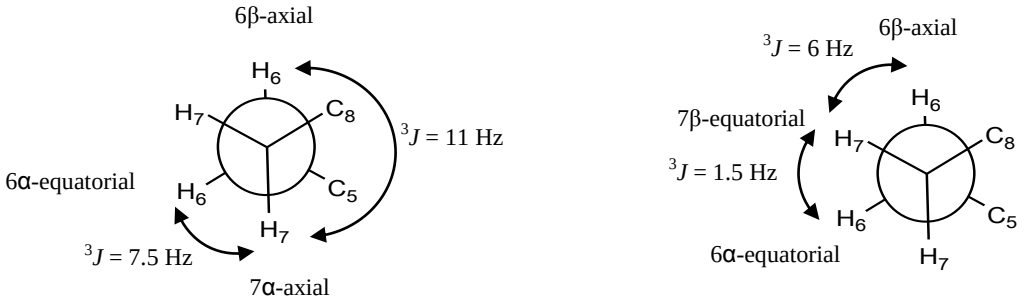

Figure 3.106 Newman projections of C-6 and C-7 of ferruginol

The chemical shift value and number of coupled protons and their coupling constants affected a shape of signal as shown in Figure 3.107. The coupling pattern of 3 non-equivalent neighboring protons is seen as a doublets of doublet of doublet (ddd). Both H-7β and H-7α displayed the ddd, but their shape was dissimilar due to different coupling constants. While the H-7β at δ 2.83 ppm (equatorial) is like four broad singlet, H-7α at δ 2.76 ppm (axial) is seen as multiplet. Methylene proton (H-6β and H-2α) displayed somewhat as a multiplet signal because it was coupled to 4-5 protons nearby, and also overlapping signal between them. As H-6 resonated more downfield than others, a coupling pattern of H-6α at δ 1.85 ppm is seen as a doublet of doublet of doublet of doublet (dddd) as shown in Figure 3.107. H-6α at δ 1.85 ppm (equatorial) was coupled to H-6β at δ 1.65 ppm with ^2J value 17 Hz, and then was further coupled to H-7α, H-5α, and H-7β with ^3J values 6, 3.5 and 2 Hz respectively.

The chemical shifts of the quaternary carbon atoms were resolved by HMBC correlations. C-13 at δ 130.9 ppm correlated to the septet signal (H-15) and dimethyl groups (H-16, and H-17), and also to a singlet aromatic proton at δ 6.62 ppm (H-14). Two carbon signals at δ 148.7 ppm, and 150.6 ppm correlated to both aromatic protons at δ 6.82 ppm (H-11) and 6.62 ppm (H-14), but only the signal at δ 148.7 ppm had a correlation to a methyl

proton at δ 1.16 ppm (H-20). Therefore, the signal at δ 148.7 ppm was assigned as C-9 while the other one was C-12 which was substituted by a hydroxyl group. Another peak at δ 127.3 ppm (C-8) was correlated to a dddd of H-6α. Two methyl carbons at δ 33.3 ppm, and 21.6 ppm had HMBC correlation to protons of each other which indicated 3-4 bond range relationship. In addition, axial methyl groups resonate upfield from equatorial methyl group on the same carbon atoms in a cyclohexane ring (Williams and Fleming, 2008). Therefore, C-19 (β-axial) would resonate at δ 21.6 ppm while equatorial methyl group (C-18) was at δ 33.3 ppm. HMBC assignments are shown in Figure 3.108.

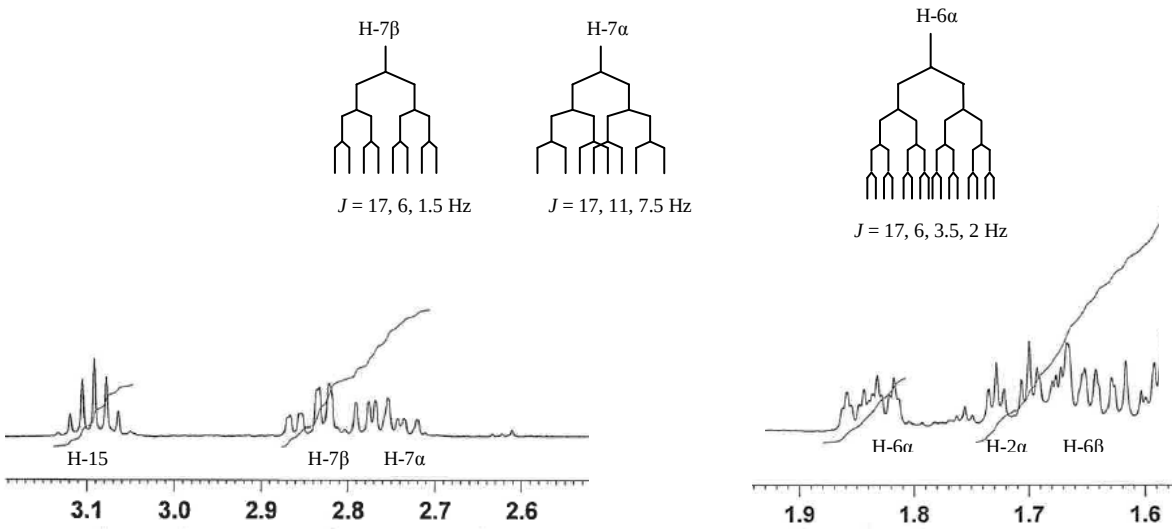

Figure 3.107 Selected ^{1}H coupling patterns of ferruginol (500 MHz in $CDCl_3$; δ in ppm)

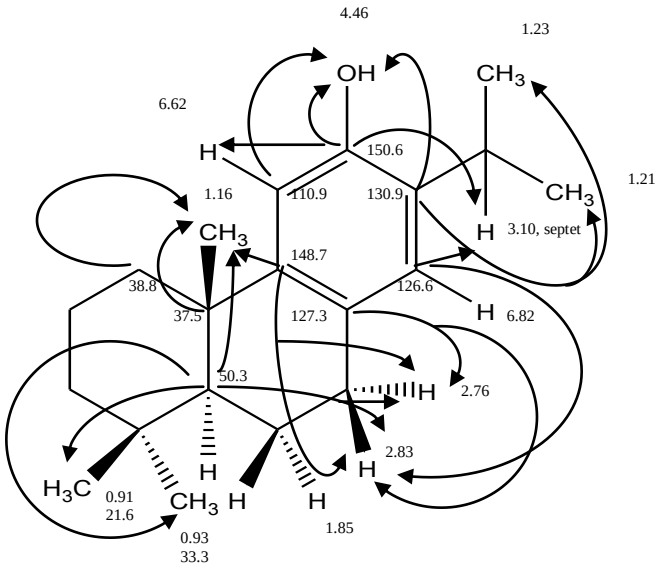

Figure 3.108 Key HMBC assignment of ferruginol

Ferruginol has previously been isolated from root parts of plants in the genus *Salvia*, for instance *S. viridis* L. (Ulubelen et al., 2000), *S. miltiorrhiza* Bunge (Lee et al., 2005), S. *cilicica* Boiss and Kotschy (Tan et al., 2002), *S. deserta* Schang (Tezuka et al., 1998). The spectroscopic data of this compound are identical to those reports.

3.8.2.2 Salvinolonyl 12-methyl ether

The MS data of salvinolonyl 12-methyl ether (Figure 3.109) gave a molecular mass of 328 and a molecular formula of $C_{21}H_{28}O_3$. ^1H and ^{13}C NMR data are shown in Table 3.34 and NMR spectra are given in Appendix 24.

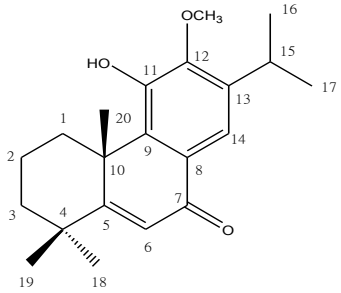

Figure 3.109 Salvinolonyl 12-methyl ether

^{13}C NMR displayed 21 signals, and corresponding DEPT-90 and DEPT-135 showed three methylene groups, nine quaternary carbon atoms, six methyl groups and three methine groups. There were three singlet signals in the deshielded region of ^1H NMR at δ 6.25 ppm, 6.47 ppm, and 7.73 ppm. Deuterium exchange indicated a hydroxyl group at δ 6.25 ppm. HMQC correlated two aromatic or alkene carbon signals at δ 115.9 ppm (C-14), and 123.6 ppm (C-6) to proton signals at δ 7.73 ppm (H-14), and 6.47 ppm (H-6) respectively. The septet signal at δ 3.25 ppm (H-15) implied the methine group of isopropyl side chain because it had COSY, and NOESY correlations to a pair of doublets at δ 1.26 ppm (H-16), and 1.28 ppm (H-17). Therefore, three out of nine positive signals from DEPT-135 were methine groups. The deshielded methyl signal at δ 3.83 ppm had a HMQC correlation to carbon at δ 61.9 ppm which indicated the methoxy substitution in this molecule. All above suggestions inferred an abietane diterpenoid skeleton.

Table 3.34 1D and 2D NMR data of salvinolonyl 12-methyl ether (^{1}H 500 MHz; ^{13}C 125 MHz in $CDCl_3$; δ in ppm; *J* in Hz)

Position	^{13}C	^{1}H	COSY	NOESY	HMBC
1	34.2	β3.27 (ddd, *J* = 14, 4, 2)	1.43*	1.43* 1.62	1.65
		α1.43* (ddd, *J* = 14, 12, 4)	3.27	3.27	
2	18.7	1.62 (m)	1.97	3.27	-
		1.97 (m)	1.43 1.62	3.27	
3	40.4	α1.43* (ddd, *J* = 14, 12, 4)	1.73	-	1.27 1.36
		β1.73 (ddd, *J* = 13, 7, 2)	1.43*	-	
4	38.1	-	-	-	1.27 1.36 6.47
5	175.3	-	-	-	1.27 1.36 1.65
6	123.6	6.47 (s)	-	1.27	1.27
7	185.4	-	-	-	7.73
8	127.4	-	-	-	6.47
9	136.7	-	-	-	1.65 6.25 7.73
10	42.2	-	-	-	1.65 6.47
11	145.8	6.25 (OH, s)	-	3.83	6.25
12	148.2	-	-	-	3.83 6.25 7.73

Table 3.34 (continued)

Position	^{13}C	^{1}H	COSY	NOESY	HMBC
13	139.7	-	-	-	1.26 1.28 3.25
14	115.9	7.73 (s)	-	1.26 1.28	-
15	26.8	3.25 (septet, *J* = 7)	1.26 1.28	1.26 1.28	1.26 1.28 7.73
16	23.6[§]	1.28 (3H, d, *J* = 7)	3.25	3.25	1.26 3.25
17	23.5[§]	1.26 (3H, d, *J* = 7)	3.25	3.25	1.28 3.25
18	33.1	α1.27 (3H, s)	-	-	1.36
19	29.3	β1.36 (3H, s)	-	1.65	1.27
20	24.8	β1.65 (3H, s)	-	1.36	1.27
Methoxyl group	61.9	3.83 (3H, s)	-	6.25	-

* Overlapped signal; [§] Interchangeable

The other singlet proton at δ 6.47 ppm (H-6) showed a NOESY correlation to a methyl signal at δ 1.27 ppm (H-19). Moreover, two quaternary carbon signals at δ 38.1 ppm (C-4), and δ 42.2 ppm (C-10) displayed HMBC correlations to H-6. The proton at δ 6.47 ppm (H-6) likely attached to the cyclohexane ring, however, it still had a HMBC correlation to an aromatic or alkene carbon at δ 127.4 ppm. These observations suggested the two aromatic protons were in the adjacent aromatic ring system with the oxo group in between.

Figure 3.110 shows certain noticeable 2D correlations of salvinolonyl 12-methyl ether. Two singlet signals of two aromatic protons suggested no correlation to each other. A singlet signal at δ 7.73 ppm (H-14) was correlated to the methine carbon of the isopropyl group at δ 26.8 ppm (C-15) by HMBC. It also had NOESY correlations to those pair of doublets at δ 1.28 ppm (H-16), and 1.26 ppm (H-17) which indicated the position of this proton in the same ring system. The methoxyl protons had a NOESY correlation to a singlet

of hydroxyl group which implied the adjacent substitution. Furthermore, NOESY also correlated this methoxyl proton signal to the septet signal. Therefore, the hydroxyl group, the methoxy group, and an aromatic proton at δ 7.73 ppm were in the same ring with isopropyl side chain attachment. In addition, the proton signal at δ 7.73 ppm (H-14) also had a HMBC correlation to a carbon signal at 185.4 ppm (C-7) which implied the ketone carbon nearby.

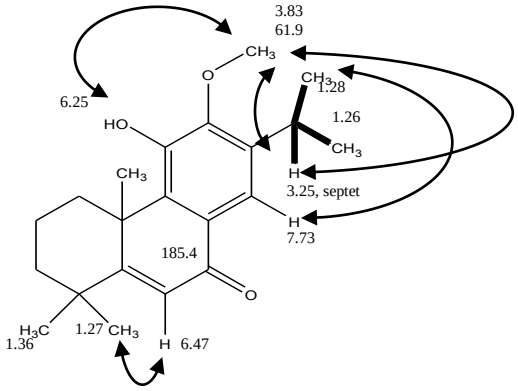

A. H-H COSY (bold line), and NOESY (arrow) correlations

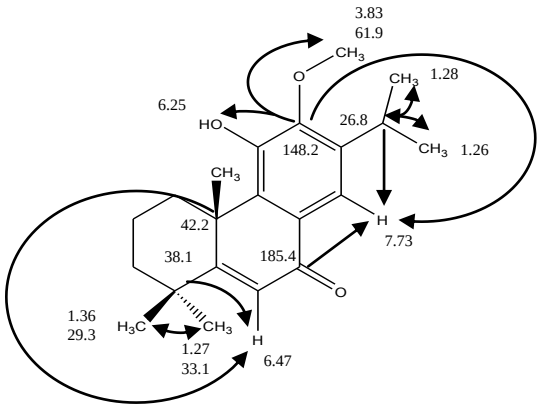

B. HMBC correlations

Figure 3.110 2D-NMR assignments from salient signals of salvinolonyl 12-methyl ether

Quaternary carbon atoms were assigned by HMBC as shown in Figure 3.111. A signal at δ 175.3 had correlations to three methyl groups at δ 1.27 ppm (H-18), 1.36 ppm (H-19), and 1.65 ppm (H-20) which implied the position of C-5. H-6 at δ 6.47 ppm exhibited HMBC correlation to a signals at δ 127.4 ppm (C-8) while C-9 at δ 136.7 ppm had 3 correlations to H-14 (7.73 ppm), hydroxyl group, and a methyl group at δ 1.65 ppm (H-20).

A carbon signal at δ 139.7 ppm was assigned as C-13 due to correlations to isopropyl side chain, H-15, H-16, and H-17.

Three methylene carbon atoms resonated at δ 18.7 ppm, 34.2 ppm, and 40.4 ppm. They correlated to six non equivalent proton signals in HMQC. Three protons coupling patterns which indicated three neighboring protons were seen in four signals from two carbon atoms at δ 34.2 ppm, and 40.4 ppm. As HMBC correlated a signal at δ 40.4 ppm to proton H-18, and H-19 as shown in Figure 3.111, therefore, this signal was assigned as C-3. Accordingly, a signal at δ 34.2 ppm would be C-1.

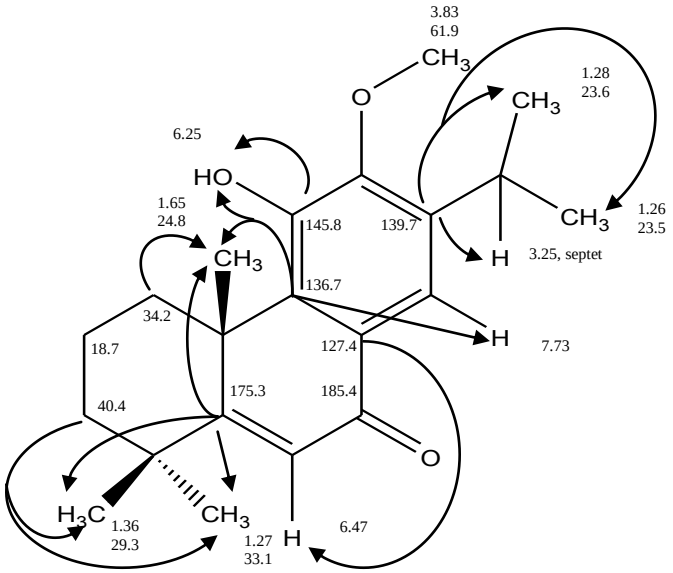

Figure 3.111 Key HMBC correlations of salvinolonyl 12-methyl ether

Each proton of C-2 (δ 18.7 ppm), at δ 1.62 ppm, and 1.97 ppm, was coupled to five adjacent protons as multiplet (m) signal as shown in Figure 3.112. Coupling patterns of three protons are seen in doublets of doublet of doublet (ddd) shape for axial-axial orientation, and doublets of triplet (dt) for equatorial-axial/equatorial one. Figure 3.112 shows the coupling shape of H-3α (axial), and H-3β (equatorial). However, two protons signals of H-1, and H-3 resonated at δ 1.43 ppm with α-axial orientation which can be seen an overlapping signal of ddd (*J* values = 14, 12, 4).

Salvinolonyl 12-methyl ether was previously reported from *S. montbretii* Benth. (Gil et al., 1994).

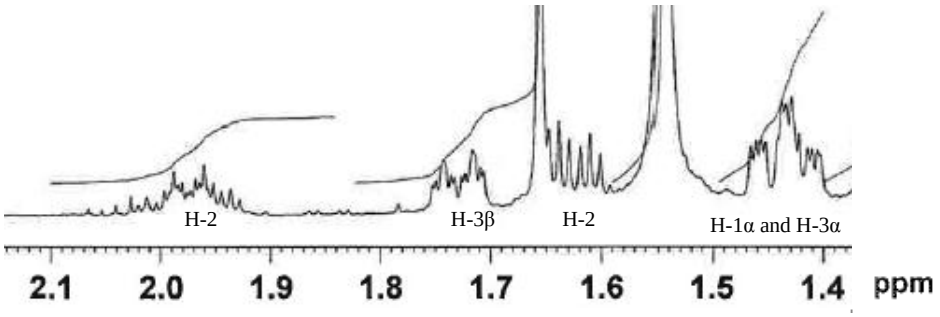

Figure 3.112 ^{1}H coupling pattern of salvinolonyl 12-methyl ether (500 MHz in $CDCl_3$)

3.8.2.3 7α-Acetoxy-14-hydroxy-8,13-abietadiene-11,12-dione

The MS data of 7α-acetoxy-14-hydroxy-8,13-abietadiene-11,12-dione (Figure 3.113) gave a molecular mass of 374 and a molecular formula of $C_{22}H_{30}O_5$. ^{1}H and ^{13}C NMR data are shown in Table 3.35 and NMR spectra are given in Appendix 25.

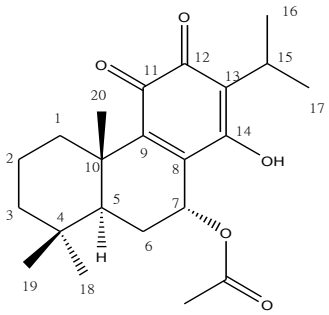

Figure 3.113 7α-Acetoxy-14-hydroxy-8,13-abietadiene-11,12-dione

^{13}C NMR displayed 22 signals, and corresponding DEPT-90 and DEPT-135 exhibited four methylene signals, nine quaternary carbon atoms, three methine groups and six methyl groups. Four singlet signals each integrating to three proton atoms were seen in ^{1}H NMR and two (3H) doublet signals. A (1H) septet at δ 3.15 ppm implied a methine proton of an isopropyl unit. There were also two signals at δ 5.92 ppm (dd), and 7.12 ppm (s). Deuterium exchange indicated that the peak at δ 7.12 ppm was a hydroxyl proton. Two ^{13}C signals at δ 183.7 ppm, and 185.4 ppm implied two carbonyl groups. A quaternary signal at δ 169.4 ppm correlated to a methyl signal at δ 2.03 ppm by HMBC suggesting an acetyl group. The presence of the isopropyl side chain and five methyl groups showed the characteristic of an abietane type diterpenoid. The molecular formula of this compound, $C_{22}H_{30}O_5$, corresponds to eight unsaturation numbers (DBE). Therefore, the above observations of four

methylene groups, three carbonyl carbon atoms with one hydroxyl group can be concluded to an abietane type containing an aromatic ring.

The key peak was the doublet of doublet ^{1}H signal at δ 5.92 ppm (H-7; ^{3}J = 4, 1.5 Hz). The small vicinal coupling constants implied the equatorial orientation of this proton. HMQC correlated this signal to a carbon signal at δ 64.5 ppm (C-7) which inferred the substitution of electronegative group, for example a hydroxyl group. The α-axial substitution of the acetyl group was verified by NOESY correlation of the -CH_3 at δ 2.03 ppm to H-5 at δ 1.49 ppm as shown in Figure 3.114A.

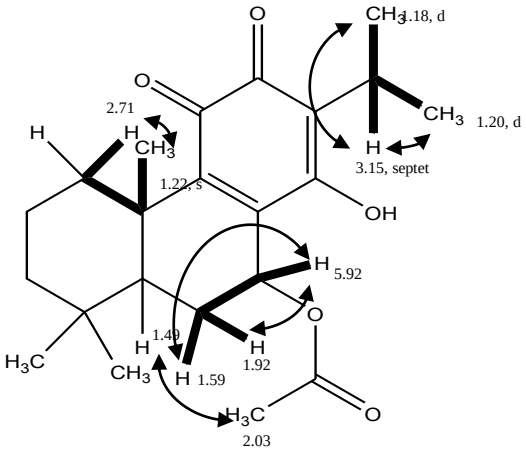

A. H-H COSY (bold line), and NOESY (arrow) correlations

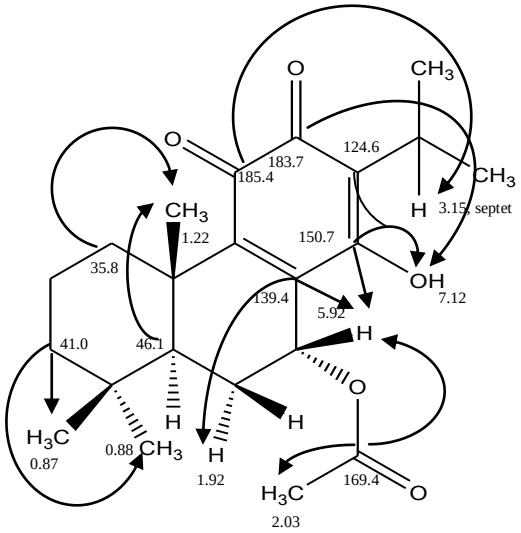

B. HMBC correlations

Figure 3.114 2D NMR assignments from salient signals of 7α-acetoxy-14-hydroxy-8,13-abietadiene-11,12-dione

Table 3.35 1D and 2D NMR data of 7α-acetoxy-14-hydroxy-8,13-abietadiene-11,12-dione (^{1}H 500 MHz; ^{13}C 125 MHz in $CDCl_3$; δ in ppm; *J* in Hz)

Position	^{13}C	^{1}H	COSY	NOESY	HMBC
1	35.8	α1.20*	1.22*		1.22
		β2.71 (dt, *J* = 13, 4, 1)	1.72		
2	18.8	α1.72 (dddd, *J* = 13, 6, 2)	1.57	-	1.49
		β1.57*	1.72	-	
3	41.0	α1.49* (br d, *J* = 13, 1)	-	-	0.87
		β1.20*	-	-	0.88
4	32.9*	-	-	-	0.87 0.88 1.22 1.49
5	46.1	α1.49* (br d, *J* = 13, 1)	-	2.03	0.87 0.88 1.22 1.59* 1.92
6	24.6	β1.59* (ddd, *J* = 15, 11, 1.5)	5.92	1.92 5.92	1.49
		α1.92 (br d, *J* = 15)	1.59*	1.59* 5.92	
7	64.5	β5.92 (dd, *J* = 4, 1.5)	1.59* 1.92	1.59* 1.92	1.49 1.92
8	139.4	-	-	-	1.92 5.92
9	149.9	-	-	-	1.22
10	39.0	-	-	-	1.22 1.49 1.57 1.59 1.92
11	185.4	-	-	-	3.15

Table 3.35 (continued)

Position	^{13}C	^{1}H	COSY	NOESY	HMBC
12	183.7	-	-	-	7.12
13	124.6	-	-	-	1.18 1.20 3.15 7.12
14	150.7	7.12 (OH, s)	-	-	3.15 5.92 7.12
15	24.1	3.15 (septet, *J* = 7)	1.18 1.20	1.18 1.20	1.18 1.20
16	19.8[§]	1.20 (3H, d, *J* = 7)	3.15	3.15	1.18 3.15
17	19.7[§]	1.18 (3H, d, *J* = 7)	3.15	3.15	1.20 3.15
18	32.9*	α0.88 (3H, s)	-	-	0.87 1.22 1.49
19	21.6	β0.87 (3H, s)	-	-	0.88 1.22 1.49
20	18.5	1.22 (3H, s)	-	-	1.49
Acetyl group	169.4	-	-	-	2.03 5.92
	21.1	2.03 (3H, s)	-	1.49	-

*Overlapped signal; [§] Interchangeable

COSY and NOESY correlated ^{1}H signal at δ 5.92 ppm to a metheylene proton at δ 1.92 ppm which further correlated to a carbon signal at δ 139.4 ppm by HMBC. Therefore, a carbon signal at δ 64.5 ppm (C-7) was in between the aromatic ring and cyclohexane ring. H-7 also had HMBC correlations to carbon signals at δ 150.7 ppm, and 169.4 ppm as shown in Figure 3.114B.

A singlet signal at δ 7.12 was assigned as a hydroxyl substitution at C-14 (δ 150.7 ppm), and correlated to ketone carbon signal at δ 183.7 ppm (C-12) by HMBC. Another ketone carbon at δ 185.4 ppm (C-11) was correlated to the septet at δ 3.15 ppm. Additionally, HMBC also displayed correlations of the septet to carbon signals at δ 150.7 ppm, and 124.6 ppm. Methyl proton at δ 1.22 ppm (H-20) displayed a HMBC correlation to a quaternary carbon at δ 149.9 ppm (C-9), and also had correlations to carbon signals at δ 35.8 ppm (C-1), 39.0 ppm (C-10), and 46.1 ppm (C-5).

Figure 3.115 shows coupling pattern of H-7 at δ 5.92 ppm. It exhibited the doublet of doublet signal with ^{3}J value 4, and 1.5 Hz which indicated the equatorial orientation. As H-5 had an α-axial orientation; therefore, H-7 would be a β-equatorial.

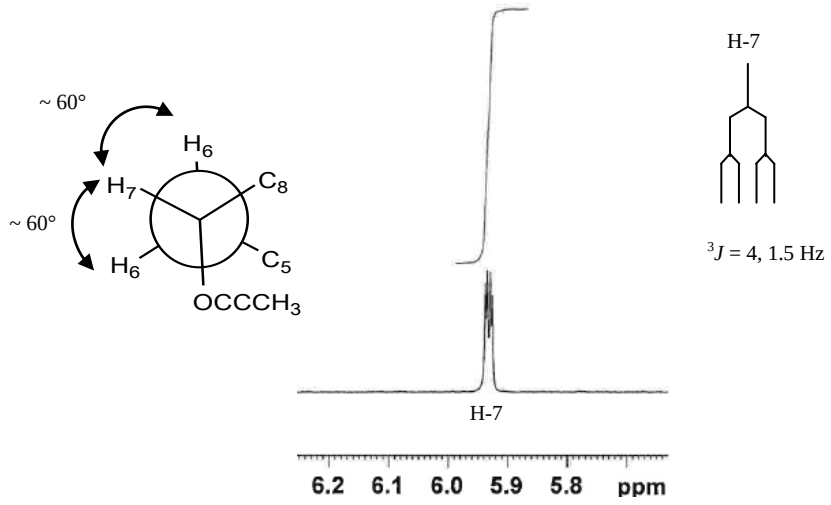

Figure 3.115 H-7 coupling pattern of 7α-acetoxy-14-hydroxy-8,13-abietadiene-11,12-dione (^{1}H NMR 500 MHz; $CDCl_3$)

A ^{1}H signal at δ 2.71 ppm (H-1) was assigned as the β-equatorial because the vicinal coupling constant were 4 and 1 Hz which referred the small dihedral angle to H-2 around 60°. Another proton of H-2 at δ 1.72 ppm (α-equatorial) exhibited a dddd (or quartet of triplet) shape which resembled to a shape of a proton (H-6α-equatorial) of ferruginol as shown in Figure 3.107. Certain signals of the methylene protons were overlapped; therefore, coupling constants were undefined. However, the orientatation (α or β) of some protons were possibly assigned from the shape of their signals. H-5 at δ 1.49 ppm displayed a broad doublet with ^{3}J value 13 Hz. The large dihedral angle (180°) indicated the axial-axial coupling constant.

3.8.2.4 7α,14-Dihydroxy-8,13-abietadiene-11,12-dione

The MS data of 7α,14-dihydroxy-8,13-abietadiene-11,12-dione (Figure 3.116) gave a molecular mass of 332 and a molecular formula of $C_{20}H_{28}O_4$. ^1H and ^{13}C NMR data are shown in Table 3.36 and NMR spectra are given in Appendix 26.

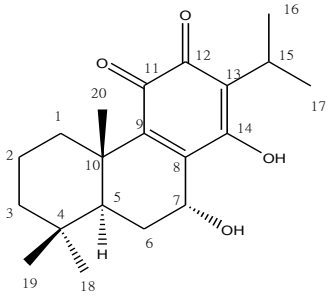

Figure 3.116 7α,14-Dihydroxy-8,13-abietadiene-11,12-dione

7α,14-Dihydroxy-8,13-abietadiene-11,12-dione and 7α-acetoxy-14-hydroxy-8,13-abietadiene-11,12-dione occurred in the same fraction in column chromatography but were separated by the solubility of 7α,14-dihydroxy-8,13-abietadiene-11,12-dione in methanol. NMR data of 7α,14-dihydroxy-8,13-abietadiene-11,12-dione showed the same pattern as 7α-acetoxy-14-hydroxy-8,13-abietadiene-11,12-dione except for a singlet ^1H proton signal at δ 3.00 ppm which was exchanged with D_2O and a signal at δ 4.72 ppm which replaced on at δ 5.92 ppm in 7α-acetoxy-14-hydroxy-8,13-abietadiene-11,12-dione. Therefore, this compound could be comprised of a hydroxyl group at C-7 instead of acetyl group as 7α-acetoxy-14-hydroxy-8,13-abietadiene-11,12-dione. This is confirmed by the MS data which shows a molecular weight of 42 mass units less than 7α-acetoxy-14-hydroxy-8,13-abietadiene-11,12-dione.

Figure 3.117 shows key signals of 7α,14-dihydroxy-8,13-abietadiene-11,12-dione. The hydroxyl signal at δ 3.00 ppm had a COSY correlation to H-7 at δ 4.72 ppm, also a HMBC correlation to C-6 at δ 25.8 ppm. In comparison with 7α-acetoxy-14-hydroxy-8,13-abietadiene-11,12-dione, a hydroxyl group substitution caused shielded effect. C-7 and H-7 resonated more upfield at δ 63.2 ppm, and δ 4.72 ppm respectively as opposed to δ 64.5 ppm, and δ 5.92 ppm in 7α-acetoxy-14-hydroxy-8,13-abietadiene-11,12-dione.

Table 3.36 1D and 2D NMR data of 7α,14-dihydroxy-8,13-abietadiene-11,12-dione (^{1}H 500 MHz; ^{13}C 125 MHz in $CDCl_3$; δ in ppm; *J* in Hz)

Position	^{13}C	^{1}H	COSY	NOESY	HMBC
1	35.8	α1.18*	-	-	1.22*
		β2.70 (dt, *J* = 13.5, 2.5)	1.18*		
2	18.8	1.70*	-	-	1.46*
		1.53*	-	-	
3	41.0	1.46*	-	-	0.90 0.98
		1.25*	-	-	
4	32.9	-	-	-	0.90 0.98 1.49*
5	45.7	α1.49* (br d, *J* = 10.5)	-	-	0.90 0.98 1.22* 1.60* 1.94
6	25.8	α1.60*	1.94	4.72	1.49* 3.00
		β1.94 (ddd, *J* = 15)	1.60*	-	
7	63.2	β4.72 (br s, *J* = 3.5, 2)	1.60* 3.00	1.60*	1.49* 1.94
		α3.00 (OH, s)	4.72	1.60* 7.20	-
8	143.2	-	-	-	1.94
9	147.8	-	-	-	1.22*
10	39.1	-	-	-	1.22* 1.49* 1.53 1.92

Table 3.36 (continued)

Position	^{13}C	^{1}H	COSY	NOESY	HMBC
11	185.0[¶]	-	-	-	3.15
12	189.1[¶]	-	-	-	3.15
13	124.2	-	-	-	1.20* 3.15
14	151.0	7.20 (OH, s)	-	3.00 4.72	3.15
15	24.0	3.15 (septet, *J* = 7)	1.20*	1.20*	1.20*
16	19.9[§]	1.20* (3H, d, *J* = 7)	3.15	3.15	1.20* 3.15
17	19.8[§]	1.20* (3H)	3.15	3.15	1.20* 3.15
18	33.1	α0.98 (3H, s)	-	-	0.90 1.22* 1.49* 1.94
19	21.7	β0.90 (3H, s)	-	-	0.98 1.22* 1.49
20	18.4	1.22* (3H)	-	-	1.49*

*Overlapped signal; [¶, §] Interchangeable

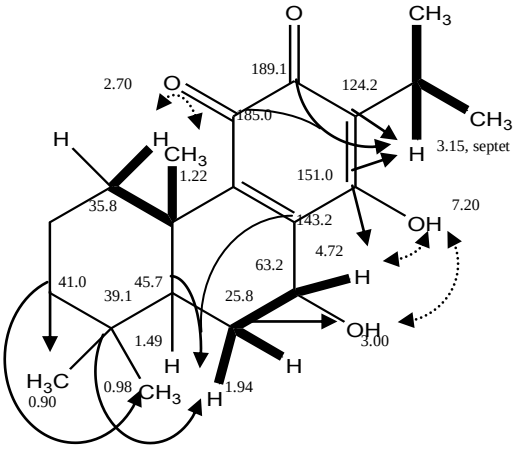

Figure 3.117 NMR assignments from salient signals of 7α,14-dihydroxy-8,13-abietadiene-11,12-dione. H-H COSY (bold line), NOESY (dot arrow), HMBC (arrow)

NMR data for 7α-acetoxy-14-hydroxy-8,13-abietadiene-11,12-dione and 7α,14-dihydroxy-8,13-abietadiene-11,12-dione are identical to published data for 7-O-acetylhorminone and horminone (Table 3.37) which is usually drawn as the *p*-quinone tautomer. HMBC correlations of 7α-acetoxy-14-hydroxy-8,13-abietadiene-11,12-dione clearly exhibited the correlation of C-14 (δ 150.4 ppm) to H-7 (δ 5.92 ppm). NOESY of 7α,14-dihydroxy-8,13-abietadiene-11,12-dione showed a correlation between the hydroxyl groups at C-14 (δ 7.20 ppm) and H-7 (δ 4.72 ppm). Both these observation are consistent with the *o*-quinone structures for 7α-acetoxy-14-hydroxy-8,13-abietadiene-11,12-dione and 7α,14-dihydroxy-8,13-abietadiene-11,12-dione which are tautomeric with 7-*O*-acetylhorminone and horminone respectively. The data presented here suggests that a significant proportion of the equilibrium mixture exists as the *o*-quinone tautomer. 7-*O*-Acetylhorminone and horminone have been reported in many *Salvia* species (Oztekin et al., 2010).

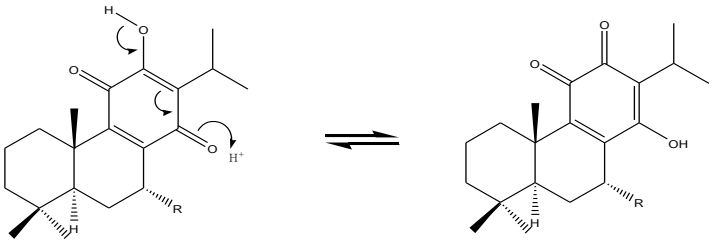

7-Acetylhorminone: R = $OCOCH_3$

Horminone: R = OH

7α-Acetoxy-14-hydroxy-8,13- abietadiene-11,12-dione: R = $OCOCH_3$

7α,14-Dihydroxy-8,13-abietadiene-11,12-dione: R = OH

Figure 3.118 Tautomers of abietane diterpenoid with quinone substitution

It is noteworthy that quinones such as these and other α,β-unsaturated carbonyl compounds, such as those depicted in Figure 1.25 (p 31), are efficient 1,4-Michael acceptors (Sharma et al., 1994) and this might explain their biological activity. In this case, a reactive nucleophile such as the cysteine–SH of a protein might attack at position 8 to yield a covalent product. As horminone is a fully substituted quinone, it is possible that this can act as a reversible 1,4-Michael acceptor as described by Avonto et al. (2011).

Table 3.37 Comparison NMR data of abietane diterpenoids with quinone substitution (δ in ppm)

Position	7α-Acetoxy-14-hydroxy-8,13-abieta-diene-11,12-dione [a]		7α,14-Dihydroxy-8,13-abietadiene-11,12-dione [a]		7-*O*-Acetylhorminone[b] (Tezuka et al., 1998)		Horminone[b] (Tezuka et al., 1998)	
	δ_C	δ_H	δ_C	δ_H	δ_C	δ_H	δ_C	δ_H
1	35.8	1.20*	35.8	1.18*	35.8	1.22	35.8	1.18
		2.71		2.70		2.73		2.70
2	18.8	1.72	18.8	1.70*	18.8	1.75	18.9	1.73
		1.57*		1.53*		1.57		1.47
3	41.0	1.49*	41.0	1.46*	41.0	1.49	41.1	1.56
		1.20*		1.25*		1.23		1.25
4	32.9*	-	32.9	-	33.0	-	33.0	-
5	46.1	1.49*	45.7	1.49*	46.1	1.48	45.7	1.54
6	24.6	1.59*	25.8	1.60*	24.6	1.61	25.8	1.61
		1.92		1.94		1.95		1.97
7	64.5	5.92	63.2	4.72	64.5	5.94	63.2	4.73
		-		3.00 (OH)		-		3.07 (OH)
8	139.4	-	143.2	-	139.4	-	143.2	-
9	149.9	-	147.8	-	150.0	-	147.8	-
10	39.0	-	39.1	-	39.1	-	39.1	-
11	183.7	-	185.0	-	183.7	-	183.9	-
12	185.4	-	189.1	-	150.8	7.18 (OH)	151.1	7.33 (OH)
13	124.6	-	124.2	-	124.7	-	124.2	-
14	150.7	7.12 (OH)	151.0	7.20 (OH)	185.4	-	189.1	-
15	24.1	3.15	24.0	3.15	24.1	3.16	24.0	3.16
16	19.8[§]	1.20	19.9[¶]	1.20*	19.7	1.19	19.8	1.21
17	19.7[§]	1.18	19.8[¶]	1.20*	19.9	1.23	19.9	1.22
18	32.9*	0.88	33.1	0.98	33.0	0.89	33.1	0.98
19	21.6	0.87	21.7	0.90	21.6	0.88	21.7	0.90
20	18.5	1.22	18.4	1.22*	18.5	1.24	18.4	1.21
Acetyl group	169.4	-	-	-	169.4	-	-	-
	21.1	2.03	-	-	21.1	2.03	-	-

*Overlapped signal; [§] [¶] Interchangeable; [a] in $CDCl_3$ 500 MHz; [b] in $CDCl_3$ 400 MHz

3.8.2.5 Microstegiol

The MS data of microstegiol (Figure 3.119) gave a molecular mass of 298 and a molecular formula $C_{20}H_{26}O_2$. ^1H and ^{13}C NMR data are shown in Table 3.38 and NMR spectra are given in Appendix 27.

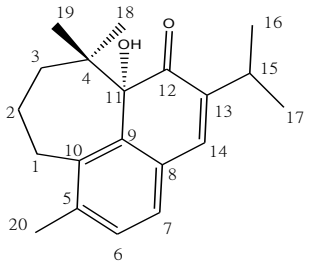

Figure 3.119 Microstegiol

The ^1H NMR, COSY, and NOESY correlations showed the characteristics of abietane diterpene skeleton type which are the septet signal of the methine proton at C-15, and two doublet signals of the methyl groups at C-16, and C-17. ^{13}C spectra displayed 20 signals with three methylene groups and eight signals of quaternary carbon atoms from DEPT-135. In the aromatic region, two protons coupled to each other as two doublet signals at δ 6.88 ppm, and 7.05 ppm (^3J value 7.5 Hz). A further singlet proton signal at δ 6.95 ppm showed a COSY correlation to the methine proton of the isopropyl group and a NOESY correlation to one of the doublet pair (H-16) as shown in Figure 3.120. In addition, this singlet proton correlated by HMBC to a carbon signal at δ 126.7 ppm which was directly attached to the aromatic proton δ 6.88 ppm (HMQC) which implied that these two rings are attached. The signal of a quaternary carbon atom at δ 206.1 ppm pointed to a ketone carbon atom which correlated (HMBC) to the septet signal at δ 3.00 ppm, an aromatic proton at δ 6.95 ppm and a singlet signal at δ 4.50 ppm which was shown to be –OH by D_2O exchange. HMBC correlations between this singlet at δ 4.50 ppm and C-11 (δ 84.4 ppm) were also observed. In addition, C-11 was further correlated to two signals of methyl groups of H-18 and H-19 by HMBC.

The aromatic proton at δ 7.05 ppm exhibited a H-H COSY correlation to a methyl singlet signal at δ 2.31 ppm. The rearranged abietane framework was assigned due to all those corresponding data. Selected 2D-NMR assignments are presented in Figures 3.120-3.121.

Table 3.38 1D and 2D NMR data of microstegiol (^{1}H 500 MHz; ^{13}C 125 MHz in $CDCl_3$; δ in ppm; *J* in Hz)

Position	^{13}C	^{1}H	COSY	NOESY	HMBC
1	27.0	α2.79 (ddd, *J* = 14, 6, 2.5)	1.41 1.78 3.59	2.31	0.78 0.79
		β3.59 (ddd, *J* = 14, 12, 2)	1.41 2.79	2.79	
2	23.5	α1.41 (m)	1.78 2.79 3.59	1.78 4.50	0.78 0.79
		1.78 (m)	1.24* 1.41 2.35 2.79 3.59	1.41	
3	42.9	2.35* (m)	1.41 1.78	-	0.78 0.79
		1.24* (m)	-	-	2.79
4	39.0	-	-	-	0.78 0.79
5	137.4	-	-	-	2.31 2.79 6.88
6	130.1	7.05 (d, *J* = 7.5)	2.31 6.88	6.88	2.31 6.88
7	126.6	6.88 (d, *J* = 7.5)	7.05	7.05	6.95 7.05
8	129.0	-	-	-	6.95 7.05
9	139.3	-	-	-	2.79 4.50 6.88 6.95

Table 3.38 (continued)

Position	^{13}C	^{1}H	COSY	NOESY	HMBC
10	143.3	-	-	-	2.31 2.79 3.59 7.05
11	84.4	4.50 (OH, s)	-	-	0.78 0.79
12	206.1	-	-	-	3.00 4.50 6.95
13	141.0[§]	-	-	-	1.14 1.19 3.00 6.88 6.95
14	140.9[§]	6.95 (s)	3.00	1.14	1.14 1.19 3.00 6.88
15	26.8	3.00 (septet, *J* = 6)	1.14 1.19 6.95	1.14 1.19	1.14 1.19
16	22.1[¤]	1.14 (3H, d, *J* = 7 Hz)	-	-	1.19 3.00
17	21.1 [¤]	1.19 (3H, d, *J* = 7)	-	-	1.14 3.00
18	21.4	α0.79 (3H, s)	-	-	0.78
19	28.0	β0.78 (3H, s)	-	-	0.79
20	21.4	2.31 (3H, s)	7.05	7.05	7.05

* Overlapped signals; [§ , ¤] Interchangeable signals

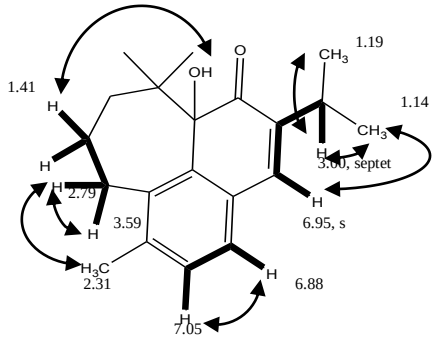

A. H-H COSY (bold line), and NOESY (arrow) correlations

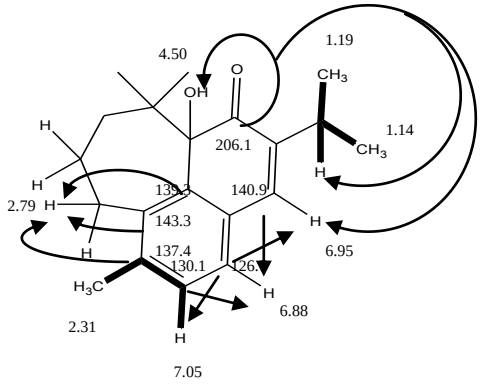

B. H-H COSY (bold line), and HMBC (arrow) correlations

Figure 3.120 2D-NMR assignments from salient signals of microstegiol.

^{13}C signals of three methylene groups correlated to 6 non-equivalent protons in HMQC. Four of them showed unclear coupling constants due to multiplet overlapping patterns. Two noticeable ^{1}H peaks at δ 2.79 ppm and δ 3.59 ppm belonged to non-equivalent proton atoms of methylene group at C-1. Each of them was coupled to only three nearby protons, and the signal at δ 2.79 ppm also had a NOESY correlation to a singlet signal at δ 2.31 ppm of C-20 (Figure 3.120A). Additionally, HMBC correlations exhibited the relation between these two protons and C-5, C-9, and C-10 (Figure 3.120B). The proton at δ 2.79 ppm was coupled as ddd (J = 14, 6, 2.5 Hz) while the other proton signal was at δ 3.59 ppm (J = 14, 12, 2 Hz). These distinctive patterns allow the configuration of these protons to be established as shown Figure 3.122. According to Karplus equation in rigid systems, the axial-axial coupling constant is large in range of 9-13 Hz due to wide dihedral angle (180°). On the other hand, the axial-equatorial and equatorial-equatorial dihedral angle is around 60°, and the vicinal coupling constant is smaller in range of 2-5 Hz (Williams and Fleming, 2002).

The other quaternary carbon atoms at δ 39.0 ppm, 84.4 ppm, 129.0 ppm, 137.4 ppm, 139.3 ppm, 141.0 ppm, and 143.3 ppm, were assigned according to HMBC correlations as shown in Figure 3.121.

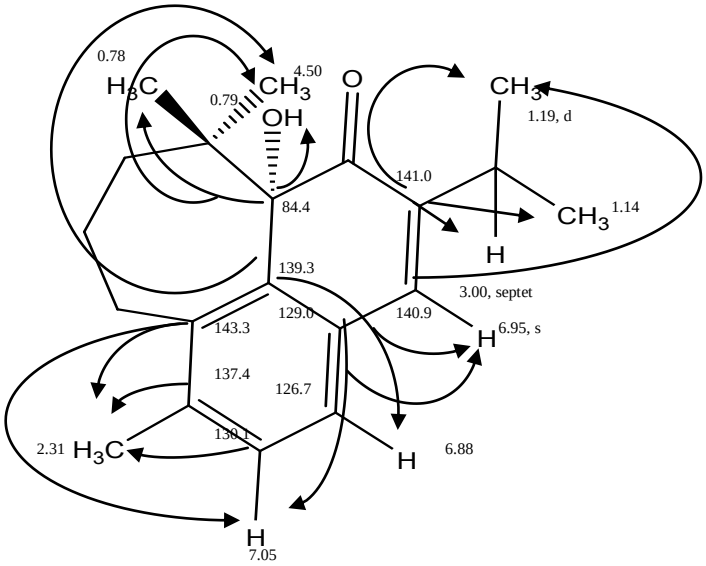

Figure 3.121 Selected HMBC correlations of microstegiol

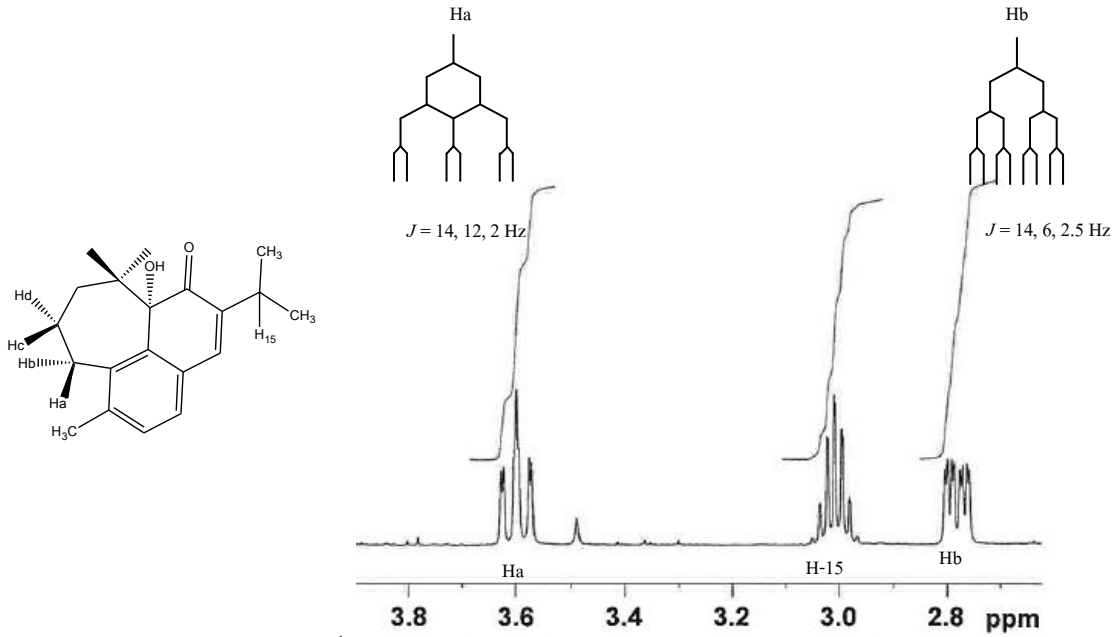

Figure 3.122 ^{1}H NMR splitting patterns of microstegiol (500 MHz in $CDCl_3$)

Microstegiol was first isolated from the aerial part of *S. microstegia* Boiss. Et Bal. (Ulubelen et al., 1992). It was also reported in root part of *S. montbretii* Benth. (Topcu and Ulubelen, 1996) and *S. viridis* L. (Ulubelen et al., 2000).

3.8.2.6 Compound 3 (1-Oxomicrostegiol; 10aS-8,9,10,10a-tetrahydro-10a-hydroxy-6,10,10-trimethyl-2-(1-methylethyl)-cyclohepta[de]naphthalene-1,7-dione)

The MS data of compound 3 (Figure 3.123) gave a molecular mass of 312 and a molecular formula of $C_{20}H_{24}O_3$. ^{1}H and ^{13}C NMR data are shown in Table 3.39 and NMR spectra are given in Appendix 28.

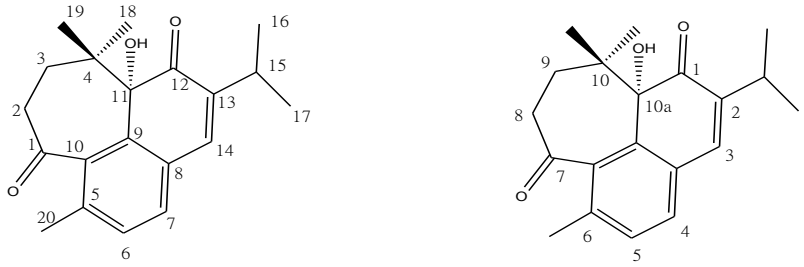

A. Diterpenoid numbering B. IUPAC numbering

Figure 3.123A-B Compound 3 (1-Oxomicrostegiol)

^{13}C NMR displayed 20 signals, and corresponding DEPT-90 and DEPT-135 showed four methine groups, two methylene groups, five methyl groups and nine quaternary carbon atoms. Two signals of quaternary carbon atom at δ 203.5 ppm, and 207.2 ppm implied two ketone groups. Three aromatic protons indicated two separate conjugated ring system because only two aromatic protons, δ 7.20 ppm, and 7.22 ppm, are coupled to each other as doublet with *J* value 7.5 Hz. A third proton in the aromatic/alkene region gave a singlet at δ 7.07 ppm. This was assigned as H-14 and showed an HMBC correlation to C-7 in the adjacent ring. In addition, the presence of two doublets of methyl group plus a septet splitting pattern indicated the isopropyl group of an abietane diterpenoid.

Deuterium exchange revealed a hydroxyl group peak as a singlet at δ 3.88 ppm. HMBC showed the correlation between a ketone peak at δ 203.5 ppm (C-12) and the hydroxyl signal. It also connected this ketone carbon to the proton singlet at δ 7.07 ppm (H-14). There was a NOESY correlation between aromatic proton at δ 7.22 ppm (H-6) and methyl group at δ 2.34 ppm (H-20). While COSY exhibited the correlation between two geminal methyl group at δ 0.80 ppm (H-19), and 1.05 ppm (H-18), one of them, δ 1.05 ppm signal, had a NOESY correlation to the hydroxyl group as shown in Figure 3.125. All assignments above suggested a rearranged abietane type which is likely to be a microstegiol framework. Key assignments of HMBC, COSY, and NOESY are shown in Figures 3.124-3.125.

Table 3.39 1D and 2D NMR data of compound 3 (1-oxomicrostegiol) (^{1}H 500 MHz; ^{13}C 125 MHz in $CDCl_3$; δ in ppm; *J* in Hz)

Position[a]	^{13}C	^{1}H	COSY	NOESY	HMBC
1	207.2	-	-	-	3.11
2	38.2	α3.11 (ddd, *J* = 14, 11.5, 2.5)	1.42 1.54 2.30	1.05 2.30	0.80 1.05
		β2.30* (ddd, *J* = 14, 5, 3)	1.42 1.54 3.11	3.11	
3	37.5	α1.42 (ddd, *J* = 14, 5, 3)	1.54 2.30 3.11	-	0.80 1.05
		β1.54* (dd, *J* = 14, 3)	1.42 2.30 3.11	-	
4	40.9	-	-	-	0.80 1.08
5	136.9	-	-	-	2.34 7.20
6	131.2	7.22 (d, *J* = 7.5)	2.34	2.34	2.34
7	129.6	7.20 (d, *J* = 7.5)	2.34	2.34	2.34 7.07
8	127.6	-	-	-	2.34 7.20 7.22
9	138.1	-	-	-	2.30 2.34 7.07
10	137.6	-	-	-	2.30 2.34 7.20 7.22

Figure 3.39 (continued)

Position[a]	^{13}C	^{1}H	COSY	NOESY	HMBC
11	81.5	3.88 (OH, s)	-	1.05	0.80 1.05 3.88
12	203.5	-	-	-	3.88 7.07
13	141.5	-	-	-	1.16 1.18 2.98
14	139.1	7.07 (s)		1.16 1.18	2.98 7.20
15	26.9	2.98 (septet, *J* = 7)	1.16 1.18	1.16 1.18	1.16 1.18 7.07
16	21.9[§]	1.16 (3H, d, *J* = 7)	-	-	1.18 2.98
17	21.5[§]	1.18 (3H, d, *J* = 7)	-	-	1.16 2.98
18	17.4	α1.05 (3H, s)	0.80	0.80 3.88	0.80 3.11
19	26.9	β0.80 (3H, s)	1.05	1.05	1.05
20	19.9	2.34 (3H, s)	7.20 7.22	7.20 7.22	7.20 7.22

[a]Diterpenoid numbering ; * Overlapped signal; [§] Interchangeable

Each proton of the methylene groups showed the three proton coupling pattern which implied the attachment of these two methylene groups. Furthermore, HMBC correlated another ketone carbon at δ 207.2 ppm (C-1) to a proton of CH_2 group (H-2α), δ 3.11 ppm, which implied the attachment in the same ring system (Figure 3.124A). The oxo-carbon at position 1 was verified by the HMBC correlation between H-2β at δ 2.30 ppm and the aromatic carbon signal at δ 138.1 ppm (C-9).

Quaternary carbon atoms were assigned according to HMBC correlations as follows: δ 136.9 ppm (C-5), 127.6 ppm (C-8), 138.1 ppm (C-9), 137.6 ppm (C-10), 81.5 ppm (C-11), and 141.5 ppm (C-13). Selected HMBC correlations are shown in Figure 3.124.

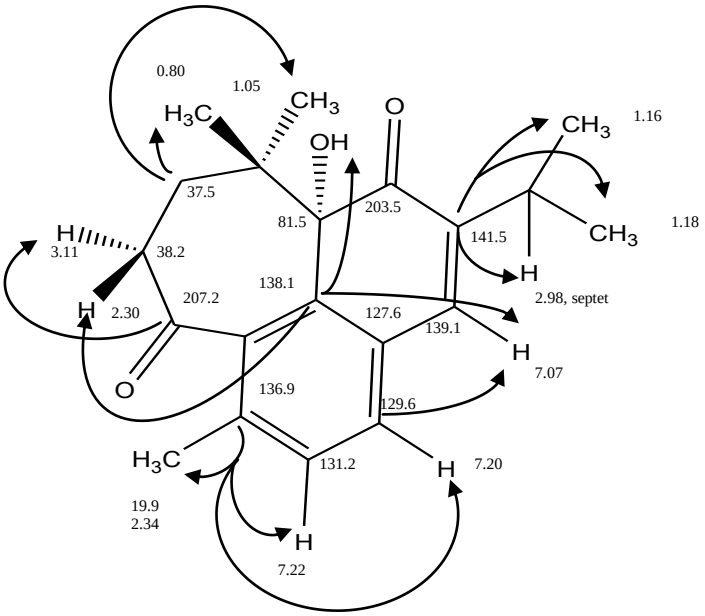

A.

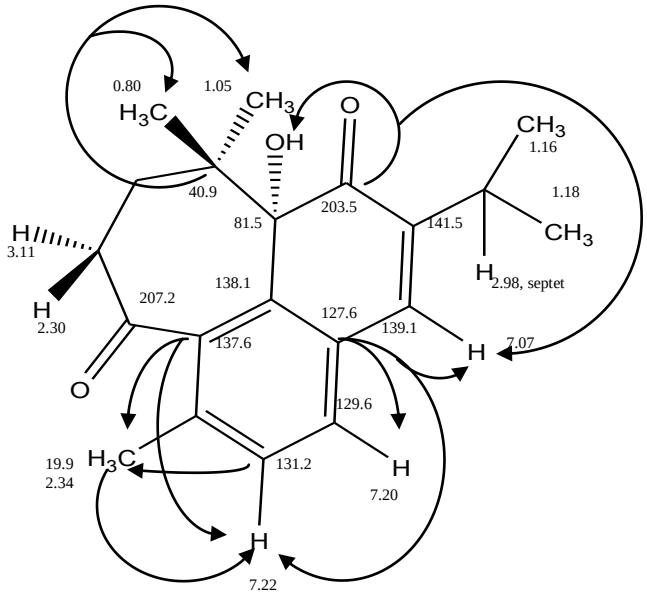

B.

Figure 3.124A-B Selected HMBC correlations of compound 3 (1-oxomicrostegiol)

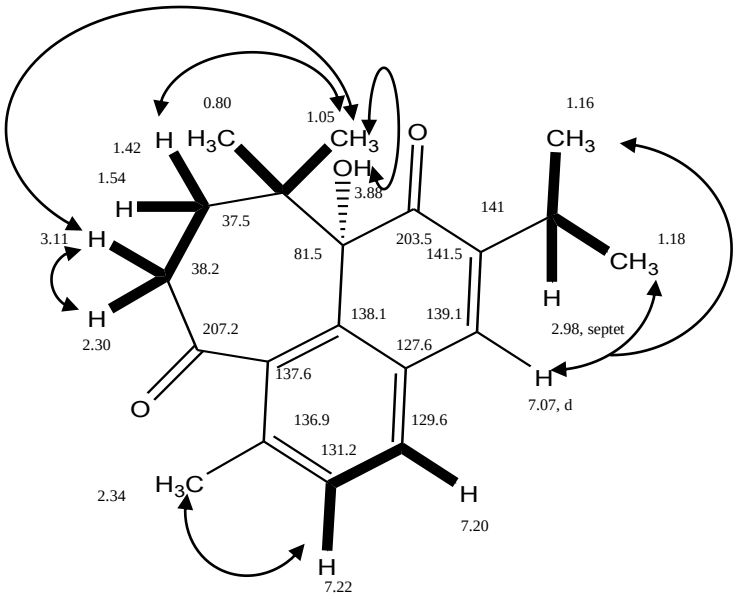

Figure 3.125 H-H COSY (bold line), and NOESY (arrow) correlations of compound 3

The ^{1}H peak at 3.11 ppm as ddd (H-2α; *J* values = 14, 11.5, 2.5 Hz) indicated an axial-axial coupling pattern as shown in Figure 3.126. The α-configuration of methyl protons (H-19) at δ 1.05 ppm was further assigned because of a NOESY correlation to H-2α.

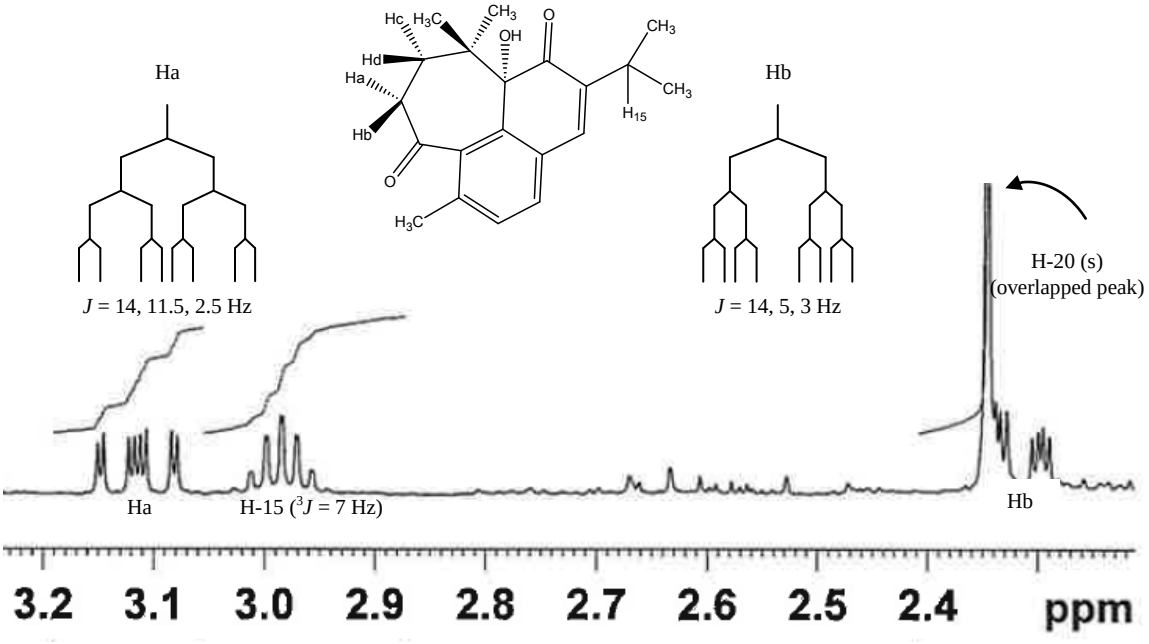

Figure 3.126 ^{1}H NMR expansion of compound 3 (500 MHz; $CDCl_3$)

Compound 3 was thus identified as 1-oxomicrostegiol established by its molecular formula $C_{20}H_{24}O_3$ (MW 312) and NMR data. It is now reported here for the first time. An isomer of this compound, 3-oxomicrostegiol, was reported from root part of *Taiwania cryptomerioides*, family Taxodiaceae (Chyu et al., 2005). Comparison of NMR spectral data of microstegiol, 1-oxomicrostegiol, and 3-oxomicrostegiol are presented in Table 3.40.

Table 3.40 Comparison NMR data of 1-oxomicrostegiol and related compounds (δ in ppm; *J* in Hz)

	Microstegiol[a]		1-Oxomicrostegiol[a] (compound 3)		3-Oxomicrostegiol[b] (Chyu et al., 2005)	
	δ_C	δ_H	δ_C	δ_H	δ_C	δ_H
1	27.0	2.79	207.2	-	24.7	3.00
		3.59				3.68
2	23.5	1.41	38.2	3.11	40.3	3.00
		1.78		2.30*		2.48
3	42.9	2.35*	37.5	1.42	210.5	-
		1.24*		1.54*		-
4	39.0	-	40.9	-	55.7	-
5	137.4	-	136.9	-	137.9	-
6	130.1	7.05 (d, 7.5)	131.2	7.22 (d, 7.5)	130.8	7.16 (d, 7.6)
7	126.7	6.88 (d, 7.5)	129.6	7.20 (d, 7.5)	127.5	7.00 (d, 7.6)
8	129.0	-	127.6	-	129.1	-
9	139.3	-	138.1	-	138.3	-
10	143.3	-	137.6	-	140.5	-
11	84.4	4.50 (OH, s)	81.5	3.88 (OH, s)	81.9	4.86 (OH, s)
12	206.1	-	203.5	-	203.5	-
13	141.0[¤]	-	141.5	-	141.2	-
14	140.9[¤]	6.95 (s)	139.1	7.07 (s)	141.1	7.04 (d, 1.2)
15	26.8	3.00 (septet, 6)	26.9	2.98 (septet, 7)	27.3	2.98 (septet, 7.2)
16	22.1[§]	1.14 (d, 7)	21.9[¶]	1.16 (d, 7)	21.5	1.17 (d, 7.2)
17	21.1[§]	1.19 (d, 7)	21.5[¶]	1.18 (d, 7)	22.0	1.20 (d, 7.2)
18	21.4	0.79 (s)	17.4	1.05 (s)	21.4	1.00 (s)
19	28.0	0.78 (s)	26.9	0.80 (s)	21.2	0.83 (s)
20	21.4	2.31 (s)	19.9	2.34 (s)	21.2	2.37 (s)

[a] 500 MHz in $CDCl_3$; [b] 400 MHz in $CDCl_3$; * Overlapped signal; [§, ¤, ¶] Interchangeable

3.8.2.7 Compound 4 (viroxocane; 3,4-dihydro-11-hydroxy-10-(1-methylethyl)-2,2,6-trimethyl-naphtha[1,8-bc]oxocin-5(2H)-one)

The MS data of compound 4 (Figure 3.127) showed a molecular mass of 312 and a molecular formula of $C_{20}H_{24}O_3$, and thus this compound is an isomer of compound 3. ^{1}H and ^{13}C NMR are shown in Table 3.41 and NMR spectra are given in Appendix 29.

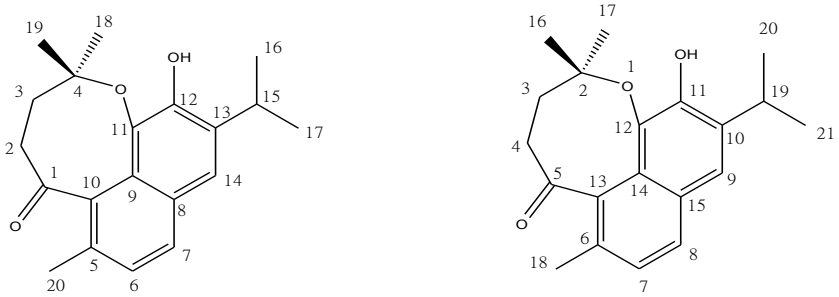

A. Diterpenoid numbering B. IUPAC numbering

Figure 3.127A-B Compound 4 (viroxocane)

Compound 4 showed the same molecular formula as compound 3 (1-oxomicrostegiol) but a difference in the quaternary carbon signals. There was the only one ketone carbon at δ 210.85 ppm, and the signal of the geminal methyl quaternary carbon atom (C-4) around δ 40 ppm was missing whilst a new quaternary signal was observed at δ 84.27 ppm. ^{13}C NMR displayed 20 signals comprised two methylene groups, four methine groups, five methyl groups, and nine quaternary carbon atoms from DEPT-90 and DEPT-135 experiments. The COSY and NOESY correlations of a septet signal at δ 3.34 ppm, and two doublets of methyl groups indicated the presence of an isopropyl side chain. The correlations between three aromatic protons at δ 7.11 ppm, 7.61 ppm, and 7.41 ppm implied two adjacent aromatic rings (Figure 3.128).

Compound 4 also showed a NOESY correlation between an aromatic proton (H-6) at δ 7.11 ppm and a methyl group (H-20) at δ 2.33 ppm (Figure 3.128A). Furthermore, the only ketone carbon at δ 210.85 ppm correlated to a methylene proton at δ 2.60 ppm by HMBC (Figure 3.129). All the above implied a rearranged abietane type which is likely an isomer of 1-oxomicrostegiol. In addition, a ^{1}H peak at δ 5.90 ppm showed no HMQC correlation, and disappeared on D_2O exchange. It was assigned as a hydroxyl substitution group at C-12 (δ 147.38 ppm).

Table 3.41 1D and 2D NMR data of compound 4 (^{1}H 500 MHz; ^{13}C 125 MHz in $CDCl_3$, δ in ppm; *J* in Hz)

Position[a]	^{13}C	^{1}H	COSY	NOESY	HMBC
1	210.85	-	-	-	2.60
2	41.20	α3.02 (ddd, *J* = 14, 10.5, 3.5)	1.60* 2.17 2.60	1.60* 2.60	-
		β2.60 (ddd, *J* = 14, 4, 4)	1.60* 2.17 3.02	1.60* 3.02	
3	35.10	α1.60* (m)	2.17 2.60 3.02	2.13 3.02	1.23 1.60* 1.62 2.60
		β2.17 (ddd, *J* = 14, 10.8, 4)	1.60* 2.60 3.02	1.60* 1.62	
4	84.27	-	-	-	1.23 1.62
5	130.37	-	-	-	2.33 7.61
6	126.27	7.11 (d, *J* = 8)	7.61	2.33 7.61	2.33 7.11 7.41 7.61
7	128.15	7.61 (d, *J* = 8)	7.11	7.11	2.33 7.41
8	126.77[¤]	-	-	-	7.41
9	126.96[¤]	-	-	-	7.41
10	132.20[¶]	-	-	-	2.33 5.90 7.11

Table 3.41 (continued)

Position[a]	^{13}C	^{1}H	COSY	NOESY	HMBC
11	132.08[¶]	-	-	-	2.33 5.90 7.11 7.41
12	147.38	5.90 (OH, s)	-	-	5.90 7.41
13	136.58	-	-	-	1.28 1.33 3.34 5.90
14	121.16	7.41 (s)	-	1.28 1.33 7.61	3.34 7.61
15	27.82	3.34 (septet, *J* = 7)	1.28 1.33	1.28 1.33	1.28 1.33 7.41
16	22.33[§]	1.33 (3H, d, *J* = 7)	-	-	1.28 3.34
17	22.29[§]	1.28 (3H, d, *J* = 7)	-	-	1.33 3.34
18	26.02	α1.23 (3H, s)	1.62	-	1.60* 1.62
19	26.24	β1.62 (3H, s)	1.23 2.17 2.30 3.02	2.17	1.23
20	18.89	2.33 (3H, s)	1.60*	1.60* 7.11	7.11

[a]Diterpenoid numbering; *Overlapped signal, [¤, §, ¶] Interchangeable

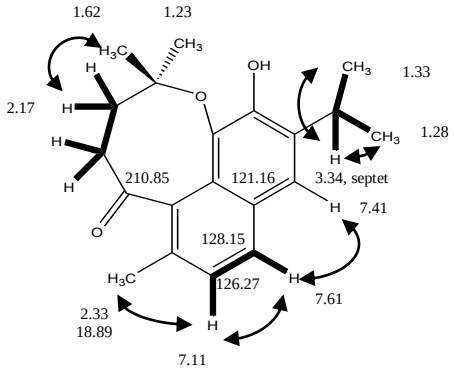

A. H-H COSY (bold line), and NOESY (arrow) correlations

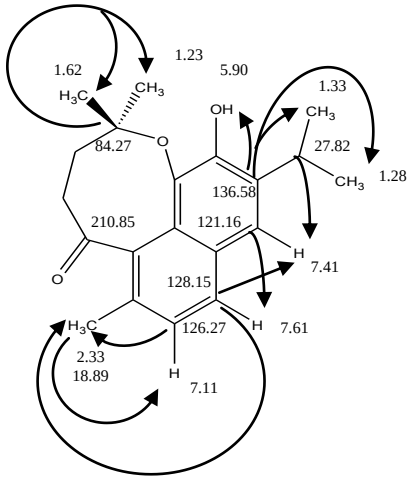

B. HMBC correlations

Figure 3.128 1D and 2D NMR assignments from salient signals of compound 4

Four ^{1}H signals of the two methylene groups indicated four non-equivalent protons. The ddd proton signal at δ 3.02 ppm was coupled to three protons nearby with coupling constant 14 Hz, 10.5 Hz, and 3.5 Hz. Both COSY correlations of these four protons and the coupling patterns indicated the adjacent attachment of two methylene groups (Figure 3.128A). The large coupling constants, 14 Hz, and 10.5 Hz inferred the geminal coupling and an axial-axial coupling constant respectively. In contrast, the geminal proton at δ 2.60 ppm, showed two smaller vicinal coupling constants at 4 Hz, and 4 Hz which implied the equatorial-axial coupling constant as described above from 1-oxomicrostegiol (Figure 3.126). In addition, H-3β at δ 2.17 ppm showed NOESY correlation to methyl protons at δ 1.62 ppm (H-18β). Therefore, the two protons (H-2) at δ 3.02 ppm, and 2.60 ppm were further assigned as H-2α (axial), and H-2β (equatorial) respectively.

The quaternary carbon atom at δ 84.27 ppm was assigned to the C-4 position because it had HMBC correlation to two methyl groups at δ 1.62 ppm, and 1.23 ppm (Figure 3.128B). However, the C-4 chemical shifts of microstegiol and 1-oxomicrostegiol are at δ 39.0 ppm, and 40.9 respectively (Table 3.40). The higher value indicates attachment to an electronegative atom which induces the deshielded effect. Quaternary carbon atoms were assigned by HMBC correlation as shown in Figure 3.129.

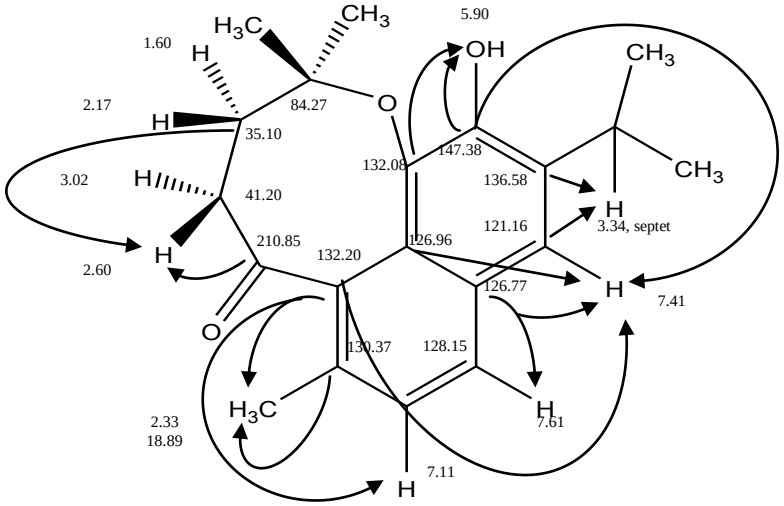

Figure 3.129 Selected HMBC correlations of compound 4

Compound 4 was thus identified as viroxocane established by its molecular formula $C_{20}H_{24}O_3$ (MW 312) and NMR data. It is now reported here for the first time. A derivative of compound 4, rabdosin D, was recently isolated from whole plant part of *Rabdosia iophanthides* (Buch.-Ham. Ex. D. Don) Hara. var. *gerardiana* (Benth.) Hara. in this family (Li et al., 2010). Another one, 10-isopropyl-2,2,6-trimethyl-2,3,4,5- tetrahydronaphtha-[1,8-bc]oxocine-5,11-diol, was reported from the roots and rhizomes of *Nardostachys chinensis* Batalin, family Valerianaceae (Zhang et al., 2005). Comparison of NMR data of compound 4 and its derivatives are shown in Table 3.42.

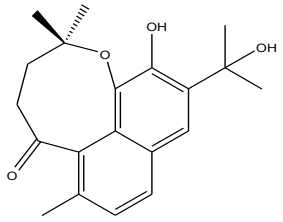

Rabdosin D

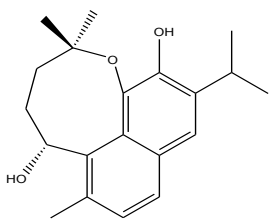

10-isopropyl-2,2,6-trimethyl-2,3,4,5-tetrahydronaphtha[1,8-bc]oxocin-5,11-diol

Figure 3.130 Derivatives of compound 4

Table 3.42 Comparison NMR data of compound 4 and its derivatives (δ in ppm; *J* in Hz)

Position	Compound 4[a]		Rabdosin D[b] (Li et al., 2010)		10-isopropyl-2,2 6-trimethyl-2, 3, 4, 5- tetrahydronaphtha-[1, 8-bc]oxocine-5,11-diol[c] (Zhang et al., 2005)	
	δ_C	δ_H	δ_C	δ_H	δ_C	δ_H
1	210.85	-	210.2	-	69.8	5.46 (dd, 6.6, 1.2)
2	41.20	α3.02 (ddd, 14, 10.5, 3.5)	41.2	3.01 (td, 14.7, 3.6)	30.6	2.03 (m)
		β2.60 (ddd, 14, 4, 4)		2.56 (dt, 15, 4.2)		2.41 (m)
3	35.10	α1.60* (m)	35.4	1.56-1.60 (m)	34.9	1.42 (m)
		β2.17 (ddd, 14, 10.8, 4)		2.07 (td, 14.6, 3.5)		1.60 (m)
4	84.27	-	84.3	-	85.1	-
5	130.37	-	131.2	-	132.8	-
6	126.27	7.11 (d, 8)	126.6	7.03 (d, 8.4)	127.1	7.08 (d, 8.4)
7	128.15	7.61 (d, 8)	128.6	7.50 (d, 8.4)	128.4	7.56 (d, 8.4)
8	126.77[¤]	-	126.1	-	129.0	-
9	126.96[¤]	-	128.2	-	128.1	-
10	132.20[¶]	-	132.3	-	131.6	-
11	132.08[¶]	-	133.4	-	131.6	-
12	147.38	-	147.4	-	148.9	-
13	136.58	-	134.5	-	136.4	-
14	121.16	7.41 (s)	120.8	7.43 (s)	123.2	7.45 (s)
15	27.82	3.34 (septet, 7)	73.6	-	28.1	3.33 (m)
16	22.33[§]	1.33 (d, 7)	29.5	1.73 (s)	22.5	1.31 (d, 6.6)
17	22.29[§]	1.28 (d, 7)	29.3	1.68 (s)	22.5	1.34 (d, 6.6)
18	26.02	α1.23 (s)	25.8	1.24 (s)	26.1	1.21 (s)
19	26.24	β1.62 (s)	26.1	1.61 (s)	25.6	1.72 (s)
20	18.89	2.33 (s)	19.0	2.32 (s)	21.1	2.29 (s)

[a]500 MHz for ^1H, 125 MHz for ^{13}C in $CDCl_3$; [b]400 MHz for ^1H, 100 MHz for ^{13}C in $CDCl_3$

[c]600 MHz for ^1H, 150 MHz for ^{13}C in $CDCl_3$; [*]Overlapped signal; [¤, ¶, §] Interchangeable

3.8.2.8 Compound 5 (viridoquinone; 5-Methyl-20-nor-abieta-1(10),6,8,13-tetraen-11,12-dione)

The MS data of compound 5 (Figure 3.131) showed a molecular mass of 296 and a molecular formula of $C_{20}H_{24}O_2$. ^1H and ^{13}C NMR data are shown in Table 3.43 and NMR spectra are given in Appendix 30.

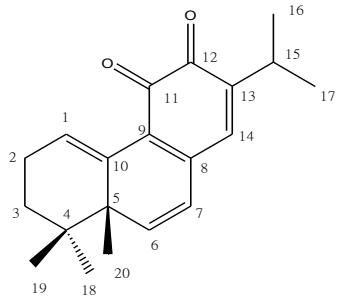

Figure 3.131 Compound 5 (viridoquinone)

^{13}C NMR displayed 20 signals, and DEPT-135 showed two methylene groups, eight quaternary carbon atoms, and 10 signals of methine and methyl groups. There were four ^1H signals that resonated in aromatic and alkene region, δ 5.97 ppm (d), 6.46 ppm (d), 6.58 ppm (s) and 6.72 ppm (t). ^1H NMR also showed the septet methine and a pair of doublet methyl groups which had correlations to each other. The presence of the isopropyl side chain and five methyl groups implied the abietane diterpenoid skeleton.

As double-bond equivalents (DBE) of the formula $C_{20}H_{24}O_2$ are nine, the structure must be an abietane diterpenoid plus 6 double bonds. Two doublet signals, δ 5.97 ppm (H-7) and 6.46 ppm (H-6) were coupled to each other with coupling constant 9.5 Hz. NOESY correlated the signal of δ 5.97 ppm (H-7) to a singlet signal at δ 6.58 ppm (H-14) which indicated adjacent rings (Figure 3.132A). There were also two quaternary carbon signals at δ 180.53 ppm, and δ 180.48 ppm which had a HMBC correlation to ^1H signal δ 6.58 ppm (H-14) as shown in Figure 3.132B. In addition, HMBC also correlated the signal C-14 (δ 137.01 ppm) to the septet signal at δ 2.95 ppm (H-15).

Table 3.43 1D and 2D NMR data of compound 5 (^{1}H 500 MHz; ^{13}C 125 MHz in $CDCl_3$; δ in ppm; *J* in Hz)

Position	^{13}C	^{1}H	COSY	NOESY	HMBC
1	134.35	6.72 (t, *J* = 4.50)	2.30*	2.30*	2.30*
2	23.84	2.30* (m)	1.26* 1.86 2.30*	0.91 1.26* 1.86 6.72	0.91 1.02 1.86 6.72
		2.30* (m)			
3	31.83	β1.86 (ddd, *J* = 14, 10, 5)	1.26* 2.30*	1.02 1.08 1.26* 2.30*	0.91 1.02 2.30*
		α1.26* (m)	1.86 2.30*	2.30*	
4	33.10	-	-	-	0.91 1.02 1.08 1.86 2.30* 6.46
5	43.37	-	-	-	0.91 1.02 1.08 5.97 6.46
6	146.57	6.46 (d, *J* = 9.5)	5.97	0.91 1.02 1.08 5.97	1.08 6.58
7	123.90	5.97 (d, *J* = 9.5)	6.46	6.46 6.58	6.58
8	137.17$^{\psi}$	-	-	-	2.30* 5.97 6.46

Table 3.43 (continued)

Position	^{13}C	^{1}H	COSY	NOESY	HMBC
9	125.41	-	-	-	2.30* 5.97 6.58 6.72
10	132.44	-	-	-	1.08 2.30* 6.46
11	180.53[¤]	-	-	-	6.58
12	180.48[¤]	-	-	-	6.58
13	146.90	-	-	-	1.10 1.12 2.95
14	137.01[Ψ]	6.58 (s)	-	5.97 1.10 1.12	2.95 5.97 6.46
15	27.18	2.95 (septet, *J* = 6)	1.10 1.12	1.10 1.12	1.10 1.12 6.58
16	21.55[§]	1.12 (3H, d, *J* = 7)	2.95	2.95	1.10 2.95
17	21.41[§]	1.10 (3H, d, *J* = 7)	2.95	2.95	1.12 2.95
18	25.74	α0.91 (3H, s)	1.02	6.46	1.02 1.86
19	24.51	β1.02 (3H, s)	0.91	6.46	0.91
20	23.44	β1.08 (3H, s)	-	6.46	2.30* 6.72

*Overlapped signal; [Ψ, ¤, §] Interchangeable

The remaining ^{1}H signal at δ 6.72 ppm showed no correlation to those described signals above. However, it resonated as triplet signal with coupling constant 4.50 Hz which referred to another two protons nearby. COSY, NOESY, and HMBC showed a strong

correlation of this triplet to methylene protons at δ 2.30 ppm (Figure 3.132A) which also showed a HMBC correlation to an adjacent methylene carbon signal at δ 31.83 ppm. The alkene proton at δ 6.72 ppm was accordingly assigned to H-1 and the double bond as Δ1(10). This implied that the C-20 methyl group, normally located at C-10 had been shifted.

Unlike the typical abietane type, a methyl singlet proton at δ 1.08 ppm (H-20) had a NOESY correlation to the alkene proton H-6 (δ 6.46 ppm) while C-20 (δ 23.44 ppm) still had HMBC correlation to methylene protons at δ 2.30 ppm. This observation suggested the rearrange diterpenoid with the substitution of C-20 at C-5 instead of C-10. Figure 3.132 shows salient correlations of this compound.

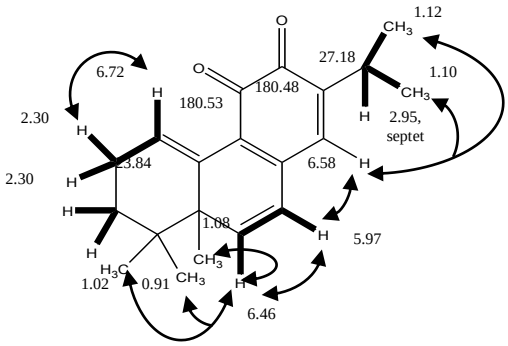

A. H-H COSY (bold line), and NOESY (arrow) correlations

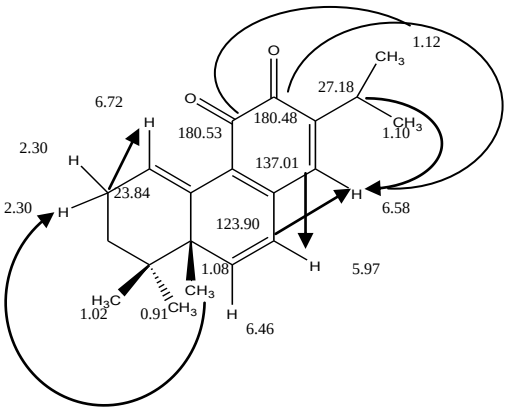

B. HMBC correlations

Figure 3.132 A-B NMR assignments from salient signals of compound 5

A quaternary carbon atom at δ 33.10 ppm (C-4) had HMBC correlations to three methyl signals, and also H-6 and H-7. A deshielded quaternary carbon atom at δ 146.90 ppm was assigned as C-13 due to HMBC correlation to isopropyl side chain, H-14, H-15, and H-16. C-9 at δ 125.41 ppm had a long range HMBC correlation to methelene protons at δ 2.30 ppm (H-2), and also to a singlet proton H-14. Figure 3.133 shows assigned HMBC correlations of compound 5.

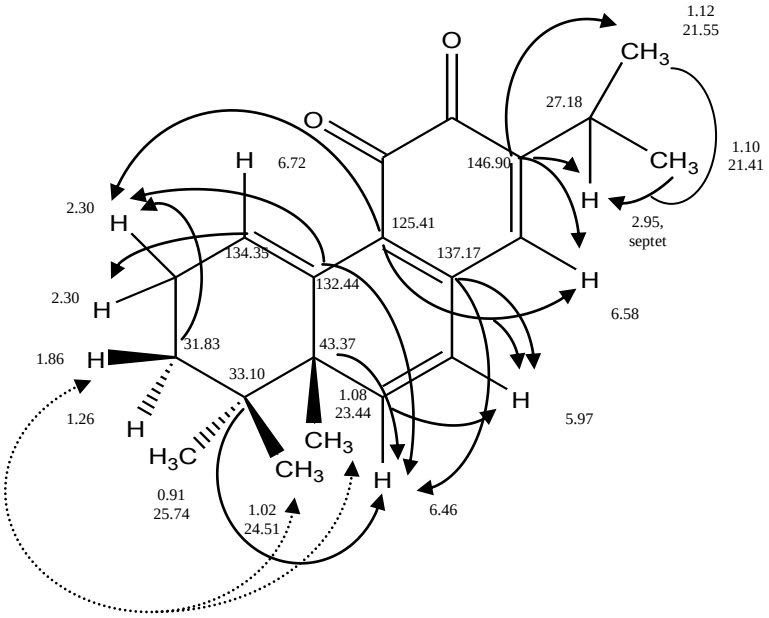

Figure 3.133 Selected HMBC (arrow), and NOESY (dot arrow) correlation of compound 5

Two carbon signals at δ 23.84 ppm, and 31.83 ppm were assigned as C-2, and C-3 respectively from NOESY and HMBC correlations. These two methylene groups comprised four non-equivalent protons. The coupling constants of H-2 were not determined due to the overlapping signals. However, one of H-3, δ 1.86 ppm, showed the coupling pattern as ddd with *J* values 14, 10 and 5 Hz. The large vicinal coupling constant indicated the axial-axial orientation to an adjacent proton. In addition, there were NOESY correlations between H_3-19, H_3-20, and H-3 which implied the β-axial orientation of signal H-3 at δ 1.86 ppm.

Compound 5 was thus identified as viridoquinone established by its molecular formula $C_{20}H_{24}O_2$ (MW 296) and NMR data. It is now reported here for the first time. A related skeleton of compound 5, salviskinone A, was recently reported from roots of *S. przewalskii* Maxim. (Ohsaki et al., 2011). It comprises *p*-quinone and a hydroxyl group as shown in Figure 3.134. NMR data are compared in Table 3.44.

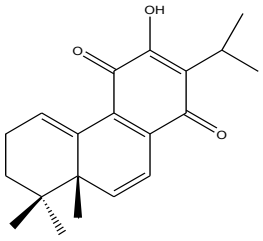

Figure 3.134 Salviskinone A

Table 3.44 Comparison NMR data of compound 5 and salviskinone A (in $CDCL_3$; δ in ppm; *J* in Hz)

Position	Compound 5		Salviskinone A (Ohsaki et al., 2011)	
	δ_C	δ_H	δ_C	δ_H
1	134.35	6.72 (t, *J* = 4.5)	137.1	6.85 (t, *J* = 4.2)
2	23.84	2.30* (m)	24.2	2.33 (m)
		2.30* (m)		2.33 (m)
3	31.83	α1.26* (m)	31.8	α1.27 (m)
		β1.86 (ddd, *J* = 14, 10, 5)		β1.88 (ddd, *J* = 13.8,10.6, 7.4)
4	33.10	-	33.0	-
5	43.37	-	43.5	-
6	146.57	6.46 (d, *J* = 9.5)	144.6	6.46 (dd, *J* = 10, 0.7)
7	123.90	5.97 (d, *J* = 9.5)	117.5	6.66 (br d, *J* = 10)
8	137.17[Ψ]	-	133.4	-
9	125.41	-	126.2	-
10	132.44	-	131.6	-
11	180.53[¤]	-	183.5	-
12	180.48[¤]	-	151.1	-
13	146.90	-	123.3	-
14	137.01[Ψ]	6.58 (s)	185.7	-
15	27.18	2.95 (septet, *J* = 6)	24.2	3.22 (septet, *J* = 7.1)
16	21.55[§]	1.12 (d, *J* = 7)	19.8	1.24 (d, *J* = 7.1)
17	21.41[§]	1.10 (d, *J* = 7)	19.9	1.24 (d, *J* = 7.1)
18	25.74	α0.91 (s)	25.6	α0.90 (br s)
19	24.51	β1.02 (s)	24.5	β1.03 (s)
20	23.44	β1.08 (s)	23.2	β1.08 (s)

*Overlapped signal; [Ψ,¤,§] Interchangeable

3.8.3 Miscellaneous

3.8.3.1 A mixture of 2-(4'-alkoxyphenyl) ethyl alkanoates

GC-CI-MS analysis of this compound was carried out by the EPSRC National Mass Spectrometry Service Centre, School of Medicine, University of Swansea. GC-CI data of this sample gave three main components of molecular mass 460, 488 and 516 which corresponded to molecular formula $C_{30}H_{52}O_3$, $C_{32}H_{56}O_3$ and $C_{34}H_{60}O_3$ respectively (Figure 3.135). ^1H and ^{13}C NMR data are shown in Table 3.45 and NMR spectra are given in Appendix 31.

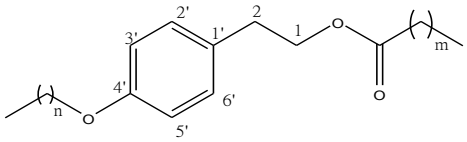

Figure 3.135 2-(4'-alkoxyphenyl) ethyl alkanoate; where m and n are the number of methylene groups of each chain. GC-CI denoted that m+n were 19 for $C_{30}H_{52}O_3$, 21 for $C_{32}H_{56}O_3$ and 23 for $C_{34}H_{60}O_3$.

^1H NMR exhibited five triplet signals, two doublet signals and peaks in alkane region as shown in Figure 3.136. The pair of doublets had COSY and NOESY correlations, and they were coupled to each other with ^3J value 8.5 Hz. ^{13}C NMR and DEPT-135 displayed two signals of methine groups at δ 115.28 ppm and 130.04 ppm which had cross-peaks to those doublets by HMQC at δ 6.75 ppm and 7.07 ppm respectively. The coupling pattern and 2D-NMR correlations implied the *para*-substitution at an aromatic ring. The chemical shifts of these protons were shielded with respect to benzene which implied the presence of a shielding substituent.

^1H NMR displayed four triplets of methylene signals at δ 2.27 ppm, 2.85 ppm, 3.64 ppm and 4.63 ppm. Two of them, δ 2.85 ppm and 4.23 ppm had COSY, NOESY, HMBC correlations, and were coupled to each other with ^3J value 7 Hz. Moreover, the triplet signal at δ 2.85 ppm had a HMBC crossed-peak to the aromatic proton at δ 7.07 ppm while the other at δ 4.23 ppm had a HMBC correlation to the only carbonyl carbon at δ 173.85 ppm. These observations implied the attachment of an ester bond to a side chain C_2H_4 of an aromatic ring. Therefore, two signals at δ 2.85 ppm and 4.23 ppm was assigned H-2 and H-1 respectively.

The carbonyl signal at δ 173.85 ppm (C-α-alkanoate) also had a HMBC correlation to a triplet signal of methylene protons at δ 2.27 ppm. This triplet was correlated to an alkane signal at δ 1.56 ppm by COSY and NOESY correlations which further had COSY and NOESY correlations to another alkane signal at δ 1.25 ppm. These two broad singlets were correlated to a group of carbon signals around δ 29-30 ppm by HMQC which were observed as methylene carbons by DEPT-135 NMR.

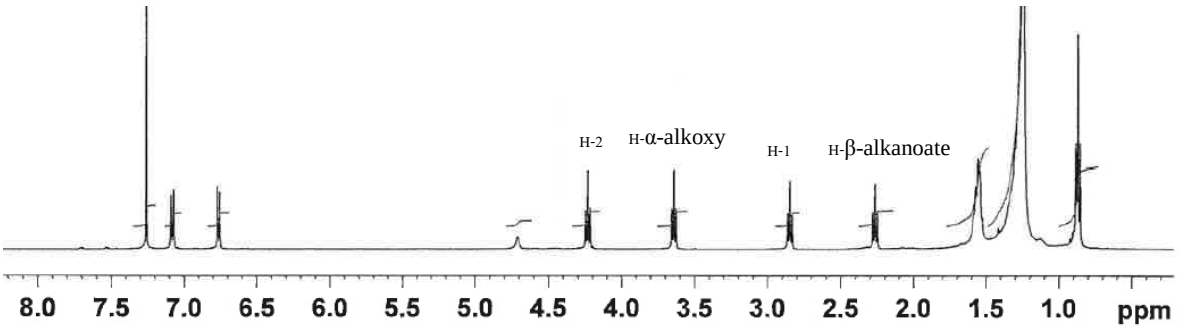

Figure 3.136 ^{1}H NMR of a mixture of 2-(4'-alkoxyphenyl) ethyl alkanoates (500 MHz; $CDCl_3$)

A triplet signal at δ 3.64 ppm showed no correlation to the other triplets but a broad singlet of alkane signals at δ 1.56 ppm. The downfield chemical shift referred an attachment to an electronegative atom and this was considered to be an oxygen atom directly attached to the aromatic ring and responsible for the shielding noted above. The integration of an upfield triplet at δ 0.88 ppm was shown as two methyl groups (6H). These observations suggested two alkane chains, one substituted via an ether link to the aromatic ring and the other as part of an alkanoate acyl moiety.

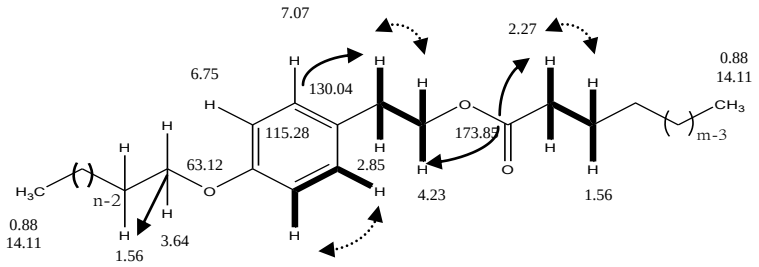

Figure 3.137 Salient correlations of 2-(4'-alkoxyphenyl) ethyl alkanoate
H-H COSY (bold line), NOESY (dot arrow), HMBC (arrow)

A fatty acid ester, 2-(4'-pentoxyphenyl) ethyl stearate, was reported from leaves and stems of *Stemodia foliosa* Benth (Scrophulariaceae) (Silva et al., 2002). In addition, a

phenolic ester, *p*-hydroxyphenylethyl docosanate was also found in the aerial of *Salvia cedronella* Boiss. (Yesilyurt et al., 2008). NMR data of this compound were identical to those published literature.

Table 3.45 1D and 2D NMR data of a mixture of 2-(4'-alkoxyphenyl) ethyl alkanoates (^{1}H, 500 MHz; ^{13}C, 125 MHz; $CDCl_3$; δ in ppm; *J* in Hz)

Position	^{13}C	^{1}H	COSY	NOESY	HMBC
α-alkanoate	173.85	-	-	-	2.27 4.23
β-alkanoate	34.26	2.27 (2H, t, *J* = 7.5)	1.56*	1.56*	-
γ-alkanoate	24.94	1.56* (2H)	1.25* 2.27	1.25* 2.27	1.25* 2.27
-CH_2-of alkanoate	29.45	1.25*	0.88	*	0.88
-CH_3 of alkanoate	14.11	0.88 (3H, t, *J* = 7)	1.25*	-	1.25*
1'	130.04*	-	-	-	2.85 4.23 6.75 7.07
2', 6'	130.04*	7.07 (d, *J* = 8.5)	6.75	6.75	2.85 4.23 6.75 7.07
3', 5'	115.28	6.75 (d, *J* = 8.5)	7.07	7.07	6.75
4'	154.16	-	-	-	6.75 7.07
1	34.34	2.85 (t, *J* = 7)	4.23	4.23	4.23 7.07
2	64.89	4.23 (t, *J* = 7)	2.85	2.85	2.85
α-alkoxy	63.12	3.64 (t, *J* = 6.5)	1.56*	1.56*	1.56*
β-alkoxy	32.80	1.56* (2H)	3.64	1.25*	3.64
-CH_2- of alkoxy	22.68	1.25-1.31*	0.88	*	0.88 1.25*
-CH_3 of alkoxy	14.11	0.88 (3H, t, *J* = 7)	1.25*	-	1.25*

*Overlapped signal

Chapter 4

In vitro testing: the protective effect of caffeic acid derivatives against UVA induced damage in human skin fibroblasts

4.1 Introduction

Solar light is the main source of the radiation which can be subdivided into three ranges of wavelengths; ultraviolet (190-400 nm), visible (400-780 nm), and infrared (780-5000 nm) radiations (Gasparro et al., 1998). More than 90% of the ultraviolet radiation in sunlight that reaches the earth is UVA (wavelength 320-400nm) whilst the rest is UVB (wavelength 290-320 nm) (Svobodova et al., 2003). Because the shorter wavelength radiation up to 310 nm can be absorbed by the ozone layer, UVC (wavelength 190-290 nm) is entirely filtered out (De Gruijl and Van de Leun, 2000). However, both UVA and UVB are potentially harmful to human health, particularly the skin (Svobodova et al., 2003). Human skin is the first barrier that comes into contact with the radiation. Acute responses include sunburn, pigmentation, hyperplasia and immunosuppression while the delayed effects such as skin ageing and cancer may occur due to chronic exposure. Nevertheless, those effects are subject to dose, time and wavelength (Gasparro et al., 1998). The intensity of radiation also varies according to latitude, altitude, season, time of day and surface reflections (Diffey, 2002). During a clear summer's day, 50-60% UV exposure occurs in the 4 hour period around noon (Diffey, 2002). UVB is considered highest during 11.00-15.00 on a daily basis while the UVA intensity is consistent throughout the day compared to UVB (Gasparro et al., 1998).

Biological peroxides, for instance, superoxide anion ($O_2 \cdot^-$) arise from the electron transport system in mitochodria and the enzyme xanthine oxidase (XO) (Trenam et al., 1992) and occur during cellular respiration and cell signaling mechanisms in all cells (Perron and Brumaghim, 2009). Reactive oxygen and nitrogen species can also be generated by skin cells, keratinocytes, fibroblasts, macrophages and melanocytes to carry out certain roles in physiological processes (Korkina and Pastore, 2008). These free radicals are automatically quenched by defense mechanisms with the aid of the natural antioxidants as shown in Figure 4.1.

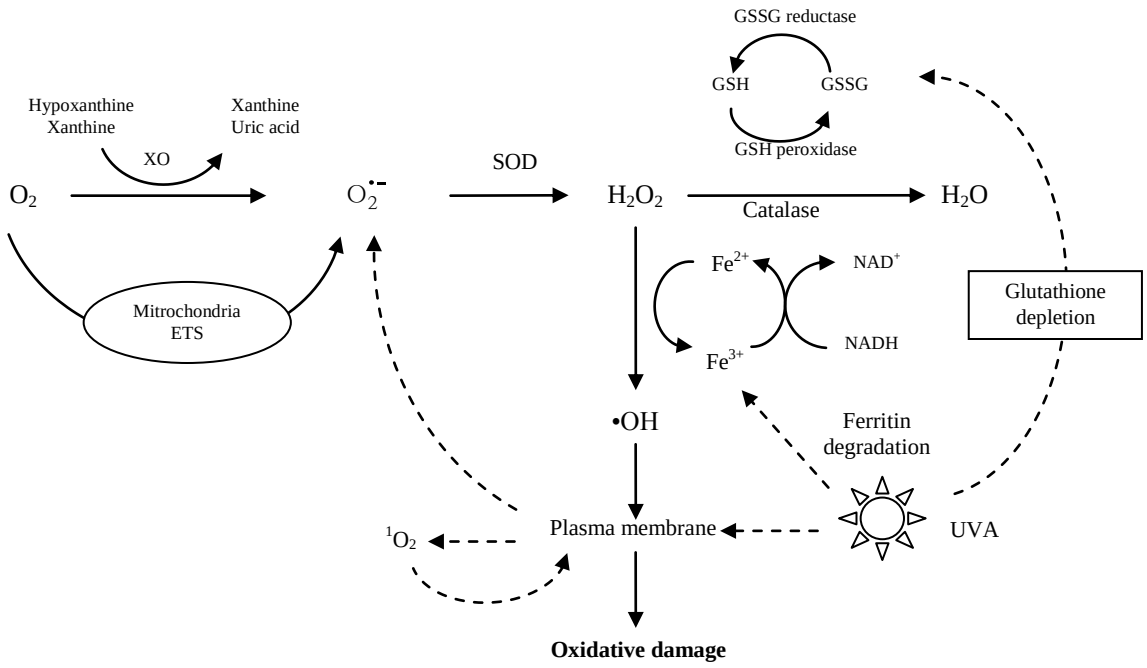

Figure 4.1 Reactive oxygen species (ROS) pathways

Superoxide dismutase (SOD) can convert superoxide anion ($O_2 \cdot^-$) to H_2O_2 which is subsequently degraded by glutathione (GSH) system and enzyme catalase into water (Bickers and Athar, 2006). Superoxide anion and hydrogen peroxide are less reactive compared to the hydroxyl radical (·OH) (Trenam et al., 1992) which can be generated from H_2O_2 by cellular reductants (NADH) involving iron (Perron and Brumaghim, 2009). The highly active hydroxyl radical reacts with lipid in plasma membrane and initiates the lipid peroxidation process (Bickers and Athar, 2006).

After UVA exposure, reactive oxygen species (ROS) such as singlet oxygen ($^1O_2$) are generated and promote biological damage to lipids and proteins in human skin fibroblasts (Vile and Tyrrell, 1995). In addition, the oxidative induction of heme oxygenase-1(HO-1), an anti-inflammatory inducible enzyme in mammalian skin, related to glutathione depletion level and singlet oxygen was observed after UVA irradiation (Tyrrell and Reeve, 2006). The transcriptional activation of HO-1 is considered as a marker of oxidative stress (Pourzand and Tyrrell, 1999). UVA also stimulated the degradation of the iron storage protein ferritin leading to iron release which could further initiate free radicals and induce oxidative damage to skin (Pourzand et al., 1999). The increase of the intracellular labile iron pool from UVA

induced membrane damage could lead to necrotic cell death in both fibroblast and keratinocyte skin cells (Zhong et al., 2004). Excess free iron could also impair the function of cells, tissues, and organs which cause iron-loading diseases such as β-thalassemia (Kalinowski and Richardson, 2005).

In the skin, natural antioxidants are distributed in the epidermal layer with the highest concentration in the deepest stratum corneum. The uppermost layer comprises mostly lipid soluble compounds, for instance, vitamin E, squalene, sterols and ubiquinol while water-soluble molecules such as vitamin C, glutathione and uric acid as well as the antioxidant enzymes, i.e. catalase, glutathione peroxidase, and superoxide dismutase (SOD) are underneath (Korkina and Pastore, 2008). Shindo et al. (1993) reported the reduction of epidermal and dermal catalase and superoxide dismutase activities and reduced levels of α-tocopherol, ubiquinol, ascorbic acid and reduced glutathione after UV irradiation in mice. Exogeneous antioxidants are required for protection if the decrease in endogeneous antioxidant levels allows a significant level of endogeneous reactive oxygen species (ROS), and hydroxyl radical formation (Trenam et al., 1992).

Radical scavenging activity and metal chelating activity of polyphenols have been extensively reported (Moridani et al., 2003; Psotova et al., 2003; Perron and Brumaghim, 2009). Both Fe(II) and Fe(III) can form complexes to deprotonated polyphenol ligands but Fe(III)-ligand complex was found to posses a greater stability over Fe(II) (Perron and Brumaghim, 2009). Figure 4.2 shows the octahedral geometry of the catechol-iron complex with three catechol groups to each ferric ion.

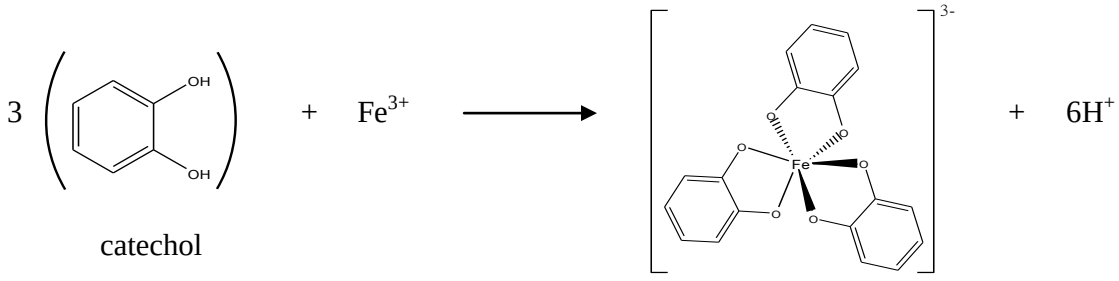

Figure 4.2 Proposed a catechol-iron complex

In this present phytochemical study, certain polyphenolic compounds were isolated from *S. viridis* L. cv. Blue Jeans that included verbascoside, rosmarinic acid, and caffeic acid. Many findings have showed the radical scavenging activity of verbascoside (Gao et al., 1999; Chiou et al., 2004; Obied et al., 2009). It was reported to protect against DNA damage from iron (II) and H_2O_2 by forming an iron-ligand complex (Zhao et al., 2005). Verbascoside protection against UVC induced necrosis was observed in keratinocytes cells (Pastore et al., 2009). Rosmarinic acid has also been reported to possess photoprotective properties on human keratinocytes against UVA (Psotova et al., 2006).

UV exposure affects keratinocytes in the epidermal skin layer as well as fibroblasts in the dermal connective tissue which may contribute to premature skin ageing (Fisher et al, 1997). Human skin has more extensive contact with UVA than with UVB or UVC. UVA can penetrate deeper into the dermal layer unlike UVB which is limited only to the epidermis (Tyrrell and Reeve, 2006). Accordingly, three isolated phenolic compounds of this plant, verbascoside, caffeic acid, and rosmarinic acid, were evaluated for their protective effect against UVA induced cell damage in human skin fibroblasts (FEK4) pretreated with those compounds.

4.2 Materials

4.2.1 Cell cultures

Human primary foreskin fibroblasts (FEK4 cells) were received from Professor Rex M. Tyrrell (University of Bath). Passages 11-16 of the FEK4 were employed in all experiments.

4.2.2 Chemicals

100% Ethanol was purchased from Fisher. Annexin V-FITC Apoptosis detection kit, sterile DMSO, and MTT were supplied from Sigma-Aldrich. Trypsin, Phosphate buffered saline (PBS), Earle's modified minimum essential medium (EMEM), 0.25% sodium bicarbonate, 2 mM L-glutamine and 50 IU/ml penicillin/ streptomycin (P/S) were obtained from Gibco (Germany). Foetal Calf Serum (FCS) was purchased from PAA Laboratories (Austria). Water was purified by Milli Q Plus PF.

4.2.3 Tested compounds

Desferrioxamine mesylate (DFO) was purchased from Ciba-Geigy laboratories (Basel, Switzerland). Rosmarinic acid, caffeic acid, and hemin were commercially supplied from Sigma-Aldrich. Verbascoside was isolated from the aerial part of *S. viridis* L. cv. Blue Jeans as described in Chapter 2. The purity of verbascoside was more than 95% monitored by ^{1}H NMR (400 MHz).

4.3 Experimental

4.3.1 Cell culture preparation procedures

All procedures were carried out under sterile conditions and equipment and fume cupboard were sterilized by spraying with 70% Ethanol. The FEK4 cell line was cultured and incubated in a humidified atmosphere at 37ºC with 5% CO_2. The FEK4 growth medium comprised 15% FCS, 10% EMEM, 2.7% sodium bicarbonate (0.25%), 1% L-glutamine (2 mM), 0.5% P/S (50 IU/ml), and 70.8% water.

4.3.1.1 Seeding FEK4 cells

A flask containing medium and FEK4 cells was placed in the fume cupboard and all the medium removed by aspiration. The cells remained adhered within the flask and were washed with 2 x 5 ml of PBS. 2.5 ml of 0.25% Trypsin solution was then added into the flask, and the flask incubated to allow all cells to detach. After 10 minutes incubation time, the cells were observed under a microscope to ensure that they were completely detached. Immediately, 5 ml of medium was added into the flask and the whole contents transferred to a falcon tube. This was centrifuged at 1200 rpm for 5 minutes. The medium was aspirated out without touching the pellet at the bottom of the tube which was carefully resuspended in 8 ml of medium to seed.

In order to control the quantity of cells on each plate, a haemocytometer was employed to determine cell number before seeding. Fifty µl of the mixture of resuspened cells and 50 µl Trypan Blue dye were added into an eppendorf tube and mixed thoroughly. Fifty µl of that mixture were dropped on to a haemocytometer slide, and observed under a microscope. The volume of cell suspension required for seeding the plate was calculated according to the number of cells counted per ml. The FEK4 were seeded onto the sterile plates as follows: 50000 cells to a 3 cm plate with 2.5 ml medium for cytotoxic, MTT and

neutral red assays and 120,000 cells to a 10 cm plate with 12 ml medium for flow cytometric analysis.

4.3.1.2 Adding compounds

Compounds were added into the medium 48 h after seeding. DFO was dissolved in water as positive control. Rosmarinic acid, caffeic acid and verbascoside were dissolved in DMSO. The final concentration of DMSO in the culture medium was less than 0.1%.

Under sterile conditions, the seeded plates were brought into the fume cupboard and the culture medium collected into a falcon tube. Compounds were added into the collected medium to the appropriate concentration. Two ml of medium with each compound was added back to each plate. All plates were further incubated for 18 h at 37ºC.

4.3.1.3 UVA treatment

All irradiations were performed with a broad-spectrum Sellas 4kW UVA lamp emission range 350-400 nm (Sellas, Germany). The UVA doses were measured using an IL1700 radiometer (International Light, Newbury, MA). Prior to irradiation, the medium from each plate was separately collected into a falcon tube. Then, all plates were washed by 2 ml PBS and 1 ml fresh PBS was added into each plate in order to maintain isotonic conditions during irradiation. Three sets of plates were treated with the same amount of each compound for 3 doses of UVA 0, 250, and 500 kJ/m^2. After irradiation, the PBS was aspirated out, and 2 ml of medium with compound from the falcon tube was added back into each plate. All plates were further incubated for a specific time post UVA treatment, e.g. 4 h and 24 h before performing an assay.

4.3.2 Cytotoxic testing

Three compounds, verbascoside, caffeic acid and rosmarinic acid, were dissolved in DMSO. Six concentrations of each compound, i.e. 12.5 µM, 50 µM, 100 µM, 200 µM, and 500 µM, were added into each plate. All plates were further incubated at 37ºC. % Enzyme activity was observed after 4 h and 18 h without irradiation by the MTT assay. The absorbance of each sample was expressed as a percentage of enzyme activity with respect to the control, and plotted on a graph of activity against concentration. Cytotoxicity of

compounds against FEK4 was reported as IC_{50} determined from the 50% enzyme activity concentration from this dose-response curve.

4.3.3 MTT assay

The MTT assay was performed under dark conditions. MTT was dissolved in PBS (5 mg/ml), and sterilized by being filtered through a 0.2 μm disposable filter unit (Ministart®, Germany). This MTT stock solution was stored at –20ºC. Serum free media (SFM) was prepared in the same way as growth medium except that no FCS was added. MTT solution was freshly prepared by mixing MTT stock solution and SFM (1:9) in a falcon tube to give a final concentration of 0.5 mg/ml. All plates were taken out of the incubator after the specified incubation time post UVA (4 h, 12 h, 18 h, and 24 h). The medium was aspirated out, 3 ml PBS was added to each plate in order to wash the residue and then aspirated out. Cells were further incubated with 0.5 ml MTT solution for 3 hours. After the incubation time, the MTT solution was aspirated out and then 0.5 ml DMSO was added to each plate. All plates were swirled by 3D rocking platform (Stuart Scientific, UK) for 5 minutes. To detect % enzyme activity, 100 μl solution from each plate was added into a 96 well microplate and the absorbance was read by VERSAmaxTM (Molecular devices, California) at 570 nm. DMSO was used as a blank. The absorbance of each sample was expressed as a percentage of enzyme activity with respect to the control without irradiation, and presented in a graph comparing activity against the intensity of UVA dose.

4.3.4 Neutral red assay

Neutral red conditioned medium (NR media) was prepared by mixing 0.5 ml of neutral red solution (0.4% in water) and 39.5 ml fresh medium, and further incubated at 37ºC for 24 h under dark conditions. Prior to using, the solution was centrifuged and filtered through a 0.2 μm disposable filter unit. The plates were taken out of the incubator at a specific incubation time post UVA (4 and 14 h). The medium was aspirated out, 3 ml PBS was added to each plate in order to wash the residue and then aspirated out. Cells were further incubated with 0.5 ml NR medium for 90 minutes at 37ºC. Fixing buffer and Lysis buffer were prepared and stored at room temperature. Fixing buffer is comprised of 10% calcium chloride and 1% formaldehyde (38%) in water. For Lysis buffer, 50 ml absolute ethanol and 19 ml glacial acetic acid were added to water to make 100 ml. After the

incubation time, the NR media was aspirated out, 0.5 ml Fixing buffer was added and left for 1 minute before being aspirated. 0.5 ml Lysis buffer was then added, and swirled by 3D rocking platform (Stuart Scientific, UK) for 10 minutes. To detect % lysosomal integrity, 200 µl solution from each plate was added into a 96 well microplate, and the absorbance was read by VERSAmaxTM (Molecular devices, California) at 560 nm. Lysis buffer was used as a blank. The absorbance of each sample was expressed as a percentage of lysosomal integrity with respect to the control without irradiation, and presented in a graph comparing activity against the intensity of UVA dose.

4.3.5 Flow cytometric analysis

At specific incubation times post UVA (4 h and 24 h), cells were collected and washed with incubation buffer (10 mM Hepes/NaOH, pH 7.4, 5 M NaCl, 100 mM $CaCl_2$). The apoptosis detection protocol was carried out as described in the Annexin V-FITC Apoptosis detection kit (Sigma). 5 x 10^5 Treated cells in 0.5 ml incubation buffer were removed into a 5 ml polystyrene round-bottom tube. 5 µl Annexin V-FITC and 10 µl Propidium iodide solution were added to each tube. The cells with both dyes were left at room temperature for 10 minutes under dark condition prior to analysis by Flow cytometry. Data analysis was performed using FACSDiva software (Becton-Dickinson, Erembodegem, Belgium).

4.3.6 Statistical analysis

Results are given as means of replicated experiments with standard deviation (SD). Statistical analysis was performed using Microsoft Excel 2003. Student's one tailed *t*-test was used to compare between sample data and control in each UVA dose unless stated otherwise. Significant difference from untreated control was reported when the p-value was less than 0.05.

4.4 Results and discussion

Three assays were performed to detect the protective effect of compounds against UVA induced cell damage. The MTT and neutral red assays are techniques for evaluating organelle function whilst flow cytometry is a precise method for analyzing the mechanism of cell death by either apoptosis or necrosis as shown in Figure 4.3.

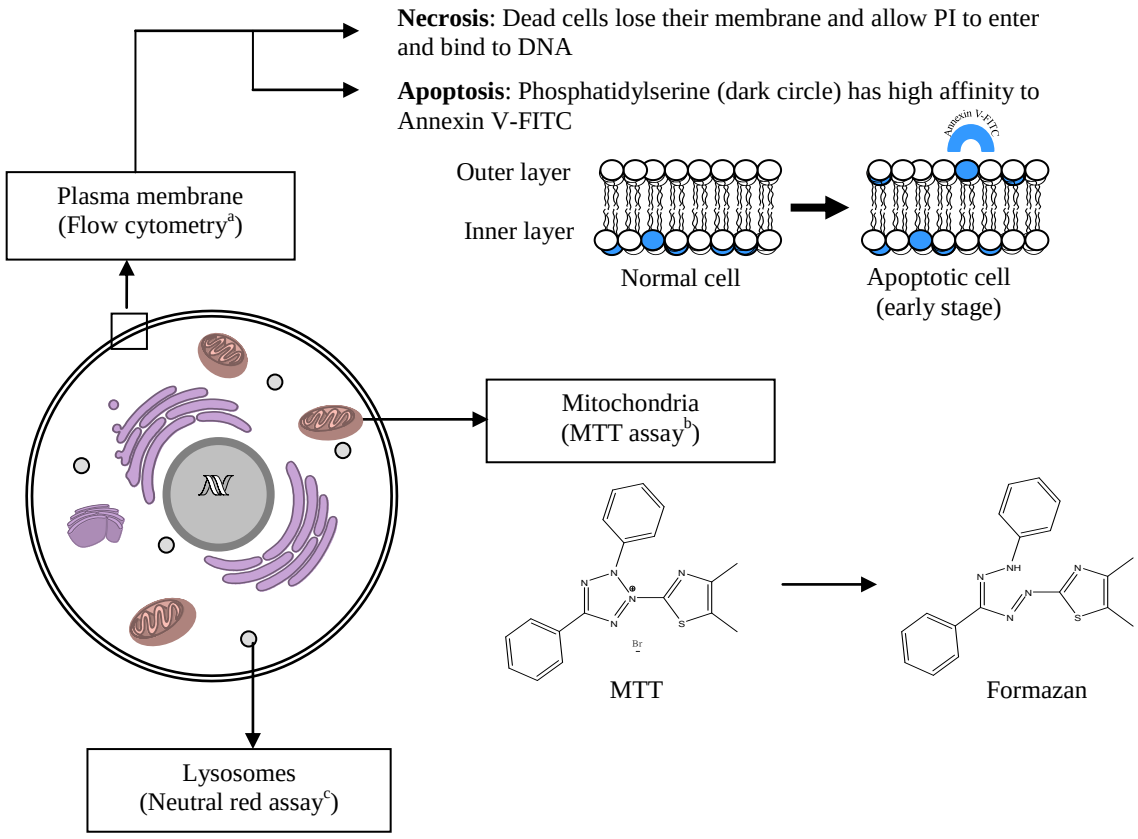

Figure 4.3 Mechanisms of action of each assay

[a]Flow cytometric analysis: Dual stained by Annexin V-FITC and propidium idodide (PI) to evaluate necrosis and apoptosis. PI enters dead cells and binds to DNA (necrosis). Annexin V is a phospholipid binding protein with a high affinity to phosphatidylserine (dark circle) which is translocated from the inner layer to the outer layer of the plasma membrane when cells are in the early stage of apoptosis (Koopman et al., 1994; van Engeland et al., 1998; Fadok et al., 2001).

[b]MTT assay: The tetrazolium salt MTT is converted into a formazan product by mitochondrial dehydrogenase enzyme of living cells (Mosmann, 1983).

[c]Neutral red assay: Neutral red is taken up by living cells and accumulated in the lysosomes (Bulychev et al., 1978).

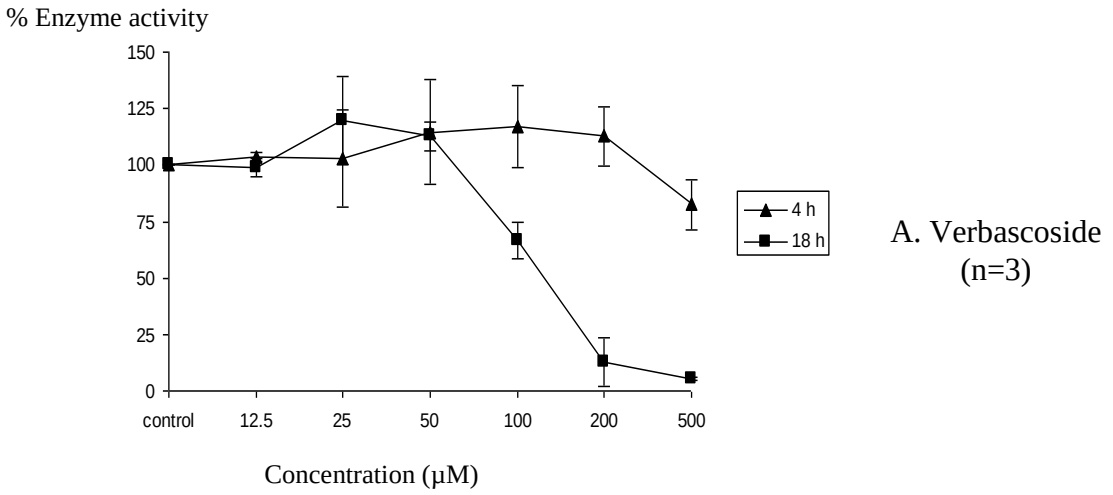

A. Verbascoside (n=3)

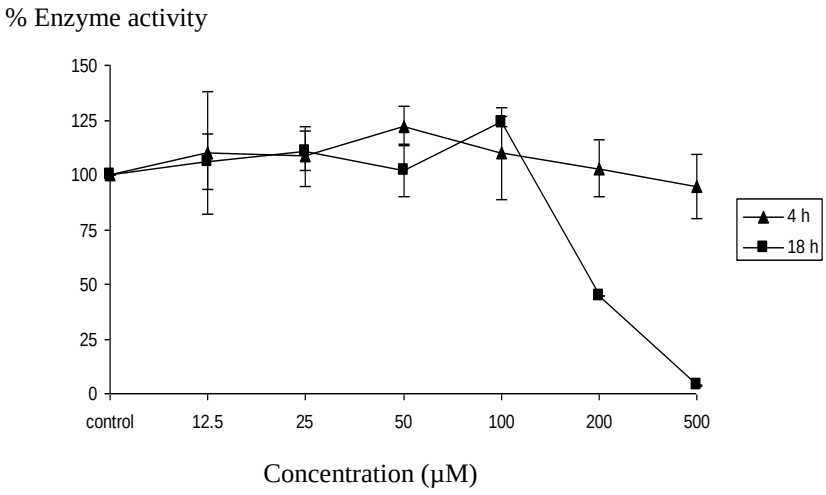

B. Caffeic acid (n=3)

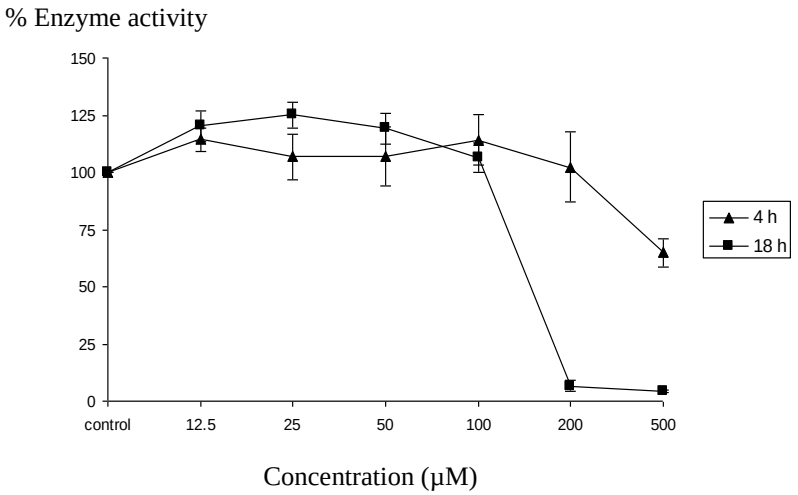

C. Rosmarinic acid (n=3)

Figure 4.4A-C. % Enzyme activity by MTT assay after pretreatment with compounds without irradiation

4.4.1 MTT assay

MTT, (3-(4,5-dimethylthiazol-2-yl)-2,5-diphenyl tetrazolium bromide), has been extensively used in cell proliferation and cytotoxicity assays (Berridge et al., 1996). This colorimetric assay was first performed by Mosmann (1983). The tetrazolium salt MTT is converted into a deep blue formazan product by mitochondrial dehydrogenase enzyme of living cells as shown in Figure 4.3.

Verbascoside, rosmarinic acid, and caffeic acid were tested for their cytotoxicity against FEK4 cells without irradiation by the MTT assay. All these compounds exhibited cytotoxicity at high concentration after 18 h incubation time as shown in Figures 4.4A-C. Results show that all three compounds are cytotoxic with IC_{50} of 125 µM for verbascoside, 150 µM for rosmarinic acid, and 195 µM for caffeic acid. In addition, decreased % enzyme activity was observed at the highest concentration (more than 200 µM) after 4 h incubation time in all tested compounds.

Two doses of UVA irradiation, 250 and 500 kJ/m^2, were used to compare the oxidative damage to human skin fibroblasts. The amount of UVA at 250 kJ/m^2 is equivalent to 70 minutes exposure to sunlight at noon during a cloudless summer day at northern latitude of 35º (Frederick and Lubin, 1988) which was considered as a physiological dose of UVA radiation (Vile and Tyrrell, 1995). After UVA irradiation, percentages of enzyme activity were decreased especially at 500 kJ/m^2 as shown in Figures 4.5-4.6. In respect of time after irradiation 4 h and 24 h, UVA at 500 kJ/m^2 killed normal cells 51.8±7.7 % at 4 h after irradiation and 78.8±8.6 % at 24 h after irradiation. Verbascoside (50 µM) pretreatment showed significant protection 24 h post UVA with 41.3±9 % enzyme activity as opposed to the control activity of 21.2±8.6 % (Figure 4.6). Caffeic acid and rosmarinic acid failed to protect the cells from UVA induced damage against UVA 500 kJ/m^2.

Since UVA induces ferritin (Ft) degradation and increases the labile iron pool (LIP) in the cytosol (Pourzand et al., 1999), DFO, which is known to be a strong iron chelator, was used as a positive control. DFO (100 µM) pretreatment for 18 h has been reported to achieve a significant reduction of Ft iron of FEK4 cells whereas hemin pretreatment (20 µM) caused iron overload and remarkably increased the intracellular level of Ft molecules (Zhong et al., 2004).

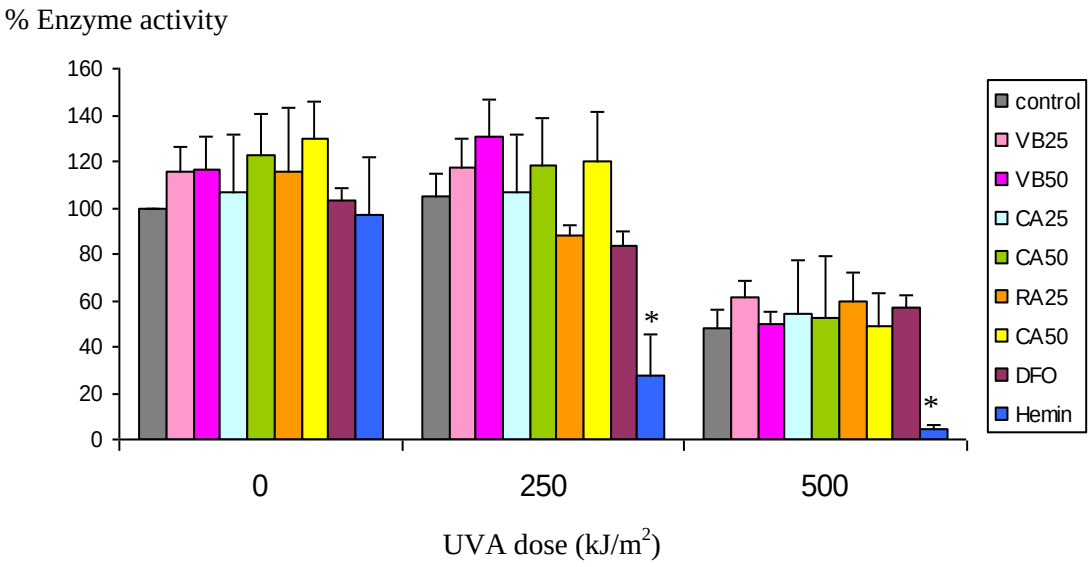

Figure 4.5 Effect of pretreatment with compounds on percentage of enzyme activity by MTT assay (n = 4) 4 hr post UVA exposure. *Significantly different from untreated control ($p<0.05$), two tailed. VB: verbascoside 25, 50 µM, CA: caffeic acid 25, 50 µM, RA: rosmarinic acid 25, 50 µM, DFO: desferrioxamine 100 µM and hemin 20 µM.

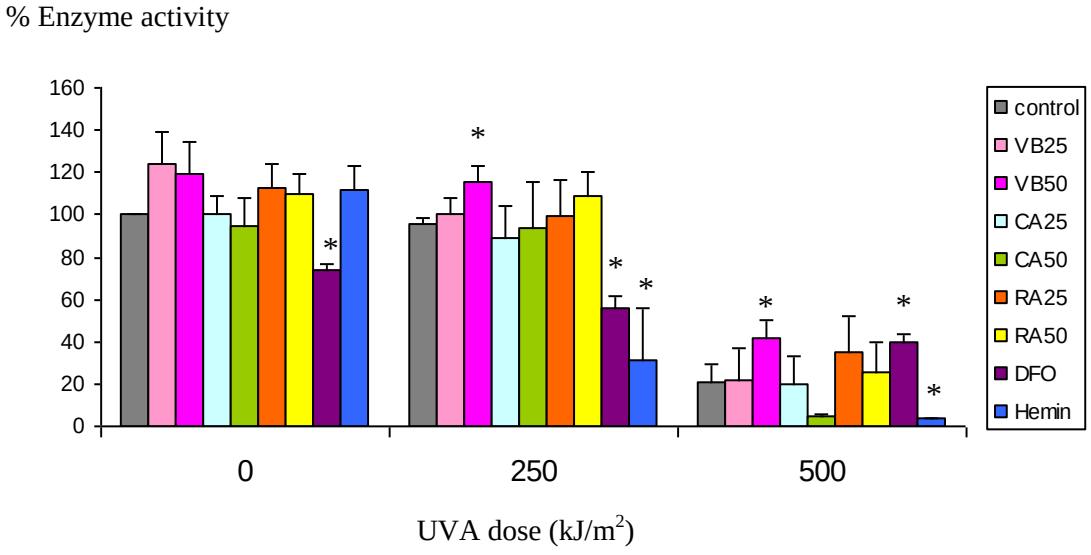

Figure 4.6 Effect of pretreatment with compounds on percentage of enzyme activity by MTT assay (n = 4) 24 hr post UVA exposure. *Significantly different from untreated control ($p<0.05$), two tailed. VB: verbascoside 25, 50 µM, CA: caffeic acid 25, 50 µM, RA: rosmarinic acid 25, 50 µM, DFO: desferrioxamine 100 µM and hemin 20 µM.

Figures 4.5-4.6 shows the corresponding protective effect of DFO. Without irradiation, percentage of enzyme activity decreased 26.2±2.8 % in DFO pretreated cells in comparison with control (100%). This result suggests that DFO depletes iron in the cell culture system and causes a reduction of enzyme activity in the normal state without irradiation. In contrast, DFO significantly protected the cell with % enzyme activity 39.7±3.5 at UVA 500 kJ/m^2 while control was at 21.2±8.6 % (Figure 4.6). This result suggests that DFO chelates a certain amount of the increased iron in the system as a result of irradiation, and shows a protective effect. On the other hand, hemin greatly showed a negative effect with less than 5% enzyme activity in any time post UVA at 500 kJ/m^2.

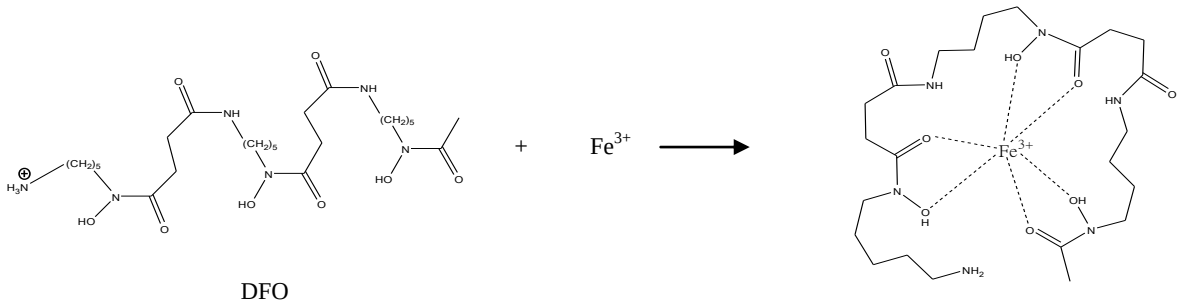

Figure 4.7 The DFO-iron complex. A strong metal chelator, desferrioxamine (DFO), binds to iron (III) in the ratio 1:1 complex which decreased the production of ROS and the oxidative stress in iron-overloaded cells (Kalinowski and Richardson, 2005).

In comparison with DFO (100 µM), a lower dose of verbascoside (50 µM) gave a similar positive result at high UVA intensity. Although the precise protective mechanism of verbascoside is still in question, the pattern of activity is somewhat consistent with iron chelation. Without irradiation, a high concentration kills cells by iron depletion (Figure 4.4A), but at lower concentrations it prevents the build up of free iron in the irradiated cells, and concomitant generation of ROS (Figure 4.6).

As can be seen in Figures 4.5-4.6 at UVA dose 250 kJ/m^2, only DFO and hemin affected cell survival. These results suggest that fibroblasts can tolerate moderate levels of UVA. In fact, Zhong et al. (2004) reported that the LIP increased 2 fold immediately after UVA irradiation at 250 kJ/m^2 but this high level gradually returned to control value within 6 h post irradiation in a fibroblast model. Therefore, injured cells could well have recovered their normal state by the time the MTT assay was carried out. However, under the iron

overload condition produced by the addition of hemin, irradiation damage seems to be irreversible as 30% enzyme activity was recorded both 4 h and 24 h post treatment with UVA at 250 kJ/m^2 (Figures 4.5-4.6).

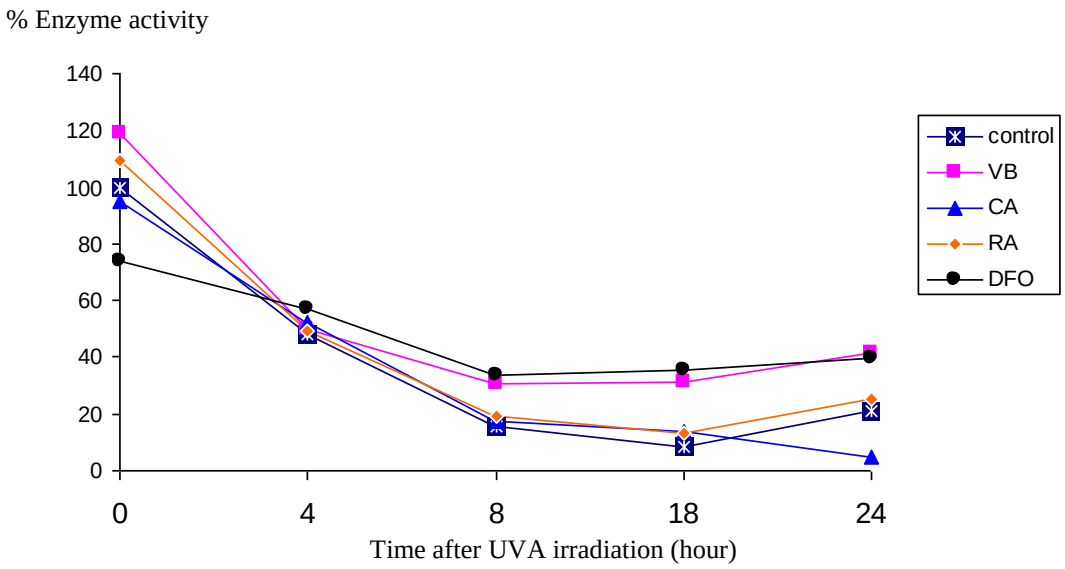

Figure 4.8 Time course of percentage enzyme activity by MTT assay (n = 4) post UVA exposure at dose of 500 kJ/m^2 after pretreatment with compounds. VB: verbascoside 50 µM, CA: caffeic acid 50 µM, RA: rosmarinic acid 50 µM, DFO: desferrioxamine 100 µM.

Figure 4.8 shows the reduction of % enzyme activity in time course experiments after irradiation at dose of 500 kJ/m^2. Caffeic acid and rosmarinic acid exhibited insignificant differences from untreated control while verbascoside and DFO showed a similar positive effect. % enzyme activity was dramatically decreased to steady state at 8 h post UVA.

The radical scavenging activity of verbascoside in vitro against DPPH (Gao et al., 1999; Chiou et al. 2004; Galvez et al., 2005; Ono et al., 2008), superoxide anion radical (Gao et al., 1999; Lee et al., 2004; Obied et al., 2009; Georgiev et al., 2011) and H_2O_2 (Obied et al., 2009) has been extensively reported. This included the inhibition of hydroxyl radical (·OH) mediated damage to pBR322 plasmid DNA via the Fenton reaction (Zhao et al., 2005), and damage to endothelial cell culture induced by Fenton's reagent (H_2O_2/Fe^{2+}) (Chiou et al., 2004). Verbascoside can form complexes with Fe(II) or Fe(III) (Zhao et al., 2005). As UVA generates both free radicals, and free labile iron (Figure 4.1), verbascoside may prevent the

increase of both deleterious factors that induce damage in cells. A lower concentration of verbascoside exhibited the same significant protection as DFO which is an iron chelator only.

4.4.2 NR assay

Neutral red (NR) is a weakly basic dye that has affinity to lysosomes of living cells (Bulychev et al., 1978). When lysosomes suffer membrane damage they are unable to retain the dyes (Basu-Modak et al., 2003). It is believed that UVA induced oxidative damage to lysosome membranes leading to ferritin (Ft) degradation and an increase in labile iron is an important contribution to cell damage by UVA (Pourzand et al., 1999). The neutral red assay was performed to evaluate any protection of lysosomes against such damage.

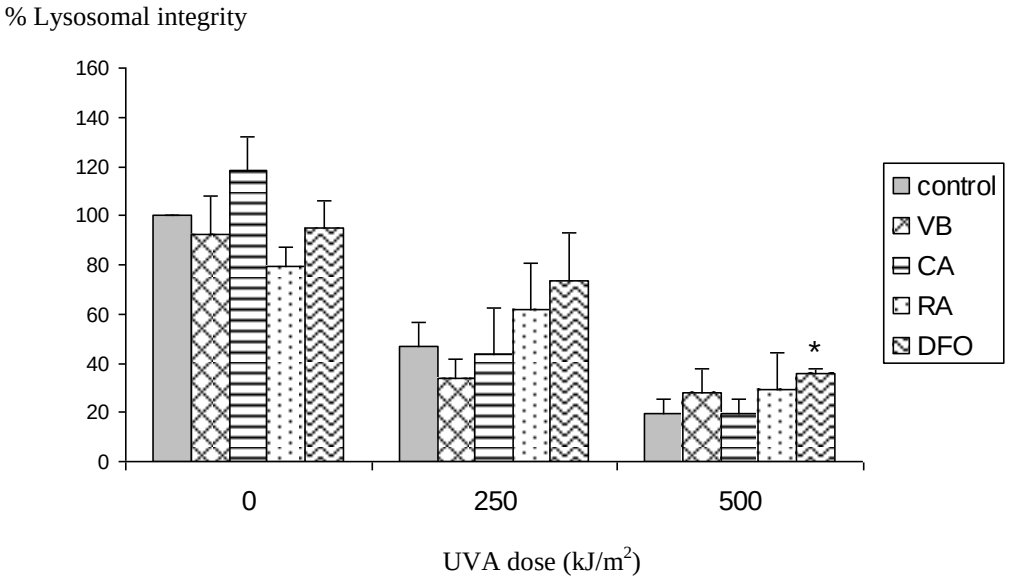

Figure 4.9 Effect of pretreatment with compounds on lysosomal integrity of cells measured 4 h post UVA by NR assay (n = 3). VB: verbascoside 50 µM, CA: caffeic acid 50 µM, RA: rosmarinic acid 50 µM, DFO: desferrioxamine 100 µM. *Significant difference from untreated control ($p<0.05$).

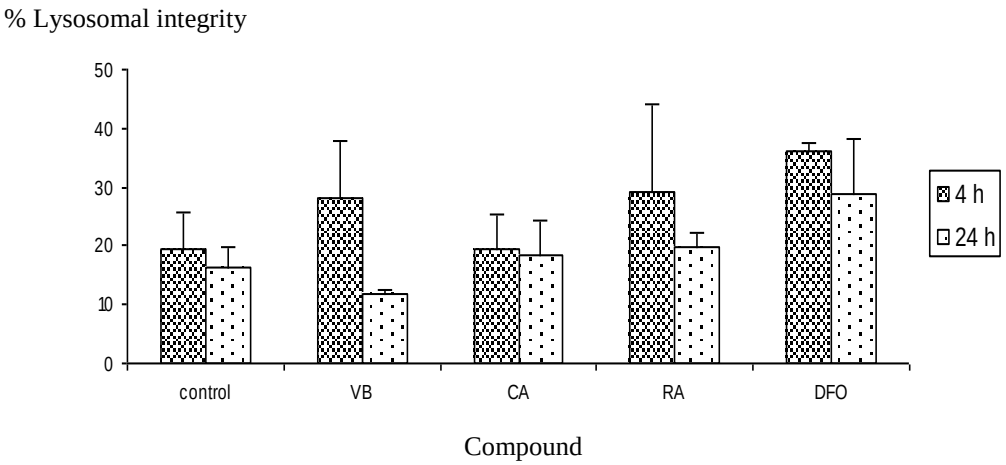

Figure 4.10 Effect of pretreatment with compounds on lysosomal integrity of cells measured at 4 h and 24 h post UVA at 500 kJ/m^2 by NR assay (n = 3). VB: verbascoside 50 µM, CA: caffeic acid 50 µM, RA: rosmarinic acid 50 µM, DFO: desferrioxamine 100 µM.

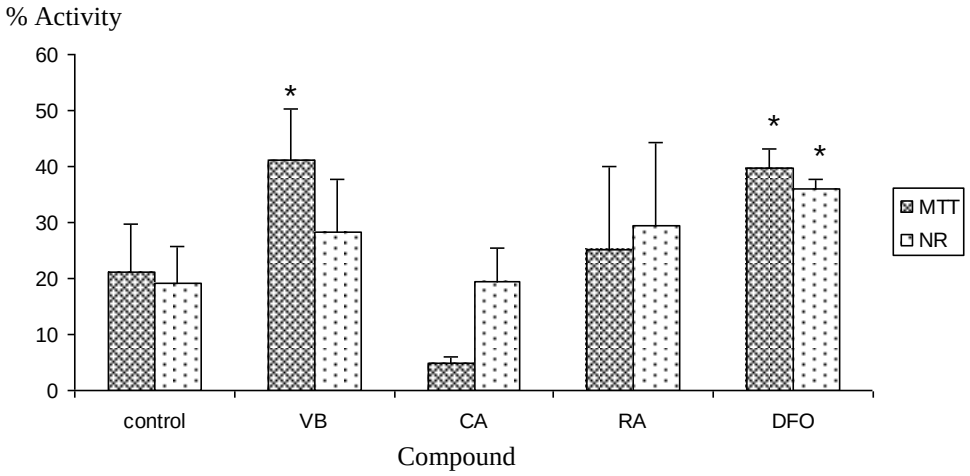

Figure 4.11 Comparison of MTT assay with NR assay to measure the effect of pretreatment with compounds on the residual activity of cells after UVA irradiation at 500 kJ/m^2. MTT assay was perform 24 h post UVA (n = 4), and NR assay was performed 4 h post UVA (n = 3). VB: verbascoside 50 µM, CA: caffeic acid 50 µM, RA: rosmarinic acid 50 µM, DFO: desferrioxamine 100 µM. *Significantly difference from untreated control ($p < 0.05$).

Figure 4.9 shows percentage of lysosomal integrity assessed by NR assay after irradiation 4 h. In comparison with the MTT assay, NR assay showed more cell damage from UVA irradiation at a dose of 250 kJ/m^2. Of the compounds used to treat the cells prior to UVA exposure, only DFO showed a significant though small level of protection. At the same UVA dose 500 kJ/m^2, the untreated control damage was 80.7±6.4 % determined by NR assay 4 h post UVA while MTT assay was 78.8±8.6 % assessed 24 h post UVA (Figure 4.11). However, the rate of survival at 24 h post UVA was steadily decreased to 15% in control cells as shown in Figure 4.10.

Verbascoside exhibited non-significant protection after 4 h post UVA (Figure 4.9) though it clearly showed less lysosomal protective effect after a longer incubation time post UVA (Figure 4.10). In comparison with untreated control, rosmarinic acid exhibited superior lysosomal protection among tested polyphenols though was not statistically significant at the number of replicates performed. On the contrary in MTT assay, verbascoside showed significant protection against mitochondrial damage induced by high UVA intensity. Figure 4.11 compares the effects of the tested compounds in the two test systems. DFO shows significant protection in both assays; verbascoside only in the MTT assay. As can be seen, lysosomes were fairly sensitive to UVA induced damage in respect of time post UVA.

4.4.3 Flow cytometric analysis

Flow cytometry is a method to analyze an individual cell by monitoring the interaction of the cell and the laser beam based on light-scattering, fluorescence and absorbance techniques (Rieseberg et al., 2001). A cell in the fluid stream flows through the focus of the laser beam and scatters the laser light. Analyzing the scattered light gives information about cell size and structure which can be changed during cell death (Darzynkiewicz et al., 1997). Morphological changes observed in cell death involve swelling, blebbing, budding, permeability alteration and shrinkage (Majno and Joris, 1995). Changes in plasma membrane properties can provide information about apoptosis, necrosis and live cells with the aid by certain dyes (Van Engeland et al., 1998).

Apoptosis, programmed cell death, is a general mechanism for removal of unwanted cells (Koopman et al., 1994). It is characterized by the shrinkage of cell with intact plasma membrane in the early stage followed by malfunctioning of the plasma membrane in the late

stage (Darzynkiewicz et al., 1997). On the other hand, necrosis (accidental cell death) is characterized by cell and mitochondrial swelling followed by the rupture of the plasma membrane (Darzynkiewicz et al., 1997). Necrosis can occur in the late stage of apoptosis (Majno and Joris, 1995).

Fadok et al. (2001) reported the role of phospholipid asymmetry for triggering recognition and removal by phagocytosis in the early stage of apoptosis. Phosphatidylserine (PS) translocates from the inner layer to the outer layer of the plasma membrane when cells are undergoing apoptosis. PS expression on the outer membrane has a high affinity with anticoagulant annexin V which can be applied to detect apoptosis by flow cytometry (Koopman et al., 1994). Annexin V labeled with fluorescein isothiocyanate (FITC) and certain dyes such as propidium iodide (PI), and ethidium bromide (EB) are used as a dual stain to differentiate between dead and apoptotic cells. Annexin V-FITC is not able to bind to the phospholipids of the plasma membrane of normal vital cells while necrotic and dead cells lose their cell membrane and take up the DNA-specific stain (PI) (Van Engeland et al., 1998).

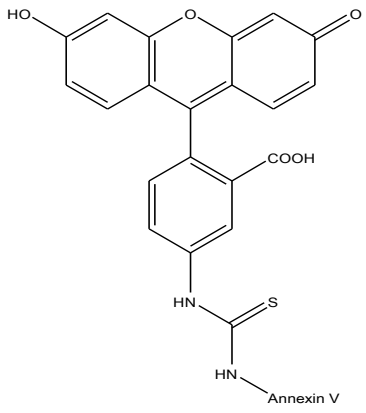

Annexin V-FITC

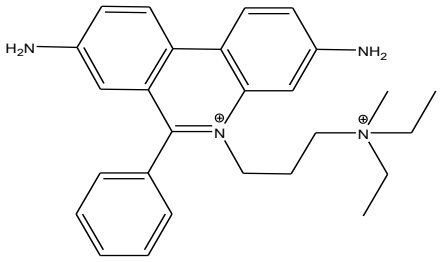

Propidium iodide (PI)

Figure 4.12 Fluorescence dyes in flow cytometric analysis. FITC (fluorescein isothiocyanate) covalently bound to primary amine of annexin V (Ormerod, 1994; Gerke and Moss, 2002). Excitation/Emission wavelengths (nm) are 495/519 for FITC and 536/617 for PI (Rieseberg et al., 2001).

The annexin V-FITC/PI apoptotic assay can quantify three kinds of cell population from a dot plot graph as demonstrated in Figure 4.13. Living cells are negative for both annexin V-FITC (AV) and PI (Q3) while the apoptotic cells are negative to PI but positive to AV (Q4). Necrotic/dead cells are positive to PI (Q1+Q2).

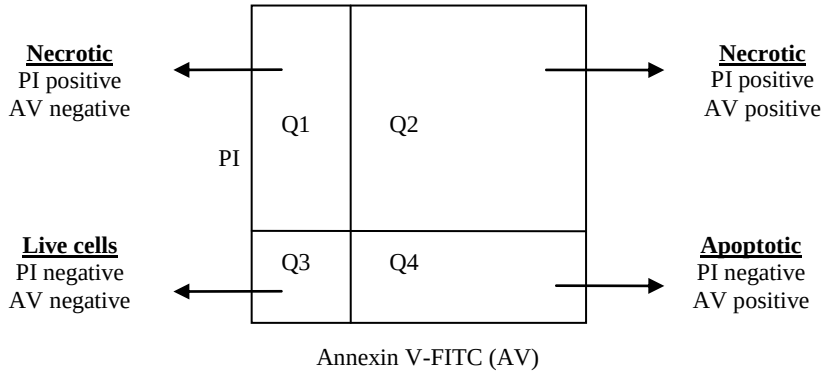

Figure 4.13 Dot plot analysis of AV/PI apoptotic assay from flow cytometry

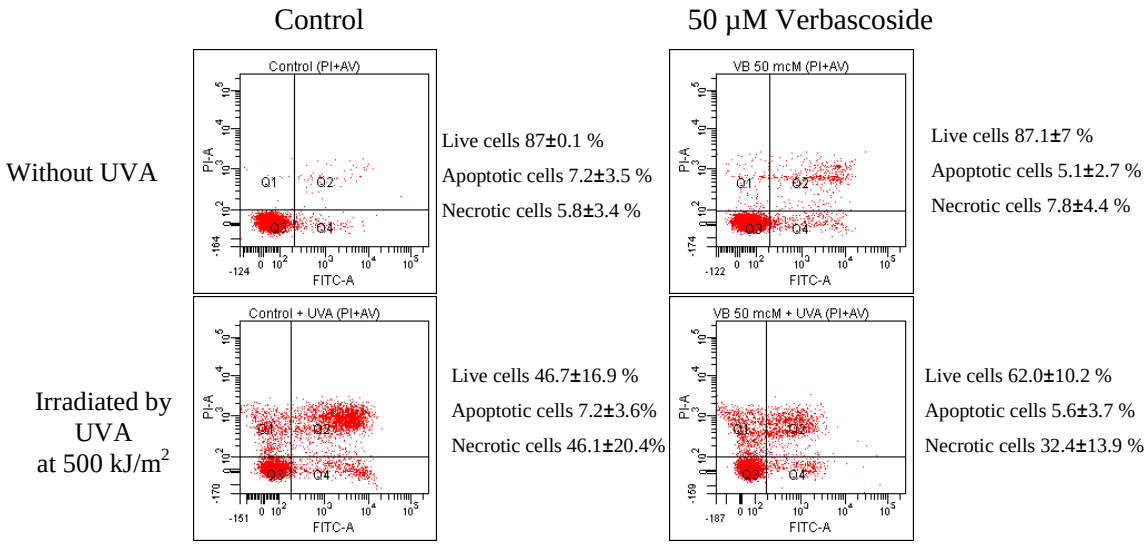

Figure 4.14 Flow cytometric analysis of control (left), and 50 µM verbascoside pretreated cells (right). Analysis was performed 24 h post UVA. Cells were irradiated by UVA at 500 kJ/m^2, and dual stained with AV and PI immediately before measurement. % Cells populations were expressed as means±SD (n = 3). Live cells (Q3), apoptotic cells (Q4), and necrotic cells (Q1+Q2). Cells without UVA (upper), Cells irradiated by UVA (lower).

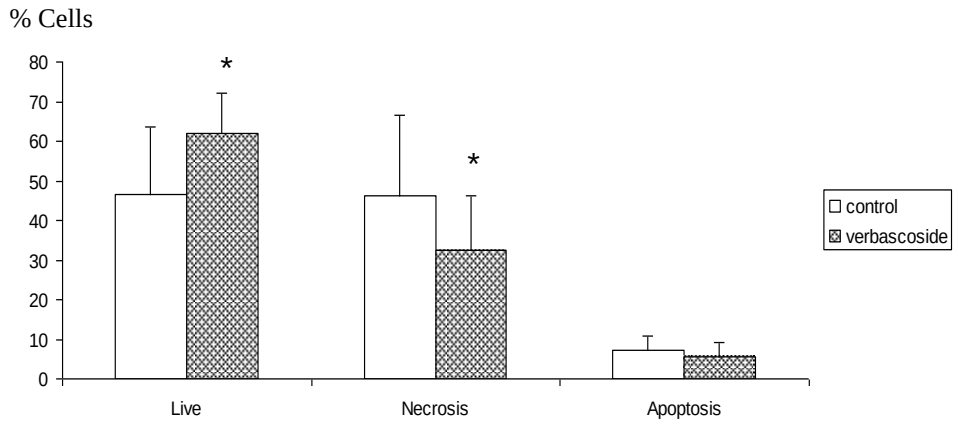

Figure 4.15 The percentages of live, necrotic, and apoptotic cells population. Flow cytometric analysis of control and 50 µM verbascoside pretreated cells. Analysis was performed 24 h post UVA. Cells were irradiated by UVA at 500 kJ/m^2, and dual stained with AV and PI immediately before measurement (n = 3). *Significantly difference from untreated control ($p<0.05$).

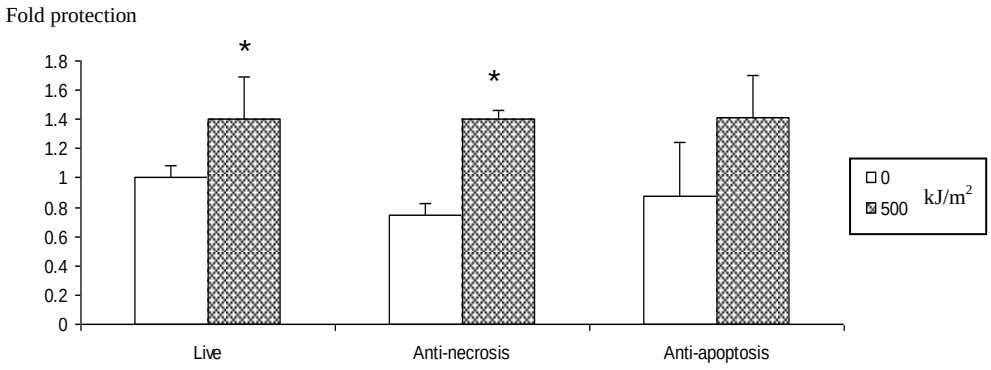

Figure 4.16 Fold protection of 50 µM verbascoside over control without UVA and irradiated by UVA at 500 kJ/m^2. Flow cytometric analysis was perform 24 h post UVA (n = 3).
* Significantly different between irradiated and non-irradiated cells ($p<0.05$).

Results of flow cytometric analysis are shown in Figures 4.14-4.15. Verbascoside pretreatment provided significant protective effect over control in terms of higher % live cells, and lower % necrotic cells. Figure 4.16 displays 1.4 fold protection accompanied by 1.4 fold anti-necrosis. Both treated- and untreated cells exhibited comparable apoptotic effect not

only without UVA irradiation but also after being irradiated as seen in Figure 4.15. % Apoptotic cells were unchanged after irradiation (Figure 4.14). This result corresponds to previous observations by the C. Pourzand and R. M. Tyrrell group (unpublished data). A higher dose of UVA failed to induce morphological changes associated with apoptosis in a human foreskin fibroblast cell line (FEK4). The resistance of skin fibroblasts to UVA mediated apoptosis was exhaustively reviewed by Pourzand and Tyrrell (1999). This could possibly be due to the increased expression of Fas receptor in adult fibroblasts, a higher level of SOD activity, the higher antioxidant capacity of the FEK4 cell and the induction of the nuclear factor kappa B (NF-κB) in this cell line.

The protective effects of verbascoside against UVC-induced and free radical mediated necrosis in a HaCaT cell model has recently been reported (Pastore et al., 2009). It inhibited cytokine-induced release of proinflammatory mediators, IP-10 and IL-8, and suppressed NF-κB and AP-1 DNA binding activity in a dose dependent manner. Therefore, the anti-necrotic effect against UVA may partly involve anti-inflammatory activity. Although short wavelength UV radiation (UVB/UVC) activated AP-1 and NF-κB and stabilized p53 transcription factor (Tyrrell, 1999), ROS may act as intracellular second messengers through the activation of certain inflammatory mediators such as nuclear factor kappa B and induce an inflammatory response (Trenam et al., 1992). However, the effective concentration of verbascoside against UVC was 200 µM which was considered a high concentration in our study. Our cytotoxicity testing showed an IC_{50} 125 µM for verbascoside in the human skin fibroblast model (FEK4). 50 µM Verbascoside was an optimum concentration for protection against UVA induced necrosis.

4.5 In vitro testing conclusions

This study showed the protective effect of verbascoside against UVA induced damage in a human skin fibroblast (FEK4) model. Two assays were introduced to detect cell function but with different sites of action. The MTT assay depends on mitochondrial enzymes of living cells while NR assay is focused at the lysosome compartment. Moreover, the precise mechanism of cell death was also analyzed by the sensitive technique of flow cytometry. Among three tested polyphenols, a major compound from *S. viridis* L. cv. Blue Jeans, verbascoside, exhibited significant protection against UVA induced mitochondrial damage and necrosis at a high intensity UVA dose (500 kJ/m^2). It exhibited 1.4 fold

protective effect against UVA induced necrosis. 50 μM Verbascoside showed the same protective effect as 100 μM DFO at UVA 500 kJ/m^2 by MTT assay. Although the precise mechanism of this action has not yet been determined, the pattern of activity is consistent with a metal chelating, radical scavenging, and anti-inflammatory activities.

Chapter 5
Conclusions

As described in Chapter 2, dried plant part of *S. viridis* L. cv. Blue Jeans, aerial and root, was extracted by two steps of solvents, acetone and methanol, collected separately, and evaporated to dryness. Both acetone and methanol crude extracts were further partitioned by three steps with petroleum ether, ethyl acetate and 1-butanol in order to classify compound corresponding to the solvent use. Eight crude fractions for each of the aerial and root parts were finally obtained from this process and certain fractions were further separated by either semi-preparative reversed-phase HPLC or open column chromatography. Three crude fractions from the aerial parts, AE (Acetone-Ethyl acetate), ME (Methanol-Ethyl acetate), and MB (Methanol-1-Butanol) were subject to further separation while four root crude fractions, RAE (Acetone-Ethyl acetate), RAP (Acetone-Petroleum ether), RME (Methanol-Ethyl acetate), and RMB (Methanol-1-Butanol), were successfully separated.

These separations yielded thirty compounds from both aerial and root parts which can be classified into three broad biosynthetic groups, terpenoids, polyphenolics, and miscellaneous. Two novel triterpenoids, lup-20(29)-ene-2α-acetate-3β-ol (compound 1) and lup-20(29)-ene-2α-ol-3β-acetate (compound 2), were isolated from the aerial parts as well as three known triterpenoids, ursolic acid, oleanolic acid and lup-20(29)-ene-2α,3β-diol. β-Sitosterol and its glucoside were also found in aerial part. Phenolic compounds comprised seven caffeic acid derivatives, five flavonoids, and a phenylethyl glycoside (salidroside) as shown in Figure 5.1. A new flavone glycoside, luteolin-7-*O*-α-rhamnopyranosyl-(1→6)-β-galactopyranoside, is reported for the first time. The major phenylpropanoid in aerial parts, verbascoside (acteoside), is also new to the genus *Salvia* as well as its methylated derivatives, leucosceptoside A and martynoside.

Three new diterpenoids, 1-oxomicrostegiol (compound 3), viroxocane (compound 4), and viridoquinone (compound 5), were found in the root part together with five known diterpenoids, ferruginol, salvinolonyl 12-methyl ether, 7α-acetoxy-14-hydroxy-8,13-abieta-diene-11,12-dione, 7α,14-dihydroxy-8,13-abietadiene-11,12-dione and microstegiol. Two caffeic acid derivatives, 1-docosyl ferulate, and 2",3"-di-*O*-acetyl-martynoside, and a mixture

of 2-(4'-alkoxyphenyl)ethyl alkanoates were isolated from the roots. Isolated compounds from roots are presented in Figure 5.2.

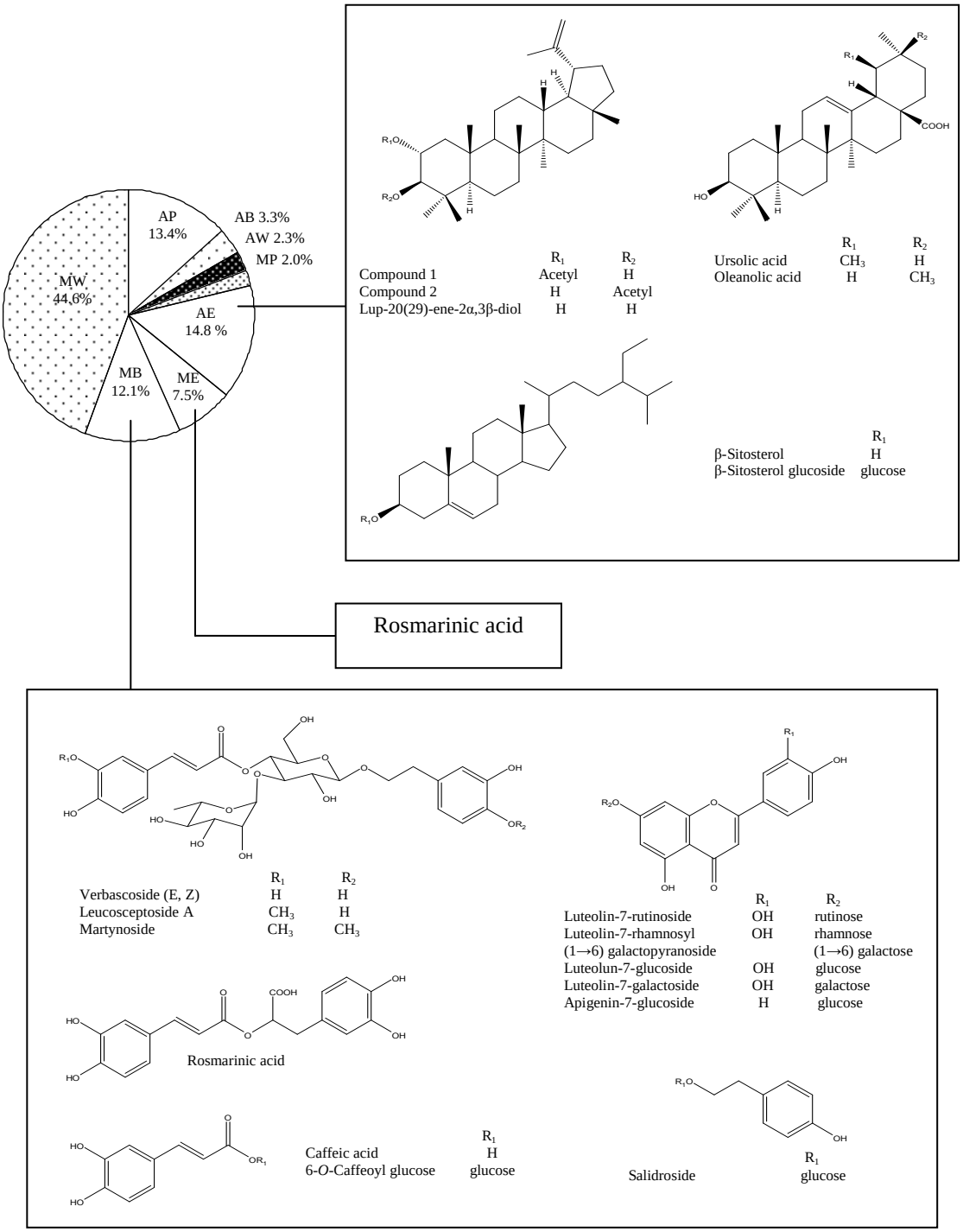

Figure 5.1 Isolated compounds from aerial part of *S. viridis* L. cv. Blue Jeans

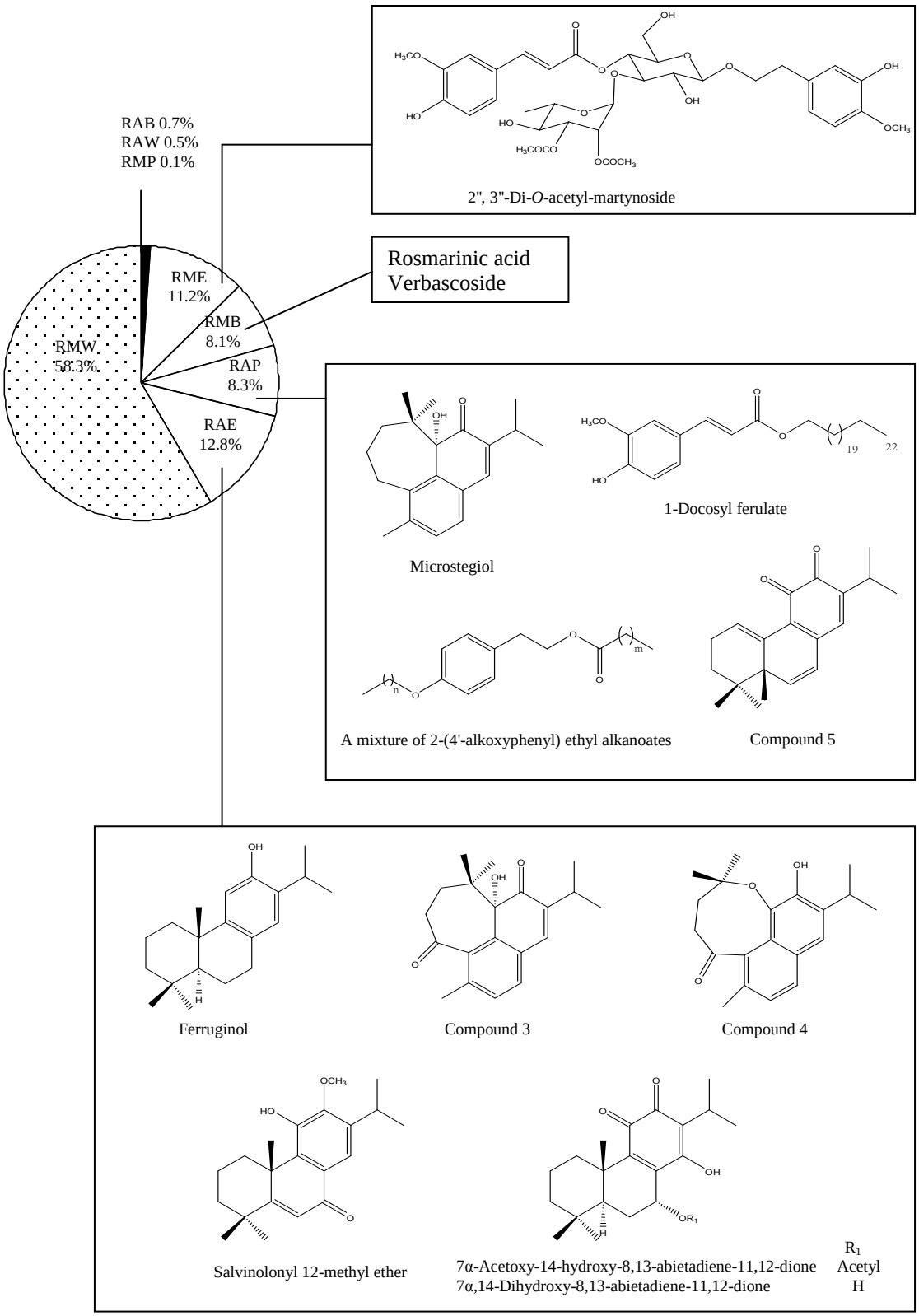

Figure 5.2 Isolated compounds from the root part of *S. viridis* L. cv. Blue Jeans

TLC-bioautographic techniques were used to screen certain activity of the eight crude fractions on a TLC plate. Antioxidant activity was based on scavenging DPPH (2, 2-Diphenyl-1-picrylhydrazyl) radical. Compounds with antiradical scavenging activity were seen a yellow band on a purple background. The strongest DPPH scavenging activity was seen in the AB (Acetone-1-Butanol) and MB (Methanol-1-Butanol) crude fractions.

Verbascoside was found as the main component in the aerial part (104 mg/ 2 g MB crude fraction; 0.06% in dried aerial). Radical scavenging activity against DPPH (Gao et al., 1999; Galvez et al., 2005), superoxide anion radical (Gao et al., 1999; Lee et al., 2004; Obied et al., 2009; Georgiev et al., 2011), H_2O_2 (Obied et al., 2009), and hydroxyl radical (·OH) (Zhao et al., 2005) have been reported. Verbascoside can also form complexes with Fe(II) or Fe(III) (Zhao et al., 2005). After UVA exposure, free radicals are generated, and could cause various biological damage such as DNA impairment leading to cancer (Svobodova et al., 2003). UVA also stimulated ferritin degradation, and leading to iron release which could further initiate free radicals and skin disorders such as psoriasis (Pourzand et al., 1999). Therefore, the protective effect of verbascoside against UVA induced damage in a human skin fibroblast model was subsequently evaluated. Other antioxidant compounds isolated from this species, rosmarinic acid and caffeic acid, were also tested to compare the protection activity.

Results showed that pretreatment with verbascoside does protect cells against UVA induced damage in a human skin fibroblast (FEK4) model. Two assays were introduced to detect cell function with different sites of action. The MTT assay depends on mitochondrial enzyme of living cells while NR assay is focused at the lysosome compartment. The precise mechanism of cell death was also analyzed by flow cytometry. Among three tested polyphenols, verbascoside exhibited the significant protection against UVA induced mitochondrial damage and necrosis at a high intensity dose of UVA (500 kJ/m^2). It exhibited 1.4 fold protective effect against UVA induced necrosis. 50 µM Verbascoside showed the same protective effect as 100 µM DFO at UVA 500 kJ/m^2 measured by MTT assay. Rosmarinic acid also showed a non-significant protective effect at high intensity UVA dose (500 kJ/m^2) while caffeic acid exhibited weak activity. Verbascoside was recently reported to posses protective effects against UVC-induced and free radical mediated necrosis in a HaCaT cell model (Pastore et al., 2009). This is the first report of verbascoside in this plant and its significant protective effect against UVA induced damage in a human skin fibroblast model.

These promising results could lead to the expansion of research and development in pharmaceutical and cosmetic areas related to dermatology. Although quite widely distributed amongst plant species, commercial verbascoside costs €115/5 mg (Extrasynthese, France, Product catalogue 2011, p 246). As a cultivated plant with a significant content of verbascoside, *S. viridis* L. could be a suitable commercial source if required.

A TLC-bioautographic technique for antibacterial activity against three Gram-positive, *Staphylococcus aureus* (ATCC 6571), *Enterococcus faecalis* (ATCC 775), *Bacillus cereus* (ATCC 2599), and three Gram-negative bacteria, *Klebsiella pneumoniae* (ATCC 9633), *Proteus vulgaris* (ATCC 4636), and *Escherichia coli* (ATCC 86), was also used to monitor the crude fractions. Aerial AE crude fraction displayed clear zones against all three Gram-positive bacteria on the agar overlay TLC plates (Figures 3.10-3.12, plate B, track 2). Further isolation of this crude fraction revealed a new antibacterial compound (lup-20(29)-ene-2α-acetate-3β-ol, compound 1) with MIC 50 µM against *Enterococcus faecalis* (ATCC 775), and 100 µM against *Staphylococcus aureus* (ATCC 6571) and *Bacillus cereus* (ATCC 2599). A new isomer, lup-20(29)-ene-2α-ol-3β-acetate (compound 2), was also active against all three Gram-positive with MIC 100 µM (Table 3.4). Two known triterpenoids, ursolic acid and oleanolic acid, also showed markedly antibacterial activity against the Gram-positive species with MIC 12.5-50 µM. Though MB crude fraction showed no clear zone, the main component, verbascoside, showed antibacterial activity against three Gram-positive with MIC 100 µM. In addition, none of crude fractions showed antibacterial activity against Gram-negative bacteria by the TLC-agar overlay assay.

Eight diterpenoids were isolated from the root crude fractions, RAE and RAP. Both these fractions showed a clear zone against three Gram-positive bacteria on the agar overlaid TLC plates (Figures 3.10-3.12, plate A, tracks 1-2). On further determination of MIC, 7α,14-dihydroxy-8,13-abietadiene-11,12-dione exhibited antibacterial against *Enterococcus faecalis* (ATCC 775) with MIC 50 µM (Table 3.4). Ferruginol also showed appreciable activity against those three Gram-positive bacteria with MIC 25-50 µM. Microstegiol was active against *Staphylococcus aureus* (ATCC 6571) with MIC 50 µM. The others were active against all three Gram-positive bacteria with MIC 100-200 µM.

References

Abe, F., Nagao, T. and Okabe, H., 2002. Antiproliferative constituents in plants 9. aerial parts of *Lippia dulcis* and *Lippia canescens*. *Biol. Pharm. Bull.*, 25, 920-922.

Abreu, M. E., Muller, M., Alegre, L. and Bosch, S. M., 2008. Phenolic diterpene and α-tocopherol contents in leaf extracts of 60 *Salvia* species. *J. Sci. Food Agric.*, 88, 2648-2653.

Ahmad, Z., Fatima, I., Mehmood, S., Ifzal, R., Malik, A. and Afza, N., 2008. New epoxydammarane triterpenes from *Salvia santolinifolia*. *Helv. Chim. Acta*, 91, 73-78.

Ahmad, Z., Mehmood, S., Ifzal, R., Malik, A., Afza, N., Ashraf, M. and Jahan, E., 2007. A new ursane-type triterpenoid from *Salvia santolinifolia*. *Turk. J. Chem.*, 31, 495-501

Akihisa, T., Ogihara, J., Kato, J., Yasukawa, K., Ukiya, M., Yamanouchi, S., and Oishi, K., 2001. Inhibitory effects of triterpenoids and sterols on human immunodeficiency virus-1 reverse transcriptase. *Lipids*, 36, 507-512.

Ali, H., Houghton, P. J. and Soumyanath, A., 2006. α-Amylase inhibitory activity of some Malaysian plants used to treat diabetes; with particular reference to *Phyllanthus amarus*. *J. Ethnopharmacol.*, 107, 449-455.

Alim, A., Goze, I., Goze, H. M., Tepe, B. and Serkedjieva, J., 2009. In vitro antimicrobial and antiviral activities of the essential oil and various extracts of *Salvia cedronella* Boiss. *J. Med. Plant. Res.*, 3, 413-419.

Alvarenga, S. A. V., Gastmans, J. P., Rodrigues, G. D. V., Moreno, P. R. H., Emerenciano, V. D. P., 2001. A computer-assisted approach for chemotaxonomic studies-diterpenes in Lamiaceae. *Phytochemistry*, 56, 583-595.

Andary, C., Wylde, R., Laffite, C., Privat, G. and Winternitz, F., 1982. Structures of verbascoside and orobanchoside, caffeic acid sugar esters from *Orobanche rapum-genistae*. *Phytochemistry*, 21, 1123-1127.

Armaka, M., Papanikolaou, E., Sivropoulou, A. and Arsenakisndary, M., 1999. Antiviral properties of isoborneol, a potent inhibitor of herpes simplex virus type 1. *Antiviral Res.*, 43, 79-92.

Astani, A., Reichling, J. and Schnitzler, P., 2010. Comparative study on the antiviral activity of selected monoterpenes derived from essential oils. *Phytother. Res.*, 24, 673-679.

Avila, J. G., De Liverant, J. G., Martinez, A., Martinez, G., Munoz, J. L., Arciniegas, A. and De Vivar, A. R., 1999. Mode of action of *Buddleja cordata* verbascoside against *Staphylococcus aureus*. *J. Ethnopharmacol.*, 66, 75-78.

Avonto, C., Taglialatela-Scafati, O., Pollastro, F., Minassi, A., Di Marzo, V., De Petrocellis, L. and Appendino, G., 2011. Michael acceptors; An NMR spectroscopic method to identify and classify thiol-trapping agents: revival of Michael acceptors for drug discovery? *Angew. Chem. Int. Ed.*, 50, 467-471.

Baker, S., Griffiths, C. and Nicklin, J., 2011. *BIOS instant notes: Microbiology* fourth ed. Garland Science, Taylor & Francis Group, LLC, USA and UK, pp 8-60.

Bakkali, F., Averbeck, S., Averbeck, D. and Idaomar, M., 2008. Biological effects of essential oils-a review. *Food Chem. Toxicol.*, 46, 446-475.

Balde, A. M., Claeys, M., Pieters, L. A., Wray, V. and Vllietinck, A. J., 1991. Ferulic acid esters from stem bark of *Pavetta owariensis*. *Phytochemistry*, 30, 1024-1026.

Baltina, L. A., Flekhter, O. B., Nigmatullina, L. R., Boreko, E. I., Pavlova, N. I., Nikolaeva, S. N., Savinova, O. V. and Tolstikov, G. A., 2003. Lupane triterpenes and derivatives with antiviral activity. *Bioorg. Med. Chem. Lett.*, 13, 3549-3552.

Bamuamba, K., Gammon, D. W., Meyers, P., Dijoux-Franca, M. G. and Scott, G., 2008. Anti-mycobacterial activity of five plant species used as traditional medicines in the Western Cape province (South Africa). *J. Ethnopharmacol.*, 117, 385-390.

Baricevic, D., Sosa, S., Loggia, R.D., Tubaro, A., Simonovska, B., Krasna, A. and Zupancic, A., 2001. Topical anti-inflammatory activity of *Salvia officinalis* L. leaves: the relevance of ursolic acid. *J. Ethnopharmacol.*, 75, 125-132.

Barnes, J., Anderson, L. A. and Phillipson, J. D., 2007. *Herbal Medicines* third ed. The Pharmaceutical Press, London, UK, pp 512-514.

Bartram, S., Jux, A., Gleixner, G. and Boland, W., 2006. Dynamic pathway allocation in early terpenoid biosynthesis of stress-induced lima bean leaves. *Phytochemistry*, 67, 1661-1672.

Baser, K. H. C., 2002. Aromatic biodiversity among the flowering plant taxa of Turkey. *Pure Appl. Chem.*, 74, 527-545.

Basu-Modak, S., Gordon, M. J., Dobson, L. H., Spencer, J. P. E., Rice-Evans, C. and Tyrrell, R. M., 2003. Epicatechin and its methylated metabolite attenuate UVA-induced oxidative damage to human skin fibroblasts. *Free Radic. Biol. Med.*, 35, 910-921.

Bayoumi, S. A. L., Rowan, M. G., Blagbrough, I. S. and Beeching, J. R., 2008. Biosynthesis of scopoletin and scopolin in cassava roots during post-harvest physiological deterioration: the E-Z-isomerisation stage. *Phytochemistry*, 69, 2928-2936.

Berridge, M. V., Tan, A. S., McCoy, K. D. and Wang, R., 1996. The biochemical and cellular basis of cell proliferation assays that use tetrazolium salts. *Biochemica*, 4, 14-19.

Bickers, D. R. and Athar, M., 2006. Oxidative stress in the pathogenesis of skin disease. *J. Invest. Dermatol.*, 126, 2565-2575.

Bozin, B., Dukic, N. M., Samojlik, I. and Jovin, E., 2007. Antimicrobial and antioxidant properties of rosemary and sage (*Rosmarinus officinalis* L. and *Salvia officinalis* L., Lamiaceae) essential oils. *J. Agric. Food Chem.*, 55, 7879-7885.

Bradford, P. G. and Awad, A. B., 2007. Phytosterols as anticancer compounds. *Mol. Nutr. Food Res.*, 51, 161-170.

Brand-Williams, W., Cuvelier, M. E. and Berset, C., 1995. Use of a free radical method to evaluate antioxidant activity. *LWT-Food Sci. Technol.*, 28, 25-30.

British Pharmacopoeia, 2008. Sage leaf and sage oil, in *British Pharmacopoeia* 2008 Volumn II. The Stationary Office, London, pp. 1913-1915.

Brusselmans, K., Vrolix, R., Verhoeven, G. and Swinnen, J. V., 2005. Induction of cancer cell apoptosis by flavonoids is associated with their ability to inhibit fatty acid synthase activity. *J. Biol. Chem.*, 280, 5636-5645.

Budzianowski, J. and Skrzypczak, L., 1995. Phenylpropanoid esters from *Lamium album* flowers. *Phytochemistry*, 38, 997-1001.

Bulychev, A., Trouet, A. and Tulkens, P., 1978. Uptake and intracellular distribution of neutral red in cultured fibroblasts. *Exp. Cell Res.*, 115, 343-355.

Burda, S. and Oleszek, W., 2001. Antioxidant and antiradical activities of flavonoids. *J. Agric. Food Chem.*, 49, 2774-2779.

Cao, E. H., Liu, X. Q., Wang, J. J. and Xu, N. F., 1996. Effect of natural antioxidant Tanshinone II-A on DNA damage by lipid peroxidation in liver cells. *Free Radic. Biol. Med.*, 20, 801-806.

Castaneda-Ovando, A., Pacheco-Hernandez, M. D. L., Paez-Hernandez, M. E., Rodriguez, J. A. and Galan-Vidal, C. A., 2009. Chemical studies of anthocyanins: a review. *Food Chem.*, 113, 859-871.

Chang, J., Xu, J., Li, M., Zhao, M., Ding, J. and Zhang, J. S., 2005. Novel cytotoxic seco-abietane rearranged diterpenoids from *Salvia prionitis*. *Planta Med.*, 71, 861-866.

Charami, M. T., Lazari, D., Karioti, A., Skaltsa, H., Litina, D. H. and Souleles, C., 2008. Antioxidant and anti-inflammatory activities of *Sideritis perfoliata* subsp. *perfoliata* (Lamiaceae). *Phytother. Res.*, 22, 450-454.

Chen, X., Ding, J., Ye, Y. M. and Zhang, J. S., 2002. Bioactive abietane and seco-abietane diterpenoids from *Salvia prionitis*. *J. Nat. Prod.*, 65, 1016-1020.

Chen, S., Zhang, D., Chen, S., Xia, T., Gao, Q., Duan, Y. and Zhang, F., 2008. Determination of salidroside in medicinal plants belonging to the *Rhodiola* L. genus originating from the Qinghai-Tibet plateau. *Chromatographia*, 65, 1016-1020.

Chiou, W. F., Lin, L. C. and Chen, C. F., 2004. Acteoside protects endotherial cells against free radical-induced oxidative stress. *J. Pharm. Pharmacol.*, 56, 743-748.

Chowdhury, A. R., Sharma, S., Mandal, S., Goswami, A., Mukhopadhyay, S. and Majumder, H. K., 2002. Luteolin, an emerging anti-cancer flavonoid, poisons eukaryotic DNA topoisomerase I. *Biochem. J.*, 366, 653-661.

Chyu, C. F., Lin, H. C. and Kuo, Y. H., 2005. New abietane and seco-abietane diterpenes from the roots of *Taiwania cryptomerioides*. *Chem. Pharm. Bull*., 53, 11-14.

Cimpoiu, C., 2006. Analysis of Some Natural Antioxidants by Thin-Layer Chromatography and High Performance Thin-Layer Chromatography. *J. Liq. Chromatogr. Relat. Technol.*, 29, 1125-1142.

Cioffi, G., Bader, A., Malafronte, A., Piaz, F. D. and Tommasi, N. D., 2008. Secondary metabolites from the aerial parts of *Salvia palaestina* Bentham. *Phytochemistry*, 69, 1005-1012.

Cushnie, T. P. T. and Lamb, A. J., 2005. Antimicrobial activity of flavonoids. *Int. J. Antimicrob. Agents*, 26, 343-356.

Da Silva Filho, A. A., de Sousa, J. P., Soares, S., Furtado, N. A., Andrade Silva, M. L. and Cunha, W. R., 2008. Antimicrobial activity of the extract and isolated compounds from *Baccharis dracunculifolia* D. C. (Asteraceae). *Z. Naturforsch*, 63, 40-46.

Darzynkiewicz, Z., Juan, G., Li., X., Gorczyca, W., Murakami, T. and Traganos, F., 1997. Cytometry in cell necrobiology: analysis of apoptosis and accidental cell death (necrosis). *Cytometry*, 27, 1-20.

De Gruijl, F. R. and Van der Leun, J. C., 2000. Environment and health: 3. Ozone depletion and ultraviolet radiation. *CMAJ*, 163, 851-855.

Delamare, A. P. L., Pistorello, I. T. M., Artico, L., Serafini, L. A. and Echeverrigaray, S., 2007. Antibacterial activity of the essential oils of *Salvia officinalis* L. and *Salvia triloba* L. cultivated in South Brazil. *Food Chem.*, 100, 603-608.

Dewick, P. M., 2009. *Medicinal Natural Products; A Biosynthetic Approach* third ed. A John Wiley and Sons Ltd, Great Britain, pp 137-310.

Diaz, A. M., Abad, M. J., Fernandez, L., Silvan, A. M., De Santos, J. and Bermejo, P., 2004. Phenylpropanoid glycosides *from Scrophularia scorodonia*: in vitro antiinflammatory activity. *Life Sci.*, 74, 2515-2526.

Diffey, B. L., 2002. Sources and measurement of ultraviolet radiation. *Methods*, 28, 4-13.

Dimas, K., Papadaki, M., Tsimplouli, C., Hatziantoniou, S., Alevizopoulos, K., Pantazis, P. and Demetzos, C., 2006. Labd-14-ene-8,13-diol (sclareol) induces cell cycle arrest and apoptosis in human breast cancer cells and enhances the activity of anticancer drugs. *Biomed. Pharmacother.*, 60, 127-133.

Dweck, A. C., 2000. The folklore and cosmetic use of various *Salvia* species, in: Kintzios, S. E. (Ed.), *Sage; The Genus Salvia.* Harwood Academic Publishers, Amsterdam, pp. 1-26.

Ellis, B. E., 1983. Production of hydroxyphenylethanol glycosides in suspension cultures of *Syringa vulgaris*. *Phytochemistry*, 22, 1941-1943.

Ellman, G., L., Courtney, K. D., Andres, V. Jr., and Featherstone, M., 1961. A new and rapid colorimetric determination of acetylcholinesterase activity. *Biochem. Pharmacol.*, 7, 88-95.

Eloff, J. N., 1998. A sensitive and quick microplate method to determine the minimal inhibitory concentration of plant extracts for bacteria. *Planta Med.*, 64, 711-713.

Fadok, V. A., De Cathelineau, A., Daleke, D. L., Henson, P. M. and Bratton, D. L., 2001. Loss of phospholipids asymmetry and surface exposure of phosphatidylserine is

required for phagocytosis of apoptotic cells by macrophages and fibroblasts. *J. Biol. Chem.*, 276, 1071-1077.

Felice, A. D., Bader, A., Leone, A., Sosa, S., Loggia, R. D., Tubaro, A. and Tommasi, N. D., 2006. New polyhydroxylated triterpenes and anti-inflammatory activity of *Salvia hierosolymitana*. *Planta Med.*, 72, 643-649.

Fisher, G. J., Wang, Z. Q., Datta, S. C., Varani, J., Kang, S. and Voorhees, J. J., 1997. Pathophysiology of premature skin aging induced by ultraviolet light. *N. Engl. J. Med.*, 337, 1419-1428.

Fontanay, S., Grara, M., Mayer, J., Finance, C. and Duval, R. M., 2008. Ursolic, oleanolic and betulinic acids: antibacterial spectra and selectivity indexes. *J. Ethnopharmacol.*, 120, 272-276.

Fredrick, J. E. and Lubin, D., 1988. Possible long term changes in biologically active ultraviolet radiation reaching the ground. *Photochem. Photobiol.*, 47, 571-578.

Fu, H., Zhang, L., Yi, T., Feng, Y. and Tian, J., 2010. Guaiane type sesquiterpenes and other constituents from *Daucus carota* L. *Biochem. Syst. Ecol.*, 38, 309-312.

Fuente, J. and Manzanaro, S., 2003. Aldose reductase inhibitors from natural sources. *Nat. Prod. Rep.*, 20, 243-251.

Gallo, M. B. C. and Sarachine, M. J., 2009. Biological activities of lupeol. *Intl. J. Biomed. Pharma. Sci*, 3 (special issue 1), 44-66.

Galvez, M., Martin-Cordero, C., Houghton, P. J. and Ayuso, M. J., 2005. Antioxidant activity of methanol extracts obtained from *Plantago* species. *J. Agric. Food Chem.*, 53, 1927-1933.

Gao, J. J., Igalashi, K. and Nukina, M., 1999. Radical scavenging activity of phenylpropanoid glycosides in *Caryopteris incana*. *Biosci. Biotechnol. Biochem.*, 63, 983-988.

Gasparro, F. P., Mitchnick, M., Nash, J. F., 1998. A review of sunscreen safety and efficacy. *Photochem. Photobiol.*, 68, 243-256.

Geetha, T. and Varalakshmi, P., 2001. Anti-inflammatory activity of lupeol and lupeol linoleate in rats. *J. Ethnopharmacol.*, 76, 77-80.

Georgiev, M., Alipieva, K. Orhan, I., Abrashev, R., Denev, P. and Angelova, M., 2011. Antioxidant and cholinesterases inhibitory activities of *Verbascum xanthophoeniceum* Griseb. and its phenylethanoid glycosides. *Food Chem.*, 128, 100-105.

Gerke, V. and Moss, S. E., 2002. Annexins: from structure to function. *Physiol. Rev.*, 82, 331-371.

Gerrish, D., Kim, I. C., Kumar, D. V., Austin, H., Garrus, J. E., Baichwal, V., Saunders, M., McKinnon, R. S., Anderson, M. B., Carlson, R., Arranz-Plaza, E. and Yager, K. M., 2008. Triterpene based compounds with potent anti-maturation activity against HIV-1. *Bioorg. Med. Chem. Lett.*, 18, 6377-6380.

Giannouli, A. L. and Kintzios, S. E., 2000. Essential oils of *Salvia* spp.: Examples of intraspecific and seasonal variation, in: Kintzios, S. E. (Ed.), *Sage; The Genus Salvia*. Harwood Academic Publishers, Amsterdam, pp 69-79.

Gil, R. R., Cordell, G. A., Topcu, G. and Ulubelen, A., 1994. Montbretol and salvinolone are identical. *J. Nat. Prod.*, 57, 181-185.

Godar, D. E., 2005. UV doses worldwide. *Photochem. Photobiol.*, 81, 736-749.

Gu, L., Wu, T. and Wang, Zhengtao, 2009. TLC bioautography-guided isolation of antioxidants from fruit of *Perilla frutescens* var. *acuta*. *LWT Food Sci. Technol.*, 42, 131-136.

Guerrero, I., Andres, L. S., Leon, L. G., Machin, R. P., Padron, J. M., Luis, J. G. and Delgadillo, J., 2006. Abietane diterpenoids from *Salvia pachyphylla* and *S. clevelandii* with cytotoxic activity against cancer cell lines. *J. Nat. Prod.*, 69, 1803-1805.

Hamburger, M. O. and Cordell, G. A., 1987. A direct bioautographic TLC assay for compounds possessing antibacterial activity. *J. Nat. Prod.*, 50, 19-22.

Hanson, J. R., 1998. Diterpenoids. *Nat. Prod. Rep.*, 15, 93-106.

Harborne, J. B. and Williams, C. A., 2000. Advances in flavonoid research since 1992. *Phytochemistry*, 55, 481-504.

Hatziantoniou, S., Dimas, K., Georgopoulos, A., Sotiriadou, N. and Demetzos, C., 2006. Cytotoxic and antitumor activity of liposome-incorporated sclareol against cancer cell lines and human colon cancer xenografts. *Pharmacol. Res.*, 53, 80-87.

Hedge, I. C., 1972. *Salvia* L., in: Tutin, T. G., Hetwood, V. H., Burges, N. A., Moore, D. M., Valentine, D. H., Walters, S. M. and Webb, D. A. (Eds.*), Flora Europaea*, vol. 3 Diapensiaceae to Myoporaceae, The Press Syndicate of the University of Cambridge Publishers, Great Britain, pp 188-192.

Herbert, J. M., Maffrand, J. P., Taoubi, K., Augereau, J. M., Fouraste, I. and Gleye, J., 1991. Verbascoside isolated from *Lantana camara*, an inhibitor of protein kinase C. *J. Nat. Prod.*, 54, 1595-1600.

Hernandez-Perez, M., Rabanal, R. M., Arias, A., de La Torre, M. C. and Rodriguez, B., 1999. Aethiopinone, an antibacterial and cytotoxic agent from *Salvia aethiopis* roots. *Pharm. Biol*., 37, 17-21.

Horiuchi, K., Shiota, S., Hatano, T., Yoshida, T., Kuroda, T. and Tsuchiya, T., 2007. Antimicrobial activity of oleanolic acid from *Salvia officinalis* and related compounds on vancomycin-resistant enterococci (VRE). *Bio. Pharm. Bull.*, 30, 1147-1149.

Houghton, P. J., Ren, Y. and Howes, M. J. R., 2006. Acetylcholinesterase inhibitors from plants and fungi. *Nat. Prod. Rep.*, 23, 181-199.

Ikeda, Y., Murakami, A. and Ohigashi, H., 2008. Ursolic acid: an anti-and pro-inflammatory triterpenoid. *Mol.Nutr. Food Res.*, 52, 26-42.

Inoue, M., Sakuma, Z., Ogihara, Y. and Saracoglu, I., 1998. Induction of apoptotic cell death in HL-60 cells by Acteoside, a phenylpropanoid glycoside. *Biol. Pharm. Bull.*, 21, 81-83.

Janicsak, G., Veres, K., Kakasy, A. Z. and Mathe, I., 2006. Study of the oleanolic and ursolic acid contents of some species of the Lamiaceae. *Biochem. Syst. Ecol.*, 34, 392-396.

Ji, L., Pan-fen, W., Rong-liang, Z., Zi-min, L. and Zhong-jian, J., 1993. Protection of Phenylpropanoid glycosides from *Pedicularis* against oxidative hemolysis in vitro. *Planta Med.*, 59, 315-317.

Jiang, R. W., Lau, K. M., Hon, P. M., Mak, T. C., Woo, K. S. and Fung, K. P., 2005. Chemistry and biological activities of caffeic acid derivatives from *Salvia miltiorrhiza*. *Curr. Med. Chem.*, 12, 237-246.

Jimenez, C. and Riguere, R., 1994. Phenylethanoid glycosides in plants: structure and biological activity. *Nat. Prod. Rep.*, 11, 591-606.

Johnson, J. J., 2011. Carnosol, a promising anti-cancer and anti-inflammatory agent. *Cancer Lett.*, 305, 1-7.

Jork, H., Funk, W., Fischer, W. and Wimmer, H., 1990. *Thin-Layer Chromatography: Reagents and Detection Methods Volume 1a Physical and Chemical Detection Methods: Fundamentals, Reagents I.* VCH Verlagsgesellschaft mbH, Weinheim, Germany.

Juergens, U. R., Stober, M. and Vetter, H., 1998. Inhibition of cytokine production and arachidonic acid metabolism by eucalyptol (1,8-cineol) in human blood monocytes in vitro. *Eur. J. Med. Res.*, 3, 508-510.

Juergens, U. R., Dethlefsen, U., Steinkamp, G., Gillissen, A., Repges, R. and Vetter, H., 2003. Anti-inflammatory activity of 1,8-cineol (eucalyptol) in bronchial asthma: a double-blind placebo-controlled trial. *Respir. Med.*, 97, 250-256.

Kabouche, A., Kabouche, Z., Ozturk, M., Kolak, U. and Topcu, G., 2007. Antioxidant abietane diterpenoids from *Salvia barrelieri*. *Food Chem.*, 102, 1281-1287.

Kalinowski, D. S. and Richardson, D. R., 2005. The evolution of iron chelators for the treatment of iron overload disease and cancer. *Pharmacol. Rev.*, 57, 547-583.

Kamatou, G. P. P., Makunga, N. P., Ramogola, W. P. N. and Viljoen, A. M., 2008. South Africa *Salvia* species: a review of biological activities and phytochemistry. *J. Ethnopharmacol.*, 119, 664-672.

Kang, D. G., Oh, H., Chung, H. T. and Lee, H. S., 2003a. Inhibition of angiotensin converting enzyme by Lithospermic acid B isolated from Radix *Salvia miltiorrhiza* Bunge. *Phytother. Res.*, 17, 917-920.

Kang, D. G., Lee, Y. S., Kim, H. J., Lee, Y. M. and Lee, H. S., 2003b. Angiotensin converting enzyme inhibitory phenylpropanoid glycosides from *Clerodendron trichotomum*. *J. Ethnopharmacol.*, 89, 151-154.

Kang, D. G., Oh, H., Sohn, E. J., Hur, T. Y., Lee, K. C., Kim, K. J., Kim, T. Y. and Lee, H. S., 2004. Lithospermic acid B isolated from Radix *Salviae miltiorrhiza* ameliorates ischemia/reperfusion-induced renal injury in rats. *Life Sci.*, 75, 1801-1816.

Karousou, R., Hanlidou, E. and Kokkini, S., 2000. The sage plants of Greece: distribution and infraspecific variation, in: Kintzios, S. E. (Ed.), *Sage; The Genus Salvia.* Harwood Academic Publishers, Amsterdam, pp 27-46.

Kavvadias, D., Monschein, V., Sand, P., Riederer, P. and Schreier, P., 2003. Constituents of Sage (*Salvia officinalis*) with in vitro affinity human brain benzodiazepine receptor. *Planta Med.*, 69, 113-117.

Kawashty, S. A. and El-Garf, I . A., 2000. The flavonoid chemosystematics of Egyptian *Verbena* species. *Biochem. Syst. Ecol.*, 28, 919-921.

Kennedy, D. O., Dodd, F. L., Robertson, B. C., Okello, E. J., Reay, J. L., Scholey, A. B. and Haskell, C. F., 2010. Monoterpenoid extract of sage (*Salvia lavandulaefolia*) with

cholinesterase inhibiting properties improves cognitive performance and mood in healthy adults. *J. Psychopharm.*, 0, 1-13.

Kim, H. J., Woo, E. R., Shin, C. G., Hwang, D. J., Park, H. and Lee, Y. S., 2001. HIV-1 interase inhibitory phenylpropanoid glycosides from *Clerodendron trichotomum*. *Arch Pharm. Res.*, 24, 286-291.

Kimura, Y., Okuda, H., Nishibe, S. and Arichi, S., 1987. Effects of caffeoyl glycosides on arachidonate metabolism in leukocytes. *Planta Med.*, 53, 148-153.

Koganov, M. M., Dueva, O. V. and Tsorin, B. L., 1999. Activities of plant-derived phenols in a fibroblast cell culture model. *J. Nat. Prod.*, 62, 481-483.

Kojima, H., Sato, N., Hatano, A. and Ogura, H., 1990. Sterol glucosides from *Prunella vulgaris*. *Phytochemistry*, 29, 2351-2355.

Kokkalou, E. and Kapetanidis, I., 1988. Flavonoids and phenolic-acids isolated from *Salvia horminum* (Lamiaceae). *Pharm. Acta Helv.*, 63, 90-92.

Kolak, U., Kabouche, A., Ozturk, M., Kabouche, Z., Topcu, G. and Ulubelen, A., 2009. Antioxidant diterpenoids from the roots of *Salvia barrelieri*. *Phytochem. Anal.*, 20, 320-327.

Koopman, G., Reutelingsperger, C. P. M., Kuijten, G. A. M., Keehnen, R. M. J., Pals, S. T. and van Oers, M. H. J., 1994. Annexin V for Flow cytometric detection of phosphatidylserine expression on B cells undergoing apoptosis. *Blood*, 84, 1415-1420.

Korkina, L. and Pastore, S., 2008. The role of redox regulation in the normal physiology and inflammatory diseases of skin. *Front. Biosci.*, E1, 123-141.

Kostyuk, V., Potapovich, A., Suhan, T., De Luca, C., Pressi, G., Toso, R. D. and Korkina, L., 2008. Plant polyphenols against UV-C-induced cellular death. *Planta Med.*, 74, 509-514.

Kumar, N. and Seshadri, T. R., 1976. New triterpene from *Pterocarpus santalinus* bark. *Phytochemistry*, 15, 1417-1418.

Kurkin, V. A., 2003. Phenylpropanoids from medicinal plants: distribution, classification, structural analysis, and biological activity. *Chem. Nat. Compd.*, 39, 123-153.

Kuzma, L., Rozalski, M., Walencka, E., Rozalska, B. and Wysokinska, H., 2007. Antimicrobial activity of diterpenoids from hairy roots of *Salvia sclarea* L.: Salvipisone as a potential anti-biofilm agent active against antibiotic resistant *Staphylococci*. *Phytomedicine*, 14, 31-35.

Lee, K. J., Woo, E. R., Choi, C. Y., Shin, D. W., Lee, D. G., You, H. J. and Jeong, H. G., 2004. Protective effect of acteoside on carbon tetrachloride-induced hepatotoxicity. *Life Sci.*, 74, 1051-1064.

Lee, S. Y., Choi, D. Y. and Woo, E. R.., 2005. Inhibition of osteoclast differentiation by tanshinones from the root of *Salvia miltiorrhiza* Bunge. *Arch. Pharm. Res.*, 28, 909-913.

Legault, J. and Pichette, A., 2007. Potentiating effect of β-caryophyllene on anticancer activity of α-humulene, isocaryophyllene and paclitaxel. *J. Pharm. Pharmacol.*, 59, 1643-1647.

Li, L., Tsao, R., Liu, Z., Liu, S., Yang, R., Young, J. C., Zhu, H., Deng, Z., Xie, M. and Fu, Z., 2005. Isolation and purification of acteoside and isoacteoside from *Plantago psyllium* L. by high-speed counter-current chromatography. *J. Chromatogr. A*, 1063, 161-169.

Li, M. H., Chen, J. M., Peng, Y., Wu, Q. and Xiao, P. G., 2008. Investigation of Danshen and related medicinal plants in China. *J. Ethnopharmacol.*, 120, 419-426.

Li, C. Y., Gao, H., Jiao, W. H., Zhang, L., Zhou, G. X. and Yao, X. S., 2010. Three new diterpenoids from *Rabdosia iophanthoides* var. *gerardiana. Helv. Chim. Acta*, 93, 450-456.

Lima, C. F., Andrade, P. B., Seabra, R. M., Fernandes-Ferreira, M. and Pereira-Wilson, C., 2005. The drinking of a *Salvia officinalis* infusion improves liver antioxidant status in mice and rats. *J. Ethnopharmacol.*, 97, 383-389.

Liu, J., 1995. Pharmacology of oleanolic acid and ursolic acid. *J. Ethnopharmacol.*, 49, 57-68.

Liu, G. T., Zhang, T. M., Wang, B. E. and Wang, Y. W., 1992. Protection action of seven natural phenolic compounds against peroxidative damage to biomembranes. *Biochem. Pharmacol.*, 43, 147-152.

Liu, P., Hu, Y. Y., Liu, C., Zhu, D. Y., Xue, H. M., Xu, Z. Q., Xu, L.M., Liu, C. H., Gu, H. T. and Zhang, Z. Q., 2002. Clinical observation of salvianolic acid B in treatment of liver fibrosis in chronic hepatitis B. *World J. Gastroenterol.*, 8, 679-685.

Loizzo, M. R., Menichini, F., Tundis, R., Bonesi, M., Conforti, F., Nadjafi, F., Statti, G., A., Frega, N. G. and Menichini, F., 2009. In vitro biological activity of *Salvia leriifolia* Benth essential oil relevant to the treatment of Alzheimer's disease. *J. Oleo. Sci.*, 58, 443-446.

Lu, Y. and Foo, L. Y., 2001. Antioxidant activities of polyphenols from sage (*Salvia officinalis*). *Food Chem.*, 75, 197-202.

Lu, Y. and Foo, L. Y., 2002. Polyphenolics of *Salvia*-a review. *Phytochemistry*, 59, 117-140.

Mahato, S. B., Kundu, A. P., 1994. ^{13}C NMR spectra of pentacyclic triterpenoids-a compilation and some salient features. *Phytochemistry*, 37, 1517-1575.

Mahato, S. B., and Sen, S., 1997. Advances in triterpenoid research, 1990-1994— review article number 118. *Phytochemistry*, 44, 1185-1236.

Majno, G. and Joris, I., 1995. Apoptosis, oncosis and necrosis, an overview of cell death. *Am. J. Pathol.*, 146, 3-15.

Mathew, J. and Thoppil, J. E., 2011. Chemical composition and mosquito larvicidal activities of *Salvia* essential oils. *Pharm. Biol.*, 49, 456-463.

Mayer, B., Baggio, C. H., Freitas, C. S., Santos, A. C. D., Twardowschy, A., Horst, H., Pizzolatti, M. G., Micke, G. A., Heller, M., Santos, E. P. D., Otuki, M. F. and Marques, M. C. A., 2009. Gastroprotective constituents of *Salvia officinalis* L. *Fitoterapia*, 80, 421-426.

Mehmood, S., Riaz, N., Nawaz, S. A., Afza, N., Malik, A. and Choudhary, M. I., 2006. New butylcholinesterase inhibitory triterpenes from *Salvia santolinifolia*. *Arch. Pharm. Res.*, 29, 195-198.

Miyase, T., Koizumi, A., Ueno, A., Noro, T., Kuroyanagi, M., Fukushima, S., Akiyama, Y. and Takemoto, T., 1982. Studies on the acyl glycosides from *Leucoseptrum japonicum* (Miq.) Kitamura et Murata. *Chem. Pharm. Bull.*, 30, 2732-2737.

Miyase, T., Ishino, M., Akahori, C., Ueno, A., Ohkawa, Y. and Tanizawa, H., 1991. Phenylethanoid glycosides from *Plantago asiatica*. *Phytochemistry*, 30, 2015-2018.

Moridani, M. Y., Pourahmad, J., Bui, H., Siraki, A. and O'Brien, P. J., 2003. Dietary flavonoid iron complexes as cytoprotective superoxide radical scavengers. *Free Radic. Biol. Med.*, 34, 243-253.

Mosmann, T., 1983. Rapid colorimetric assay for cellular growth and survival: application to proliferation and cytotoxicity assays. *J. Immunol. Methods*, 65, 55-63.

Moujir, L., Navarro, A. M. G., Andres, L. S. and Luis, J. G., 1996. Bioactive diterpenoids isolated from *Salvia mellifera*. *Phytother. Res.*, 10, 172-174.

Murai, M., Tamayama, Y. and Nishibe, S., 1995. Phenylethanoids in the herb of *Plantago lanceolata* and inhibitory effect on arachidonic acid-induced mouse ear edema. *Planta Med.*, 61, 479-480.

Nikolova, M. T., Grayer, R. J., Genova, E. and Porter, E. A., 2006. Exudate flavonoids from Bulgarian species of *Salvia*. *Biochem. Syst. Ecol.*, 34, 360-364.

Ninomiya, K., Matsuda, H., Shimoda, H., Nishida, N., Kasajima, N., Yoshino, T., Morikawa, T. and Yoshikawa, M., 2004. Carnosic acid, a new class of lipid absorption inhibitor from sage. *Bioorg. Med. Chem. Lett.*, 14, 1943-1946.

Nishimura, H., Sasaki, H., Inagaki, N., Chin, M. and Mitsuhashi, H., 1991. Nine phenethyl alcohol glycosides from *Stachys sieboldii*. *Phytochemistry*, 30, 965-969.

Obied, H. K., Prenzler, P. D., Konczak, I., Rehman, A. and Robards, K., 2009. Chemistry and bioactivity of olive biophenols in some antioxidant and antiproliferative in vitro bioassays. *Chem. Res. Toxicol.*, 22, 227-234.

Ohsaki, A., Kawamata, S., Ozawa, M., Kishida, A., Gong, X. and Kuroda, C., 2011. Salviskinone A, a diterpene with a new skeleton from *Salvia przewalskii*. *Tetrahedron Lett.*, 52, 1375-1377.

Ono, M., Oda, E., Tanaka, T., Iida, Y., Yamasaki, T., Masuoka, C., Ikeda, T. and Nohara, T., 2008. DPPH radical-scavenging effect on some constituents from aerial parts of *Lippia triphylla*. *J. Nat. Med.*, 62, 101-106.

Orhan, I., Kartal, M., Naz, Q., Ejaz, A., Yilmaz, G., Kan, Y., Konuklugil, B., Sener, B. and Choudhary, M. I., 2007. Antioxidant and anticholinesterase evaluation of selected Turkish *Salvia* species. *Food Chem.*, 103, 1247-1254.

Ormerod, M. G., 1994. An introduction to fluorescence technology, in: Ormerod, M. G. (Ed.), *Flow cytometry: A Practical Approach* second ed. Oxford University Press Inc., New York, pp 27-43.

Owen, R.W., Haubner, R., Mier, W., Giacosa, A. Hull, W. E., Spiegelhalder, B. and Bartsch, H., 2003. Isolation, structure elucidation and antioxidant potential of the major phenolic and flavonoid compounds in brine olive drupes. *Food Chem. Toxicol.*, 41, 703-717.

Oztekin, N., Baskan, S., Kepekci, S. E., Erim, F. B. and Topcu, G., 2010. Isolation and analysis of bioactive diterpenoids in *Salvia* species (*Salvia chionantha* and *Salvia*

kronenburgii) by micellar electrokinetic capillary chromatography. *J. Pharm. Biomed. Anal.*, 51, 439-442.

Pan, Z. H., Wang, Y. Y., Li, M. M., Xu, G., Peng, L. Y., He, J., Zhao, Y., Li, Y. and Zhao, Q. S., 2010. Terpenoids from *Salvia trijuga*. *J. Nat. Prod.*, 73, 1146-1150.

Pastore, S., Potapovich, A., Kostyuk, V., Mariani, V., Lulli, D., De Luca, C. and Korkina, L., 2009. Plant polyphenols effectively protect HaCaT cells from ultraviolet C-triggered necrosis and suppress inflammatory chemokine expression. *Ann. N. Y. Acad. Sci.*, 1171, 305-313.

Pavia, D. L., Lampman, G. M., Kriz, G. S. and Vyvyan, J. R., 2009. *Introduction to spectroscopy* fourth ed. Brooks/Cole, Cengage Learning, USA, pp 242-244.

Peana, A. T., D'Aquila, P. S., Panin, F., Serra, G., Pippia, P. and Moretti, M. D. L., 2002. Anti-inflammatory activity of linalool and linalyl acetate constituents of essential oils. *Phytomedicine*, 9, 721-726.

Pennacchio, M., Syah, Y. M., Alexander, E. and Ghisalberti, E. L., 1999. Mechanism of action of verbascoside on the isolated rat heart: increases in level of prostacyclin. *Phytother. Res.*, 13, 254-255.

Perron, N. R. and Brumaghim, J. L., 2009. A review of the antioxidant mechanisms of polyphenol compounds related to iron binding. *Cell Biochem. Biophys.*, 53, 75-100.

Perry, N. B., Anderson, R. E., Brennan, N. J., Douglas, M. H., Heaney, A. J., McGimpsey, J. A. and Smallfield, B. M., 1999. Essential oils from Dalmatian sage (*Salvia officinalis* L.): variations among individuals, plant parts, seasons, and sites. *J. Agric. Food Chem.*, 47, 2048-2054.

Perry, N. S. L., Houghton, P. J., Theobald, A., Jenner, P. and Perry, E. K., 2000. In –vitro inhibitioin of human erythrocyte acetylcholinesterase by *Salvia lavandulaefolia* essential oil and constituent terpenes. *J. Pharm. Pharmacol.*, 52, 895-902.

Perry, N. S. L., Houghton, P. J.,Jenner, P., Keith, A. and Perry, E. K., 2002. *Salvia lavandulaefolia* essential oil inhibits cholinesterase in vivo. *Phytomedicine*, 9, 48-51.

Petersen, M. and Simmonds, M. S. J., 2003. Rosmarinic acid. *Phytochemistry*, 62**,** 121-125.

Petersen, M., Abdullah, Yana, benner, J., Eberle, D., Gehlen, K., Hucherig, S., janiak, V., Kim, K. H., Sander, M., Weitzel, C. and Wolters, S., 2009. Evolution of rosmarinic acid biosynthesis. *Phytochemistry*, 70, 1663-1679.

Pettit, G. R., Numata, A., Takemura, T., Ode, R. H., Narula, A. S., Schmidt, J. M., Cragg, G. M. and Pase, C. P., 1990. Antineoplastic agents, 107. Isolation of acteoside and isoacteoside from *Castilleja linariaefolia*. *J. Nat. Prod.*, 53, 456-458.

Pietta, P. G., 2000. Flavonoids as antioxidants. *J. Nat. Prod.*, 63, 1035-1042.

Pitarokili, D., Tzakou, O., Loukis, A. and Harvala, C., 2003. Volatile metabolites from *Salvia fruticosa* as antifungal agents in soilborne pathogens. *J. Agric. Food Chem.*, 51, 3294-3301.

Pourzand, C. and Tyrrell, R. M., 1999. Apoptosis, the role of oxidative stress and the example of solar UV radiation. *Photochem. Photobiol*., 70, 380-390.

Pourzand, C., Watkin, R. D., Brown, J. E. and Tyrrell, R. M., 1999. Ultraviolet A radiation induces immediate release of iron in human primary skin fibroblasts: The role of ferritin. *Proc. Natl. Acad. Sci. USA*, 96, 6751-6756.

Psotova, J., Lasovsky, J. and Vicar, J., 2003. Metal-chelating properties, electrochemical behavior, scavenging and cytoprotective activities of six natural phenolics. *Biomed. Papers*, 147, 147-153.

Psotova, J., Svobodova, A., Kolarova, H. and Walterova, D., 2006. Photoprotective properties of *Prunella vulgaris* and rosmarinic acid on human keratinocytes. *J. Photochem. Photobiol. B.*, 84, 167-174.

Raman, A., Weir, U. and Bloomfield, S. F., 1995. Antimicrobial effects of tea-tree oil and its major components on *Staphylococcus aureus*, *Staph. Epidermidis* and *Propionibacterium acnes*. *Lett. Appl. Microbiol.*, 21, 242-245.

Rauter, A. P., Branco, I., Lopes, R. G., Justino, J., Silva, F. V. M., Noronha, J. P., Cabrita, E. J., Brouard, I. and Bermejo, J., 2007. A new triterpenoid and anticholinesterase activity of *Salvia sclareoides*. *Fitoterapia*, 78, 474-481.

Ravn, H., Nishibe, S., Sasahara, M. and Xuebo, L., 1990. Phenolic compounds from *Plantago asiatica*. *Phytochemistry*, 29, 3627-3631.

Reich, E. and Schibli, A., 2007. *High-Performance Thin-Layer Chromatography for the analysis of medicinal plants*. Thieme Medical Publishers, New York.

Ren, Y., Houghton, P. J., Hider, R. C. and Howes, M. J. R., 2004. Novel diterpenoid acetylcholinesterase inhibitors from *Salvia miltiorhiza*. *Planta Med.*, 70, 201-204.

Rhee, I. K., van Rijn, R. M. and Verpoorte, R., 2003. Qualitative determination of false-positive effects in the Acetylcholinesterase assay using Thin Layer Chromatography. *Phytochem. Anal.*, 14, 127-131.

Rice-Evans, A.C., Miller, N. J. and Paganga, G., 1996. Structure-antioxidant activity relationships of flavonoids and phenolic acids. *Free Radic. Biol. Med.*, 20, 933-956.

Rieseberg, M., Kasper, C., Reardon, K. F. and Scheper, T., 2001. Flow cytometry in biotechnology. *Appl. Microbiol. Biotechnol.*, 56, 350-360.

Robards, K., 2003. Strategies for the determination of bioactive phenols in plants, fruit and vegetables. *J. Chromatogr. A.*, 1000, 657-691.

Robbins, R. J., 2003. Phenolic acids in foods: an overview of analytical methodology. *J. Agric. Food Chem.*, 51, 2866-2887.

Romussi, G., Ciarallo, G., Bisio, A., Fontana, N., Simone, F. D., Tommasi, N. D., Mascolo, N. and Pinto, L., 2001. A new diterpenoid with antispasmodic activity from *Salvia cinnabarina*. *Planta Med.*, 67, 153-155.

Roth, B. L., Baner, K., Westkaemper, R., Siebert, D., Rice, K. C., Steinberg, S., Ernsberger, P. and Rothman, R. B., 2002. Salvinorin A: A potent naturally occurring nonnitrogenous κ opioid selective agonist. *Proc. Natl. Acad. Sci. USA*, 99, 11934-11939.

Saija, A., Tomaino, A., Trombetta, D., Pasquale, A. D., Ucella, N., Barbuzzi, T, Paolino, D. and Bonina, F., 2000. In vitro and in vivo evaluation of caffeic acid and ferulic acids as topical photoprotective agents. *Int. J. Pharm.*, 199, 39-47.

Saito, N. and Harborne, J. B., 1992. Correlations between anthocyanin type, pollinator and flower colour in the Labiatae. *Phytochemistry*, 31, 3009-3015.

Sanchez-Rabaneda, F., Jauregui, O., Lamuela-Raventos, R. M., Bastida, J., Viladomat, F. and Codina, C., 2003. Identification of phenolic compounds in artichoke waste by high-performance liquid chromatography-tandem mass spectrometry. *J. Chromatogr. A*, 1008, 57-72.

Saracoglu, I., Inoue, M., Calis, I. and Ogihara, Y., 1995. Studies on constituents with cytotoxic and cytostatic activity of two Turkish medicinal plants *Phlomis armeniaca* and *Scutellaria salvifolia*. *Biol. Pharm. Bull.*, 18, 1396-1400.

Sato, Y., Suzaki, S., Nishikawa, T., Kihara, M., Shibata, H. and Higuti, T., 2000. Phytochemical flavones isolated from *Scutellaria barbata* and antibacterial activity against methicillin-resistant *Staphylococcus aureus*. *J. Ethnopharmacol.*, 72, 483-488.

Savelev, S. U., Okello, E. J. and Perry, E. K., 2004. Butyryl- and acetyl-cholinesterase inhibitory activities in essential oils of *Salvia* species and their constituents. *Phytother. Res.*, 18, 315-324.

Scalbert, A., Johnson, I. T. and Saltmarsh, M., 2005. Polyphenols: antioxidants and beyond. *Am. J. Clin. Nutr.*, 81, 215S-217S.

Scholey, A. B., Tildesley, N. T. J., Ballard, C. G., Wesnes, K. A., Tasker, A., Perry, E. K. and Kennedy, D. O., 2008. An extract of *Salvia* (sage) with anticholinesterase properties improves memory and attention in healthy older volunteers. *Psychopharmacology*, 198, 127-139.

Senatore, F., Rigano,D., Formisano, C., Grassia, A., Basile, A. and Sorbo, S., 2007. Phytogrowth inhibitory and antibacterial activity of *Verbascum sinuatum*. *Fitoterapia*, 78, 244-247.

Seyoum, A., Asres, K. and El-Fiky, F. K., 2006. Structure-radical scavenging activity relationships of flavonoids. *Phytochemistry*, 67, 2058-2070.

Shai, L. J., Mcgaw, L. J., Aderogba, M. A., Mdee, L. K. and Eloff, J. N., 2008. Four pentacyclic triterpenoids with antifungal and antibacterial activity from *Curtisia dentate* (Burm.f) C. A. Sm. leaves. *J. Ethnopharmacol.*, 119, 238-244.

Sharma, S., Mesic, T. M. and Martin, R. A., 1994. Thiophilic reactions of pseudopterolide: potential implications for its biological activity. *Tetrahedron*, 50, 9223-9228.

Shindo, Y., Witt, E. and Packer, L., 1993. Antioxidant defense mechanisms in murine epidermis and dermis and their responses to ultraviolet light. *J. Invest. Dermatol.*, 100, 260-265.

Shoyama, Y., Matsumoto, M. and Nishioka, I., 1987. Phenolic glycosides from diseased roots of *Rehmannia glutinosa* var. *purpurea*. *Phytochemistry*, 26, 983-986.

Siciliano, T., De Tommasi, N., Morelli, I. and Braca, A., 2004. Study of flavonoids of *Sechium edule* (Jacq) Swartz (Cucurbitaceae) different edible organs by liquid chromatography photodiode array mass spectrometry. *J. Agric. Food Chem.*, 52, 6510-6515.

Siebert, D. J., 1994. *Salvia divinorum* and salvinorin A: new pharmacologic findings. *J. Ethnopharmacol.*, 43, 53-6.

Silva, L. L. D., Nascimento, M., Silva, D. H. S., Furlan, M. and Bolzani, V. D. S., 2002. Antibacterial activity of a stearic acid derivative from *Stemodia foliosa*. *Planta Med.*, 68, 1137-1139.

Sivropoulou, A., Nikolaou, C., Papanikolaou, E., Kokkini, S., Lanaras, T. and Arsenakis, M., 1997. Antimicrobial, cytotoxic, and antiviral activities of *Salvia fluticosa* essential oil. *J. Agric. Food Chem.*, 45, 3197-3201.

Somova, L. I., Shode, F. O. and Mipando, M., 2004. Cardiotonic and antidysrhythmic effects of olenolic and ursolic acids, methyl maslinate and uvaaol. *Phytomed.*, 11, 121-129.

Sultana, N. and Ata, A., 2008. Oleanolic acid and related derivatives as medicinally important compounds. *J. Enzyme Inhib. Med. Chem.*, 23, 739-756.

Svobodova, A., Psotova, J. and Walterova, D., 2003. Natural phenolics in the prevention of UV-induced skin damage. A review. *Biomed. Papers*, 147, 137-145.

Szakiel, A., Ruszkowski, D., Grudniak, A., Kurek, A., Wolska, K. I., Doligalska, M. and Janiszowska, W., 2008. Antibacterial and antiparasitic activity of oleanolic acid and its glycosides isolated from Marigold (*Calendula officinalis*). *Planta Med.*, 74, 1709-1715.

Tabanca, N., Demirci, B., Baser, K. H. C., Aytac, Z., Ekici, M., Khan, S. I., Jacob, M. R. and Wedge, D. E., 2006. Chemical composition and antifungal activity of *Salvia macro-chlamys* and *Salvia recognita* essential oils. *J. Agric. Food Chem.*, 54, 6593-6597.

Tan, N., Kaloga, M., Radtke, O. A., Kiderlen, A. F., Oksuz, S., Ulubelen, A. and Kolodziej, H., 2002. Abietane diterpenoids and triterpenoic acids from *Salvia cilicica* and their antileishmanial activities. *Phytochemistry*, 61, 881-884.

Tasdemir, D., Donmez, A. A., Calis, I. and Ruedi, P., 2004. Evaluation of biological activity of Turkish plants. Rapid screening for the antimicrobial, antioxidant, and acetylcholinesterase inhibitory potential by TLC-bioautographic methods. *Pharm. Biol.*, 42, 374-383.

Tewtrakul, S., Miyashiro, H., Nakamura, N., Hattori, M., Kawahata, T., Otake, T., Yoshinaga, T., Fujiwara, T., Supavita, T., Yuenyongsawad, S., Rattanasuwon, P. and Dej-Adisai, S., 2003. HIV-1 integrase inhibitory substances from *Coleus parvaifolius*. *Phytother. Res.*, 17, 232-239.

Tezuka, Y., Kasimu, R., Li, J. X., Basnet, P., Tanaka, K., Namba, T. and Kadota, S., 1998. Constituents of roots of *Salvia deserta* Schang. (Xinjiang-Danshen). *Chem. Pharm. Bull.*, 46, 107-112.

Tholl, D., 2006. Terpene synthases and the regulation, diversity and biological roles of terpene metabolism. *Curr. Opin. Plant Biol.*, 9, 297-304.

Tong, X., Van Dross, T. V., Abu-Yousif, A., Morrison, A. R. and Pelling, J. C., 2007. Apigenin prevents UVB-induced cyclooxygenase 2 expression: coupled mRNA stabilization and translational inhibition. *Mol. Cell. Biol.*, 27, 283-296.

Topcu, G., 2006. Bioactive triterpenoids from *Salvia* species. *J. Nat. Prod.*, 69, 482-487.

Topcu, G. and Goren, A. C. 2007. Biological activity of diterpenoids isolated from Anatolian Lamiaceae plants. *Rec. Nat. Prod.*, 1, 1-16.

Topcu, G., Turkmen, Z., Ulubelen, A., Schilling, J. K. and Kingston, D. G. I., 2004. Highly hydroxylated triterpenes from *Salvia kronenburgii*. *J. Nat. Prod.*, 67, 118-121.

Topcu, G., Turkmen, Z., Schilling, J. K., Kingston, D. G. I., Pezzuto, J. M. and Ulubelen, A., 2008. Cytotoxic activity of some Anatolian *Salvia* extracts and isolated abietane diterpenoids. *Pharm. Biol.*, 46, 180-184.

Topcu, G. and Ulubelen, A., 1996. Abietane and rearranged abietane diterpenes from *Salvia montbretii*. *J. Nat. Prod.*, 59, 734-737.

Toth, E., Toth, G., Mathe, I. and Blunden, G., C., 2007. Martynoside, forsythoside B, ladanein and 7a-acetoxyroyleanone from *Ballota nigra* L. *Biochem. Syst. Ecol.*, 35, 894-897.

Trenam, C. W., Blake, D. R. and Morris, C. J., 1992. Skin inflammation: reactive oxygen species and the role of iron. *J. Invest. Dermatol.*, 99, 675-682.

Tzakou, O., Pitarokili, D., Chinou, I. B., Harvala, C., 2001. Composition and antimicrobial activity of the essential oil of *Salvia ringens*. *Planta Med.*, 67, 81-83.

Tyrrell, R. M., 1999. Redox regulation and oxidant activation of heme oxygenase-1. *Free Rad. Res.*, 31, 335-340.

Tyrrell, R. M. and Reeve, V. E., 2006. Potential protection of skin by acute UVA irradiation-from cellular to animal models. *Prog. Biophys. Mol. Biol.*, 92, 86-91.

Ulubelen, A., 2003. Cardioactive and antibacterial terpenoids from some *Salvia* species. *Phytochemistry*, 64, 395-399.

Ulubelen, A. and Brieskorn, C. H., 1975. Pentacyclic triterpene acids-micromeric acid from *Salvia horminum*. *Phytochemistry*, 14, 820-821.

Ulubelen, A., Brieskorn, C. H. and Ozdemir, N., 1977. Triterpenoids of *Salvia horminum*, constitution of a new diol. *Phytochemistry*, 16, 790-791.

Ulubelen, A., Topcu, G., Tan, N., Lin, L. J. and Cordell, G. A., 1992. Microstegiol, a rearranged diterpene from *Salvia microstegia*. *Phytochemistry*, 31, 2419-2421.

Ulubelen, A., Topcu, G., Eris, C., Sonmez, U., Kartal, M., Kurucu, S. and Bozok-Johansson, C., 1994a. Terpenoids from *Salvia sclarea*. *Phytochemistry*, 36, 971-974.

Ulubelen, A., Topcu, G. and Olcal, S., 1994b. Rearranged abietane diterpenes from *Teucrium divaricatum* subsp. *villosum*. *Phytochemistry*, 37, 1371-1375.

Ulubelen, A., Topcu, G. and Johansson, C. B., 1997. Norditerpenoids ansd diterpenoids from *Salvia multicaulis* with antituberculous activity. *J. Nat. Prod.*, 60, 1275-1280.

Ulubelen, A., Topcu, G., Chai, H. B. and Pezzuto, J. M., 1999. Cytotoxic activity of diterpenoids isolated from *Salvia hypargeia*. *Pharm. Biol.*, 37, 148-151.

Ulubelen, A., Oksuz, S., Kolak, U., Bozok-Johansson, C., Celik, C. and Voelter, W., 2000. Antibacterial diterpenes from the roots of *Salvia viridis*. *Planta Med.*, 66, 458-462.

Van Engeland, M., Nieland, L. J. W., Ramaekers, F. C. S., Schutte, B. and Reutelingsperger, C. P. M., 1998. Annexin V-affinity assay: a review on an apoptosis detection system based on phosphatidylserine exposure. *Cytometry,* 31, 1-9.

Vile, G. F. and Tyrrell, R. M., 1995. UVA radiation-induced oxidative damage to lipids and proteins in vitro and in human skin fibroblasts is dependent on iron and singlet oxygen. *Free Radic. Biol. Med.*, 18, 721-730.

Volkman, J. K., 2005. Sterols and other triterpenoids: source specificity and evolution of biosynthetic pathways. *Org. Geochem.*, 36, 139-159.

Wada, S., Iida, A. and Tanaka, R., 2001. Screening of triterpenoids isolated from *Phyllanthus flexuosus* for DNA topoisomerase inhibitory activity. *J. Nat. Prod.*, 64, 1545-1547.

Walker, K., 2002. *Salvia viridis* Annual Clary, in: Preston, C. D., Pearman, D. A. and Dines, T. D. (Eds.), *New Atlas of the British and Irish Flora*. Oxford University Press, Oxford, p 531.

Walker, J. B., Sytsma, K. J., Treutlein, J. and Wink, M., 2004. *Salvia* (Lamiaceae) is not monophyletic: implications for systematic, radiation, and ecological specializations of *Salvia* and tribe Mentheae. *American J. Bot.*, 91, 1115-1125.

Wang, M, Li, J., Rangarajan, M., Shao, Y., LaVoie, E. J., Huang, T. C. and Ho, C. T., 1998. Antioxidative phenolic compounds from sage (*Salvia officinalis* L.). *J. Agric. Food Chem.*, 46, 4869-4873.

Wang, Y., Song, D., Li, Z., Yuan, T., Zhang, H., Pei, Y., Jing, Y. and Hua, H., 2009a. Triterpenoids isolated from the aerial parts of *Salvia chinensis*. *Phytochemistry Lett.*, 2, 81-84.

Wang, H., Ding, Y., Zhou, J., Sun, X. and Wang, S., 2009b. The in vitro and in vivo antiviral effects of salidroside from *Rhodiola rosea* against coxsackievirus B3. *Phytomed.*, 16, 146-155.

Wang, J. W. and Wu, J. Y., 2010. Tanshinone biosynthesis in *Salvia miltiorrhiza* and production in plant tissue cultures. *Appl. Microbiol Biotechnol.*, 88, 437-449.

Williams, H. D. and Fleming, I., 2008. *Spectroscopic Methods in Organic Chemistry* sixth ed. McGraw Hill Education, UK, pp 62-179.

Winkel-Shirley, B., 2001. Flavonoid biosynthesis. A colorful model for genetics, biochemistry, cell biology, and biotechnology. *Plant Physiol.,* 126, 485-493.

Wolfle, U., Esser, P. R., Diman-Haarhaus, B., Martin, S. F., Lademann, J. and Schempp, C. M., 2011. UVB-induced DNA damage generation of reactive oxygen species, and inflammation are effectively attenuated by the flavonoid luteolin in vitro and in vivo. *Free Radic. Biol. Med.,* 50, 1081-1093.

Wolska, K. I., Grudniak, A. M., Fiecek, B., Kraczkiewicz-Dowjat, A. and Kurek, A., 2010. Antibacterial activity of oleanolic and ursolic acids and their derivatives. *Cent. Eur. J. Biol.*, 5, 543-553.

Xiong, Q., Hase, K., Tezuka, Y., Tani, T., Namba, T. and Kadota, S., 1998. Hepatoprotective activity of phenylethanoids from *Cistanche deserticola*. *Planta Med.,* 64, 120-125.

Xu, G., Peng, L. Y., Weng, Z. Y., Zhao, Y., Li, X. L., Zhao, Q. S. and Sun, H. D., 2006. Two new abietane diterpenoids from *Salvia yunnanensis*. *Planta Med.*, 72, 84-86.

Xu, G., Yang, J., Wang, Y. Y., Peng, L. Y., Yang, X. W., Pan, Z. H., Liu, E. D., Li, Y. and Zhao, Q. S., 2010. Diterpenoid constituents of the roots of *Salvia digitaloides*. *J. Agric. Food Chem.*, 58, 12157-12161.

Yamada, Y., Yasui, H. and Sakurai, H., 2006. Suppressive effect of caffeic acid and its derivatives on the generation of UVA-induced reactive oxygen species in the skin of hairless mice and pharmacokinetic analysis on organ distribution of caffeic acid in ddY mice. *Photochem. Photobiol.*, 82, 1668-1676.

Yamamoto, H. and Ogawa, T., 2002. Antimicrobial activity of perilla seed polyphenols against oral pathogenic bacteria. *Biosci. Biotechnol. Biochem.*, 66, 921-924.

Yesilyurt, V., Halfon, B., Ozturk, M. and Topcu, G., 2008. Antioxidant potential and phenolic constituents of *Salvia cedronella*. *Food Chem.*, 108, 31-39.

Yu, P., Hu, C., Meehan, E. J. and Chen, L., 2007. X-ray crystal structure and antioxidant activity of salidroside, a phenylethanoid glycoside. *Chem. Biodiv.*, 4, 508-513.

Zarzuelo, A., Jimenez, I., Gamez, M. J., Utrilla, P., Fernadez, I., Torres, M. I. and Osuna, I., 1996. Effects of luteolin-5-rutinoside in streptozotocin-induced diabetic rats. *Life Sci.*, 58, 2311-2316.

Zhang, H. J. and Li, L. N., 1994. Salvianolic acid I: a new depside from *Salvia cavaleriei. Planta Med*., 60, 70-72.

Zhang, Y., Lu, Y., Zhang L., Zheng, Q. T., Xu, L. Z. and Yang, S. L., 2005. Terpenoids from the roots and rhizomes of *Nardostachys chinensis*. *J. Nat. Prod.*, 68, 1131-1133.

Zhang, J. J., Wang, Y. L., Feng, X. B., Song, X. D. and Liu, W. B., 2011. Rosmarinic acid inhibits proliferation and induces apoptosis of hepatic stellate cells. *Biol. Pharm. Bull.*, 34, 343-348.

Zhao, C., Dodin, G., Yuan, C., Chen, H., Zheng, R., Jia, Z. and Fan, B. T., 2005. "In vitro" protection of DNA from Fenton reaction by plant polyphenol verbascoside. *Biochim. Biophys. Acta*, 1723, 114-123.

Zhao, G. R., Zhang H. M., Ye, T.X., Xiang, Z. J., Yuan, Y. J., Guo, Z. X. and Zhao, L. B., 2008. Characterization of the radical scavenging and antioxidant activities of danshensu and salvianolic acid B. *Food Chem. Toxicol.*, 46, 73-81.

Zhao, Y., Yang, G., Ren, D., Zhang, X., Yin, Q. and Sun, X.., 2011. Luteolin suppresses growth and migration of human lung cancer cells. *Mol. Biol. Rep.*, 38**,** 1115-1119.

Zhong, J. L., Yiakouvaki, A., Holley, P., Tyrrell, R. M. and Pourzand, C., 2004. Susceptibility of skin cells to UVA-induced necrotic cell death reflects the intracellular level of labile iron. *J. Invest. Dermatol.*, 123, 771-780.

Ziegler, H. L., Franzyk, H., Sairafianpour, M., Tabatabai, M., Tehrani, M. D., Bagherzadeh, K., Hagerstrand, H., Staerka, D. and Jaroszewskia, J. W., 2004. Erythrocyte membrane modifying agents and the inhibition of *Plasmodium falciparum* growth: strcture-activity relationships for betulinic acid analogues. *Bioorg. Med. Chem.*, 12, 119-127.

Ziyan, L., Yongmei, Z., Nan, Z., Ning, T. and Baolin, L., 2007. Evaluation of the antiinflammatory activity of luteolin in experimental animal models. *Planta Med.*, 73, 221-226.

Appendices

Appendix 1 NMR spectra of caffeic acid

Appendix 1.1 ^{1}H NMR spectrum of caffeic acid (500 MHz; CD_3OD)

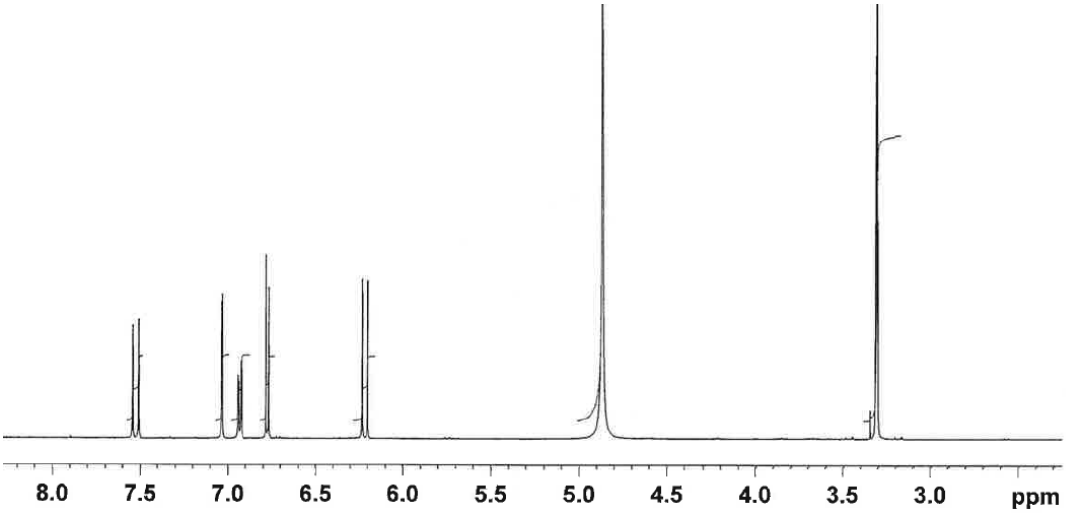

Appendix 1.2 COSY spectrum of caffeic acid (500 MHz; CD_3OD)

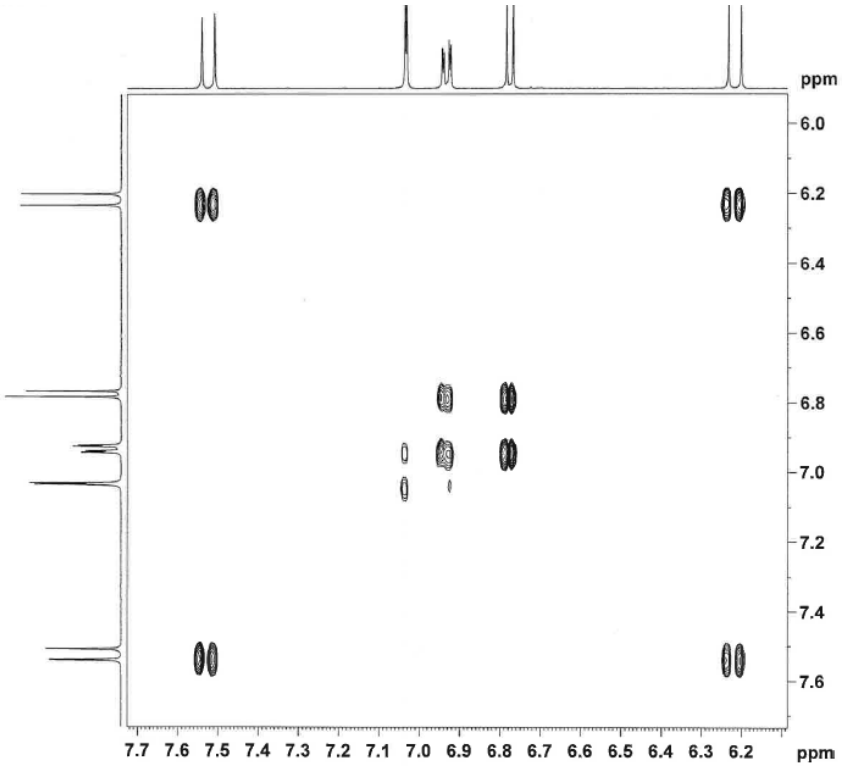

Appendix 1.3 ^{13}C NMR spectrum of caffeic acid (125 MHz; CD_3OD)

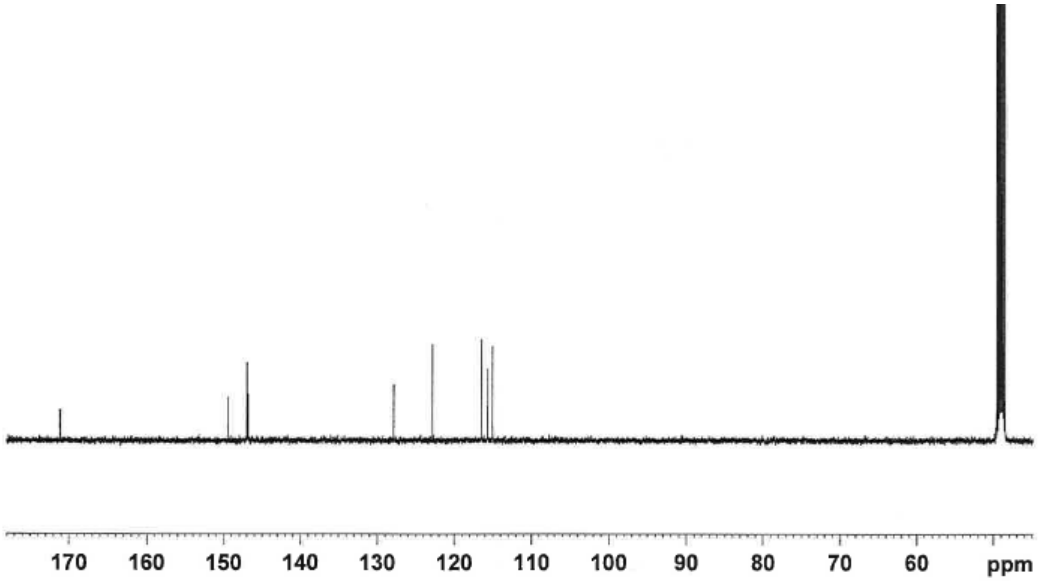

Appendix 1.4 HMQC spectrum of caffeic acid (500 MHz for ^{1}H; 125 MHz for ^{13}C; CD_3OD)

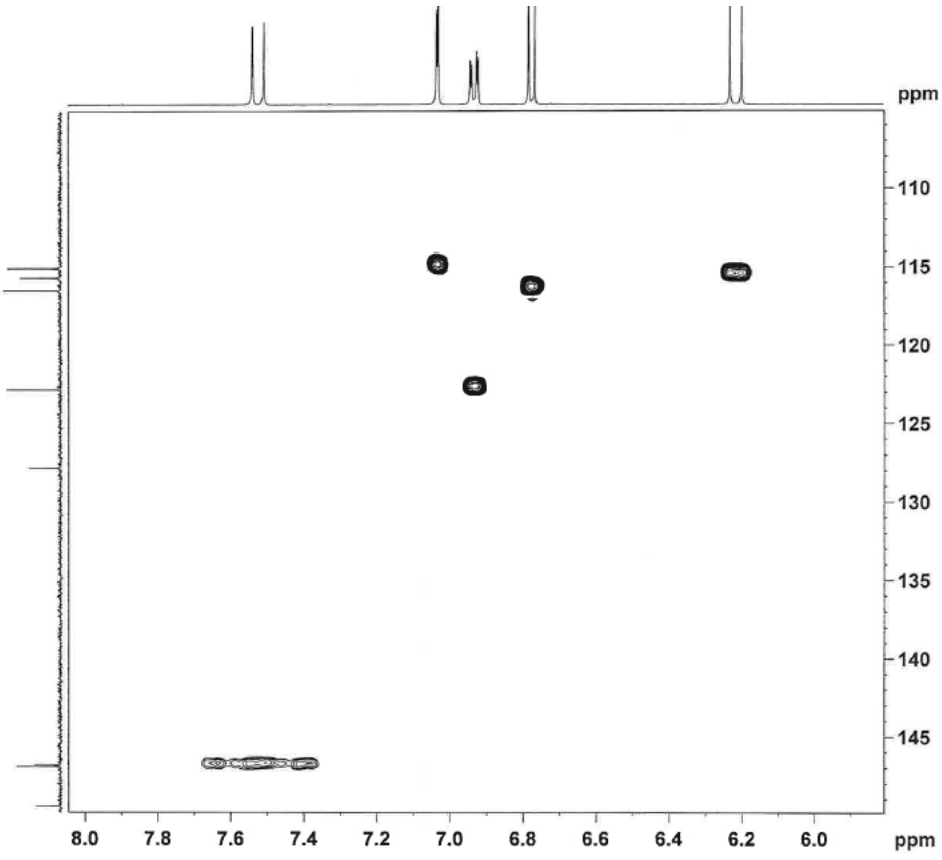

Appendix 1.5 HMBC NMR spectrum of caffeic acid (500 MHz for ^{1}H; 125 MHz for ^{13}C; CD_3OD)

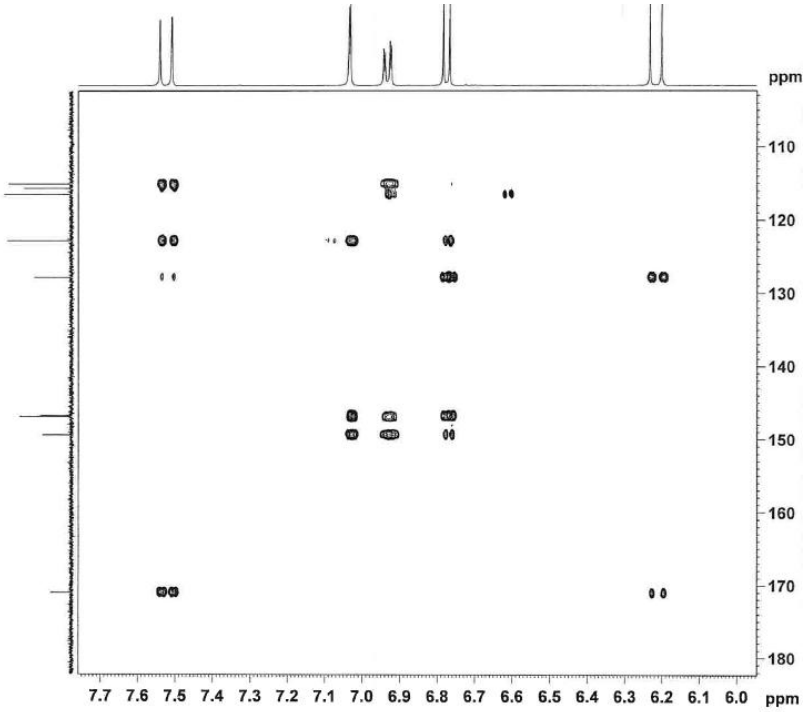

Appendix 1.6 NOESY spectrum of caffeic acid (500 MHz; CD_3OD)

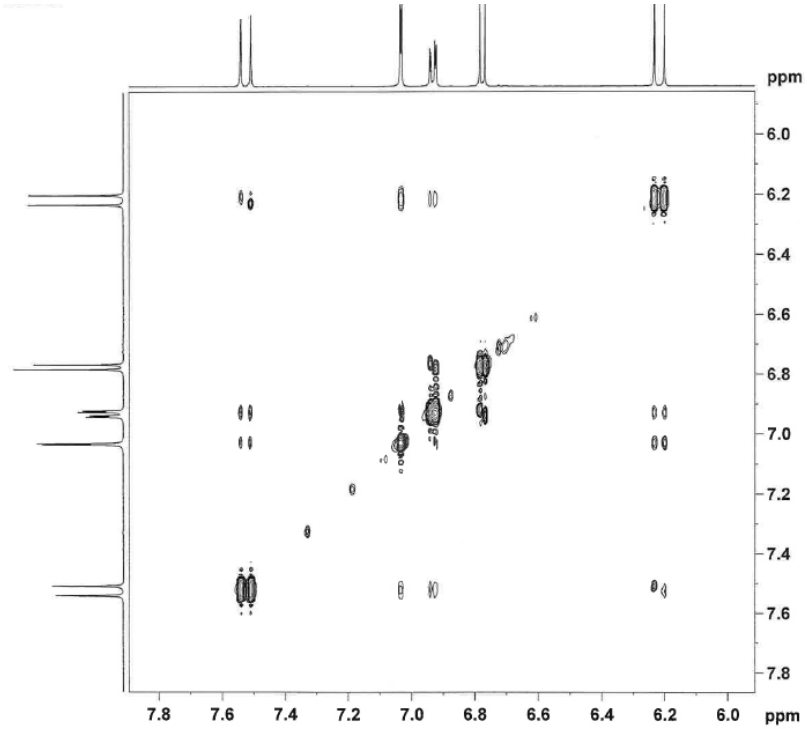

Appendix 2 NMR spectra of trans-verbascoside

Appendix 2.1 ^{1}H NMR spectrum of trans-verbascoside (400 MHz; CD_3OD)

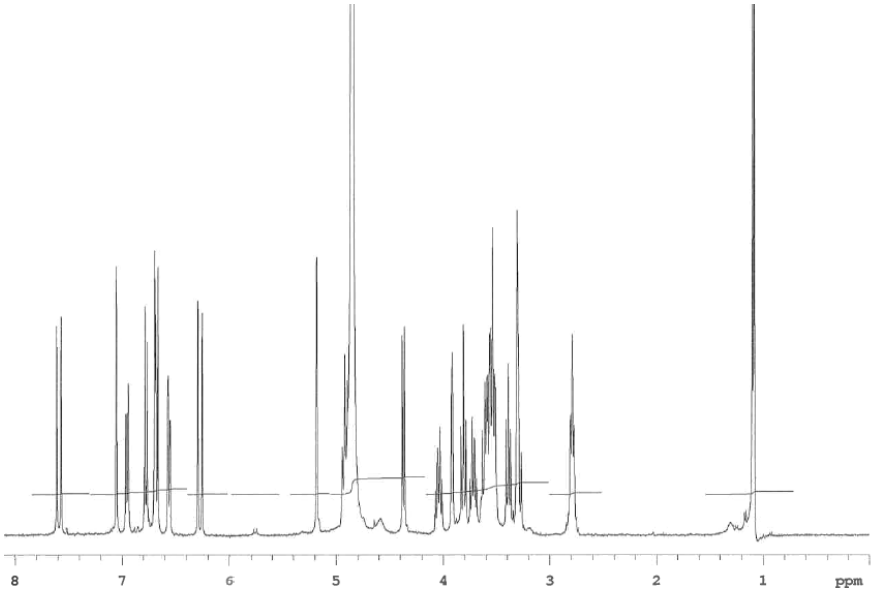

Appendix 2.2 COSY spectrum of trans-verbascoside (100 MHz; CD_3OD)

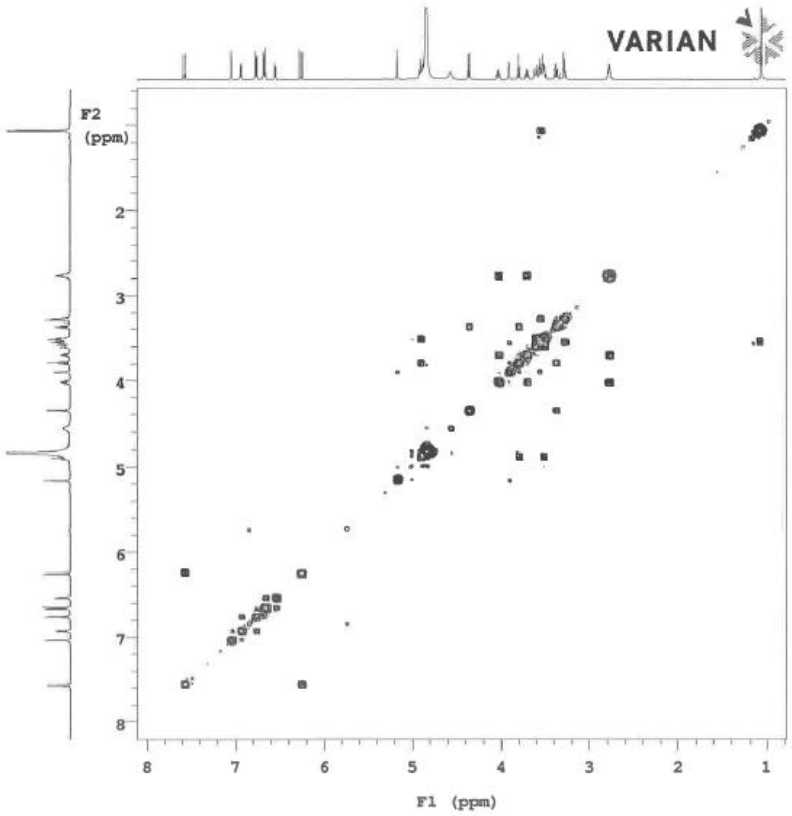

Appendix 2.3 ^{13}C NMR spectrum of trans-verbascoside (100 MHz; CD_3OD)

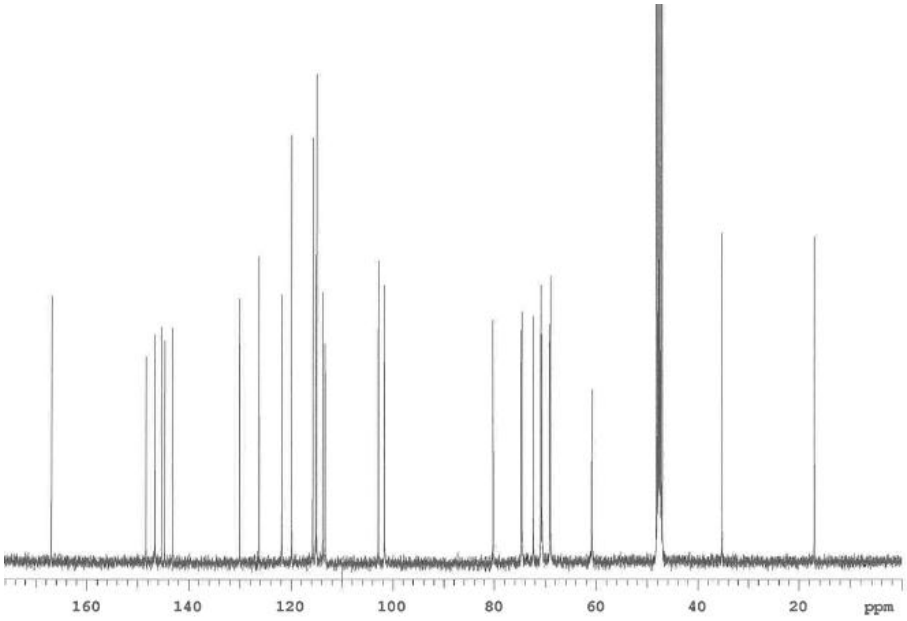

Appendix 2.4 HMQC spectrum of trans-verbascoside (400 MHz for ^{1}H; 100 MHz for ^{13}C; CD_3OD)

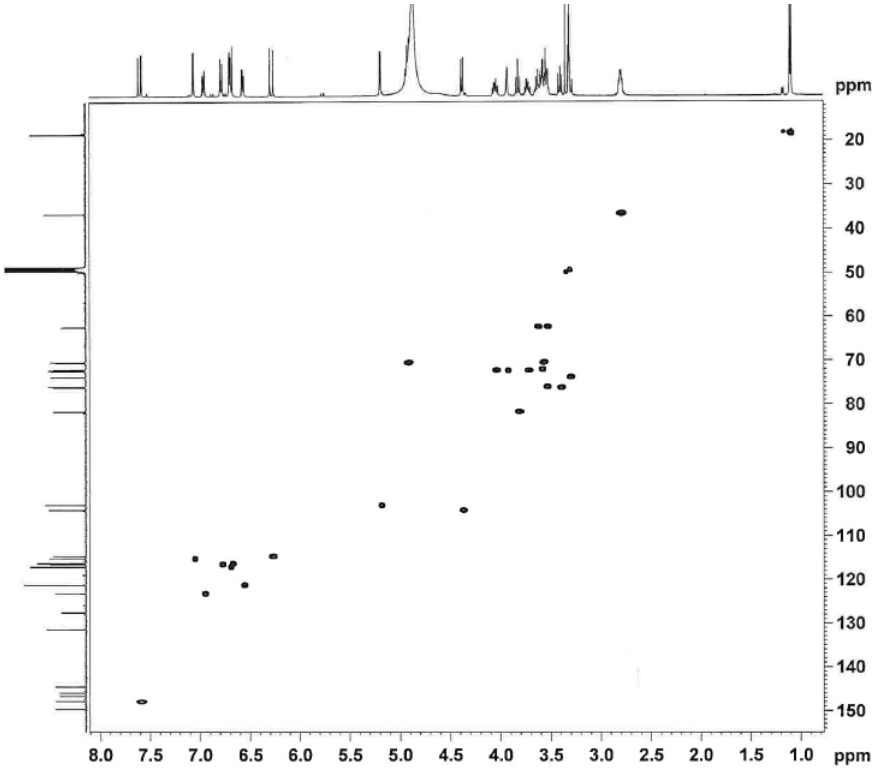

Appendix 2.5 HMBC spectrum of trans-verbascoside (400 MHz for ^{1}H; 100 MHz for ^{13}C; CD_3OD)

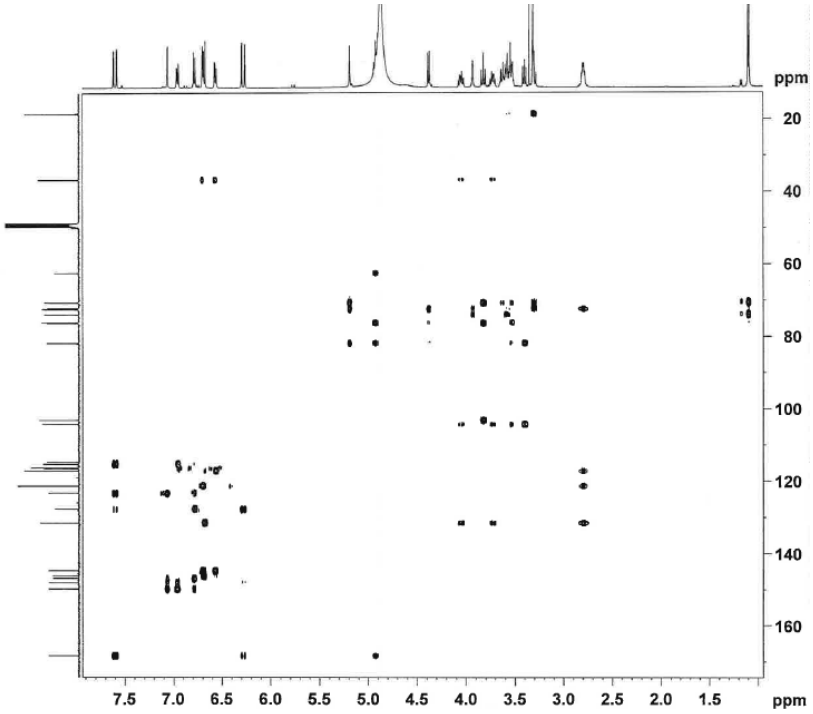

Appendix 2.6 NOESY spectrum of trans-verbascoside (400 MHz; CD_3OD)

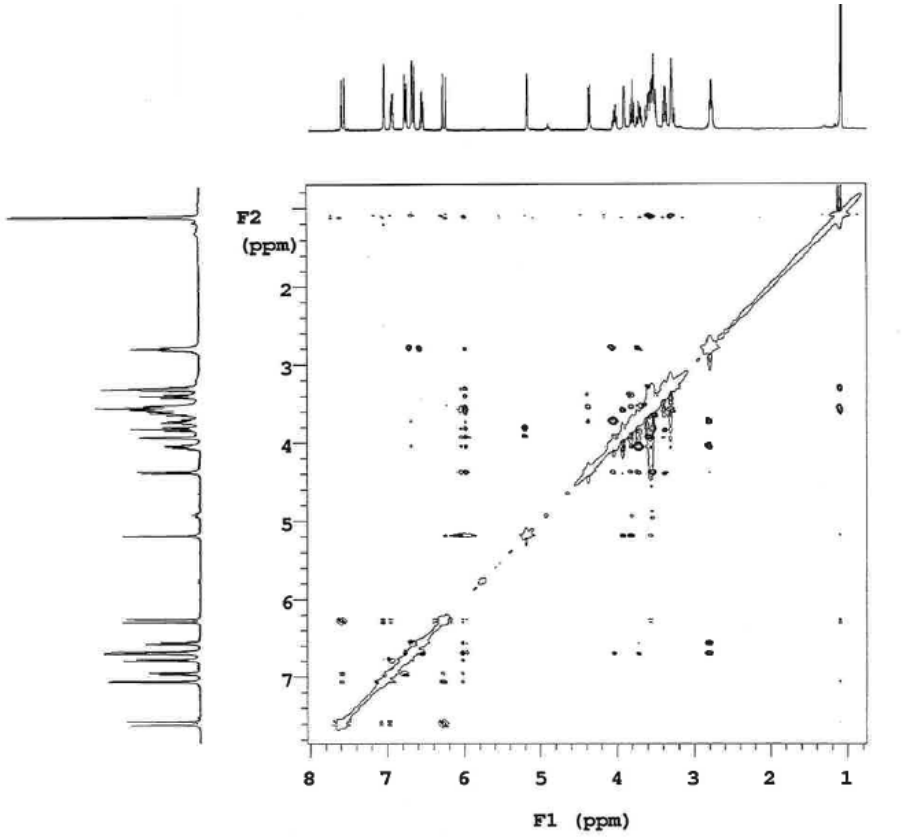

Appendix 3 NMR spectra of a mixture of trans- and cis-verbascoside

Appendix 3.1 ^{1}H NMR spectrum of a mixture of trans- and cis-verbascoside (400 MHz; CD_3OD)

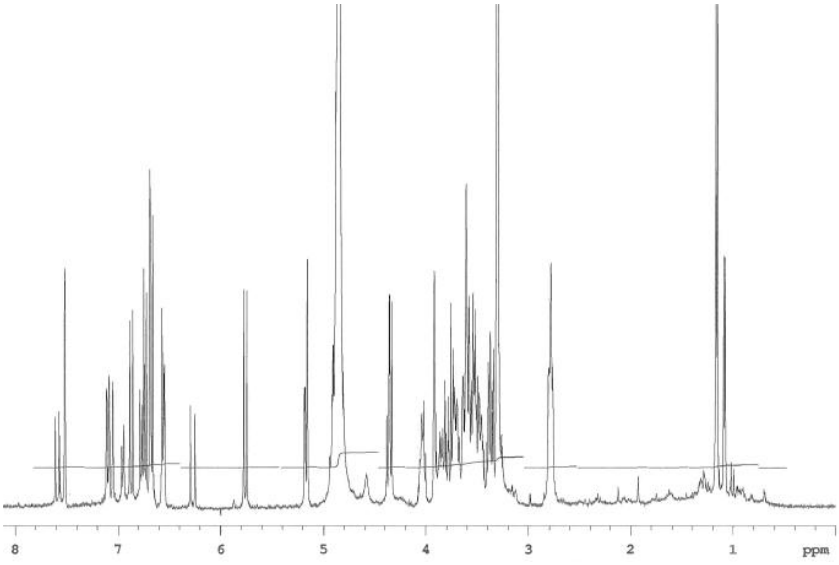

Appendix 3.2 H-H COSY spectrum of a mixture of trans- and cis-verbascoside (400 MHz; CD_3OD)

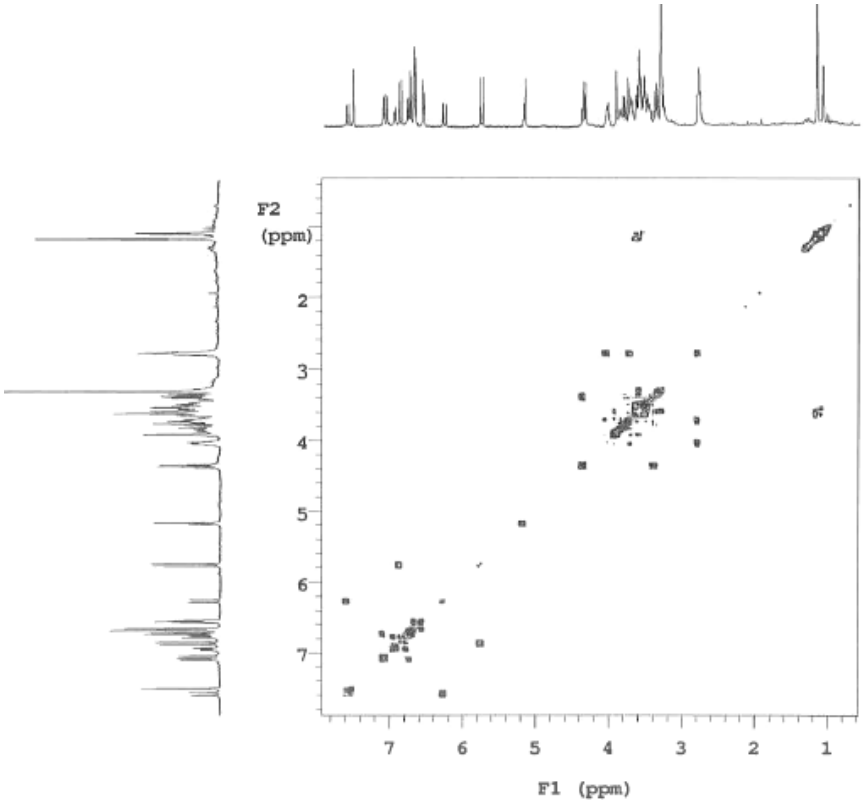

Appendix 3.3 HMQC expansion spectrum of a mixture of trans- and cis-verbascoside (400 MHz for ^{1}H; 100 MHz for ^{13}C; CD_3OD)

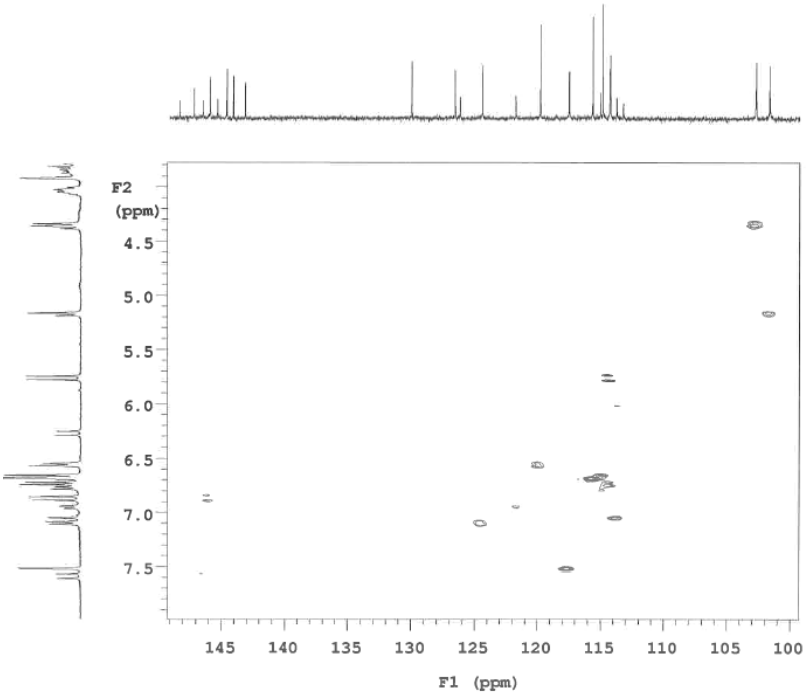

Appendix 3.4 NOESY spectrum of a mixture of trans- and cis-verbascoside (400 MHz; CD_3OD)

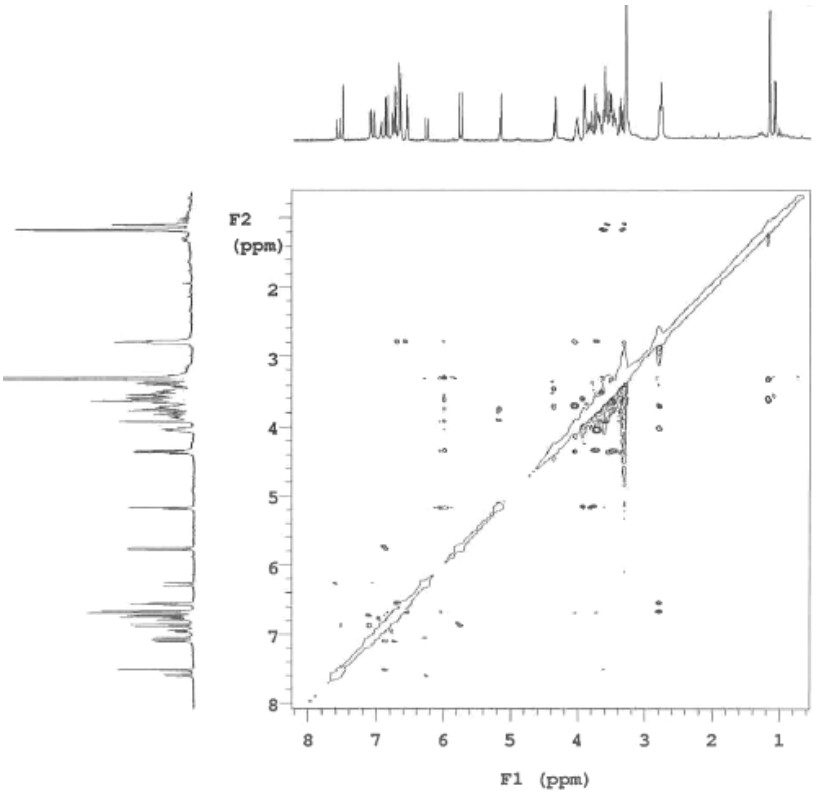

Appendix 4 NMR spectra of leucosceptoside A

*Judging from the NMR spectra, this material was about 90% pure.

Appendix 4.1 ^{1}H NMR spectrum of leucosceptoside A (500 MHz; CD_3OD)

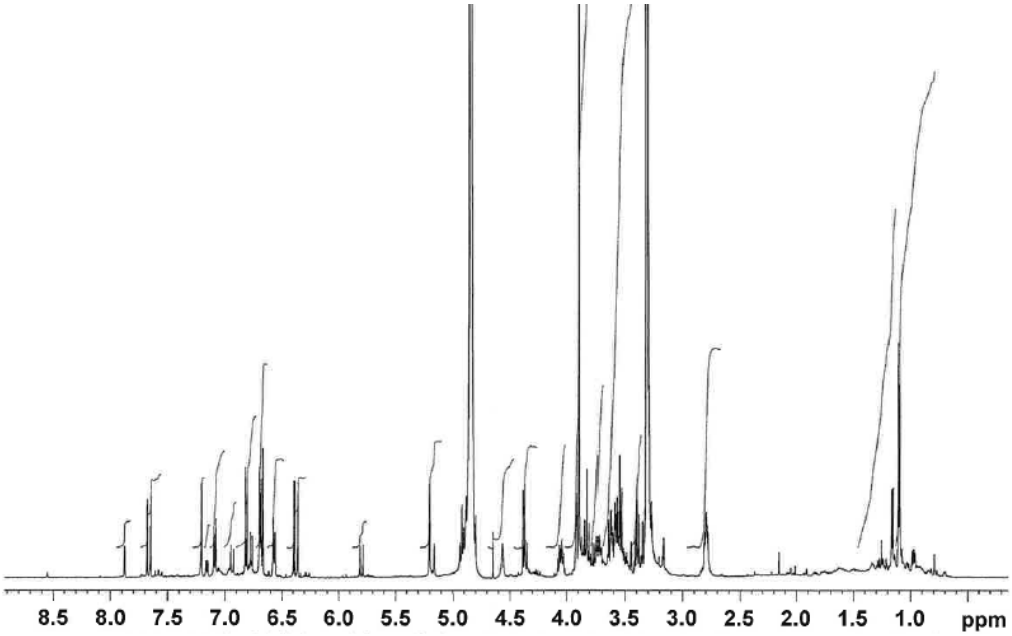

Appendix 4.2 COSY spectrum of leucosceptoside A (500 MHz; CD_3OD)

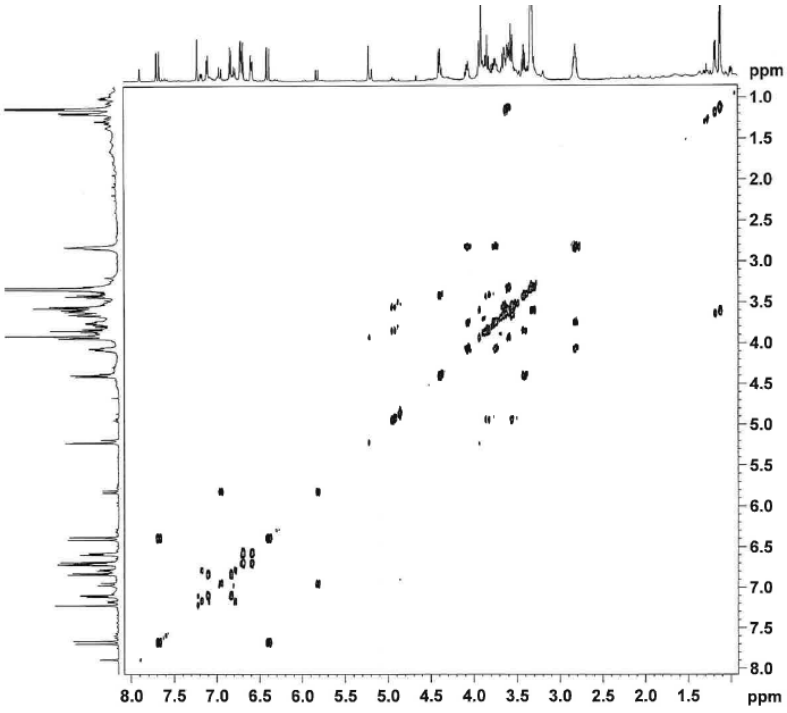

Appendix 4.3 ^{13}C NMR spectrum of leucosceptoside A (125 MHz in CD_3OD)

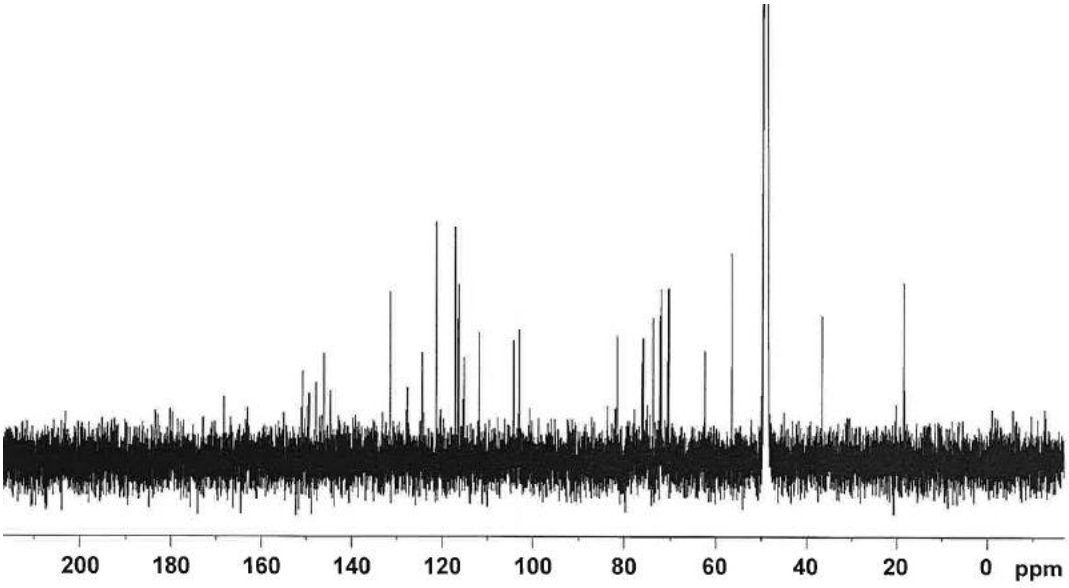

Appendix 4.4 HMQC of leucosceptoside A (500 MHz for ^{1}H; 125 MHz for ^{13}C; CD_3OD)

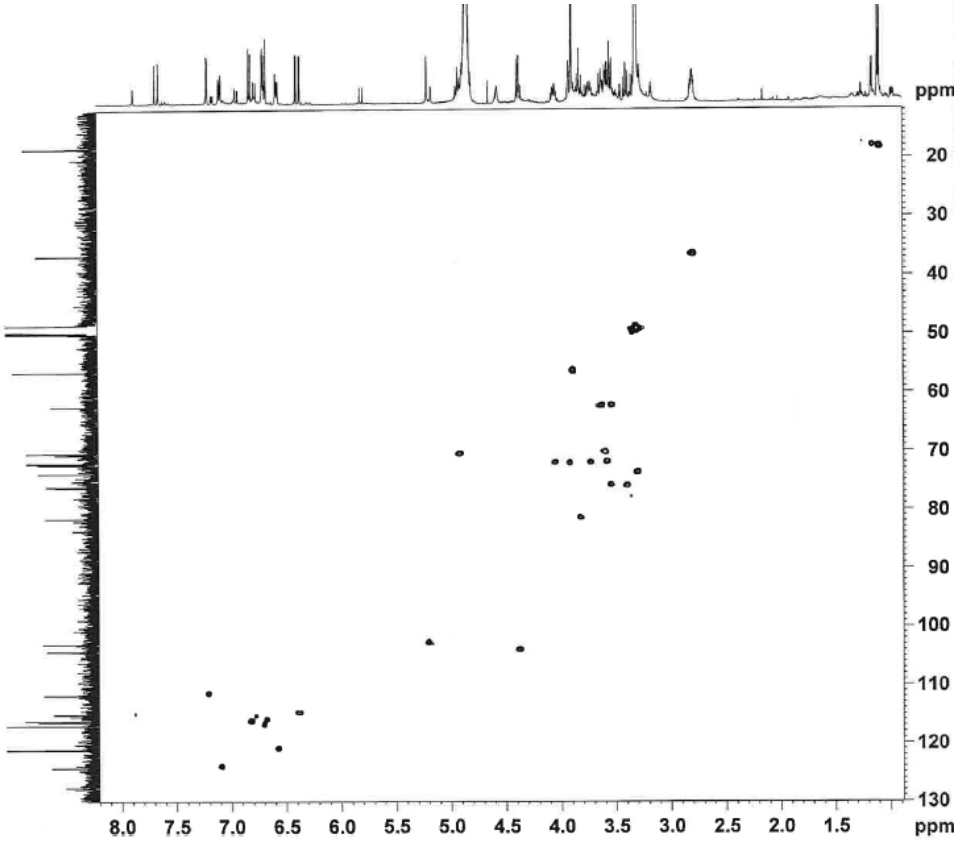

Appendix 4.5 HMBC spectrum of leucosceptoside A (500 MHz for ^{1}H; 125 MHz for ^{13}C; CD_3OD)

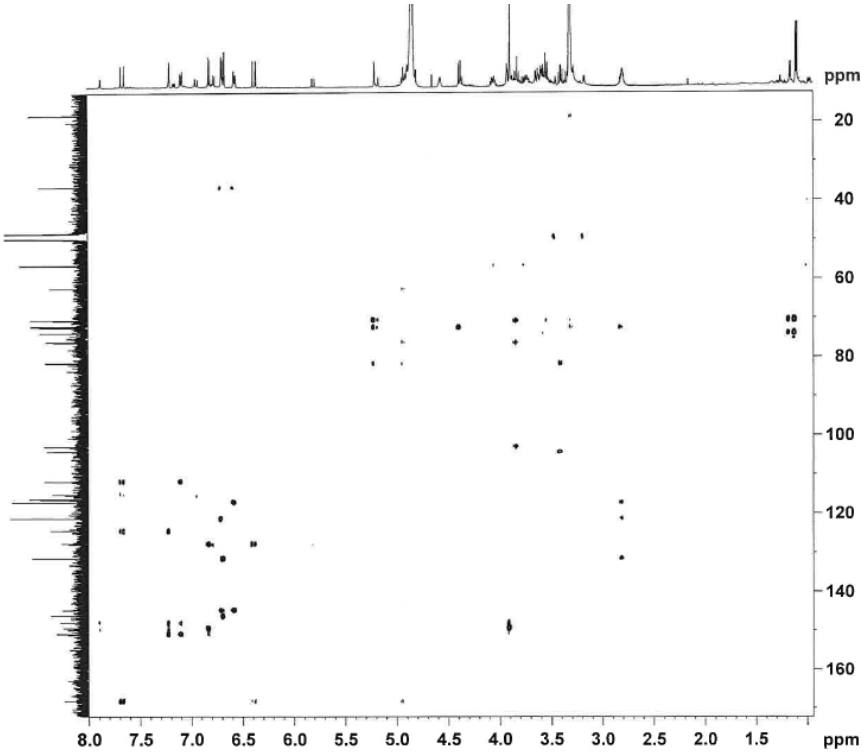

Appendix 4.6 NOESY spectrum of leucosceptoside A (500 MHz; CD_3OD)

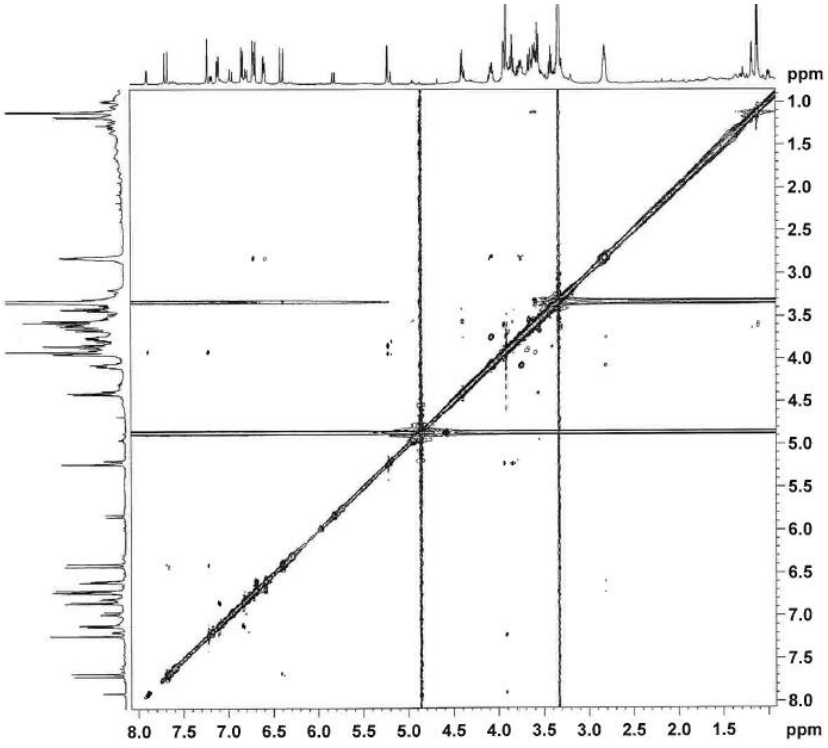

Appendix 5 NMR spectra of martynoside

*Judging from the NMR spectra, this material was about 90% pure.

Appendix 5.1 ^{1}H NMR spectrum of martynoside (500 MHz; CD_3OD)

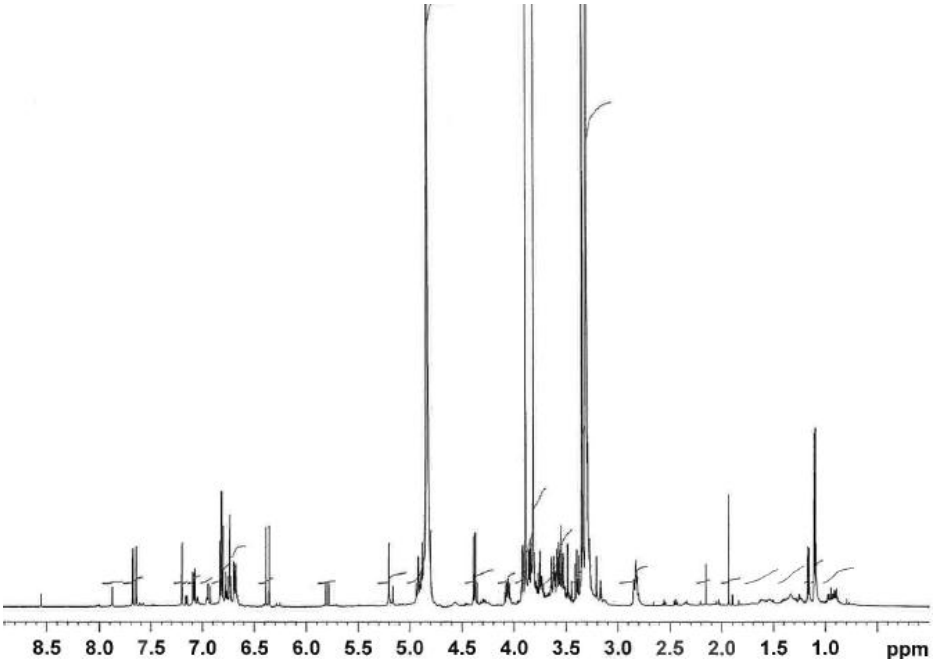

Appendix 5.2 COSY spectrum of martynoside (500 MHz; CD_3OD)

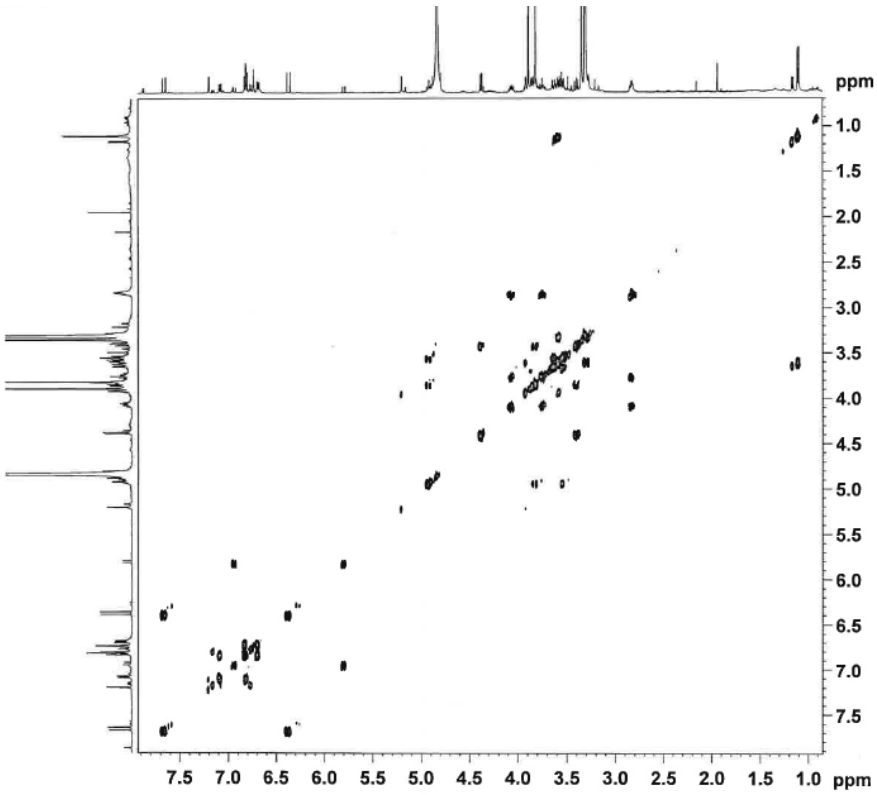

Appendix 5.3 ^{13}C NMR spectrum of martynoside (125 MHz; CD_3OD)

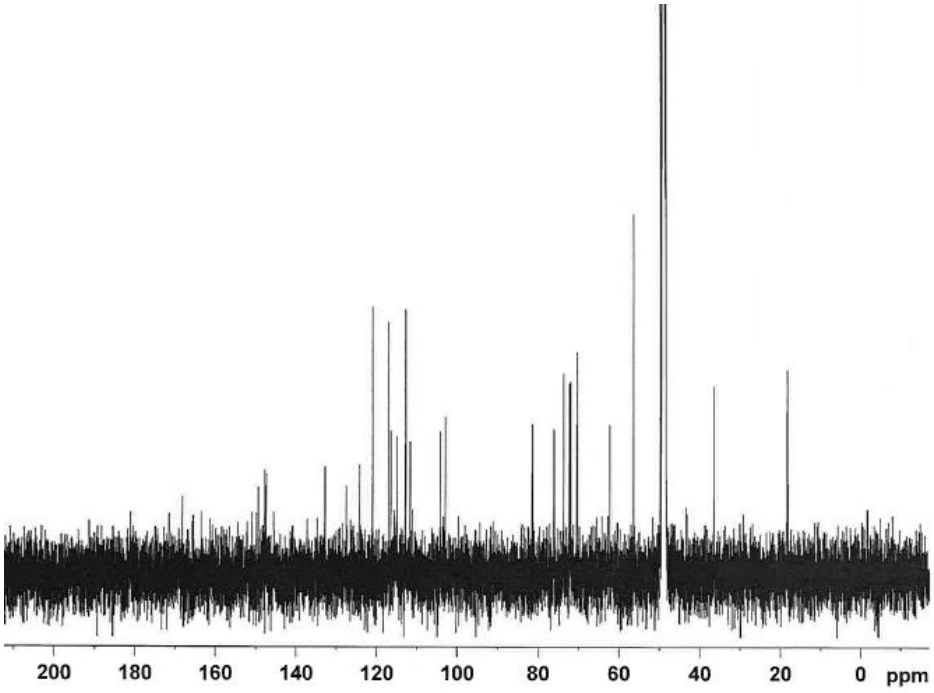

Appendix 5.4 HMQC spectrum of martynoside (500 MHz for ^{1}H; 125 MHz for ^{13}C; CD_3OD)

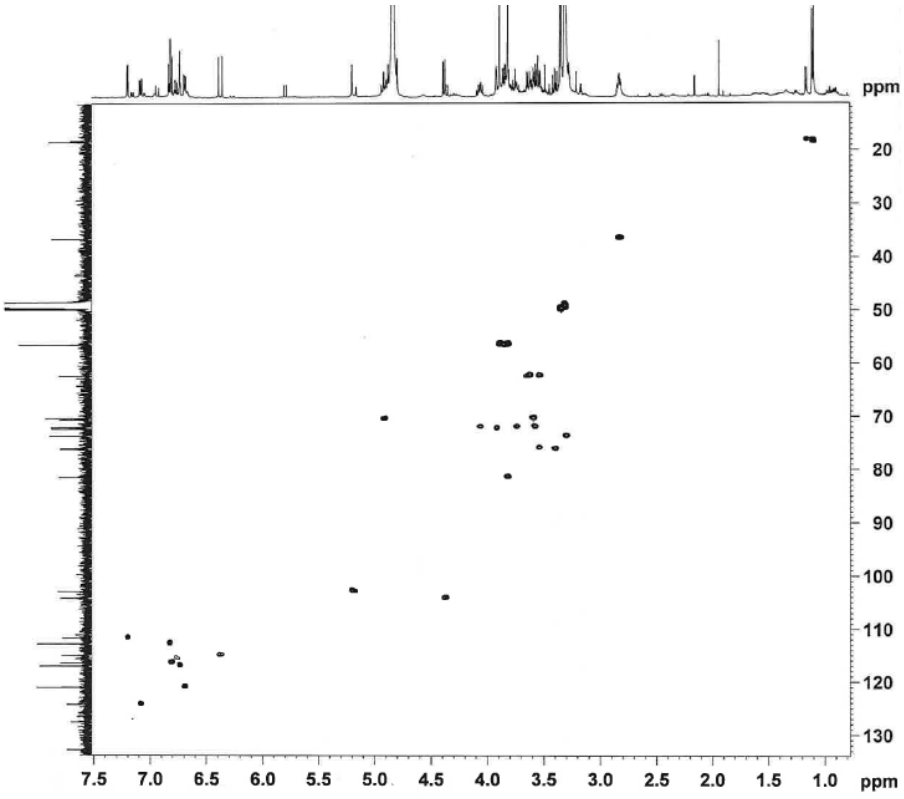

Appendix 5.5 HMBC spectrum of martynoside (500 MHz for ^{1}H; 125 MHz for ^{13}C; CD_3OD)

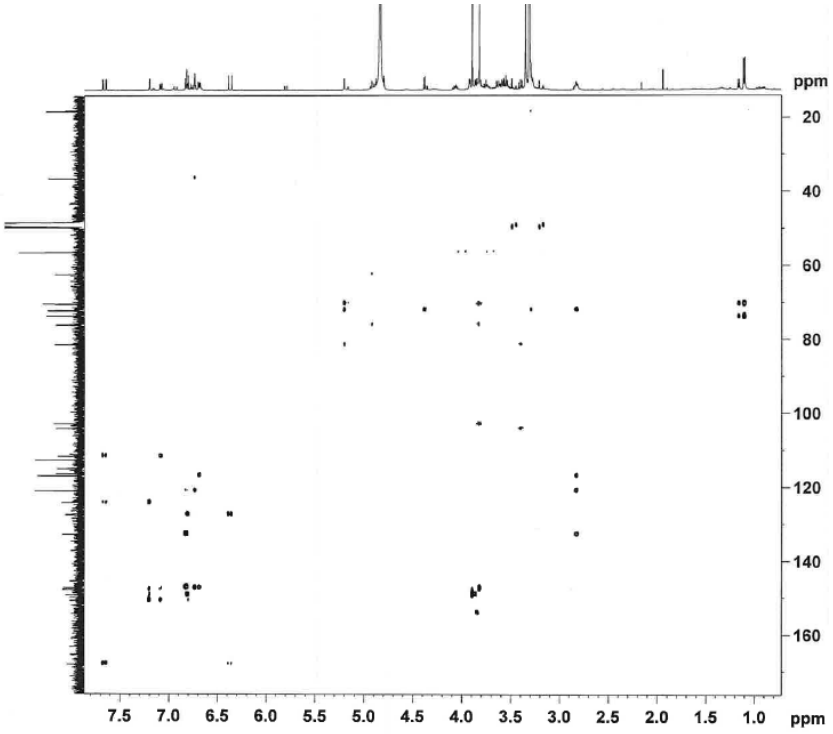

Appendix 5.6 NOESY spectrum of martynoside (500 MHz; CD_3OD)

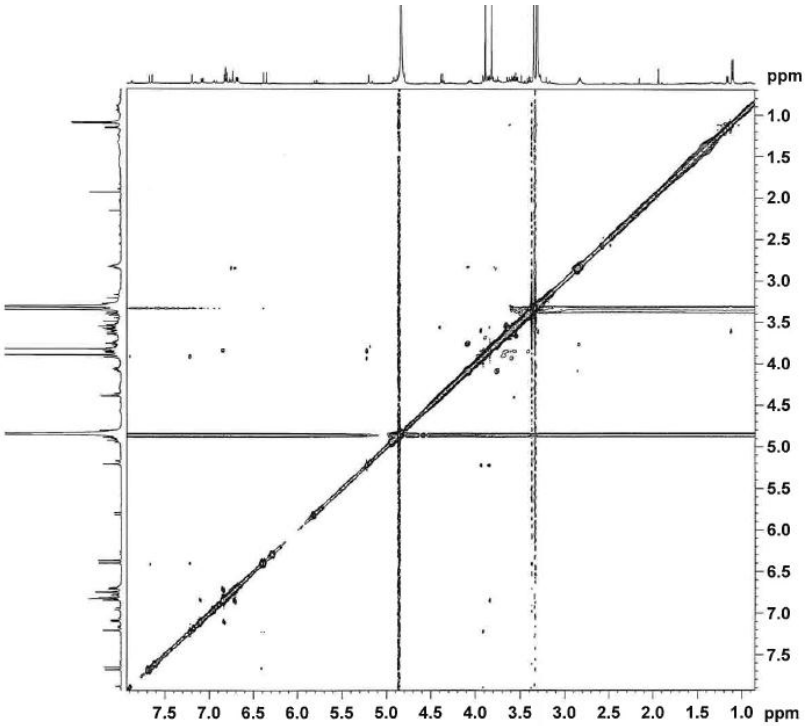

Appendix 6 NMR spectra of rosmarinic acid

Appendix 6.1 ^{1}H NMR spectrum of rosmarinic acid (500 MHz; CD_3OD)

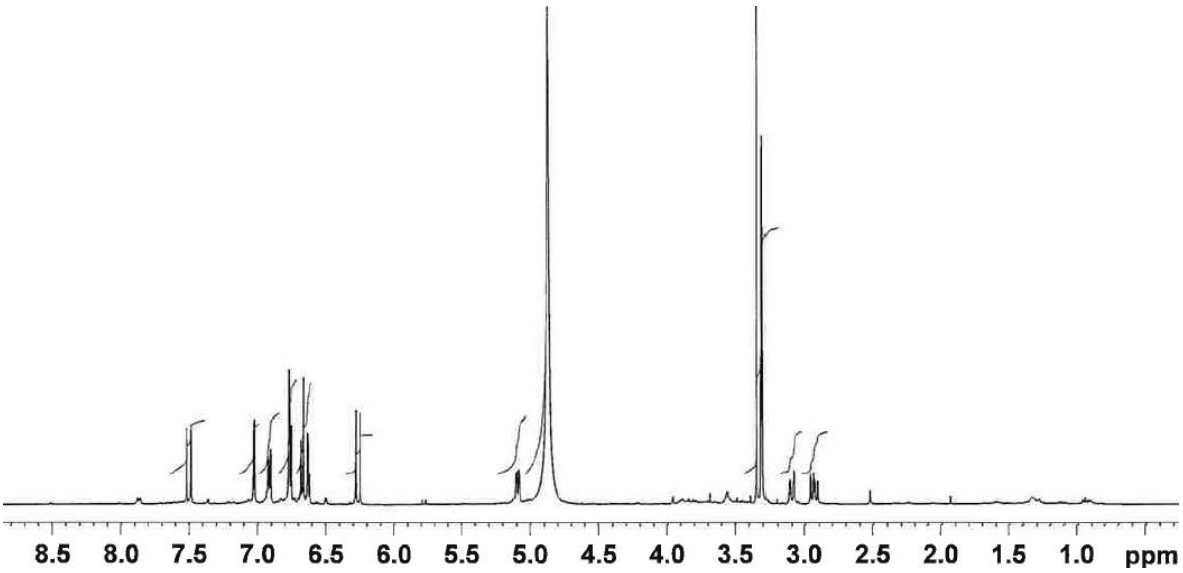

Appendix 6.2 COSY spectrum of rosmarinic acid (500 MHz; CD_3OD)

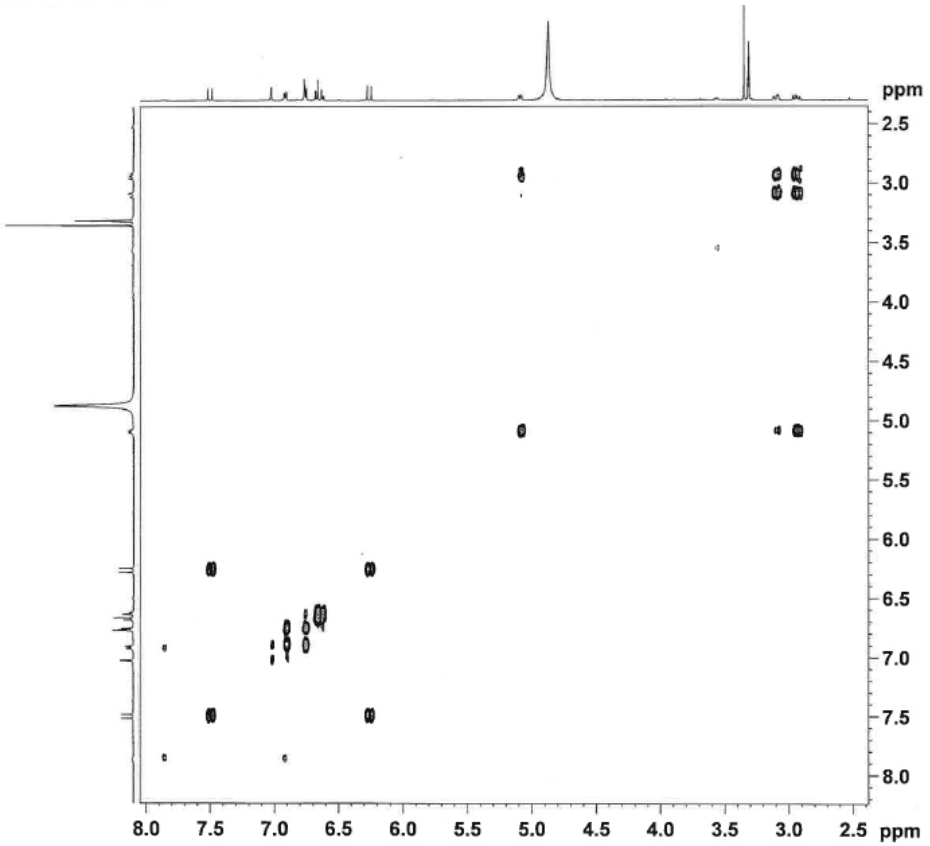

Appendix 6.3 ^{13}C NMR spectrum of rosmarinic acid (125 MHz; CD_3OD)

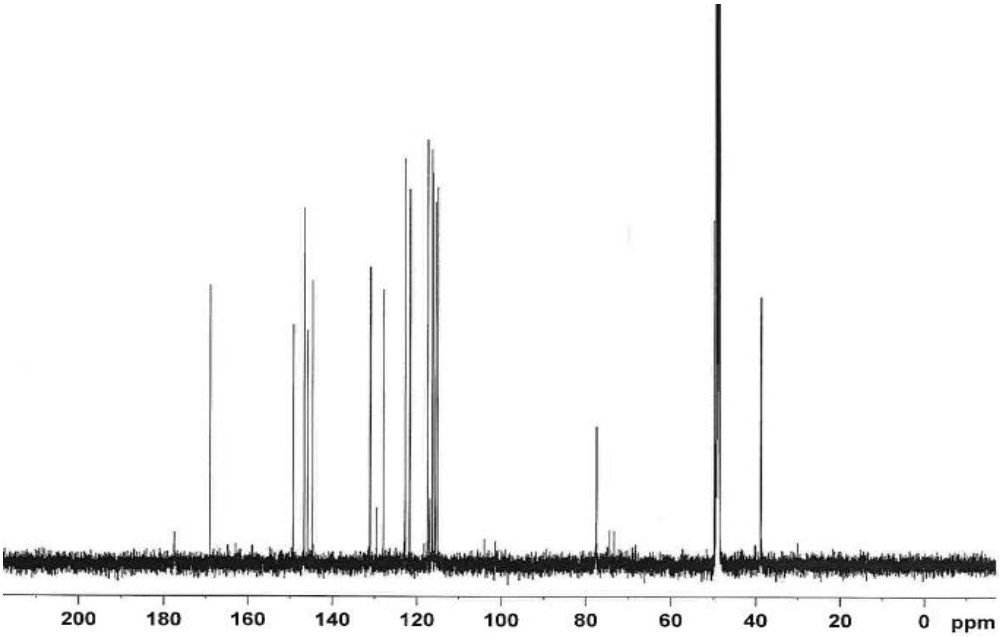

Appendix 6.4 HMQC spectrum of rosmarinic acid (500 MHz for ^{1}H, 125 MHz for ^{13}C; CD_3OD)

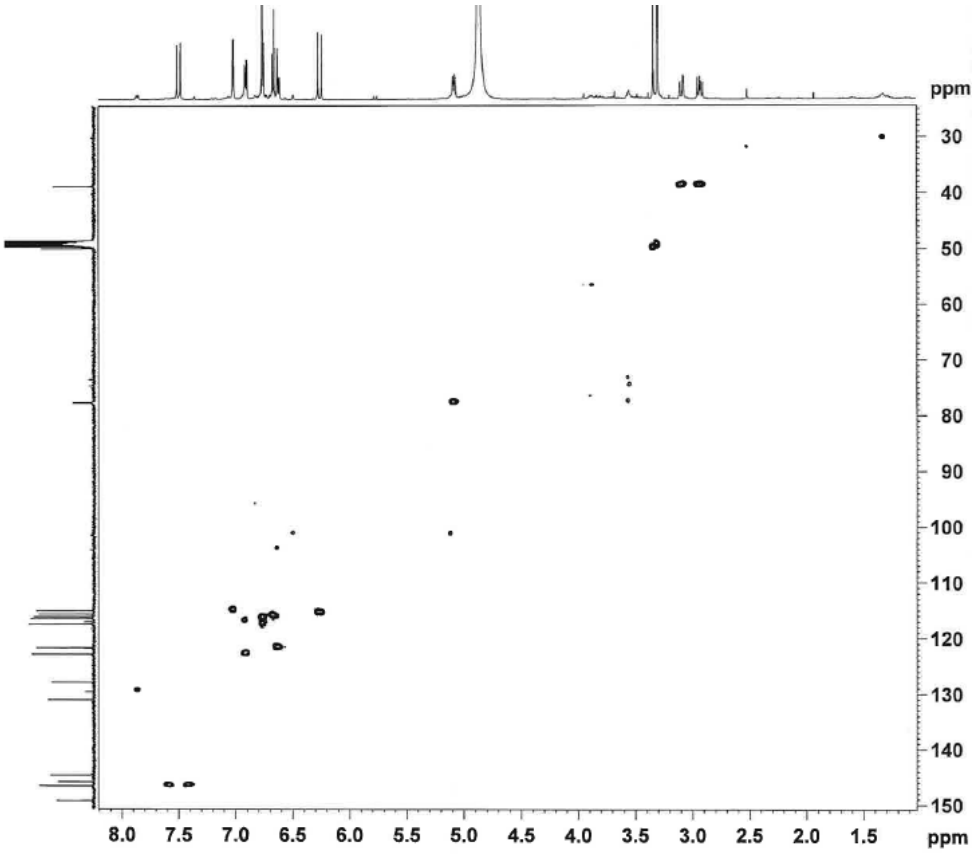

Appendix 6.5 HMBC spectrum of rosmarinic acid (500 MHz for ^{1}H, 125 MHz for ^{13}C; CD_3OD)

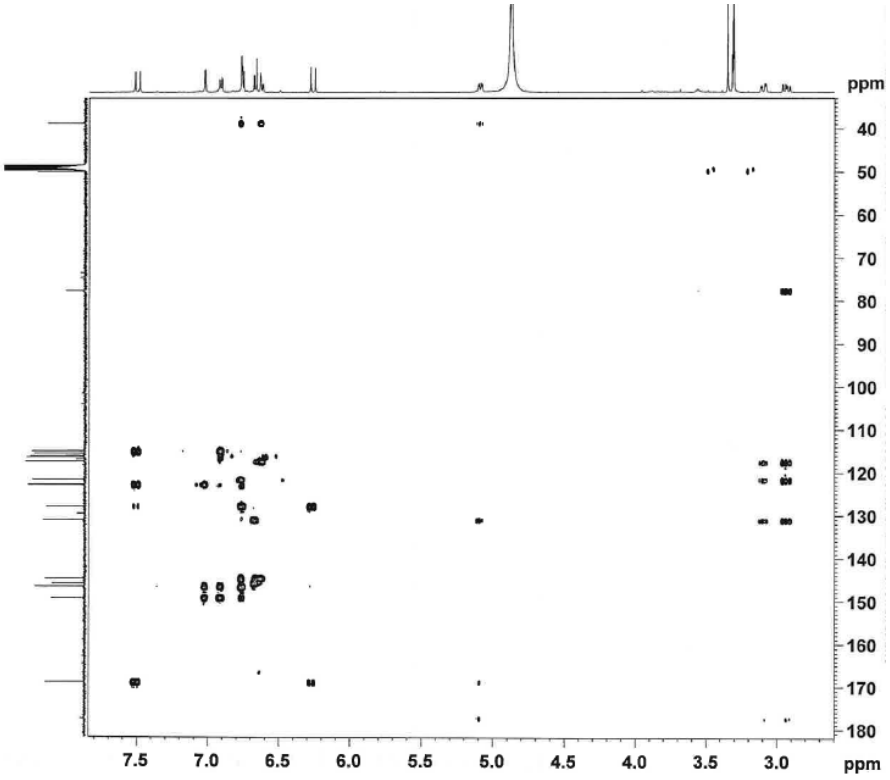

Appendix 6.6 NOESY spectrum of rosmarinic acid (500 MHz; CD_3OD)

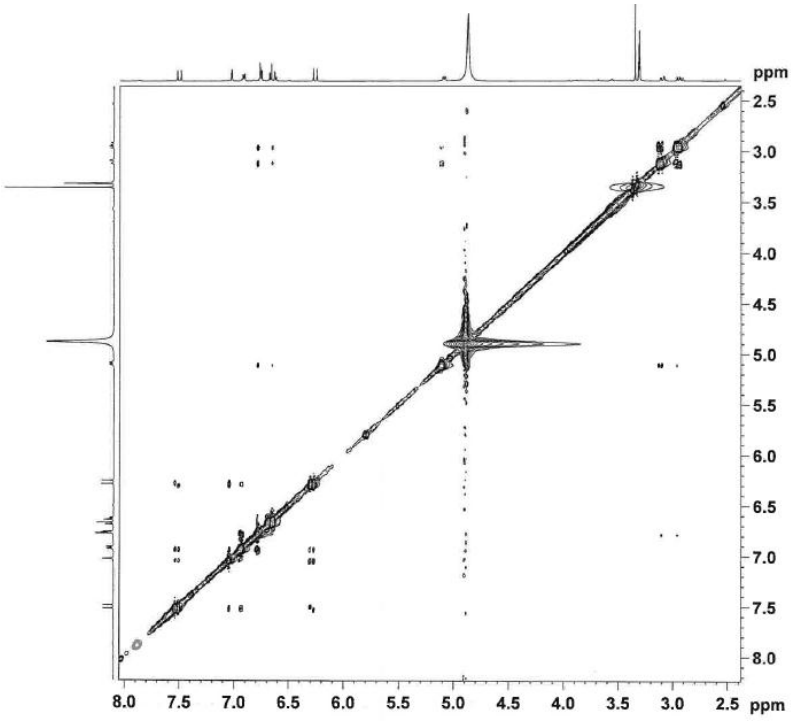

Appendix 7 NMR spectra of 6-*O*-caffeoyl-glucose

*Judging from the NMR spectra, this material was about 80% pure.

Appendix 7.1 ^{1}H NMR spectrum of 6-*O*-caffeoyl-glucose (500 MHz; CD_3OD)

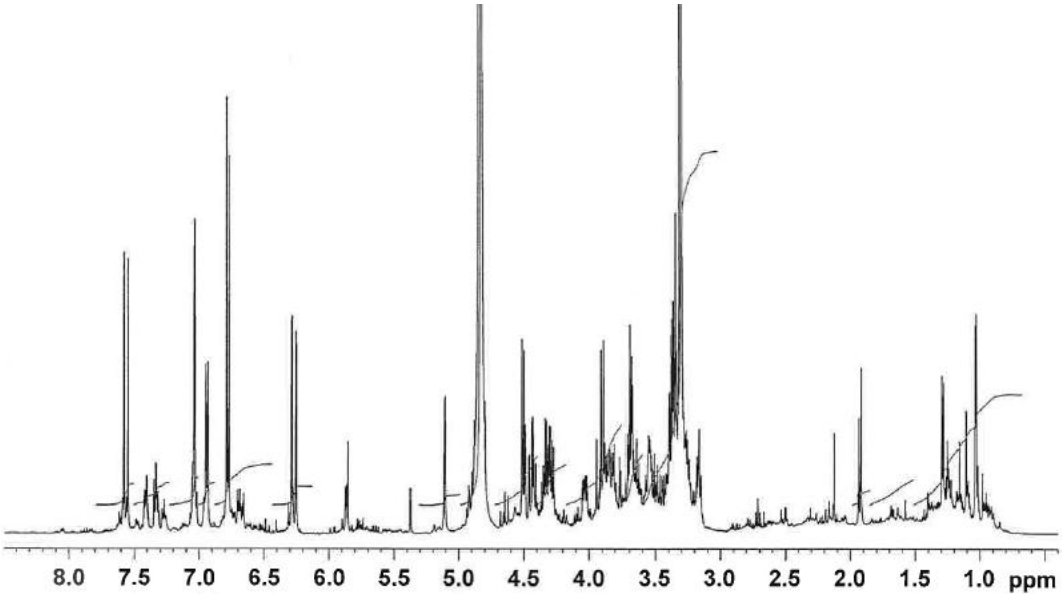

Appendix 7.2 COSY spectrum of 6-*O*-caffeoyl-glucose (500 MHz; CD_3OD)

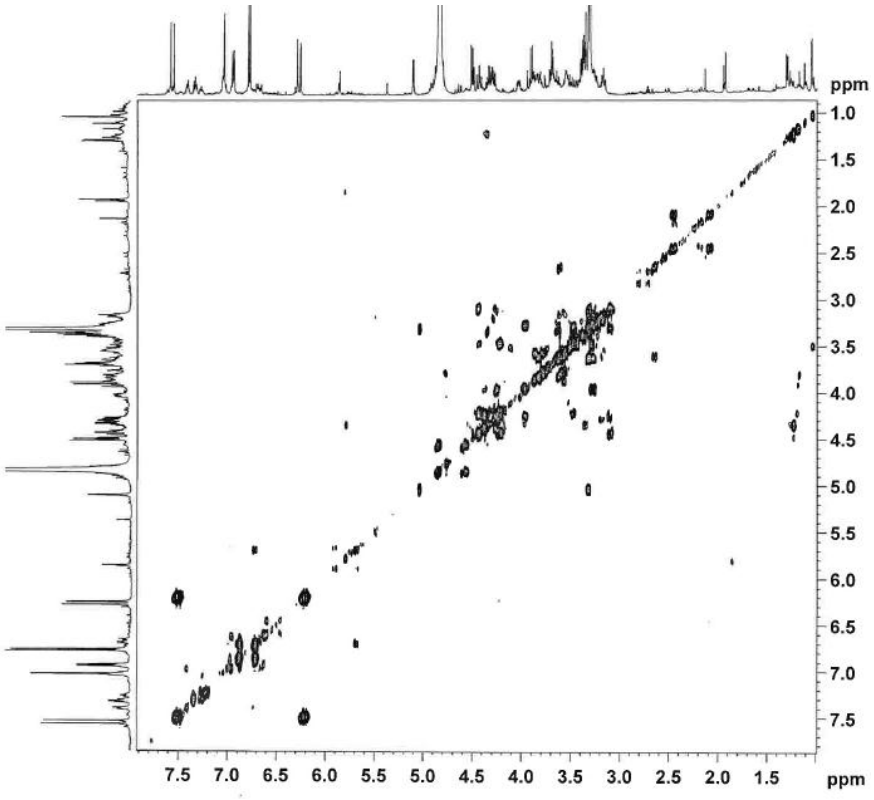

Appendix 7.3 ^{13}C NMR spectrum of 6-*O*-caffeoyl-glucose (500 MHz; CD_3OD)

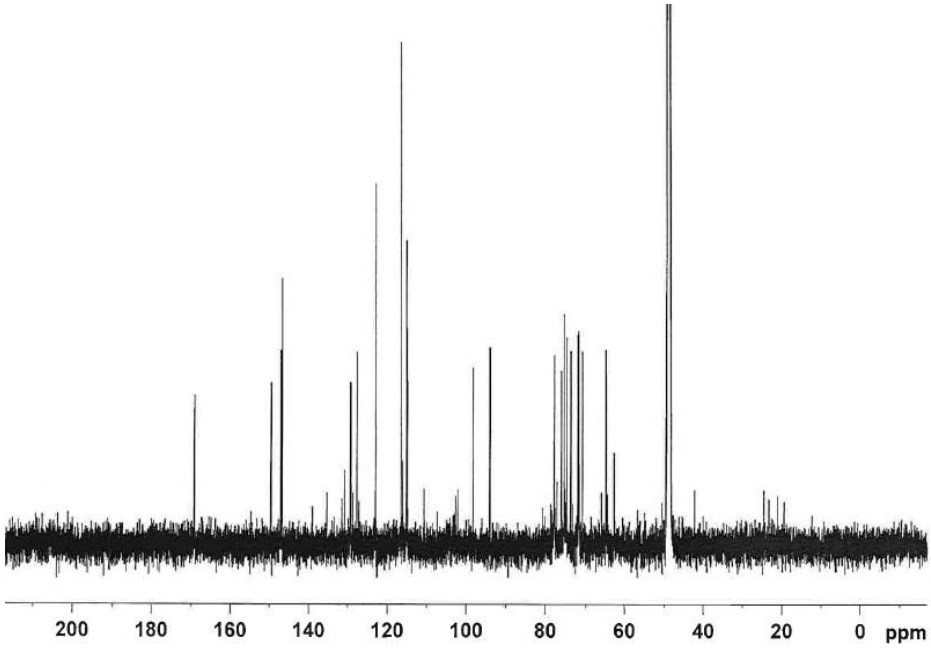

Appendix 7.4 HMQC spectrum of 6-*O*-caffeoyl-glucose (500 MHz for ^{1}H, 125 MHz for ^{13}C; CD_3OD)

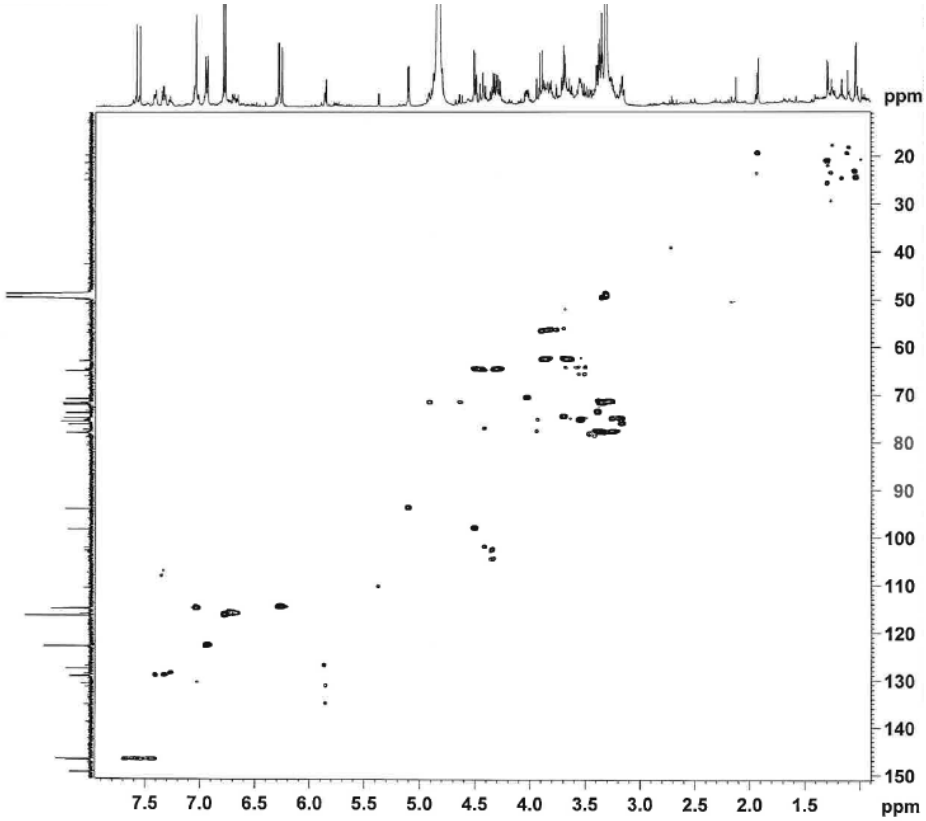

Appendix 7.5 HMBC spectrum of 6-*O*-caffeoyl-glucose (500 MHz for ^{1}H, 125 MHz for ^{13}C; CD_3OD)

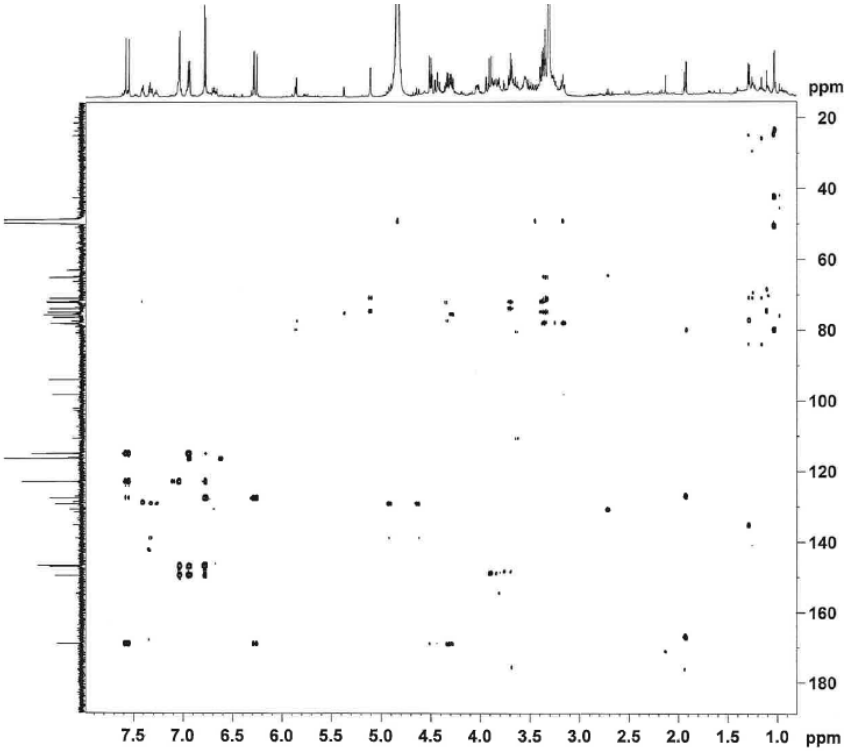

Appendix 7.6 NOESY spectrum of 6-*O*-caffeoyl-glucose (500 MHz; CD_3OD)

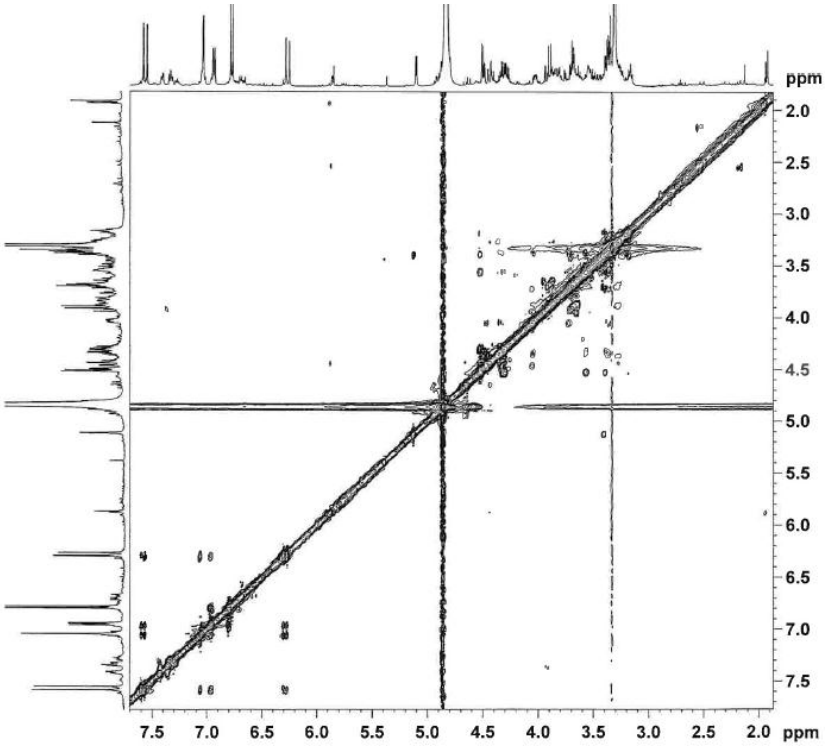

Appendix 8 NMR spectra of luteolin-7-*O*-glucopyranoside

*Judging from the NMR spectra, this material was about 85% pure.

Appendix 8.1 ^{1}H NMR spectrum of luteolin-7-*O*-glucopyranoside (500 MHz; DMSO-d6)

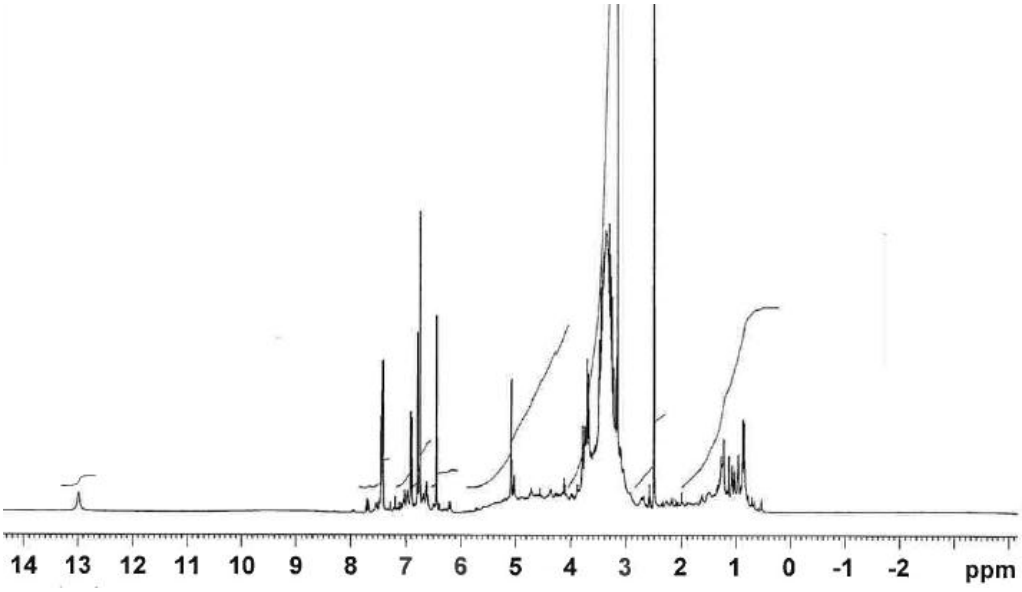

Appendix 8.2 COSY spectrum of luteolin-7-*O*-glucopyranoside (500 MHz; DMSO-d6)

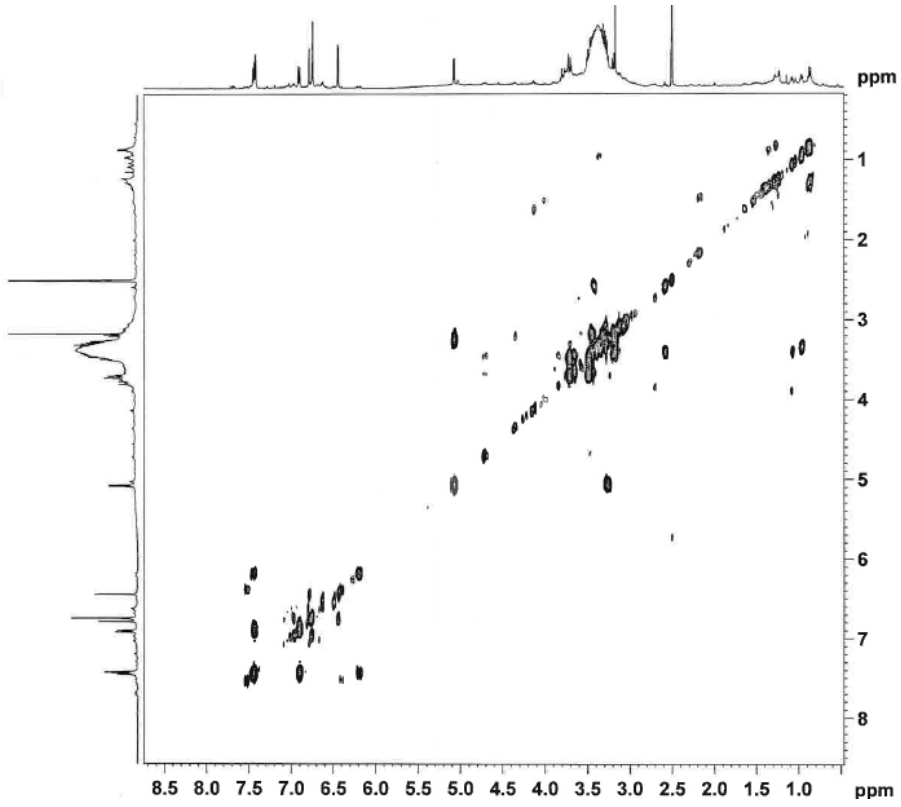

Appendix 8.3 ^{13}C NMR spectrum of luteolin-7-*O*-glucopyranoside (125 MHz; DMSO-d6)

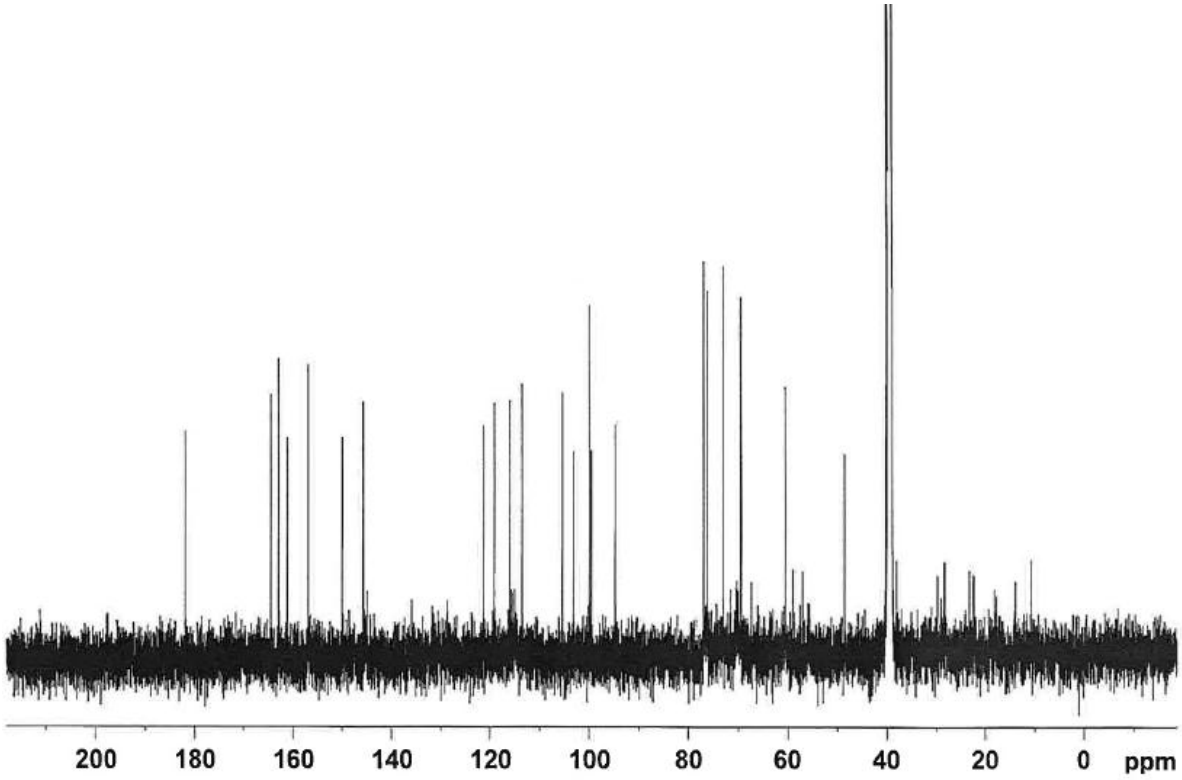

Appendix 8.4 HMQC spectrum of luteolin-7-*O*-glucopyranoside (500 MHz for ^{1}H, 125 MHz for ^{13}C; DMSO-d6)

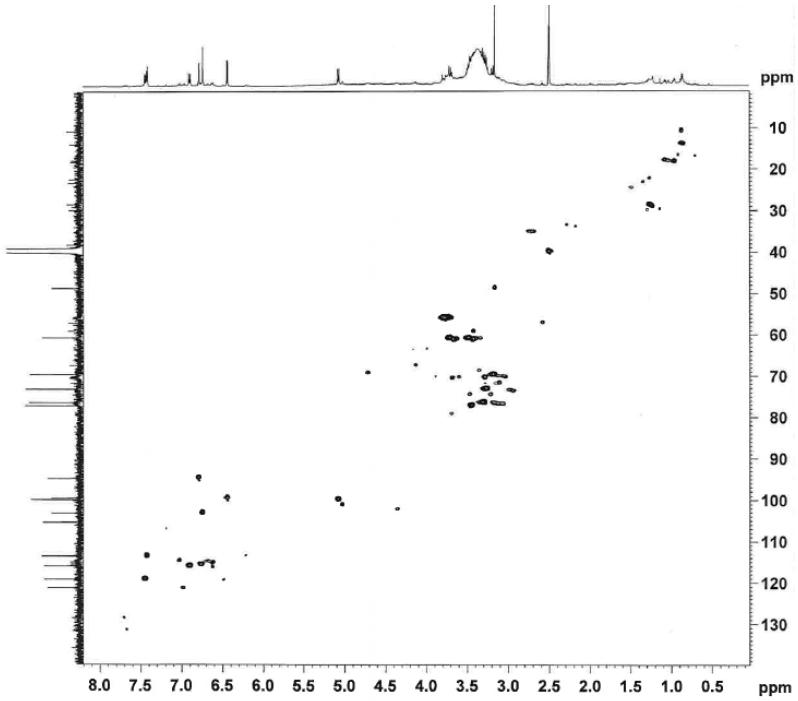

Appendix 8.5 HMBC spectrum of luteolin-7-*O*-glucopyranoside (500 MHz for ^{1}H, 125 MHz for ^{13}C; DMSO-d6)

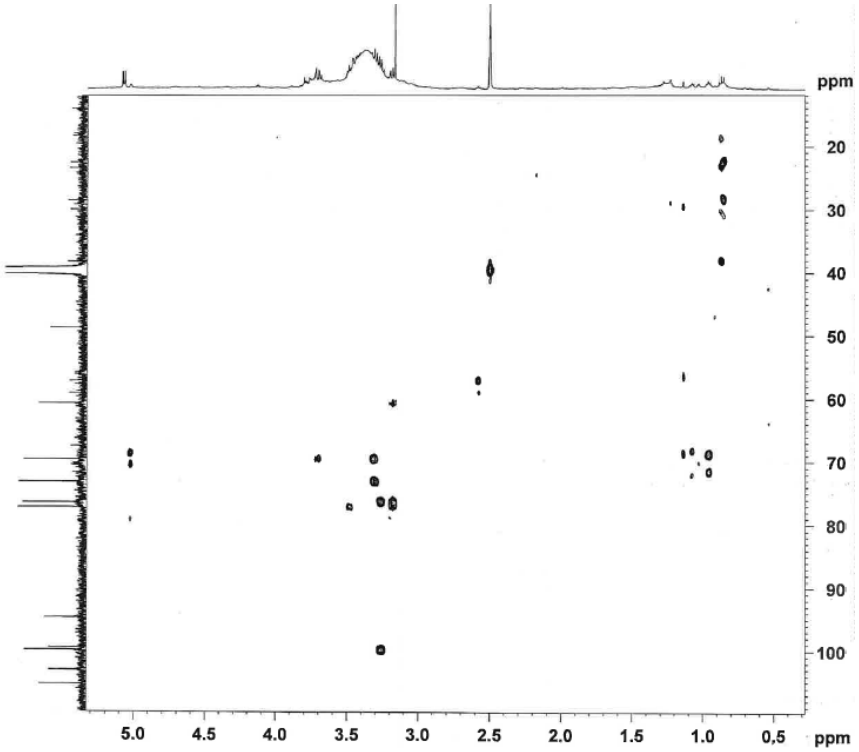

Appendix 8.6 NOESY spectrum of luteolin-7-*O*-glucopyranoside (500 MHz in DMSO-d6)

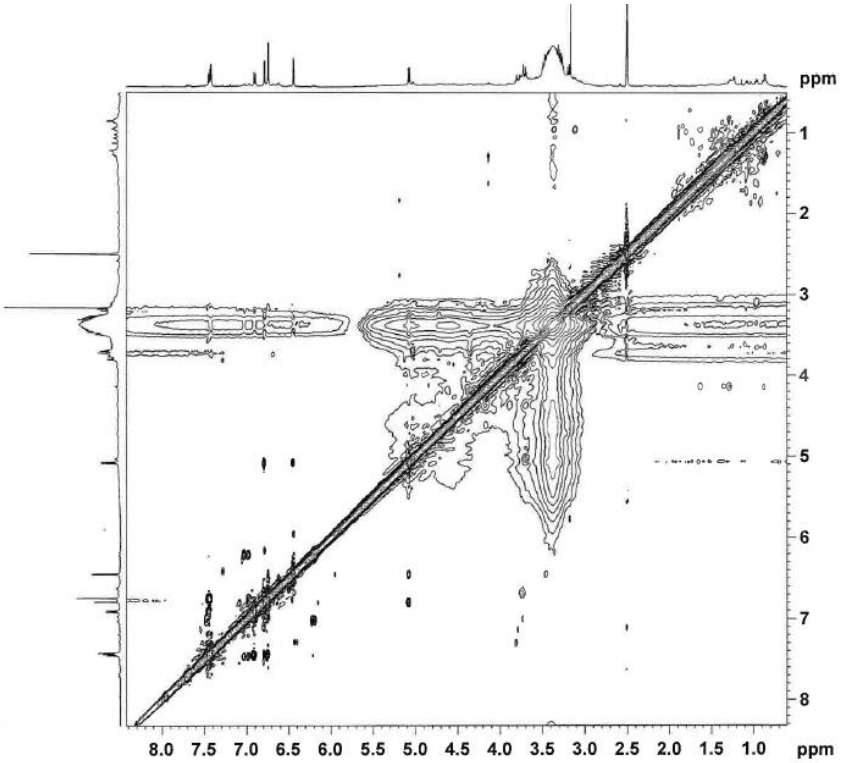

Appendix 9 NMR spectra of luteolin-7-*O*-galactopyranoside

*Judging from the NMR spectra, this material was about 90% pure.

Appendix 9.1 ^{1}H NMR spectrum of luteolin-7-*O*-galactopyranoside (500 MHz; CD_3OD)

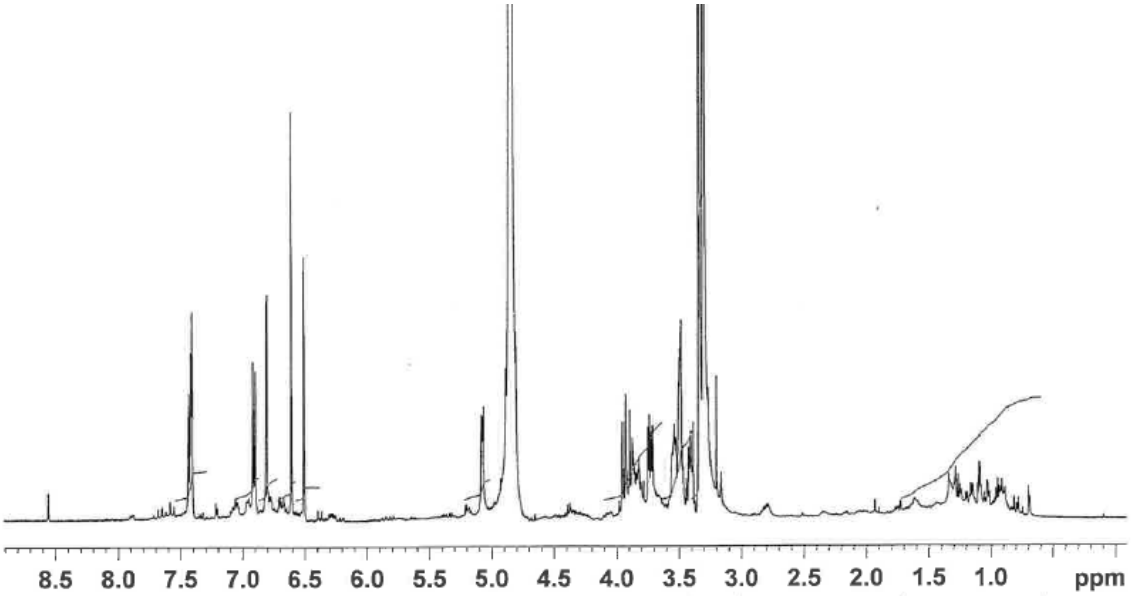

Appendix 9.2 COSY spectrum of luteolin-7-*O*-galactopyranoside (500 MHz; CD_3OD)

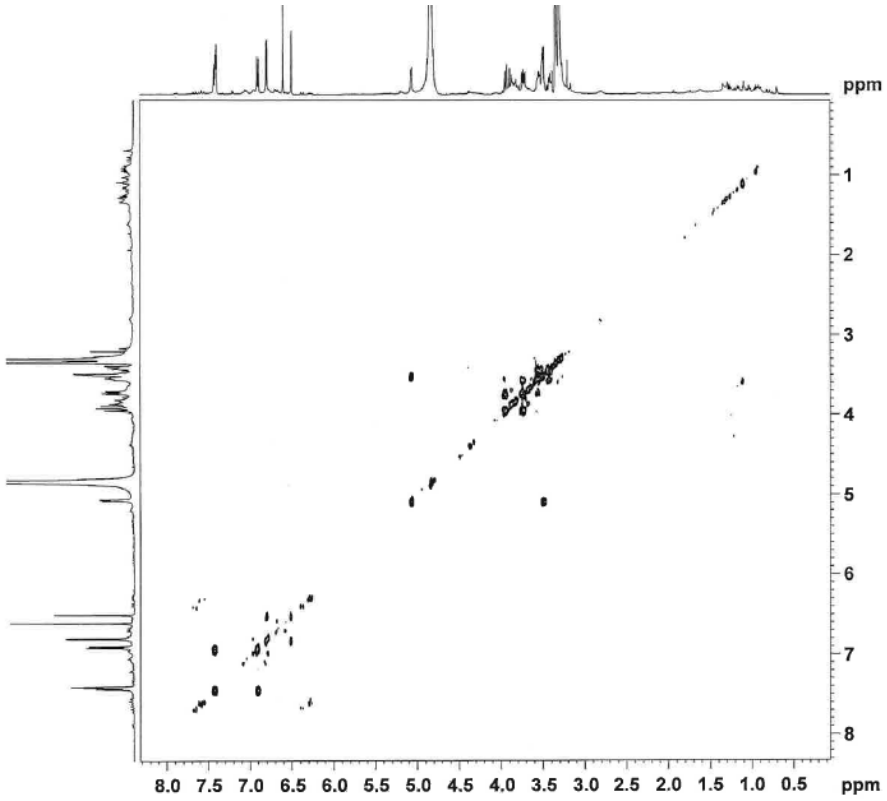

Appendix 9.3 ^{13}C NMR spectrum of luteolin-7-*O*-galactopyranoside (125 MHz; CD_3OD)

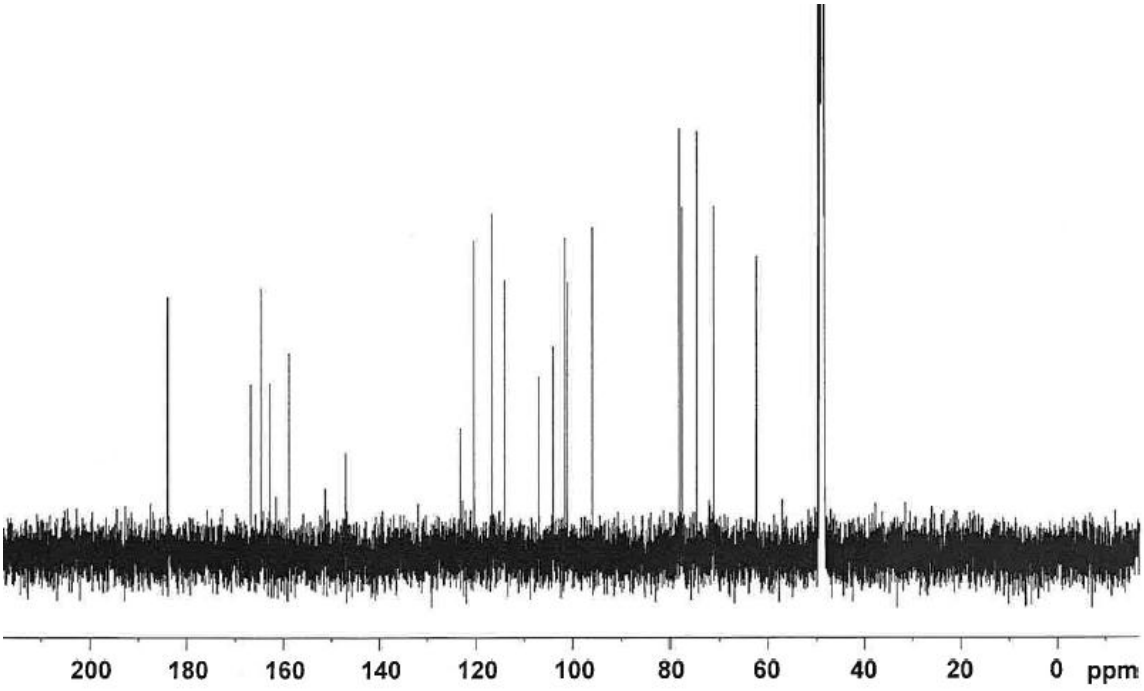

Appendix 9.4 HMQC spectrum of luteolin-7-*O*-galactopyranoside (500 MHz for ^{1}H, 125 MHz for ^{13}C; CD_3OD)

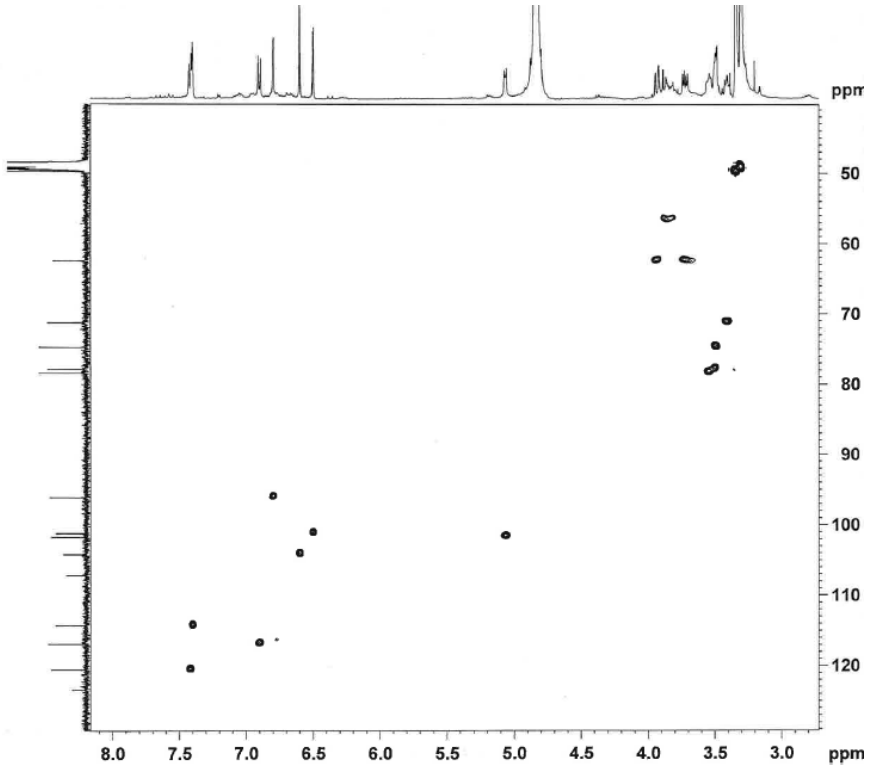

Appendix 9.5 HMBC spectrum of luteolin-7-*O*-galactopyranoside (500 MHz for ^{1}H, 125 MHz for ^{13}C; CD_3OD)

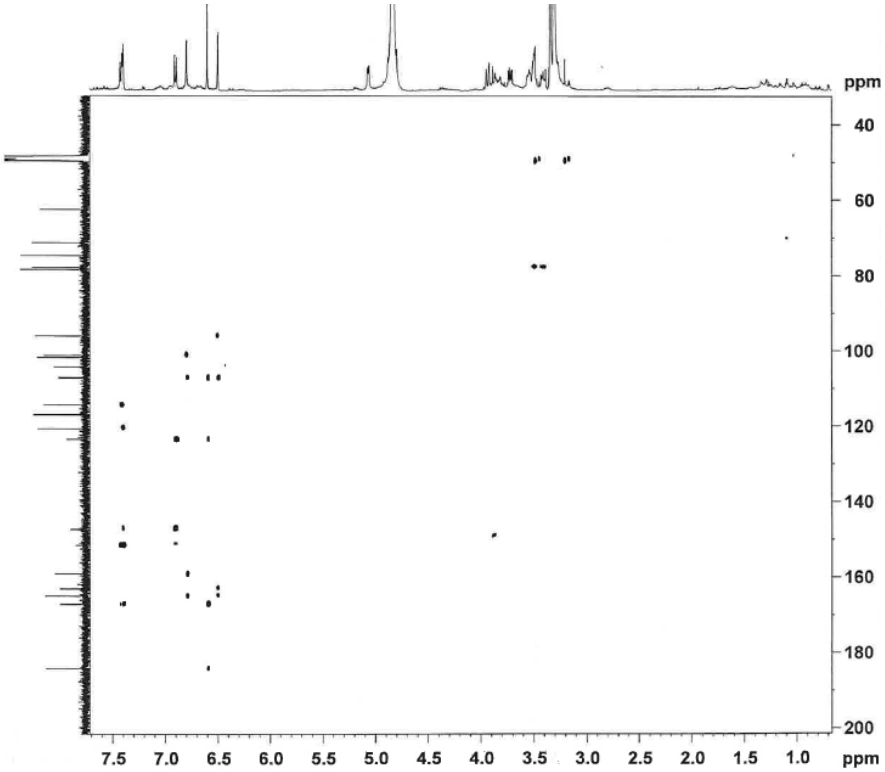

Appendix 9.6 NOESY spectrum of luteolin-7-*O*-galactopyranoside (500 MHz in CD_3OD)

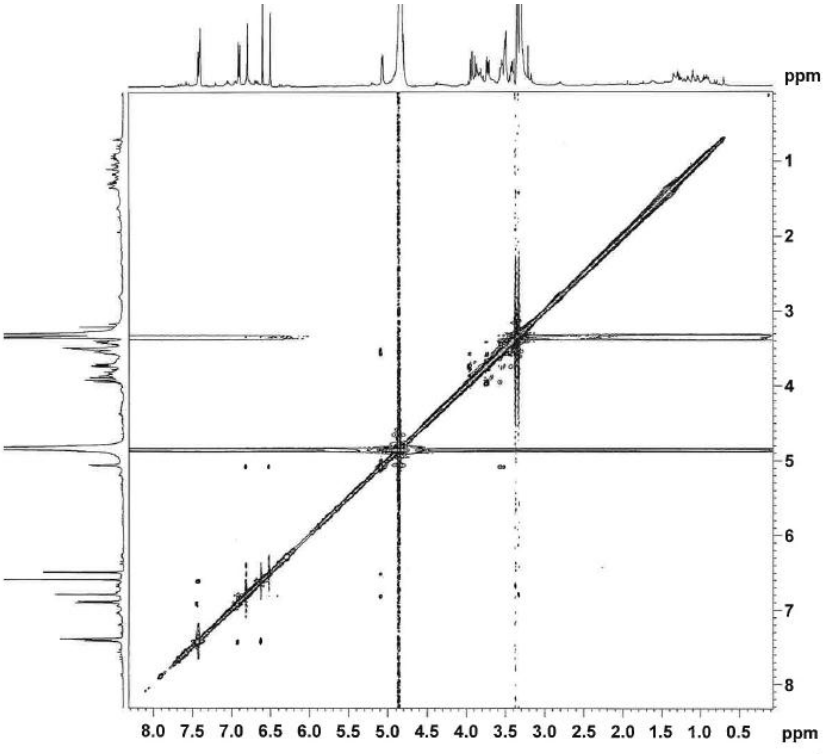

Appendix 10 NMR spectra of luteolin-7-*O*-rutinoside

Appendix 10.1 ^{1}H NMR spectrum of luteolin-7-*O* -rutinoside (500 MHz; DMSO-d6)

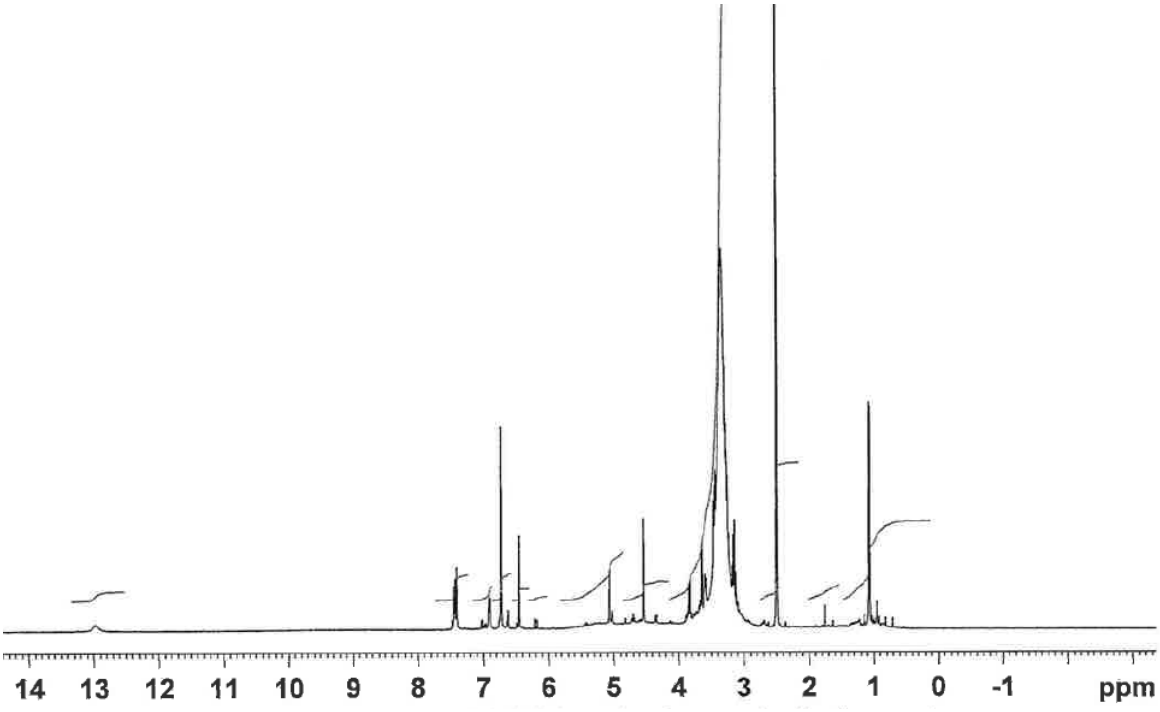

Appendix 10.2 COSY spectrum of luteolin-7-*O* -rutinoside (500 MHz; DMSO-d6)

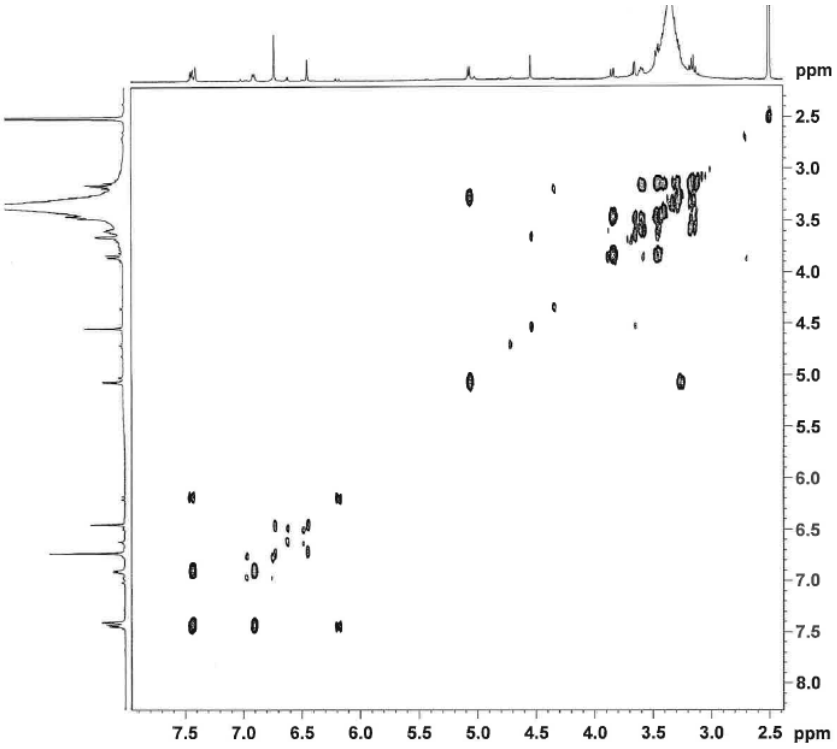

Appendix 10.3 ^{13}C NMR spectrum of luteolin-7-*O* -rutinoside (125 MHz; DMSO-d6)

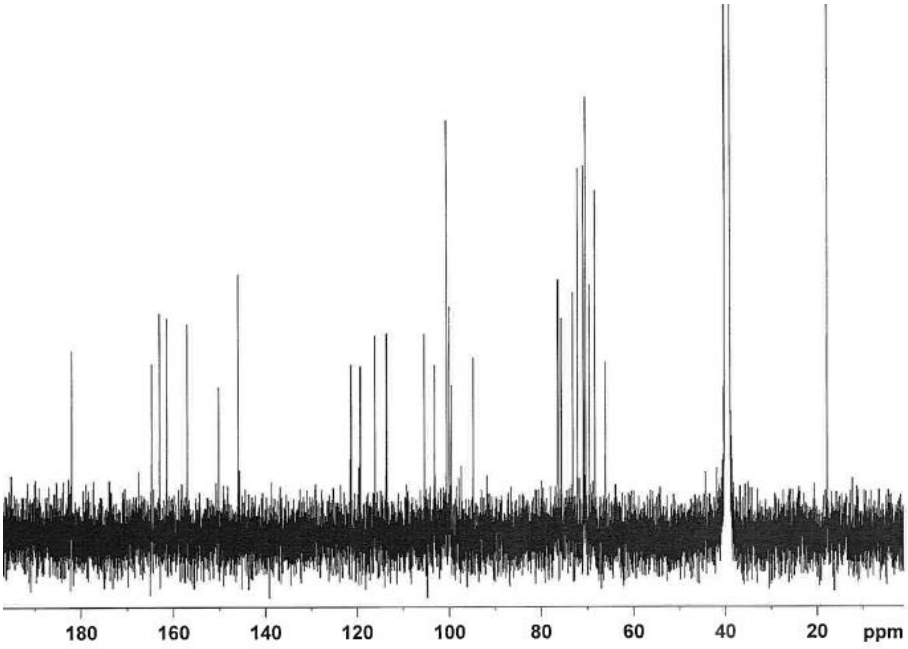

Appendix 10.4 HMQC spectrum of luteolin-7-*O*-rutinoside (500 MHz for ^{1}H, 125 MHz for ^{13}C; DMSO-d6)

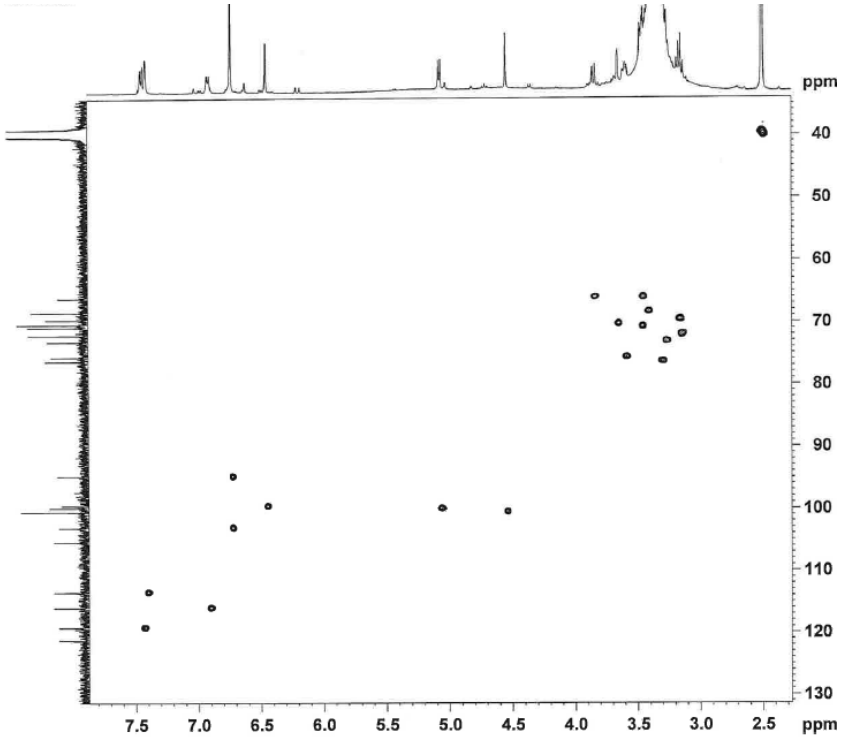

Appendix 10.5 HMBC spectrum of luteolin-7-*O*-rutinoside (500 MHz for ^{1}H, 125 MHz for ^{13}C; DMSO-d6)

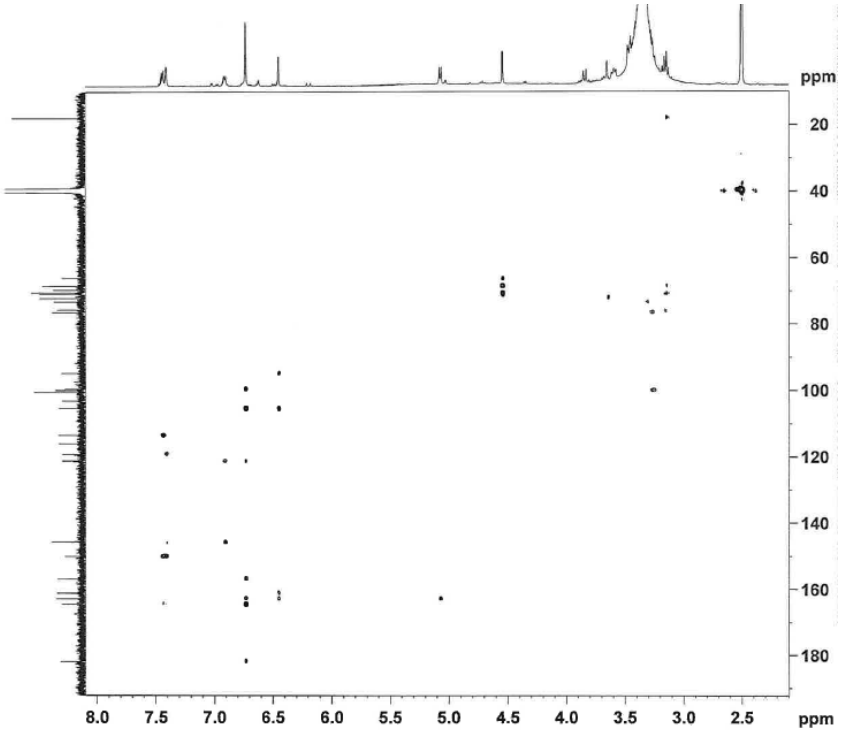

Appendix 10.6 NOESY spectrum of luteolin-7-*O* rutinoside (500 MHz; DMSO-d6)

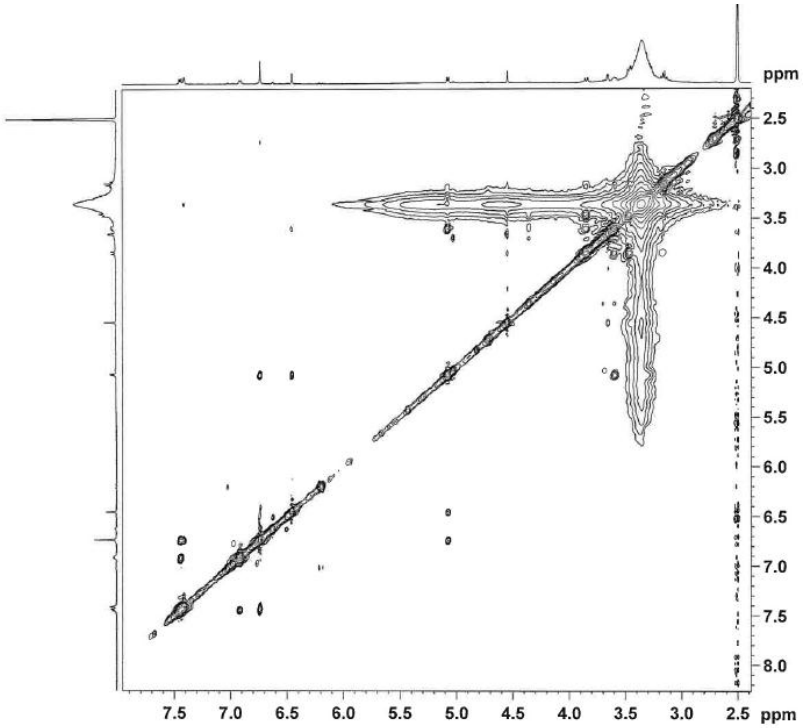

Appendix 11 NMR spectra of luteolin-7-*O*-α-rhamnopyranosyl-(1→6)-β-galactopyranoside

Appendix 11.1 ^{1}H NMR spectrum of luteolin-7-*O*-α-rhamnopyranosyl-(1→6)-β-galactopyranoside (500 MHz; CD_3OD)

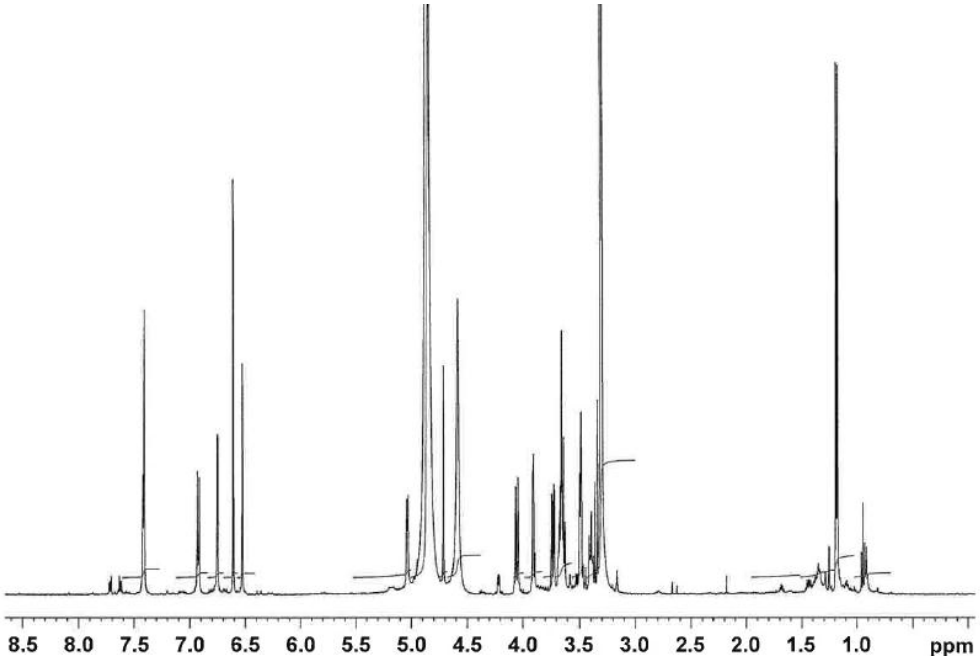

Appendix 11.2 COSY spectrum of luteolin-7-*O*-α--rhamnopyranosyl-(1→6)-β-galactopyranoside (500 MHz in CD_3OD)

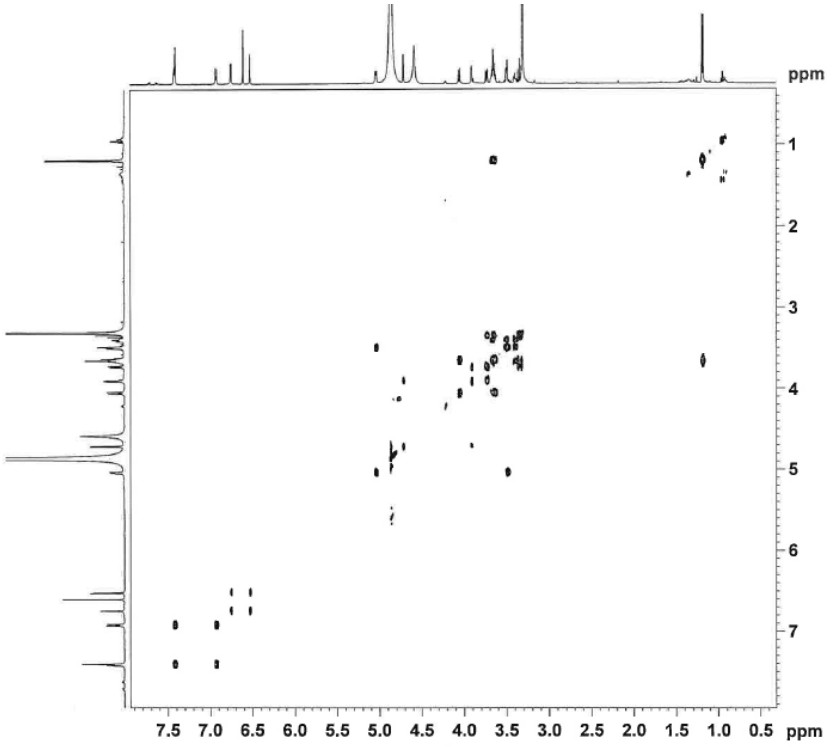

Appendix 11.3 ^{13}C NMR spectrum of luteolin-7-*O*-α-rhamnopyranosyl-(1→6)-β-galactopyranoside (125 MHz in CD_3OD)

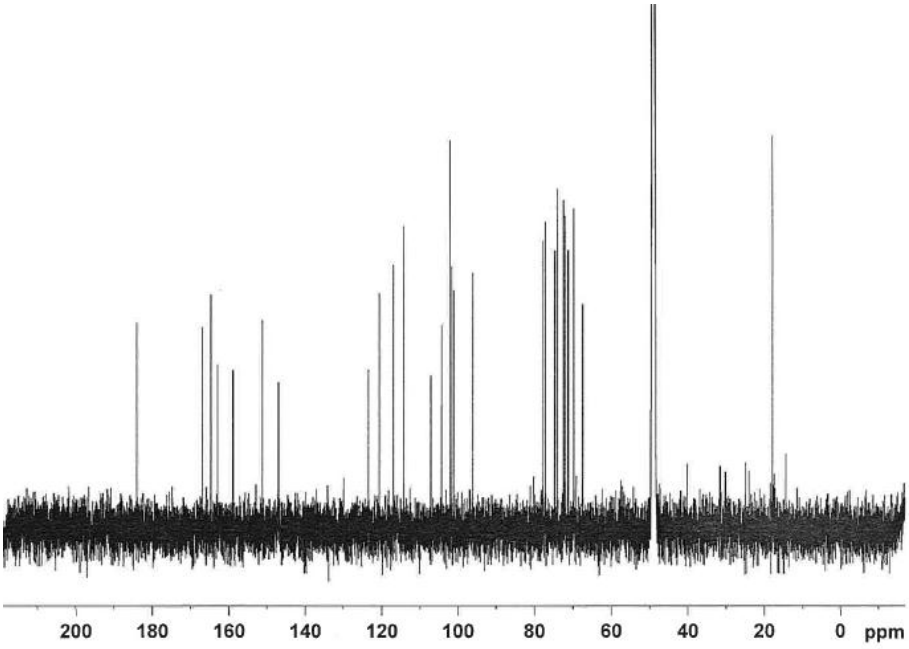

Appendix 11.4 HMQC spectrum of luteolin-7-*O*-α-rhamnopyranosyl-(1→6)-β-galactopyranoside (^1H, 500 MHz; ^{13}C, 125 MHz in CD_3OD)

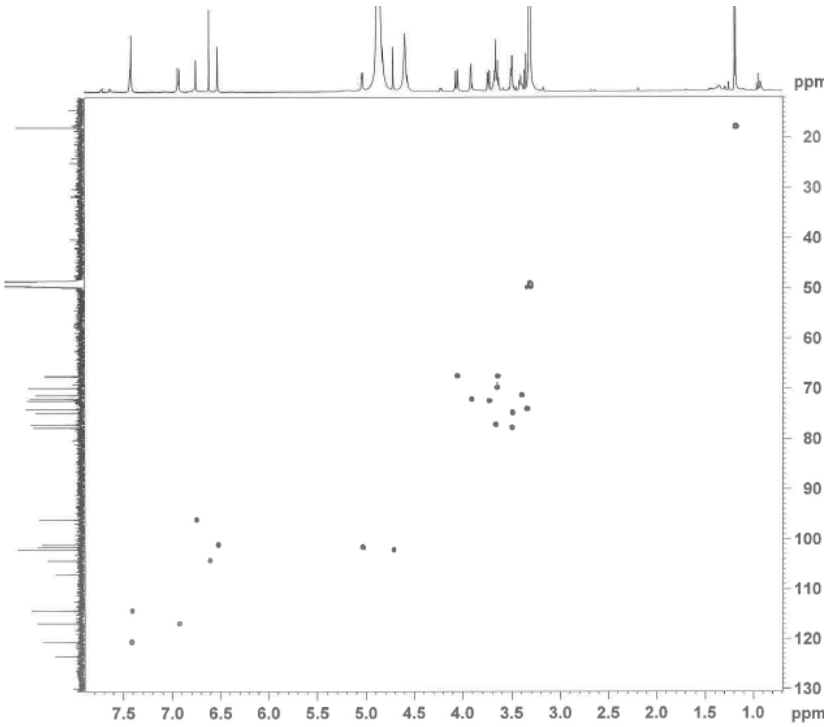

Appendix 11.5 HMBC spectrum of luteolin-7-*O*-α-rhamnopyranosyl-(1→6)-β-galactopyranoside (^{1}H, 500 MHz; ^{13}C, 125 MHz in CD_3OD)

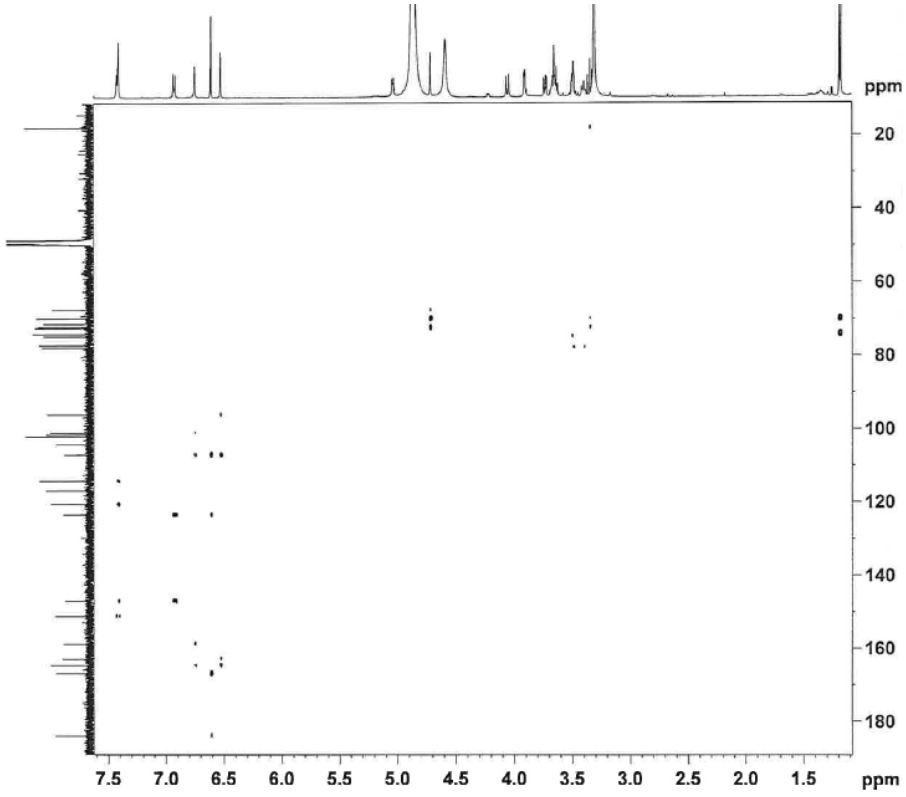

Appendix 11.6 NOESY spectrum of luteolin-7-*O*-α-rhamnopyranosyl-(1→6)-β-galactopyranoside (500 MHz in CD_3OD)

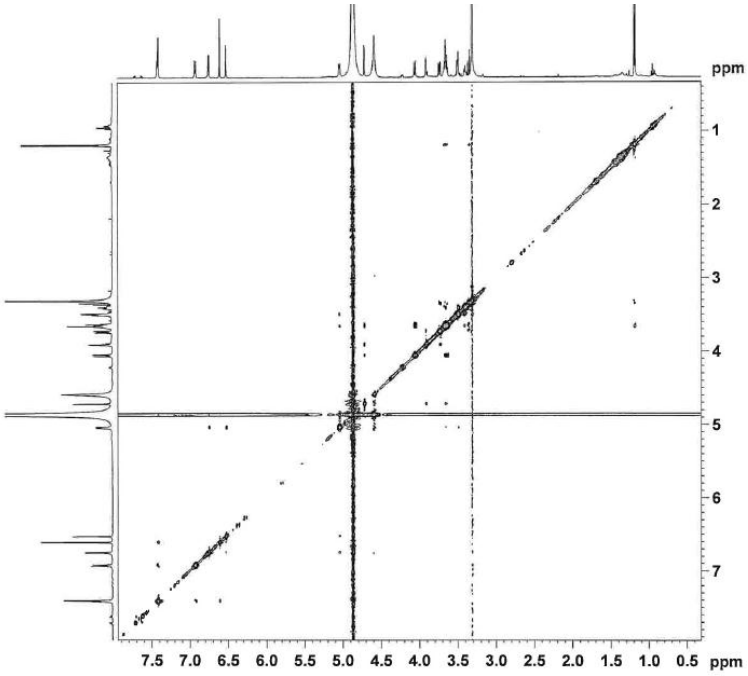

Appendix 12 NMR spectra of apigenin-7-*O*-glucopyranoside

Appendix 12.1 ^{1}H NMR spectrum of apigenin-7-*O*-glucopyranoside (500 MHz; CD_3OD)

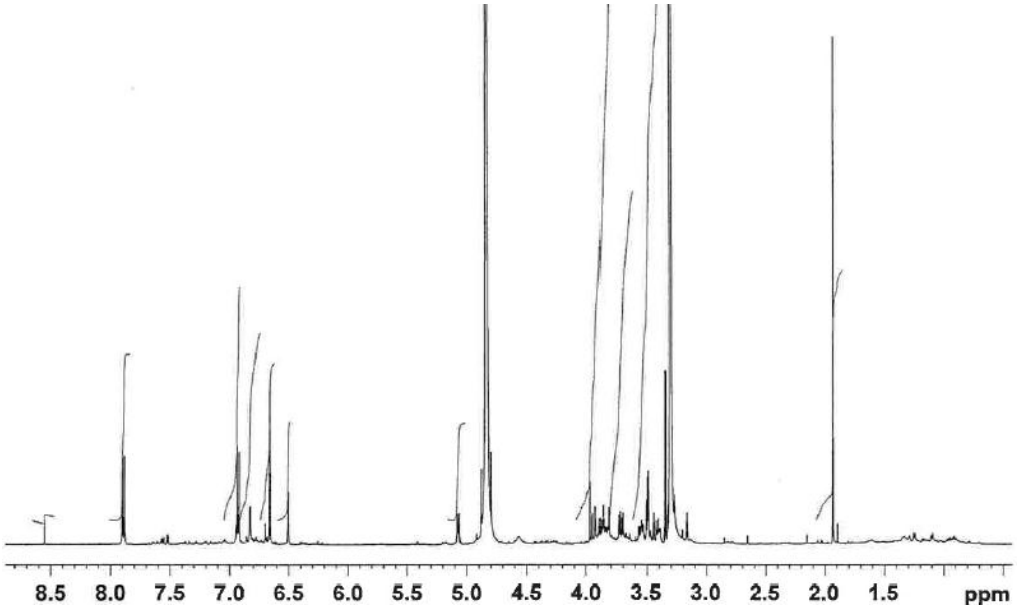

Appendix 12.2 COSY spectrum of apigenin-7-*O*-glucopyranoside (500 MHz in CD_3OD)

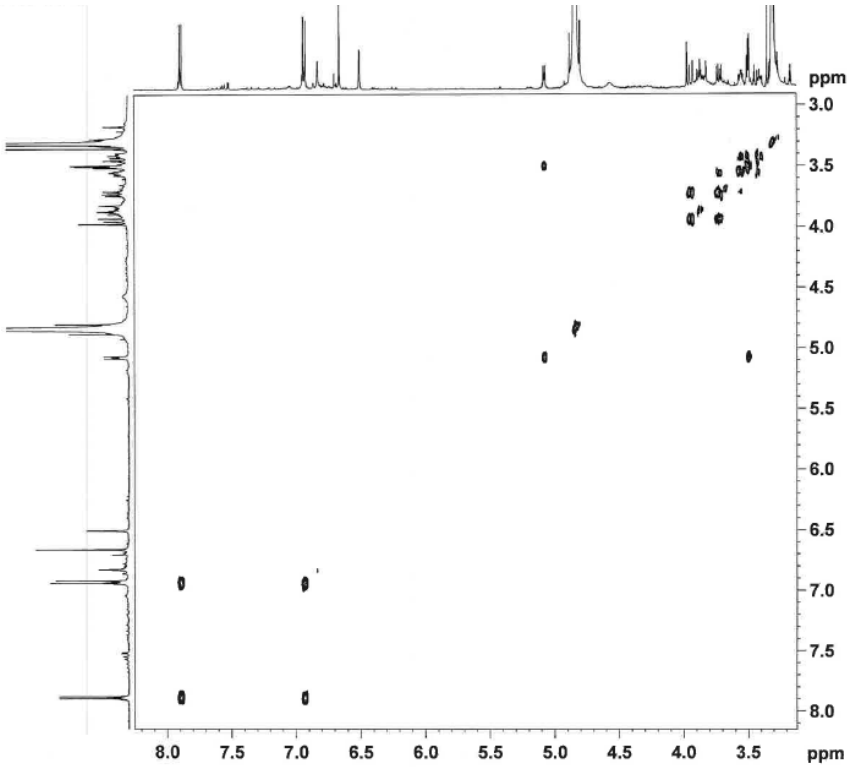

Appendix 12.3 ^{13}C NMR spectrum of apigenin-7-*O*-glucopyranoside (125 MHz; CD_3OD)

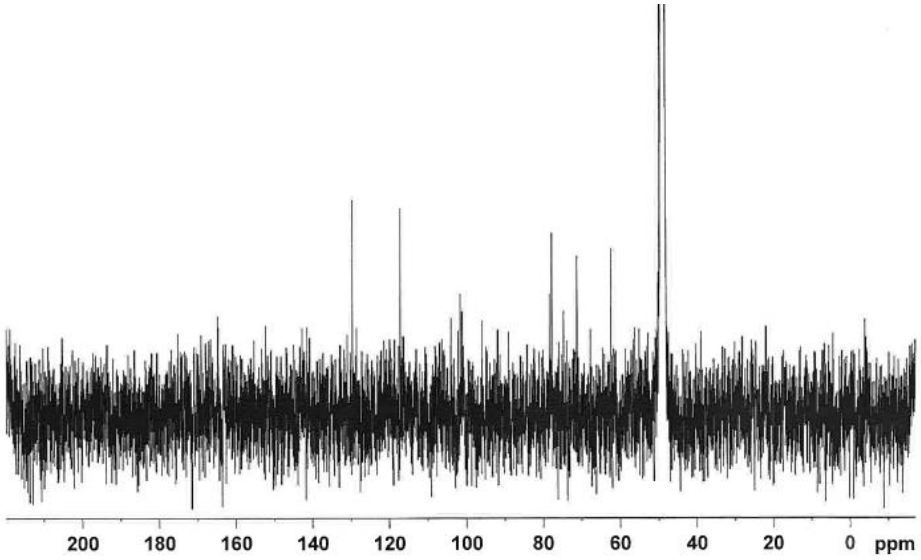

Appendix 12.4 HMQC spectrum of apigenin-7-*O*-glucopyranoside (500 MHz for ^{1}H, 125 MHz for ^{13}C; CD_3OD)

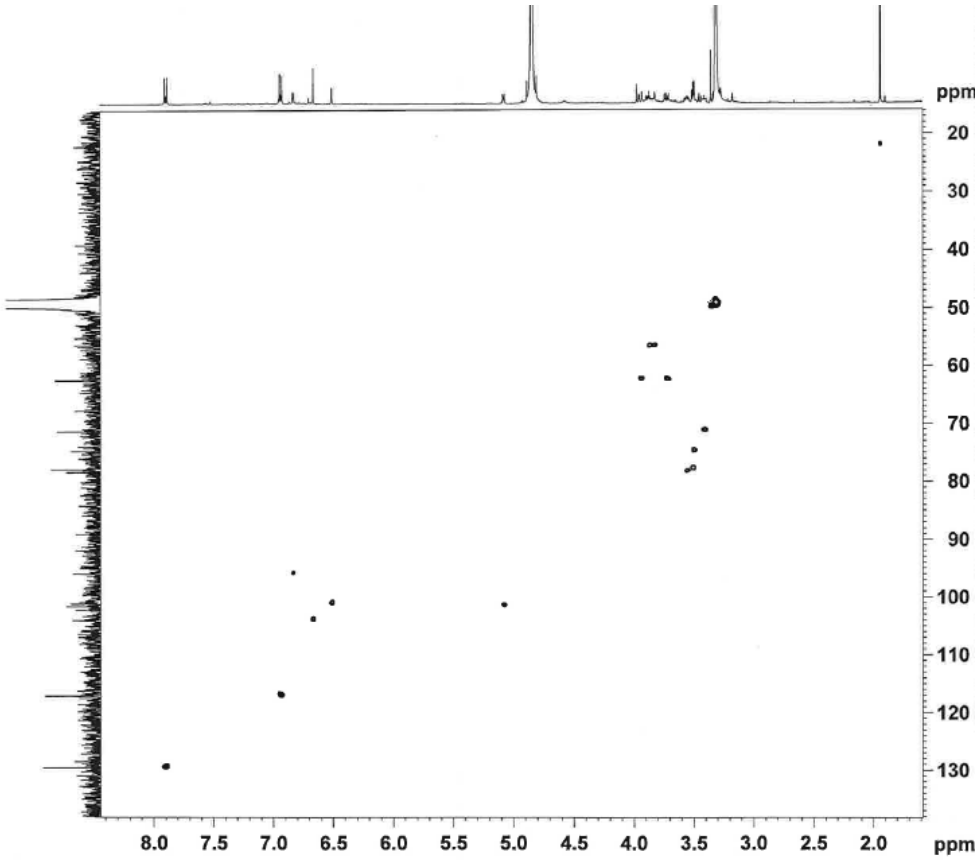

Appendix 12.5 HMBC spectrum of apigenin-7-*O*-glucopyranoside (^{1}H, 500, MHz; ^{13}C, 125 MHz in CD_3OD)

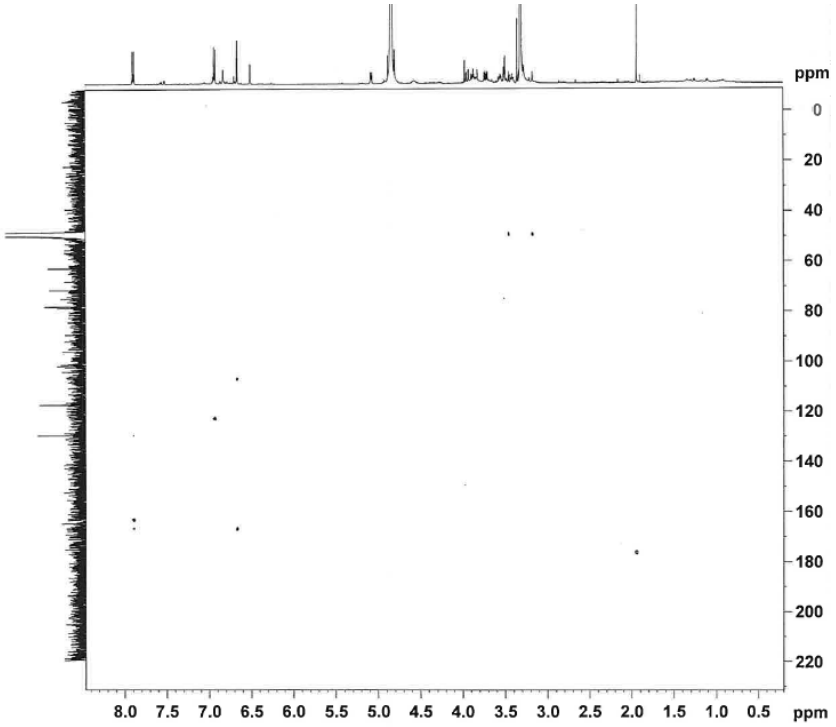

Appendix 12.6 NOESY spectrum of apigenin-7-*O*-glucopyranoside (500 MHz; CD_3OD)

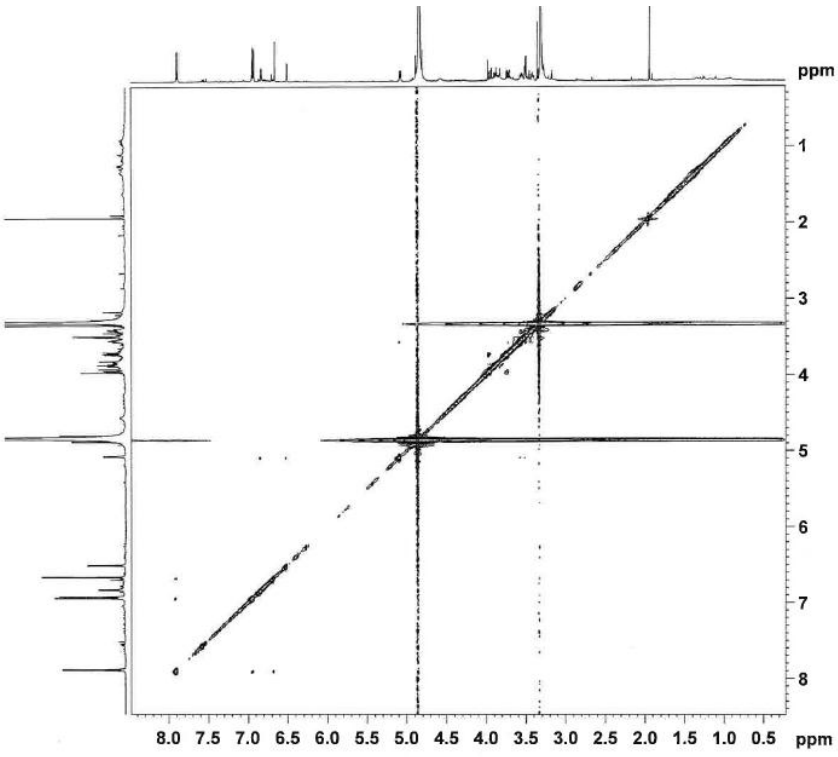

Appendix 13 NMR spectra of ursolic acid

Appendix 13.1 ^{1}H NMR spectrum of ursolic acid (500 MHz; a mixture of CD_3OD and $CDCl_3$)

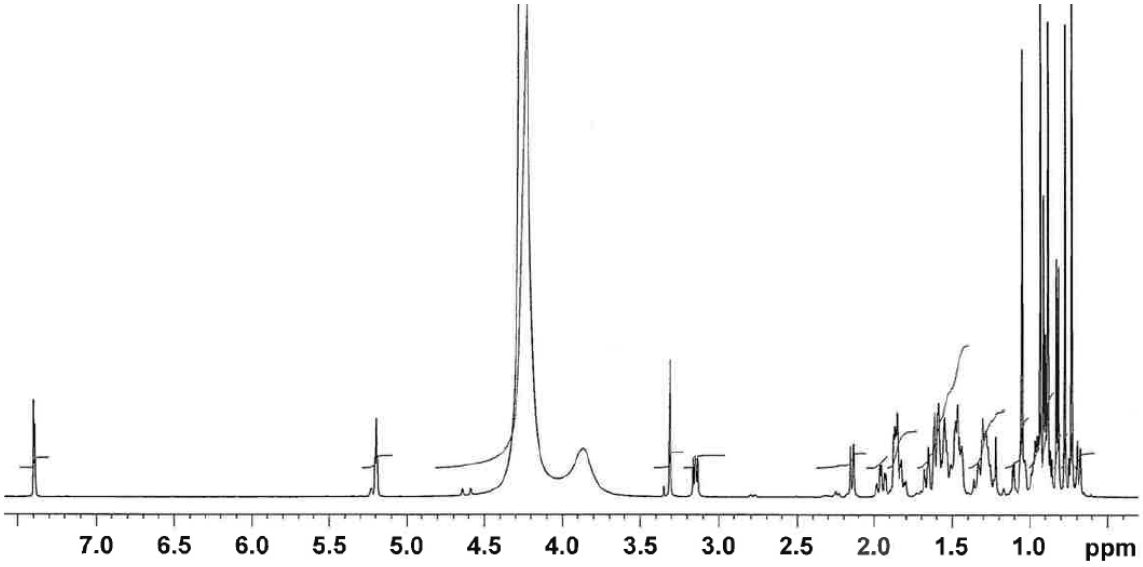

Appendix 13.2 COSY spectrum of ursolic acid (500 MHz; a mixture of CD_3OD and $CDCl_3$)

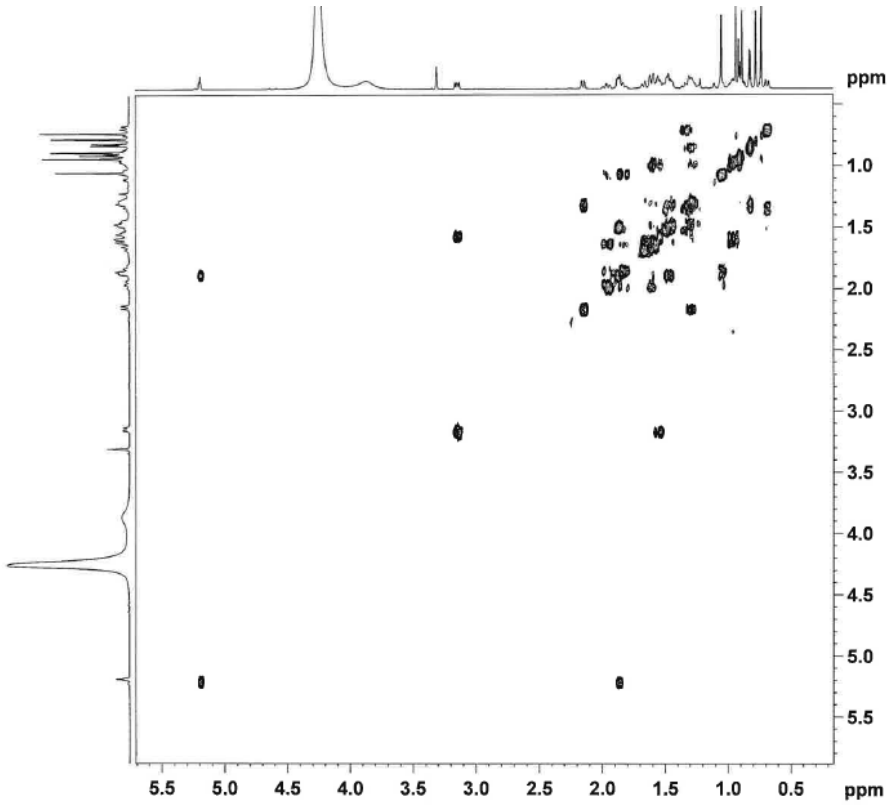

Appendix 13.3 ^{13}C NMR spectrum of ursolic acid (125 MHz; a mixture of CD_3OD and $CDCl_3$)

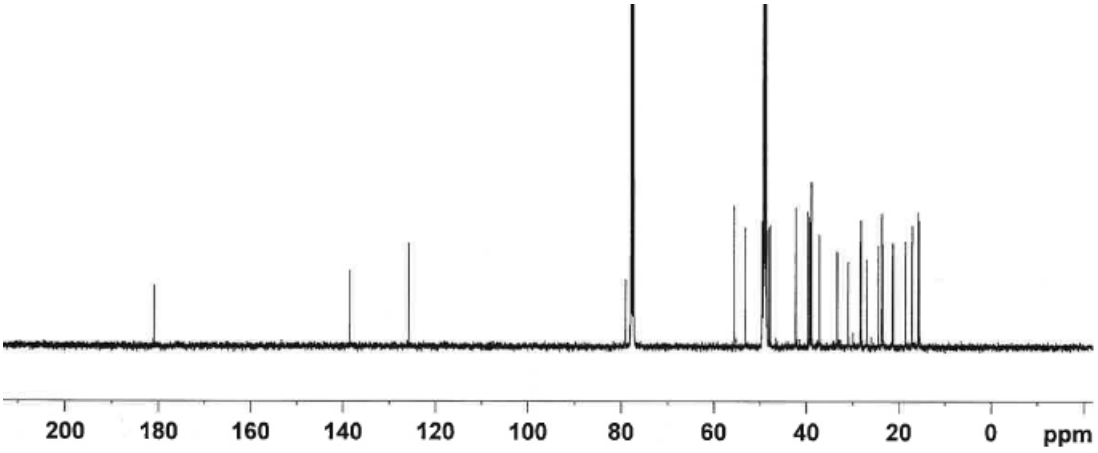

Appendix 13.4 HMQC spectrum of ursolic acid (500 MHz for ^{1}H, 125 MHz for ^{13}C 125 MHz; a mixture of CD_3OD and $CDCl_3$)

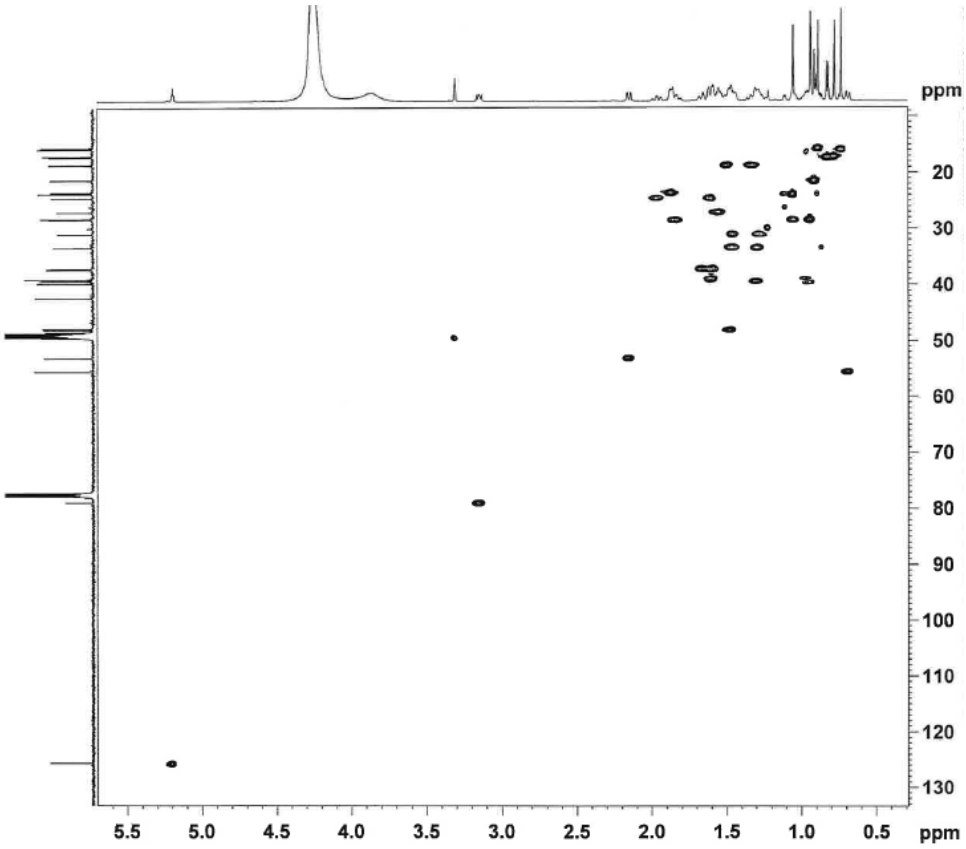

Appendix 13.5 HMBC spectrum of ursolic acid (500 MHz for ^{1}H, 125 MHz for ^{13}C 125 MHz; a mixture of CD_3OD and $CDCl_3$)

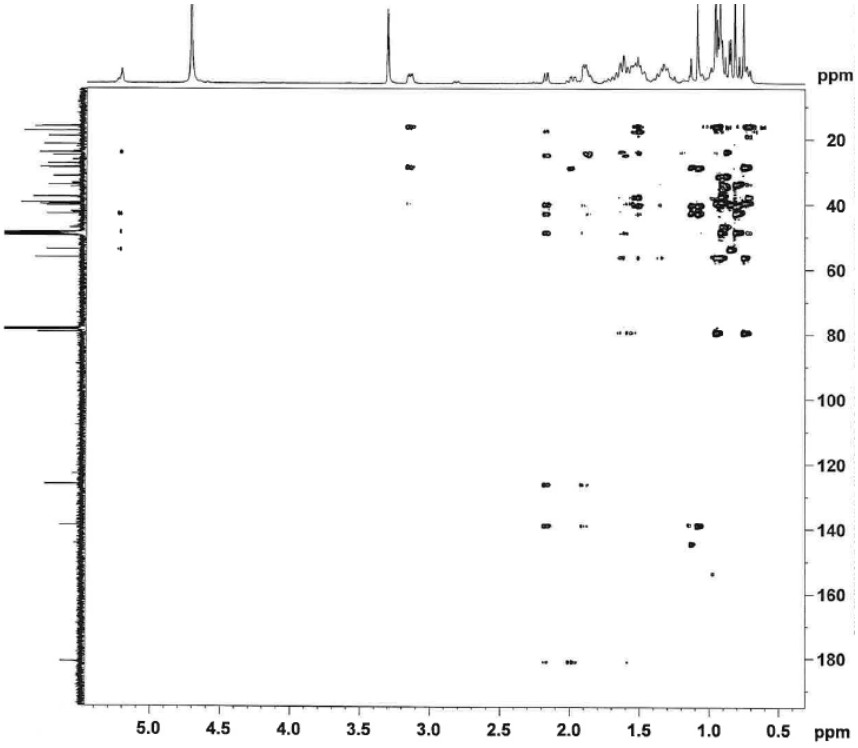

Appendix 13.6 NOESY of ursolic acid (500 MHz; a mixture of CD_3OD and $CDCl_3$)

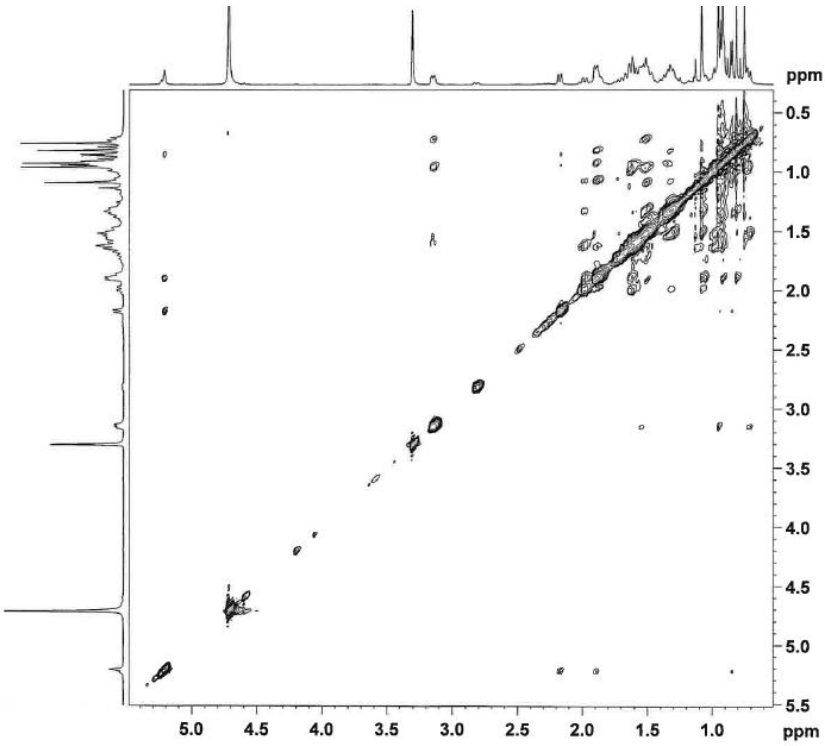

Appendix 14 NMR spectra of oleanolic acid

*Judging from the NMR spectra, this sample was about 70% pure, with ursolic acid as the major impurity.

Appendix 14.1 ^{1}H NMR spectrum of oleanolic acid (500 MHz; a mixture of CD_3OD and $CDCl_3$)

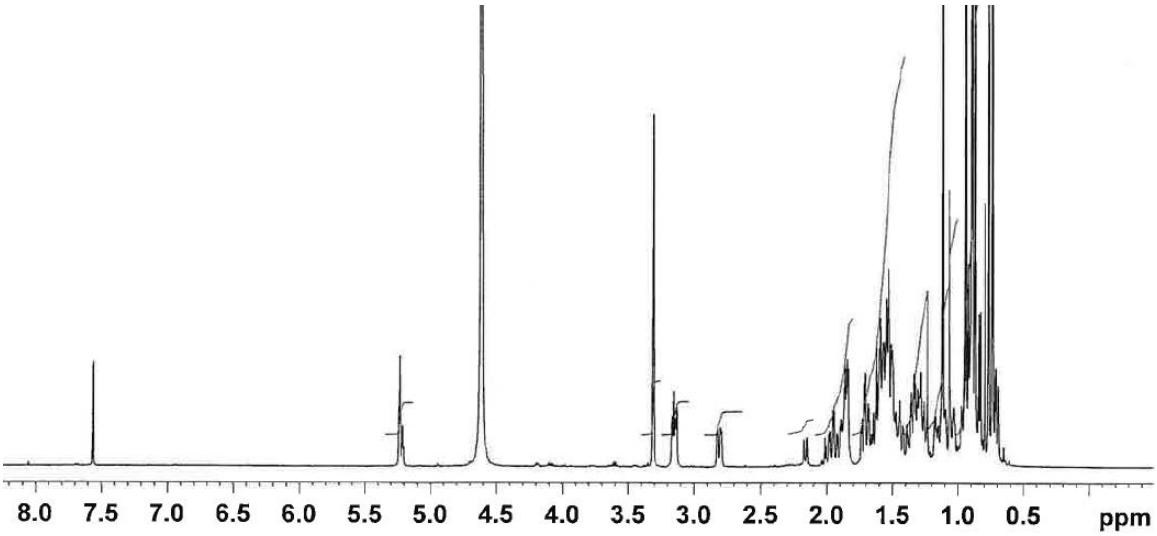

Appendix 14.2 COSY spectrum of oleanolic acid (500 MHz; a mixture of CD_3OD and $CDCl_3$)

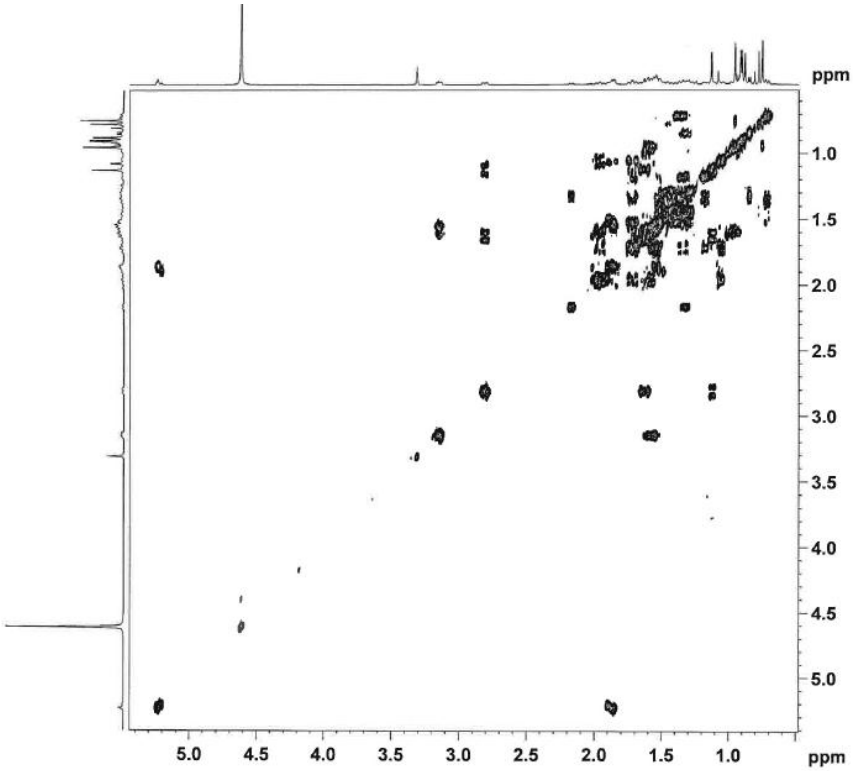

Appendix 14.3 ^{13}C NMR spectrum of oleanolic acid (125 MHz; a mixture of CD_3OD and $CDCl_3$)

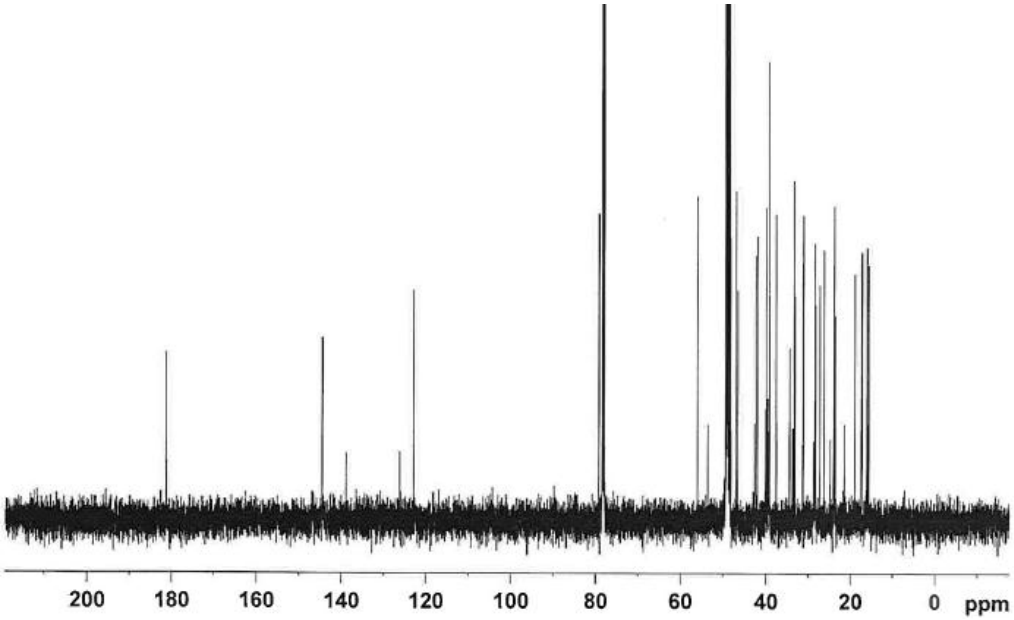

Appendix 14.4 HMQC spectrum of oleanolic acid (500 MHz for ^{1}H, 125 MHz for ^{13}C 125 MHz; a mixture of CD_3OD and $CDCl_3$)

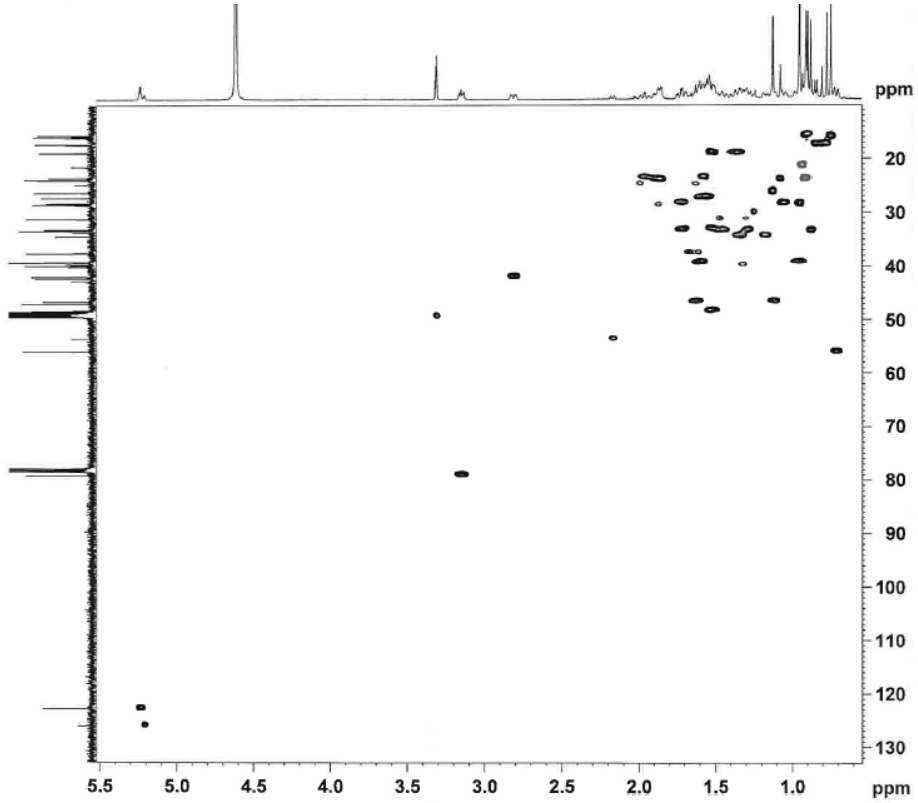

Appendix 14.5 HMBC spectrum of oleanolic acid (500 MHz for ^{1}H, 125 MHz for ^{13}C 125 MHz; a mixture of CD_3OD and $CDCl_3$)

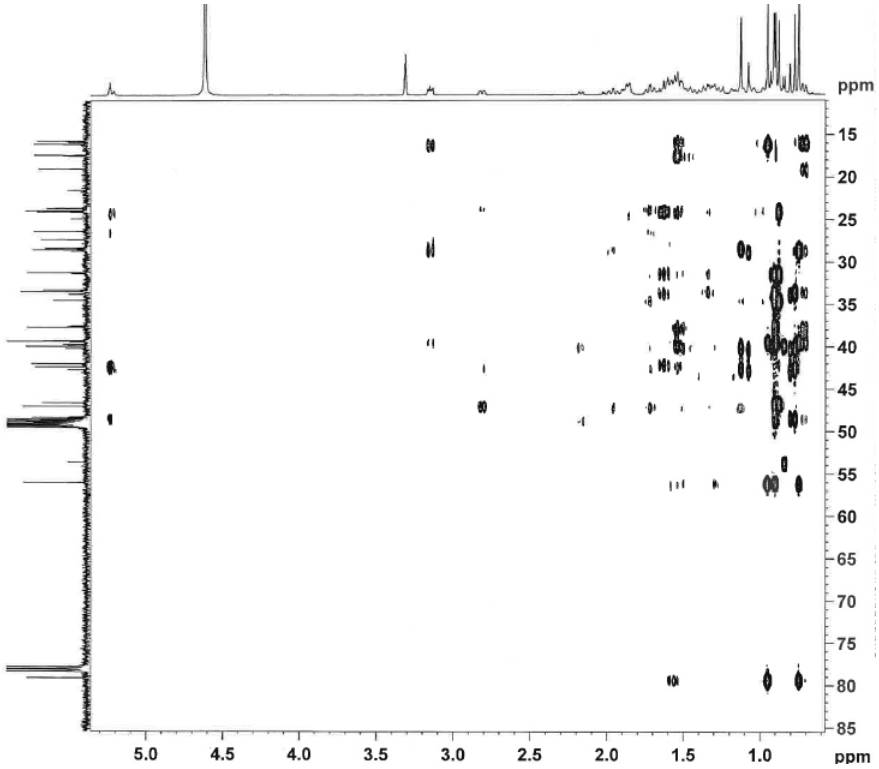

Appexdix 14.6 NOESY spectrum of oleanolic acid (500 MHz; a mixture of CD_3OD and $CDCl_3$)

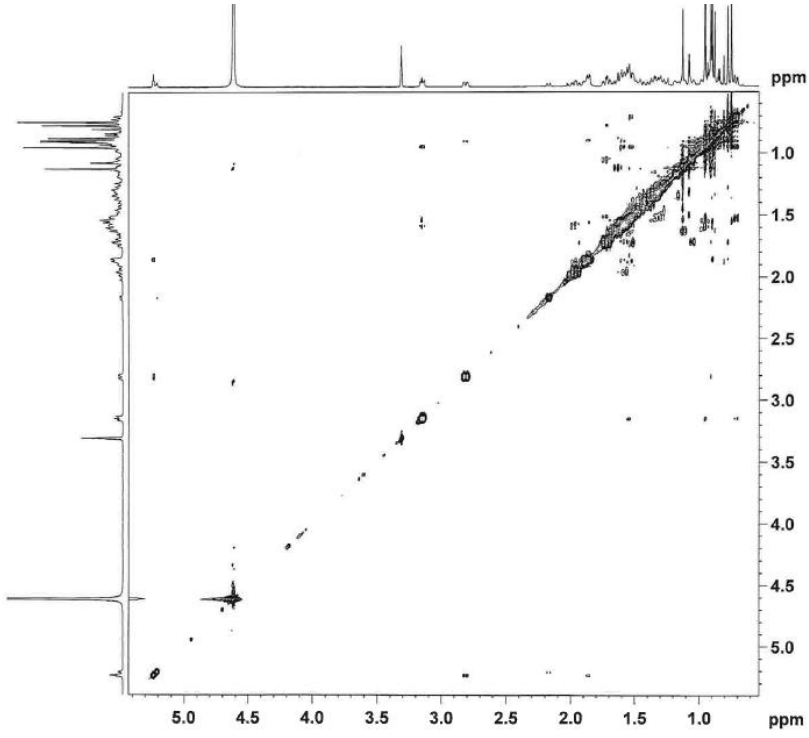

Appendix 15 NMR spectra of lup-(20)29-ene-2α,3β-diol

Appendix 15.1 ^{1}H NMR spectrum of lup-(20)29-ene-2α,3β-diol (500 MHz; $CDCl_3$)

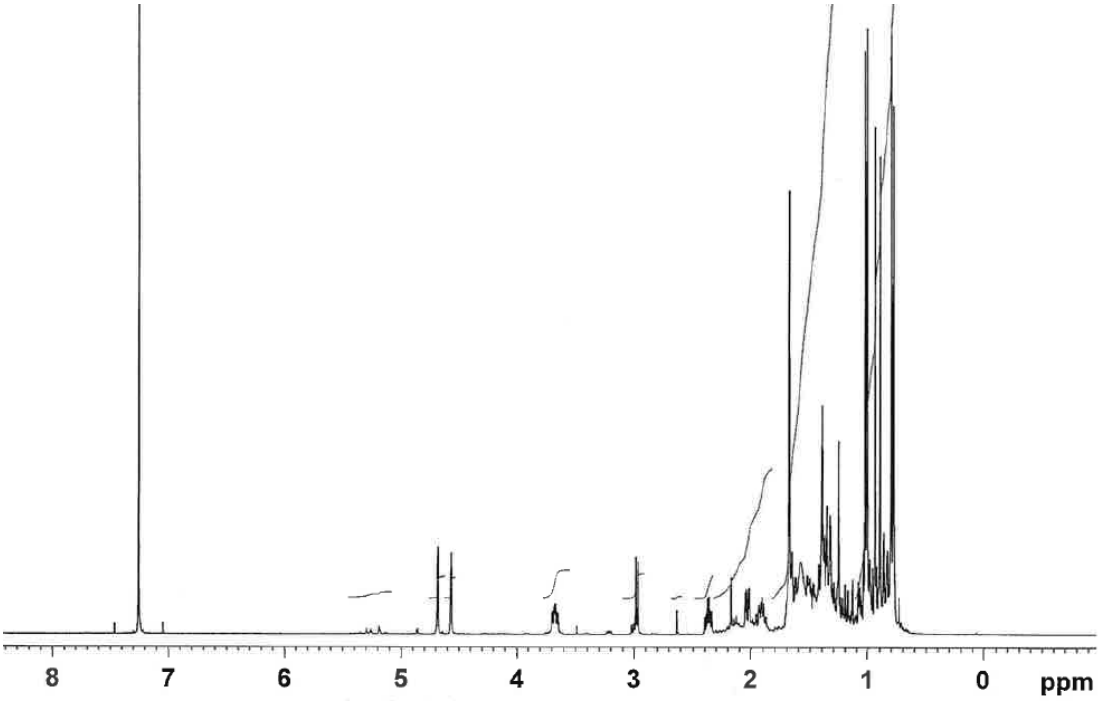

Appendix 15.2 COSY spectrum of lup-(20)29-ene-2α,3β-diol (500 MHz; $CDCl_3$)

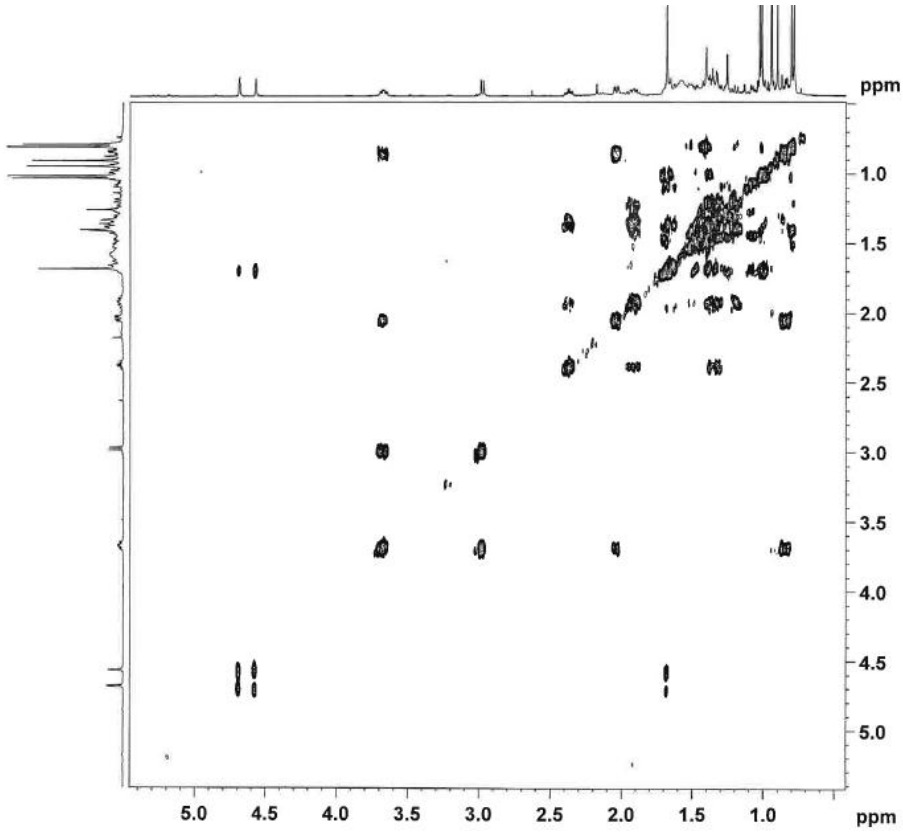

Appendix 15.3 ^{13}C NMR spectrum of lup-(20)29-ene-2α,3β-diol (125 MHz; $CDCl_3$)

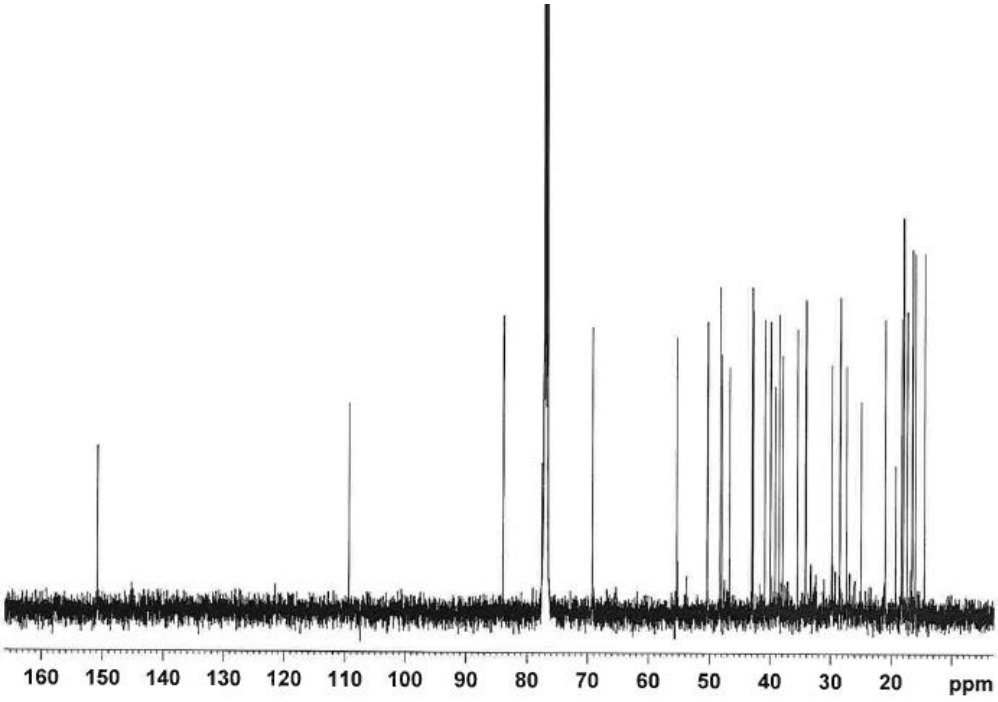

Appendix 15.4 HMQC spectrum of lup-(20)29-ene-2α,3β-diol (500 MHz for ^{1}H, 125 MHz for ^{13}C 125 MHz; $CDCl_3$)

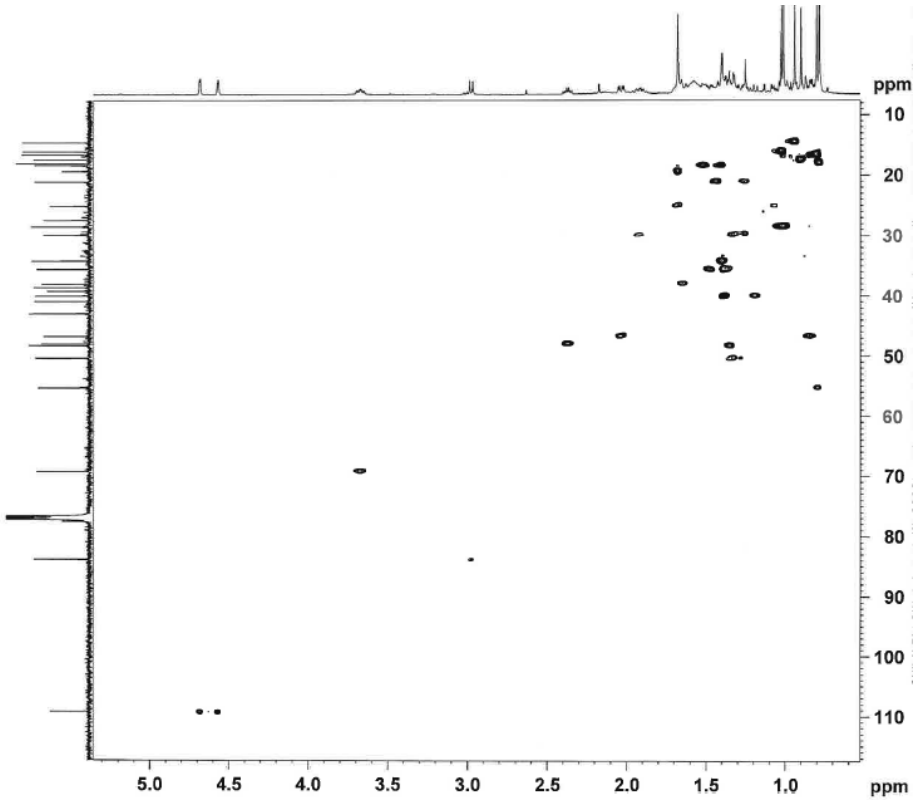

Appendix 15.5 HMBC spectrum of lup-(20)29-ene-2α,3β-diol (500 MHz for ^{1}H, 125 MHz for ^{13}C 125 MHz; $CDCl_3$)

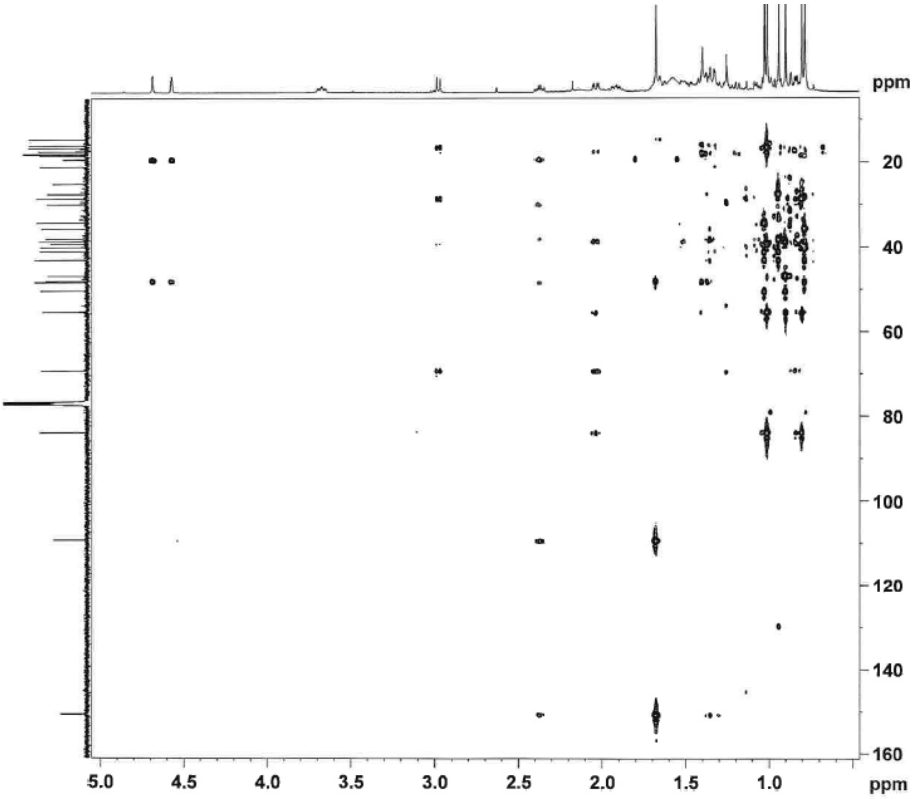

Appendix 15.6 NOESY spectrum of lup-(20)29-ene-2α,3β-diol (500 MHz; $CDCl_3$)

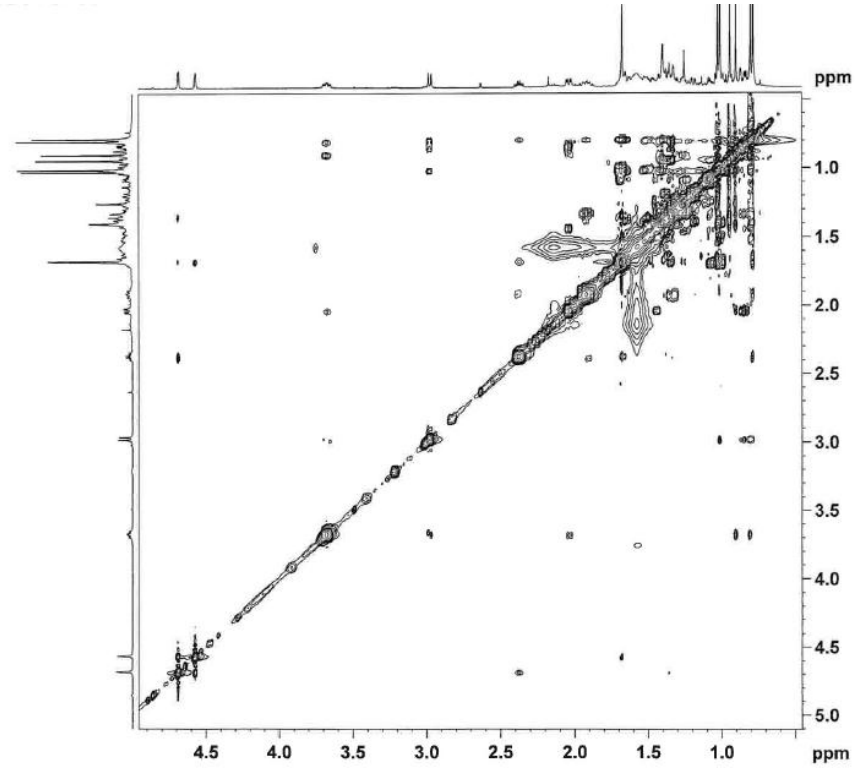

Appendix 16 NMR spectra of compound 1 (lup-(20)29-ene-2α-acetate-3β-ol)

*Judging from the NMR spectra, this sample was about 95% pure.

Appendix 16.1 ^{1}H NMR of compound 1 (lup-(20)29-ene-2α-acetate-3β-ol) (500 MHz; $CDCl_3$)

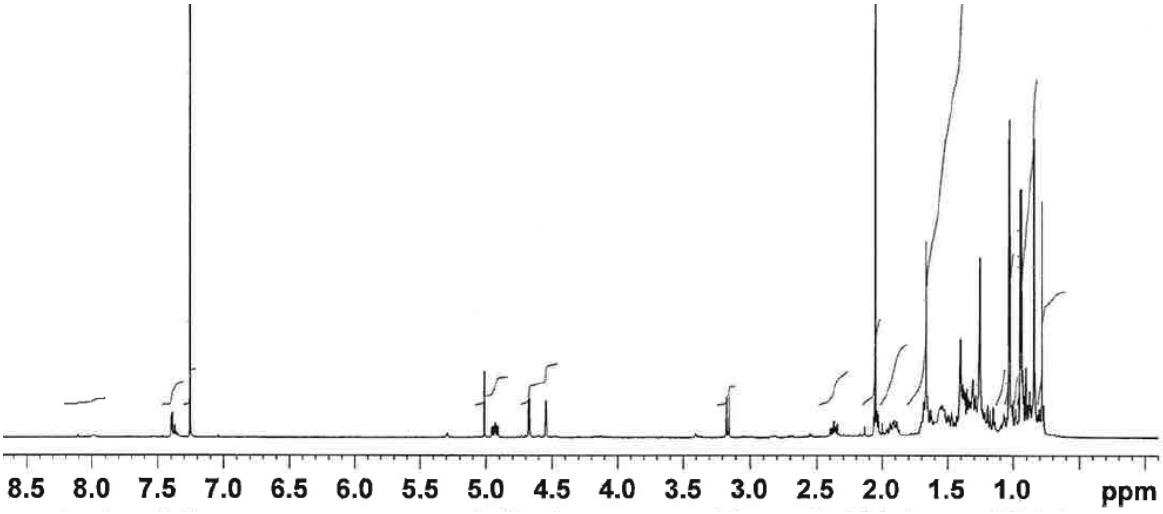

Appendix 16.2 COSY spectrum of compound 1 (lup-(20)29-ene-2α-acetate-3β-ol) (500 MHz in $CDCl_3$)

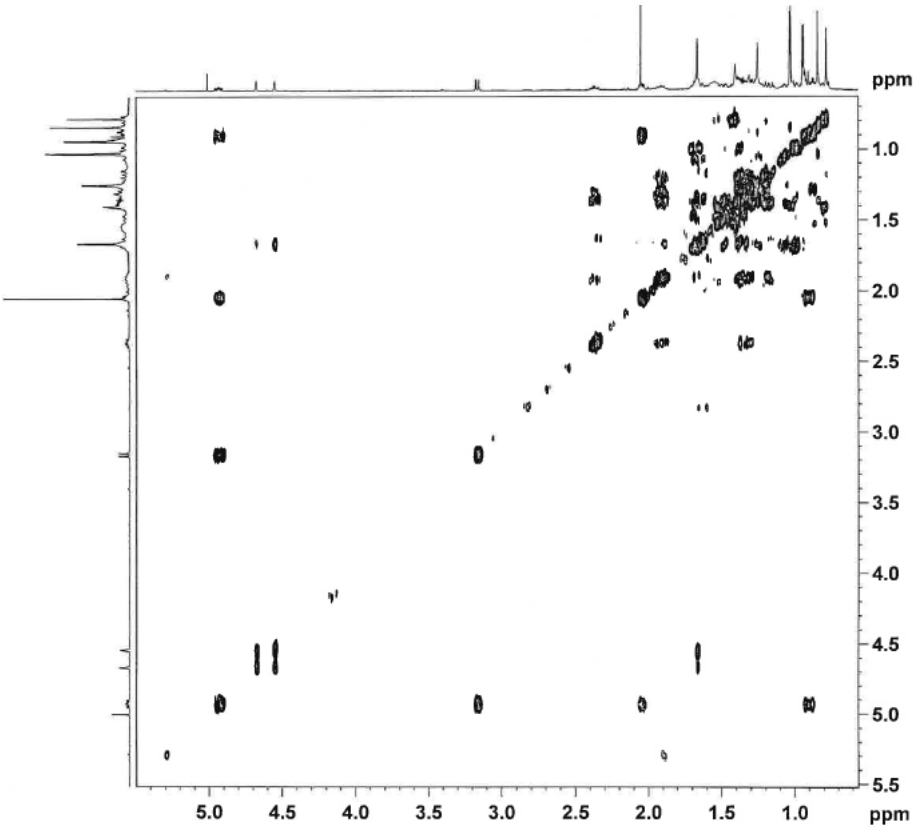

Appendix 16.3 ^{13}C NMR of compound 1 (lup-(20)29-ene-2α-acetate-3β-ol) (125 MHz; $CDCl_3$)

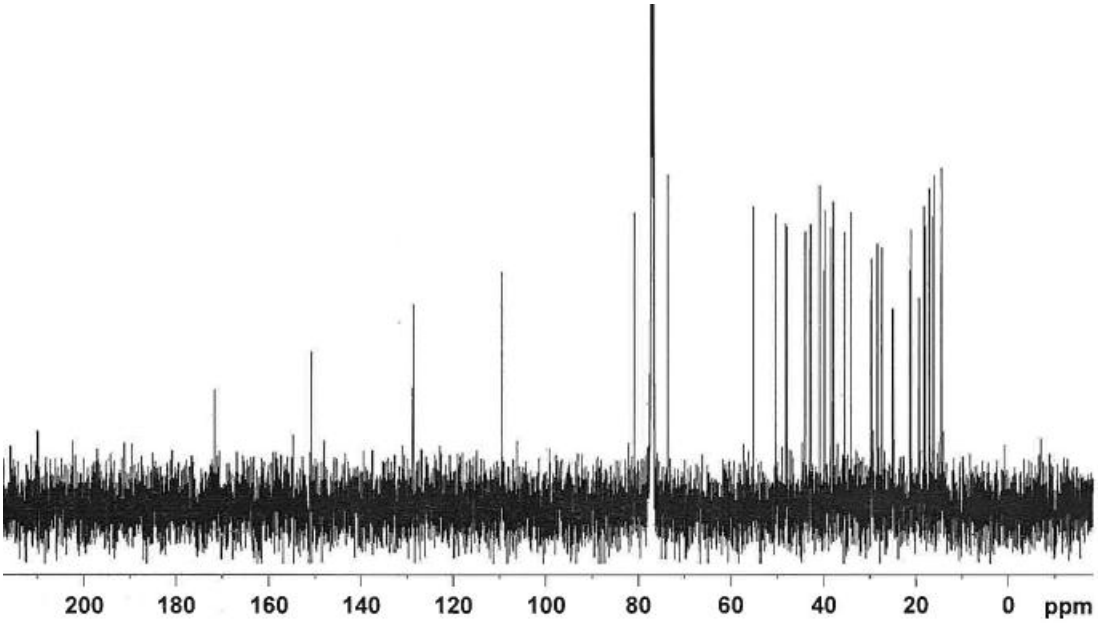

Appendix 16.4 HMQC spectrum of compound 1 (lup-(20)29-ene-2α-acetate-3β-ol) (500 MHz for ^{1}H, 125 MHz for ^{13}C 125 MHz; $CDCl_3$)

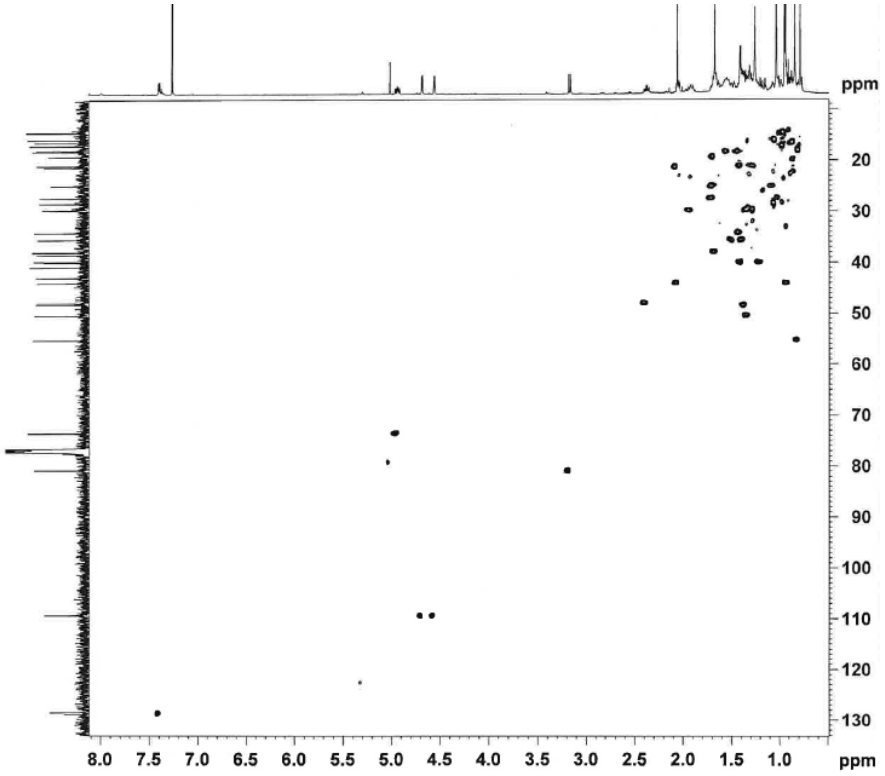

Appendix 16.5 HMBC spectrum of compound 1 (lup-(20)29-ene-2α-acetate-3β-ol) (500 MHz for ^{1}H, 125 MHz for ^{13}C 125 MHz in $CDCl_3$)

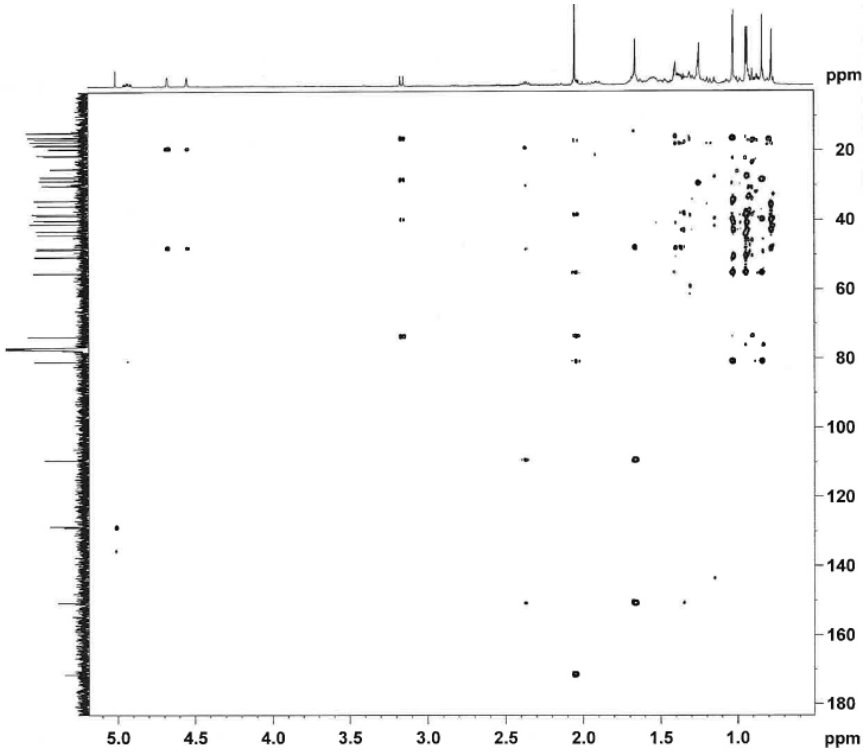

Appendix 16.6 NOESY spectrum of compound 1 (lup-(20)29-ene-2α-acetate-3β-ol) (500 MHz; $CDCl_3$)

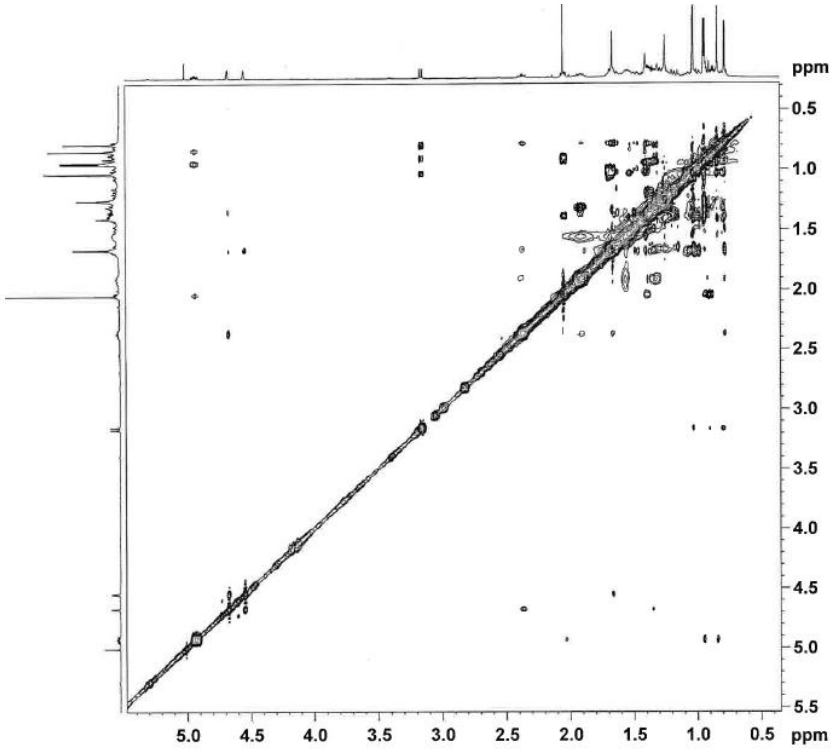

Appendix 17 NMR spectra of compound 2 (lup-(20)29-ene-2α-ol-3β-acetate)

*Judging from the NMR spectra, this sample was about 95% pure.

Appendix 17.1 ^{1}H NMR spectrum of compound 2 (lup-(20)29-ene-2α-ol-3β-acetate) (500 MHz; $CDCl_3$)

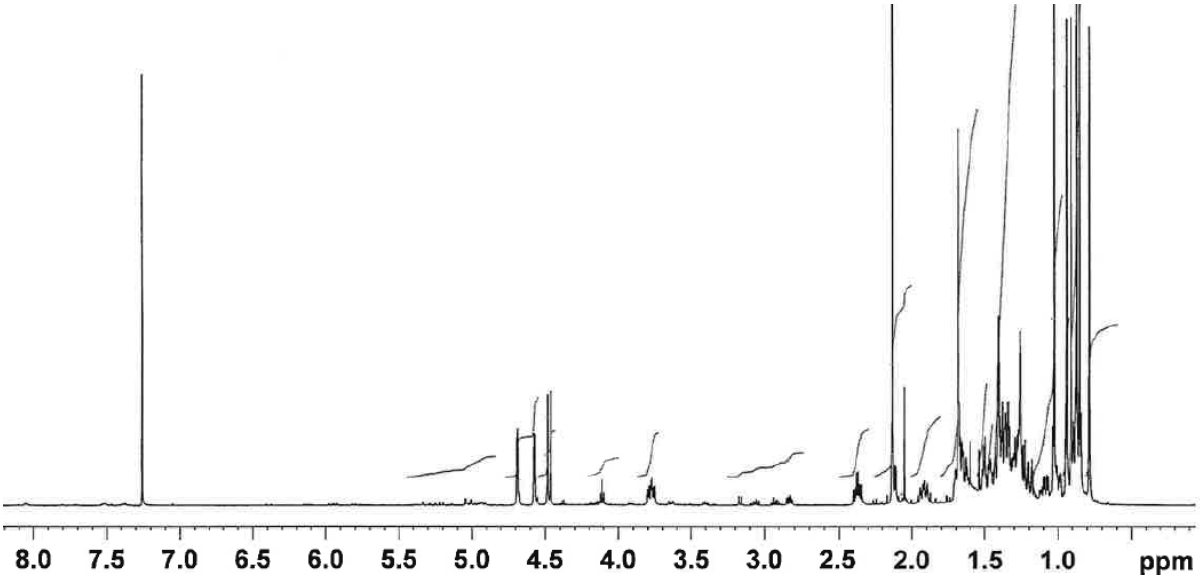

Appendix 17.2 COSY spectrum of compound 2 (lup-(20)29-ene-2α-ol-3β-acetate) (500 MHz in $CDCl_3$)

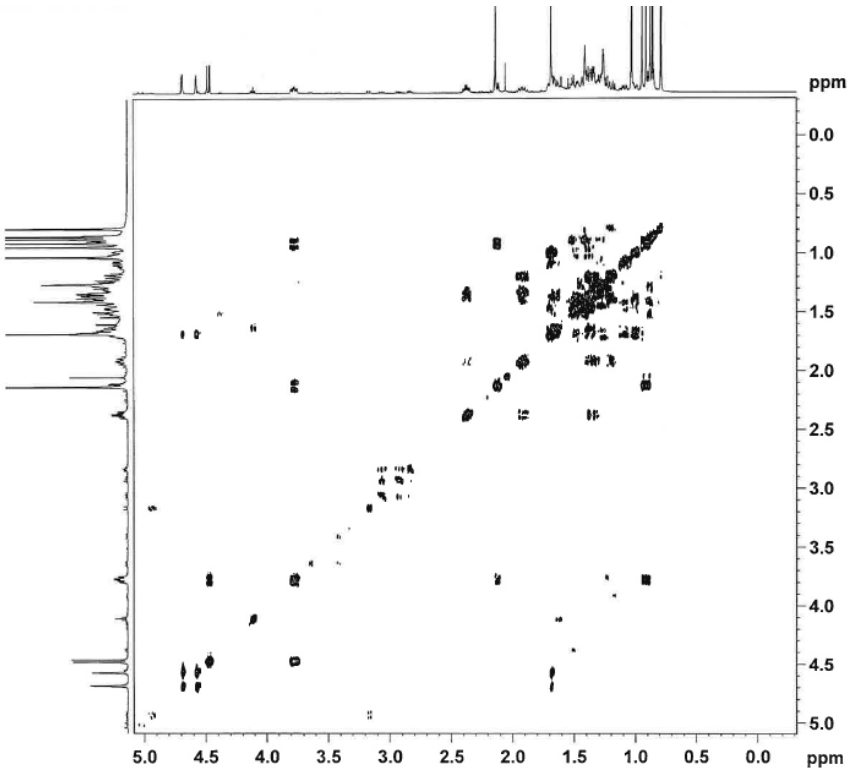

Appendix 17.3 ^{13}C NMR spectrum of compound 2 (lup-(20)29-ene-2α-ol-3β-acetate) (125 MHz; $CDCl_3$)

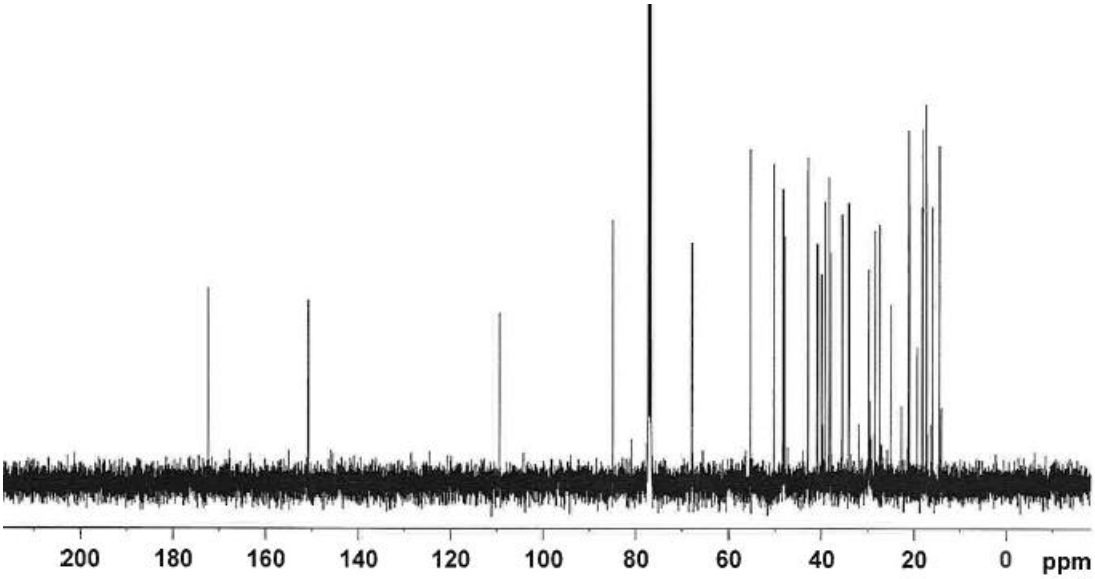

Appendix 17.4 HMQC spectrum of compound 2 (lup-(20)29-ene-2α-ol-3β-acetate) (500 MHz for ^{1}H, 125 MHz for ^{13}C; $CDCl_3$)

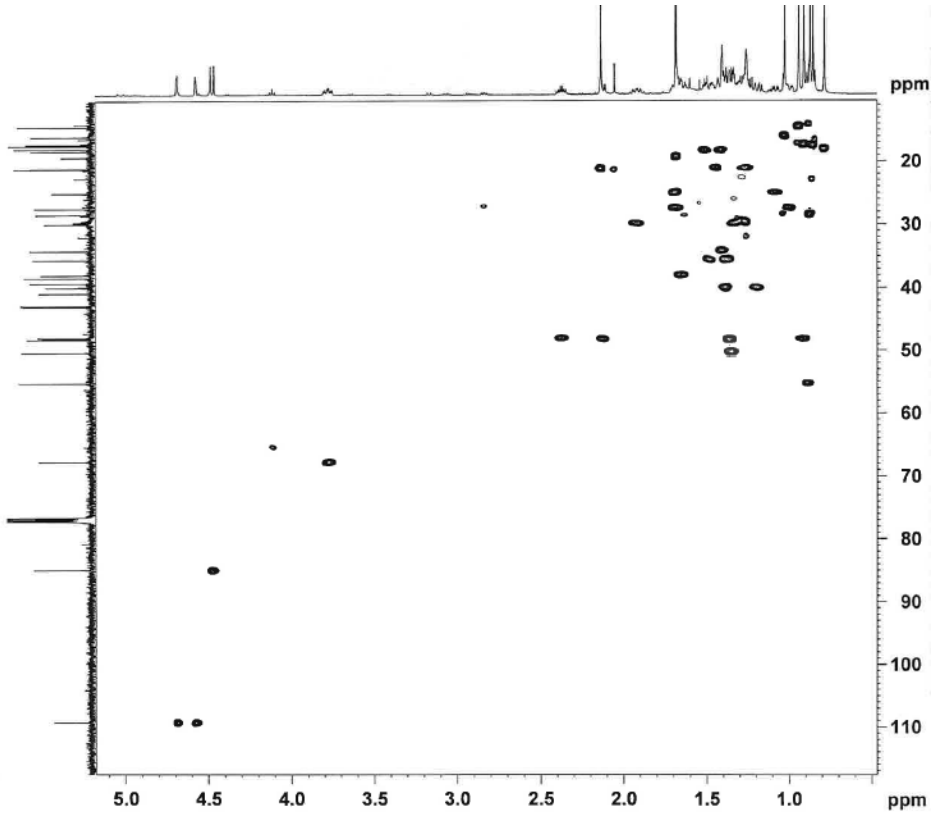

Appendix 17.5 HMBC spectrum of compound 2 (lup-(20)29-ene-2α-ol-3β-acetate) (500 MHz for ^{1}H, 125 MHz for ^{13}C; $CDCl_3$)

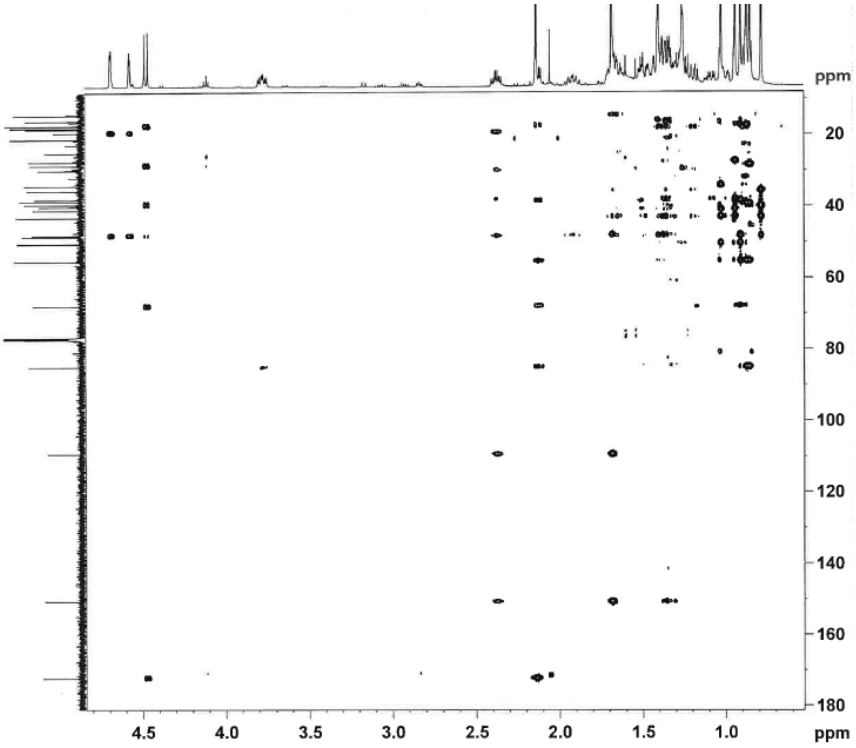

Appendix 17.6 NOESY spectrum of compound 2 (lup-(20)29-ene-2α-ol-3β-acetate) (500 MHz; $CDCl_3$)

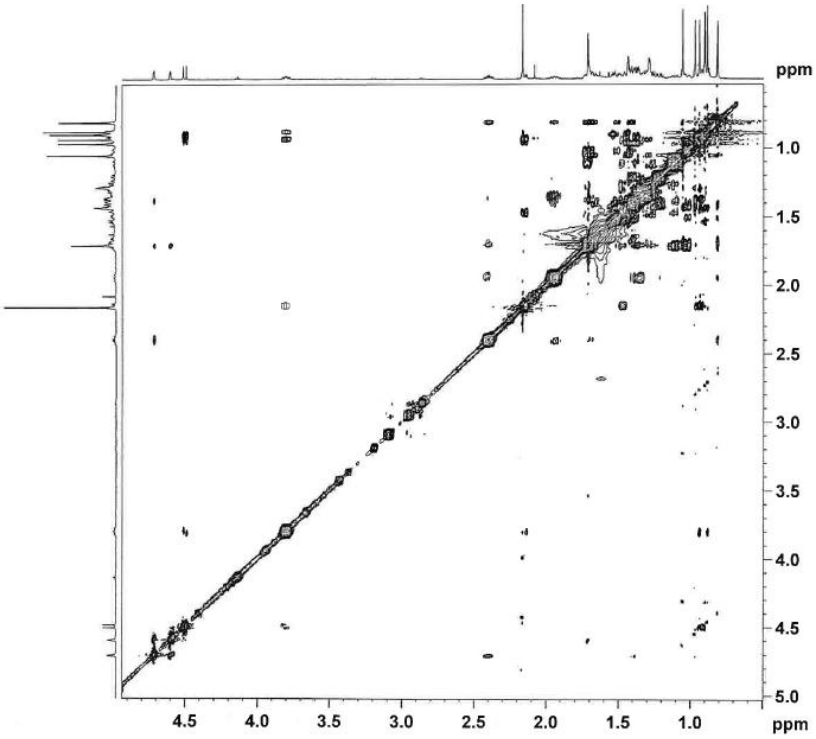

Appendix 18 NMR spectra of β-sitosterol

Appendix 18.1 ^{1}H NMR spectrum of β-sitosterol (500 MHz; $CDCl_3$)

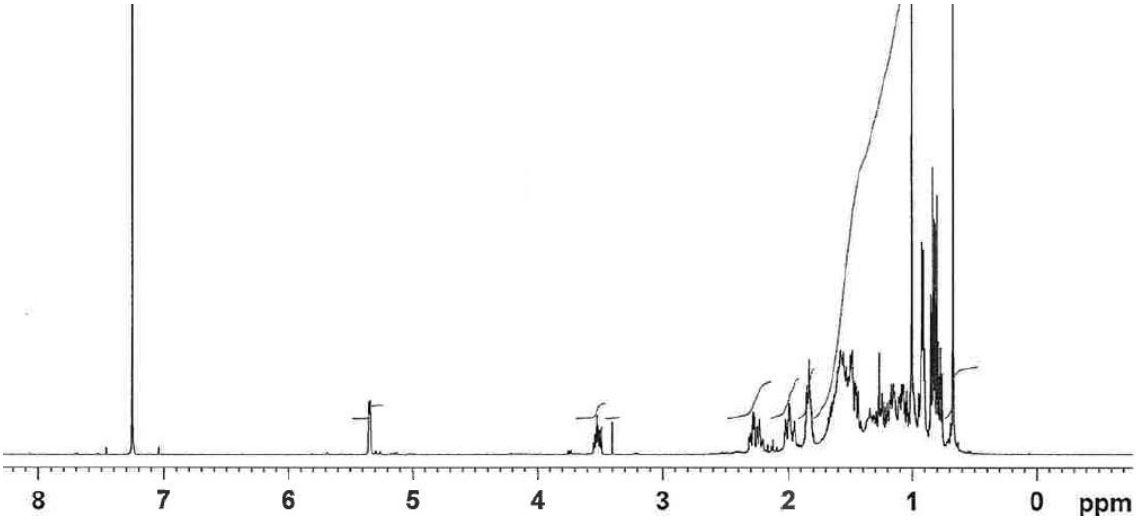

Appendix 18.2 COSY spectrum of β-sitosterol (500 MHz; $CDCl_3$)

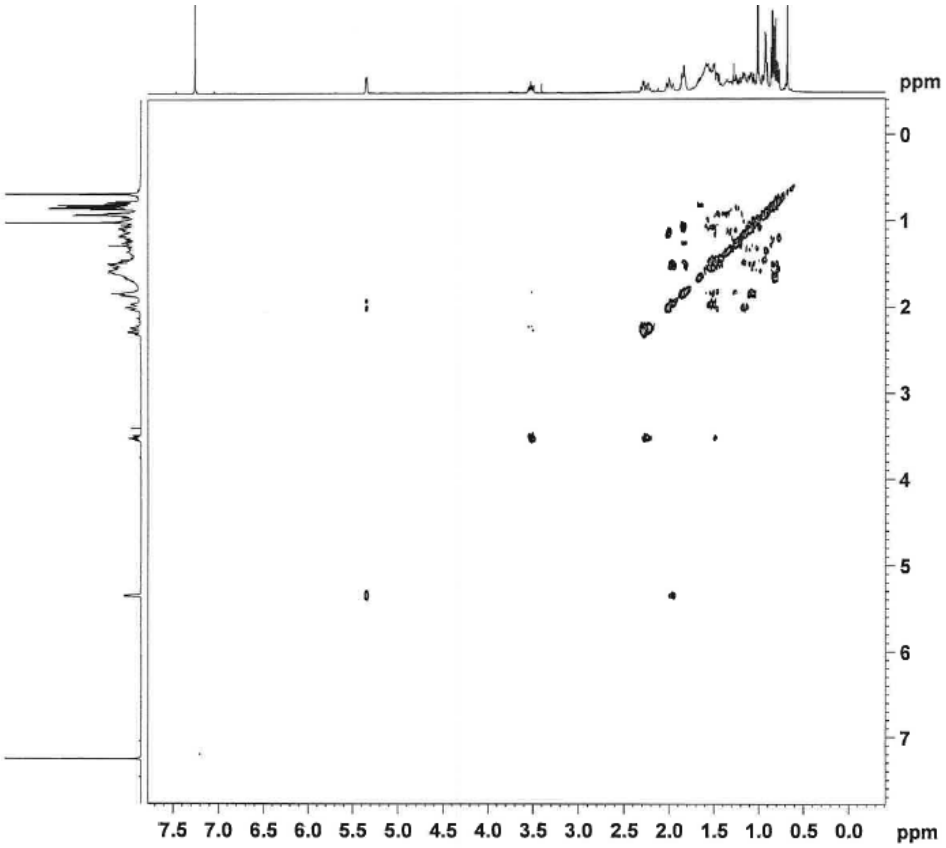

Appendix 18.3 ^{13}C NMR spectrum of β-sitosterol (125 MHz; $CDCl_3$)

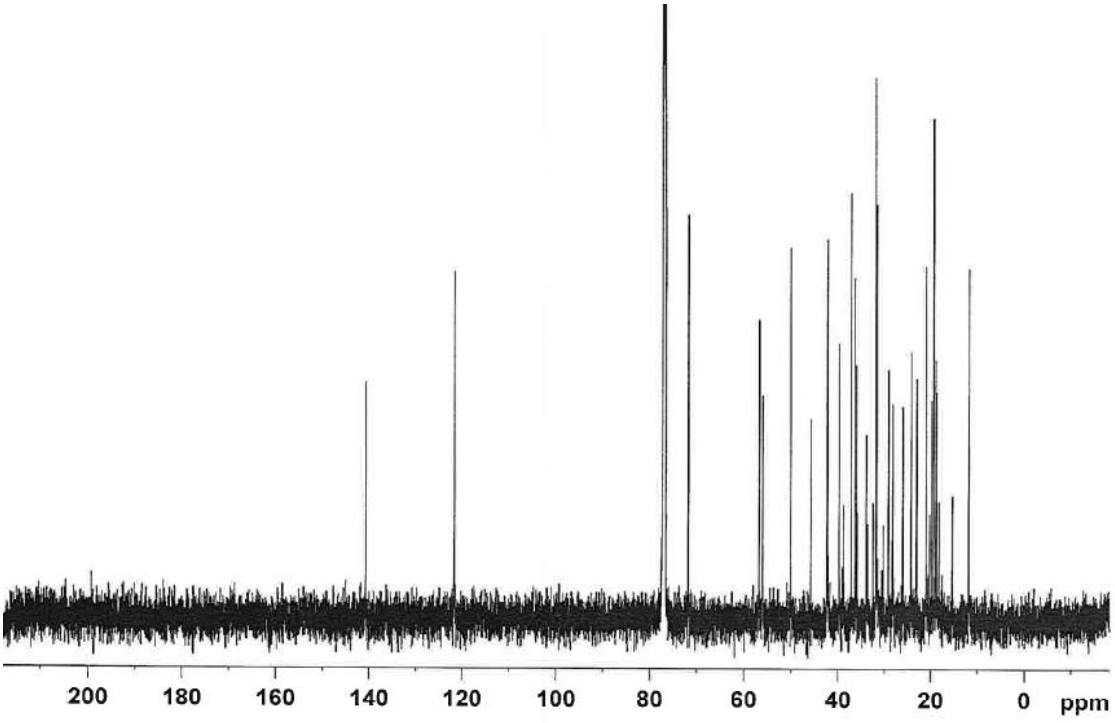

Appendix 18.4 HMQC spectrum of β-sitosterol (500 MHz for ^{1}H, 125 MHz for ^{13}C; $CDCl_3$)

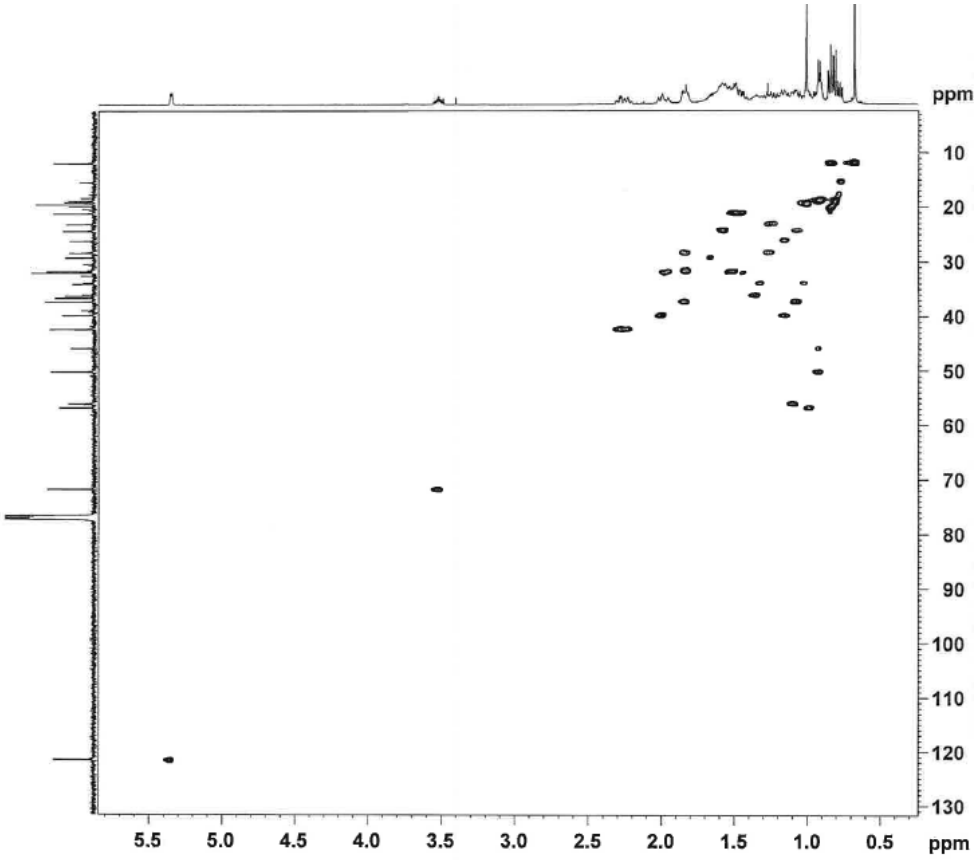

Appendix 18.5 HMBC spectrum of β-sitosterol (500 MHz for ^{1}H, 125 MHz for ^{13}C; $CDCl_3$)

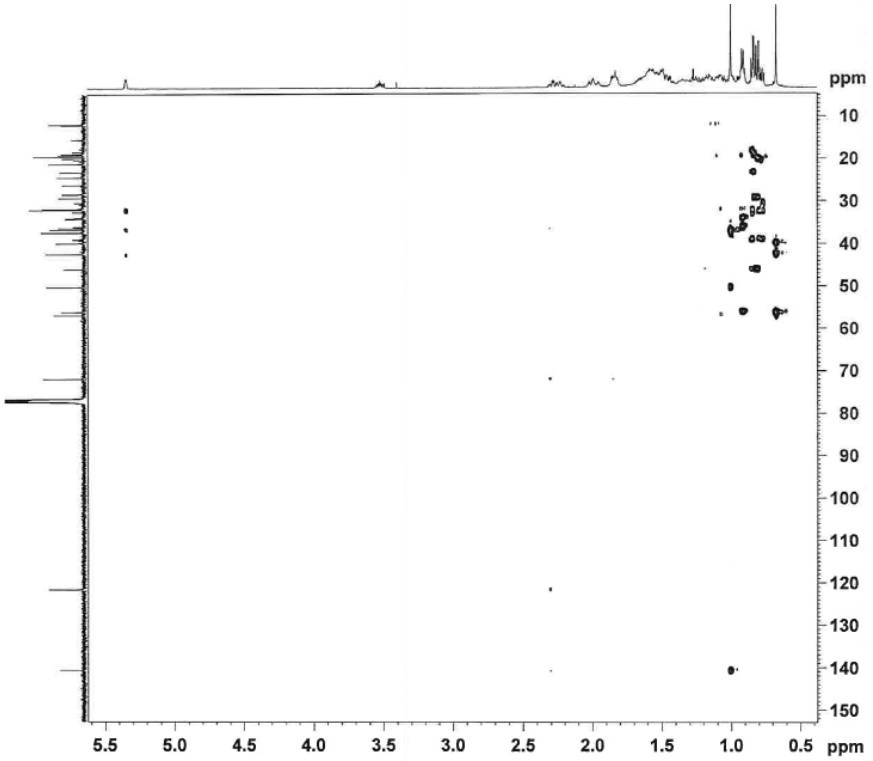

Appendix 18.6 NOESY spectrum of β-sitosterol (500 MHz; $CDCl_3$)

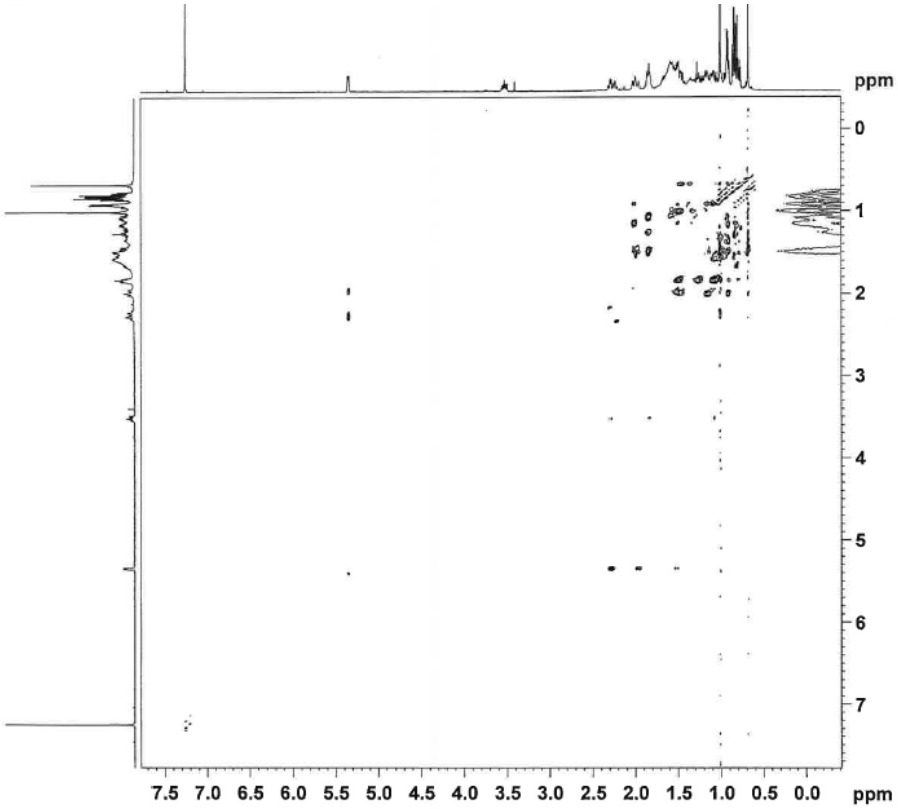

Appendix 19 NMR spectra of β-sitosterol glucoside

Appendix 19.1 ^{1}H NMR spectrum of β-sitosterol glucoside (500 MHz; mixture of $CDCl_3$ and CD_3OD)

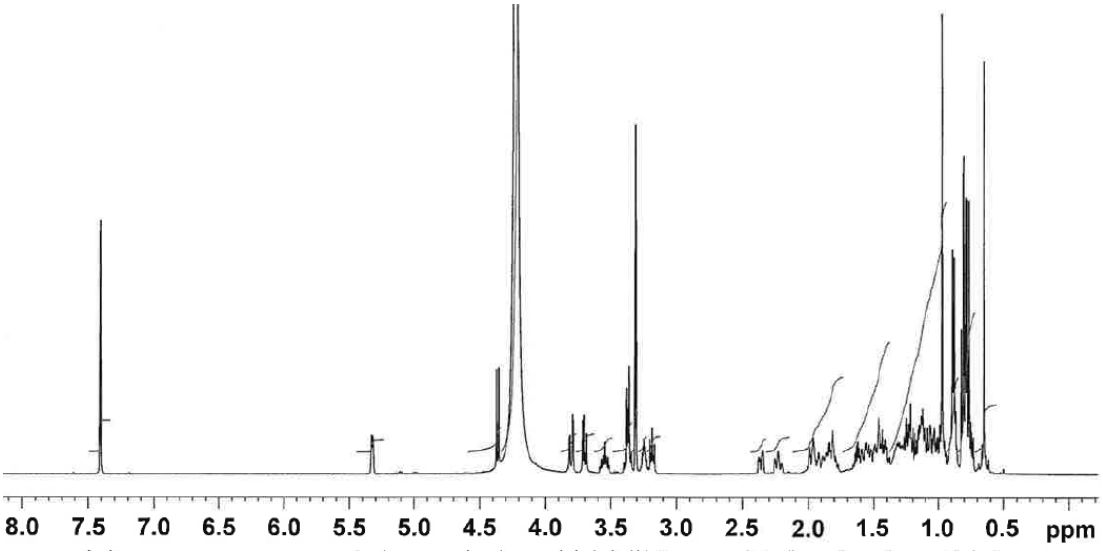

Appendix 19.2 COSY spectrum of β-sitosterol glucoside (500 MHz; mixture of $CDCl_3$ and CD_3OD)

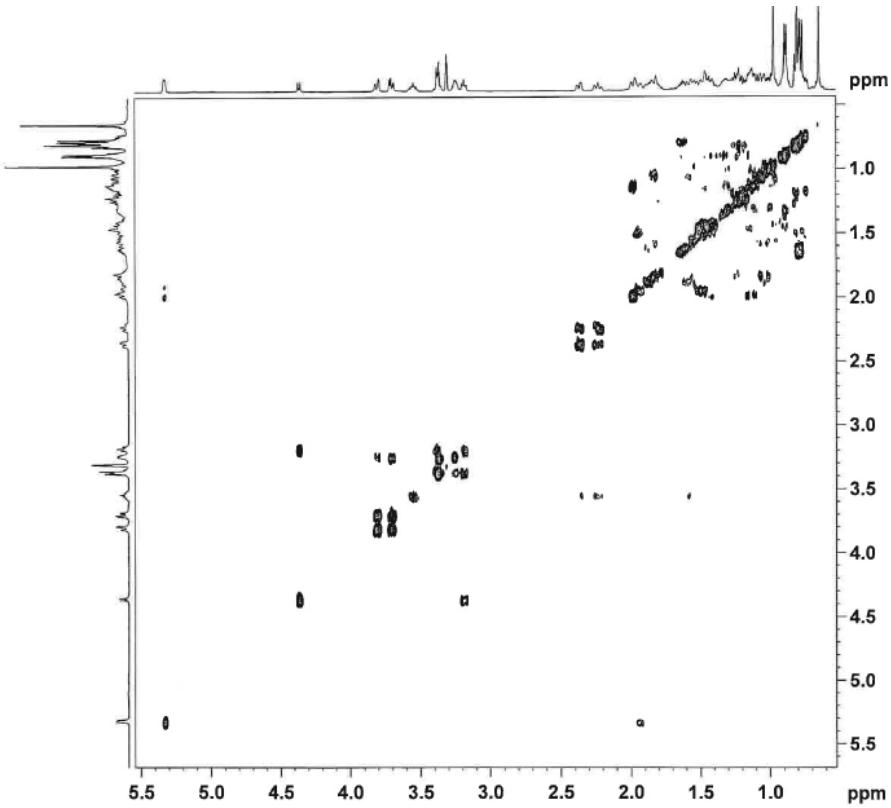

Appendix 19.3 ^{13}C NMR spectrum of β-sitosterol glucoside (125 MHz; mixture of $CDCl_3$ and CD_3OD)

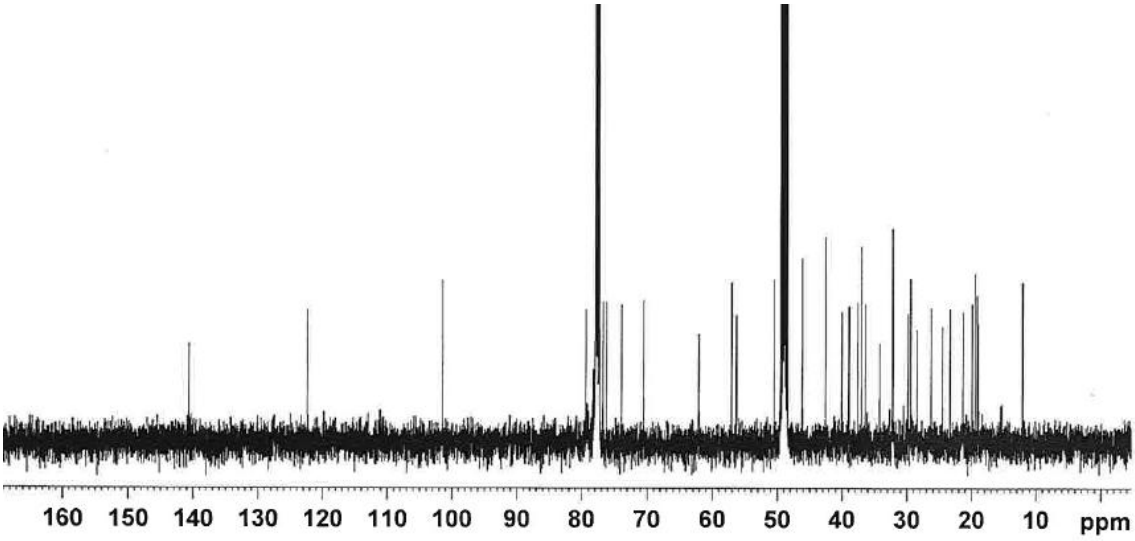

Appendix 19.4 HMQC spectrum of β-sitosterol glucoside (500 MHz for ^{1}H, 125 MHz for ^{13}C; mixture of $CDCl_3$ and CD_3OD)

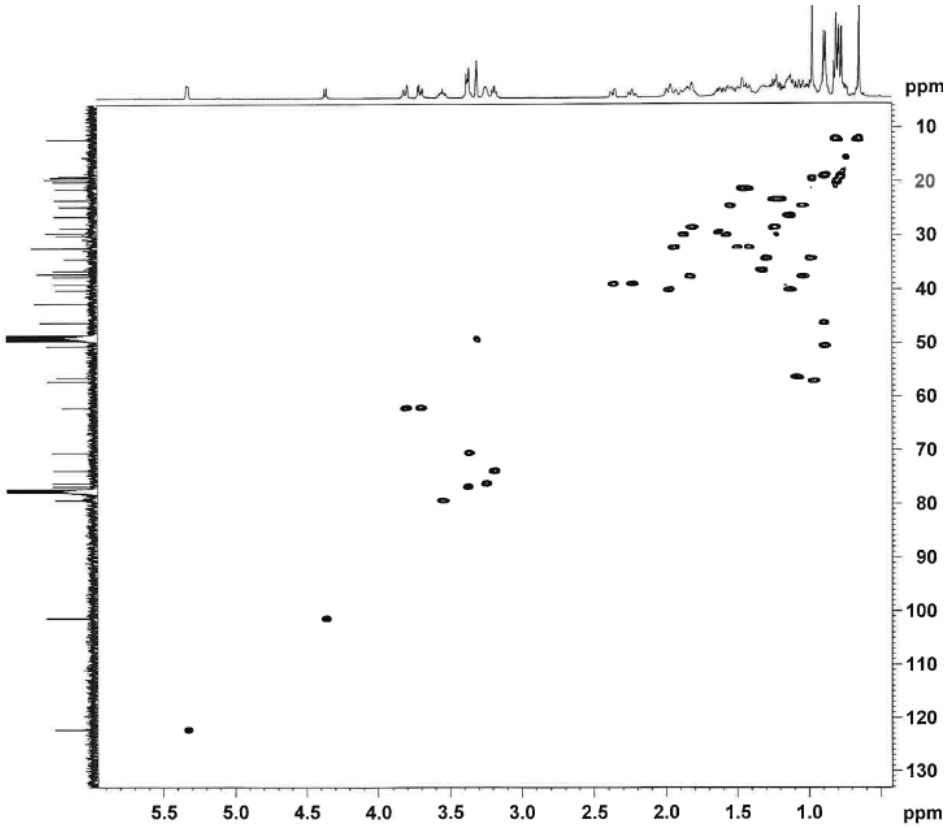

Appendix 19.5 HMBC spectrum of β-sitosterol glucoside (500 MHz for ^{1}H, 125 MHz for ^{13}C; mixture of $CDCl_3$ and CD_3OD)

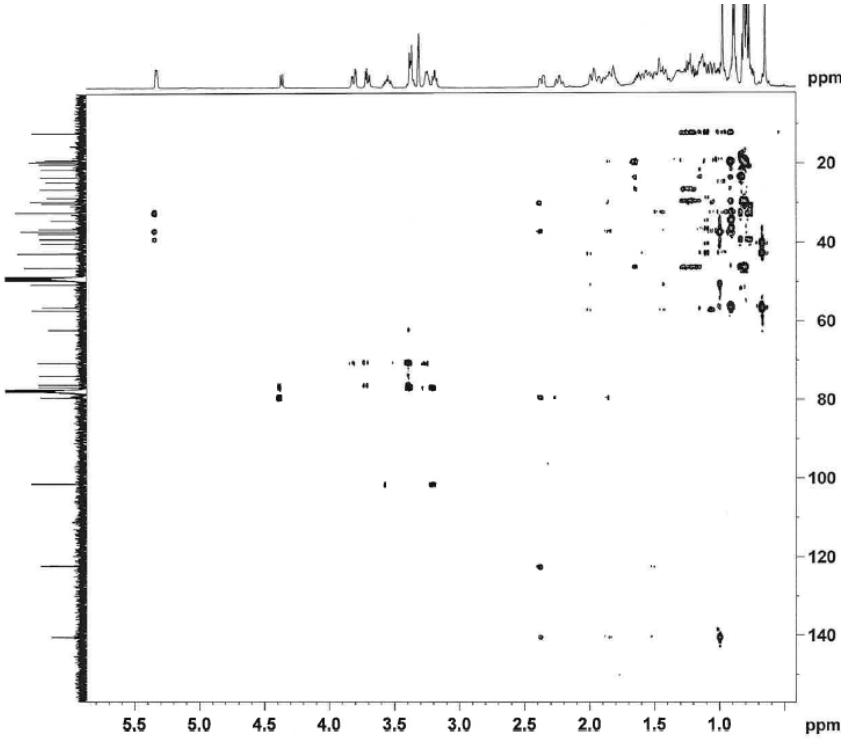

Appendix 19.6 NOESY spectrum of β-sitosterol glucoside (500 MHz in mixture of $CDCl_3$ and CD_3OD)

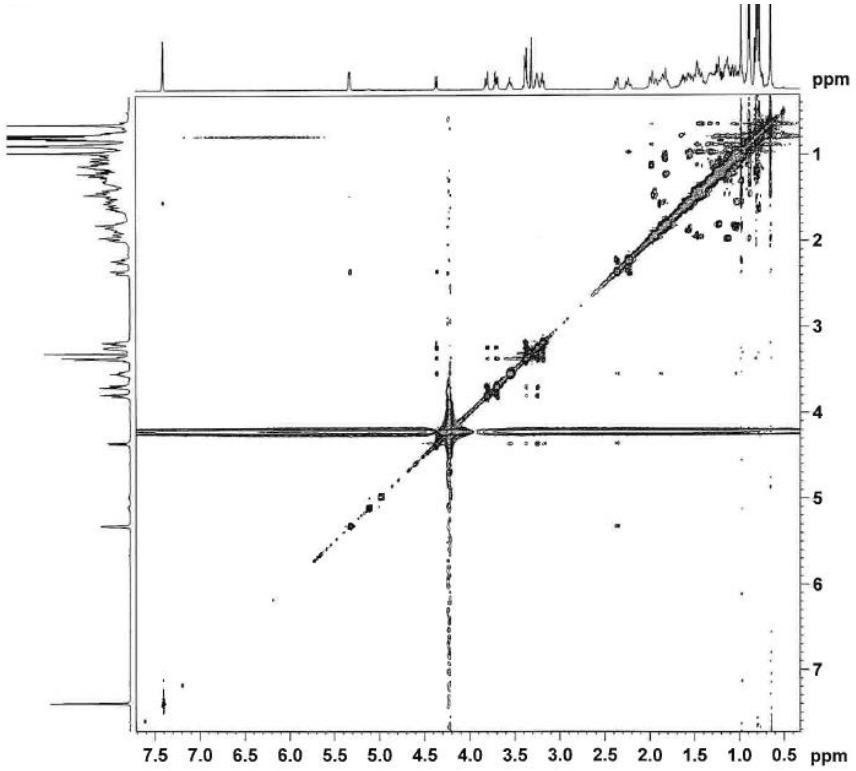

Appendix 20 NMR spectra of salidroside

*Judging from the NMR spectra, this sample was about 80% pure.

Appendix 20.1 ^{1}H NMR spectrum of salidroside (500 MHz; CD_3OD)

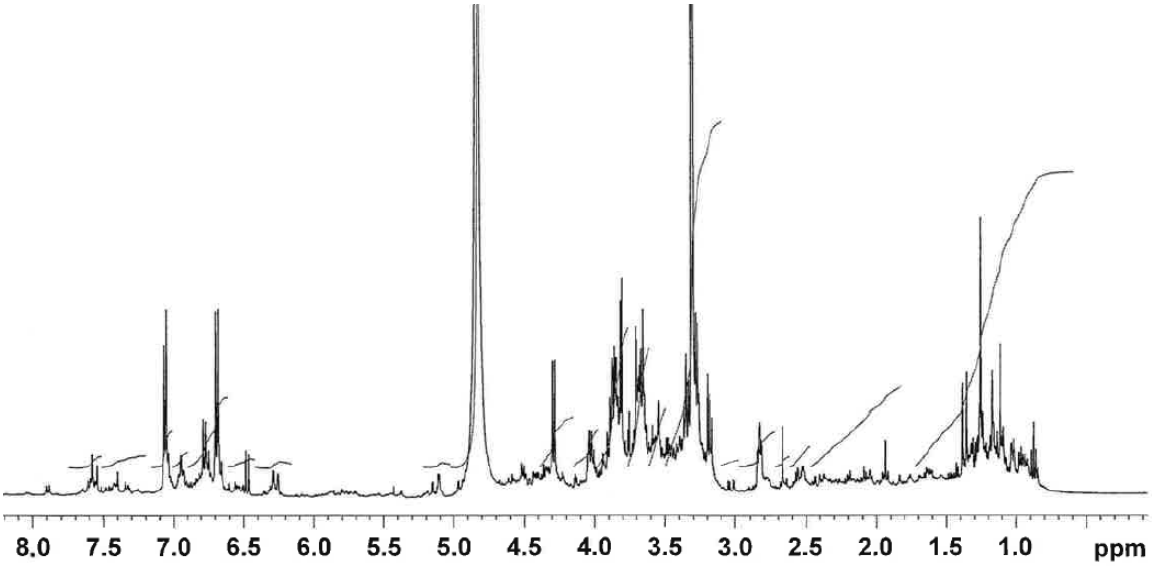

Appendix 20.2 COSY spectrum of salidroside (500 MHz; CD_3OD)

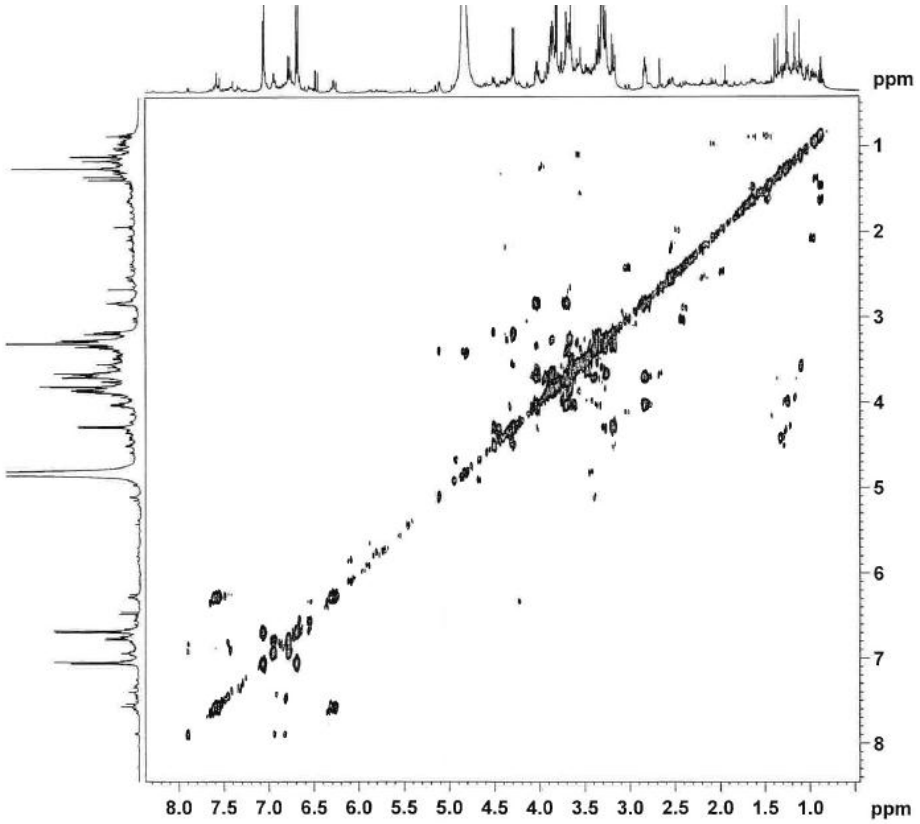

Appendix 20.3 ^{13}C NMR spectrum of salidroside (125 MHz; CD_3OD)

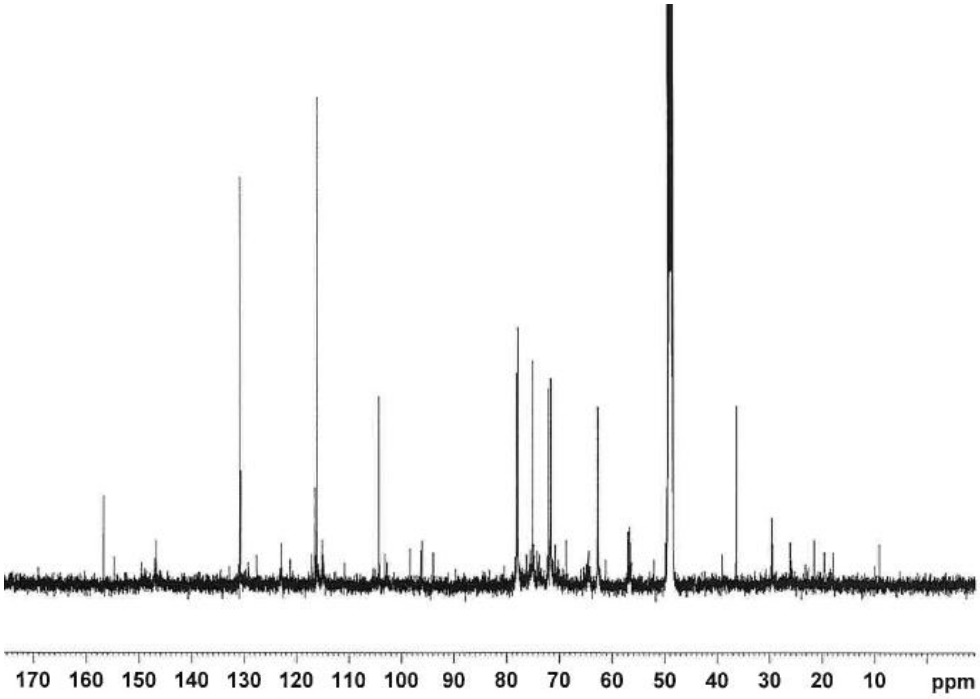

Appendix 20.4 HMQC spectrum of salidroside (500 MHz for ^{1}H, 125 MHz for ^{13}C; CD_3OD)

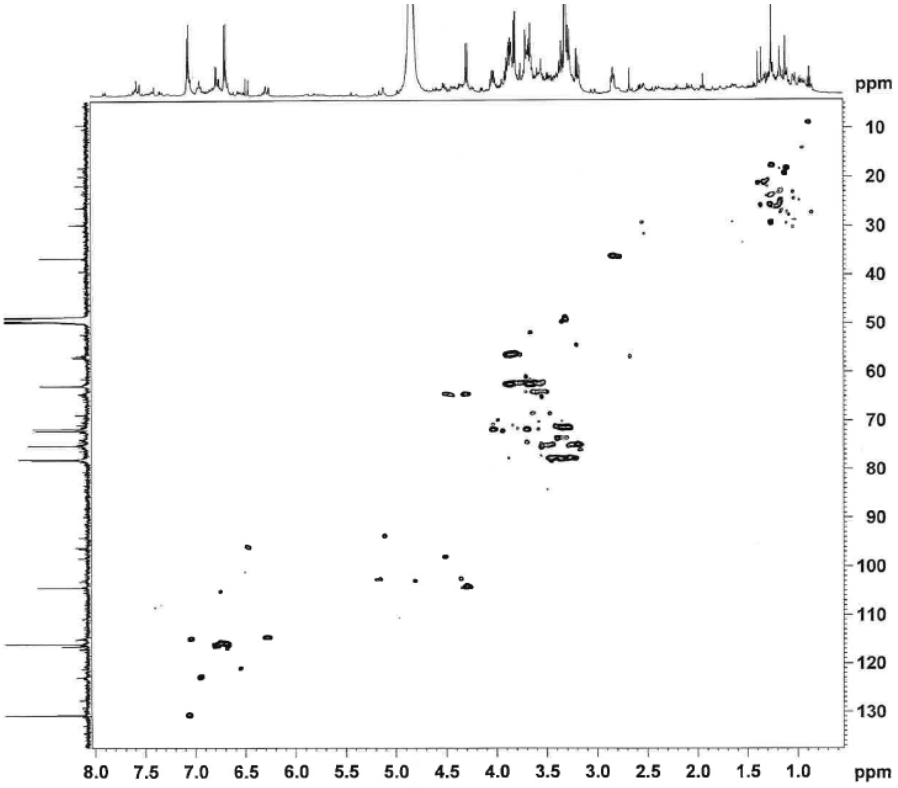

Appendix 20.5 HMBC spectrum of salidroside (500 MHz for ^{1}H, 125 MHz for ^{13}C; CD_3OD)

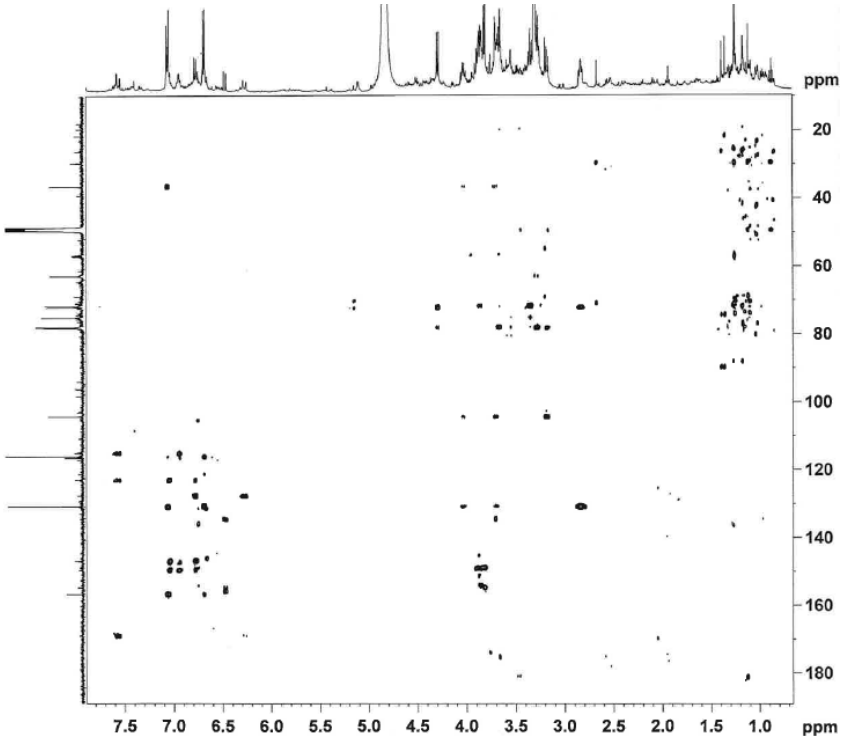

Appendix 20.6 NOESY spectrum of salidroside (500 MHz; CD_3OD)

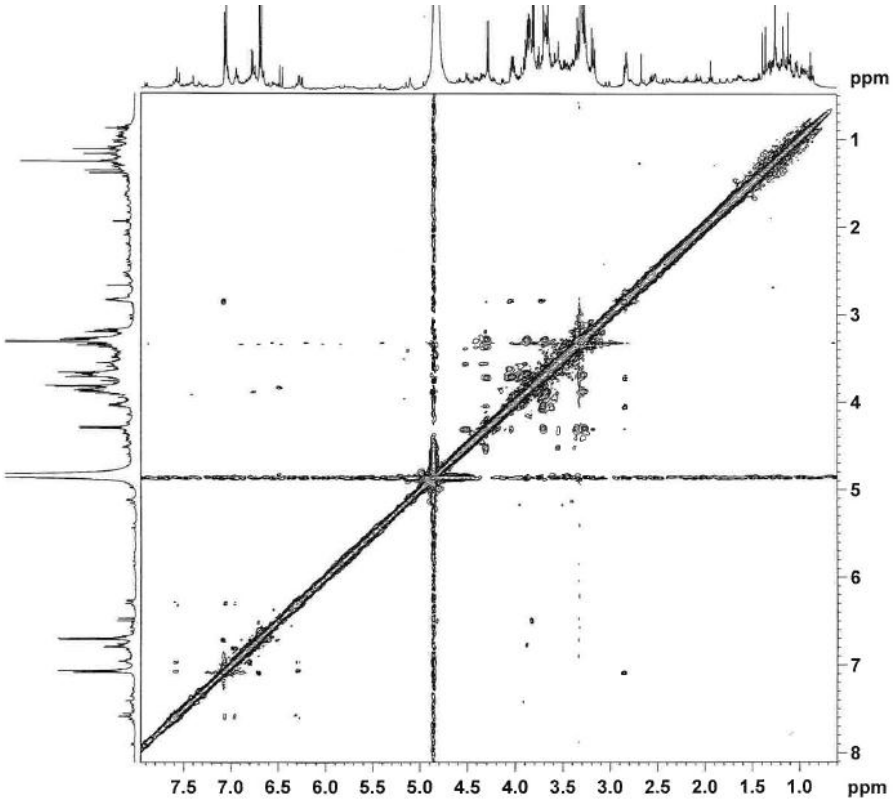

Appendix 21 NMR spectra of 2",3"-di-*O*-acetyl-martynoside

*Judging from the NMR spectra, this sample was about 95% pure.

Appendix 21.1 ^{1}H NMR spectrum of 2",3"-di-*O*-acetyl-martynoside (500 MHz; $CDCl_3$)

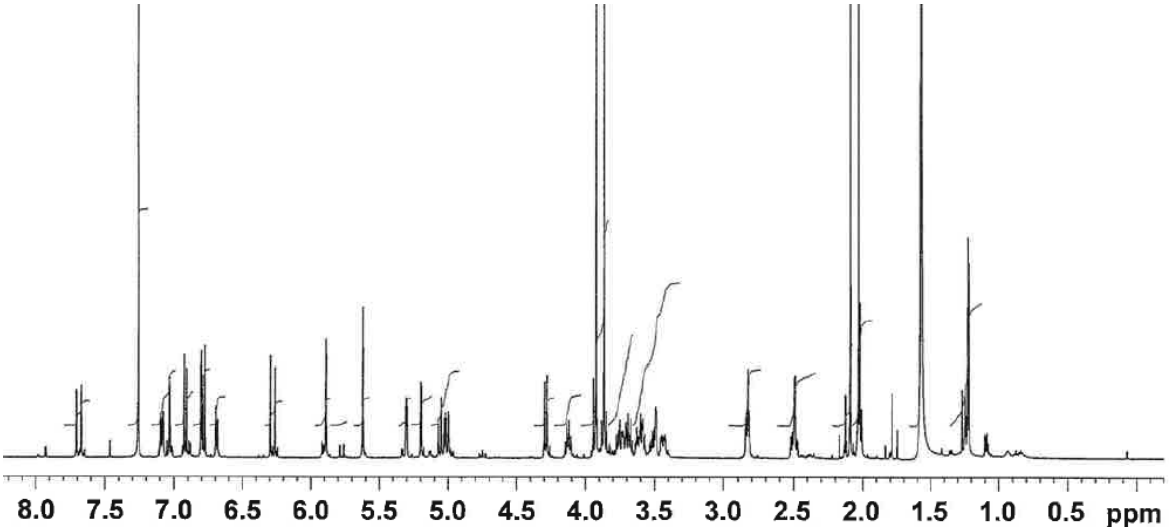

Appendix 21.2 COSY spectrum of 2",3"-di-*O*-acetyl-martynoside (500 MHz ; $CDCl_3$)

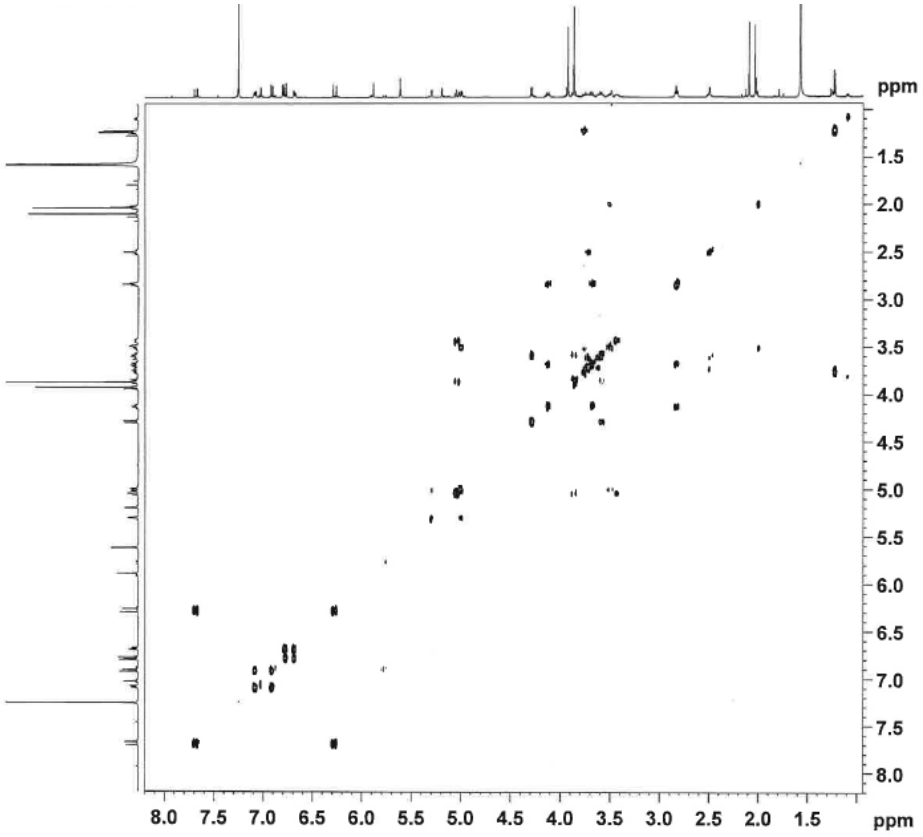

Appendix 21.3 ^{13}C NMR spectrum of 2",3"-di-*O*-acetyl-martynoside (125 MHz; $CDCl_3$)

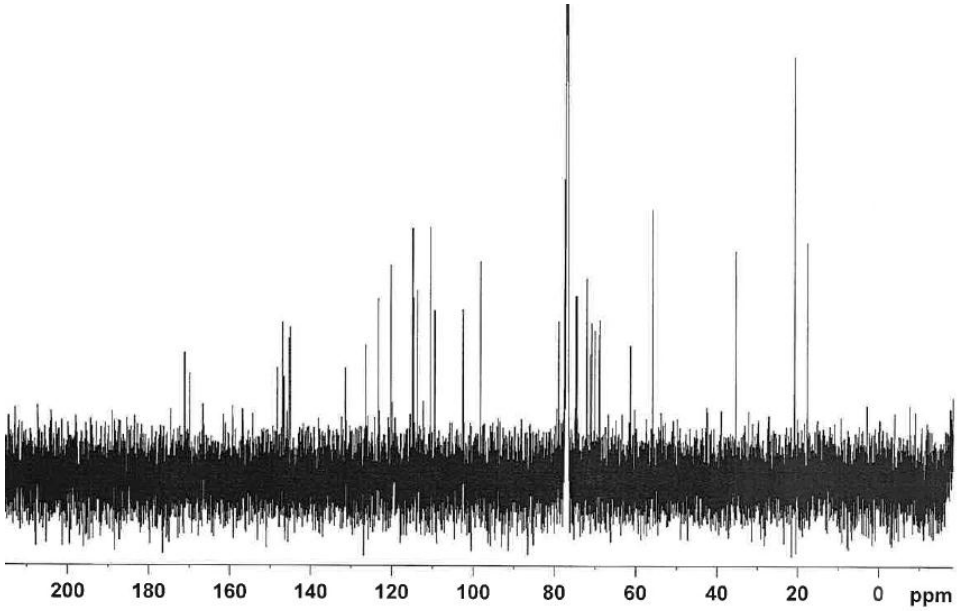

Appendix 21.4 HMQC spectrum of 2",3"-di-*O*-acetyl-martynoside (^1H, 500 MHz; ^{13}C, 125 MHz in $CDCl_3$)

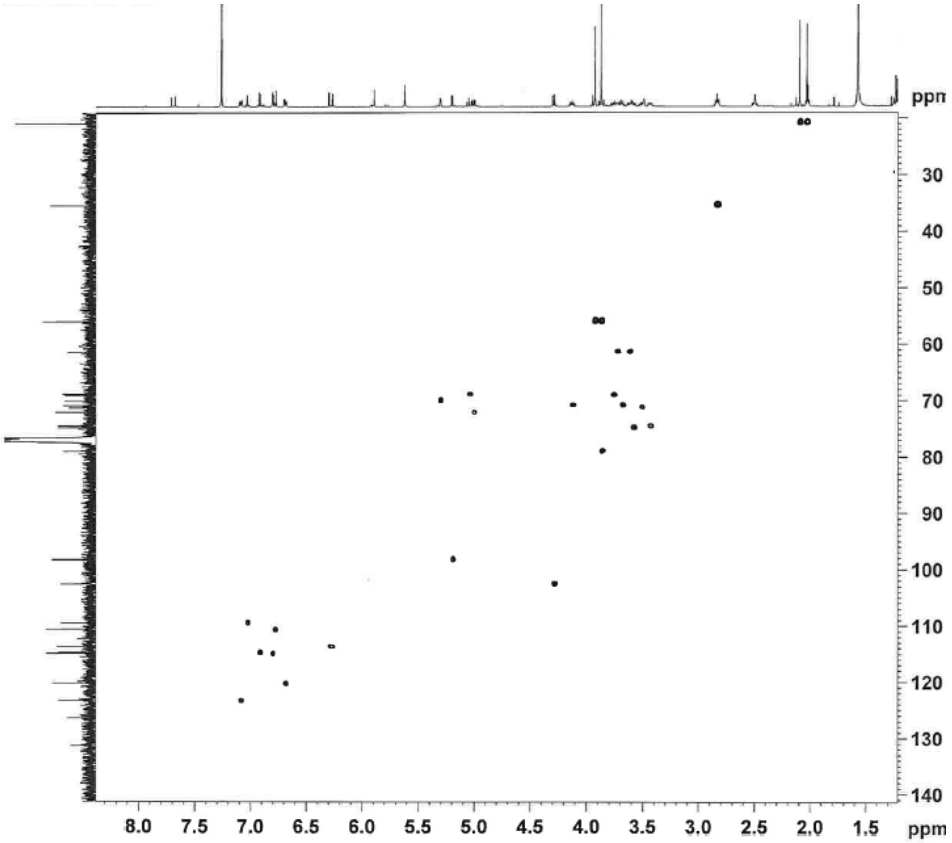

Appendix 21.5 HMBC spectrum of 2",3"-di-*O*-acetyl-martynoside (^{1}H, 500 MHz; ^{13}C, 125 MHz in $CDCl_3$)

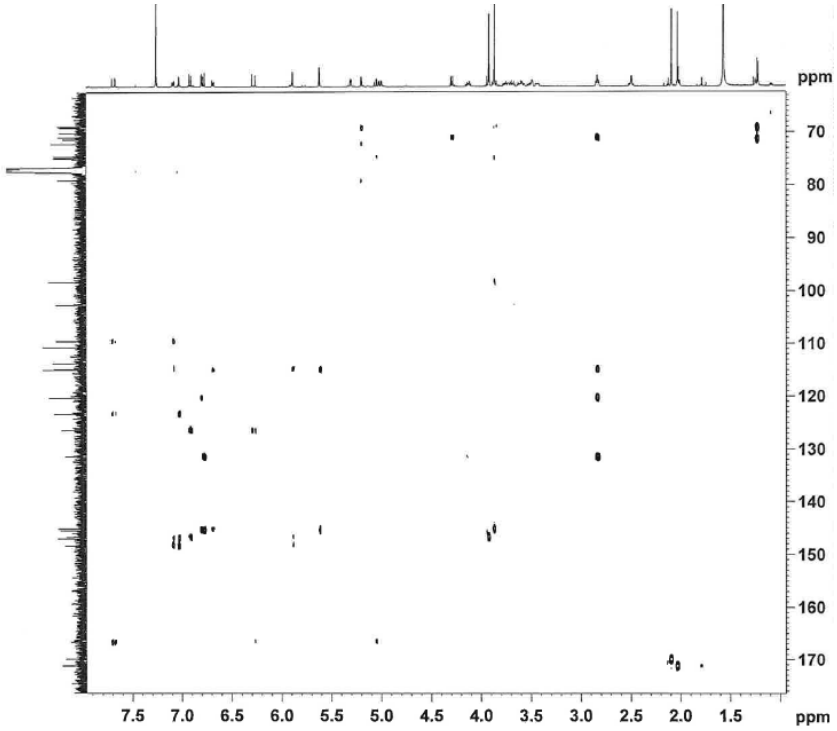

Appendix 21.6 NOESY spectrum of 2",3"-di-*O*-acetyl-martynoside (500 MHz in $CDCl_3$)

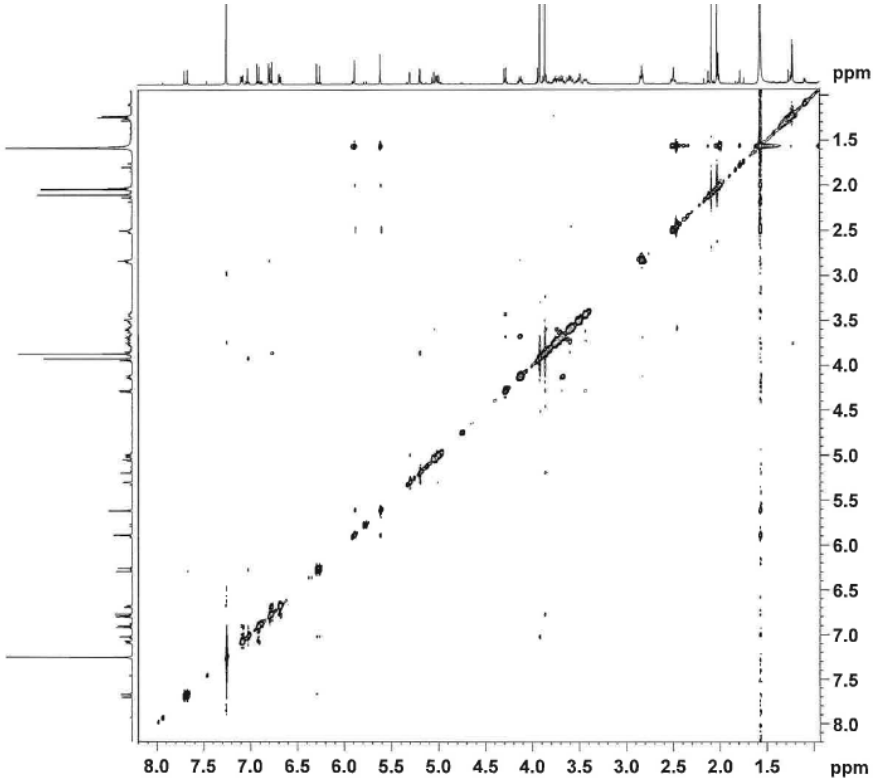

Appendix 22 NMR spectra of 1-docosyl ferulate

Appendix 22.1 ^{1}H NMR spectrum of 1-docosyl ferulate (500 MHz; $CDCl_3$)

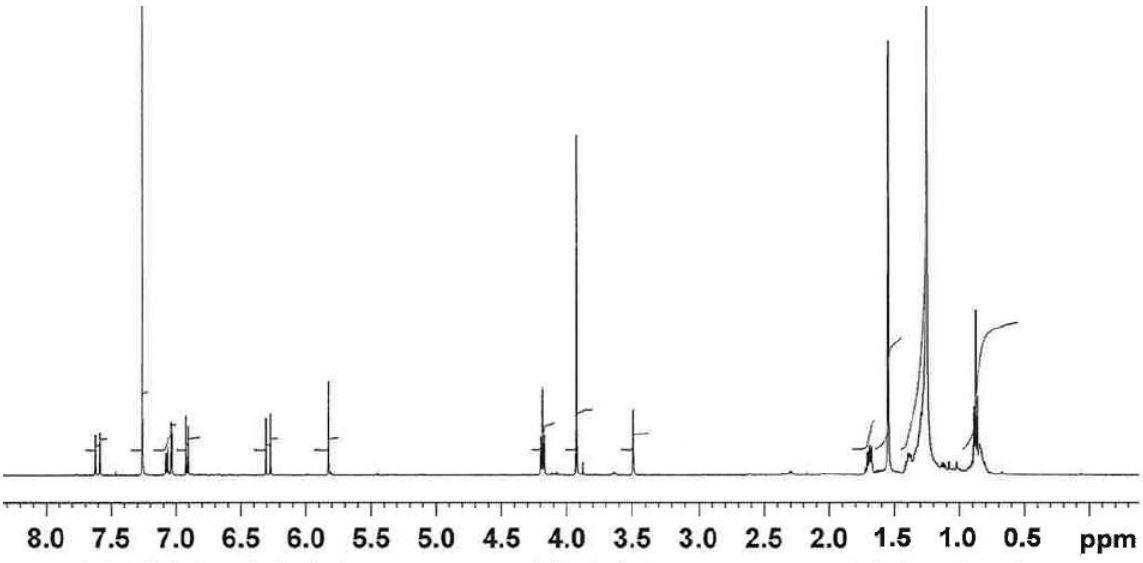

Appendix 22.2 COSY spectrum of 1-docosyl ferulate (500 MHz; $CDCl_3$)

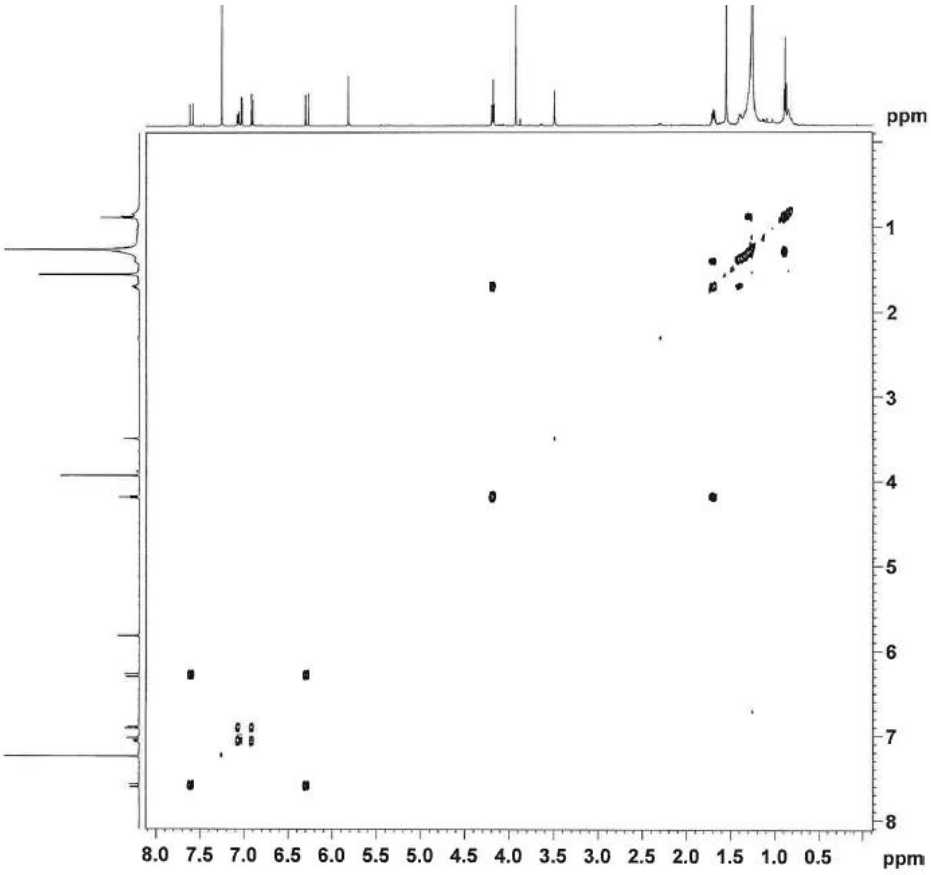

Appendix 22.3 ^{13}C NMR spectrum of 1-docosyl ferulate (125 MHz; $CDCl_3$)

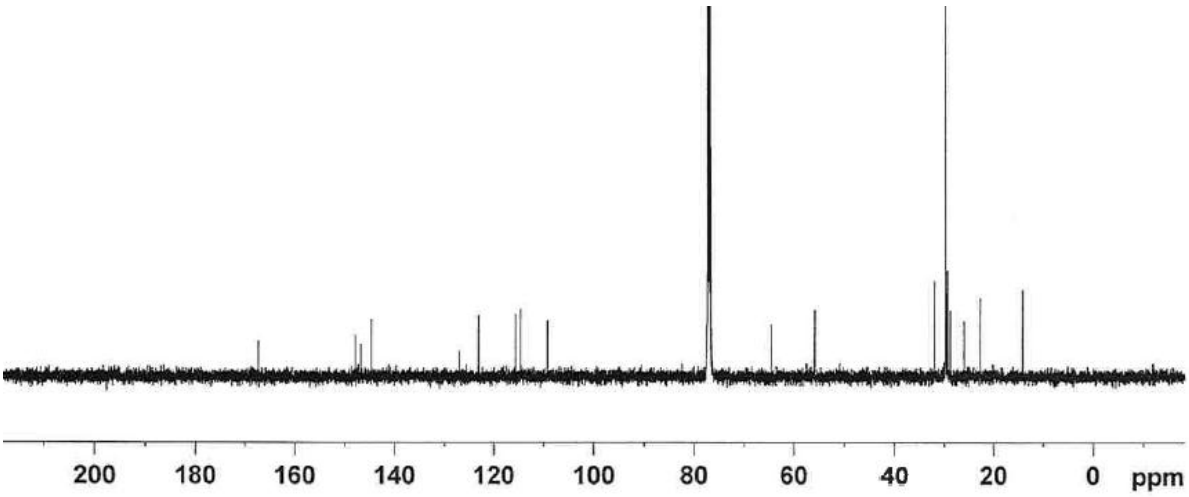

Appendix 22.4 HMQC spectrum of 1-docosyl ferulate (500 MHz for ^{1}H, 125 MHz for ^{13}C; $CDCl_3$)

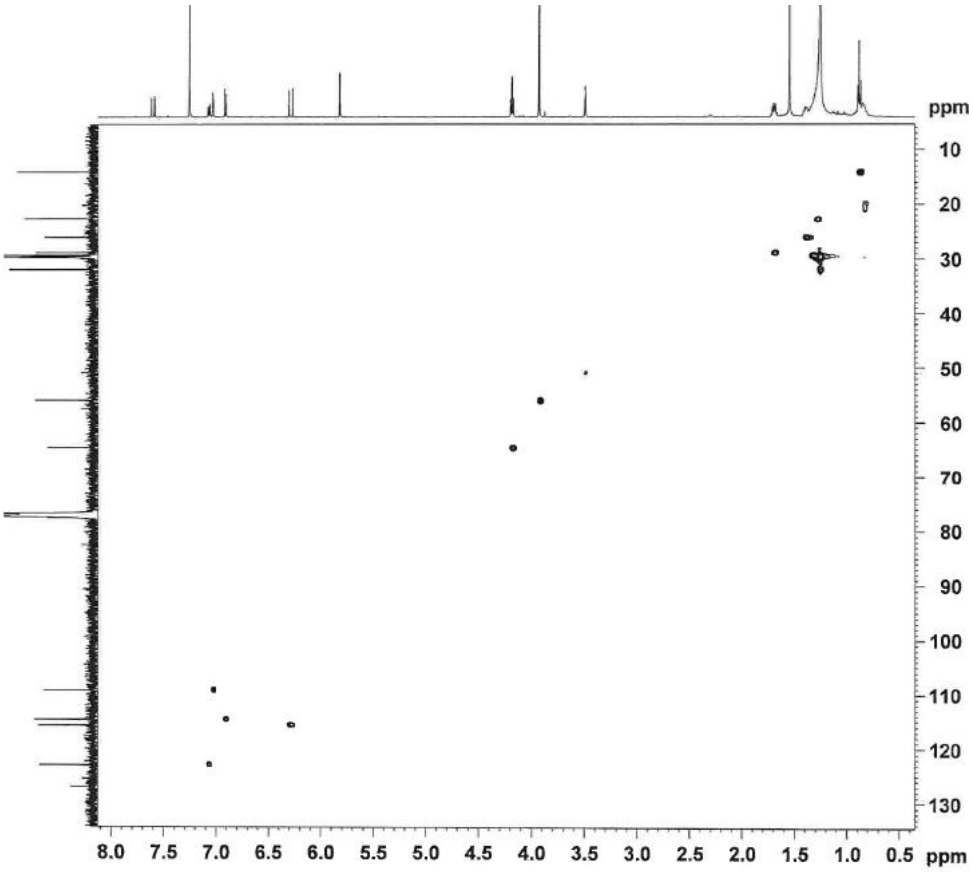

Appendix 22.5 HMBC spectrum of 1-docosyl ferulate (500 MHz for ^{1}H, 125 MHz for ^{13}C; $CDCl_3$)

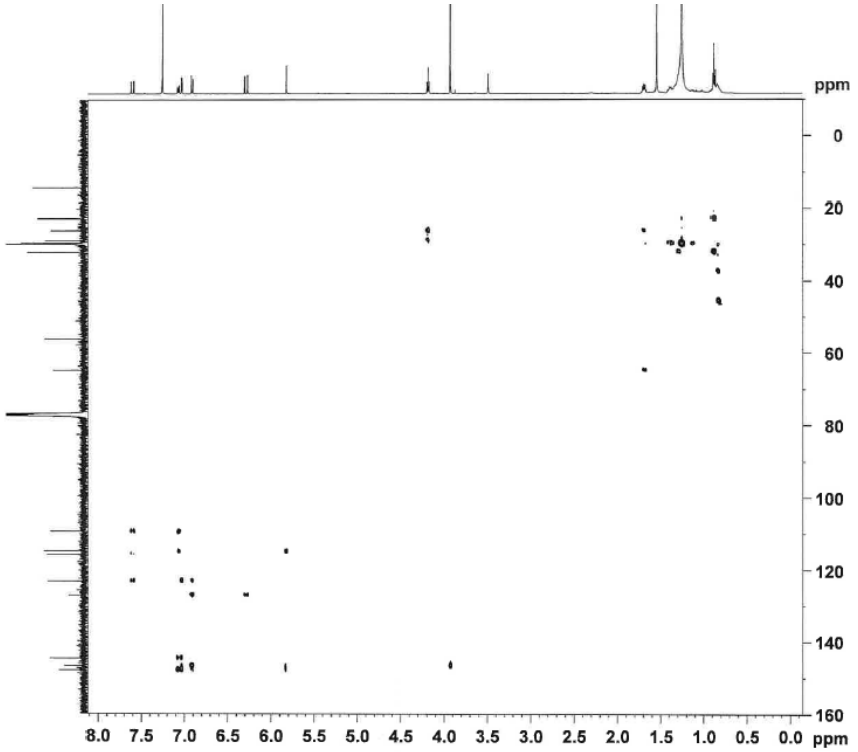

Appendix 22.6 NOESY spectrum of 1-docosyl ferulate (500 MHz; $CDCl_3$)

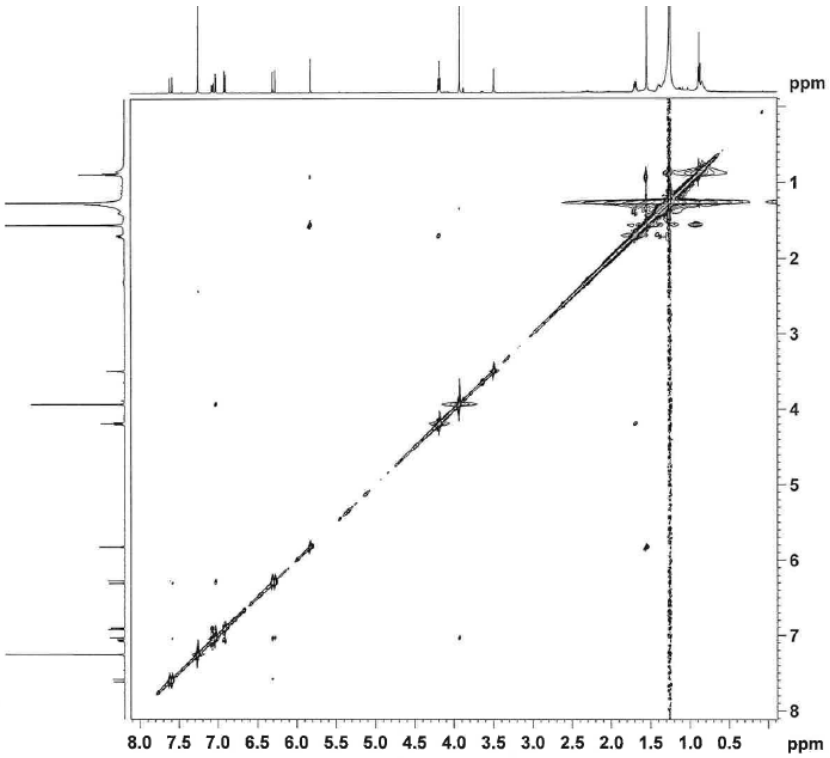

Appendix 23 NMR spectra of ferruginol

*Judging from the NMR spectra, this material was about 90% pure, with plasticiser (phthalate) as the major impurity.

Appendix 23.1 ^{1}H NMR spectrum of ferruginol (500 MHz; $CDCl_3$)

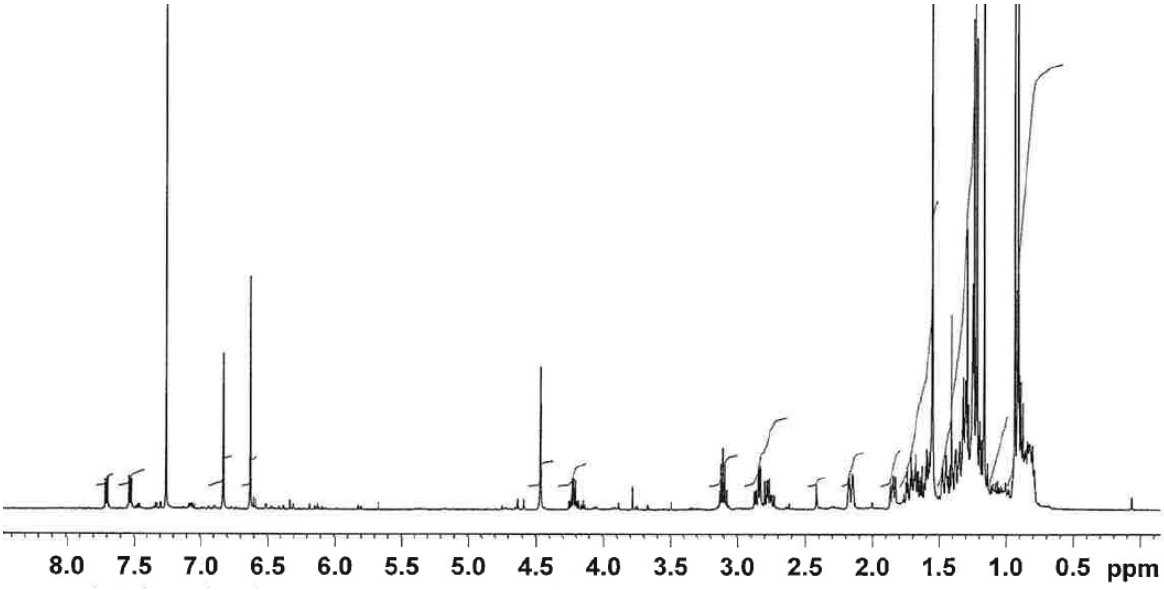

Appendix 23.2 COSY spectrum of ferruginol (500 MHz; $CDCl_3$)

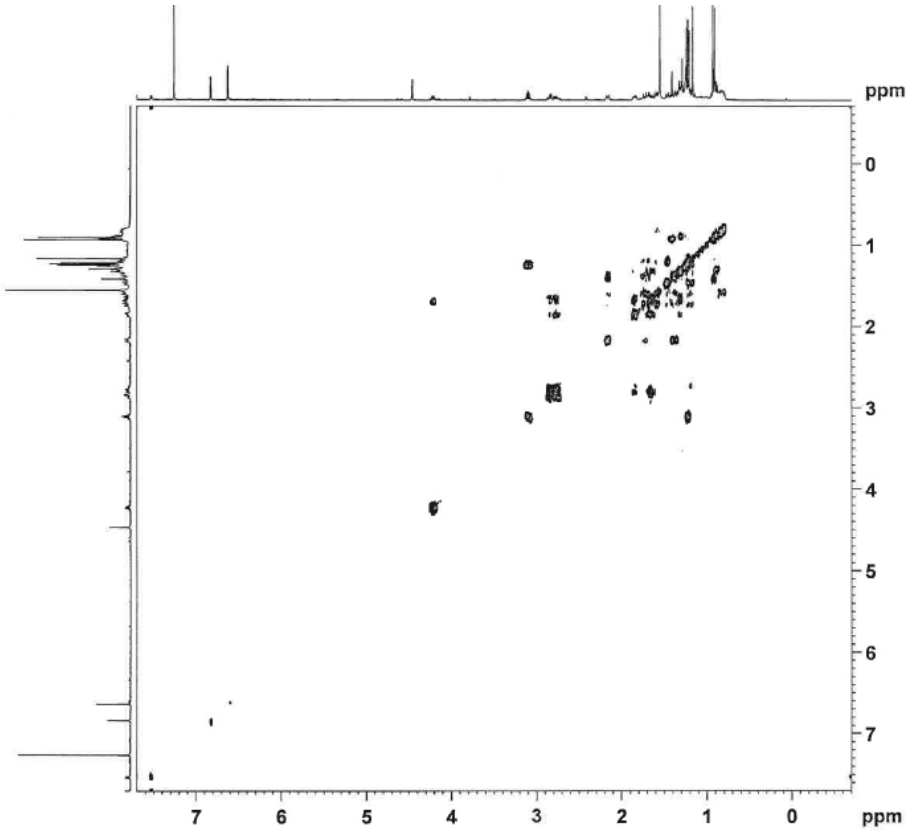

Appendix 23.3 ^{13}C NMR spectrum of ferruginol (125 MHz; $CDCl_3$)

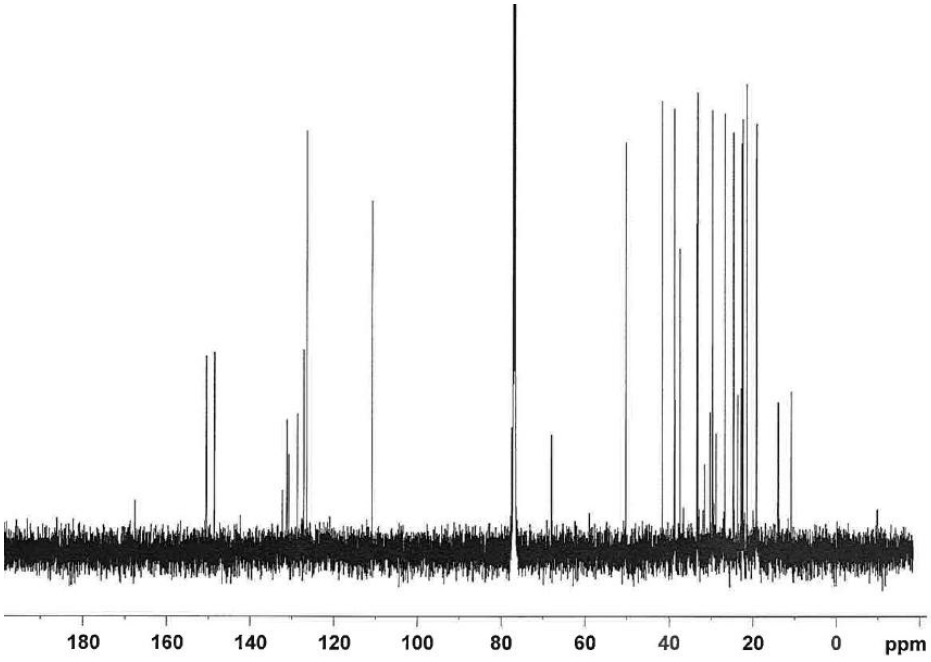

Appendix 23.4 HMQC spectrum of ferruginol (500 MHz for ^{1}H, 125 MHz for ^{13}C; $CDCl_3$)

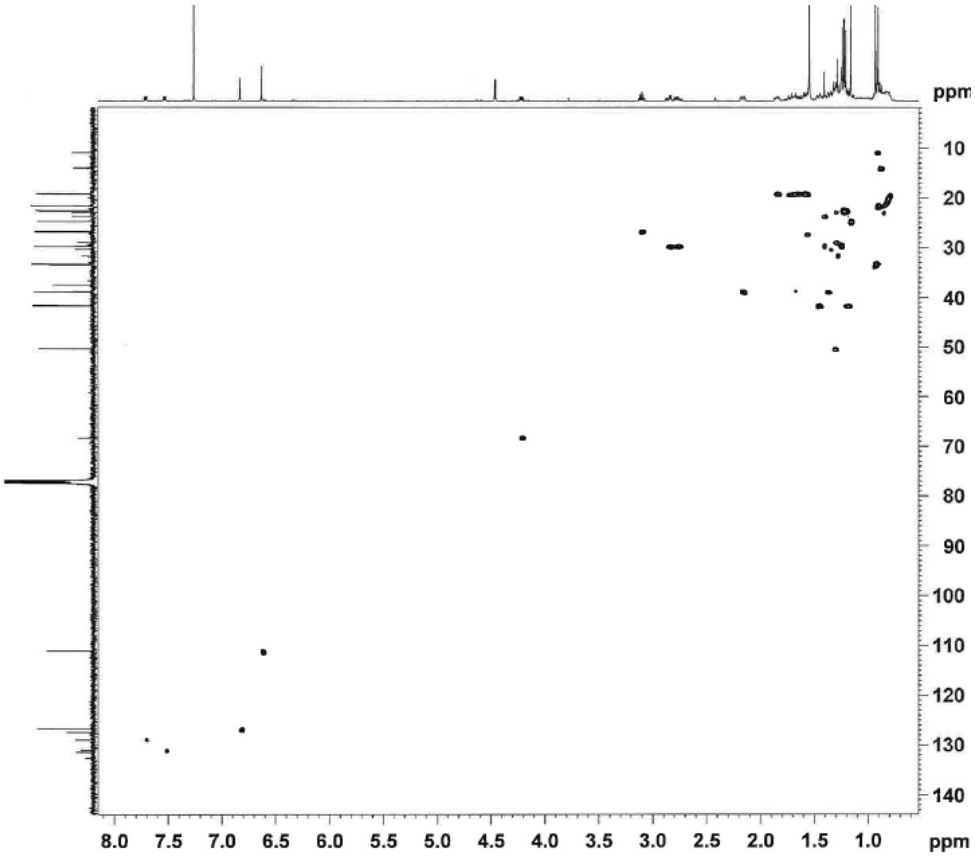

Appendix 23.5 HMBC spectrum of ferruginol (500 MHz for ^{1}H, 125 MHz for ^{13}C; $CDCl_3$)

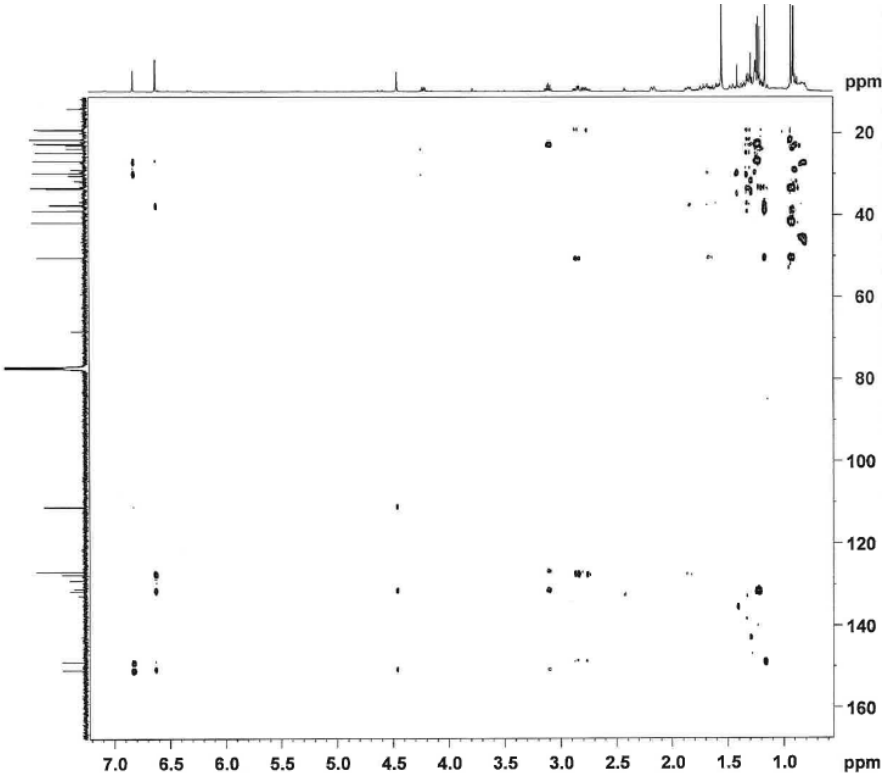

Appendix 23.6 NOESY spectrum of ferruginol (500 MHz; $CDCl_3$)

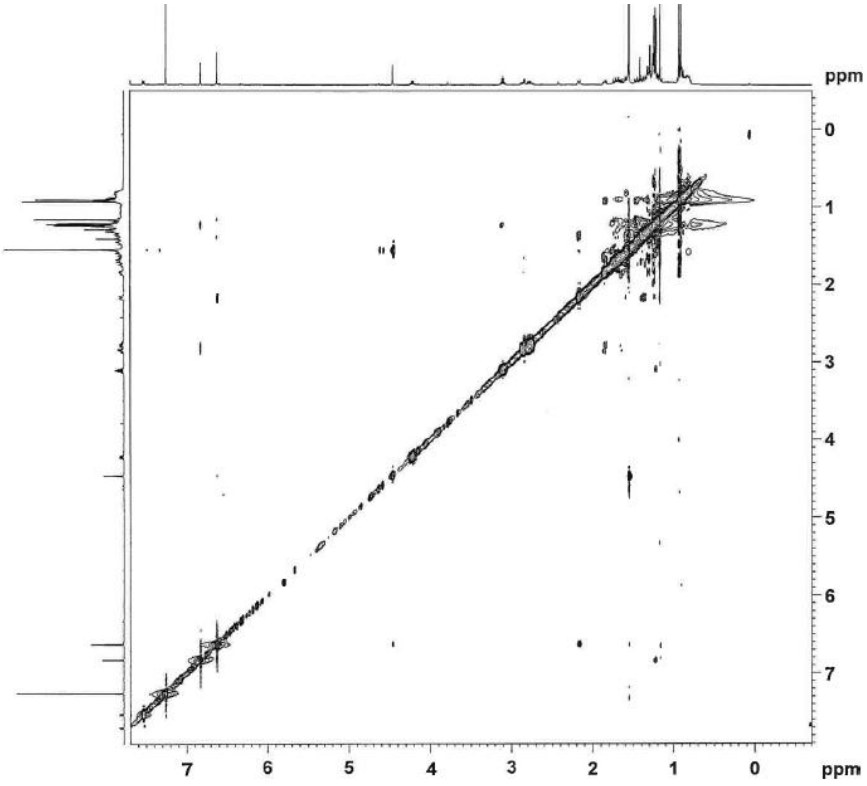

Appendix 24 NMR spectra of salvinolonyl 12-methyl ether

Appendix 24.1 ^{1}H NMR spectrum of salvinolonyl 12-methyl ether (500 MHz; $CDCl_3$)

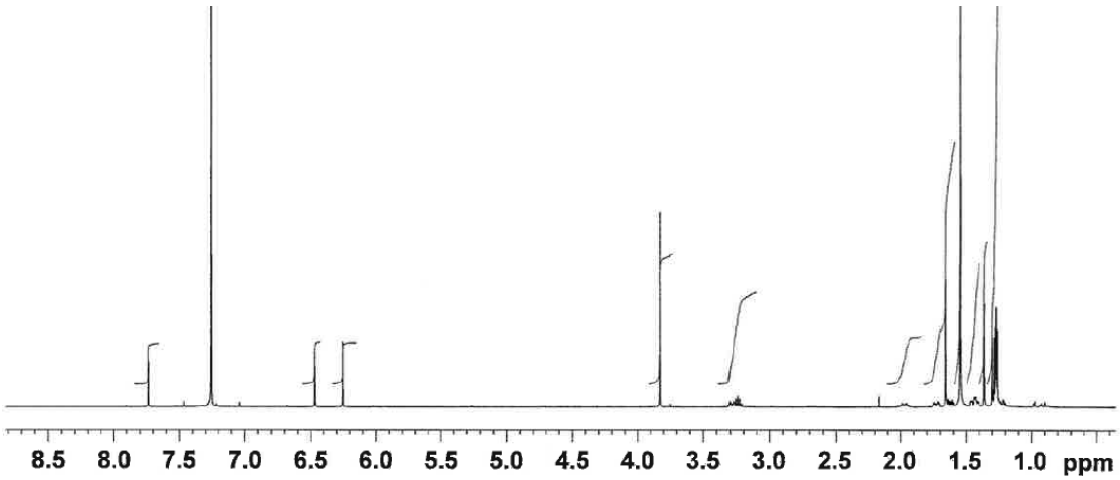

Figure 24.2 COSY spectrum of salvinolonyl 12-methyl ether (500 MHz; $CDCl_3$)

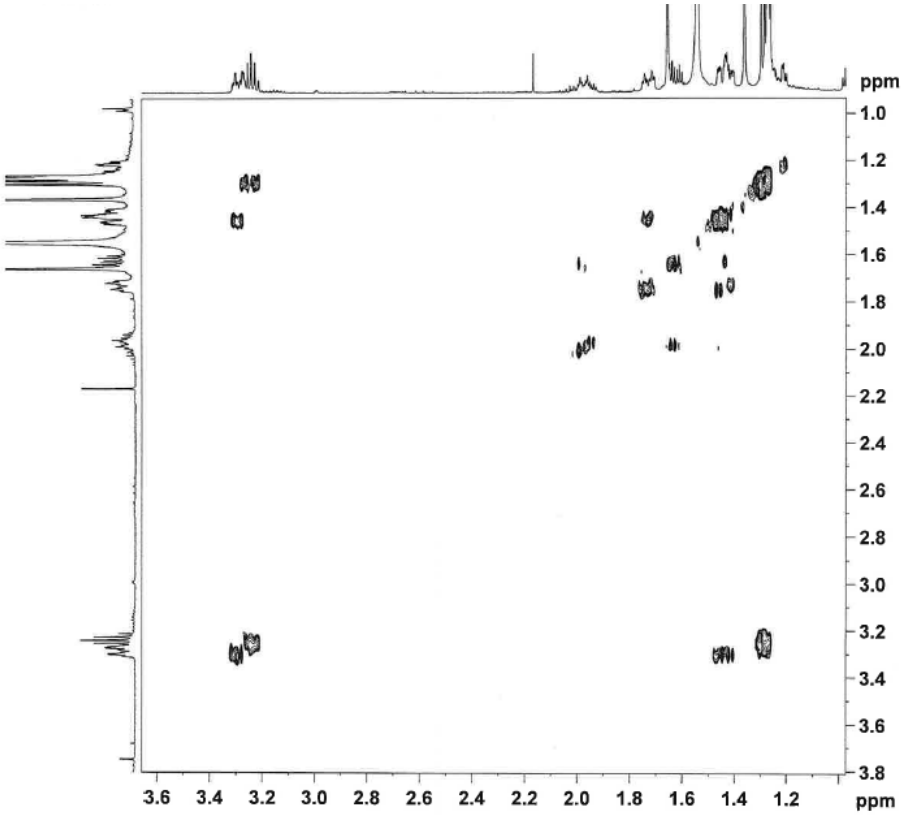

Appendix 24.3 ^{13}C NMR spectrum of salvinolonyl 12-methyl ether (125 MHz; $CDCl_3$)

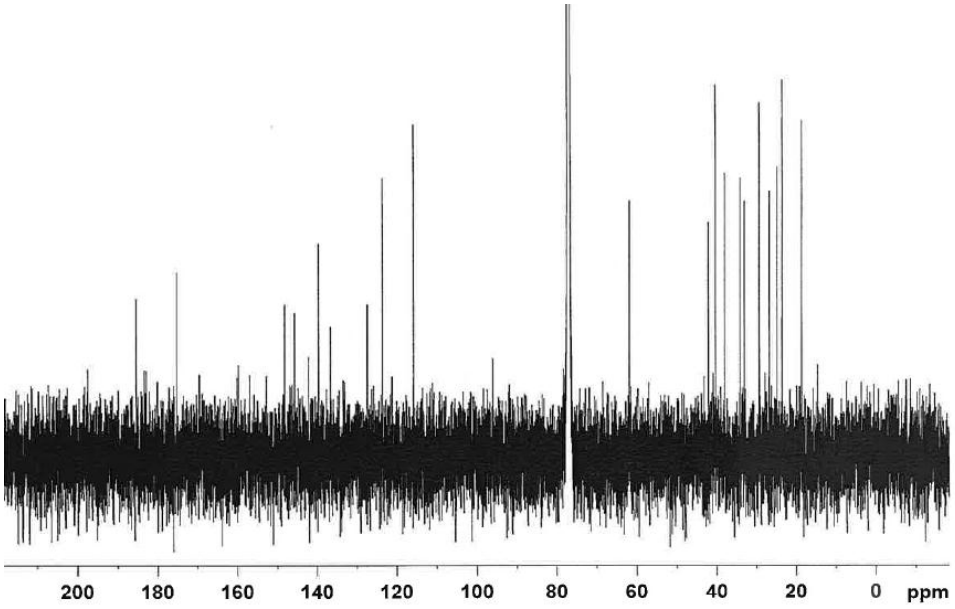

Appendix 24.4 HMQC spectrum of salvinolonyl 12-methyl ether (500 MHz for ^{1}H, 125 MHz for ^{13}C; $CDCl_3$)

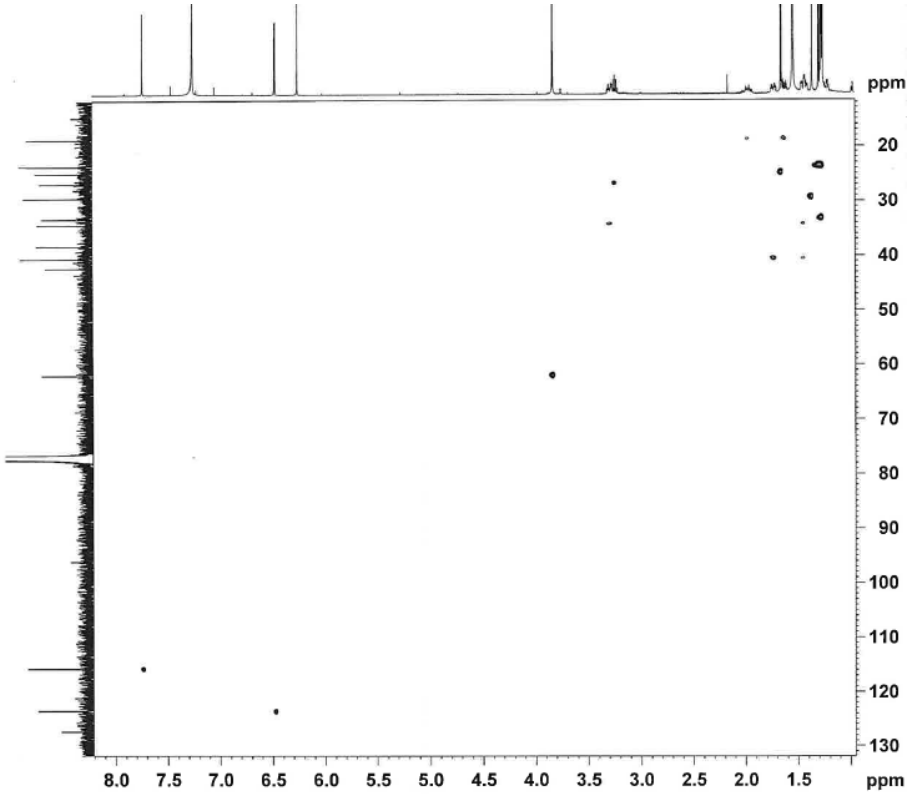

Appendix 24.5 HMBC spectrum of salvinolonyl 12-methyl ether (500 MHz for ^{1}H, 125 MHz for ^{13}C; $CDCl_3$)

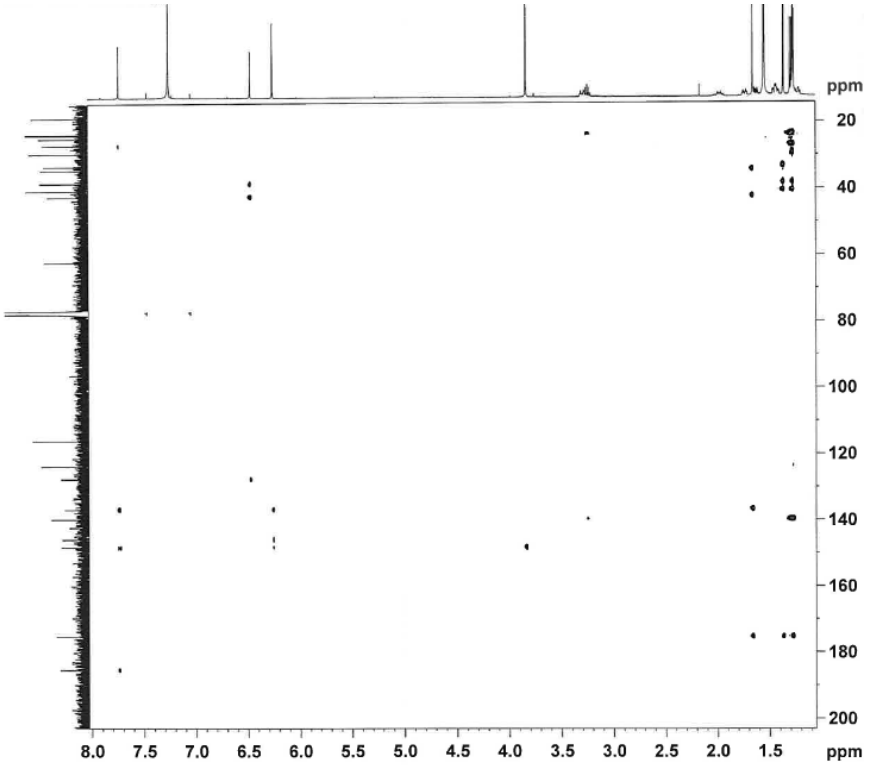

Appendix 24.6 NOESY spectrum of salvinolonyl 12-methyl ether (500 MHz; $CDCl_3$)

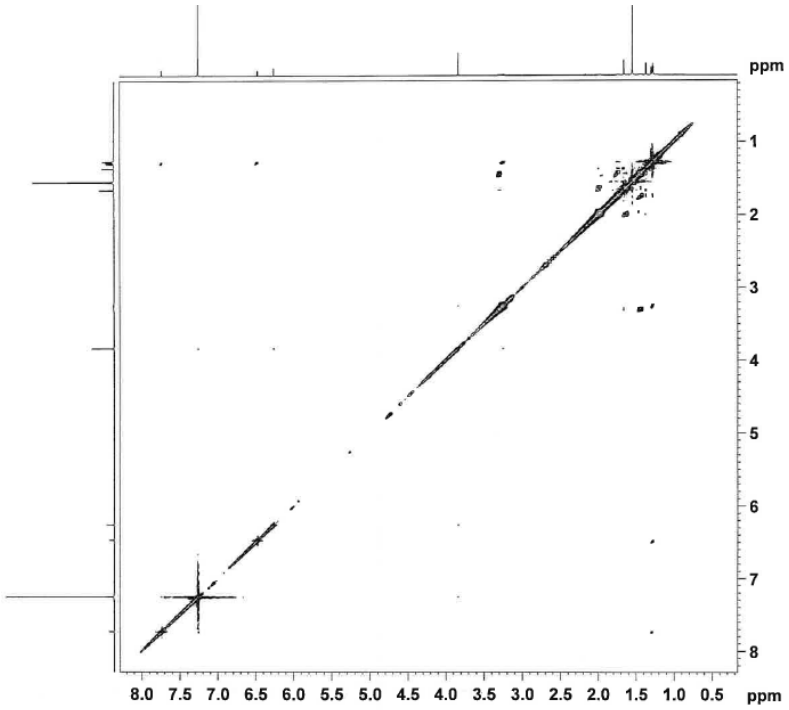

Appendix 25 NMR spectra of 7α-acetoxy-14-hydroxy-8,13-abietadiene-11,12-dione

Appendix 25.1 ^{1}H NMR spectrum of 7α-acetoxy-14-hydroxy-8,13-abietadiene-11,12-dione (500 MHz; $CDCl_3$)

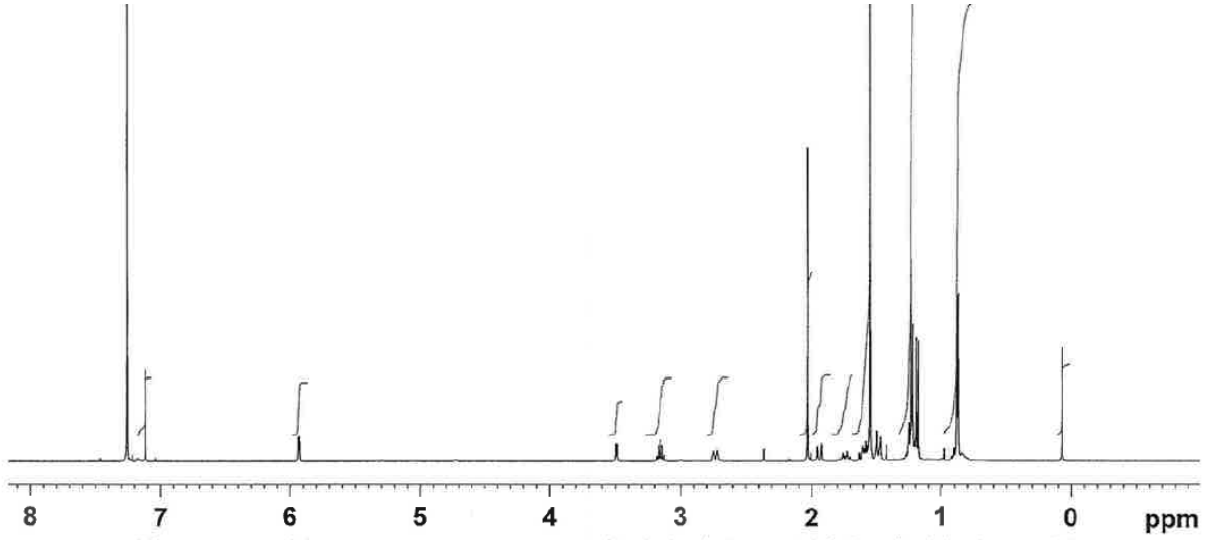

Appendix 25.2 COSY spectrum of 7α-acetoxy-14-hydroxy-8,13-abietadiene-11,12-dione (500 MHz; $CDCl_3$)

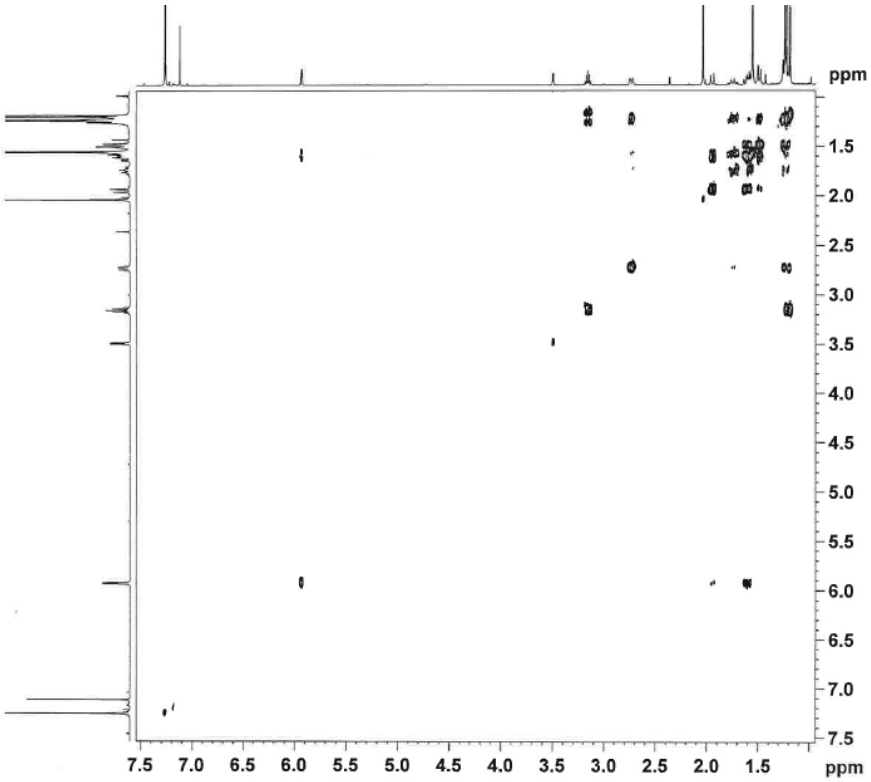

Figure 25.3 ^{13}C NMR spectrum of 7α-acetoxy-14-hydroxy-8,13-abietadiene-11,12-dione (125 MHz; $CDCl_3$)

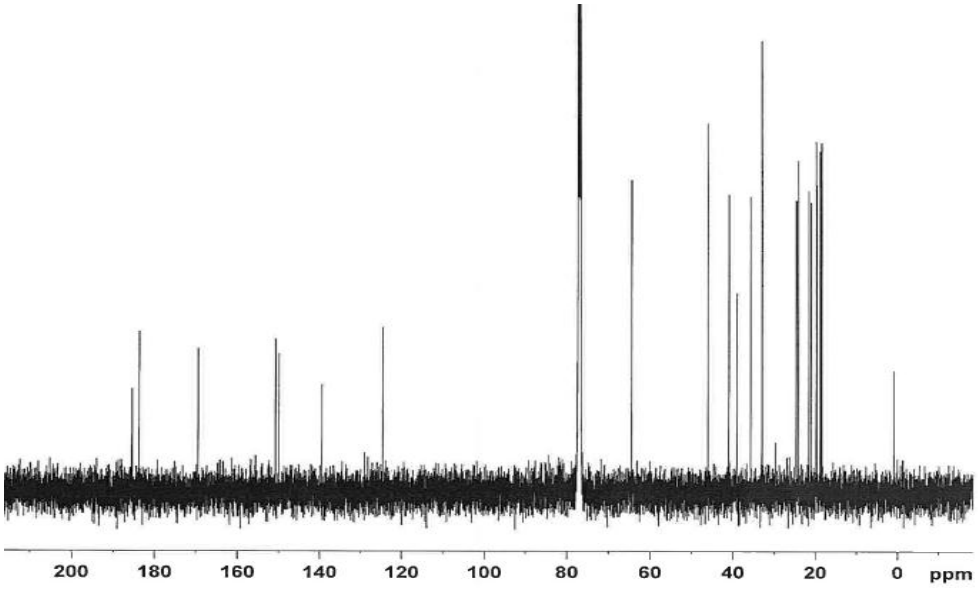

Appendix 25.4 HMQC spectrum of 7α-acetoxy-14-hydroxy-8,13-abietadiene-11,12-dione (500 MHz for ^{1}H, 125 MHz for ^{13}C; $CDCl_3$)

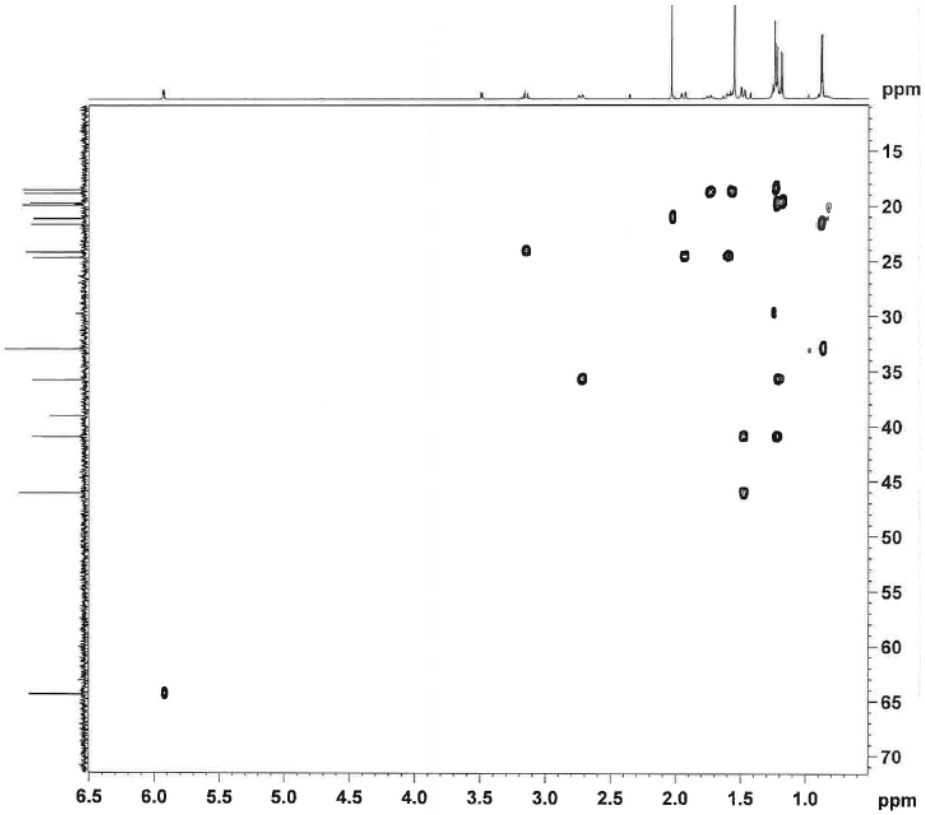

Appendix 25.5 HMBC spectrum of 7α-acetoxy-14-hydroxy-8,13-abietadiene-11,12-dione (500 MHz for ^{1}H, 125 MHz for ^{13}C; $CDCl_3$)

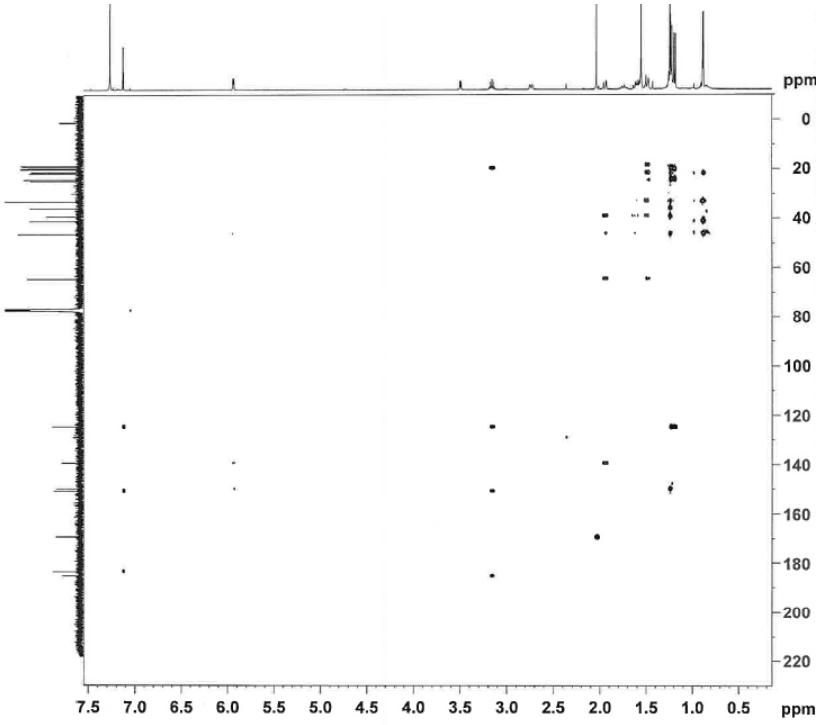

Appendix 25.6 NOESY spectrum of 7α-acetoxy-14-hydroxy-8,13-abietadiene-11,12-dione (500 MHz; $CDCl_3$)

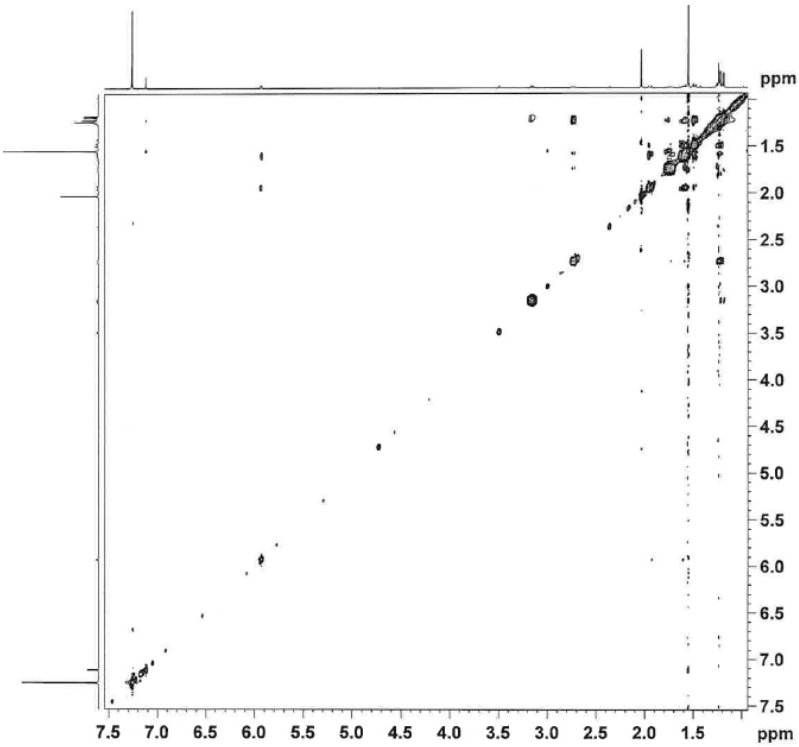

Appendix 26 NMR spectra of 7α,14-dihydroxy-8,13-abietadiene-11,12-dione

*This material was about 60% pure, with 7α-acetoxy-14-hydroxy-8,13-abietadiene-11,12-dione and plasticiser (phthalate) as the major impurities.

Appendix 26.1 ^{1}H NMR spectrum of 7α,14-dihydroxy-8,13-abietadiene-11,12-dione (500 MHz; $CDCl_3$)

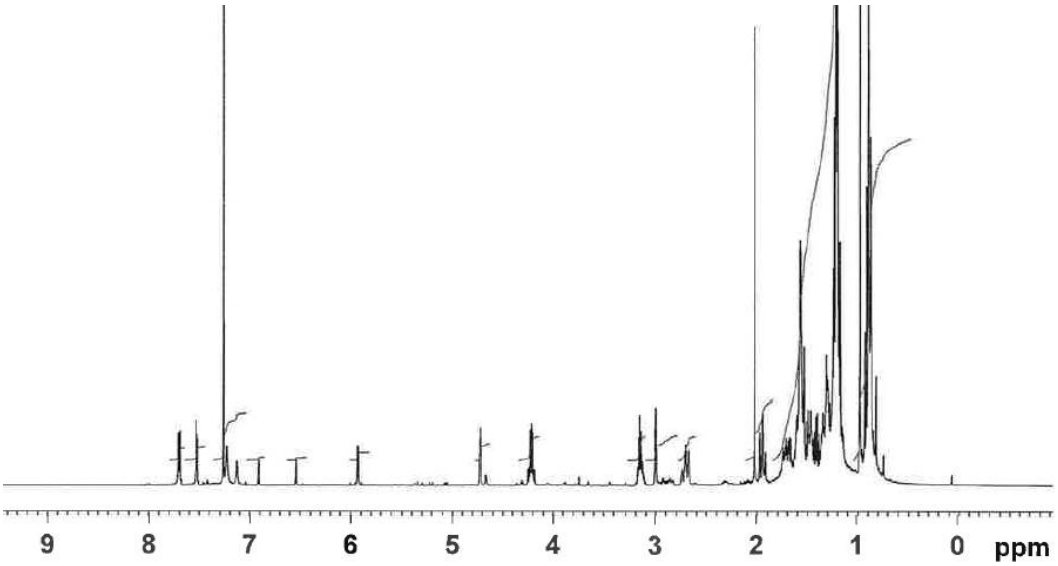

Appendix 26.2 COSY spectrum of 7α,14-dihydroxy-8,13-abietadiene-11,12-dione (500 MHz; $CDCl_3$)

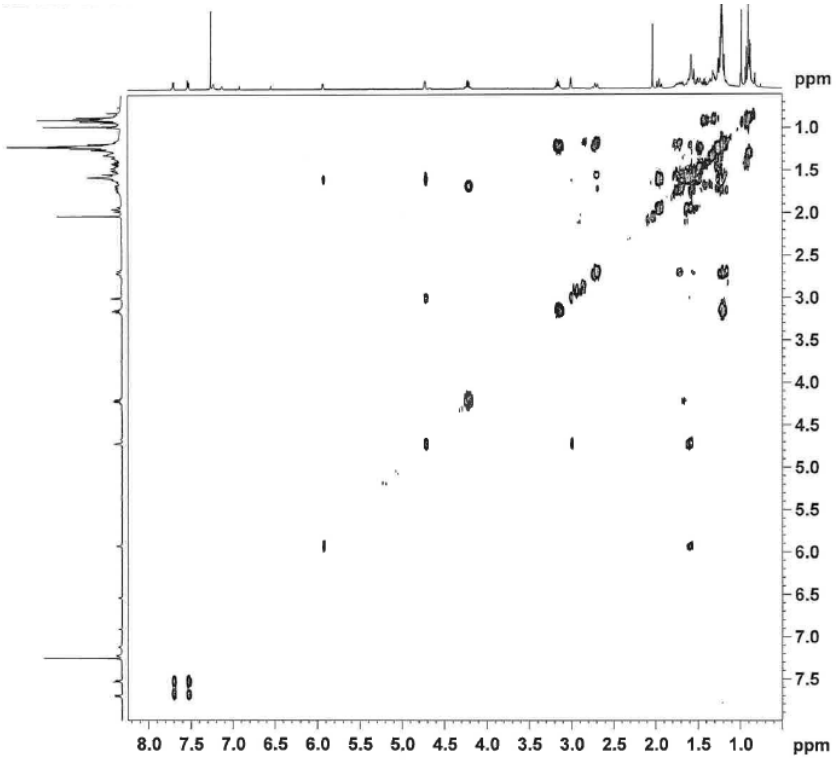

Appendix 26.3 ^{13}C NMR spectrum of 7α,14-dihydroxy-8,13-abietadiene-11,12-dione (125 MHz; $CDCl_3$)

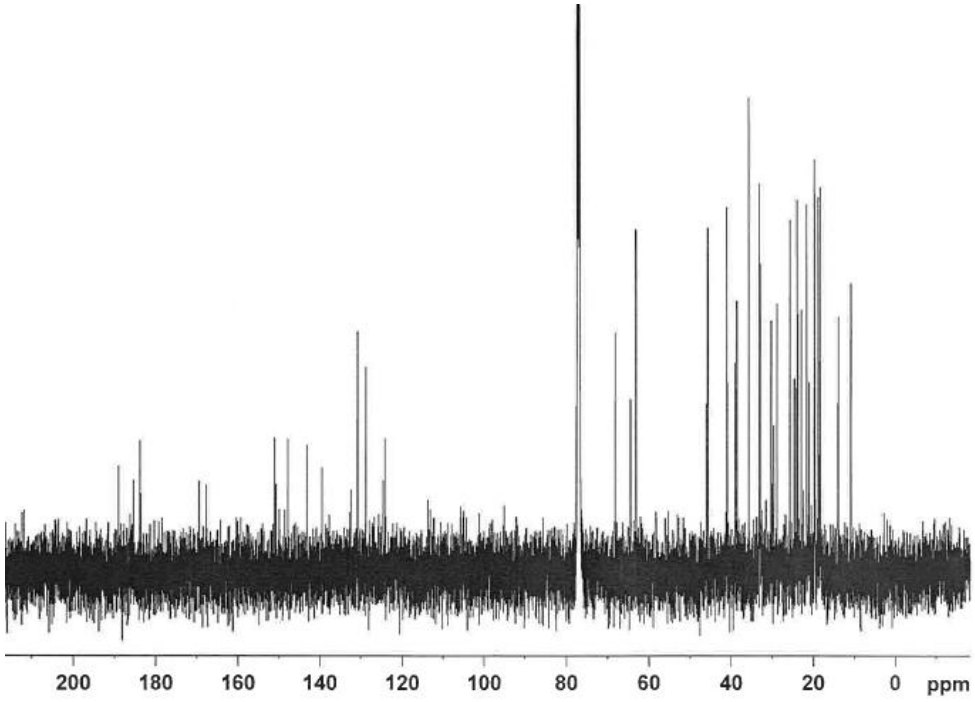

Appendix 26.4 HMQC spectrum of 7α,14-dihydroxy-8,13-abietadiene-11,12-dione (500 MHz for ^{1}H, 125 MHz for ^{13}C; $CDCl_3$)

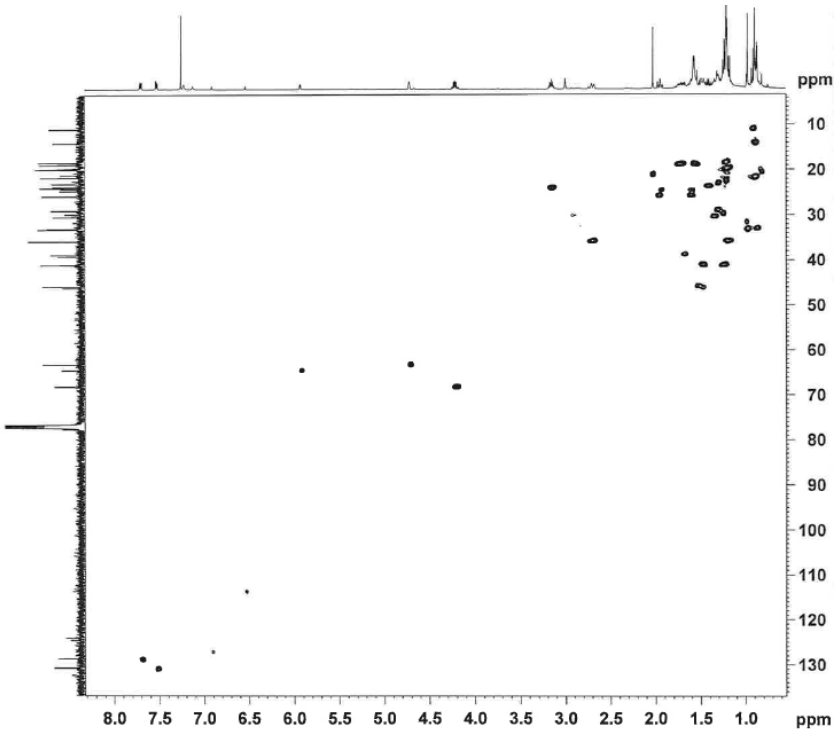

Appendix 26.5 HMBC spectrum of 7α,14-dihydroxy-8,13-abietadiene-11,12-dione (500 MHz for ^{1}H, 125 MHz for ^{13}C; $CDCl_3$)

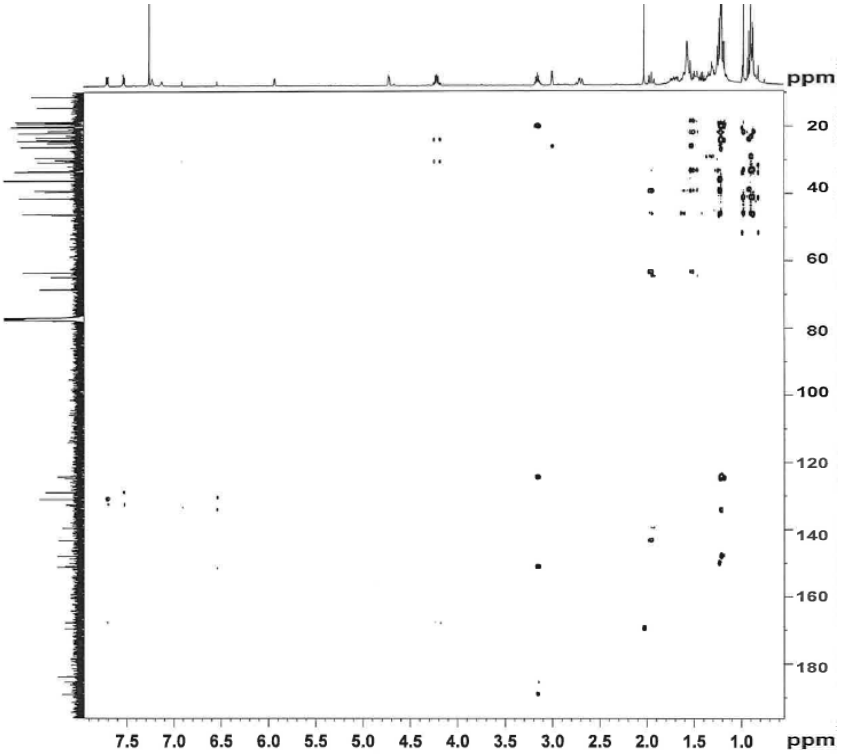

Appendix 26.6 NOESY spectrum of 7α,14-dihydroxy-8,13-abietadiene-11,12-dione (500 MHz; $CDCl_3$)

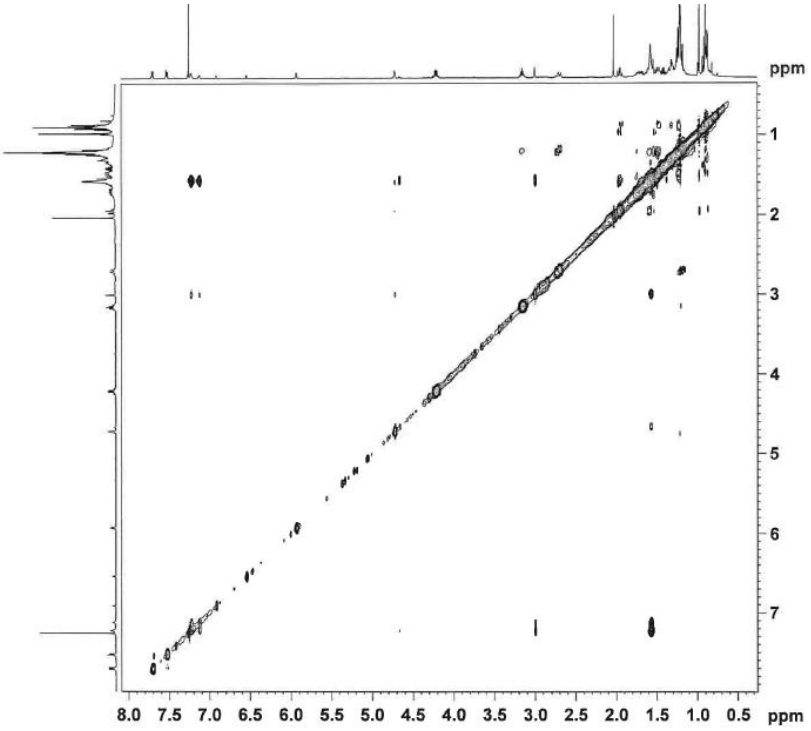

Appendix 27 NMR spectra of microstegiol

*This material was about 95% pure, with plasticiser (phthalate) as the major impurity.

Appendix 27.1 ^{1}H NMR spectrum of microstegiol (500 MHz; $CDCl_3$)

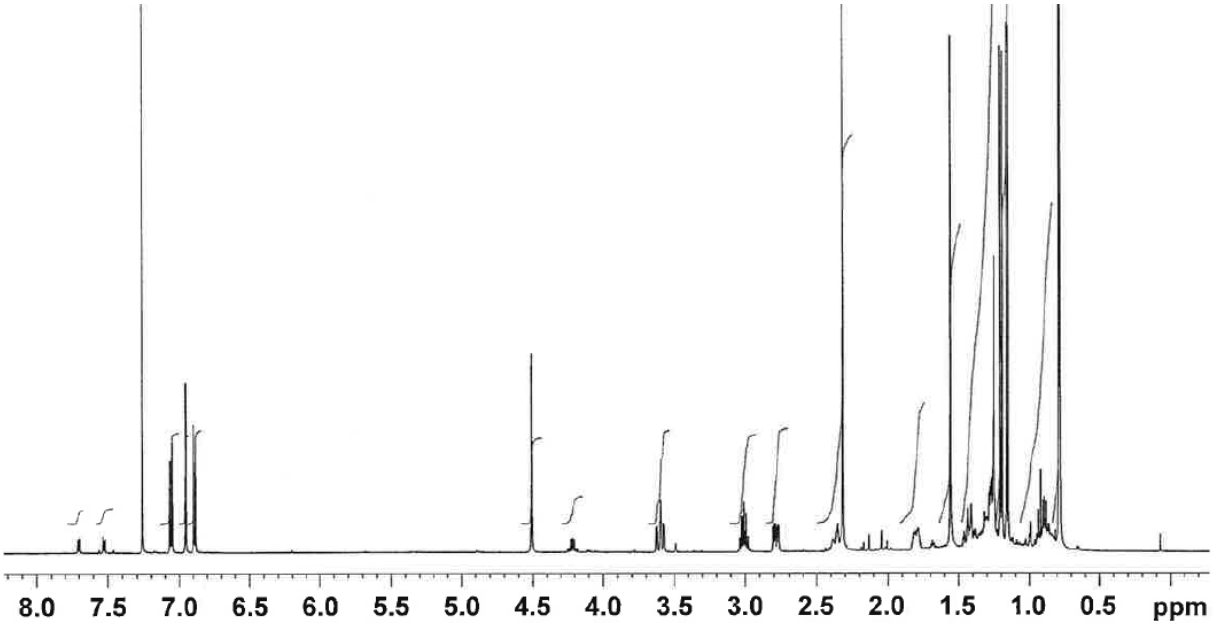

Appendix 27.2 COSY spectrum of microstegiol ($CDCl_3$; 500 MHz)

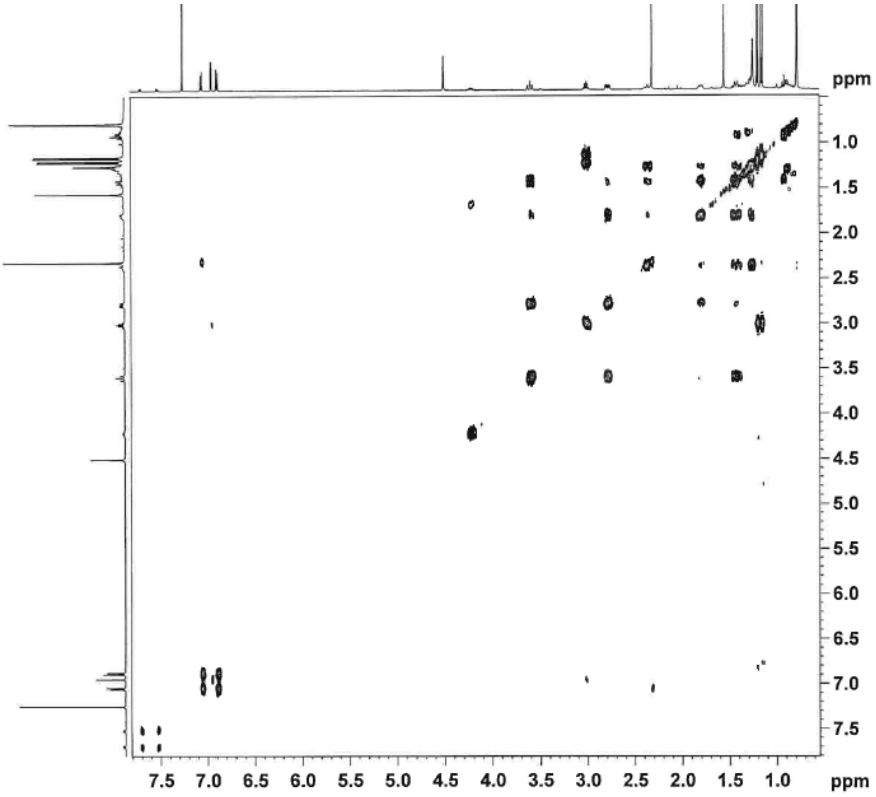

Appendix 27.3 ^{13}C NMR spectrum of microstegiol (125 MHz; $CDCl_3$)

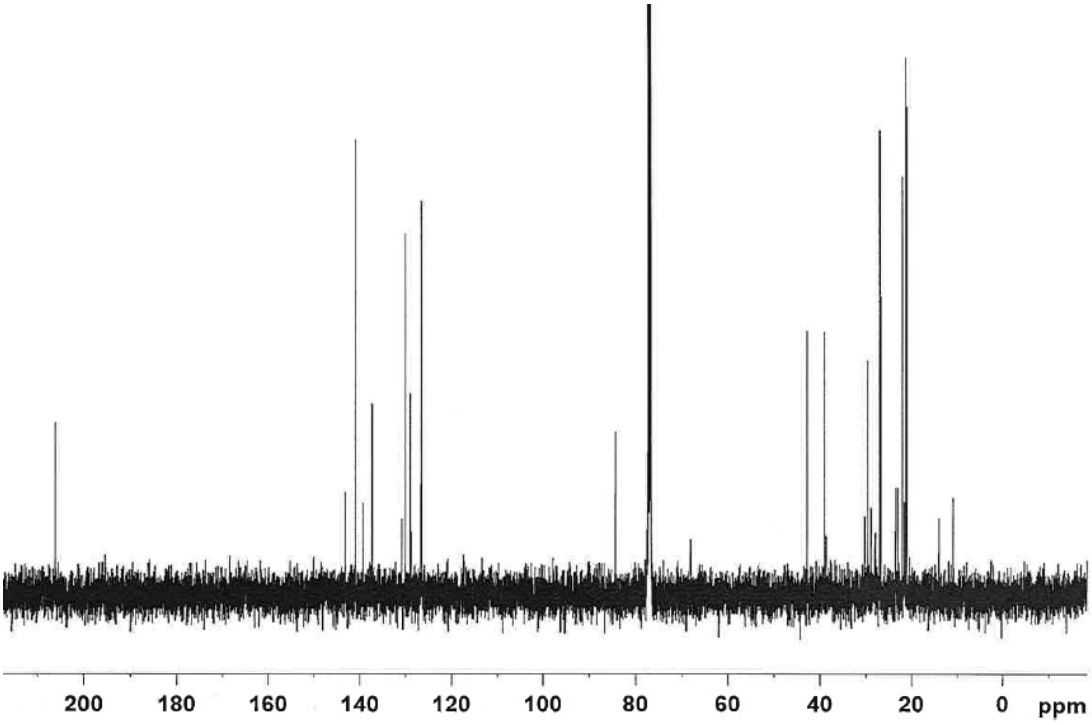

Appendix 27.4 HMQC spectrum of microstegiol (500 MHz for ^{1}H, 125 MHz for ^{13}C; $CDCl_3$)

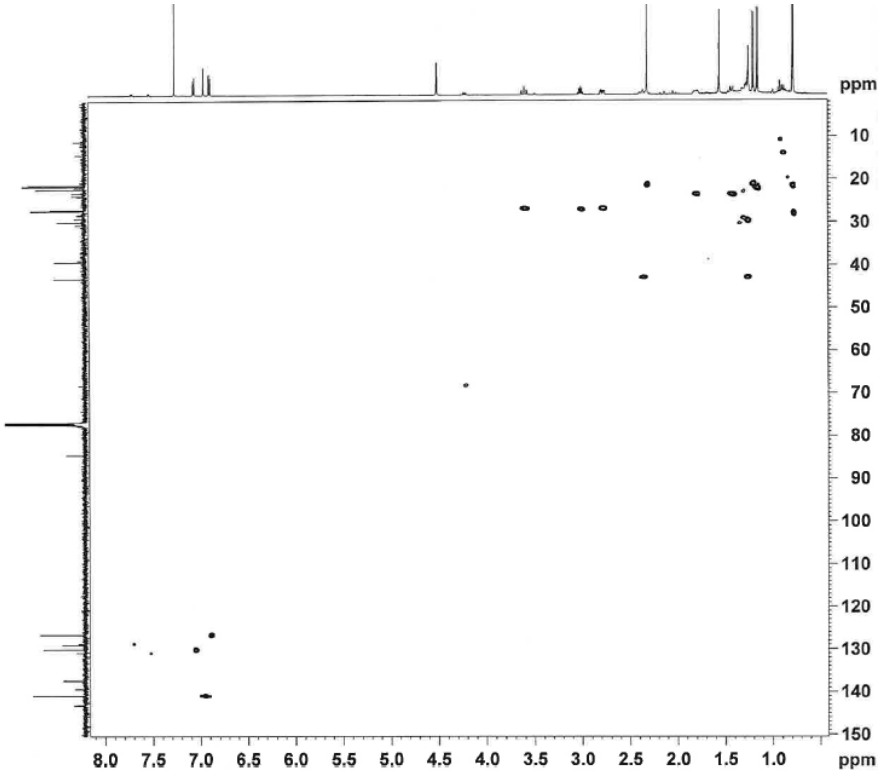

Appendix 27.5 HMBC spectrum of microstegiol (500 MHz for ^{1}H, 125 MHz for ^{13}C; $CDCl_3$)

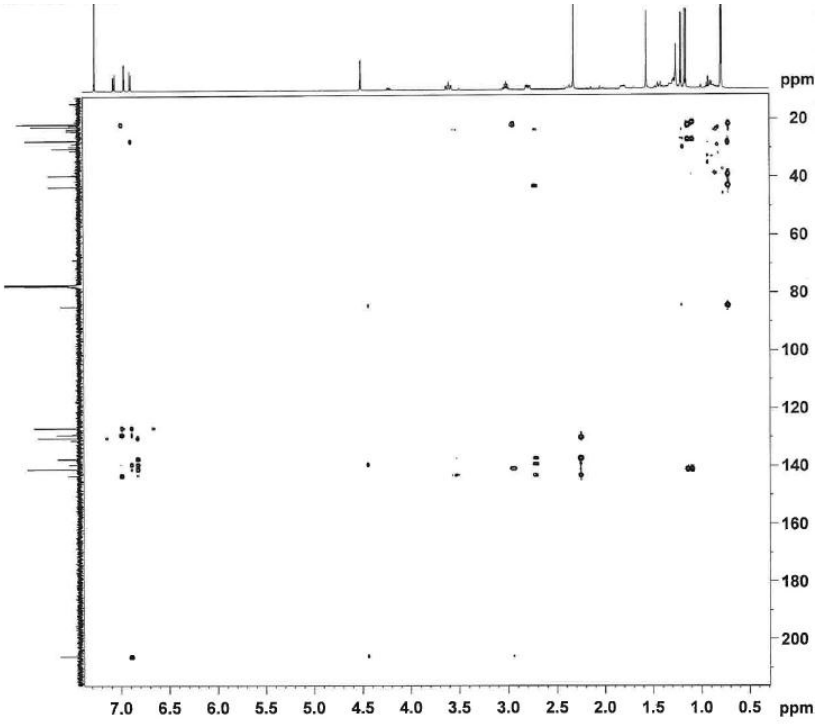

Appendix 27.6 NOESY spectrum of microstegiol (500 MHz; $CDCl_3$)

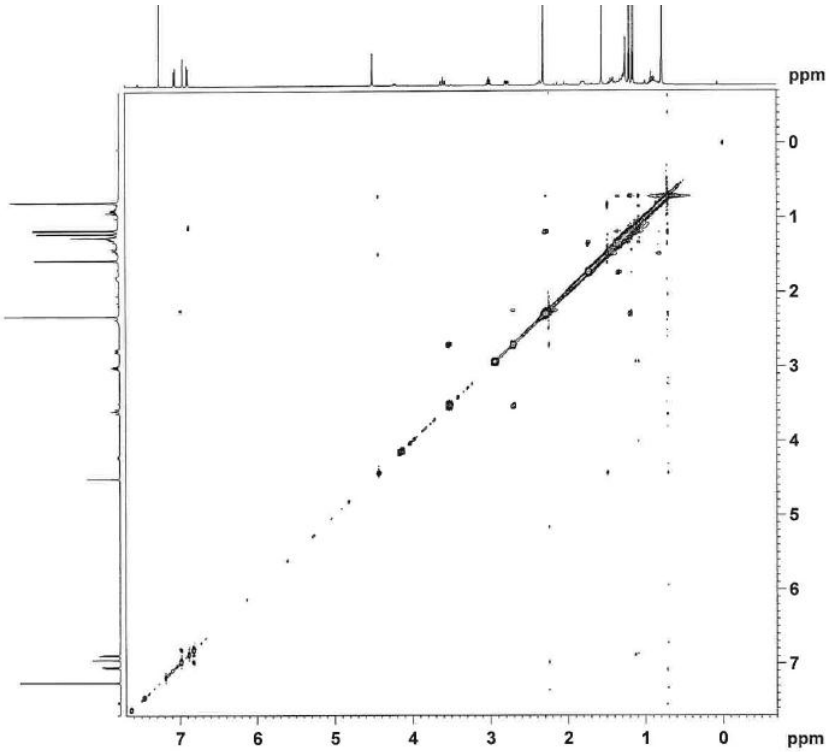

Appendix 28 NMR spectra of compound 3 (1-oxomicrostegiol)

Appendix 28.1 ^{1}H NMR spectrum of compound 3 (1-oxomicrostegiol) (500 MHz; $CDCl_3$)

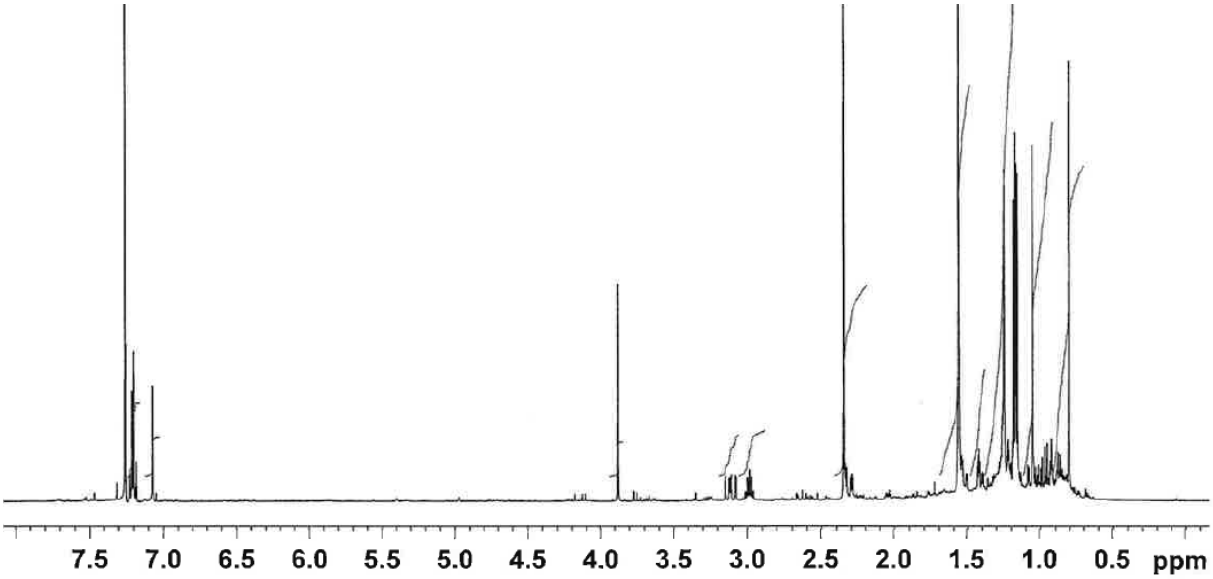

Appendix 28.2 COSY spectrum of compound 3 (1-oxomicrostegiol) (500 MHz; $CDCl_3$)

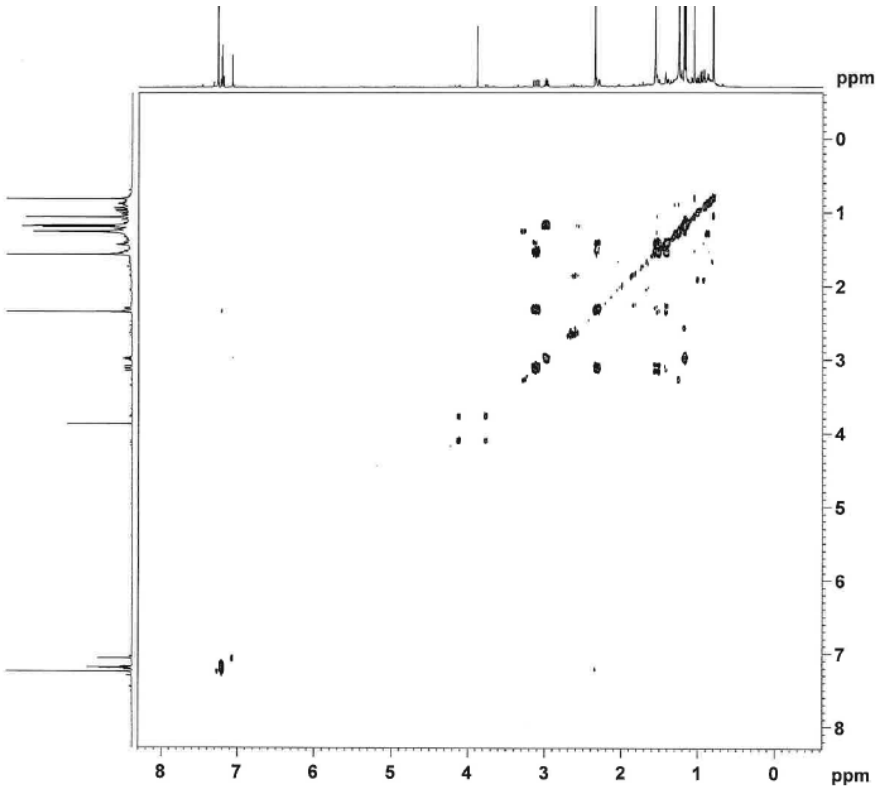

Appendix 28.3 ^{13}C NMR spectrum of compound 3 (1-oxomicrostegiol) (125 MHz; $CDCl_3$)

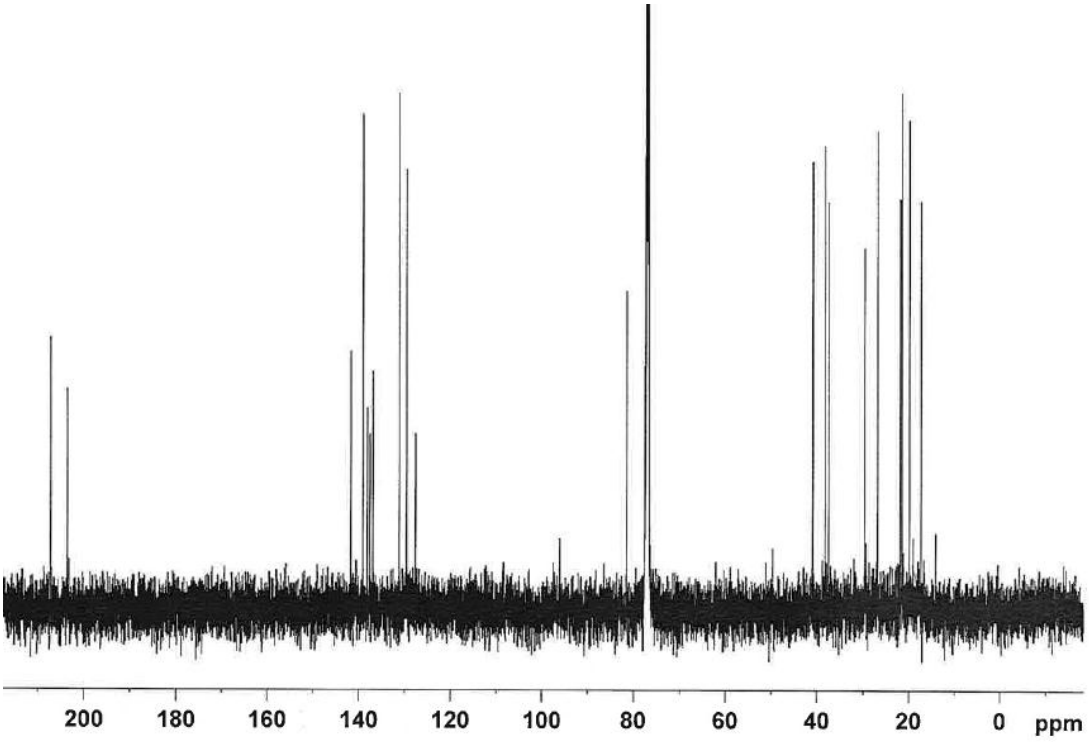

Appendix 28.4 HMQC spectrum of compound 3 (1-oxomicrostegiol) (500 MHz for ^{1}H, 125 MHz for ^{13}C; $CDCl_3$)

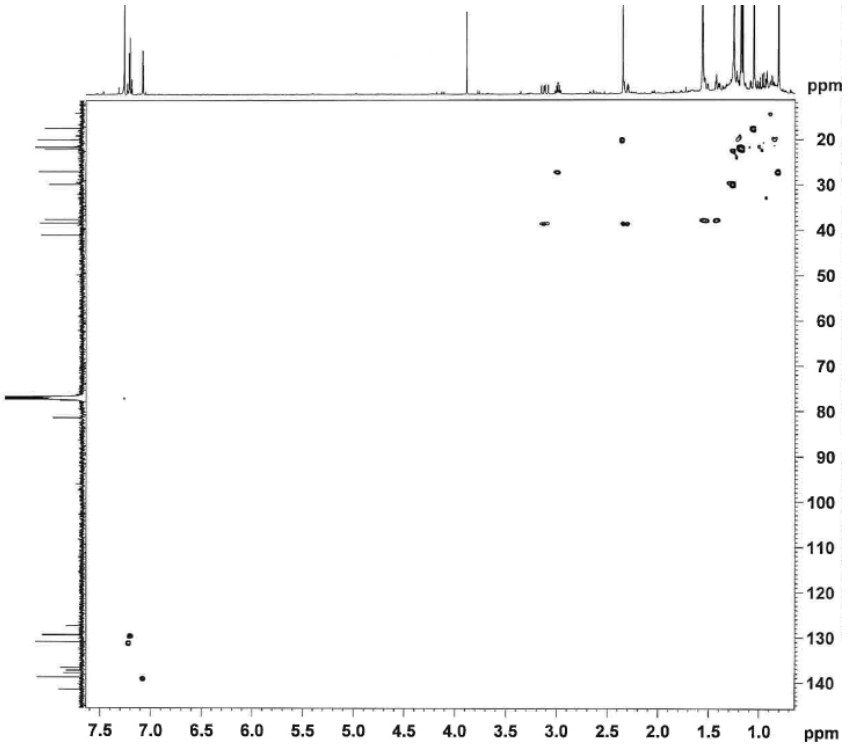

Appendix 28.5 HMBC spectrum of compound 3 (1-oxomicrostegiol) (500 MHz for ^{1}H, 125 MHz for ^{13}C; $CDCl_3$)

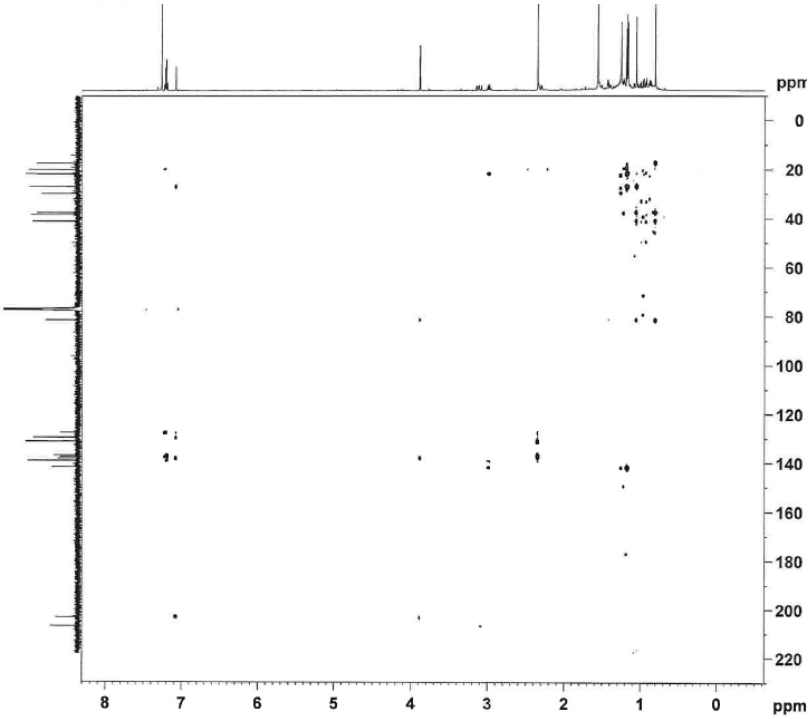

Appendix 28.6 NOESY spectrum of compound 3 (1-oxomicrostegiol) (500 MHz; $CDCl_3$)

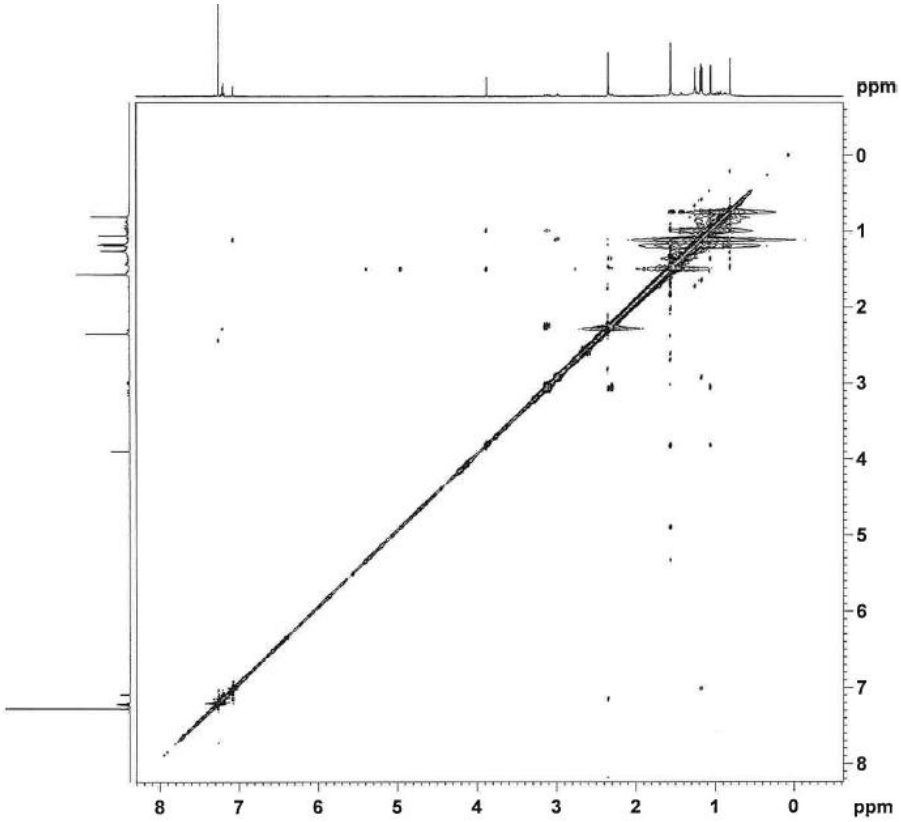

Appendix 29 NMR spectra of compound 4 (viroxocane)

*Judging from the NMR spectra, this sample was about 95% pure.

Appendix 29.1 ^{1}H NMR spectrum of compound 4 (viroxocane) (500 MHz; $CDCl_3$)

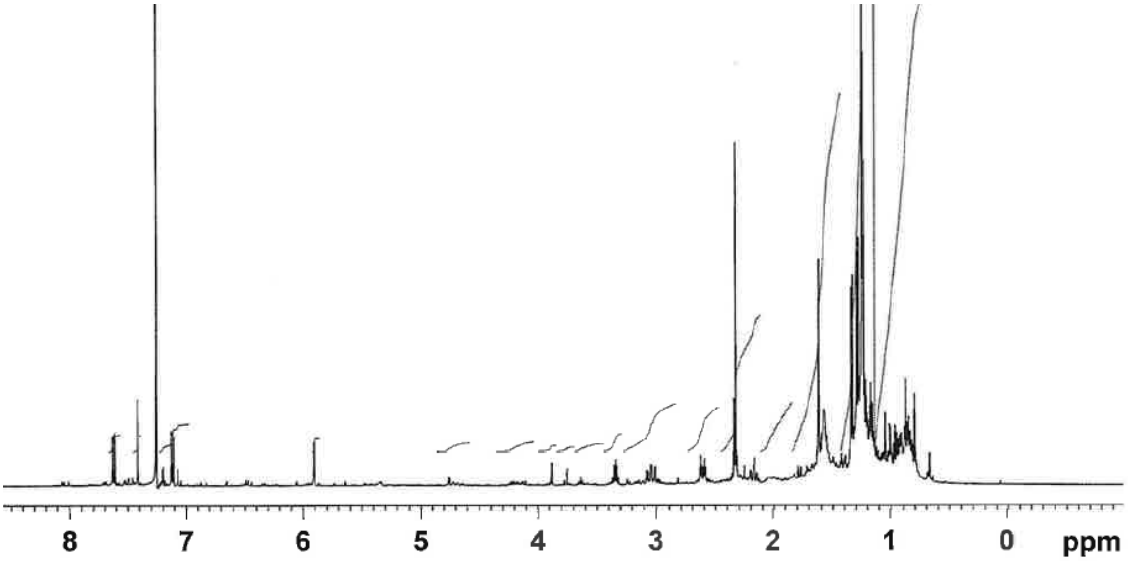

Figure 29.2 COSY NMR spectrum of compound 4 (500 MHz; $CDCl_3$)

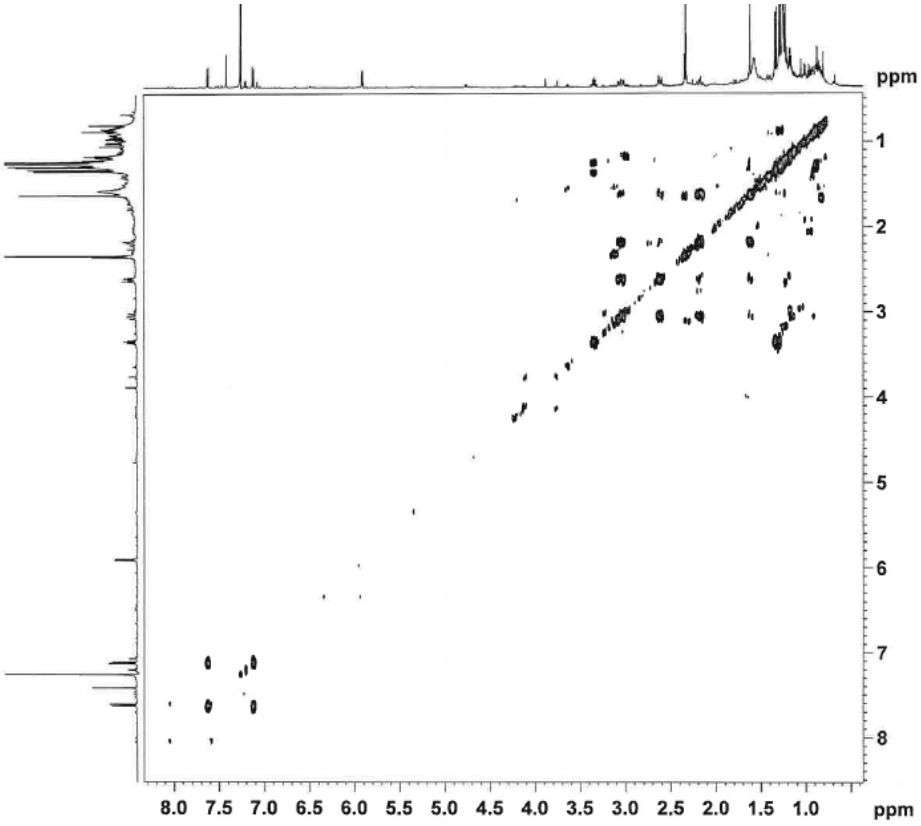

Appendix 29.3 ^{13}C NMR spectrum of compound 4 (viroxocane) (125 MHz; $CDCl_3$)

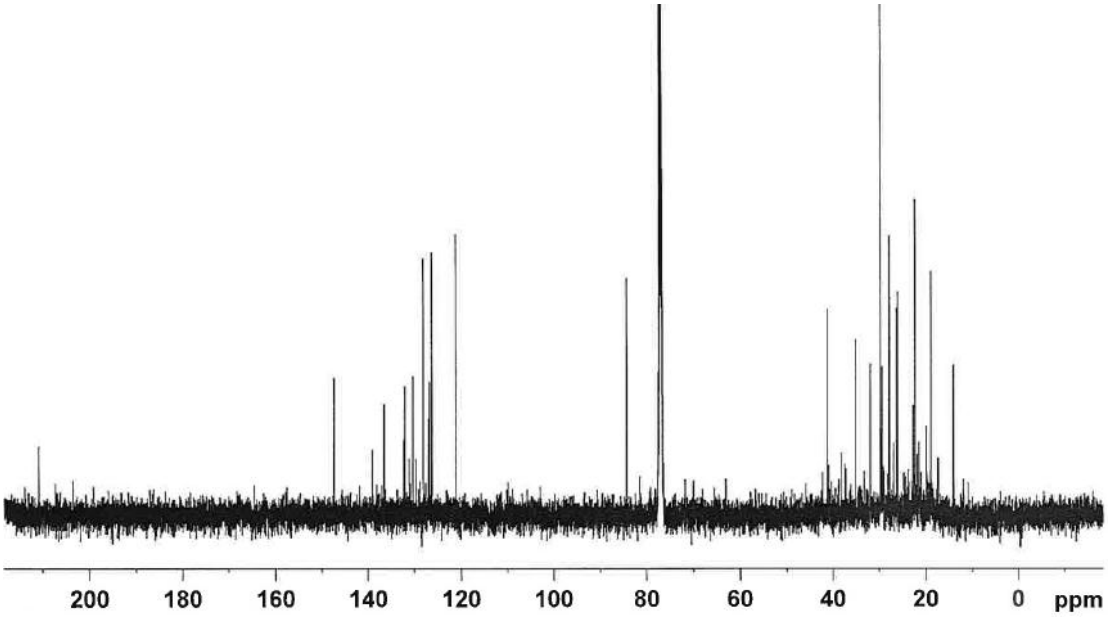

Appendix 29.4 HMQC spectrum of compound 4 (viroxocane) (500 MHz for ^{1}H, 125 MHz for ^{13}C; $CDCl_3$)

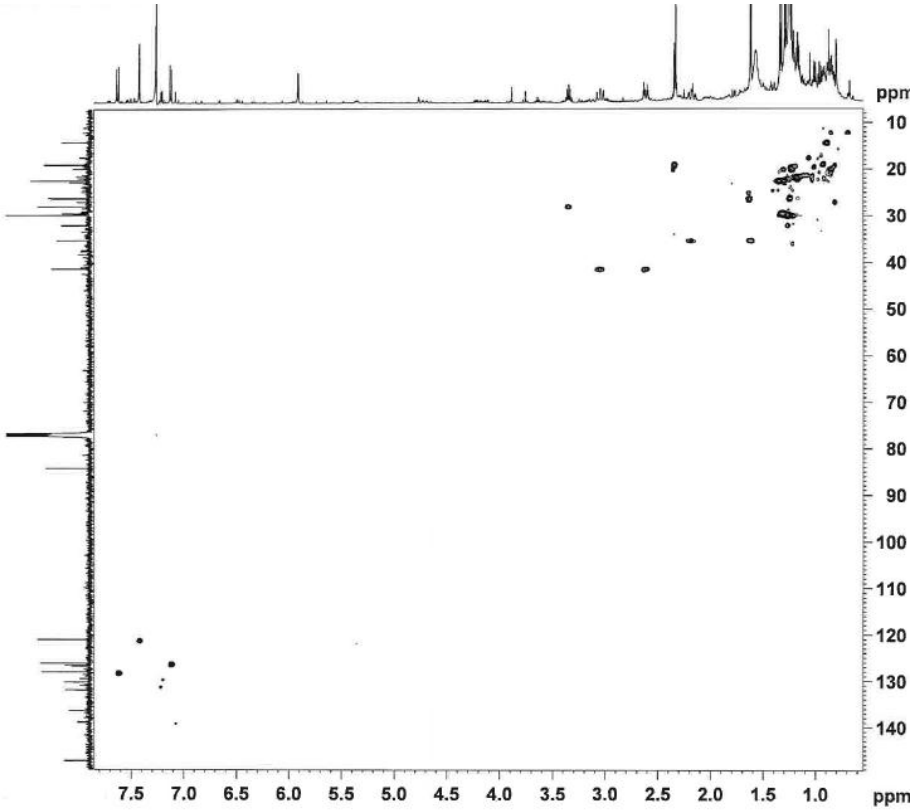

Appendix 29.5 HMBC spectrum of compound 4 (viroxocane) (500 MHz for ^{1}H, 125 MHz for ^{13}C; $CDCl_3$)

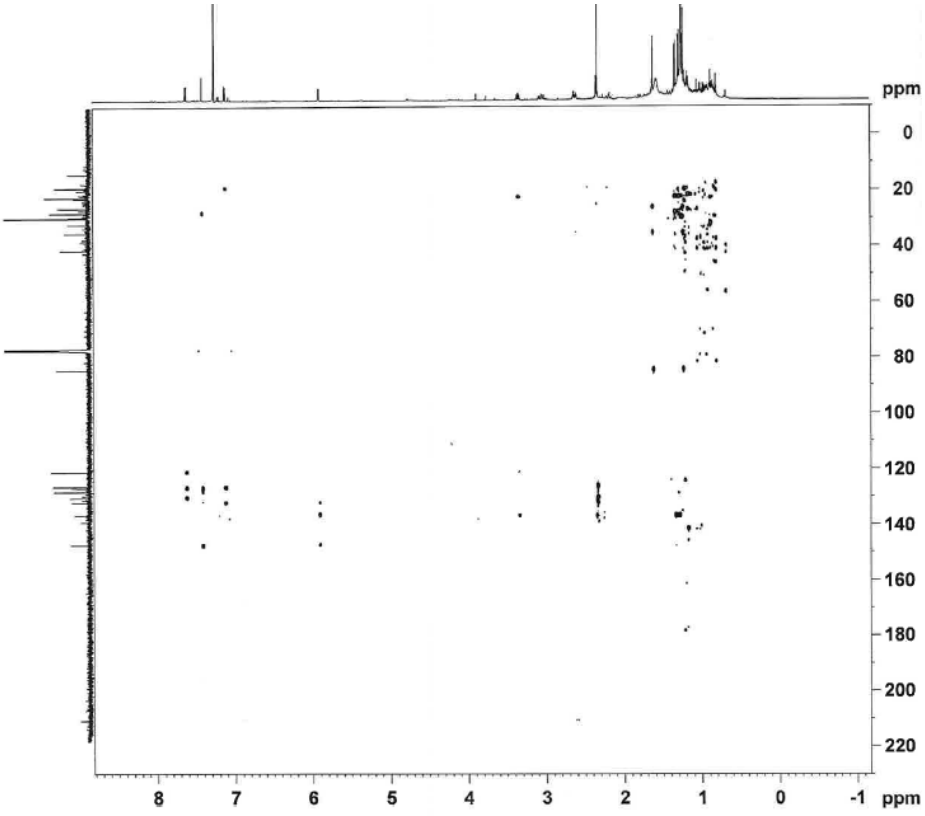

Appendix 29.6 NOESY spectrum of compound 4 (viroxocane) (500 MHz; $CDCl_3$)

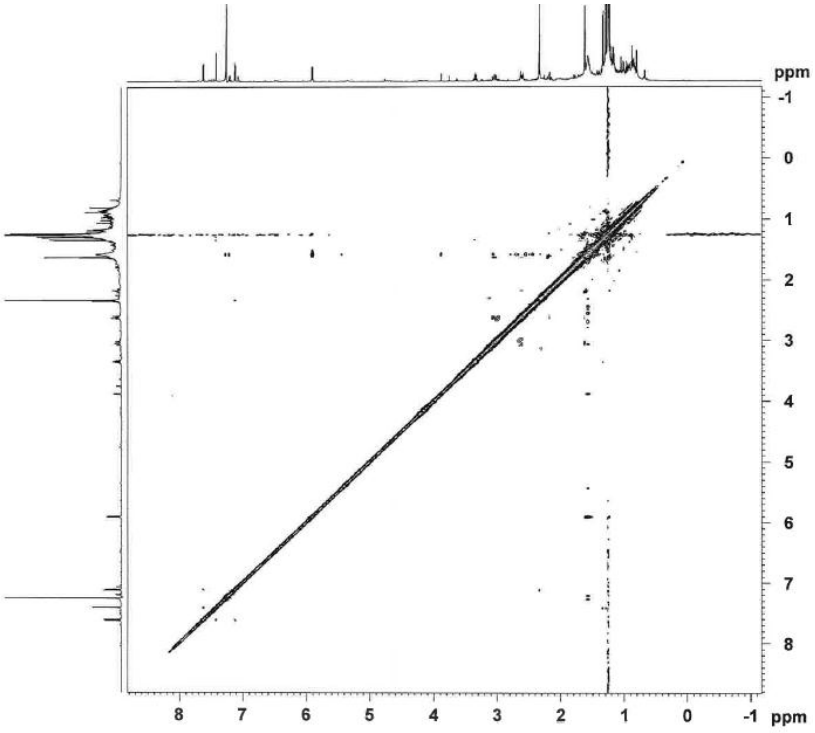

Appendix 30 NMR spectra of compound 5 (viridoquinone)

*This material was about 85% pure, with plasticiser (phthalate) as the major impurity.

Appendix 30.1 ^{1}H NMR spectrum of compound 5 (viridoquinone) (500 MHz; $CDCl_3$)

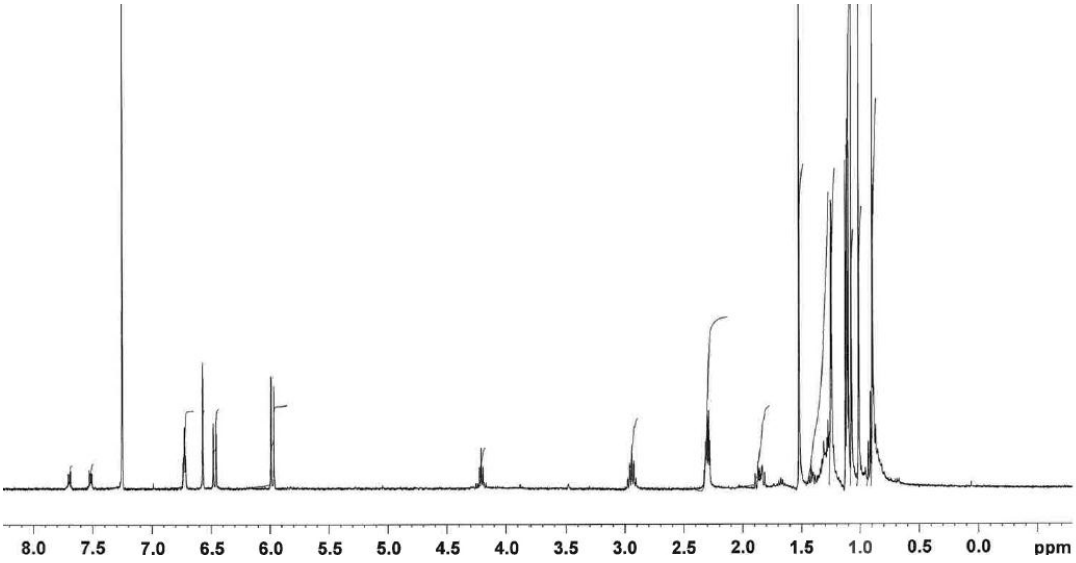

Appendix 30.2 COSY spectrum of compound 5 (viridoquinone) (500 MHz; $CDCl_3$)

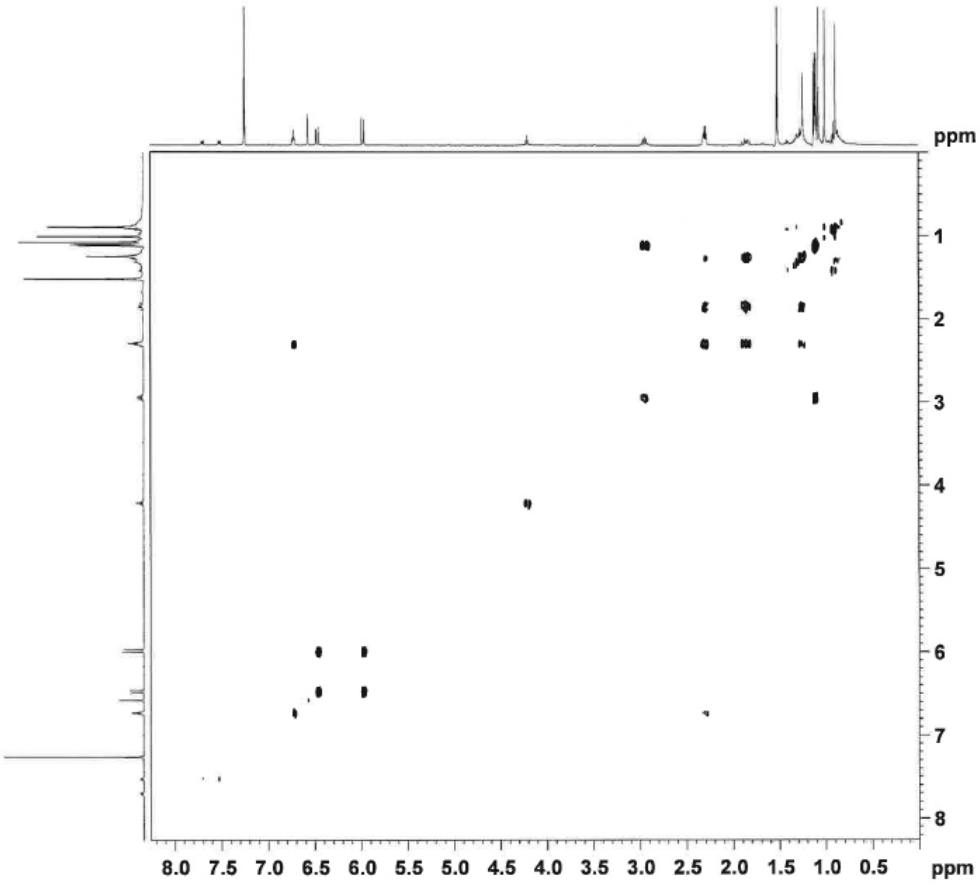

Appendix 30.3 ^{13}C NMR spectrum of compound 5 (viridoquinone) (125 MHz; $CDCl_3$)

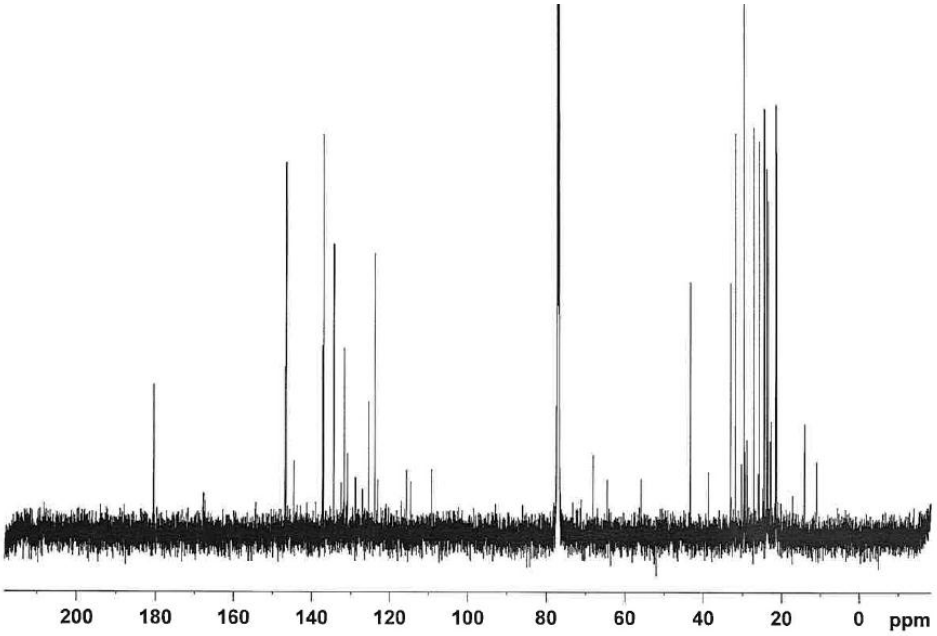

Appendix 30.4 HMQC spectrum of compound 5 (viridoquinone) (500 MHz for ^{1}H, 125 MHz for ^{13}C; $CDCl_3$)

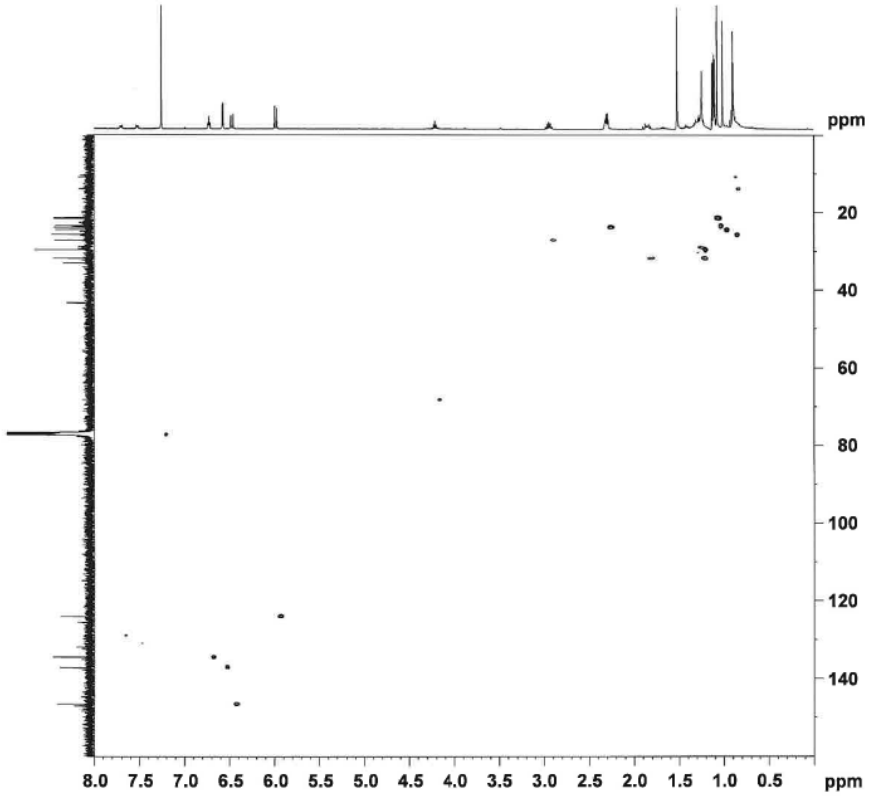

Appendix 30.5 HMBC spectrum of compound 5 (viridoquinone) (500 MHz for ^{1}H, 125 MHz for ^{13}C; $CDCl_3$)

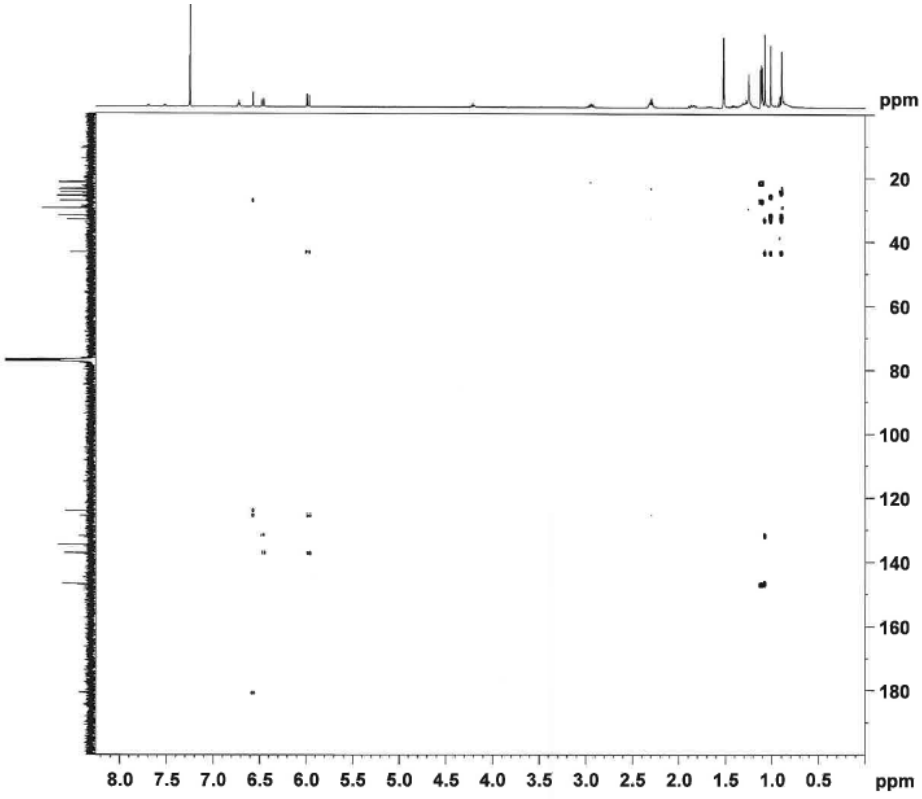

Appendix 30.6 NOESY spectrum of compound 5 (viridoquinone) (500 MHz; $CDCl_3$)

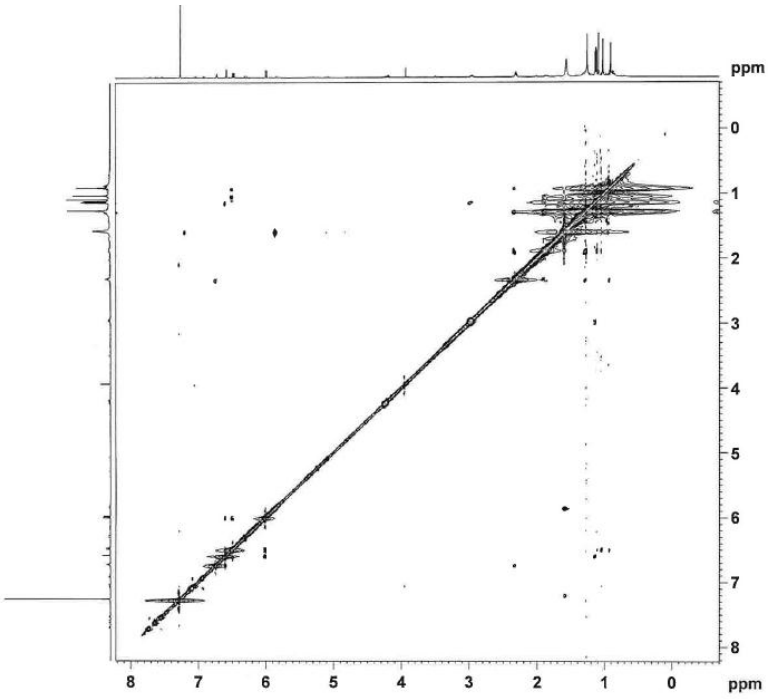

Appendix 31 NMR spectra of a mixture of 2-(4'-alkoxyphenyl) ethyl alkanoates

Appendix 31.1 ^{1}H NMR spectrum of a mixture of 2-(4'-alkoxyphenyl) ethyl alkanoates (500 MHz; $CDCl_3$)

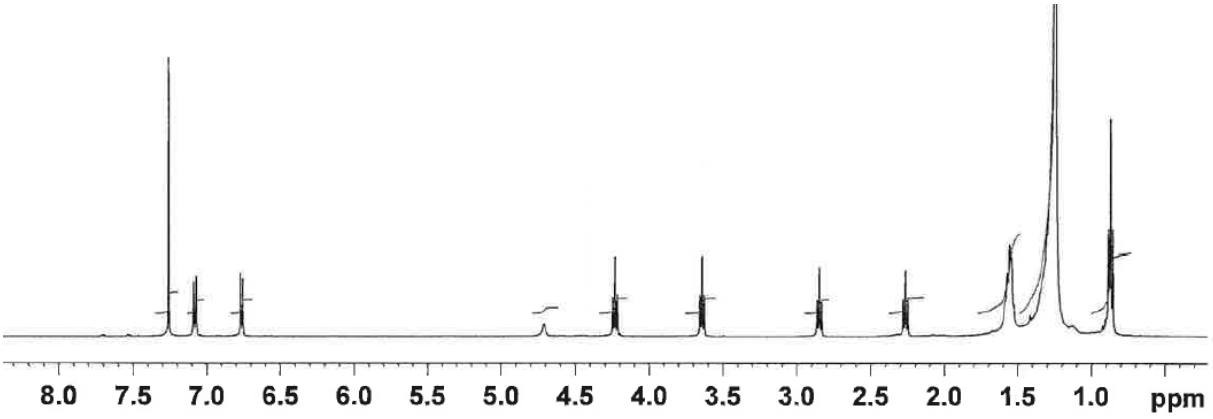

Appendix 31.2 COSY spectrum of a mixture of 2-(4'-alkoxyphenyl) ethyl alkanoates (500 MHz; $CDCl_3$)

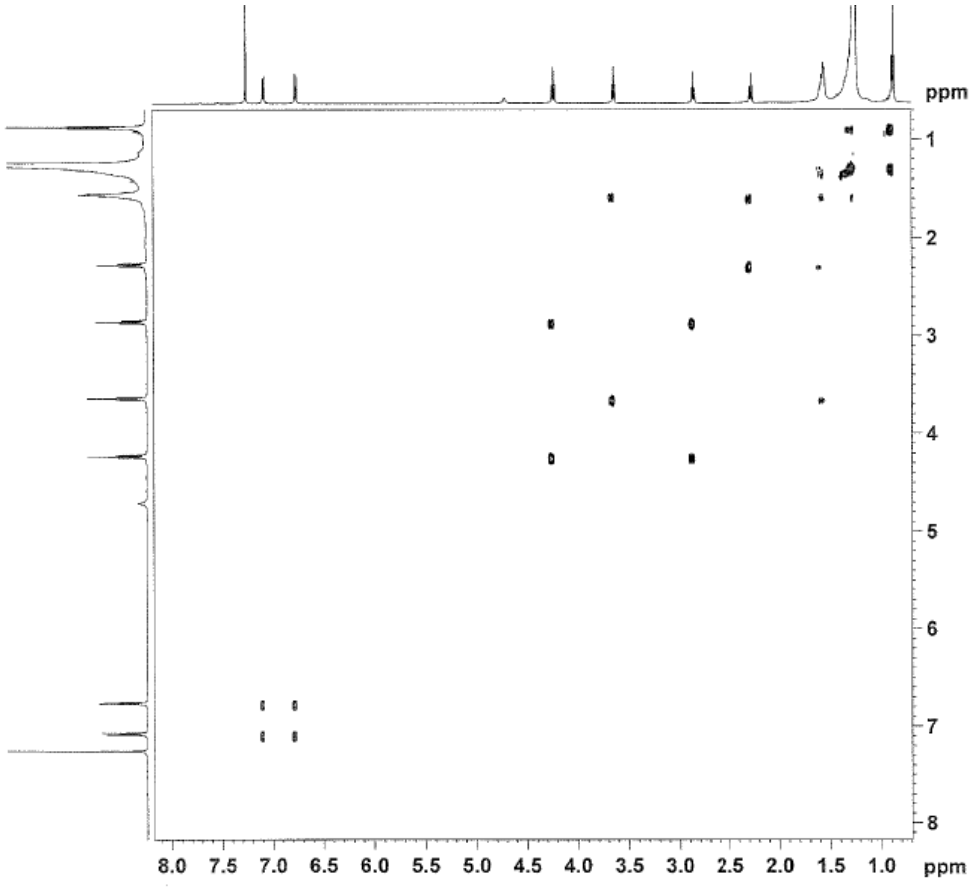

Appendix 31.3 ^{13}C NMR spectrum of a mixture of 2-(4'-alkoxyphenyl) ethyl alkanoates (125 MHz; $CDCl_3$)

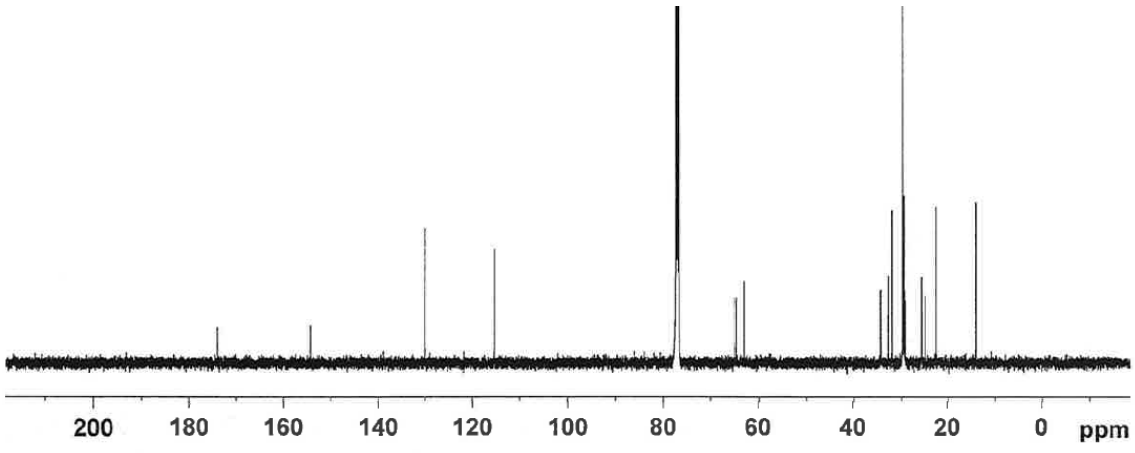

Appendix 31.4 HMQC spectrum of a mixture of 2-(4'-alkoxyphenyl) ethyl alkanoates (500 MHz for ^{1}H, 125 MHz for ^{13}C; $CDCl_3$)

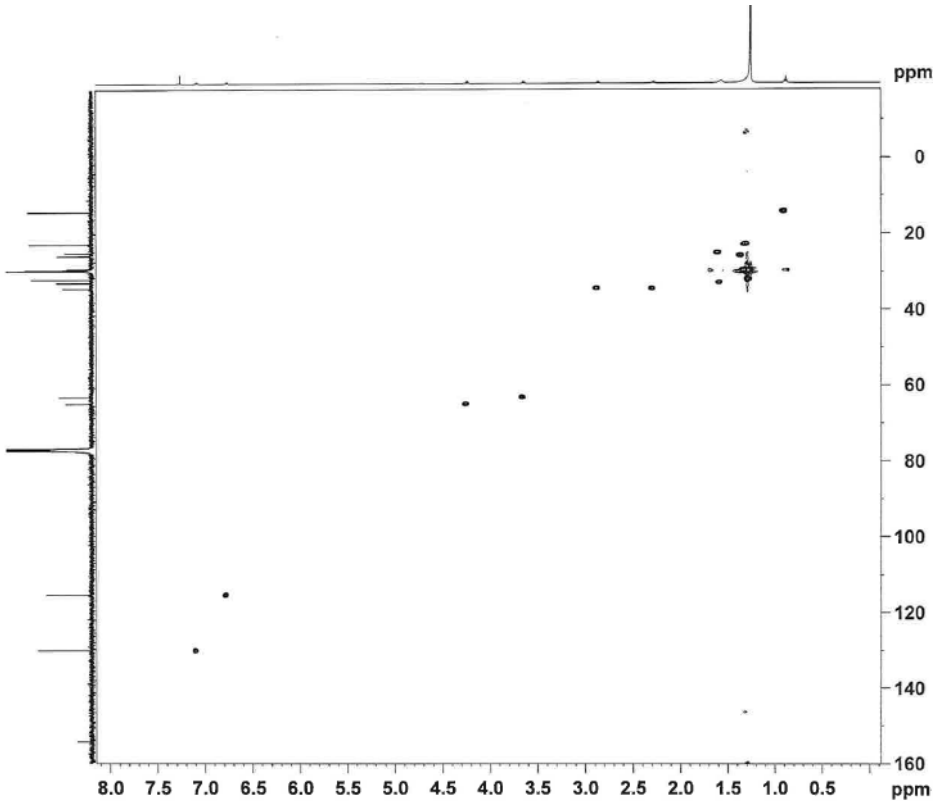

Appendix 31.5 HMBC spectrum of a mixture of 2-(4'-alkoxyphenyl) ethyl alkanoates (500 MHz for ^{1}H, 125 MHz for ^{13}C; $CDCl_3$)

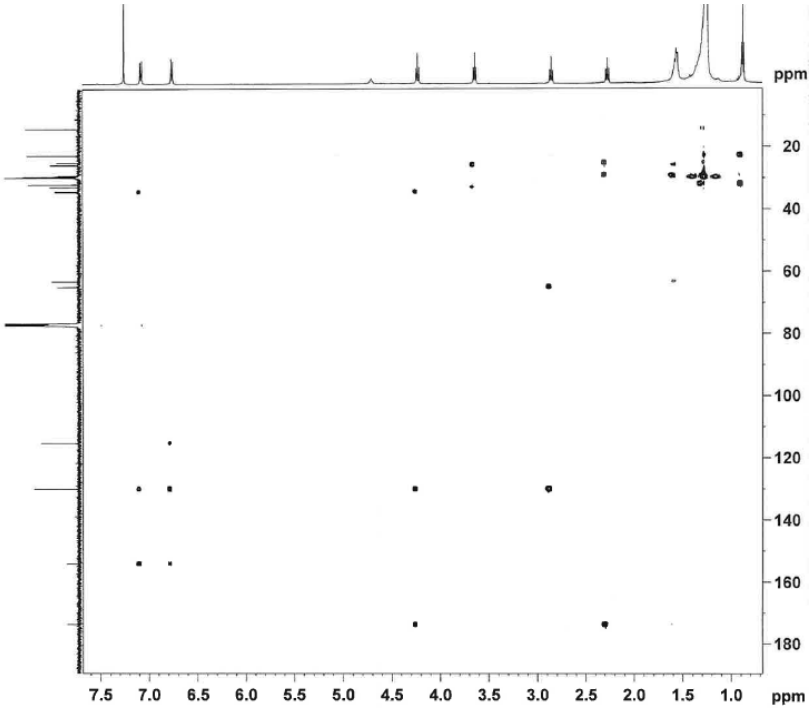

Appendix 31.6 NOESY spectrum of a mixture of 2-(4'-alkoxyphenyl) ethyl alkanoates (500 MHz in $CDCl_3$)

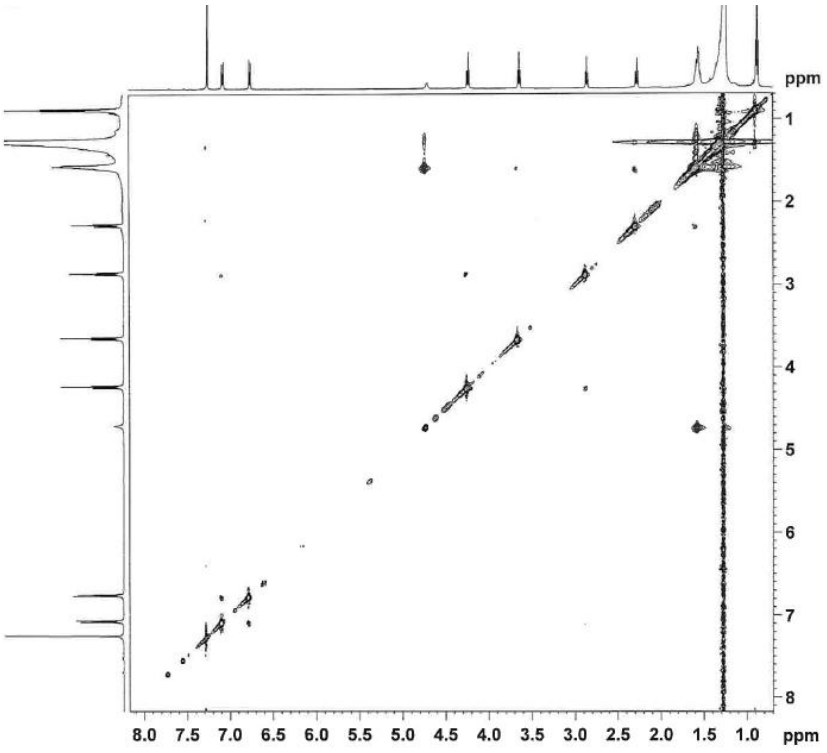

Appendix 32 Abstracts and presentations from this work

Appendix 32.1 Trends in natural products research (12th-14th April 2010), The Phytochemical Society of Europe, De Montfort University, Leicester, UK.

Phenylpropanoid glycosides from *Salvia horminum* L.

Supattra Rungsimakan, Charareh Pourzand, Michael G Rowan,

Department of Pharmacy and Pharmacology,University of Bath, Bath BA2 7AY, United Kingdom

sr322@bath.ac.uk

Many plants of genus *Salvia* in family Lamiaceae have been extensively investigated for their active biological compounds. *Salvia horminum* L. (Synonym *S. viridis* L.) is one of many sages that is used as traditional medicine, for example, an infusion of leaves as a gargle for sore gums[1]. In this study, *S. horminum* L. was investigated for its compounds as well as bioactivity. A TLC-chemoautographic method was used as a preliminary test for antioxidant activity of a crude extract. Compounds that possess this activity were seen as yellow bands or spots on a purple background in visible light shortly after a developed TLC plate was sprayed with DPPH (2, 2-Diphenyl-1-picrylhydrazyl) solution[2]. Verbascoside (acteoside) was the major compound isolated from this bioactivity-guided fractionation by using semi-preparative HPLC on a C-18 reversed-phase column. Cis-verbascoside was further separated by semi-preparative HPLC on a pentafluorophenyl column. Their structures were elucidated by HRMS and Nuclear Magnetic Resonance spectroscopy. They are now reported in *Salvia* species for the first time. Preliminary in vitro testing of verbascoside has been carried out in human skin fibroblast (FEK4) cell cultures. Fifty µM verbascoside showed protection against UV-A (wavelength 320-400 nm) induced cell damage.

[1] Dweck, A. C. (2000) The folklore and cosmetic use of various *Salvia* species, in: Kintzios, S. E. (Ed.), *Sage; The Genus Salvia.* Harwood Academic Publishers, Amsterdam.

[2] Cimpoiu, C. (2006) Analysis of some natural antioxidants by Thin-Layer Chromatography and High Performance Thin-Layer Chromatography. *J. Liq. Chromatogr. Relat. Technol.*29: 1125-1142.

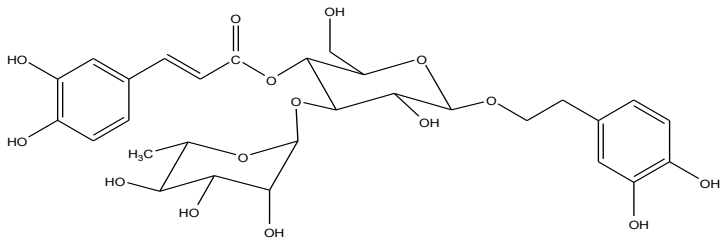

Figure 1. Verbascoside

Appendix 32.2 The international conference on natural products (24th-27th May 2011), University Paul Sabatier, Toulouse, France.

Protective effect against UVA induced cell damage of phenolic compounds from *Salvia viridis* L. cv. Blue Jeans

Supattra Rungsimakan, Charareh Pourzand, and Michael G Rowan

Department of Pharmacy and Pharmacology,University of Bath, Bath, BA2 7AY, United Kingdom

sr322@bath.ac.uk

Plants of the genus *Salvia* are well known to possess a wide range of phenolic compounds of various structural types. Many of which have shown interesting biological properties such as anti-inflammatory[1], antibacterial[1], antiviral[1], cardiovascular[2], and anti-lipid-peroxidation[2] activities. Dihydroxy phenols of the catechol type are known to form co-ordination complexes with iron in both the Fe(II), and Fe(III) oxidation states[3]. Ultraviolet light present in sunlight is known to cause oxidative damage to cells, a process that is also thought to involve iron catalysed reactions of the Fenton type[4]. Thus polyhydroxy phenols that possess both antioxidant and iron chelating activity may afford protection against such damage.

In this study, we have isolated, and identified a wide range of phenolic compounds from aerial parts of the species *Salvia viridis* L. cv. Blue Jeans (Synonym *S. horminum* L.) using column chromatography, semi-preparative reversed phase HPLC and spectroscopic methods of structure elucidation. Compounds isolated include: caffeic acid, rosmarinic acid, 6-*O*-caffeoyl-glucose, verbascoside (acteoside), leucosceptoside A, martynoside, apigenin-7-glucoside, luteolin-7-glucoside, luteolin-5-glucoside, luteolin-5-rutinoside and salidroside. We have tested three of these compounds, caffeic acid, rosmarinic acid and verbascoside for their cytotoxicity and for their protective effect against UVA (wavelength 320-400 nm) damage of cultured human fibroblast cells. All compounds were added into cell cultures 18 hours before UVA irradiation. % Cell viability was detected 24 hours after irradiation by MTT method, and flow cytometry analysis. 50% Growth inhibition concentration (IC_{50}) was also determined after 18 hours incubation period without irradiation.

Results show that all these compounds are cytotoxic with IC_{50} of 180 µM for caffeic acid, 150 µM for rosmarinic acid, and 125 µM for verbascoside. However, at lower concentrations all protect the cells against the effects of UV irradiation; survival of the cells is significantly higher than control at concentration of 50 µM for verbascoside. Flow cytometry analysis showed 1.5 fold protection of verbascoside pretreated cells over control at UVA dose 500 kJ/m^2. Furthermore, percentage of necrosis was 1.4 fold less than control while percentages of apoptosis were comparable. Although we have not yet determined the precise mechanism of action, this pattern of activity is consistent with iron chelation which at high concentration kills cells by iron depletion, but at lower concentrations prevents the build up of free iron in the cells, and concomitant generation of reactive oxygen species (ROS).

[1] Petersen, M., and Simmonds, M. S. J., 2003. Rosmarinic acid. *Phytochemistry*, 62**,** 121-125.

[2] Jiang, R. W., Lau, K. M., Hon, P. M., Mak, T. C., Woo, K. S., and Fung, K. P., 2005. Chemistry and biological activities of caffeic acid derivatives from *Salvia miltiorrhiza*. *Curr. Med. Chem.*, 2**,** 237-246.

[3] Perron, N. R., and Brumaghim, J. L., 2009. A review of the antioxidant mechanisms of polyphenol compounds related to iron binding. *Cell Biochem. Biophys.*, 53, 75-100.

[4] Pourzand, C., Watkin, R. D., Brown, J. E. and Tyrrell, R. M., 1999. Ultraviolet A radiation induces immediate release of iron in human primary skin fibroblasts: The role of ferritin. *Proc. Natl. Acad. Sci. USA*, 96**,** 6751-6756.